

WOFEX 2012

proceedings of the 10th annual workshop

Faculty of Electrical Engineering and Computer Science,
VŠB – Technical University of Ostrava

ISBN 978-80-248-2769-8

WOFEX 2012

<http://wofex.vsb.cz/2012/>

10th annual workshop,
Ostrava, 11th – 12th September 2012
Proceedings of papers

Organized by

VŠB – Technical University of Ostrava
Faculty of Electrical Engineering and Computer Science



WOFEX 2012

© Michal Krátký, Jiří Dvorský, Pavel Moravec, editors

ISBN 978-80-248-2769-8

This work is subject to copyright. All rights reserved. Reproduction or publication of this material, even partial, is allowed only with the editors' permission.

Faculty of Electrical Engineering and Computer Science,
VŠB – Technical University of Ostrava

Page count: 688
Impression: 200
Edition: 1st
First published: 2012

This proceedings was typeset by PDFL^AT_EX.
Printed and bound in Tiskárna Tiskservis, gen. Sochora 1764, 708 00 Ostrava-Poruba,
Czech Republic.

Published by Faculty of Electrical Engineering and Computer Science, VŠB – Technical
University of Ostrava

Preface

The workshop WOFEX 2012 (PhD workshop of Faculty of Electrical Engineering and Computer Science) was held on September 11th – 12th, 2012 at the VŠB – Technical University of Ostrava. The workshop offers an opportunity for students to meet and share their research experiences, to discover commonalities in research and studentship, and to foster a collaborative environment for joint problem solving. PhD students are encouraged to attend in order to ensure a broad, unconfined discussion. In that view, this workshop is intended for students and researchers of this faculty offering opportunities to meet new colleagues.

This book of proceedings includes 106 papers of faculty PhD students and 6 papers of external authors. The proceedings of WOFEX 2012 are also available at WOFEX Web site <http://wofex.vsb.cz/2012/>. I would like to thank the authors and the Organizing Committee from Department of Computer Science, namely Jiří Dvorský and Pavel Moravec, for their arduous editing work.

September 2012

Michal Krátký
Program Committee Chair
WOFEX 2012

Organization

Program Committee

Chair:

Michal Krátký (VŠB – Technical University of Ostrava)

Members:

Pavel Brandštetter (VŠB – Technical University of Ostrava)

Zdeněk Dostál (VŠB – Technical University of Ostrava)

Petr Chlebiš (VŠB – Technical University of Ostrava)

Stanislav Rusek (VŠB – Technical University of Ostrava)

Václav Snášel (VŠB – Technical University of Ostrava)

Vilém Srovnal (VŠB – Technical University of Ostrava)

Vladimír Vašínek (VŠB – Technical University of Ostrava)

Organizing Committee

Jiří Dvorský (VŠB – Technical University of Ostrava)

Pavel Moravec (VŠB – Technical University of Ostrava)

Kateřina Kašparová (VŠB – Technical University of Ostrava)

Lenka Skanderová (VŠB – Technical University of Ostrava)

Workshop Location:

Campus of VŠB – Technical University of Ostrava

17. listopadu 15, 708 33 Ostrava–Poruba, Czech Republic

11th – 12th September 2012

<http://wofex.vsb.cz/2012/>

Table of Contents

WOFEX Workshop

Study Programme P2649 Electrical Engineering

Electrical Power Engineering (3907V001)

Assessment of LED Tubes Usage in Luminaires Designed for Linear Fluorescent Lamps	3
<i>Zbyněk Carbol, Jan Šumpich, and Karel Sokanský</i>	
Shall We Reduce Levels of Luminances on the Roads in the Near Future?	9
<i>Daniel Diviš</i>	
Energy Calculation of a Train Ride	14
<i>Maroš Ďurica</i>	
Backup Alternatives for 110 kV Lines	20
<i>Vít Houdek</i>	
Construction of Model Antiphase Eliminator	26
<i>Viktor Pokorný</i>	
Complaints of Customers on Power Quality in the Czech Republic	32
<i>Petr Rozehnal</i>	
Statistical Evaluation of the Operation of Photovoltaic Power Plant	37
<i>Martin Smoček</i>	
The Issue of the Operation of Heating System	43
<i>Jaroslav Sojka</i>	
Implementation of the New Power Supply and Propulsion Concept for Steel Materials Stress Testing Device	49
<i>Peter Staš, Martin Marek, and Michal Šofer</i>	
The Monitoring System of Energetically Self-sufficient “SMART” House	55
<i>Jindřich Stuchlý</i>	
Modeling of Electromagnetic Fields in the Vicinity of the Rail	61
<i>Pavel Svoboda and Lukáš Paulinský</i>	
Trial Run of Public Lighting in Insular Mode	67
<i>Jaroslav Šnobl</i>	
MCA Evaluation of Heating Systems, Measurement of Energy Balance as Tool for Improvement Usability	73
<i>Jan Šrámek</i>	

Estimation of Voltage Unbalance in High Power Systems Supplying AC Electric Railways	79
<i>Tien Trung Vo</i>	
Using the Dynamic Model to the Transition of Traditional Distribution Network to Smart Grid	84
<i>Marián Uher</i>	
Production and Quality of Wind Energy	90
<i>Jan Unger</i>	
Laboratory Research on Production of Hydrogen in the Electrolyzer	96
<i>Jan Vaculík</i>	
Energy Accumulation of Photovoltaic Power Plant to Suppress the Negative Back Effects Caused by the Operation	102
<i>Jakub Vramba</i>	
Heating with Heat Pumps	108
<i>Petr Zach</i>	

Electrical Machines, Apparatus and Drives (2642V004)

Data Collection System for Application Artificial Neural Networks in Controlled Drives	114
<i>Pavel Bílek</i>	
Simulation of Sensorless Vector Control of Induction Motor using Kalman Filter by HIL Method	120
<i>Marek Dobrovsky</i>	
Magnetic Properties of Core for Toroidal Transformers Made from Thin Low-loss Sheets and Thermal Influence on Resulting Transformer Idle Current	126
<i>Aleš Folvarčný</i>	
Vector Control of AC Drives Using Fractional Order Controllers	132
<i>Jiří Friedrich</i>	
Computational Simulation of Electromagnetic and Electrostatic Lenses Used in Electron Microscopes	138
<i>Regina Holčáková</i>	
Control Unit for Reversible Voltage Inverter	143
<i>Michal Hromják</i>	
Sensorless Control Simulation of Switched Reluctance Motor Using HIL Method	149
<i>Petr Krňa</i>	

Dynamic Voltage Restorer 154
Lukáš Odlevák

Design of Synchronous Machine with Permanent Magnets Using FEM ... 159
Ladislav Slíva

Electronics (2612V015)

Second Order Low-Pass and High-Pass Filter Designs Using Method of Synthetic Immittance Elements 165
Lukas Klein

Analysis of FFT Algorithms for DSP Texas Instruments 171
Josef Opluštil

Simulations of the Frequency Converter 177
Josef Opluštil and Roman Šprlák

Thermal Field of Heat Sink 183
Roman Šprlák

Design and Construction Power Converter with the Aid of 3D CAD System 189
Martin Tvrdoň

Technical Cybernetics (2612V045)

Nonparametric Predictive Inference as an Alternative to the Kaplan-Meier Estimator in Survival Analysis 195
Kateřina Janurová

Interdisciplinary Approach to Renewable Energy Storage Global Planning 201
Filipe Campos, Radim Hercík, Lili Nemeč, and Alejandro Santana – Alonso

Topology of Fuel Cell Laboratory Pilot Extension 207
Kristýna Friedrišchková and Bohumil Horák

Testing of Dynamic Behavior of PMU and the Results of the Basic Tests . 213
Marek Horinek and Petr Bilik

Built-in Smartphone Accelerometer Motion Pattern Recognition Using Wavelet Transform 220
Jakub Jirka and Michal Prauzek

Handheld Vital Function Monitoring Device 227
Jan Kijonka and Marek Penhaker

An Approach to Knowledge Adaptation of Regulator in PID Control with PLC Implementation 233
Jiri Kocian and Jiri Koziorek

Energy Storage Utilizing Hydro Pump and Battery Technologies	239
<i>Jaromír Konečný, Simon Holmbacka, Dorotea Bueno Silva, Roman Chvialek, and Amer Kareem Kareem</i>	
The Application for Hybrid Power System Data Evaluation	245
<i>Jakub Maňas</i>	
The Concept of Application for Intelligent Building Management on a “SaaS” Platform	251
<i>Petr Pětvaldský and Petr Bilík</i>	
PMU Data Stream Generator for Testing of Transmission Properties in PMU Virtual Networks	257
<i>Pavel Řepka and Petr Bilík</i>	
Statistical Evaluation of Compression Methods for Storing Binary Image into Memory of Microprocessor	262
<i>Roman Slabý</i>	
Wireless System for Biotelemetry	267
<i>Martin Stankus</i>	
Methodology for Assessing Efficiency of a Photovoltaic Plant	273
<i>Michal Tutsch</i>	
Improving the Quality of Hospital Care by Using RFID Technology	279
<i>Lucie Valová</i>	
Measurement of Thermal Boreholes with Programmable Logical Controller of B&R and Sensors with Interface of 1-Wire	285
<i>Tomas Vavrla and Jiri Koziorek</i>	
Implantation System for the Real Usage as the Educational Support	291
<i>Karel Vlach, Jakub Jirka, Viktor Michna, and Radka Pustková</i>	
Using Improved Methodology for Detailed Investigating and Evaluating the Results of In-situ Thermal Response Test Experiments	297
<i>Petr Vojčínák</i>	
The Computer Based Vectorcardiography Monitoring System with Driven Right Leg Circuit	303
<i>Michal Vozda, Barbora Hrvolova, Jana Krohova, Maros Smondrk, and Marek Penhaker</i>	
Study Programme P1807 Computer Science, Communication Technology and Applied Mathematics	
Informatics (1801V001)	
Index-based N-gram Extraction from Large Document Collections	309
<i>Václav Bašniar</i>	

Processing of Range Query Using SIMD and GPU	314
<i>Pavel Bednář</i>	
Parking Lot Detection System Based on the Heat Transfer	320
<i>Radovan Fusek, Karel Mozdřeň, and Milan Šurkala</i>	
Detection of Vehicles on Parking Lots from Multiple Images via Graph Cuts	325
<i>Michael Holuša</i>	
Knowledge-base Approach to Software-process Development	331
<i>Michal Košinár</i>	
Using Prolog to Detect Resource Conflict in Processes Modelled using EPC	337
<i>Jakub Macek</i>	
Deductive Reasoning in High-order Logic	343
<i>Marek Menšík, Lukáš Vích, and Luboš Chupáč</i>	
Mean Shift and Anisotropic Diffusion	349
<i>Karel Mozdřeň, Radovan Fusek, and Milan Šurkala</i>	
Image Segmentation Utilizing Multiple Mean – Shift Executions	355
<i>Milan Šurkala, Karel Mozdřeň, and Radovan Fusek</i>	
Computational and Applied Mathematics	
(1103V036)	
Application of Edge-magic Total Labelings	361
<i>Ondrej Grunt</i>	
Parallel Implementation of Domain Decomposition Solvers	367
<i>Václav Hapla, Michal Merta, and David Horák</i>	
Numerical Solution of Stokes – Brinkman Equations Using the Mixed Finite Element Method	373
<i>Martin Hasal and Pavel Burda</i>	
Preconditioning for Block Matrices and Applications	379
<i>Rostislav Hrtus, Radim Blaheta, and Petr Byczanski</i>	
Hybrid Total FETI Method	385
<i>Marta Jarošová, Tomáš Kozubek, Martin Menšík, and Alexandros Markopoulos</i>	
Solution of Contact Problems with Level Set Based Conditions of Non-interpenetration	392
<i>Petr Kotas</i>	
Improving the Probabilistic Prediction Model of the Phadiatop Test by Data Pre-processing	399
<i>Pavčina Kuráňová, Pavel Praks, and Zdeňka Hajduková</i>	

Semi-Smooth Newton Method for 2D Contact Problems with Tresca and Coulomb Friction	405
<i>Kristina Motyčková and Radek Kučera</i>	
The Polynomials in Barzilai-Borwein Algorithm	411
<i>Lukáš Pospíšil</i>	
Ant Colony Optimization for Traffic Routing on a Dynamic Network with Anti-Congestion Measures	417
<i>Lukas Rapant</i>	
Parallel Mesh Multiplication for Petascale Systems	423
<i>Aleš Ronovský, Pavla Kabelíková, and Vít Vondrák</i>	
Discrete-Time Markov Chains in Reliability Analysis	429
<i>Pavel Skalný</i>	
Parallelization of MULTIDIS Code for Nonadiabatic Molecular Dynamics on European Supercomputers	435
<i>Martin Stachoň</i>	
Elastic Image Registration with Rigid Parts Solved by TFETI	441
<i>Alena Vasatová</i>	
Modelling of Risk to Safety Personnel in Process Industries by Simulation Method	447
<i>Adam Zdráhala</i>	
Communication Technology (2601V018)	
Polyaniline – Electrical Resistance	453
<i>Jiří Bocheza and Stanislav Hejduk</i>	
Study of Edge Detection Algorithms	458
<i>Miroslav Bureš and Jaroslav Zdrálek</i>	
Software for Visualization of Measured Data from Mach – Zehnder Interferometer	464
<i>Jan Doricak, Stanislav Kepak, and Jakub Cubik</i>	
FBG Temperature Sensor with Two Braggs Gratings with Mutually Overlapping Spectra	470
<i>Marcel Fajkus, Andrej Liner, and Martin Papes</i>	
Comparison of Communication via IR and Visible Light Spectrum in Mobile Indoor FSO Networks	476
<i>Stanislav Hejduk, Jiri Bocheza, Jan Vitasek, and Karel Witas</i>	
The Method for Real-time Content Transmission Measurement in Mobile Networks	482
<i>Lukas Kapicak and Pavel Nevlud</i>	

New Method of Analysis of Crystallizer Temperature Profile Using Optical Fiber DTS	488
<i>Petr Koudelka, Jan Látal, Jan Vitásek, Martin Pápeš, and Andrej Líner</i>	
Practical Simulation Phenomenon of the Helmholtz Coils and Its Calculation	494
<i>Lukáš Paulinský and Pavel Svoboda</i>	
CUDA Attacks and Their Effect on Security in SIP	500
<i>Jan Rozhon, Karel Tomala, and Martin Mikulec</i>	
Development and Implementation of IP Telephony Solution on Embedded Platform and Integration of YANG/NETCONF to OpenWRT	506
<i>Jakub Safarik, Jiri Vychodil, and Pavol Partila</i>	
The USRP Devices in LabVIEW	512
<i>Martin Tomis</i>	
The Radiation Pattern Shaping of Power LED Diode	518
<i>Jan Vitásek, Stanislav Hejduk, Artem Ganiyev, Jan Látal, and Jiří Bocheza</i>	
External Authors	
High-resolution Images Reconstruction Based on the Standard Thermograms	526
<i>Miroslaw Lasar</i>	
Photo and Thermal Image as an Additional Information for the Point Cloud Data	532
<i>Paweł Michalski</i>	
Thermal Analysis of Induction Motor	538
<i>Piotr Mynarek and Marcin Kowol</i>	
The Possibility of the Implementation of the Gaussian Puff Model in the Parallel Architecture	542
<i>Tomasz Przybyła</i>	
Effect of Rounding Duty Cycle on the PWM Modulation	546
<i>Tomasz Pyka</i>	
Detection and Classification of Two-dimensional Images Based on the Hilbert Method of Digital Optical	550
<i>Stawomir Stemplewski and Adam Sudol</i>	

BIOM Workshop

Finding and Recommendation of Suitable Persons in Social Networks	559
<i>Alisa Babskova</i>	
Similarity Measurement of Text Documents using Signatures	564
<i>Petr Berek, Jan Platoš, and Václav Snášel</i>	
Non-negative Matrix Factorization as Massively Parallel Algorithm for Brain Computer Interfaces	570
<i>Pavel Dohnálek</i>	
Hardware, Software, Questionnaires and Conferences for the Handicapped	576
<i>Jaroslav Hořejší</i>	
Methodology for Estimating Working Time Effort in the Software Projects	581
<i>Ondřej Koběorský, Jakub Štolfa, and Martin Kopka</i>	
Using Case-based Reasoning with Time-warped Data Collections	586
<i>Tomáš Kocyan</i>	
Estimation of the Project or Use Case Parameters Using SOM and Fuzzy Rules	592
<i>Martin Kopka, Jakub Štolfa, and Ondřej Koběorský</i>	
Analysis of Web Pages Using Schema.org Collection	598
<i>Jonáš Krutíl, Miloš Kudělka, and Václav Snášel</i>	
Compression – based Similarity	604
<i>Michal Průlepek, Jan Platoš, and Václav Snášel</i>	
Business Process – Formal Modeling in Graphical Ontology Tool – Functional View	610
<i>Jakub Štolfa</i>	
EEG Cognitive Action Recognition Based on Singular Value Decomposition Accelerated by GPU	616
<i>Lukáš Zaorálek</i>	

SoftComp Workshop

From Petri Nets to Octave Modules	625
<i>Stanislav Böhm and Ondřej Meca</i>	
Floreon JavaScript Framework for Data Visualization in Web Application	631
<i>Patrik Dubec and Jan Plucar</i>	
Current Trends in Object Constraint Language (OCL) Use	637
<i>Adam Farnik</i>	
Detecting Frayed Edge in Steel Plate using Multi Scale Retinex Algorithm	643
<i>Michal Holíš and Martin Plaček</i>	
Investigation on Evolutionary Algorithms Dynamics	650
<i>Lenka Skanderová</i>	
Dynamic Control of Adaptive e-Learning	656
<i>Ondřej Takács, Jana Šarmanová, and Kateřina Kostolányová</i>	
P Systems for Traffic Flow Simulation	662
<i>Lukáš Vojáček, Zbyněk Janoška, and Jiří Dvorský</i>	

Author Index

WOFEX Workshop



Assessment of LED Tubes Usage in Luminaires Designed for Linear Fluorescent Lamps

Zbyněk Carbol, Jan Šumpich, and Karel Sokanský

Department of Electrical Power Engineering, FEECS,
VŠB – Technical University of Ostrava, 17. listopadu 15, 708 33 Ostrava – Poruba
{zbynek.carbol, jan.sumpich, karel.sokansky}@vsb.cz

Abstract. In this paper, authors are trying to complexly assess usage of LED tubes as replacement of linear fluorescent tubes. In the first part, advantages of LED tubes deployment are shortly described. Then comparison of electrical parameters is done, followed by thermal measurement held in dust-proof luminaire. Based on this, confirmation of useful lifetime is provided. Light sources were measured in louvre luminaire to compare luminances and light intensity distribution curves. With measured data, authors made economic analysis of three different lighting systems. Finally paper compares project expenses of using conventional and LED tubes in these installations, including payback period calculation.

1 Introduction

European Union and hunger for economical savings are forcing society to use highly effective light sources with small power consumption and maintenance cost. Linear tubes are widely used for more than 70 years, nowadays the most efficient version on market is T5. But there is still majority of older T8 systems in operation, most of LED tubes are therefore designed to replace them. Usage LED technology provides customers many benefits, such as:

- High lumen efficiency- LED tubes have integrated driver and their overall lumen efficiency is ca. 95 lm/W, value for T8 tubes with inductive driver, depending on tube type, is between 70 and 80 lm/W.
- Flicker effect removal- light sources based on LED technology are reducing or removing disturbing light flickering caused by low electricity quality, because LEDs are powered by direct current from stabilized current source.



Fig. 1. Measured tubes - discharge, LED transparent, LED diffuse

- Instant luminous flux start and turn ON/OFF cycle independency- discharge tube's lifetime is strongly dependent on number of switching and

moreover their light output became stable after 5 minutes minimum. LED tubes aren't affected by these phenomenons and therefore its usage with presence sensor to reach energy savings is possible.

- Low temperature operation- LED tubes are capable of working in very low ambient temperature, what is increasing efficiency and lifetime of LEDs. These tube's operation is independent on working position.
- Long lifetime- lifetime of LED tubes provided by manufacturers or resellers is usually between 25 and 50 thousand hours, based on L80 or L70 calculation. Discharge tube's lifetime on inductive ballast is about 15 000 hrs.

Some other important advantages and disadvantages are closely described in next chapters. Comparison was made on sample of several 1200mm long tubes – discharge, LED with transparent and diffused cover.

2 Electrical parameters

Replacing linear fluorescent tubes by LED tubes is in practice very simple operation. Modern LED tubes doesn't require change of luminaire's wiring, just use special igniter, which shorts its circuit. This connection prevents electrical shock hazard, when previous versions could cause injury when installing new tube.

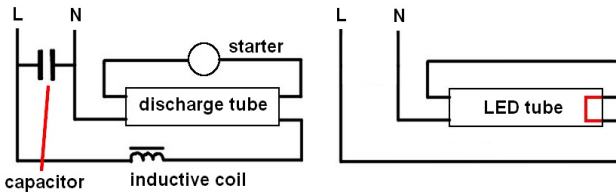


Fig. 2. Standard fluorescent lamp connection, recommended connection of LED tube

Some LED tube producers/sellers don't provide installation manual or claim, that except of short-circuit starter installation, no further modification is needed. After this installation of LED tube in luminaire (connection diagram fig. 2 left), very low power factor was measured. This was caused by compensating capacitor, which is present in some luminaires to compensate low power factor of induction ballast. When capacitor is removed, power factor increases.

Table 1. Electrical parameters of tubes in same luminaire

	P (W)	cos φ / λ (-)	S (VA)
fluorescent tube 2x36W	84,6	0,92 inductive	92,0
LED tube 2x18W	32,5	0,23 capacitive	141,3
LED tube 2x18W (condenser disconnected)	32,3	0,92 inductive	35,1

This overcompensation cause higher losses in supplying line and can cause malfunction of circuit protection devices or resonance phenomenon in local power grid. Moreover LED tubes are not suitable to be used with electronic ballast.

By LED tubes deployment in old luminaires, original ES declaration of conformity from luminaire's manufacturer is no longer valid, because its parameters and/or wiring were changed by using improper light source. From that point, responsibility for luminaire operation and safety passes to person who changed sources or LED tubes manufacturer.

3 Thermal measurements

Desired result of this measurement was confirmation of declared LED tubes lifetime. For this purpose, dust-proof luminaire was chosen, because no air exchange is possible, thus cooling of LED tubes is complicated.

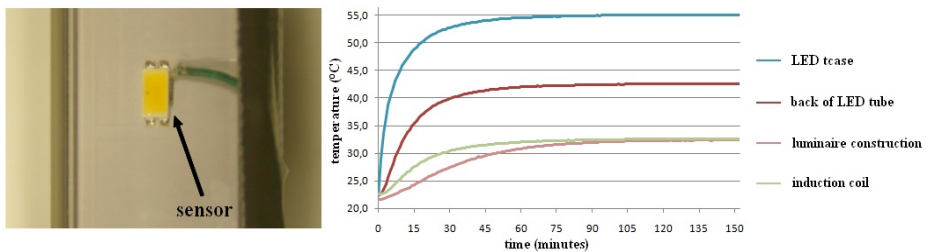


Fig. 3. tcase sensor, heating diagram

Measured t-case reached (in ambient $t=23^{\circ}\text{C}$) 55°C , estimated PN junction temperature is ca. 60°C . Even if ambient temperature was 50°C , maximum temperature approved by LED tubes manufacturer, t-case temperature wouldn't exceed 85°C . Based on similar SMD LED's aging characteristics, estimated lifetime is conclusively above 50 000 hours.

4 Light output change using LED tubes

The most important parameters of light sources are parameters that characterize light output. For these measurements was used surface mounted luminaire with aluminium louvre, which is widely used in offices and school classes.

4.1 Luminous intensity curves change

Luminous intensity curves determine illuminance level and uniformity on task plane. Fig. 4 shows significant change in magnitude and directional distribution of light. If LED tubes are installed in existing lighting system, this replacement will cause decrease of monitored parameters and if area was not previously over-lighted, then will not pass through hygienic requirements.

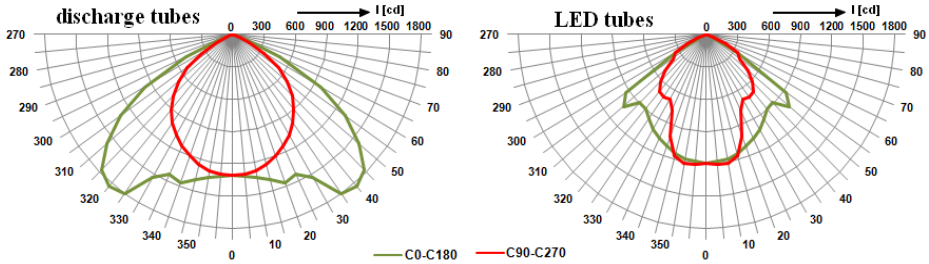


Fig. 4. Luminous intensity curves of LLX236Al with different tubes

Fig. 4 also proves, that original data from luminaire’s manufacturer can’t be used for project calculation, new measurement with LED tubes needs to be done.

4.2 Luminous flux behavior

With change of luminous intensity distribution curves is connected change of luminous flux and related parameters, such as efficiencies.

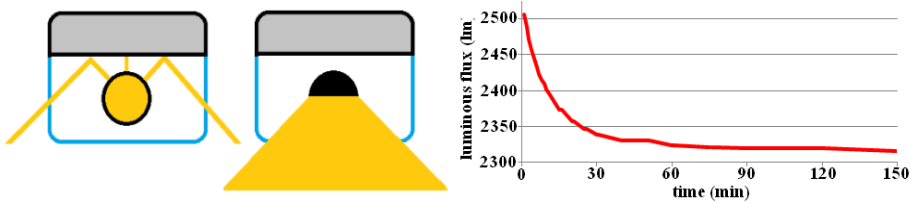


Fig. 5. Luminous intensity curves of LLX236Al with different tubes

Fig. 5 (left) shows princip of luminaires optical efficiency increase using LED tubes. Rays are going directly out of the luminaire and their energy is not decreased by reflections inside of luminaire.

Table 2. Optical and electrical parameters of different tubes in Modus LLX236Al luminaire

	luminous flux [lm]	input power [W]	optical efficiency [-]	luminous efficiency [lm/W]
luminaire with 2x36W discharge tubes	3690	84,6	0,61	43,6
luminaire with 2x18W LED tubes (transparent)	2330	32,5	0,75	71,8

Although LED tubes are in luminaire much more efficient, absolute luminous output is ca. 30% less, as shown in table 2. Nowadays LED tubes can’t reach higher luminous flux (input power), because of poor cooling performance.

4.3 Luminance

Despite of lower luminous flux of LED tubes, high luminance of LED chips can cause higher glaring. This parameters can't be qualified by valid standards, therefore just results of measurement are provided.

Table 3. Luminance characteristics of measured tubes

	luminous flux [lm]	maximal luminance [kcd/m ²]	average luminance [kcd/m ²]
fluorescent tube 36W/840	3010	16	13
LED tube transparent 18W	1560	4 400	n/a
LED tube diffuse 18W	1450	200	15

Problem is caused by extremely high maximum luminance of LED chips, diffuse and transparent tube luminance images are shown on fig. 6 (left).

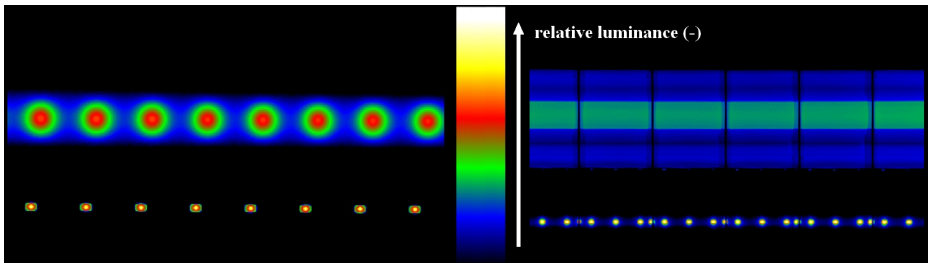


Fig. 6. Luminance camera images

Fig. 6 (right) shows luminance analysis of fluorescent and transparent LED tube in louvre luminaire. LED tube doesn't use optical system of luminaire, therefore high contrast to reflector in background is visible.

5 Economic analysis

Main reason for buying expensive LED tubes is definitely savings in consumed energy. This comparison was made in 3 different projects considering new installation of lighting system:

- Class/office lighting system, average operation time 4 hours/day, 5days/week
- Warehouse lighting system, average operation time 12 hours/day, 7days/week
- Underground car park lighting system, average operation time 24 hours/day

Because LED tube's luminous flux is lower, to reach same illuminance was in every installation needed to use 30% more LED luminaires.

Financial input data are: electricity price 4k/kWh, LED tube 120cm 18W (lifetime 50 000 hrs) 1500 k/pcs, fluorescent tube 36W (lifetime 15 000 hrs) 50k/pcs, luminaire price 750k/pcs, tube/luminaire replacement/installation 50k/each.

For comparison was chosen lighting system with 100 luminaires with fluorescent lamps, respectively 130 luminaires with LED tubes.

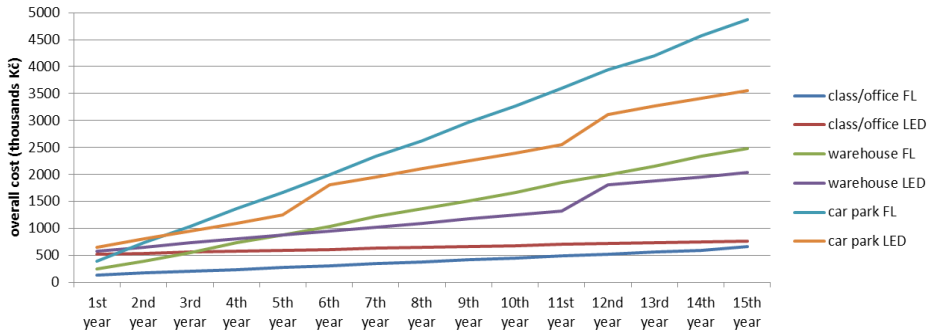


Fig. 7. Economic comparison of overall cost

Overall cost (investment, energy, maintenance) comparison between fluorescent lamps (FL) and LED tubes is shown on fig. 7. Investment payback period is shortest in third case – nonstop operation – 3 years. Warehouse’s payback period is 6 years. In first case payback period doesn’t come in evaluated time period (15 years).

6 Conclusion

The objective of this article is to assess LED tubes as replacement of T8 fluorescent:

In electrical connection, it’s necessary to confirm proper connection, without compensation condenser.

From thermal point of view, cooling of LEDs in tube is sufficient to reach useful lifetime as declared, 50 000 hours. Question is, if driver, installed in tube will not cause earlier malfunction.

Optical properties of LED tubes changes completely appearance and light output of luminaire. Therefore new measurement or project calculation is needed before LED tubes are installed. For interior workplaces lighting, authors recommend only diffuse LED tubes to reduce possible glaring.

Last but not least is economic aspect: to reach maximum acceptable payback period 10 years, minimal 3 000 lighting hours per year, resp. 8 hours a day, is needed. Concluding all facts, LED tubes are capable to replace T8 discharge tubes, but further multi-aspect appraisal of each project is needed. Generally it’s worth to deploy LED tubes in long time operation lighting systems with lower requirements on quality of light (because of glare).

Acknowledgement

This research was supported by SGS project SP2011/135: Optimization electrical energy consumption using modern light sources.

Shall We Reduce Levels of Luminances on the Roads in the Near Future?

Daniel Diviš

Department of Electrical Power Engineering, FEECS,
VŠB – Technical University of Ostrava, 17. listopadu 15, 708 33 Ostrava – Poruba
daniel.divis@vsb.cz

Abstract. This paper describes the latest knowledge of mesopic vision. Some manufacturers and operators of public lighting systems want to reduce luminance levels using modern light sources (LED). These manufacturers claim that the human eyes are adapted to the mesopic vision luminances (0.005 cd m^{-2} - 5 cd m^{-2}) on lit roads by public lighting. Human eyes use cones and rods receptors in these levels of luminance. Rods are more sensitive in the shorter wavelengths region of incident visible radiation that is emitted by diodes instead of high pressure sodium lamps. These are currently used in public lighting dominantly. Although all standards and instrumentation are adapted to human eye sensitivity for daytime (photopic) vision, so some manufacturers and operators public lighting systems want to reduce luminance on the roads. Article describes the controversy between the requirements of luminance levels on the roads with the latest knowledge in this area.

Keywords: Mesopic vision, Public lighting system, LED, S/P ratio

1 Introduction

In the paper we explore the latest knowledge in the field of mesopic vision and their practical use in assessing and evaluating the luminance on roads with a security in mind. There are several unspecified factors that influence our perception of movement on the roads. The most fundamental seems to be determination of adaptation luminance. For evaluation is also important to know what lamp is used in lighting luminaire.

2 Mesopic vision

Mesopic vision of man is in the area between the day (photopic) and night (scotopic) vision. The range of luminance in which humans use mesopic vision is as follows: $0,005 \text{ cd}\cdot\text{m}^{-2}$ - $5 \text{ cd}\cdot\text{m}^{-2}$.. Typical example of how our eyes use mesopic vision is outdoor street lighting, where the road surface reflectance in the range $0.05 \div 0.25$,

for the practical purposes usually uses the value 0.07. The luminance of the road is in these values. In the vision of both types of photoreceptors, we can define the rate at which they are involved in the vision - S / P ratio (CIE 191-2010).

2.1 Application of the mesopic photometry

Known factors:

- adaptation luminance defining spectral sensitivity of human eye $V''(\lambda)$,
- S / P ratio of light sources,
- procedure for calculating the L_{mes} based on S / P ratio and L_p photometric luminance.

Unknown factor:

- visual adaptation field - what it involves and how to define it?

2.2 S/P ratio [3]

It is the ratio of contribution scotopic to photopic of vision.

$$S / P \text{ ratio} = \frac{K'_m \int_0^\infty S_\lambda(\lambda) V'(\lambda) d\lambda}{K_m \int_0^\infty S_\lambda(\lambda) V(\lambda) d\lambda} \tag{1}$$

where:

K_m 683 lm / W

K'_m 1700 lm / W

S_λ spectral distribution of light source

$V(\lambda)$ spectral curve of the photopic vision

$V'(\lambda)$ spectral curve scotopic vision

If S/P ratio will be greater than 1, then mesopic luminance caused by a photopic luminance value will increase and conversely if the S/P ratio will be less than 1 then mesopic perceived luminance will be lower.

International commission on illumination CIE recommended for the conversion to use the system Mes2 describing the process mesopic spectral sensitivity. Other calculation models that are currently used for determining the mesopic luminance: USP, Move and Mes1.

Table 1. Percentage differences between photopic luminance and perceived luminance in mesopic vision for light sources with different S/P ratio [1]

S/P	Adaptation photopic luminance (cd-m-2)		
	0,03	0,3	3
0,65	-24 %	-10 %	-3 %

1,00	0 %	0 %	0 %
1,35	20 %	9 %	3 %
2,15	61 %	28 %	9 %

Table 2. Light sources and their S/P ratio

Light source	S/P ratio [-]	Note
Low pressure sodium lamp	0,25	-
High pressure sodium lamp	0,40-0,76	2000 K
Mercury lamp	1,18	3500 K
Incandescent lamp	1,41	2850 K
Fluorescent lamp - cool white	1,58	5000 K, triphosphor
Fluorescent lamp - cool white	1,70	5000 K, Ra 90
LED - neutral white	1,68	4180 K
Fluorescent lamp - daylight	1,72-2,22	-
Induction lamp	1,83	4866 K
LED - cool white	2.50	6000 K

2.5 Examples of determination of adaptation luminance

In foveal vision applied cones only, which are located in the central hole - yellow spot. Rods are not in the central hole. In peripheral vision are active rods photoreceptors which are most densely located along the edge of the retina.

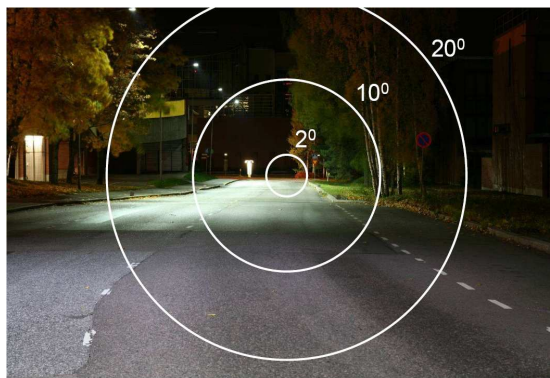


Fig. 1. Observed situation I [2]

The differences in the luminance at those figures are due to various situations that may occur in sight of the driver, the differences can amount to tens of percent. The decrease of the average luminance of the adaptation of the observer 2 ° through 10 °, 20 ° to the whole area being evaluated is approximately 66% according to [2].

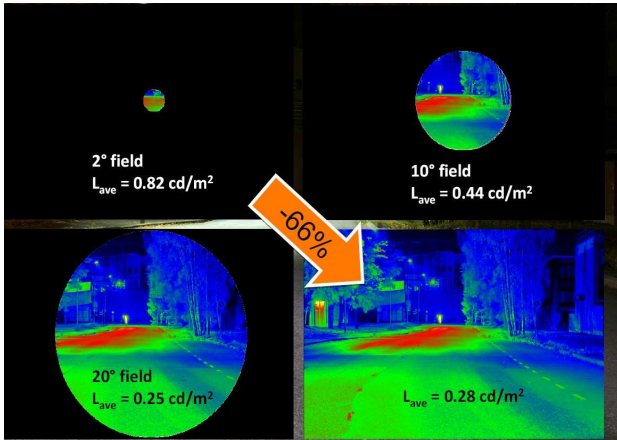


Fig. 2. The average luminance for different fields of view [2]

Fig. 2 illustrates the road with dark environment (trees). There are no trees in Fig. 3 and there is road between the buildings with relatively bright facade, so drop in average luminance between the first areas and the fourth is down by 31%.

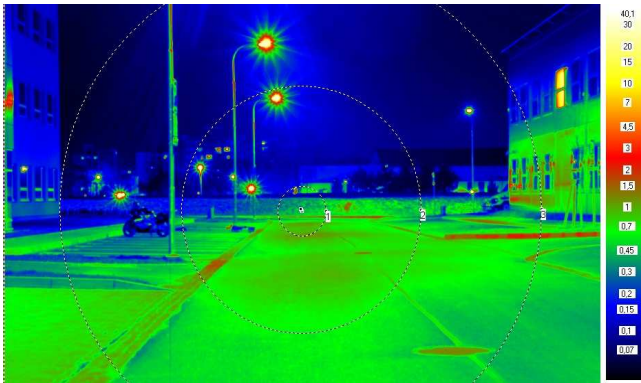


Fig. 3. Observed situation II

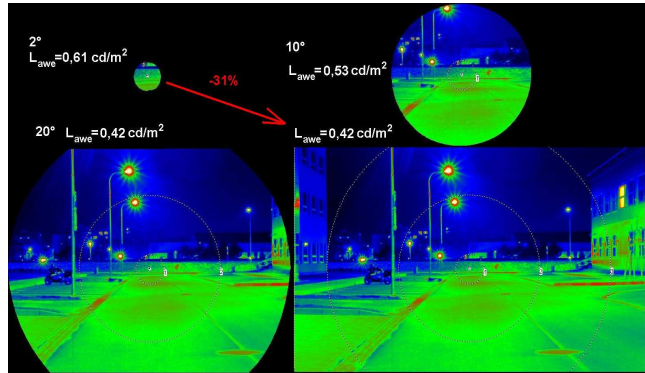


Fig. 4. Luminance conditions for various communication fields of vision

3 Conclusion

Although modern LED lamps are more efficient in mesopic perception, it is not possible to reduce the levels of luminance and illuminance on the road with a regard to safety on the roads because we can not specify the adaptation luminance (foveal vision -cones, peripheral vision - rods). S/P ratio is understood as an integral whole retina, but the critical detail is perceived as photopic foveal to the 2°. Increasing the S/P ratio (color temperature sources) affects the increase perception in the mesopic vision area, but not in the area of critical detail. It follows that we can not reduce the luminance. The issue of the luminance adaptation area on is still in solution. We consider the behavior of the eye in the dynamic mode as totally unexplored area - the time change luminance adaptation through which it passes as a driver while driving.

Acknowledgment

The article was created by the project SGS - New options for LED technology in lighting, project number SP 2012/160.

References

1. Gašparovský, D., Smola, A.: Návrh umelého osvetlenia interiérov a exteriérov, Bratislava: SEZ-KEZ, 2011. s. 262. ISBN 978-80-8106-046-5.
2. Halonen, L., Puolakka, M.: CIE system for mesopic photometry, CIE introductory tutorial & workshop on mesopic photometry, p. 35 Vienna 2012
3. CIE 191:2010 Recommended system for mesopic photometry based on visual performance, ISBN 9783901906886

Energy Calculation of a Train Ride

Maroš Ďurica

Department of Electrical Engineering, FEECS,
VŠB – Technical University of Ostrava, 17. listopadu 15, 708 33 Ostrava – Poruba
d.maros@seznam.cz

Abstract. Energy consumption is related to basic technical parameters which depend on a type of a train and a track. Owing to this, speed and acceleration of a train, rolling resistance, aerodynamic resistance can be calculated from basic formulae based on traction data. A basic element of the calculation is a matrix of train speed and a matrix of lengths of individual train tracks. The overall calculation needs two forms of input data: the train data and the track data.

Keywords: Energy calculation, energy consumption, aerodynamic resistance, acceleration, matrix, driving resistance, rolling resistance, railroad tracks

1 Introduction

Railways play a significant role in the European transport network. They represent a significant transport mean as well as a large investment on the part of society. Development of the future transport network and the wise use of resources require that this network is utilized in an appropriate manner. A significant factor for evaluation of a part of the transport network is a problem of railway transport energy consumption. In this paper, the calculation has been used for an analysis of several actual problems connected with transport by train and the relation to energy consumption.

2 Electric Traction Power Supply

Power supply of an electric traction covers a field of energy consumption and losses of operated railway vehicles. A train run energy consumption calculation can be performed as follows:

- Time integration based on the vehicle input.
- Determination of consumption based on traction work and loss components. We need to calculate the consumption for the traction work and coverage of energy losses in the traction unit arising from irregular motion. The motion is divided to the starting, constant speed running and braking phases. Furthermore, we need to take into account heating in winter and consumption of auxiliary circuits – drives of the railway vehicle equipment.

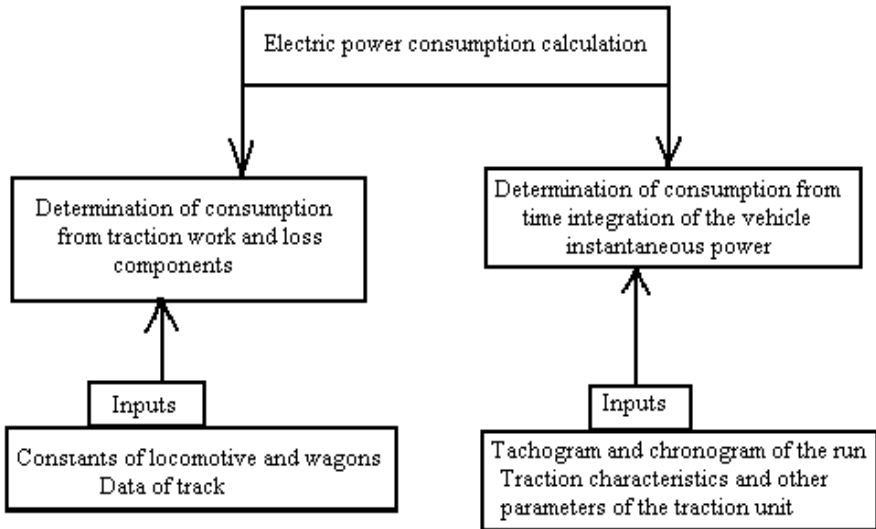


Fig. 1. Railway vehicle power consumption calculation

3 Data traction vehicles

For the calculation we use E669.2-type locomotive (Fig.2) with the coefficient of traction equation:

$$a = 3.8 + 0.02 \cdot V + 0.0004 \cdot V^2 \quad (\text{N} \cdot \text{kN}^{-1}, \text{km} \cdot \text{h}^{-1}) \quad (1)$$



Fig. 2. E669.2 - type locomotive, 3kV voltage, Co 'Co' undercarriage

Basic data:

Manufacturer -	Škoda Plzeň
Year of manufacture -	1963 - 1965
Continuous power -	2610 kW
Consumption of auxiliary drives (compressor, air conditioning, lighting, heating and bat. recharging) -	52.2 kW
Running time of auxiliary drives -	0.8 h
Coefficient of rotating masses -	1.25
Electric hot-air heating of the locomotive -	10kW
Running time of heating -	3 h
Adhesion weight -	120 t
Nominal efficiency -	88%
Undercarriage of the locomotive -	Co 'Co'
Electric system -	3 kV DC

4 Railroad Track Data

To calculate the power consumption, Bohumín – Čadca No.320 (Czech Railways nomenclature) segment of the railroad is used.

Table. 1. Data of Bohumín – Čadca No.320 railroad track

Section No.	Station	Distance (km)	Max. Speed (km/h)	Reduced gradient (N/kN)
1	Bohumín	0	40	0,85
2		1,182	110	6,21
3	Dolní Lutyně	4,052	110	4,16
4		7,902	60	2,16
5	Dětmarovice	8,494	100	3,14
6	Karviná hl.n.	15,223	40	3,99
7	Karviná -Darkov	17,544	50	3,32
8	Louky nad Olší	23,631	100	2,33
9	Chotěbuz	26,322	100	3,33
10		28,574	60	3,43
11	Český Těšín	29,682	80	3,15
12		31,248	80	3,27
13		32,414	80	4,28
14		33,616	70	0,75
15	Ropice zastávka	34,264	80	4,38
16	Třinec - konská	36,444	100	3,13
17	Třinec	37,106	80	5,21
18	Vendryně	37,874	70	7,5
19	B. nad Olší	44,055	100	12,3
32	Čadca	68,842	80	0

5 Energy Consumption Calculation

For the electric energy consumption calculation, the Canadian production software Mathcad is used which can perform calculations, draw graphs and work with a text. All calculations are performed using commands of libraries, whereas the given expressions are written in usual forms as fractions, matrices.

The solution: In the Bohumín - Čadca segment, there are 32 values of vehicle speeds arranged to the matrix marked as V1. V2 matrix is the square of V1 matrix. These values have been substituted into the equation of the E 669.2 locomotive driving resistance. And then we have obtained a matrix Po.

$$V1 := \begin{pmatrix} 40 & 110 & 110 & 60 \\ 100 & 40 & 50 & 100 \\ 100 & 60 & 80 & 80 \\ 80 & 70 & 80 & 100 \\ 80 & 70 & 100 & 70 \\ 70 & 70 & 80 & 70 \\ 70 & 80 & 70 & 70 \\ 70 & 80 & 80 & 80 \end{pmatrix} \quad V2 := \begin{pmatrix} 1600 & 12100 & 12100 & 3600 \\ 10000 & 1600 & 2500 & 10000 \\ 10000 & 3600 & 6400 & 6400 \\ 6400 & 4900 & 6400 & 10000 \\ 6400 & 4900 & 10000 & 4900 \\ 4900 & 4900 & 6400 & 4900 \\ 4900 & 6400 & 4900 & 4900 \\ 4900 & 6400 & 6400 & 6400 \end{pmatrix}$$

$$Po = 3.8 + 0.02 \cdot V1 + 0.0004 \cdot V2 \quad (\text{N} \cdot \text{kN}^{-1}, \text{km} \cdot \text{h}^{-1}) \quad (2)$$

$$p = Po + psred \quad (\text{N} \cdot \text{kN}^{-1}) \quad (3)$$

$$Wt = p \cdot 2.725 \quad (\text{W} \cdot \text{h} / \text{t} \cdot \text{km}) \quad (4)$$

$$Wt \text{ total} = Wt / \text{efficiency} \cdot \text{track} \quad (\text{W} \cdot \text{h} / \text{t} \cdot \text{km}) \quad (5)$$

$$Po = \begin{pmatrix} 5.24 & 10.84 & 10.84 & 6.44 \\ 9.8 & 5.24 & 5.8 & 9.8 \\ 9.8 & 6.44 & 7.96 & 7.96 \\ 7.96 & 7.16 & 7.96 & 9.8 \\ 7.96 & 7.16 & 9.8 & 7.16 \\ 7.16 & 7.16 & 7.96 & 7.16 \\ 7.16 & 7.96 & 7.16 & 7.16 \\ 7.16 & 7.96 & 7.96 & 7.96 \end{pmatrix} \quad Wt = \begin{pmatrix} 16.596 & 46.462 & 40.875 & 23.435 \\ 35.262 & 22.428 & 24.852 & 33.055 \\ 35.78 & 26.897 & 30.275 & 30.601 \\ 33.354 & 21.554 & 33.627 & 35.234 \\ 38.614 & 39.949 & 60.222 & 48.397 \\ 63.711 & 63.982 & 68.889 & 60.168 \\ 63.438 & 60.168 & 60.74 & -15.259 \\ -14.007 & -9.919 & -5.014 & 21.691 \end{pmatrix}$$

Regarding the fact that the traction resistances in the track stages are constant, we can add them up and obtain a matrix p which is then used for the calculation of the specific consumption Wt. The sum of all elements of the specific energy consumption matrix $\Sigma Wt = 1096.04 \text{ W} \cdot \text{h} / \text{t} \cdot \text{km}$.

The result is the total specific energy consumption for steady speed:

$$Wt_{\text{total}} = 18.092 \text{ W}\cdot\text{h} / \text{t}\cdot\text{km}.$$

In the following part of the calculation we take into account losses caused by acceleration, braking and power consumption of the vehicle auxiliary circuits and heating.

$$W_{\text{start}} = 1.072 \cdot 0.01 \cdot (\zeta / \text{track}) \cdot V^2 \cdot (1 + (P_o + p_{\text{sred}} / p_{\omega \text{ start}}) \cdot (1 / \eta - 1)) \quad (6)$$

$$(\text{W} \cdot \text{h} / \text{t} \cdot \text{km})$$

$$p_{\omega \text{ start}} = 102 \cdot \zeta \cdot \omega_{\text{start}} \quad (\text{N} / \text{kN}) \quad (7)$$

$$W_{\text{stop}} = 1.072 \cdot 0.01 \cdot (\zeta / \text{track}) \cdot V^2 \cdot (1 - (P_o + p_{\text{sred}} / p_{\omega \text{ stop}})) \quad (8)$$

$$(\text{W} \cdot \text{h} / \text{t} \cdot \text{km})$$

$$p_{\omega \text{ stop}} = 102 \cdot \zeta \cdot \omega_{\text{stop}} \quad (\text{N} / \text{kN}) \quad (9)$$

According to Table 1, the specific energy losses for 32 starts = 39.61 W·h / t·km and for 32 stops = 5.23 W·h / t·km.

Specific energy consumption of auxiliary drives:

$$W_{\text{pp}} = \text{Consumption of auxiliary drives} \cdot \text{Running time of auxiliary drives} \cdot \quad (10)$$

$$1000 / \text{locomotive weight} \cdot \text{track} \quad (\text{W} \cdot \text{h} / \text{t} \cdot \text{km})$$

The specific energy consumption of auxiliary drives is 5.055 W·h / t·km.

Specific energy consumption for heating:

$$W_{\text{pt}} = \text{Consumption for heating} \cdot \text{Running time of heating} \cdot 1000 / \text{locomotive} \quad (11)$$

$$\text{weight} \cdot \text{track} \quad (\text{W} \cdot \text{h} / \text{t} \cdot \text{km})$$

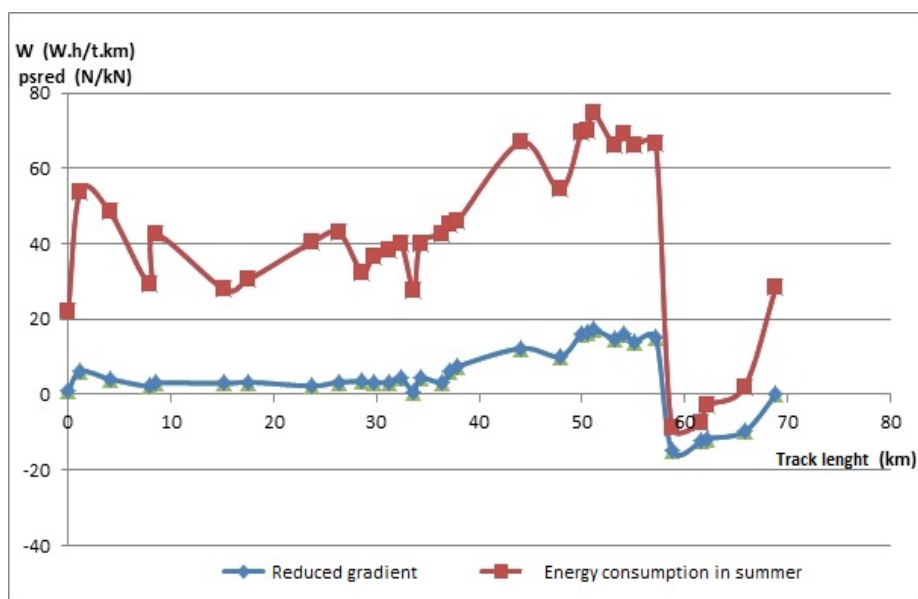
The specific energy consumption for heating is 3.632 W·h / t·km.

The specific energy consumption calculation for the locomotive collector: In summer, the sum of all components is 67.98 W.h / t.km. In winter, the specific energy consumption for heating needs to be added.

6 Conclusion

In this paper, the problem of calculating the specific energy consumption for the selected traction vehicle - E669.2-type locomotive running on the Bohumín – Čadca track segment (No.320 - Czech Railways nomenclature) is solved. Of all the energy losses, the loss at start has the biggest influence on the resulting electric energy consumption, because the locomotive stops at every stop of this track segment. Furthermore, there is an unfavourable profile of this track segment with a relatively large reduced gradient in the second half of the track segment. I have verified the calculation correctness by the specific power consumption nomogram for type trains which corresponds to P_n through freight train.

Fig. 3. Graph of the relation of the energy consumption in summer and the reduced gradient on the track length.



References

1. http://en.wikipedia.org/wiki/ČSD_Class_E_669
2. Prof.Ing.Paleček, J., CSc: Elektroenergetika v dopravě, studijní materiály k přednáškám, VŠB – Technical University of Ostrava, Winter Semester 2010.

Backup Alternatives for 110 kV Lines

Vít Houdek

Department of Electrical Power Engineering, FEECS,
VŠB – Technical University of Ostrava, 17. listopadu 15, 708 33 Ostrava – Poruba
vit.houdek@centrum.cz

Abstract. The article analyses the alternatives of backup for 110 kV lines. We not only describe various types of back-ups, but also present theoretical calculations of probability failure-free operation and evaluate ranking of different backup options. It is specified and documented by line back up calculated values.

Keyword: Backup, probability of failure-free operation, reliability scheme, maintenance, RCM, backup capability

1 Introduction

Electricity is a very important need to people's lives. Therefore it is very important to ensure the reliable distribution. This reliable and safe function ensures the distribution system that follows the rules for the operation of the grid. In the event of a power distribution company loses profit for distribution and sale of electric energy. Today can also be sanctioned for the undelivered electricity customers. Important activity to maintain reliability and safety is maintenance. Distribution system maintenance is performed according to a number of preventive maintenance. To optimize the maintenance is now performed Reliability Centered Maintenance (RCM). This type of maintenance depends on the technical condition and importance of equipment. This article outlined the importance of the lines and its backup alternatives.

2 Importance of Line

Importance of a 110 kV line can be determined by carrying capacity, load or losses. It is better to determined importance of line by backup capability. Backup alternatives for a failed line must be specified. Power can be supplied by another 110 kV line or an MV line. However, some 110 kV lines have no backup. If a line fails,

localization of a failure and manipulations to deal with failure, either manual or remote, must be carried out. In terms of reliability, manipulation time is important for the calculation.

2.1 Method of Reliability Schemes

To calculate backup capability, we use probability of failure-free operation R (-) evaluated in the following equation:

$$R = 1 - \frac{\lambda \cdot \tau}{8760} \quad (-; \text{year}^{-1}, \text{hour}) \quad (1)$$

Failure rate λ (year^{-1}) and mean failure time τ (hour) must be determined. With a modified reliability schemes method, the final reliability parameters can be obtained by means of gradual simplification of reliability scheme. The method diversifies three basic types of connecting two elements:

- Series connection of elements
- Parallel connection of elements – hot reserve
- Parallel connection of elements – cold reserve

A method correspond to ČEZ 22/80 regulation was used for calculation (no using maintenance to calculation).

Series connection of elements

Equations for calculating the probability of failure-free operation:

$$\lambda = \lambda_1 + \lambda_2 \quad (\text{year}^{-1}, \text{year}^{-1}, \text{year}^{-1}) \quad (2)$$

$$\tau = \frac{(\lambda_1 \cdot \tau_1 + \lambda_2 \cdot \tau_2)}{\lambda} \quad (\text{hour}; \text{year}^{-1}, \text{hour}) \quad (3)$$



Fig.1 Series connection of elements

Parallel connection of elements – hot reserve

Equations for calculating the probability of failure-free operation:

$$\lambda = \frac{1}{8760} \cdot (\lambda_1 \cdot \lambda_2 \cdot (\tau_1 + \tau_2)) \quad (\text{year}^{-1}; \text{year}^{-1}, \text{hour}) \quad (4)$$

$$\tau = \frac{(\lambda_1 \cdot \lambda_2 \cdot \tau_1 \cdot \tau_2)}{8760 \cdot \lambda} \quad (\text{hour}; \text{year}^{-1}, \text{hour}) \quad (5)$$

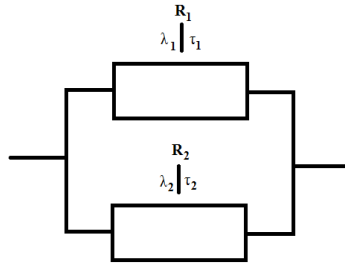


Fig. 2 Parallel connection – hot reserve

Parallel connection of elements – cold reserve

This scheme is for determinate probability with manipulation. Equations for calculation formulas are combination of serial and parallel connection. Firstly is calculated parallel combination. Then is calculated serial combination with parallel results and parameters of manipulation. Failure rate of manipulation corresponds with failure rate of the first element manipulation takes place if the first element fails.

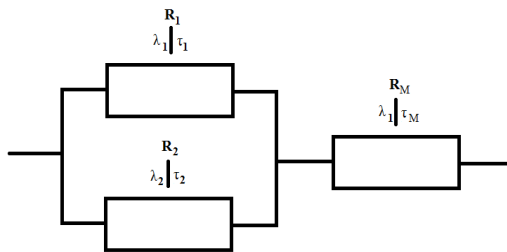


Fig. 1 Parallel connection – cold reserve

2.2 Probability of Failure-Free Operation

Input parameters were calculated from the failure database at the Department of Electrical Power Engineering. These parameters are collected during a long-term monitoring and recording of failures. To calculate probability of failure-free operation, we used failure rate and mean failure time input values from Tab.1 [1]

Tab. 1 Input parameters

	λ (year ⁻¹)	τ (hour)
HV line	0.282 / 100 km	3.155
MV line	3.623 / 100 km	18.759
HV/MV transformer	0.048	74.892

To calculate the probability of failure-free operation were created 5 models of backups:

- No backup
- Backup by HV line of the same length
- Backup by HV line of 1.5 multiple of its length
- Backup by MV line of the same length
- Backup by MV line of 1.5 multiple of its length.

Every backup has two options (besides – no backup). One option is without manipulation (hot reserve), second is with manipulation (cold reserve). The parameters were chosen to enable comparison:

- Manipulation time: 7 minutes (backup by HV), 20 minutes (backup by MV),
- Line length which is backed: 100 km (basic length).

No backup

Model has only one element (Fig.4). The calculation is very simply (1).

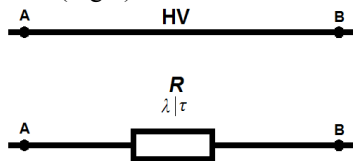


Fig. 4 No backup – electrical and reliability schemes

$$R = 0.999\ 996\ 234$$

Backup by HV line of the same length

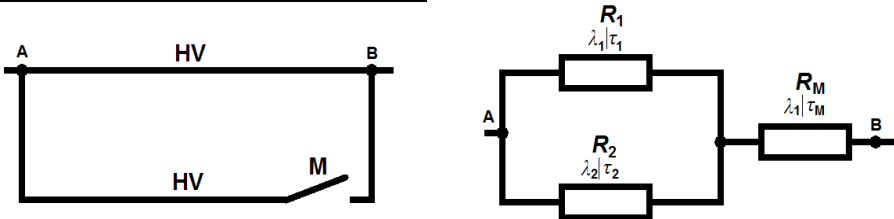


Fig. 5 HV backup – electrical and reliability schemes

This is typical for twin line. This backup has two options – with and without manipulation. For calculation probability we used reliability scheme (Fig.5).

Without manipulation $R = 0.999\ 999\ 989$

With manipulation $R = 0.999\ 996\ 234$

Backup by HV line of 1.5 multiple of its length

The schemes (Fig.5) and calculations are the same as the previous backup. Only length of backup line is 150 km.

Without manipulation $R = 0.999\ 999\ 985$

With manipulation $R = 0.999\ 996\ 229$

Backup by MV line of the same length

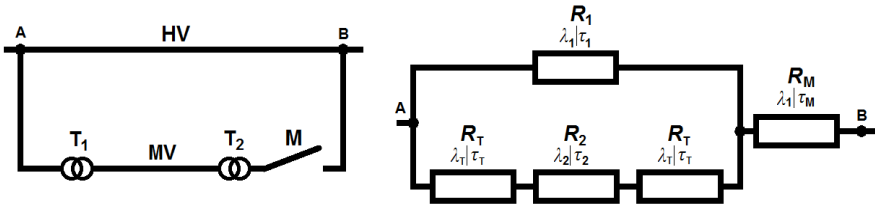


Fig. 6 MV backup – electrical and reliability schemes

This backup has two options – with and without manipulation. Firstly we calculate serial connection (MV line and two transformers), then parallel connection with HV line.

Without manipulation $R = 0.999\ 999\ 129$
 With manipulation $R = 0.999\ 988\ 398$

Backup by MV line of 1.5 multiple of its length

The schemes (Fig.6) and calculations are the same as the previous backup. Only length of backup line is 150 km.

Without manipulation $R = 0.999\ 998\ 735$
 With manipulation $R = 0.999\ 988\ 004$

3 Backup Alternatives

With help of probability of failure-free operation we can evaluate ranking of all backup options. The best backup is provided by backup without manipulation – hot reserve, second is backup with manipulation - cold reserve. The worst option is a line without backup. Options using the HV line are better than the options MV backup. Depending on the failure probability we evaluated backup capability by method from our department. Most backups in distribution networks are cold reserves requiring manipulation time, therefore results of hot reserves – without manipulation will not be included in the assessment of backup alternatives.

The HV abbreviation in Tab. 2 means that the backup is via HV line, $l_1 = l_2$ means that the lengths of the backed up line and the backup lines are the same, $l_1 < l_2$ means that the length of the backup line is 1.5 longer than that of the backed up line. Backups using MV lines are marked MV. The MAN abbreviation means that the backup is with manipulation.

Tab. 2 Backup capability

Backup type	Backup capability
HV $l_1 = l_2$ MAN	100 %
HV $l_1 < l_2$ MAN	90 %
MV $l_1 = l_2$ MAN	70 %
MV $l_1 < l_2$ MAN	60 %
NO	0 %

Conclusion and Acknowledgment

This article describes the backup of 110 kV. For different backup options is determined backup capability. It's calculated by method of probability of failure-free operation. The best backup capability has HV line with same length – the backup capability is 100 %. The worst is HV line without backup – the backup capability is 0 %. Better backup capabilities have backups with same length as line which we backup. MV backups are worse then HV backups. The method of backup capability evaluation has to be extended with carrying capacity of the backup line. All the backups evaluated in this article can carry full loads.

This work was supported by the Czech Science Foundation (No.GAČR 102/09/1842), Ministry of Education, Youth and Sports of the Czech Republic (No. SP2012/188). and by the project ENET (Research and Development for Innovations Operational Programme No. CZ.1.05/2.1.00/03.0069).

The results of the thesis are published in conferences proceedings:

- EPE 2012, Brno: VUT Brno, ISBN 978-80-214-4514-7
- ELNET 2011, Ostrava: VŠB-TU Ostrava, ISBN 978-80-248-25106

References

1. Tůma, J., Rusek, S., Martínek, Z. Chemišinec, I., Goňo, R. Spolehlivost v elektroenergetice. 2006, Praha. ISBN 80-239-6483-6
2. Sojka, J., Houdek, V., Rusek, S., Goňo, R. - Priorities of Faults on HV Lines. In ELNET 2011. 2011, Ostrava, 8-13, ISBN 978-80-248-25106
3. Pravidla provozování DS 2011, ČEZ distribuce a.s.

Construction of Model Antiphase Eliminator

Viktor Pokorný

Department of Electrical Power Engineering, FEECS,
VŠB – Technical University of Ostrava, 17. listopadu 15, 708 33 Ostrava – Poruba
viktor.pokorny.st@vsb.cz

Abstract. Nowadays, human health and wellbeing are the priorities connected with every human activity. One of the inseparable factors which has unfavorable effect on human organism is the noise around us. The main producers of noise emissions are electrical devices, for example transformers. Human physiology is not adapted to noise emissions. Science and research bring new possibilities how to resist these unfavorable impacts. One of the possibilities is the elimination of noise using antiphase.

Key words: Anti-phase, transformer, noise, acoustic signal

1 Introduction

The aim of this research is to create functional system which eliminates the noise of electrical devices. This system works on active basis, therefore it process parasitic signal itself and use it for elimination of the noise. On the first stage it focuses on elimination of energetic devices with great intensity of noise but with small frequency deviations.

Methods of elimination can be divided into three basic systems: constructional, passive systems, active systems.

Active systems are devices capable of eliminating noise, such as using anti-phase. [1.]

2 Antiphase

To understand the system is important to know basic, namely waves alone. Phase of the wave is a dimensionless quantity that determines the relation variable waves, (e.g. displacement noise) at that place and time and to the state variables characteristic waves in temporal and spatial origin. Dependence characteristic of variables determines the shape of „waves” regardless of its dissemination. Phase is a parameter, which depends on the timing characteristic values in a fixed location, which the wave passes, respectively spatial field characteristic values for a fixed moment in time. Noise so we can capture by the curve demonstrate displacement in time. Anti-phase is turning the current signal o 180°.

The result of the exact anti-phase is an absolute deduction of both signals and therefore their complete elimination. [2]

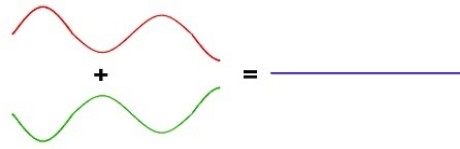


Fig. 1. Generating of antiphase wave

3 Purpose of the noise-elimination of the electrical equipment.

The initial equipment will be tested transformers to eliminate by using anti-phase. Their constant frequency noise is very ideal for sampling and subsequent rotation the signal to the anti-phase. The result will be possible limitations of a majority in the meantime use the anti-noise measures and restrictions of noise enclosure of buildings.

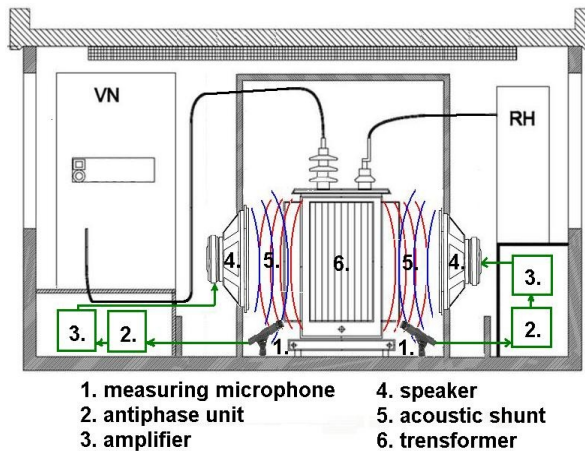


Fig. 2. Elimination of the transformer noise by anti phase.

After refinement of the system may be subject to certain physical conditions applied to almost any electrical equipment. Everything depends on the speed of sampling and capabilities of the right anti-phase waves. It depends to some extent on the frequency diversity of parasitic noise.

4 Measurement and acoustic testing

The measurements carried out on four transformers installed at the VSB – Technical University of Ostrava. This is the core three-phase transformers old design. These transformers are not equipped with active cooling – fans that would participate in making some noise. Transformer cover was opened and the microphone scans the noise that is reduced to the closest possible distance in order to eliminate environmental influences. For this reason it is also used for directional microphone.

Scanned signal by quality microphone is then sent to quality sound card that it digitizes and this signal is sent to a computer thru USB interface. It works only during the measurement as a digital recording device. Fig.3. shown a simple block diagram of the recording of measuring device, which is the source of the analyzed signals.

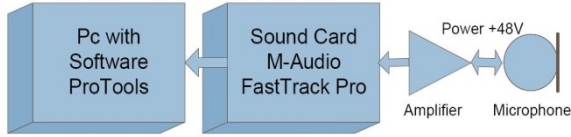


Fig. 3. Block diagram of recording devices for spectral analysis

For measurements were selected randomly three transformers, which are long-term measurement of noise intensity depending on load. Therefore, the results are taken as in no-load state and also in loaded state. Subsequent analysis of the transformers seem numbered T615/1 of its parameters are 1000kVA , 10kV/400V, 50Hz. In the first case, the transformer worked to 7% of maxi-mal load, the measured noise reached 74,7dB when the housing is closed and 75,65dB for open. The latter was loaded transformer 480A per phase, it means 48% load of the total power. Measured noise reached very similar values as the unload state, 76,8dB for closed housing and 78,3dB for open.

4.1 Spectral analysis of transformer T615 in the loaded state

Whole system is spectrally ease after loading the transformer and carrier frequency noise remains 100Hz. There are core to de-saturate the load transformer and thus also to mention upper harmonic. This state war confirmed by spectral analysis of the transformer in loaded state, see Fig.4.

The size of the transformer noise depends on the magnetic flux, it depends on the voltage and then idle current. The noise of the transformer is strongly associated with the magnetization process. Saturation of the transformer core idling is higher and is given to the design, construction and the type metal.

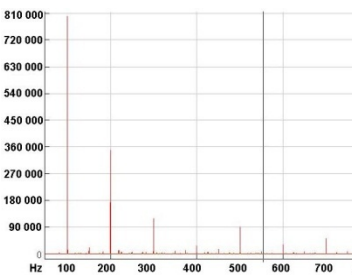


Fig. 4. Spectral analysis of the loaded transformer T615

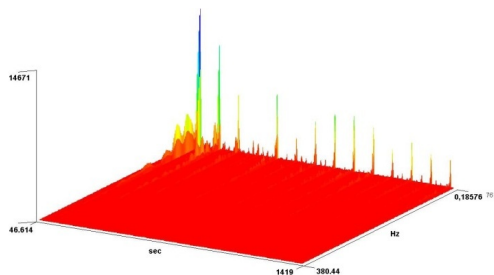


Fig. 5. Spectrogram loaded transformer T615

It is clear from these measurements, that entire system to eliminate noise using antiphase transformer is designed entirely to eliminate the noise around 100Hz. This applies to the measurement of transformers, in the case of transformers using active cooling would be difficult to analyze the situation of the fan noise.

5 Construction of Antiphase model

After spectral analysis of transformers noise it was concluded that this device will be constructed to eliminate the strongest frequency component which is frequency 100Hz. As the test could not take place on the transformer itself due to safety reasons, the special measurement workplace simulating the actual noise of transformer must have been created. The base comprise of two stands with identical speakers attached. One of these simulates the noise of transformer and the second stand produces antiphase which causes acoustic short. There are different types of schematic connections applied on the stands and acoustic efficiency, consumption of the system and other quantities are tested.

5.1 Schematic proposal of prototype

On the first stage the simple system which would verify functionality of all basic components was proposed. It is a system which works with computer simulation only. This simulation sends 100Hz frequency signal to one linear amplifier. Amplifier intensify signal to speaker to 78dB which is actual transformer noise intensity. Computer sends the identical signal 100Hz from the second channel, but this one is turned 180 degrees. This signal is again increased by linear amplifier and it is sent to second, opposite speaker.

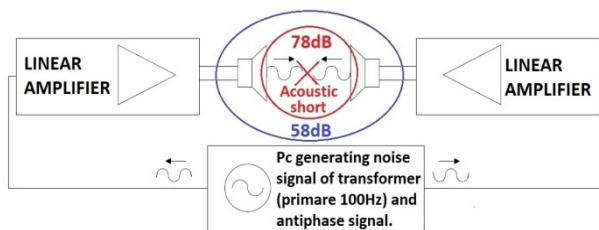


Fig. 6. Block diagram of the prototype Anti-Phase eliminator.

On the second stage the system is supplied with designed microphone which receives noise emissions. These noise emissions are again produced by the right part of circuit that is supplied with computer which in this phase transmits the actual transformer noise record to amplifier. The amplifier intensify the signal to speaker to 78dB measured value of transformer acoustic emissions. So the right part of circuit simulates the actual transformer. The left part of circuit starts with microphone designed by us, and it receives transformer sound closely. Received acoustic signal is sent to SQN unit which is analog device turning microphone phase in actual time so it

works as phase control. In this unit we can also partly adjust frequency extent. In our case any intervention is unwanted - apart from turning the phase. Turned signal goes to linear amplifier which intensify signal to speaker system to performance we need. If the specific distance of speaker systems is kept, there is an acoustic short and therefore unwanted acoustic emissions are eliminated.

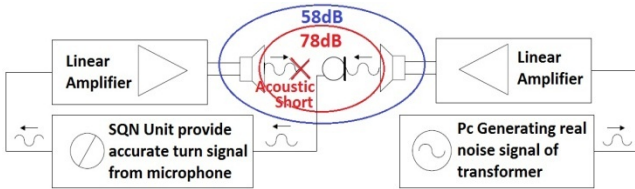


Fig. 7. Block diagram of the prototype Anti-Phase eliminator.

The proposal of schemes showed how the model will be designed so now the construction itself can be introduced. The model required great amount of wood construction material, the specific approach was chosen. The whole construction is made of wood waste, it is assumed that after series of tests and measurements it will not be used in operation and anti-phase eliminator will be professionally constructed again based on the same model. The chosen method is more economic and environmental friendly. The construction itself consist of two identical stands which are equipped with identical speaker systems.

The present model is based on scheme 1 see fig. 6, it is a connection testing the system in simplified frequency zone and only in simulating computer mode. The Carlsbro PA1670 was used as a terminal amplifier. Also, special computer audiocard M-audio FasTrack Pro is used in the system. On fig. 8 the whole physical construction is shown. The model is ready to start with tests and measurements, and if these test are successful and if model works in these conditions, the second stage will start – connection according to scheme see fig. 7 and another series to tests and measurements will follow.

6 Conclusion

If the certain physical conditions are kept, the system after improvement could be applied to any electrical equipment. This process is depended on a speed of sampling and ability to apply the right antiphase wave. There could be also influence of frequency heterogeneity of parasitic noise. The ambition of the project is to use this application for an elimination of noise various electrical equipments.

Acknowledgement

This contribution was prepared in the framework of re-search project SP2012/53

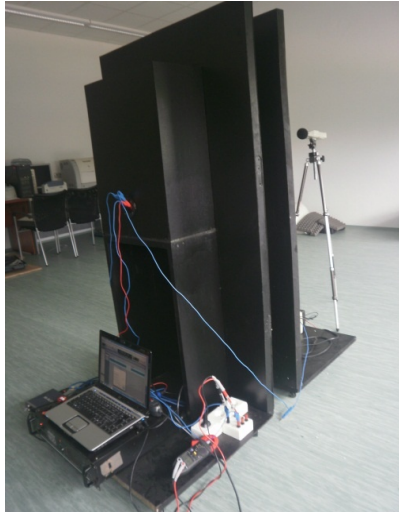


Fig. 8. Model Anti-Phase eliminator for measuring the intensity of noise.

References

1. Chmelík, K.. (2003) *DC and commutator electrical machinery, general machinery*, VŠB – Technical University of Ostrava., ISBN 80-248-0314-3
2. Chu M.; (2001) http://gilmore2.chem.northwestern.edu/tech/anr_tech.htm, Accessed on: 2010-04-19
3. Krejci, P.; Prokop, L. & Misak, S.(2009) *Analysis of Long Time WPP Power Flows Measurement. In RUSEK, Stanislav, GONO, Radomir (ed.)*. 10th International Scientific Conference Electric Power Engineering 2009., ISBN 978-80-248-1947-1, p. 373-378
4. Manwell J.F ;McGowan J.G & Rogers A.L, (2002) *Wind energy explained, design and application*, University of Massachusetts, Amherst, USA., ISBN 13: 978-0-471-49972-5 (H/B)
5. Tomlinson H.; (2009) <http://www.mefeedia.com/>– Anti-noise by Tomlinson Holman, Accessed on: 2010-05-15

Complaints of Customers on Power Quality in the Czech Republic

Petr Rozehnal

Department of Electrical Power Engineering, FEECS,
VŠB – Technical University of Ostrava, 17. listopadu 15, 708 33 Ostrava – Poruba
petr.rozehnal1@vsb.cz

Abstract. Power Quality is an important factor for the performance of electrical equipment. Violation of power quality parameters causes a complaint to the power quality. Complaints supplied electricity is a common problem of electricity distributors. Distribution companies must deal with these complaints and remove the causes of poor power quality. To reduce the number of complaints is necessary to monitor electrical power distribution companies because they must find the cause, evaluate and then make corrections. In the Czech Republic carried out the evaluation of power quality parameters in accordance with European standard ČSN EN50160.

Keywords: Complaints, distribution companies, telephone, correspondence, e-mail, fax, personal contact, location, customer

1 Introduction

Electric power in people's lives, are part of everyday life. The use of electric energy in industry and households is necessary to deliver electricity from points of production to point of consumption. The advantage of power is the ability to transport from place of production to point of consumption and also on long distances, where it can be converted to another type of energy.

With the ability to transport over long distances is required to transport electricity from points of production to point of consumption with the least losses, with no power outages and also to sinusoidal electric energy supplied was not deformed or otherwise damaged to various disturbances or disorders on the network.

Power Quality is evaluated according to EN 50160, according to which the voltage value of 13 parameters. By following these power quality parameters is essential for proper functioning appliances.

Distribution companies in the Czech Republic monitored power quality parameters. A major problem faced by distribution companies, the claim to power quality. Distribution of these complaints addressed.

Complaints about the quality of electric energy by customers, distribution companies are trying to solve as soon as possible, as losses from distribution companies may be large. These claims can be substantiated or unsubstantiated by customers. However, once it is determined that the complaint is well founded, formed distribution companies not only technical but also economic losses.

2 Reasons for complaints about the quality of electricity

The grounds of complaint on the quality of electric power are several. Among the reasons that may lead to claims for power quality, harmonics include the creation of a network, voltage fluctuations, voltage unbalance, and interruption of electricity supply to customers.

All these causes, which are the cause of the complaints about power quality can lead to large losses on the part of consumers of electricity, as the supplier of electricity.

All claims arising from the quality of electricity must be certified supplier of electric energy, which determines whether it is a legitimate reason to claim the power quality.

The validity of the claim to power quality electricity supplier informs the consumer of electricity and if it is a legitimate complaint, it must implement corrective action. All the quality parameters of electricity, which are compared with a complaint on the quality of electricity are given in ČSN EN 50160.

3 Methods of complaints Power Quality

In the Czech republic there are several companies that deal with the supply of electricity. These companies must address the issue of complaints per day of electricity. In modern times, the development of communication between distribution companies and energy consumers. Since 2004, leading distribution of documentation on how to report o complaints and the time resolution of this claim, but also whether it is justified or unjustified claims.

Complaints of electricity are done in several ways. The most advanced means of communication between customers and distribution companies in the electricity complaints if you call us. This is mainly due to the fact that customers are electricity used in previous years, when people did not have so many communication options (internet, fax, etc). Another reason is that in the event of total power failure, telephone contact is the only way to report failure distributor of electricity.

To evaluate ways of using communications to claim the quality of supplied electricity is based on data-but or distribution of electricity, which are collected from 2004 to now during this period, there were altogether over 13,497 complaints about the quality of electrical energy with the fact that they were to evaluate the use 11794 as the rest of the complaints was not mentioned, what the source of complaint is, or was shown the place where she complained about the quality of electricity.

Table 1. Type of communication between the customer and the customer electricity

Type	2004	2005	2006	2007	2008	2009	2010	2011	Celkem	%
Phone	177	223	876	1037	1119	1282	1501	1195	7410	62,83
Correspondence (letter)	94	26	195	278	177	137	106	110	1123	9,52
Email	18	13	142	233	190	231	246	277	1350	11,45
Internet (Web site)	5	0	10	12	28	42	34	73	204	1,73
Fax	0	2	10	11	8	2	1	1	35	0,30
Personal contact	161	60	85	80	127	137	152	152	954	8,09
Internal Group	0	6	5	13	60	37	75	161	357	3,03
IVR	0	0	0	0	0	0	3	1	4	0,03
Contracting partner	0	3	18	34	39	72	77	76	319	2,70
Not specified	4	0	1	0	4	17	5	7	38	0,32
Total	459	333	1342	1698	1752	1957	2200	2053	11794	

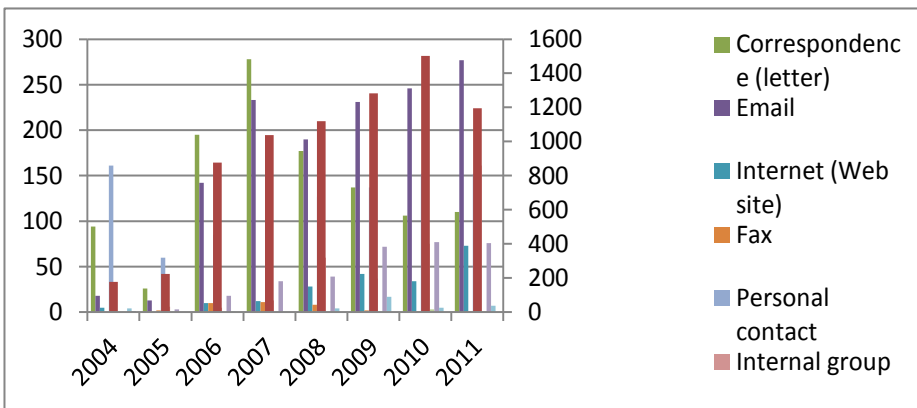


Fig. 1. Show the types of complaints, communications power quality

Table 1 shows the number of complaints in the period 2004 - 2011. From this perspective it is clear that the number of complaints is increasing every year. The lowest number of complaints was in the years 2004 and 2005. Since 2006, the number of complaints about the quality of electricity increases. In 2005, the number of recorded complaints about the quality of electricity in 1342 and in 2011 was the 2053rd.

From Table 1 and Figure 1 shows that most complaints were made telephone contact with 62.83%. It is evident from Table 1 that after the telephone contact more customers prefer a complaint by e-mail communication (11.45%). This is followed by a corresponding claim (9.52%) and claims for personal contact at the branch (8.09%). The least used form of complaint is via the website (1.73%), followed by fax (0.3%) or the controller (0.03%). Another way to claim power quality is the use of contractor distributor of electricity (2.7%). The last item in Table 11 is 0.32%

unknown mode of communication. This is because the electricity distributor has not identified a way to report complaints on the quality of power supply. Table 1 is also apparent that all of the methods of communication in all years researched at a similar level of use compared with other methods of communication utilized.

5 Electricity complaint

Customer's power is often claimed by the quality of electrical energy. Since 2004, electricity distributors gradually the number of complaints recorded power quality. During the period 2004-2011 there were 11,794 power quality complaints. All these complaints were the former regions and the claim of the power quality.

Table 2. Complaints to the power quality in the years 2004 to 2011

Place	2004	2005	2006	2007	2008	2009	2010	2011
ZCE	116	107	234	273	263	291	296	280
SCE	214	79	220	256	209	237	355	284
SME	132	67	287	358	499	477	496	444
STE	0	29	346	473	490	576	682	620
VCE	0	51	255	338	293	376	367	424
Total in year	462	333	1342	1698	1754	1957	2196	2052

In Table 2 are shown the numbers of power quality complaints. From the table 2 shows that from the perspective of total number of complaints is the quality of electricity every year complaints more power quality. The exception is the year 2011, when was the number of complaints of the quality of electricity less than 1.22% in 2010. It is evident from Table 2 that most power quality complaints during the reporting period was in the Central Bohemia region with 620 complaints on the quality of electrical energy, then north Moravian region with 444 power quality complaints and East County with 424 complaints on the quality of electricity.

6 Conclusion

The paper summarizes the reasons for and methods of power quality complaints. They are given various forms of communication, which consumers use to power quality complaints in 2004 - 2011. The results of individual research communications indicate that the most common means of communication between customer and distributor of electricity if you call us. The paper shows that the development of electronic means of communication, when the total research effort, it was found that electronic communication is the second most common way to report the claim to power quality. Contrast sharply declining claims on power quality, which are made by mail, but even so, the use of correspondence in power quality complaint is the third

most used method of communication used. Another method by which customers are abandoning personal contact at a branch distributor of electricity, in 2011, the number of complaints by two-thirds less than in 2004. However, the number of complaints still made personal contact at a branch distributor's power ranking fourth in the most commonly used methods of communication in a claim on power quality.

Further in the paper the numbers of complaints on the quality of electricity carried out between 2004 - 2011. Of the complaints made that the number of complaints about the quality of electricity is increasing every year.

Distribution companies are trying to reduce the number of complaints about the quality of electricity. For this reason alone distribution company carries out monitoring of electrical networks, and when it detects a problem with the power quality, performs correction.

7 Acknowledgment

This work was supported by the Czech Science Foundation (No. GA ČR 102/09/1842) and by the Ministry of Education, Youth and Sports of the Czech Republic (No. SP2012/188)

8 References

- [1] Rozehnal P., Cumpelik R., Krejci P., Evaluation of selected parameters of quality of electric energy distribution network. Conference "EPE 2011", Kouty nad Desnou, p 584-587, ISBN 978-80-248-2393-5
- [2] Gono, R., Kratky, M., Rusek, S.: Analysis of Distribution Network Failure Databases. In *Przegląd elektrotechniczny*, 2010, vol. 86, čís. 8/2010, s. 168-171, 4 s. ISSN 0033-2097
- [3] Rozehnal.P, Krejci.P., Monitoring Methods of Power Quality Complaints. Conference „EPE2012“, Brno, p 403-406, ISBN 978-80-214-4514-7

Statistical Evaluation of the Operation of Photovoltaic Power Plant

Martin Smoček

Department of Electrical Power Engineering, FEECS,
VŠB – Technical University of Ostrava, 17. listopadu 15, 708 33 Ostrava – Poruba
martin.smocek@vsb.cz

Abstract. Photovoltaic power plants are sources that are highly dependent on meteorological conditions. This is reflected in stochastic change of power produced. Change produced power also causes a change of voltage in the connection point. The paper deals with evaluating the operation of photovoltaic power plants, specifically relationships between operating parameters. The result is their mutual functional dependence. Dates of operation are evaluated based on the mathematical apparatus.

1 Introduction

The introduction of this article explains the basic mathematical terms, based on the theory of statistics. In the next chapters is a description of data processing, statistical evaluation process and determination of final results from the operation of photovoltaic power plants. The processing and evaluation of data was used Excel and math software Statgraphic.

2 Theory of statistic

Mathematical Statistics is the science that deals with variable of data which showing random character. It deals with issues of data acquisition, their analysis and role in the formulation of conclusions about experiments or deciding based on data. Statistical methods allow model the interdependence between the groups of data. In energetics the groups of data are representing by measured physical quantities and time. [4]

Outliers are the values of variables that are extremely different from other values and thus affect the representativeness of the diameter. For identify outliers using the visual assessment and mathematical methods. [2], [3]

Regression means a systematic change variables (independent variable) caused changes in other variables (dependent variable), which can be expressed by mathe-

mathematical functions. Most often it is possible to meet with a linear regression model. Based on regression analysis is possible to determine interval and point estimates.

[4]

Point and interval estimates based on regression analyzes provide an estimate of one parameter depending on another with a specific accuracy. Specifically, it is the determination of the conditional mean and estimates of individual values. In both cases it is possible to obtain point and interval estimations.

3 Description of measured data

The data were measured on photovoltaic power plant continuously for one month. Specifically, it was in April 2011. Data was recording by network analyzer with time steps one minute. The data set contains a total of 43 128 records. Measured variables are active power P , reactive power Q , voltage at the connection U and current I .

4 Analyzing the data file

Data analysis can be divided into three phases and that filtering, processing and final evaluation. In Fig. 1 is an example of measured quantities during one day in unsuitable weather conditions.

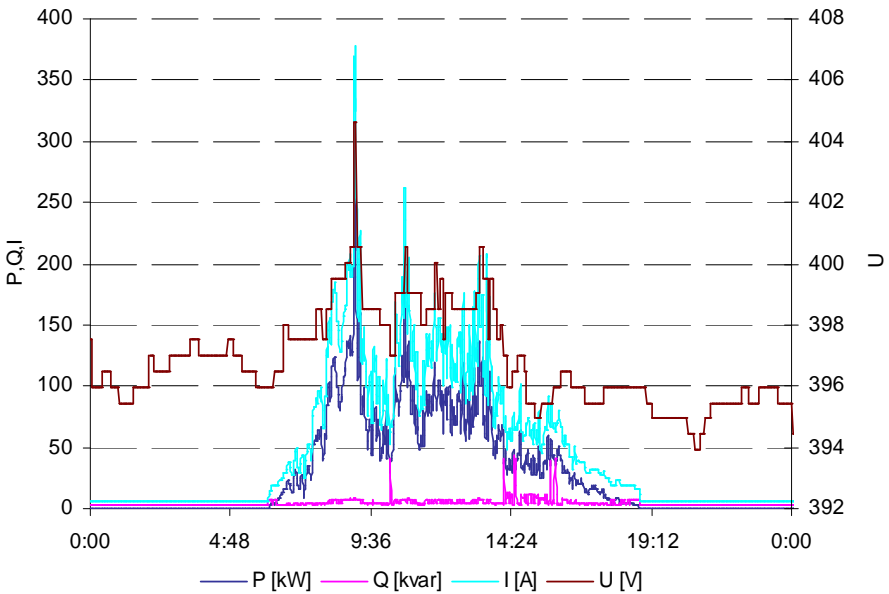


Fig. 1 Curve of P , Q , U and I in one day for unsuitable weather conditions

Data source [1]

In Fig. 1 may be the observed correlation of all measured parameters. Under suitable weather conditions this dependence is more pronounced. It can be stated that the study of relations of measured values is warranted.

4.1 Filtered data

From the graph in Fig. 1 can be noted that the data file contains a record from the night, when produced power is zero. Photovoltaic power plant is idle. This data for further evaluation are filtered from the data file. Now the data file has only 23 257 records.

Next is important to identify outliers using standard mathematical procedures. For the identification were used methods of distance 1.5 times of the interquartile range from the lower and upper quartile and distance MAD „ z " coordinate with parameter 3. File size of the data after removing outliers is in the Tab. 1.

Tab. 1 Percentage of outliers

Values	P	Q	U	I
Original data file	43 128			
Data file with $P>0$	23 257			
Data file with $P>0$ and without	19 700	22 126	19 357	19 918
Percentage of outliers (%)	15	5	17	14

4.2 Verification of dependence of the measured parameters

If the data file is filtered from undesirable values and the values of remote observation, it is possible to verify whether there is a statistical correlation between the monitored parameters. It suffices to verify only relationship between active power P and voltage U . If there is dependence between these quantities will also be a relationship between the other measured parameters. This statement is evident from the theory of electrical engineering.

Verification of statistical dependence consists in the distribution of the data file (P and U) into three groups according to the power range. Power range is defined by three equal intervals. Evaluation was performed by Kruskal-Wallis test. Null hypothesis is to verify the equality of medians of voltage for the respective power supply range. The test was rejected. This means that the medians of voltage are different and therefore there is a statistically significant relationship between produced power and changing the voltage levels at the connection with 95% confidence level.

4.3 Regression analysis

Regression analysis determined the functional dependence between the variables being monitored. In this study is defined the dependence $P = f(U)$. The most important parameter for regression analysis is a modified index of determination R^2 , which

indicates the quality of the regression model. Specifies how many percentage variance of dependent variable is explained by model and how much remains unexplained. Another important parameter is the correlation coefficient, which indicates a linear relationship between variables.

Software Statgraphics offers four types of alternative models with correlations above 0.9 and a modified index of determination more than 88%. Was selected a linear regression function from Tab. 2.

Tab. 2 Suitable alternative regression models from Statgraphic

<i>Model</i>	<i>Correlation</i>	<i>R-Squared</i>
Reciprocal-X	-0,9420	88,74 %
Logarithmic-X	0,9418	88,69 %
Square root-X	0,9416	88,67 %
Linear	0,9415	88,64 %

Correlation box (scatter graph) shows the relationship between the independent variable U and dependent variable P . Examples of such correlation box including a description is shown in Fig. 2. Methods for identifying outliers which were carried out in Section 4.1 are not suitable for regression analysis. There would be an excessive increase in the number of outliers and in many cases it was the wrong decision. For this reason, Fig. 2 does not respect the outliers identified in Section 4.1. A better method is the visual assessment. The blue ovals in Fig. 2 show the possible points of outliers.

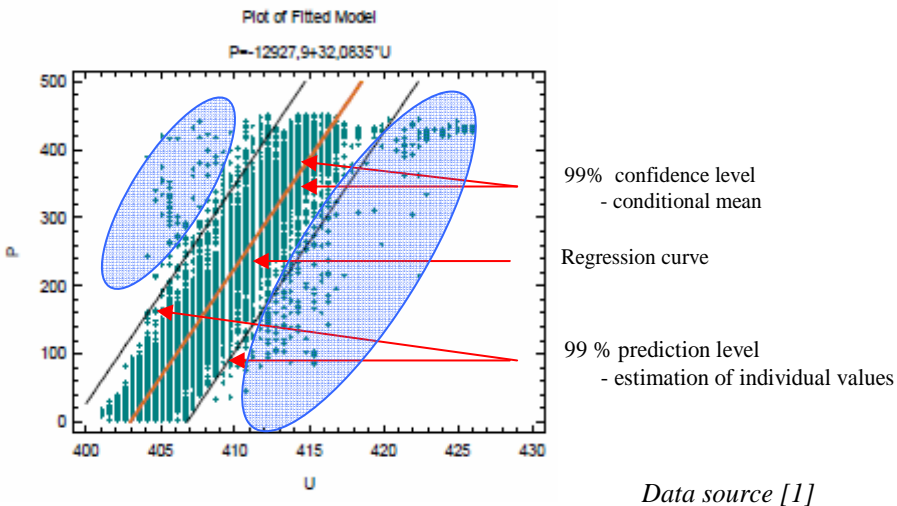


Fig. 2 Correlation box dependence $P = f(U)$ with outliers with 99% prediction levels

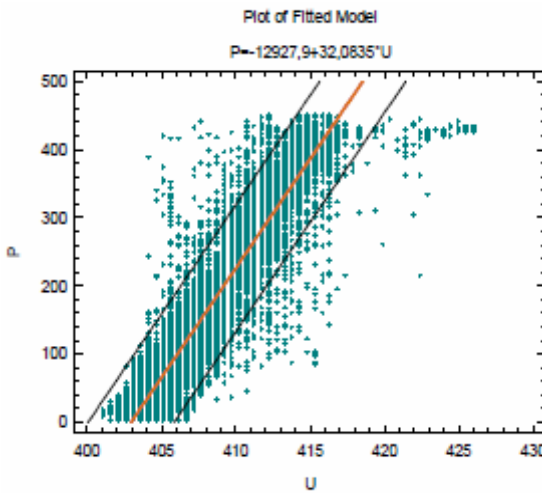
The emergence of remote observation points, shown in blue ovals in Fig. 2, not yet identified and therefore these values must be taken into account as actual operating

parameters. With regard to their low frequency can be described as irrelevant and not essential to the final evaluation.

Regression function of this model is:

$$P = -12927,9 + 32,0835 \cdot U \quad (\text{kW}; \text{V}).$$

Prediction levels in model show expected values for active power P . On Fig. 2 is set 99% prediction intervals for new observations and 99% confidence intervals for the mean of many observations. For the purpose of this evaluation is sufficient 95% prediction level (in the technique commonly used), which is shown in Fig. 3.



Data source [1]

Fig. 3 Correlation box dependence $P = f(U)$ with outliers with 95% prediction levels

4.3 Interval and point estimates

Interval and point estimates are the result of use of the entire regression analysis. This is a prediction of the expected values of the dependent variable in the selected independent variables.

Tab. 3 and interval estimates for 410 V and 420 V from the Statgraphic

		95,00%		95,00%	
	<i>Predicted</i>	<i>Prediction</i>	<i>Limits</i>	<i>Confidence</i>	<i>Limits</i>
<i>X</i>	<i>Y</i>	<i>Lower</i>	<i>Upper</i>	<i>Lower</i>	<i>Upper</i>
410,0	226,229	133,381	319,218	225,608	226,991
420,0	547,134	454,198	640,07	545,211	549,057

Point estimate

Estimate individual value

Conditional mean

Conditional mean:

It can be argued that the average value of active power is 547 kW, when the voltage is 410 V. With 95% confidence it will mean value of active power in the range from 545 to 549 kW in the selected voltage 410 V.

Estimate individual value:

It can be said that the value of active power is 547 kW, when the voltage is 410 V. With 95% confidence it will value of active power in the range from 454 to 640 kW in the selected voltage 410.

5 Conclusion

The work refers to possible definition of functional dependencies between quantities measured on photovoltaic power plant with a certain probability and reliability. Example of evaluation and formulation of conclusion is in the Chapter 4.3. This study will further explore other relationships between the variables being monitored, also precisising and improving the results of this prediction.

Acknowledgements

This work was supported by the Czech Science Foundation (No. GA ČR 102/09/1842), by the Ministry of Education, Youth and Sports of the Czech Republic (No. SP2012/188) and by the project ENET (Research and Development for Innovations Operational Programme (No. CZ.1.05/2.1.00/03.0069).

Reference

- [1] HRADÍLEK, Z. – ŠUMBEA, T. Simulator for Prediction of Energy Obtained from Wind Power Plants. International Scientific Conference Electric Power Engineering 2011; (EPE 2011), 2011.
- [2] BRIŠ, R. Statistics 1. Study materials VŠB – TU Ostrava.
- [3] BRIŠ, R. – Litschmanová, M. Statistic 1. Study materials VŠB – TU Ostrava.
- [4] Litschmanová, M. Statistic 1. Study materials VŠB – TU Ostrava.

The Issue of the Operation of Heating System

Jaroslav Sojka

Department of Electrical Power Engineering, FEECS,
VŠB – Technical University of Ostrava, 17. listopadu 15, 708 33 Ostrava – Poruba
sojka.jaroslav@email.cz

Abstract. Post is a preview into the heat-engineering, where I began working full-time at a heating company. In this paper are the basic concepts, methods of production heat and types of heat supply, technology and types of heat networks. As an author I want to focus on the issues of heat losses in heat networks.

Keywords: Heat-engineering, heat exchanger station, primary and secondary supply, heat take-off, heat feeder, steam, hot-water, heat-water

1 Introduction

Heat-engineering is the one of energy sector (power engineering, gas engineering and heat-engineering), engaged in production, distribution and sale of heat energy.

These three sectors covered by the law of the Czech Republic No. 458/2000 Coll. on business conditions and public administration sectors in energetic and amending certain laws (just longer Energy law). This law defines and regulates the conditions of business, state administration and regulation in this threes energy sectors, as well as the rights and obligations of natural and legal persons involved. Heat is devoted to Chapter II, Part 3, Sections § 76 - § 89 of this Act. The law is effective from 1 January 2001.

2 Heat-Engineering in Czech Republic

Czech Republic belongs to countries with a high proportion of intensive industrial sectors (mining, metallurgy, automobile, heavy industry). This sector, along with the cities, creates a high demand for sufficient quantities of energy. One of these forms of energy is heat [6].

Heat-engineering - system centralized heat supply (SCZT), started to develop since 1930. The main reason for building heating system was the first expansion of manufacturing in cities (large amount of heat needed for the technology), new heating for residential buildings, the development of electricity and the need to solve the problem with transportation, storage of fuel (coal) and last but not least, limiting dispersion of flue gases after combustion.

2.1 Basic concepts

The need for heat: is given by the heat input in watts [W, kW, MW] and heat extraction in [MWh / day, MWh / month, MWh / year].

Heat Capacity: amount of heat is connected per hour [MW].

Heat take-off: the amount of heat required for some longer time period [MWh / day, MWh / month, MWh / year].

Heat consumption: the amount of heat actually consumed in a given time period [MWh / day, MWh / month, MWh / year].

Combined Heat and power plant (CHP): is the production of electricity and heat energy.

Boiler room: a room or a separate structure, where is located the boiler for production hot water or steam, if used for heating, is also sometimes uses the term heating plant.

3 Sources, production and technology of heat supply

Types of sources, where is the heat energy producing, are condensing power plants, nuclear power plants, heating plants, small municipal heating plants, gas boiler and cogeneration units. Fuels used in sources for producing are mainly brown and black coal, natural gas and biomass. For producing of heat is also used waste combustion in refuse incinerating plant Transfer medium is used (hot water, heat water and steam).

Heat supply areas are the cities, city districts, settlements, houses, industrial enterprises and social construction. Used method for storage of heat networks are (distribution pipeline above the ground, under the ground in hot-water tunnel manhole and insulated piping).

3.1 Production of heat energy

Heat is mainly produced in CHP plants, which convert available resources into heat. It serves for the central or local heating and service hot water (STW).

Separate production of heat in heat and power plants can be divided into:

- heat-water production

Water is heated to a temperature of 120°C. The advantages are less loss of water during transport to the place of consumption. The disadvantage is the need of more powerful pumps and pipes.

- hot-water production

Water temperature reaches temperatures of 120-180°C.

Higher heat losses are compensated by using short lines and a weaker pump, which consumes not too much energy.

- steam production

The steam is heated to 180-240°C and requires no pump, because for her transport is used her pressure. The steam on their way heating circuit cools, thereby forming a

water condensate. Water condensate is transported back to plant, its own pressure or by pump.

Combined production of heat and electricity in power plants can be divided:

- steam extraction turbine
- back-pressure steam turbine
- gas turbine
- gas motors (cogeneration)

From an economic and ecological point of view is effective to generate heat and electricity in one place. Sources are used to roughly 30% better.

3.3 Supply of heat energy

The medium, that carries heat energy, depends on the mode of transport of heat and service hot water (SHW) from power station to consumers.

This medium can be water or steam. Heat is distributed either centrally or locally.

Types supply of heat:

- central supply of heat (CZT)
- decentral supply of heat (DZT)

Type of heat supplies by the heat supplier:

- primary supply of heat
- secondary supply of heat

Central supply of heat

The system includes interconnected heat production, heat networks, reduction and heat exchanging station and consumer devices. This is the supply of heating and STW centrally for the needs of home and industrial enterprises.

3.4 Heat networks

Equipment for the transport heat energy from the source to the customers. They also include heat exchanger station and reducing station, where is the delivery heat energy governing the values that are required for consumer devices (pressure reduction, etc.).

Heat networks and supply of heat can be divided:

- **Primary distribution network of heat energy** – part of the heat network between the sources of heat energy and the heat exchanging station (which ended in the heat exchanger).

If the supplier delivers heat energy only to the exchanger station, where will transfer heat to the customer then this supply is called the ***primary supply***.

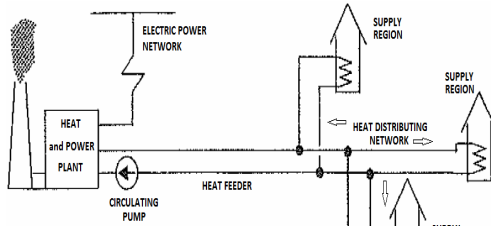


Fig.1. Primary supply of Heat [5]

- **Secondary distribution net-work of heat energy** – part of the heat network between heat exchanging station and customers.

If the supplier delivers heat energy up to the place of consumption of the customer (residential exchangers station or directly to the apartment to the customer), then this supply of heat is called the *secondary supply*.

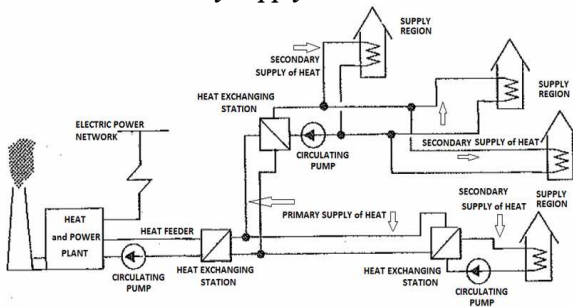


Fig.2. Secondary supply of Heat [5]

Heat energy is transmitted by:

- *steam piping*

The advantage of steam is her pressure energy that ensures the flow in pipes. The temperature of steam in the steam line is up to 240 °C and a pressure of up to 1.8 MPa. The steam is pumped either directly for technological purposes, or at heat exchanging stations where is adjusting the parameters used for heating or for production service hot water.

- *hot-water lines*

To transport the hot water are needed circulating pumps, which are usually located in the factory (heat and power plant). The water pressure reaches 2.5 MPa. Water is heated up to 180 ° C and distributed insulated hot-water directly to customers or to heat exchanging stations. Water that has passed heat returns to the heating plant, which heats up again and the cycle repeats.

- *heat-water lines*

The water in the heat-water lines up to 110 °C and 1,6 MPa pressure. In some cases, the temperature is lowered to 95 °C and pressures to 0.6 MPa. This allows direct connection of consumer devices without having to use the heat exchanging station.

3.5 Heat exchanging station

The maximum temperature for heating and SHW is $95\text{ }^{\circ}\text{C}$, the temperature should therefore be adjusted from the primary network. For this purpose, a heat exchanging station containing heat exchangers. In these devices, water is heated and circulated separately at the heat exchanging station and the consumer.

In Pressure - dependent heat exchanging station is the internal heating network to heat buildings directly connected to the primary heat supply. The connection is done using loops, reducing valves, pumps and mixing ejectors. Heating appliances are hydraulically connected and influenced by the primary heat supply.

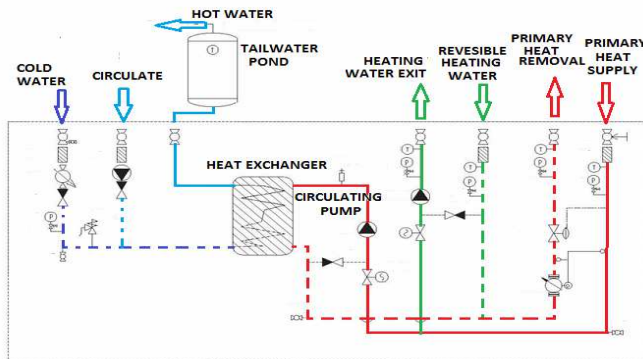


Fig.3. Pressure – dependent heat exchanging station [3]

In Pressure – independent heat exchanging station is internal heating network to heat buildings connected through a heat exchanger and completely done in the hydraulic supply from the primary heat.

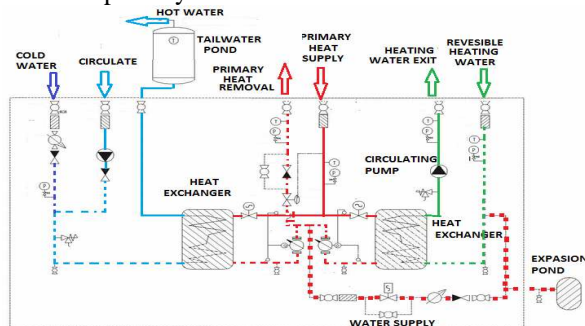


Fig.4. Pressure - independent heat exchanging station [3]

Decentral supply of heat

In this case, the heat source located in the place of consumption. For example, residential house with a gas boiler for heating and hot water is a typical example of DZT. Object that has a boiler or other source of heat and hot water.

Heating-system losses

They are much more pronounced in the CZT because the heat transfer medium it overcomes much greater distance and the heat losses are inevitable. In DZT, heat transfer medium it overcomes a much shorter distance and his temperature is lower at source, so the losses are lower. Steam piping, hot-water and heat-water lines, are insulated but heat loss cannot be completely avoided. Losses also occur in the exchangers stations. Heat, from the primary heat distribution network to the secondary part, simply lost. Heat networks are placed under the ground, which significantly eliminates losses.

4 Conclusions

Currently underway in the field of high ecological and rationalization in order to restore the grid and to minimize heat loss of "conversion" (transition from steam to hot water supply). In the field continues in development of heat networks and attempt to connect to other customers from the household use and industrial enterprises. Heat-engineering depends on the main raw material for production of heat - brown coal. According to [7] in 2012 was mined 42 million tons / year of brown coal in 2020 would be 32 million tons / year and in 2050 only 10 million tons / year. From this perspective, the heat-engineering will increase demands for ensuring the supply of new fuels and huge investment in upgrading facilities. Help for heat-engineering may be using [4]:

- Creating space for heat-engineering adaptation to new conditions (small co-generation and local resources, modernization of plants and heat networks)
- Economic empowerment by local heating heat
- State Energy Policy
- Removing barriers to energy recovery of municipal waste and public education

Acknowledgement

This work was supported by the Czech Science Foundation (No. GA ČR 102/09/1842), the Ministry of Education, Youth and Sports of the Czech Republic (No. SP2012/188) and by the project ENET (No. CZ.1.05/2.1.00/03.0069).

References

1. Cikhart, J., a kolektiv, Soustavy centralizovaného zásobování teplem, Praha, 1977,
2. Kadrožka, J., Ochrana, L., Teplárenství, Brno 2001, ISBN 80-7204-222-X.
3. Fiedler, J., Odborný kurz teplárenství pro pracovníky společnosti ČEZ Teplárenská.
4. Hájek, M., Aktuální situace v teplárenství a SEK, Teplárenské sdružení ČR, 2011.
5. Karafiát, J., Teplárenství, ORTEP, 2001
6. Kaufmann, P., Vývoj teplárenství v České republice, Teplárenské sdružení ČR.
7. Topolánek, M., Problémy českého teplárenství, Drážďany 2011.

Implementation of the New Power Supply and Propulsion Concept for Steel Materials Stress Testing Device

Peter Staš¹, Martin Marek¹, and Michal Šofer²

¹Department of Electrical Power Engineering, FEECS,
VŠB – Technical University of Ostrava, 17. listopadu 15, 708 33 Ostrava – Poruba
{peter.stas, martin.marek}@vsb.cz

²Department of Mechanics of Materials, Faculty of Mechanical Engineering,
VŠB – Technical University of Ostrava, 17. listopadu 15, 708 33 Ostrava – Poruba
michal.sofer@vsb.cz

Abstract. The paper deals with steel materials contact stress testing device. Main idea which supports the innovation of the device stems in the necessity of new effective approaches for contact stress material testing because older version of the device was not capable to perform tests with all necessary parameters. With respect to the tests requirements, we have proposed a solution, which allows performing of the contact stress tests in the wide range of parameters. Project is realized via cooperation of the Department of the Electrical Power Engineering and Department of the Mechanics of the Materials.

Keywords: Contact stress, control system, propulsion system.

1 Introduction

Steel materials contact stress testing is significant for example in railway transport. Wheels of the railway machines are exposed to strong mechanical stress during their lifetime. Increased stress results into deformation and damage of the materials. Nowadays, it is standard to test crucial mechanical parts of the railway machines before their introduction to service. Therefore, contact stress material testing pose key element in the reliability and safety of the personal as well as goods railway transport.

First of all, purpose of the tests is revelation of the structural and further failures, which have to be made in sufficient advance. Quality of the stress tests is strongly influenced with the properties of the testing device. Hence, it is necessary to perform tests using devices, which allow setting up of all desired parameters with high precision in a full range and so positively influence results of the tests.

2 Stress of the steel materials

Steel disorders are due to different causes but mostly from forces acting on the rolling parts during acceleration and braking. Forces induce microstructural transformation of the material resulting into creation of rifts, shifts and loss of the surface materials. More information about steel material damage can be found in the literature [1].

These effects are undesirable and therefore we have to prevent them. Hence, it is important to continue and improvement and the development of the testing devices.

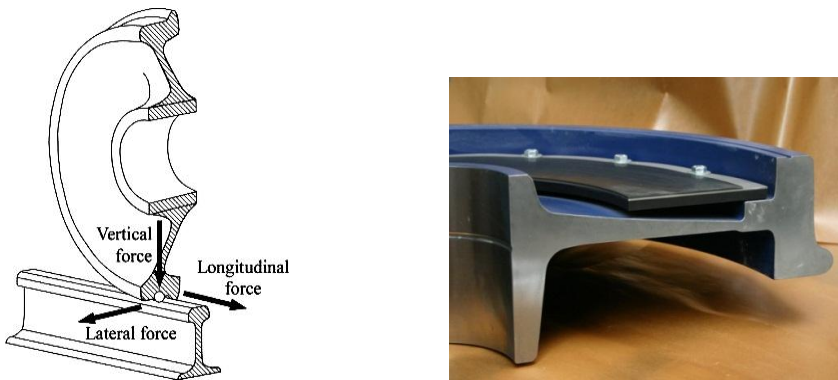


Fig. 1. Forces, which act between a wheel and a line (left) [7] and wheel cross section (right)

2.1 Basic principles of the tests and requirements for the device

Tests of the stress are performed according to demands of the applicant. Railway transport machines tests are performed using two circle-shaped specimens of the specific diameter.

Specimen's surfaces touch tightly with outer surfaces. Depending on the test type, they rotate at the same or different speed and so simulate movement of the wheel on the surface of the railway line. First specimen represents wheel, second represents the line.

Before the start of the test, desired pressure force between the specimens is set up. During testing, a finite number of rotations are performed. At the end of the test, surface changes of the material, change of the diameter and mass decrease are examined. More information can be found in the literature [1, 3].

Requirements on the device set-up. With respect to different types of the exams to be performed on the machine, it is avoidable to set up different parameters. Most important parameters are pressure force between specimens, adjustment of the housing for different dimensions and shapes of the specimen and independent set – up of the rotational speed for both specimens. The latter parameter depends on the power supply system and operation of asynchronous electric engines. New concept of the

testing device was designed for to fulfil all requirements put on the power supply and asynchronous engine operation system.

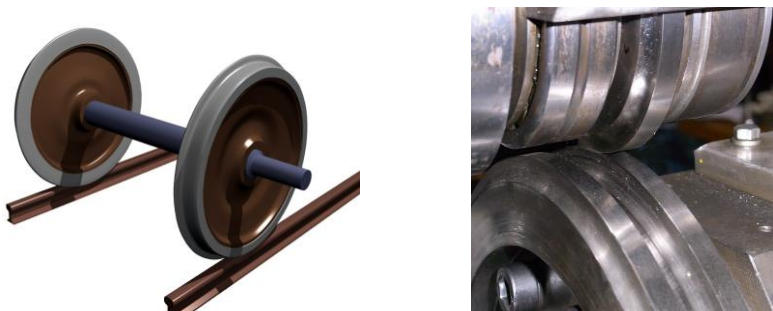


Fig. 2. Wheels used in railway carriages [8] and specimens of the steel materials during the test (TOURS machine)

3 The tours testing device

The TOURS contact stress testing device is located in the premises of the Technical University of Ostrava. Increasing demands on the tests forced us to perform reconstruction of the device, which will guarantee higher degree of the flexibility of the propulsion system.

3.1 Original technical design of the TOURS device

The propulsion system of the original device was based on utilization of one asynchronous engine (AE) of output power equal to 2,2 kW. This AE powered and control via frequency converter. The engine was directly connected with a worm gear system and the gear system was connected via shaft with tested specimen. Rotation of the second specimen was realized via mechanical transmission using the same AE.

Types of the material stress tests. The device allowed performing of two types of the tests:

- a) With free hobbling of the material,
- b) with forced over thrust.

Second tests were realized via different diameters of the tested specimens or via change of the mechanic gear. The change of the mechanic gear was not practical because specific tests required specific additional gears.

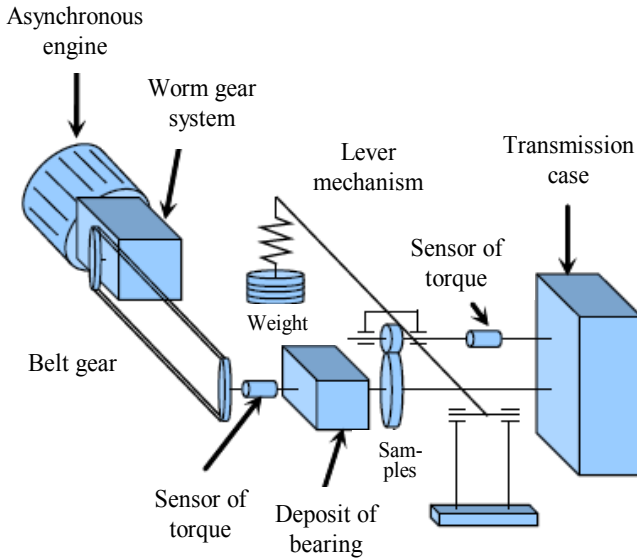


Fig. 3. Diagram of the testing machine TOURS (old solutions) [3]

3.2 New technical design of the TOURS device

Sustainment of the world trends in the development and use of the contact stress material testing devices requires modernizing of the traction system of the TOURS device. This means modernization of power supply unit, engine and gear unit and control system.

Part of the device, which contained AE with frequency converter and gear unit, was not modified because it fulfilled all tests requirements. This part will be further referred to as “first traction unit”.

Second specimen traction system realized using mechanical gears was replaced with new technical proposal.

“Second traction unit” is realized using AE with electrical power 3 kW. It is powered using frequency converter. Frequency converter is also used in the process of testing device controlling and data collection. Both specimens’ traction systems are independent. Such a technical solution is sufficient for current as well as future use.

Testing device required careful choice of the AE. AE is planned to be exposed to high load at low revolution speed and it will be thermally loaded during long – duration tests (typically about 6 hours). Therefore, several tests were performed in cooperation with SIEMENS company tests of the AE thermal load during different operational modes of the stress testing device. More information about these tests and diagnostic of induction machine can be found in literature [4, 5].

Types of the tests. The innovated device allows performing of the same tests as the previous version of the device but with wider spectrum of the testing parameters.

This has positively influenced possibilities of the tests which now fulfil all requirements of the producers of the wheels (original technical design of the testing device allowed to set up parameters only finitely).



Fig. 4. Contact stress testing device after innovation

Requirements for the choice of the AE. Selection of the new AE had to consider technical parameters of the original parts of the testing device as well as economical cost.

Decision guidelines:

Testing device must have two types of elastic coupling with torque moment equal to 300 Nm and 150 Nm, maximum diameter of the steel specimen is equal to $d = 85$ mm, steel specimen contact surface width: $h = 10$ mm, maximum AE's rpm $n = 500$ r/min.

On the base of these requirements and measurements in the SIEMENS company, following AE was chosen:

Electrical power: $P = 3$ kW, number of poles: $n = 6$, nominal moment: $M = 30$ Nm.

Software control and data collection. Frequency converter of the second traction unit is controlled via special software installed on a PC workstation. Simple parameters of the frequency converter can be also set – up directly from the control panel but connection with PC via RS-232 allows to store information about engine mo-

ment, rpm, engine temperature etc., which are important for final evaluation of the contact stress tests.

Software also allowed fluent start of the tests and as a result the specimens are not during the start of the independent specimen traction system. Naturally, this all have positively influence the accuracy of the results.

Conclusion

Purpose of the paper is to briefly familiarize a reader with the research in contact stress material testing in the Czech Republic and with possibilities of detection of materials defects using the described device.

Czech Republic belongs to leaders in area of construction of railway wheels. Goal is to achieve world standards and to continue with further research.

The results of work are published in conference proceedings:

13th International Scientific Conference Electric Power Engineering 2012, Brno University of Technology, vol. 2012/2, pages 1031-1035, ISBN 978-80-214-4514-7.

Acknowledgements

This work was supported by the SGS projects SP2012/53 and SP2011/157.

References

1. Koan-Son, B., Keiji, K., Tsunamitsu, N. – An experimental investigation of transient traction characteristics in rolling-sliding wheel/rail contacts under dry-wet conditions Wear, 16th International Conference on Wear of Materials, 2007
2. Kůs, V. – Vliv polovodičových měničů na napájecí soustavu, BEN – technická literatura, ISBN 80-7300-062-8, Praha, 2002
3. Halama, R. – Experimentální poznatky a fenologické modelování cyklické plasticity kovů, Habilitační práce, VŠB – TU Ostrava, 2009
4. Staš, P. – Design of electric drive for testing system of steel materials, Diplomová práce, VŠB – TU Ostrava, 2010
5. Mišák, S., Sokanský, K., Chmelík, K., Foldyna, J.: THE DIAGNOSTIC OF INDUCTION MACHINES WITH USING METHOD OF MEASURING MAGNETIC FIELD, Wien, Austria., DAAAM International, 2006, DAAAM International Vienna, p. 35-40, ISBN 3-901509-57-7
6. Mišák, S., Mach, V.: THE DIAGNOSTIC OF SURGE PHENOMENA AT WINDINGS OF ELECTRIC MACHINES WITH USING PROGRAM EMTP-ATP, Wien, Austria., DAAAM International, 2006, DAAAM International Vienna, p. 156-162, ISBN 3-901509-57-7
7. Fig. 1 [online]. [cit. 2012-02-26]. Available WWW: <http://origin-ars.sciencedirect.com/content/image/1-s2.0-S0013794409002707-gr5.jpg>
8. Fig. 2 [online]. [cit. 2012-08-06]. Available WWW: <http://www.starmans.net/en/magnetic-particle-testing-of-railway-wheels.html>

The Monitoring System of Energetically Self-sufficient “SMART” House

Jindřich Stuchlý

Department of Electrical Power Engineering, FEECS,
VŠB – Technical University of Ostrava, 17. listopadu 15, 708 33 Ostrava – Poruba
jidrich.stuchly.st@vsb.cz

Abstract. In recent years there has been put a focus on self-sufficient objects at different voltage levels. This trend might help faster growing source of electricity, among which could be included without any doubt photovoltaic and wind power plants, which are currently applied in different voltage levels. The combination of these renewable energy sources can be achieved by direct local consumption of produced energy or storage of energy in a battery bank or other systems, especially for the lower performance of production units.

Keywords: renewable sources, hybrid system, monitoring system, smart house

1 Introduction

In year 2011 was built the pilot project of energy conception to power supply self-sufficient house by electrical and solar energy [1]. As the sources for this project were used renewable energy sources only. The main aim for this year is creating the monitoring and control system for the self-sufficient house.

1.1 Smart grid conception of smart house

The project was built wind and photovoltaic power plant as sources of electric and solar energy shown in Fig.1.

This created a basic platform for research in stand-alone system area in different power levels. The comprehensive monitoring and control system will be able to define the basic operating parameters of individual components and whole system as well.

Along with the established monitoring and control system will be possible to determine the overall efficiency of the system, define the contribution of individual resources within the long time period and specify the usability for proposed energy conception for any place around the world.



Fig. 1. Smart grid conception of smart house in university campus (hybrid system)

2 Sources and inverter's parameters

In a conception of hybrid system have been used 2 strings of photovoltaic's power plant - 2kWp each, wind power plant with installed electrical power 12kW and solar collector of absorption area 2,53m². The accumulation bank consists of 24 batteries of nominal voltage 2V. The sources parameters are in Table 1.

Table 1. Sources parameters

Type of source	Type	Nominal value
Photovoltaic power plant 1 – tracker	Monocrystalline technology	2 kWp
Photovoltaic power plant 2 – fixed installations	Polycrystalline technology	2 kWp
Wind power plant	Synchronous generator with permanent magnet (SGPM)	12 kW
Solar collector	Flat selective collector	2,53 m ²
Batteries	Lead acid	840 A·h

Table 2. Inverter’s parameters

Type of inverter	Quantity	Type	Nominal power output
Sunny boy	1	SMA SB2100tl	1950 W
Windy boy	4	SMA WB5000A	5000 W
Sunny Island	1	SMA SI3324	3300 W
Windy boy protection box	3	SMA WBPB 600	2000 – 6000 W

These inverters are responsible for operation and control of hybrid system. They take part in forming an inseparable part of the system and consequently the system could not work basically without these elements. One of the basic steps in the beginning of building this system was current availability of suitable inverters and then their exact parameterization in collection with their use as a stand-alone system and debugging the whole system. The inverter’s parameters are in Table 2.

2.1 Measurement modules

For the measuring of voltage and current will be used following modules in Table 3.

Table 3. Measurement modules Parameters

Type of module	Quantity	Type	Input signal	Max. Output signal
Voltage converter	13	SCM-101	$\pm 300/600$ V	± 10 V
Voltage converter	1	MACX MCR-UI-UI	± 48 V	± 10 V
Current converter	12	SCM111	$\pm 12/25$ A	± 10 V
Current converter	1	LEM-Isens-02-2,5	$\pm 2,5$ A	± 10 V
Current converter	1	LEM-Isens-01-105	± 105 A	$\pm 14,5$ V

3 Hybrid system

The measurement system was created for the energy conception. The measurement system can define voltage, current and consequently the electrical power output. This measurement will be carried out for individual components of the wind and photovoltaic power plants in order to optimize energy conversion chain and to contribute increasing the overall efficiency of system. For the part of solar energy is expected to measure the basic quality parameters of solar collector as well as for the electric power part.

The monitoring system will be used for an assessment of meteorological conditions in order to assign the overall efficiency of the proposed concept of operation for different operational and climatic conditions.

All the results of measuring will be saved for subsequent post-processing to the database and will be published by means of requested steps via web browsing interface on the internet domain.

Using the control system will be possible to take control of the basic operating conditions of the concept of energetically self-sufficient “SMART” house. Using the remote administration can be controlled the basic operating conditions created by the web interface and control via PDA communicators.

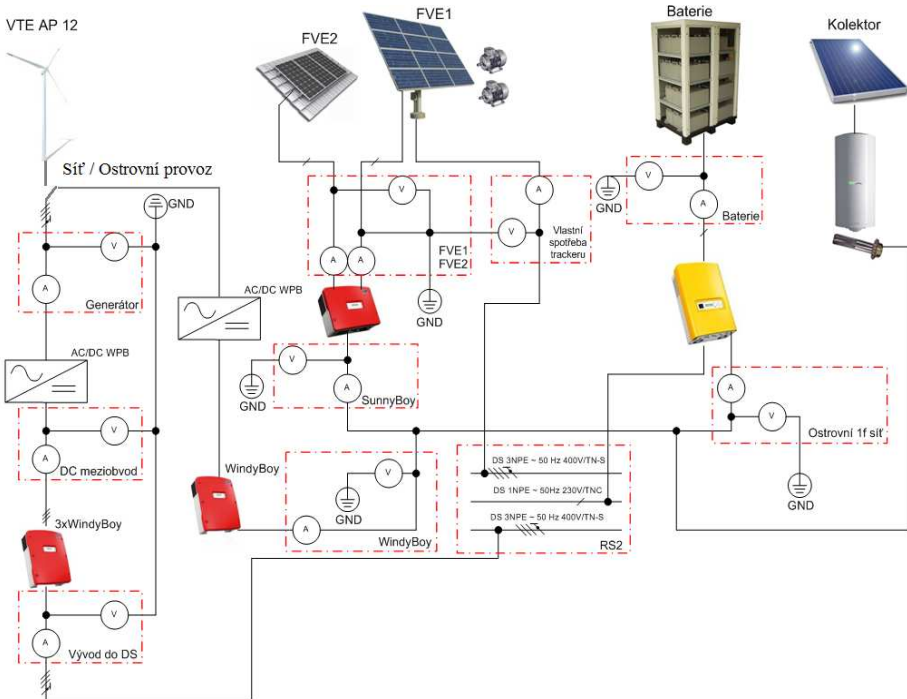


Fig. 2. Block scheme of hybrid system

That block scheme describes the electrical connections between the individual elements of the hybrid system.

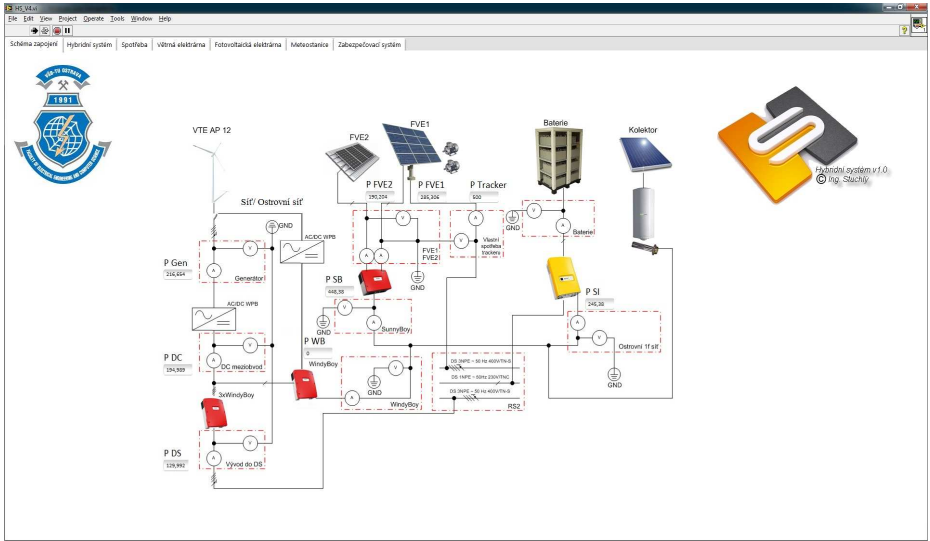


Fig. 3. LabView example visualization tools for virtual instrumentation of hybrid system – The main screen.

In Fig. 3. can be seen the welcome screen of monitoring system, where are the essential parameters of hybrid system. Basically it is a block scheme with marked measuring points of electric power and solar energy. The individual measuring points are assigned for the clarity of actual measured values.

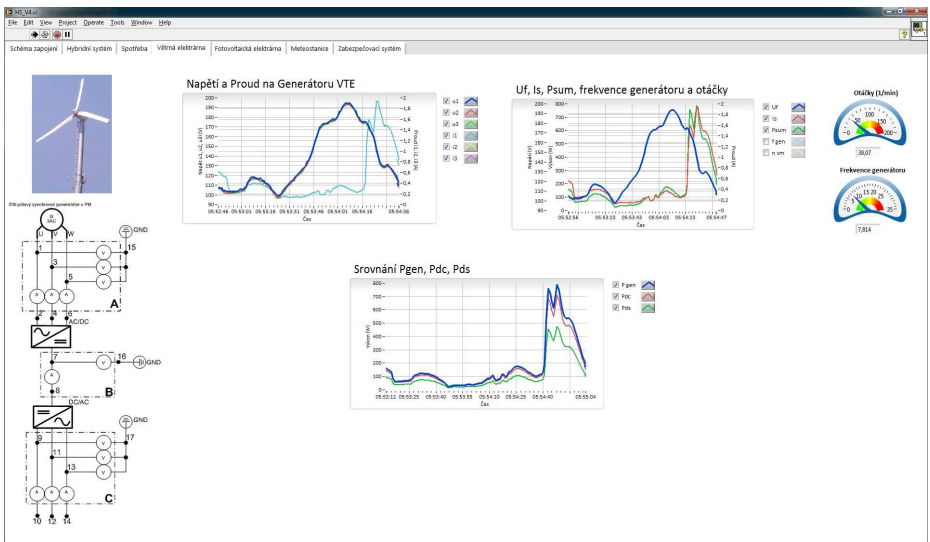


Fig. 4. LabView example visualization tools for virtual instrumentation of hybrid system – The Wind power plant parameters.

Fig.4. represents the operating parameters of Wind power plant type AP 12. The individual graphs represent the measuring points (blocks) with the possibility of dis-

playing all parameters or just those parameters which are interesting for the user by using the tick boxes.

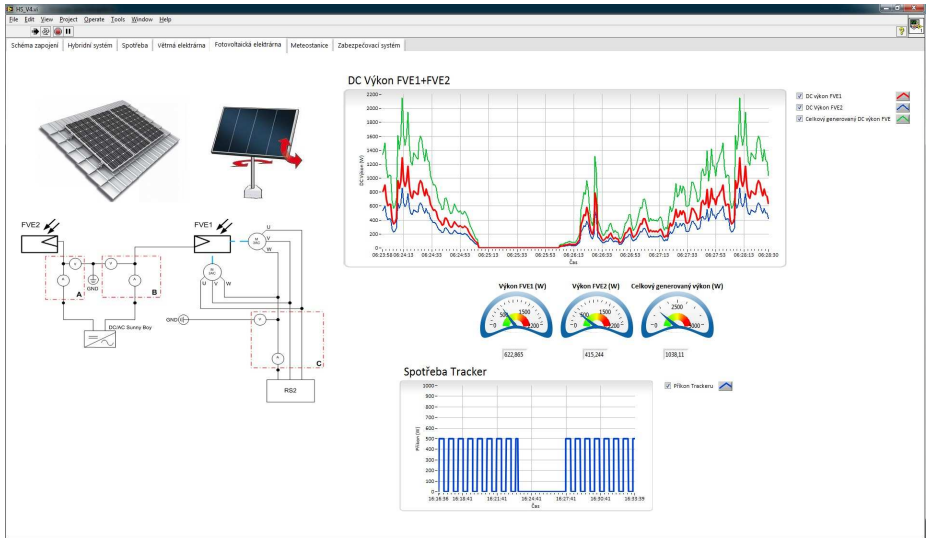


Fig.5. LabView example visualization tools for virtual instrumentation of hybrid system – The Photovoltaic power plant parameters.

Fig.5. displays the actual parameters of both parts of the Photovoltaic power plant and then its own consumption of the tracker.

Acknowledgment

This paper was created with the support by project SGS nr. SP2012/53.

Conclusion

This pilot project of energetically self-sufficient “SMART” house is the basic conception unit for smart grids region [2]. The output of the measurement will be used as a basic database for artificial intelligence methods and modified results to exact place can be apply anywhere in the world.

References

[1] L. PROKOP, S. MIŠÁK – Off – grid energy concept of family house, EPE2012, Brno, Czech rep.
 [2] A. DAS, V. BALAKRISHNAN – Sustainable energy future via grid interactive operation of spv system at isolated remote island – *Renewable and Sustainable Energy Reviews* 09/2012

Modeling of Electromagnetic Fields in the Vicinity of the Rail

Pavel Svoboda and Lukáš Paulinský

Department of Electrical Engineering, FEECS,
VŠB – Technical University of Ostrava, 17. listopadu 15, 708 33 Ostrava – Poruba
svo288@vsb.cz

Abstract. This article describes modeling of electromagnetic fields in the vicinity of the rail. The results of simulations are shown for some values of electric current. To perform these simulations the COMSOL software was used. This software works with finite elements method.

1 Introduction

In electric traction, we need to know the magnitude of leaking current and its distribution in the ground. This fact can relate with determination of other parameters of electric traction. These parameters have practical function for power circuits as well as for signaling, safety and communication circuits. These parameters are used for determination of transmission function, distribution of electric current between ground and rails, for determination of corrosion danger and for correct adjustment of signaling and safety circuits.

Artificial electric fields arise in vicinity of electrical sources which are supported by insufficiently isolated power sources or from sources which are using ground as a backward conductor. These electrical fields may arise form galvanic cells which can be caused by chemical dirt on surface of conductors.

Electromagnetic issues, linked with solving of current fields in railway traction, works with electrical current and density of electrical current which is relative to electromagnetic intensity and potential, respectively. [1]

2 Performance in COMSOL

Comsol Multiphysics software solves physical issues, which are described by partial differential equations, by finite elements method. Whole procedure is composed of definition of environment and bordering conditions on surfaces, edges or points of the model. By these, the model is prepared to generation of computing network (meshing). In the nodes of the network the data will be computed. We can show results of simulation like color maps, isolines, steamlines, arrows et cetera. [2]

2.1 Disposal layout of the rail

For illustration, the model is solved in 3D like on figure 1.

For our simulation, we created 1m of rail. This rail was fed by electrical current from 100A to 1000A with 100A step. Our interest was in distribution of electrical field in rail and the vicinity of this rail. Therefore we made cylinder of air around the rail in our model.

In Comsol software the current values were set as a current density which was computed from current and volume of the rail.

Computation network was set to 720000 degrees of freedom (figure 2). The time demand for this simulation was approximately 120 minutes.

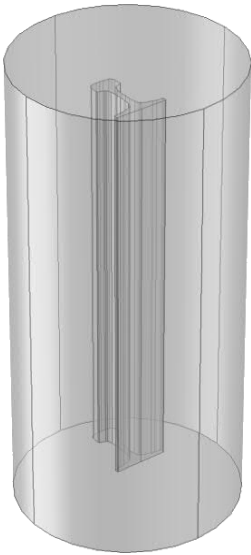


Fig. 1 Disposal layout

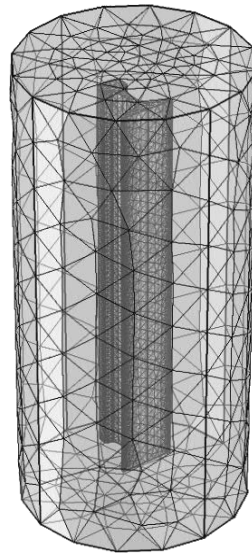


Fig. 2 Model with computation network

2.2 Resolution

For clarity, the distribution of magnetic induction and intensity of magnetic field is shown in three cases – 100A, 500A and 1000A. Other results of simulation are summarized in table below. All of the results are shown like cross-sections. A plane of the cut goes through the center of the rail.

2.3 Current 100A

The distribution of the electromagnetic field for DC current 100A is shown below. The maximum value of magnetic induction (Figure 3) on borders of the rail is 0.0312T. The value of magnetic induction in the middle of the rail is approximately 0.01T. In the picture, the distribution of magnetic induction around the rail is also obvious.

The intensity of the magnetic field (Figure 4) has its top at 187.3A/m. In the middle of the rail, the intensity of the electromagnetic field is almost one-third of the top value.

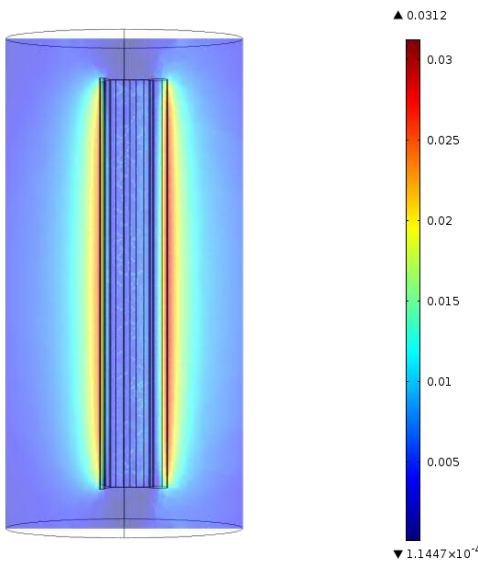


Fig. 3 Distribution of magnetic induction for 100A

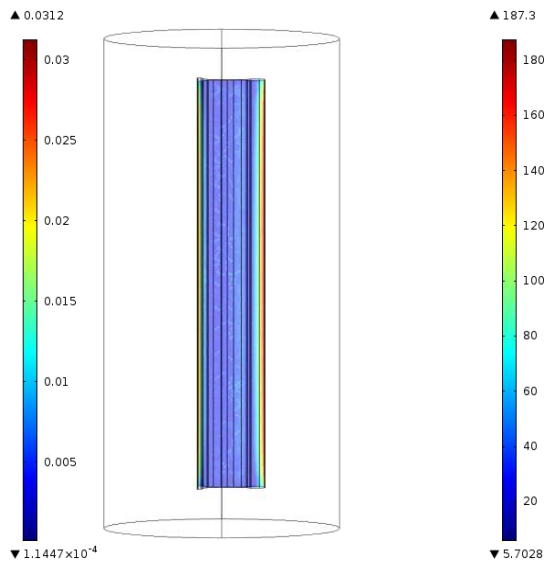


Fig. 4 Distribution of intensity of magnetic field for 100A

2.4 500A current

The distribution of magnetic induction for 500A is shown in figure 5. The maximum value is almost ten times higher than in the last case - 0.2723T. In the middle of the rail, it is 0.07T which is 7 times bigger than in last case.

The top value of intensity of the magnetic field grew up to 916.95A/m (figure 6). In the middle of the rail the intensity of magnetic field is approximately 400A/m.

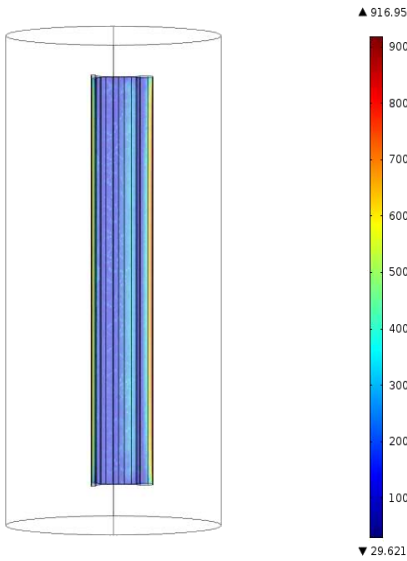


Fig. 5 Distribution of magnetic induction for 500A

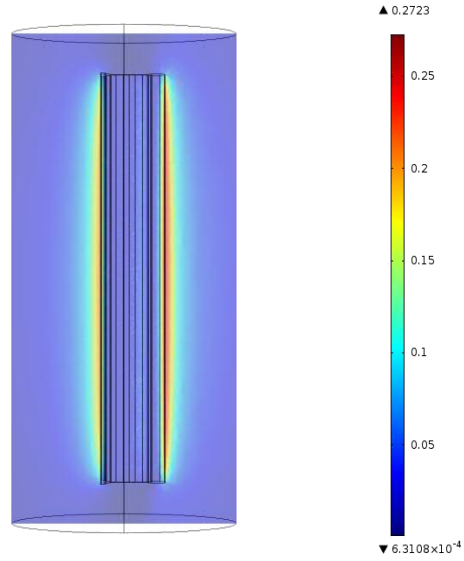


Fig. 6 Distribution of intensity of magnetic field for 500A

2.5 Current 1000A

1000A was our maximum value of DC current which caused the top value of magnetic induction 0.77T and magnetic induction in the middle of the rail was 0.2T (figure 7).

Intensity of the magnetic field reaches 1930.8A/m at the borders which is ten times higher than for 500A. In the middle of the rail there is 800A/m. This value is only twice as higher as in the last case.

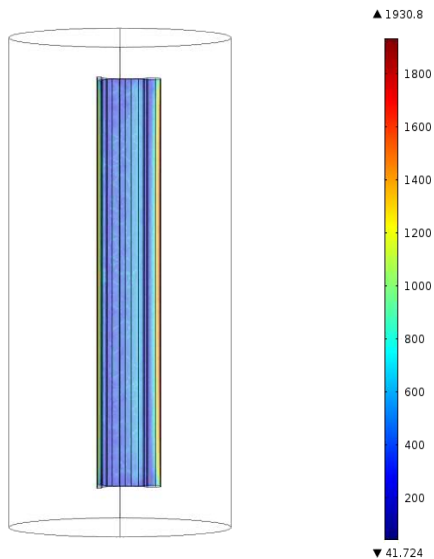


Fig. 7 Distribution of magnetic induction for 1000A

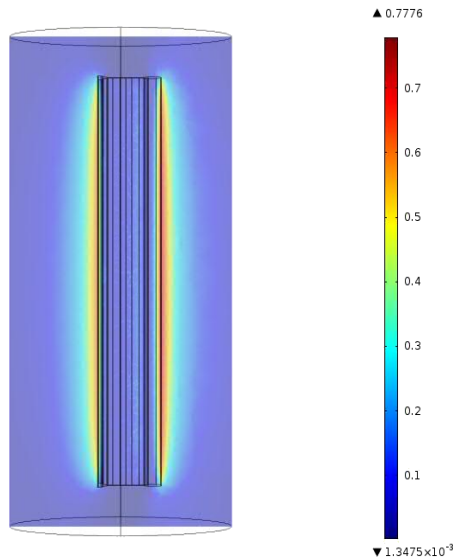


Fig. 8 Distribution of intensity of magnetic field for 1000A

2.6 Summary of the results

Table. 1 Summary of the results

Current	Maximum values		Values in the middle	
	B (T)	H (A/m)	B (T)	H (A/m)
100 A	0,031	187,3	0,01	60
200 A	0,067	367,82	0,02	130
300 A	0,12	531,13	0,035	190
400 A	0,21	717,28	0,05	300
500 A	0,27	916,95	0,07	400
600 A	0,36	1062,9	0,1	460
700 A	0,51	1278,8	0,15	520
800 A	0,6	1482,4	0,156	600
900 A	0,68	1666,6	0,178	710
1000 A	0,77	1930,8	0,2	800

The table shows all the results from the simulations. The maximum values of the magnetic induction and intensity of the magnetic field are the top values from the rail and they were reached on the edges of the rail. Magnetic induction in the middle of the rail is from three to four times lower as the magnetic induction on the edge of the rail. Top values of intensity of the magnetic field are 2.5 times higher than the values in the middle of the rail.

3 Conclusion

Our next task is to solve the rail for alternating current with the same values as in these simulations and to obtain the magnetic field for different frequencies. Following these simulations we would like to create a model with variable subsurface and to investigate the distribution of the magnetic and electric field outside the rail.

Acknowledgement

This article results from the project SGS FEI, VŠB-TU SP 2012/41 and the project MŠMT of Czech Republic and MO of Russian Federation KOTAKT II: LH 11125 Investigation of the current ground field in the vicinity of electrical railways.

References

1. IVÁNEK, L., *Modely a přenosové parametry pro šíření zpětných proudů v elektrické trakci*, Habilitační práce, VŠB-TUO, Ostrava 1998.
2. Promotion materials by Comsol Multiphysics, [online], c 2008-2011, last revision 1.4.2012 [quotes 12.7.2012], available from: < <http://www.humusoft.cz/produkty/comsol/comsol/> > .

Trial Run of Public Lighting in Insular Mode

Jaroslav Šnobl

Department of Electrical Power Engineering, FEECS,
VŠB – Technical University of Ostrava, 17. listopadu 15, 708 33 Ostrava – Poruba
jaroslav.snobl@vsb.cz

Abstract. The LED luminaires with their parameters are able to replace conventional luminaires with high pressure sodium lamps in public lighting area at the present time. The LED luminaires have one big advantage in comparison to other types of luminaires available on the current market. They have lower power consumption and there is an expectation that power consumption will be reduced to the half in the future. It leads to the possibility of using renewable energy sources in lighting area. We have prepared the analysis of the potential usage of renewable resources for LED luminaires in the future which is based on evaluation of data obtained from our model system.

1 Introduction

In recent years there was a presentation of a scientific project at the EPE conference to build up two separate poles with LED lights. Those LED lights would be powered by electricity generated from renewable sources. The project was put into operation in the beginning of the year and the data relating to produced and consumed energy was collected during the whole year.

2 System description

The system consists of two wind power stations with a top power of 200 Wp and 300 Wp and the output voltage of 12 V. In addition the system consists of two photovoltaic panels (mono-crystalline and polycrystalline) with a maximum output of 130 Wp. For those two units were chosen two different types of wind motors, first one is a horizontal propeller engine (see Fig. 1) which starts at higher wind speeds (about 4 m / s) and second one is a vertical (see Fig. 1) which can produce electricity at lower wind speeds (about 3 m / s). Those two motors charge special charging Saft batteries with a total capacity of 360 Ah. The flow of power is controlled by a control device for optimization of battery load. The output of the control device is lead to the inverter 12V DC / 230 V AC for powering of PHILIPS Mini-Iridium lights with LED light source (light emitting diodes) 31 W and CPO (metal halide lamp) 45 W. The switch of lights is realized by decreasing voltage of the photovoltaic Panels. The decrease is connected with decrease of solar radiation.



Fig. 1. Vertical (left) and Horizontal propeller (right) wind turbine

3 Evaluation of measured data

The main objective of this project was to determine whether the current configuration of system components is able to consistently and reliably supply the selected lamp lighting. Configuration of the system and the flows of electricity from wind and solar power batteries to the battery and then to the lights is shown in Fig. 2.

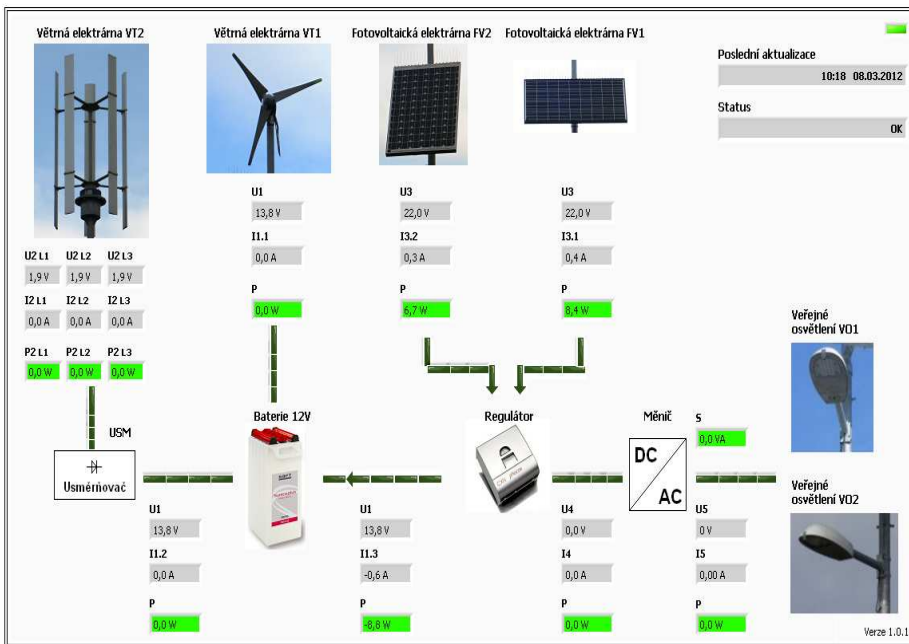


Fig. 2. The concept of the power system of public lighting

The currently available data are from May 2011 to February. The Table 1 shows the monthly totals of the energy from two wind and two photovoltaic power stations - shortcuts to the titles are the very same as in the Fig. 2. The total produced energy equals to the sum of them. The last column indicates the power consumption of both lights, need to be noted the consumption is related to the amount of electricity available in packs. The average monthly consumption of LED lamps is about 10 720 Wh, monthly consumption of both lamps is 28 358 Wh (expected time of active lighting is 4150 hours per year).

Table 1. Table showing the energy which is produced monthly from the individual components

month	VT1 (Wh)	VT2 (Wh)	VF1 (Wh)	VF2 (Wh)	electric energy produced (Wh)	consumption of public lighting (Wh)
April 2011	435,4	43,3	3821,8	3253,2	7553,7	6332,5
May 2011	-3,9	66,6	8538,2	7465,0	16065,9	13321,1
June 2011	0,0	110,6	8544,7	7322,5	15977,7	14417,0
July 2011	-0,2	62,0	7605,3	6519,2	14186,3	12134,8
Augt 2011	0,0	47,3	8864,7	7655,0	16566,9	14255,9
Sep 2011	0,0	13,6	6960,3	5940,6	12914,5	11108,3
Oct 2011	0,0	56,0	5996,8	4957,4	11010,2	9887,8
Nov 2011	0,0	330,8	4749,1	3886,2	8966,0	7971,8
Dec 2011	0,0	552,0	3628,2	2906,4	7086,6	6196,2
Jan 2012	104,0	610,0	3615,4	2883,0	7212,3	5164,6
Feb 2012	130,5	474,9	2821,8	2300,9	5728,2	-

As is shown in the Table 1 the total energy produced does not cover the energy needs for lighting during the whole night in any month and consumption of electrical energy for lighting copies produced energy which is distributed primarily from photovoltaic panels (Fig. 3).

Table 2. The total production of electric energy

wind	3,04 kWh	2,46 %
sun	120,61 kWh	97,54 %

Additionally you can see that inputs from the wind power stations are marginal in comparison to total energy inputs. In numbers there are 2,5% produced by winter power stations to 97,5% produced by photovoltaic panels. When we calculate the efficiency of the produced and taken electricity it takes us about 80%. To overall effect, however, we have to include individual elements of the system (rectifier,

battery, inverter, control device) and after that the real effectiveness of the system will be approximately 60%.

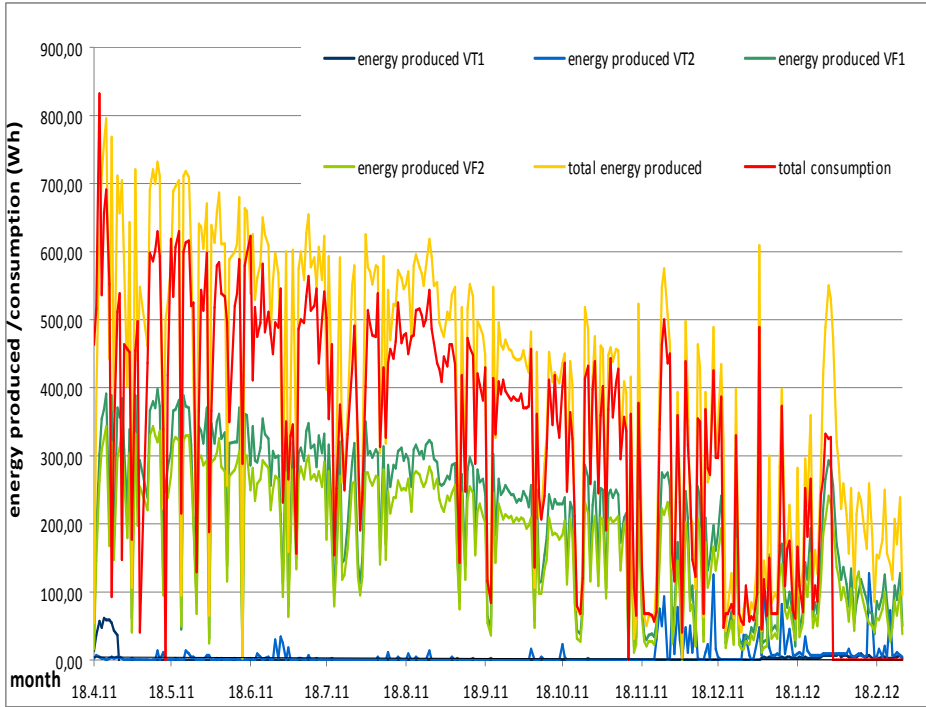


Fig. 3. Summaries of produced and consumed electric power

During the first ten observed months there were made about 123 kWh of electricity and consumed about 101 kWh. The average daily value of the electricity produced is 392 Wh. If we take into account the initial estimate (1368 Wh per day) which was used in the planning phasis of the project, the difference is 976 Wh.

4 Evaluation of working of public lighting

Taking into account the lighting time for public lighting in individual months, the ranges are from 6,9 h per day in the summer months to 15,3 h per day in the winter months. The above mentioned data shows that the system in current arrangement is not able to supply (with exception of one month) the energy required for night lighting. As shows the Table 3 the critical period is the winter period, when the street lighting is in use more than 12 hours per day.

Table 3. Table of monthly balances of public lighting energy supply and consumption

month	average operating time (hours)	total energy supplied (kWh)	necessary energy for public lighting (kWh/month)
April 2011	9,6	4,532	23,643
May 2011	7,9	9,639	20,124
June 2011	6,9	9,586	17,015
July 2011	7,1	8,511	18,165
August 2011	9,0	9,940	22,963
September 2011	11,0	7,748	27,094
October 2011	13,0	6,606	33,004
November 2011	14,4	5,379	35,465
December 2011	15,3	4,251	38,977
January 2012	14,6	4,327	37,113
February 2012	13,3	3,436	31,627

If we would accept the optimal arrangement of wind turbines and second lamp would be fitted with LED of a power of 31 W (instead with the current CPO), then we would have the balanced energy system in individual months. The real effectiveness of the system is about 60%.

5 Conclusion

Based on current data we can conclude that the concept of the system of powering two lamps in mentioned arrangement is insufficient, because to the whole system does not contribute two wind power stations. If the potential power delivery of wind turbines is taken into account (which can deliver energy in range from 600 to 800 Wh per day) it would be possible to supply two LED lights with total input of 62 W. Lamps with this input are already on the market and can be used to illuminate communications of the lower classes, ie. class S4 and S5.

It is also important to note that further increasing of installed capacity of renewable resources is no longer possible due to limited design options for street lighting poles, ie. for wind power of higher output and larger areas of photovoltaic panels would be need more robust poles that would have to have higher demands for fixation

Acknowledgement

This article was prepared under the project SP2012/160 "New possibilities of LED technology in lighting," and under the project SP2012/53 "Monitoring and control system of energy self-sufficient SMART house".

References

1. Sokanský, K., Novák, T., Šnobl, J.: Vývojové trendy LED svítidel pro veřejné osvětlení. Světlo 2011 - 19. mezinárodní konference, 2011, Praha, Czech republic, pp. 196-198, ISBN 978-80-248-2480-2
2. Novák, T., Mišák, S., Sokanský, K.: Využití obnovitelných zdrojů energie pro napájení svítidel veřejného osvětlení. 11th International Scientific Conference Electric Power Engineering 2010; (IEEE EPE 2010), pp. 253-256, ISBN 978-80-214-4094-4
3. Mišák, S., Prokop, L.: Analýza technických a ekonomických parametrů hybridních systémů. 11th International Scientific Conference Electric Power Engineering 2010; (IEEE EPE 2010), pp. 295-300, ISBN 978-80-214-4094-4
4. Mlčák, T., Mišák, S., Bača, Z., Hrbáč, R.: Provozní parametry větrné elektrárny, Sborník mezinárodní konference EPE 2011, VŠB - TU Ostrava, 2011, ISBN 978-80-248-2393-5

MCA Evaluation of Heating Systems, Measurement of Energy Balance as Tool for Improvement Usability

Jan Šrámek

Department of Electrical Power Engineering, FEECS,
VŠB – Technical University of Ostrava, 17. listopadu 15, 708 33 Ostrava – Poruba
jan.sramek@vsb.cz

Abstract. The paper deals with comparison of not only alternate and renewable sources for heating. The assessment focuses on a real property and six optional heating systems. Those are currently available on common basis and utilized in practice. The scope includes most common systems as well as alternate ones. Optimization of heating system designed for a particular property enables objective assessment of all options by means of MCA (multi-criteria analysis) methods in accordance with selected and precisely defined criteria. The next aim of this paper is to compile an instrument for measurement on the real object and receive realistic data from whole heating season for improvement of usability.

Key words heating, heating systems, heat accumulation, MCA evaluation

1 Introduction

The aim of this paper is to present options for selection of the most convenient method for heating depending on selected criteria and their importance.

That is followed by description of the MCA methodology used for assessment and software used to generate final solution in the analysis.

The criteria selected are compared against chosen and duly described assessment criteria, with clarification of obtaining their values as well as determination of criteria weights.

In the second part of this paper is described preparation of measurement in real object for obtain energy balance of heat pump and help us for improving usability.

2 MCA evaluation of heating systems

For the evaluation was chosen property which is represented by a low-energy building located within the area of Jeseníky; close to the town of Bruntál. The building has been designed as a single floor house with the total built-up area of 239 m². Heat loss calculated for this building equals to 7.14 kW at the calculation temperature of -18 °C. Heat losses have been calculated in compliance with ČSN EN 12 831 standard from 2005. [3],[5]

2.1 Description of heating systems assessed

Assessment using the MCA method is conducted by the most common and available heating methods designed on an actual family house

Table 1. Chosen variant of heating systems

No.	Heating Systems	Primary Energy Sources	Prepare of DHW
1	Air/Water Heat Pump	Low-potential	Primary source
2	Ground/Water Heat Pump	Low-potential	Primary source
3	Automatic Biomass Boiler, Solar Collectors	Biomass and Solar Energy	Primary and electric energy
4	Natural Gas Heating- Condensation System	Natural Gas	Primary source
5	Electric Heating Convectors	Electric energy	Primary source
6	Electric Radiant Heating	Electric energy	Primary source

Now after chosen of heating systems we have to choose methodology of MCA.[1],[2]

2.2 Assessment methodology

Assessment of chosen options is performed using the MCA8 decision making software used for support of multicriteria decisioning and it has been developed at Vysoká škola báňská-Technical University of Ostrava. [1],[2]

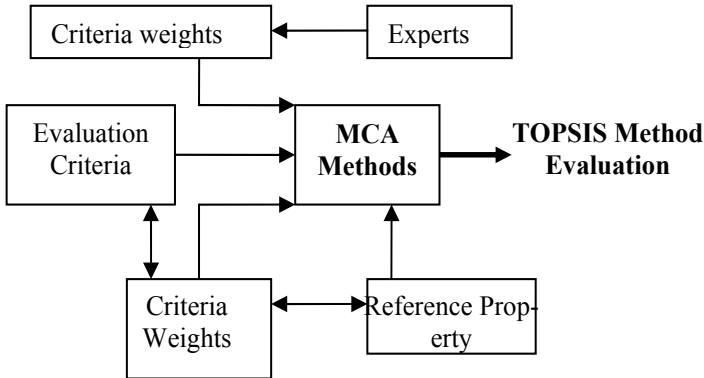


Fig 1. Diagram of methodology

2.3 Evaluation criteria and values

Solutions chosen for evaluation are subject to examination with respect such criteria, which strive towards reflection of real requirements for heating systems. For legibility purposes, those criteria have been included in Table 2; including stated criterion preferences and units.

Individual heating solutions shall be assigned with relevant values to be obtained, so each solution is provided with at least three alternates conducted (different suppliers/manufacturers of heating system). The resultant criterion value will be determined using data obtained in relevance to design of heating system on the reference building. We will use the Median function to eliminate extremes among values and obtain a representative resultant value for a specific criterion. Data used for criteria No.1, No.2, No.3 and No. 5 have been adopted from practical experience, whereas the life criterion has been derived mainly from technical literature. [1],[4]

Table 2. Criteria

No .	Criteria	Index	Value	Criteria preference
1	Investment costs	N_i	CZK	Min.
2	The energetic overview price	N_e	CZK/MWh	Min.
3	Profitability	N_p	Thousands CZK	Max.
4	Lifetime	N_l	Year	Max.
5	Environmental impact	N_{envi}	mg/m^3	Min.

2.4 Determination of criteria weights

Values of weights obtained come from 12 (twelve) experts addressed and it is necessary to point out that opinions of experts with regards to criteria importance are almost identical, yet values of weights assigned showed certain significant differences in some cases. To ensure the necessary objectivity, values of criteria weights are presented on anonymous basis. There is also an intention of further extension of the group of experts concerned in order to secure the maximally relevant ratio of criteria weights to enable future elaboration on these issues. [1],[2]

Table 3. Used weights of criteria received from experts

No.	Criteria	Preference	Weight for evaluation
1	Investment costs	Min.	26
2	The energetic overview price	Min.	22
3	Profitability	Max.	28
4	Lifetime	Max.	15
5	Environmental impact	Min.	9
SUMMARY			100

2.5 Result of evaluation by MCA method

Transformation of all input values enables us to obtain results of evaluation using the MCA TOPSIS method, which referred to the criteria entered, their values and weights obtained to show a clear dominance by heat pump systems (as shown in Tab. 4) using low-potential energy. [1],[2]

Table 4. Received results of MCA analyses

No.	Heating Systems	Evaluation
1	Ground/Water Heat Pump	0,598
2	Air/Water Heat Pump	0,574
3	Automatic Biomass Boiler, Solar Collector	0,558
4	Natural Gas Heating Condensation System	0,527
5	Electric Radiant Heating	0,41
6	Electric Heating Convectors	0,393

3 Measurement of energy balance

The object in village Mala Roudka was chosen for measurement of energy balance. Point of interest on this object is his usability during a heating season and also obviously by wrongly designed nominal power of air/water heat pump.

3.1 Current status of the heating system and target of measurements

Actual status of heating system in a chosen object is air/water heat pump with nominal output heat power 10,2 kW (Fig. 2.) which secures heating and preparing part of hot domestic water. Heat loss of the object is calculated according to [5] is 15 kW. The aim of measurement is determination of actual energy balance between heat source (heat pump) and usability of building (heat demands) and outside weather conditions. For receiving data with maximum objectivity is necessary to execute a measurement for complete heating season, during period Autumn-January 2012/2013.



Fig. 2. Current unsatisfactory status of heating installation.

3.2 Measurements tools

For realization of measurements is chosen heat meter with recording possibility. According to flow rate of heating media (water) and difference of temperature in the supply and return pipe meter calculates amount of consumed heat. The aim of measurement is also executes secondary measurement of consumption of electric energy by heat pump and other electric equipment installed in the heating system. The meter has many functions which will be helpful in our analyses as flow rate, operation hours of heating system and etc.

4 Conclusion

The aim of whole realization of this measurement is to obtain real data of energy balance from air/water heat pump and also to discover real coefficient of performance. On the basis of obtained values we can design steps for usability of actual heat-

ing system e.g. by better accumulation of the heat. We expect realization and installation of measurements probably during October 2012. We will have complete data for analysis during summer 2013.

Acknowledgements

This work was supported by the Czech Science Foundation (102/09/1842), by the Ministry of Education, Youth and Sports of the Czech Republic (SP2012/188) and by the project ENET (Research and Development for Innovations Operational Programme (CZ.1.05/2.1.00/03.0069).

Publications

1. ŠRÁMEK, Jan. HRADÍLEK, Zdeněk. MCA methods evaluation of alternative heating system application. In. Proceedings of the 13th International Scientific Conference EPE 2012 May 23-25, 2012 Brno, Czech Republic. ISBN: 978-80-214-4514-7
2. ŠRÁMEK, Jan. MCA methods evaluation of alternative heating system application. In. Proceedings of the 1th Conference Progress 2012. Ostrava, Czech Republic. ISBN: 978-80-248-2666-0
3. ŠRÁMEK, Jan. HRADÍLEK, Zdeněk. Improvement efficiency of the design heating. In. Proceedings of the Conference ELNET 2011. Ostrava-Poruba. Czech Republic. ISBN: 978-80-248-2510-6

References

- [1] ŠRÁMEK, Jan. HRADÍLEK, Zdeněk. MCA methods evaluation of alternative heating system application. In. Proceedings of the 13th International Scientific Conference EPE 2012 May 23-25, 2012 Brno, Czech Republic. ISBN: 978-80-214-4514-7
- [2] ŠRÁMEK, Jan. MCA methods evaluation of alternative heating system application. In. Proceedings of the Conference Progress 2012. Ostrava, Czech Republic. ISBN: 978-80-248-2666-0
- [3] HRADÍLEK, Zdeněk. Energetika průmyslových a distribučních sítí. 1. vyd. 2008. ISBN 987-80-7225-291-6.
- [4] DAHLSVEEN, Trond. *Energetický audit a certifikácia budov*. 2008 Bratislava. ISBN 978-80-8076-063-2
- [5] ČSN EN 12831 (06 0206). Praha: Český normalizační institut, c2005. 76s.

Estimation of Voltage Unbalance in High Power Systems Supplying AC Electric Railways

Tien Trung Vo

Department of Electrical Engineering, FEECS,
VŠB – Technical University of Ostrava, 17. listopadu 15, 708 33 Ostrava – Poruba
vo.tienTrung@yahoo.com

Abstract. Electric railway loads are supplied by the three phase power system represent one of the main sources of voltage unbalance perturbation in the grid. The power system configuration and the load conditions influence the degree of this power quality perturbation. This present paper deals with the problems raised by the practical determination of the voltage unbalance in conformity with the standards. Availability of voltage unbalance is measured and investigated on performance of power system network in České Budějovice in Czech Republic.

Keywords: Power quality, Voltage unbalance, Traction network

1 Introduction

The electric railway systems are supplied by the high voltage power network. In three-phase power systems the generated voltages are sinusoidal and equal in magnitude, with the individual phases 120 apart. However, the resulting power system voltages at the distribution end and the point of utilization can be unbalanced for several reasons. Voltage unbalance occurs in electrical power supply systems due to the asymmetry of the equipment on the one hand and the asymmetry of load states on the other. The main influencing factor with regard to the equipment can be overhead lines. Because of the geometric arrangement, the different mutual influence and the difference phase-to-earth capacity to asymmetries. With regard to system perturbations, the asymmetrical load states cause the asymmetries. In low voltage systems they occur mainly due to the loads connected between the phase-conductor and the neutral conductor. At the medium and high voltage levels the loads operated between the two conductors form the rare loads.

2 Definition of Voltage Unbalance

In a three-phase system, the degree of voltage unbalance is expressed by the ratio (in percent) between the RMS values of the negative sequence component and the positive sequence component of the voltage. The NEMA (National Equipment Manufacturer's Association) definition of voltage unbalance, also known as the line voltage unbalance rate (LVUR), is given by formula:

$$\%LVUR = \frac{\text{max voltage deviation from avg line voltage}}{\text{avg line voltage}}$$

Effects of voltage unbalance: The main effect of voltage unbalance is motor damage from excessive heat. Voltage unbalance can create a current unbalance 6 to 10 times the magnitude of voltage unbalance. In turn, current unbalance produces heat in the motor windings that degrades motor insulation causing cumulative and permanent damage to the motor. This scenario would result to expensive facility downtime due to motor failures.

Standardizations: The emitted interference of an individual disturbance should not exceed a value of $k_U = 0.7\%$ in the area of the asymmetry. The compatibility level for medium and high voltage systems is stipulated as 2%. The 10-minute average of the negative sequence component of the voltage in a three phase system is less than 2 percent of the phase voltage of the nominal voltage (95 percent value during a measurement period of one week). This value is given in EN 61000-2-2 and EN 61000-2-4. EN 50160 also stipulates a value of 2%. Ten-minute mean-value intervals should be assessed to determine the level. The interference immunity for electrical equipment is stipulated as 2% according to EN 50178. EN 50178 also stipulates an asymmetry for the ratio of the voltage of the zero phase-sequence system to the voltage of the positive sequence system. A limit of 2% is also stipulated for this quantity.

Reduction of voltage unbalance: A number of technical options may be considered in order to reduce existing or potential unbalance in a supply system as connection of disturbing loads to a different supply point, rearrangement of phase connections of one or more loads, connection of disturbing load at a higher voltage level, provision of phase balancing or filtering equipment.

3 Example of measurement and calculation

In this section, a numerical example is shown and calculated for voltage unbalance in power system network in České Budějovice in Czech Republic. Measurement and calculation have been performed in high power supplying 110kV for three node of the grid that are Skoda, Velesin and Lipno substation.

The simple diagram for measurement and calculation is shown in figure 1.

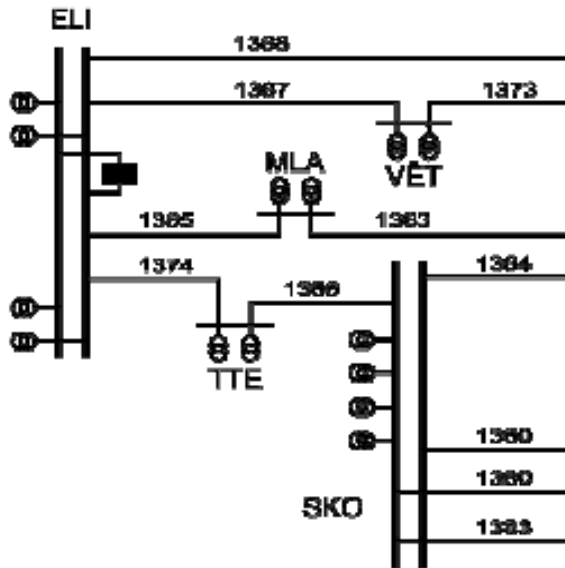


Fig.1 Simple diagram Lipno (ELI), Velesin (TTE) and Skoda.

Availability of measurement has been performed for one week. The RMS of voltage is measured 10-minute average.

Calculation of voltage unbalances in 110kV high power systems supplying.

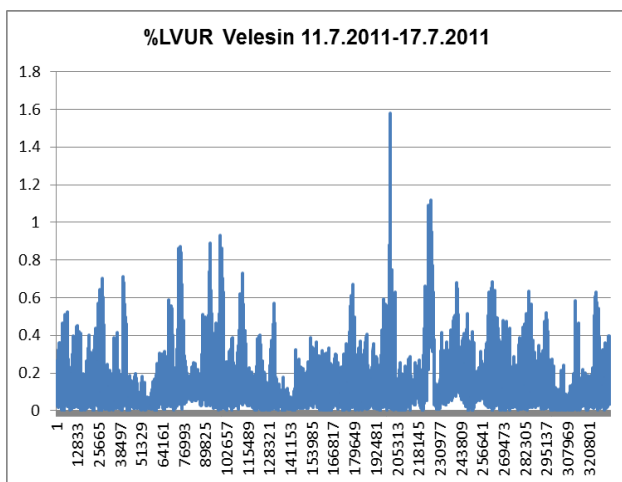


Fig.2 Voltage unbalance in 110kV Velesin substation

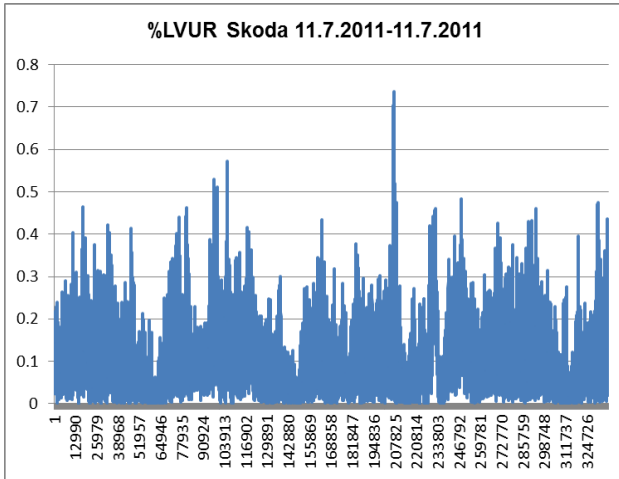


Fig.3 Voltage unbalance in 110kV Skoda substation

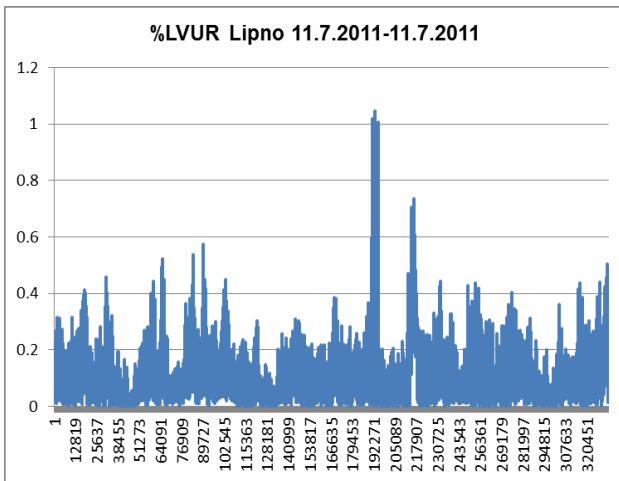


Fig.4 Voltage unbalance in 110kV Lipno substation

4 Conclusion

This paper present results of measurement and calculation the voltage unbalance in high power supplying electric railways. Objective of this Study was to measure and compare with standards. In order to reduce voltages unbalance on the traction power systems distribution network.

Measurement and calculation results are shown that the most of voltage unbalance percent in 110kV Velesin substation: %PVUR = 1.578512%; in Skoda substation: %PVUR = 0.736695%; in Lipno substation: %PVUR = 1.047143%;

Evaluation of measured data resulted in an information that the voltage unbalance on the measured high power supplying electric railways meets specified conditions by standards for the operation of distribution systems. With regard to the measurements taken into other lines, we can conclude that generalize for the entire railway network in Czech Republic.

References

1. Josef Paleček, Václav Kolář, Vítězslav Stýskala, Bogdan Fukala: Operating AC Electric Railway from the Point of View of EMC – Harmonics Spreading in 110. Proceeding 13th International Scientific Conference on Electric Power Engineering 2012, MAY 23-25, 2012 Brno, CZECH REPUBLIC Pages: 361-366, ISBN 978-80-214-4514-7.
2. M. H. J. BOLLEN: Definitions of Voltage Unbalance. IEEE Power Engineering Review, November 2002, 0272-1724/02/\$17.00©2002.
3. K. KARWOWSKI, A. SZELAG: modern electric traction. Gdansk university of technology 2009. ISBN 83-911669-7-X.

Using the Dynamic Model to the Transition of Traditional Distribution Network to Smart Grid

Marián Uher

Department of Electrical Power Engineering, FEECS,
VŠB – Technical University of Ostrava, 17. listopadu 15, 708 33 Ostrava – Poruba
Marian.uher@vsb.cz

Abstract. This article describes solving problems of power flow optimizing in an existing distribution network that will be gradually transformed into so called Smart Grid. There is also included possibility of calculating complex AC networks, the methods used to solve this problem. This article also describes the dynamic model of behavior of distribution network. This is the software developed for solving of operating states of current distribution network, which will be revitalized to Smart Grid as the first in Czech Republic. Development stages of the dynamic model, the possibility of its use and the other intended applications are contained.

Keywords: Smart Region, Smart Grid, Dynamic model

1 Introduction

High-quality supply of electricity is already an essential part of everyday life. Scientists involved in power flow optimizing in ac networks for many years. Many optimization techniques were invented and several algorithms solving this problem were examined.

As examples might be shown iterative methods, including the fundamental Gauss-Seidel [1], which shows simple calculation algorithm, but due to its low potential of convergence is not commonly used. Another iterative method used to solve of power flow calculation in ac network is Newton-Rhapson's one [2], which shows much powerful ability of convergence for the same configuration of analyzed network, but it requires greater claim on computer technology due to Jacobian of partial derivatives calculating necessity. To je take důvod k vývoji zjednodušených metod jako je zjednodušená NR metoda [3]. This is the reason for development of simplified method such as Simplified Newton-Rhapson method [3].

Optimal power flow calculation can be performed by other methods such as linear programming [4], Newton based methods [5], interior point methods [6] or the non-interior point methods.

In the case of changing the current distribution network to the Smart Grid technology [7], knowledge of power conditions is basic assumption of right solution. CEZ group has started construction of the first Smart Grid in the Czech Republic as part of its pilot project called Smart Region in the Futur/e/motion initiative. Therefore they allocate a part of the existing electricity grid in the eastern Bohemia for this purpose. To revitalize this devoted part of network and for power flow analysis so-called dynamic model was developed on VSB-Technical university of Ostrava Department of electrical power. It is complex software which mathematically calculates the behavior of devote distribution network on voltage level of MV and LV.

2 Optimization of power flow in the devoted distribution network

2.2 Solved stages of Smart Region power flow optimization

The task of first stage of power flow analysis in devoted part of current distribution network was the deployment of long-term measurements to typed daily load diagrams determining. These typed load diagrams were later used as a source of data for offline analysis of the upcoming dynamic model.

Another main object of this stage was to create an equivalent mathematical model of the prepared Smart region network. For this purpose software ATPDraw was used. It is the simulation software for analysis of electromechanical processes, which is based on structure of programming language FORTRAN.

Next stages task was to create a user interface of mathematical model. For this purpose software LabView was used.

The experimental measurements, which were realized in the area of Smart region has become to subject of next stages of Smart Region power flow optimizing. In this stage the following measurement was realized:

- Simulation of metal ground connecting on a 35kV side of transformer 110/35 kV (different tuning of shunt reactor)
- Simulation of metal ground connecting on 10kV of transformer 35/10 kV
- Long-term measuring of power loading of transformer T 32, 35/10 kV

The measurements relating to the metal ground faults were realized to control of correctness of mathematical model, respectively to control correct capacity modeling respectively (measuring of the capacity network current).

In case of long-term transformer loading measurement, the data of measurement on secondary side of transformer 6.3 kV·A, 35/10 kV was statistically analyzed. This transformer supplies a number of the other distribution transformers 10/0,4 kV, which supplies mostly flat buildings or family houses. Respectively the data of complex time period of one month was analyzed. Than the resultant measured load diagram was compared with the typed daily load diagrams relevant to Smart Region area. Namely:

TDD4 – consumption of electricity without heat utilization, and TDD East Bohemia. The data was analyzed and compared by the statistic methods. By the analysis of variance and median comparison was found, that the data is not identical statistically. But graph in Fig.1 shows curve similarity of measured power curve with TDD4 curve. It is possible to say, that this type of power load is majority represented in this area.

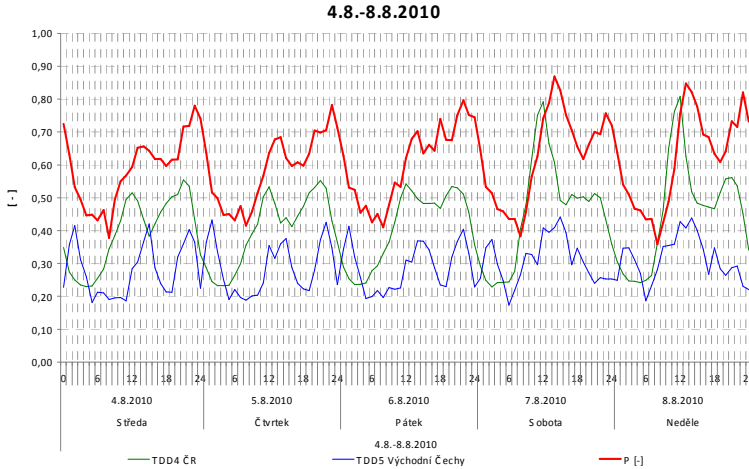


Fig. 1. The resulting waveforms of TDD

One of the stages in development of the dynamic model and the Smart Region were cogeneration unit integration. Three units of cogeneration in total installed power capacity of 3920 kW (total heat power 4351 kW) will be built in the Smart Region area. The cogeneration unit with installed power of 800 kW has been installed and now it is in trial operation. The other two units of 1560 kW will follow. Cogeneration unit has been already implemented to the dynamic model environment. It was a model of four-pole synchronous machine of 1500 kV·A, working on voltage level of 400 V. The model of cogeneration unit was created by a controlled model of synchronous machine with mechanic power regulation on its shaft as an input value to keep terminal voltage constant.

Optimization of power supply operating includes an analysis of transient conditions. Also computational core of the dynamic model was modified for this purpose as shown Fig. 2. Using this menu it is possible to simulate this type of faults:

1. Symmetrical faults
 - 3phase short-circuit
 - 3phase ground fault
2. Asymmetrical faults
 - 2phase short circuit
 - 2phase ground fault

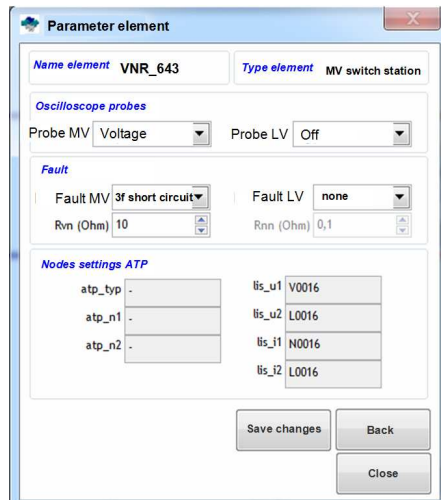


Fig.2. Bookmark for settings faults conditions in an environment of Dynamic Model

The user receives information about the progressions of the variable such as voltage, current or frequency, of rotation speed in case of cogeneration unit. It is possible to follow time sequence of selected variable signals. Basic mathematical operations with these signals such as sum, difference, product and calculation of TRMS) is allowed by using of post-processing.

Perfect communication between production and consumers of electricity is the basic building block of Smart Grid philosophy. The information about current power consumption is given not only to final users, but mainly to electric power control center by so called smartmeters. For possibility of online power flow analysis in the Smart Region area the data from smartmetering was implemented into the environment of the dynamic model. Incoming data was also modified, because of their form of 15minutes record of energy and voltage values, while the dynamic model processes data in form of one hour record of electric power and voltage values.

2.2 Aims of next solution

The next stage of development of the dynamic model will be based on the so called complex solver of occurring events. The priority of warning messages, which is able to generate by the dynamic model (transformer overload, line overload, overvoltage etc.), will be pre-determined. If the occurring event became (operating or fault one), several possibilities of network topologies changes will be suggested and calculated by the dynamic model. Then there will be made a calculating of the weighted average of their generated warnings messages. Final options of analyzed network will be select by user according this weighted average of warning messages.

Another stage of innovation will involve the integration of renewable sources of electrical power into the environment of the dynamic model. Therefore it is necessary to create the models of renewable sources such as wind turbine or solar plants. These models will be implemented to the mathematical model of analyzed network, and also computational core of the dynamic model system will be modified accordingly. There is also expected with the connection of the dynamic model to the system of climatic conditions prediction. As shown in Fig. 3., approximate power consumption of analyzed network will be known, and using the prediction system also amount of energy produced by renewable source will be known for several hours in advance. The user receives information about what amount of electric energy must be produced by the other sources.

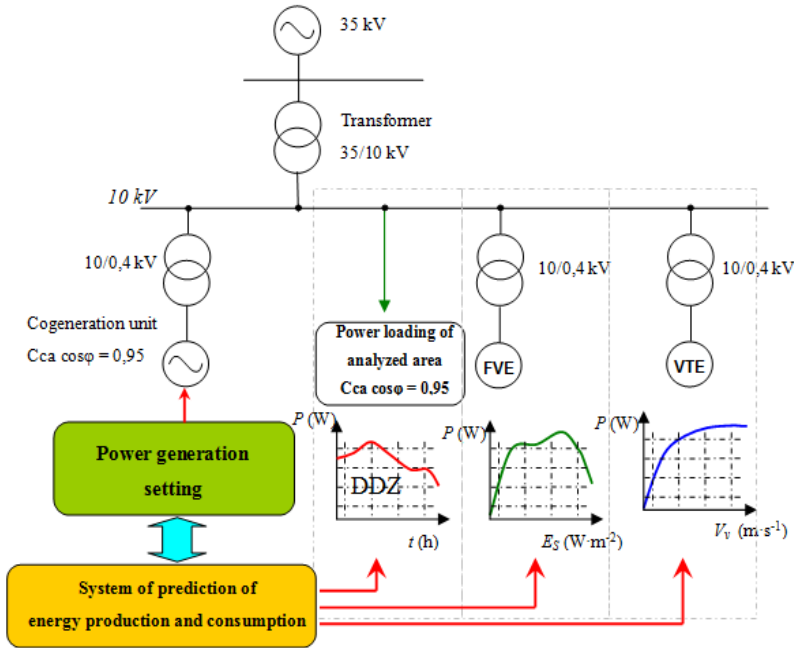


Fig.3. Philosophy of renewable sources including

Conclusion

The performance of power flow optimization using the dynamic model is carried out in several stages. Some of them are already realized.

The main task of the first stages was to create the equivalent model of real devote distribution network, which is currently rebuilding to Smart Grid technology.

The subject of second stage of development was to create the user interface for presenting calculated results. Also realizing of experimental measurements in the area of smart region was task of this stage.

While last and very important stage has lead to implementation of data from smartmetering, which are necessary for so called online analysis.

The aim of the next stages of the dynamic model development is to create the complex solver of occurring events and inclusion of renewable source of energy.

Publications

1. Uher, M.: Optimalizace provozu sítí s obnovitelnými zdroji s využitím dynamického modelu. In sborníku, VŠB - Technická univerzita Ostrava, Ve sborníku EPE 2011, 2011, VŠB - Technická univerzita Ostrava, 978-80-248-2393-5
2. Uher, M., Mišák, S.: Smart Region Operation Optimizing Using Dynamic Model. In sborníku EPQU, Lisabon:, 2011
3. Uher, M.: Optimalizace provozu sítí s obnovitelnými zdroji s použitím Dynamického modelu, Ostrava:, VŠB - Technická univerzita Ostrava, Workshop Doktorandů 2011, 978-80-248-2378-2
4. Uher, M.: Optimizing Power Flow in the Smart Region. Ve sborníku WOFEX, Ostrava:VŠB - Technická univerzita Ostrava, 2011, 978-80-248-2449-9

References

1. Saadat H. Power system analysis. McGraw-Hill; 2004.
2. Mehdi Dehghan, Behnam Hashemi, Iterative solution of fuzzy linear systems. Applied mathematics and computation, 2005
3. Thanatchai Kulworawanichpong. Simplified Newton–Raphson power-flow solution method. Electrical Power and Energy Systems, 2009.
4. Alsac O, Stott B. Optimal load flow with steady state security. IEEE Trans Power Apparatus System 1974; PAS 93:745–54.
5. Sun DI, Ashley B, Brewer B, Hughes A, Tinney WF. Optimal power flow by Newton approach. IEEE Trans Power Apparatus System 1984; PAS 103:2864–80
6. Dillon TS. Computational methods for solution of the optimal power flow problem. In: 4th International symposium on large engineering system, Calgary, 1982.
7. Ipakchi A, Grid of future, Power and Energy Magazine, IEEE 2009, New York 2009 ISSN: 1540-7977

Production and Quality of Wind Energy

Jan Unger

Department of Electrical Engineering, FEECS,
VŠB – Technical University of Ostrava, 17. listopadu 15, 708 33 Ostrava – Poruba
jan.unger@vsb.cz

Abstract. This article is about current status of wind power engineering not only in Czech republic but in whole world. We can notice increasing number of newly built wind powerstations in last years which has a result in increase of total number of operating wind turbines. There exist different types of used systems which are producing electric energy, but all of them have influence to quality of produced electric energy. Parameters of this energy are measured, analyzed and evaluated according ČSN EN 50160.

1 Introduction

Renewable energy sources are increasingly being incorporated into the energy system, especially in terms of the clean energy production compared to fossil and nuclear fuels, and also because of the support from EU which is bigger and bigger. These resources are not dependent on fuel supplies from unstable sources and on the sun and wind availability.

Usage of renewable options are limited on certain levels in Czech republic. This is a result of the lack of locations which are suitable for OZE construction, territorial limits, which are given by law (protected landscape areas, national parks, historical sites, military areas, etc.), and restrictions connected with social and psychological nature (attitude residents, impact on landscape character).

Reliability of electricity supply from renewable sources is important in terms of distribution and transmission networks. Stochastic and unstable supply of electricity have results in higher demands on the operating reserve and the constant increase of installed capacity from renewable energy sources is threatening the stability of electric networks.

2 Wind Energy in Czech Republic

The most significant development and construction of wind turbines in our area was in 2006 and 2007, when it doubled the amount of installed capacity. On the other hand, wind energy had significant decrease in last few years when comparing to the global trend of increasing the share of electricity generated from renewable resources.

There was installed 23 MW of wind energy in 2010, which is 45% less than in 2009. In 2011 were installed only 2 MW. This number is the smallest since 2004 and speaks about the fact that even political support is still very low. This could be changed if the government would accept law about supported energy resources and other law standards related to this field. At the end of 2010 was installed 1727 MW in solar energy.

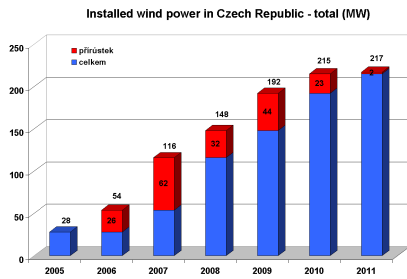


Fig. 1. Installed wind power in Czech Republic

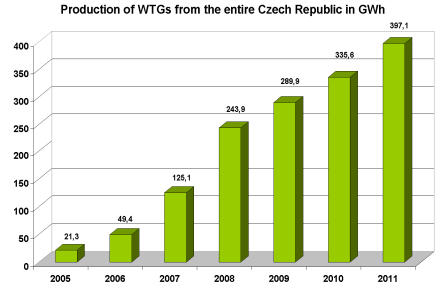


Fig. 2. Production of WTGs from the entire CR in GWh

The total electric energy produced in 2011 was 397 GWh, which is roughly equal coverage of consumption in 113,000 households.

3 Wind Energy in Europe

According to statistics from Europe and the world is more than evident that the development of wind energy, unlike the CR, is certainly not in decline. Rather the opposite.

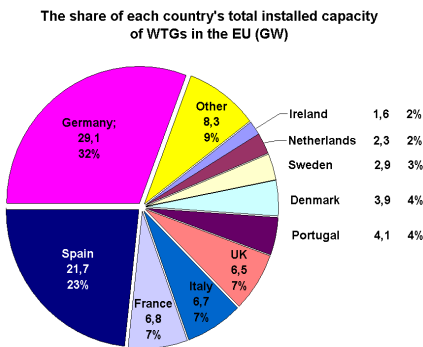


Fig. 3. The share of each country's total installed capacity of WTGs in the EU (GW)

New sources of energy put into operation and decommissioning in the EU in 2011 (MW)

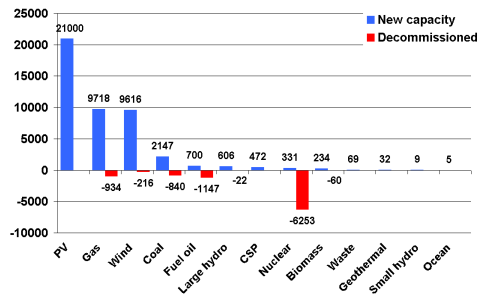


Fig. 4. New sources of energy put into operation and decommissioning in the EU in 2011 (MW)

There were added another 9,616 MW wind installations in Europe, which is almost the same number, which was in 2010. The installations were 21,4% of the totally installed capacity of all electricity resources last year.

The increase was also recorded on offshore wind farms, which increased in Europe over the last year by 866 MW. Overall capacity was increased by offshore installations to 3814 MW and more 2400 MW are in construction. Europe has totally over 97 GW in wind energy (EU has 94 GW).

4 Wind Energy in the World

World statistics achieved the value of 238.3 GW in the wind energy at the end of 2011, new installations exceeded 41 GW in 2011, which represents an annual increase of 20,9 %. Between the states with the largest amount of installations belongs China (62,733 MW), USA (46,919 MW), Germany (29,060 MW), Spain (21,674 MW) and India (16,084 MW). It is interesting that wind energy overrun half of installed capacity in nuclear energy last year, which is now 368 GW.

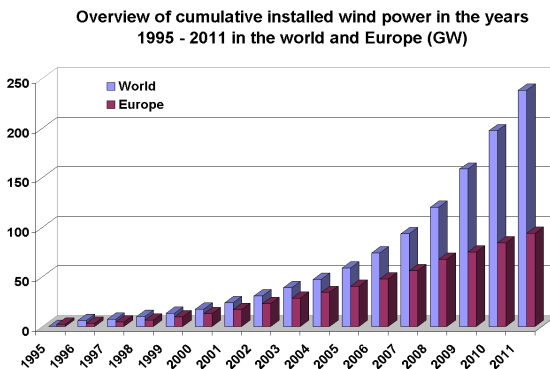


Fig. 5. Overview of cumulative installed wind power in the years 1995 - 2011 in the world and Europe (GW)

5 Analysis of the Influence the Wind Power on the Network

Currently the most of the wind farms in the Czech Republic are equipped with asynchronous generators as a source of electrical energy. For wind power plants of small and medium-power up to about 300 kW are used most often asynchronous generators with squirrel rotor connection to the grid through the thyristor trigger or asynchronous generators with switching the number of poles. The advantage of these systems is their relatively simple construction and low maintenance requirements. Their disadvantage is the low efficiency of the system especially at lower wind speeds, because the active power supply is conditioned by over synchronous speed of asynchronous generator. Other disadvantages include the lack of reactive power compensation,

which is in the most cases designed as a stepped switching and unwanted transients that are associated with switching asynchronous generator to the grid, respectively with connection of compensation equipment. If thyristor trigger control is used as a switching device it is possible to optimize current surge accompanying the connection by changing the angle of semiconductor devices. However, if happens at the moment of connection of the wind farm to the grid a sharp change of torque on the shaft of the motor due to strong wind turbulence, wind flow, the control system is not able to respond to this change and the connection is not fully optimized. This causes deformation of the machines current and the corresponding voltage distortion at the connection of wind power plants. Deformation of voltage and current is further enhanced if the power of the wind taken out to the grid connection point by long cable line. If the mount point of wind power is selected as an end in a radar grid arrangement, it may affect the voltage of the system at a given point.

For large wind power (hundreds of kW, units of MW) are currently the most used management systems with asynchronous generator with wound (slip-ring rotor) which uses the drive co-operation with heat recovery unit. It is a system in the cascade connection. Using a wind power control system with a frequency converter is possible to use better energy of wind flowing and guarantee stable supply of electricity into the grid.

If the system operates in a cascade, the generator stator is directly connected to the electricity grid (via LV/MV transformer) and wound rotor generator is powered by the drive. The process of this device is provided on multiprocessor basis. Management system evaluates wind speed and the engine's torque. Momentary characteristic of the engine is adapted to this. The voltage and current course on the generator rotor is controlled to maximize the use of wind energy, provided the minimum negative impact on the grid. Capacity which is driven by the inverter is fractional comparing to capacity of power generator, and therefore effects may be small on distribution network. The control system also ensures connecting to the network with minimal impact on current and generator operation without significant surge events. In modern wind turbines is used switching stator Y-D to reduce current surges.

5.1 Reversing the effects of the power network

It is necessary to limit the retroactive effects of local plants to avoid disturbing of the other customers and operations in the PDS. It is necessary to proceed from reverse effects and their permissible limits principles.

The factories can be connected without further control of reverse effects can if the ratio of short-circuit network performance S_{kV} to the rated output device S_{rA} is greater than 500.

If you leave your equipment to verify in a respected institute, it is possible to include to the assessment of the connection conditions favorable factor S_{kV}/S_{rG} (<500), where the apparent S_{rG} generator output/production units is. For wind power you need to submit a certificate, test report, etc. on the rear of the expected impacts.

The individual assessment of the connection of one or more of their own plants in a single point of common coupling must be based on the following boundary conditions.

Deviation of voltage

Allowed deviation of voltage for a common point in the supply network is $\Delta u_{\max,nn} \leq 3\%$, and for a common point in the supply network voltage and 110 kV $\Delta u_{\max,vn} \leq 2\%$.

Voltage fluctuations (flicker)

For the assessment of one or more plants in one place forwarding is needed with regard to fluctuations in voltage causing flicker to observe at point of common coupling low voltage and high voltage threshold level of long-term perception of flicker $P_{lt} \leq 0,46$ and in point of common coupling limit of 110 kV $P_{lt} \leq 0,37$.

In factory with more of individual devices is necessary to calculate separately for each P_{lt} and the resulting value for flicker in the point of common coupling determined by:

Harmonics and interharmonics

Harmonics and interharmonics are generated mainly in devices with inverters or frequency converters, but also by other sources of generators forming an interface with the grid. Harmonic and interharmonic currents emitted by these devices must indicate the manufacturer, for example, type test report.

6 Conditions for Connection

To prevent the introduction of reverse voltage to the PDS network is needed to ensure the technical measures in order to connect to the network's own production PDS was possible only when all phases of the network are under voltage.

6.1 Connection of synchronous generators

The synchronous generator has to have a synchronization device which can be observed the following conditions for synchronization:

- voltage difference $\Delta U < \pm 10\% U_n$
- difference frequency $\Delta f < \pm 0,5\% Hz$
- phase difference $< \pm 10^\circ$

Depending on the ratio of the impedance of the generator may be necessary to avoid unacceptable effects on the network re-set for switching narrower limits.

6.2 Connection of asynchronous generators

Asynchronous generators ups drive must be connected without tension at speeds within 95 % to 105 % of synchronous speed. For asynchronous generators capable of close system, which is not connected without tension, to be followed as switching conditions for synchronous generators.

6.3 Connecting plants with the inverters, eventually frequency converter

Inverters may be actuated only when the AC side is energized. For custom made with inverter capable of operating the island that are not switched without tension, it is necessary to comply with applicable switching for synchronous generators.

7 Conclusion

Power Quality is not only determined by the quality of supply, but also the reliability of power supply. In this context, an important criterion for planning production and consumption of electricity. Some types of renewable resources. Especially those required for its operation some kind of fuel are characterized by great irregularity of supply. For this reason, consideration of replacement of a significant proportion of electricity consumption by these sources problematic. One of the ways to assess the feasibility of using renewable potential is to compare the overall performance of these sources at different times of the energy diagram.

The impact of the electricity produced wind power plant, which is connected to the electricity grid is dependent on the hardness of the network and the active and reactive power wind turbines. Voltage quality can influence the correct choice of site for a common connection point. With regard to emissions and their harmonics and multiples are particularly problematic and odd harmonics are dependent on their own production facilities, but may also contribute to a negative power factor correction device on the network.

Acknowledgement

This work was supported by the Czech Science Foundation (No. GA ČR 102/09/1842) and by the Ministry of Education, Youth and Sports of the Czech Republic (No. SP2012/188).

References

- [1] Unger, J., Krejci, P.: Influence of Wind Power Plants on Power System, EPE 2012, s. 529-533
- [2] Hradilek Z., Sumera T.: In Reliability od Electrical Power Supplies from Renewable Sources, EPE 2010, s. 401 – 406
- [3] URL: <www.csve.cz>

Laboratory Research on Production of Hydrogen in the Electrolyzer

Jan Vaculík

Department of Electrical Power Engineering, FEECS,
VŠB – Technical University of Ostrava, 17. listopadu 15, 708 33 Ostrava – Poruba
jan.vaculik@vsb.cz

Abstract. This paper elaborates on the hydrogen technology with respect to electrical power accumulation in hydrogen via Hogen GC 600 electrolyser. The measurements contained in the paper illustrate laboratory research of hydrogen generation in the electrolyser which are being taken at the Fuel Cells Laboratory, VŠB – Technical University of Ostrava.

1 Introduction

Electrolyser is, in terms of efficiency, the weakest element of electrical power hydrogen accumulation cycle. For this reason we have focused our attention on research aiming at enhancing the efficiency of connected Hogen GC 600 electrolyser. During last research we have found that the total efficiency of our island hydrogen system is less than 9 %. This very low efficiency is caused by production cycle of hydrogen. Our current research consists in the effort to improve the efficiency of used hydrogen generator (electrolyzer) Hogen GC600, because this electrolyzer is the least efficient part of hydrogen storage system.

2 Electrical power hydrogen accumulation

To accumulate electrical power with help of hydrogen technologies and at the same time use the advantage of zero-emission renewable energy sources (RES), hydrogen must be generated by water electrolysis. An osmotic unit in an electrolyser processes modified water at the time of low load in electricity system or with use of electrical power from photovoltaic panels (at the Fuel Cells Laboratory, VŠB-TU).

Generated hydrogen can be stored in cylinders with laminated walls. The inner wall is made of stainless steel to resist effects of pressurized hydrogen; the outer wall is made of steel suitable for necessary pressures. Produced hydrogen is then stored in pressurized containers with laminated walls. The inner wall of the container is made of stainless steel to withstand the effects of hydrogen pressure. The outside of this container is made of steel suitable for required hydrogen pressures. The electrolyser used in our laboratory is able to compress gas, therefore there is no need for a compression unit.

Hydrogen generation cycle contains two basic procedures:

- a) **generation** – H₂O electrolysis takes place in an electrolyser which transforms electrical energy into chemical one the basis of synthetically produced fuel – hydrogen
- b) **storing**, transportation of hydrogen resp.

3 Electrolysers

Hydrogen is acquired in a process of decomposition of demineralized water – electrolysis. If the energy used for the hydrogen production is generated with renewable energy sources, such as wind power generator or photovoltaics (at VŠB-TU) and burning of fossil fuels is avoided, the process of hydrogen generation is very clean and emission-free (no CO₂, SO₂, NO_x etc. emissions).

Electrolyser is a series of cathodes and anodes immersed in water with added electrolyte (often KOH potassium hydroxide) to increase conductivity.

A polymeric electrolyte with ion exchange membrane seems to be very promising. Porous electrode layers are applied on both sides of the membrane and the current is conducted with H₃O⁺ ion at the cathode and OH⁻ ion at the anode. The thickness of the membranes is >1mm. [1]

4 Efficiency research

The task of laboratory measurements was to analyse the changes of efficiency of Hogen GC 600 electrolyser with different pressures on the electrolyser panel (fig. 1). The pressure can be adjusted within the span 3 – 13,8 bar. Hydrogen flow within the span 0 – 300 cm³ / min and 0 – 600 cm³ / min is also dependent on the set pressure. The level of the flow is displayed on the flowmeter connected between the electrolyser and the hydrogen-storing cylinders. At the same time the data on the flow are stored in a computer with expert software. The data can be further analysed for needed overview and graphs. [2]

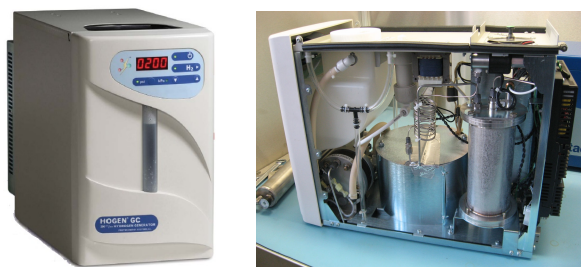


Fig. 1. Hogen GC600 Electrolyser

4.1 Measurements in 30-minute periods

The needed measurements are in Tab. 1-5 informing on values in given time periods and also average values of adjusted criteria.

Table 1. Adjusted value 7 bar

	Time (s)	Consumption (Wh)	Volume H ₂ (litry)	EEQ (Wh)	Efficiency (%)	Hydrogen pressure (bar)
7 bar	0	0	0,00	0,00	0,00	5,93
	300	48	1,75	5,62	11,70	5,93
	600	94	4,58	14,70	15,64	5,93
	900	132	8,68	27,87	21,11	5,93
	1200	169	12,28	39,42	23,33	6,00
	1500	198	15,45	49,60	25,05	6,00
	1800	233	18,7	60,03	25,76	6,00
Average		124,86	8,78	28,18	17,51	5,96

Table 2. Adjusted value 8 bar

	Time (s)	Consumption (Wh)	Volume H ₂ (litry)	EEQ (Wh)	Efficiency (%)	Hydrogen pressure (bar)
8 bar	0	0	0,00	0,00	0,00	6,07
	300	46	3,09	9,92	21,56	6,07
	600	88	7,02	22,54	25,61	6,07
	900	121	10,96	35,18	29,08	6,07
	1200	159	14,54	46,68	29,36	6,21
	1500	203	18,66	59,90	29,51	6,21
	1800	232	21,55	69,18	29,82	6,21
Average		121,29	10,83	34,77	23,56	6,13

Table 3. Adjusted value 9 bar

	Time (s)	Consumption (Wh)	Volume H ₂ (litry)	EEQ (Wh)	Efficiency (%)	Hydrogen pressure (bar)
9 bar	0	0	0,00	0,00	0,00	6,21
	300	45	3,71	11,91	26,47	6,27
	600	74	6,47	20,77	28,07	6,27
	900	104	9,7	31,14	29,94	6,34
	1200	137	12,95	41,57	30,65	6,34
	1500	175	16,04	51,49	29,42	6,34
	1800	200	19,08	61,25	30,63	6,34
Average		105,00	9,71	31,16	24,98	6,30

Table 4. Adjusted value 10 bar

	Time (s)	Consumption (Wh)	Volume H₂ (litry)	EEQ (Wh)	Efficiency (%)	Hydrogen pressure (bar)
10 bar	0	0	0,00	0,00	0,00	6,34
	300	35	3,95	12,68	36,23	6,41
	600	64	6,78	21,77	34,01	6,41
	900	84	9,66	31,01	36,92	6,41
	1200	113	12,08	38,78	34,32	6,48
	1500	143	15,78	50,66	35,43	6,48
	1800	176	18,80	60,35	34,29	6,48
	Average	87,86	9,58	30,75	30,17	6,43

Table 5. Adjusted value 13,79 bar

	Time (s)	Consumption (Wh)	Volume H₂ (litry)	EEQ (Wh)	Efficiency (%)	Hydrogen pressure (bar)
13,79 bar	0	0	0,00	0,00	0,00	6,76
	300	36	3,57	11,46	31,84	6,83
	600	70	7,18	23,05	32,93	6,83
	900	96	10,25	32,91	34,28	6,83
	1200	131	13,88	44,56	34,01	6,96
	1500	165	16,92	54,32	32,92	6,96
	1800	190	20,30	65,17	34,30	6,96
	Average	121,29	10,30	33,07	28,61	6,88

4.2 Measurement evaluation

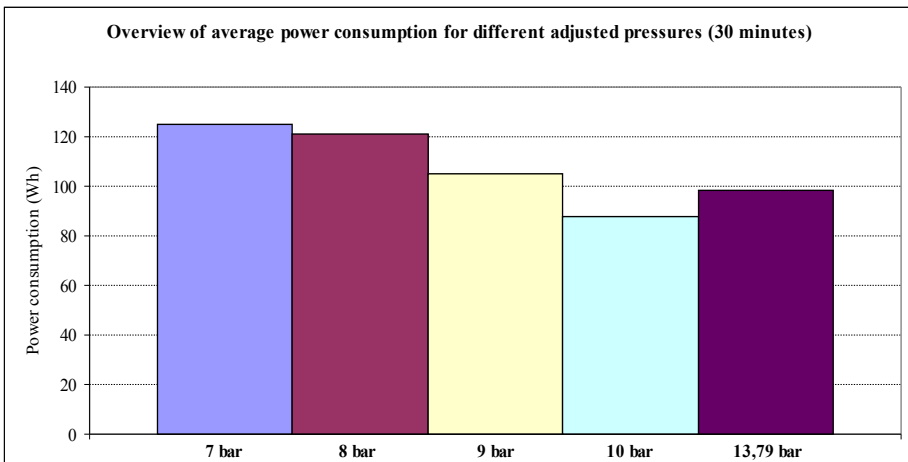
Graphics and table images illustrate generation cycle of hydrogen in Hogen GC 600. The starting value of pressure is 7 bar (so-called „cold“ condition) and the maximum value is 13.79 bar. Other adjusted values are taking into account a warmed up electrolyser with pre-heated water which means higher efficiency of the process.

Tab. 6 shows comparison of average values of all measure pressures. The most important indicator was efficiency which proved to be highest with pressure adjusted on 10 bar.

Efficiency is closely connected with another critical parameter - electrical power consumption during the generation cycle. As graph 1 shows, consumption decreases with rising pressure manually adjusted on the electrolyser unit. Consequently, hydrogen generated during electrolysis is compared with equivalent energy quantum (EEQ).

Table 6. Average measurement values

30 minutes	Criteria				
	Consumption (Wh)	H ₂ volume (litry)	EPA (Wh)	Efficiency (%)	Hydrogen pressure (bar)
7 bar	124,86	8,78	28,18	17,51	5,96
8bar	121,29	10,83	34,77	23,56	6,13
9 bar	105,00	9,71	31,16	24,98	6,30
10 bar	87,86	9,58	30,75	30,17	6,43
13,79 bar	98,29	10,30	33,07	28,61	6,88

**Graph 4.** Overview of average electricity

5 Conclusion

The research principle was to adjust different pressures which the electrolyser span allows. In this case the span was 7 – 13,79 bar. Each pressure was adjusted for a period of 30 minutes.

In the course of measurements a few machine failures occurred resulting in breakdown condition. The machine would cut off due to low-quality water or low level of water. A warning would flash on the display calling for immediate service - repeated pressurizing cycle. Each of those failures caused increase in power consumption and therefore decrease in efficiency at particular pressure. Such failures are irrelevant to the focus of our research and therefore can be neglected at data processing.

In all aspects the least efficient seems to be the pressure value of 7 bar. Up to 10 bar the efficiency continuously grows and the power consumption falls. With pressure adjusted on 10 bar, the electrolyser works most efficiently disproving the pre-

sumption that an electrolyser works best at maximum pressure 13,79 bar. As for poor parameters of 7 bar pressure, the fact that it is a starting value and reaction water is still cold could misrepresent the findings.

Acknowledgements

This work was supported by the Ministry of Education, Youth and Sports of the Czech Republic (No. SP2012/188) and by the Czech Science Foundation (No. GAČR 102/09/1842).

References

1. HOGEN® GC 300 and 600 Laboratory hydrogen generators User's Manual
2. BALAJKA, Jiří. Vodík a jiné nové nosiče energie. Bratislava : ALFA, 1982. 312 s.

Energy Accumulation of Photovoltaic Power Plant to Suppress the Negative Back Effects Caused by the Operation

Jakub Vramba

Department of Electrical Power Engineering, FEECS,
VŠB – Technical University of Ostrava, 17. listopadu 15, 708 33 Ostrava – Poruba
vramba@seznam.cz

Abstract. Photovoltaic power plants are categorized as ecological and renewable sources of electricity. With their growing number, however, increase the negative feedback effects on connection point caused by their operation. With using the optimal system, it is possible to realize the requirements of the operator of distribution system into which the photovoltaic power plants power is taken out. Among the major negative feedback effects are changes in voltages, instability and quality of power energy deliveries. A possible solution presents an accumulation of electrical energy to reduce the undesirable feedback effects. In this article are defined the basic parameters of the accumulation facilities operated by photovoltaic power plant in order to reduce the negative feedback effects of photovoltaic power plants and improve the security and reliability of power system in which is the power taken out.

Keywords: Photovoltaic power plant, Voltage change, Power factor

1 Introduction

The voltage change is one of the most important negative feedback effects induced by the operation of FVE connection point. The voltage change in the distribution network occurs due to power changes of connected sources and loads. The voltage change in one node is reflected in voltage changes in the other network nodes. Recently, we have come across with a large number of diffuse sources in practice. In these networks, the problem is specified to comply with changes in voltage. According to the operating rules of a distribution system, Annex 4 cannot increase the tension caused by the operation of generating plants connected to the worst case in the connection point exceed $\Delta u_{NN} \geq 3 \%$ compared with the voltage without connection. The limit value of 3% is related to the permanent operating voltage. The compliance of the prescribed conditions prevents the introduction of significant voltage changes. It helps to control and stabilize the voltage at all points in the network. [1] Another problem is the power supply PV power plant in the neutral power factor. By PPDS.4 is it 0,95-1 inductive and 0,95-1 capacitive power factor. [1] The operating mode PVP expects the annual utilization of installed capacity from 900 to 1 100 hours per year. This means that the plant is operated for most of the time with a lower or minimum power. This results in the production operation with capacitive power factor - the supply of capacitive reactive power into the grid. The capacitive power factor causes greater variation voltages in the connection point. [2]

2 Analysis operation FVE 70 kWp

FVE is located in the Czech Republic and has an installed capacity of 70 kWp. There is the monocrystalline technology used and the power is led by NN (400/230 V) radial network. Network model is created by using the software E-vlivity. E-vlivity allow you to simulate the voltage conditions in the network with an installed FVE power plant before and after connection.

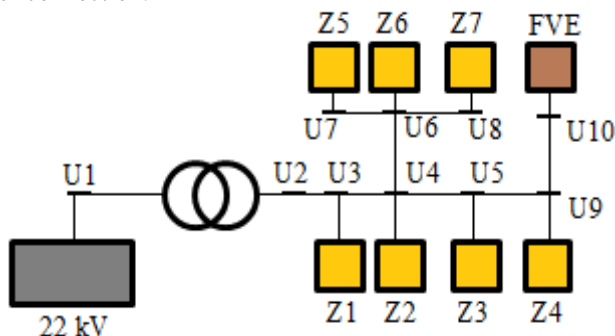


Fig.1 connection diagram ($S_k=0,25 \text{ MV}\cdot\text{A}$) [3]

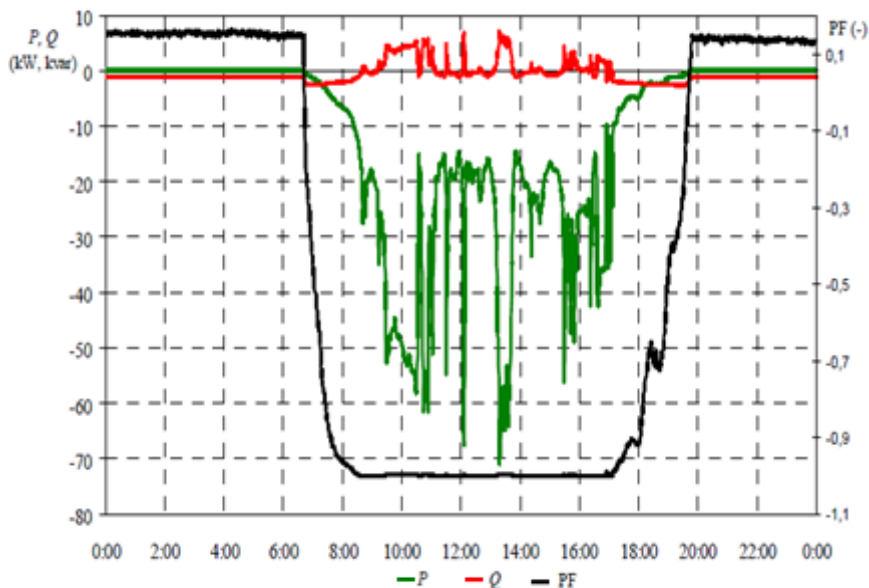


Fig.2 power ratios FVE

In Fig. 2 you can see, how the power FVE conditions can dynamically change in a cloudy day. These power conditions have negative effects on the change in a voltage connection point. In comparison with the resulting changes in the values voltage for node U10 cloudy and clear days are graphically illustrated in Fig.3.

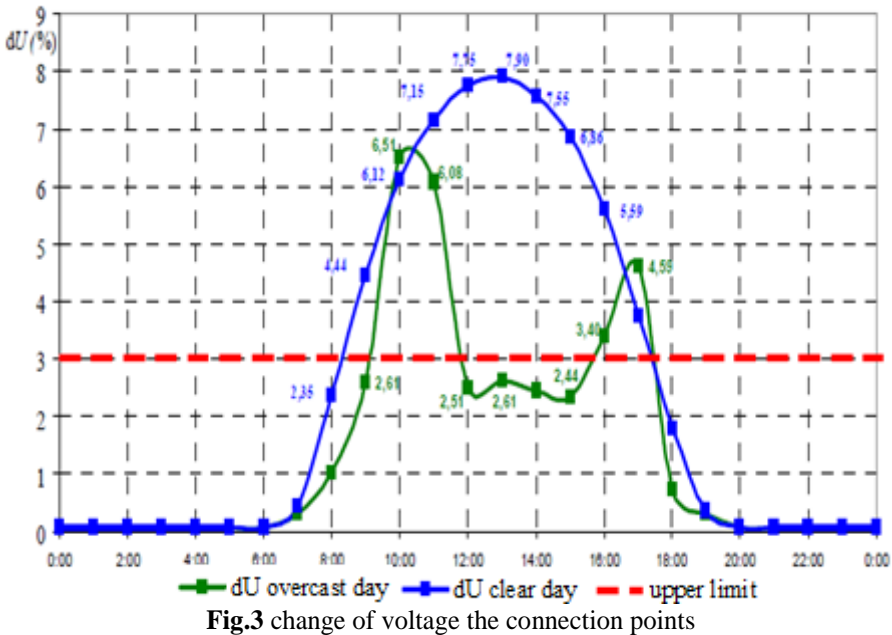


Fig.3 change of voltage the connection points

Fig. 3 shows the voltage change during one day of the operation FVE. The greatest change occurred about one o'clock in the afternoon. The value is closer to 8% at maximum power FVE and 45% network load. To comply with the requirement of 3% FVE would have to work up to 30% of its maximum capacity. In 90% of the network load according to the results software E-rlivy voltage change could be up to 14%. Fig.4 [2] [3]

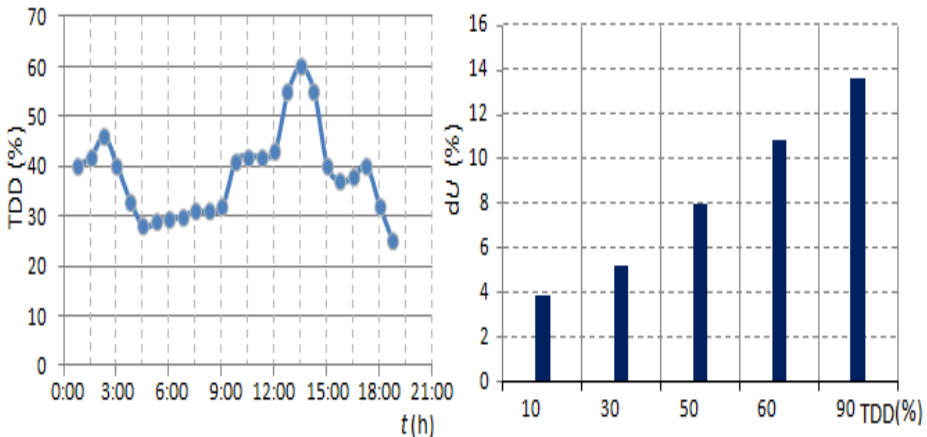


Fig.4 changes in voltage at node U10, max power FVE and changing the network load [4]

3 Accumulation of electrical energy

The results of the chapter two are visible crossing limit values determined by the standard EN 50160 and PPDS. Specifically:

- Deviation supply voltage
- Fast voltage changes
- Changes voltage at maximum and variable power

The reason for installing accumulation device is the suppression of reverse effects on the distribution system. Accumulation device is able to accumulate power peaks and also subsidize power decreases during the day. FVE is supplemented by energy accumulation with the storage battery which offers several options for configuring the operation of the electric battery with FVE.

3.1 Powers accumulation

This option involves the removal of rapid change power FVE and related changes voltage. It serves to cover declines and capture power peaks. In this case it is used the performance version of the battery. It has a short charging and discharging times, which carry a large number of cycles and high performance. The advantage is a smaller capacity battery. The battery absorbs rapid changes in the supplied power during cloudy days. Eliminates rapid changes in voltage Fig.5. The advantage of this system accumulation is the removal of rapid changes in flow power. Fluctuations and overflows into the 22 kV power grid. Working conditions FVE with power accumulations:

During the first operating state, when power FVE is small. Total power FVE is used for charging accumulation device. The estimated charging energy efficiency is 0.9.

During the second operating condition, the power of FVE is used for charging accumulation device and remaining part is supplied to electrical network. The charging power is controlled so that the power of battery was sufficient during sudden loss of power FVE. With the increasing power, FVE increases the size of the accumulated electric energy. During rapid loss of power, FVE is power supplied to the electricity grid funded from the battery. The power system is controlled by the size and duration changes and the battery charge. For longer lasting power drop, FVE is power supplied from the battery gradually reduced. When the power is restored, electricity from photovoltaic power plant system performance is increased and power peaks are dampened and used to charge batteries. For long loss of power FVE is battery disconnected. Rapid declines power FVE from the battery is replaced. Energy battery is reduced to the desired level. Reduction energy of battery is necessary to ensure the ability to accumulate power peaks FVE the following day.

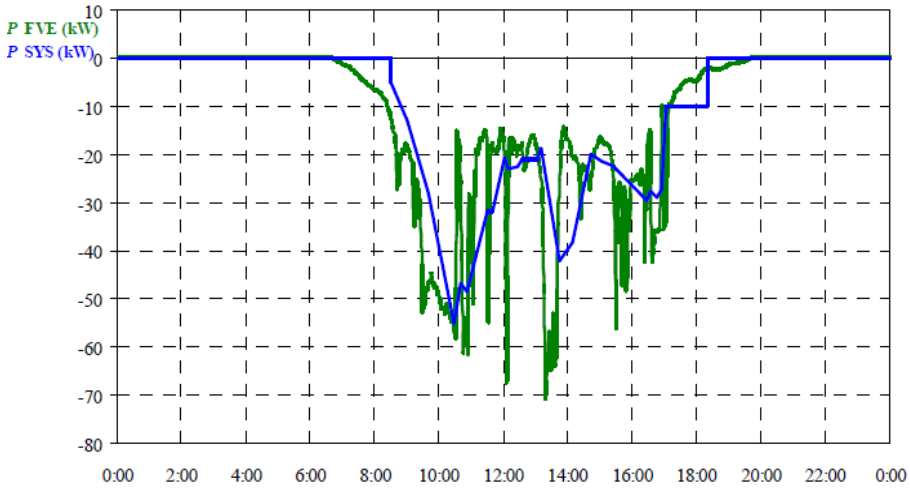


Fig.5 powers of accumulation

3.2 Energy accumulation

The variant energy accumulation is used to accumulate energy of FVE for use during the peak of a daily load diagram. It is also used to supply power to grid in a selected time interval.

The energy version of an accumulator has a longer charge and discharge times. The energy version of an accumulator has less power, but high capacity batteries. The big advantage of the energy version is the possibility to predict the power supply, the possibility to remove rapid changes in the network flow of power and changes voltage in node U10. It allows an even supply of electricity to the grid with the power factor equal to one. The disadvantage of this version is the high cost of batteries.

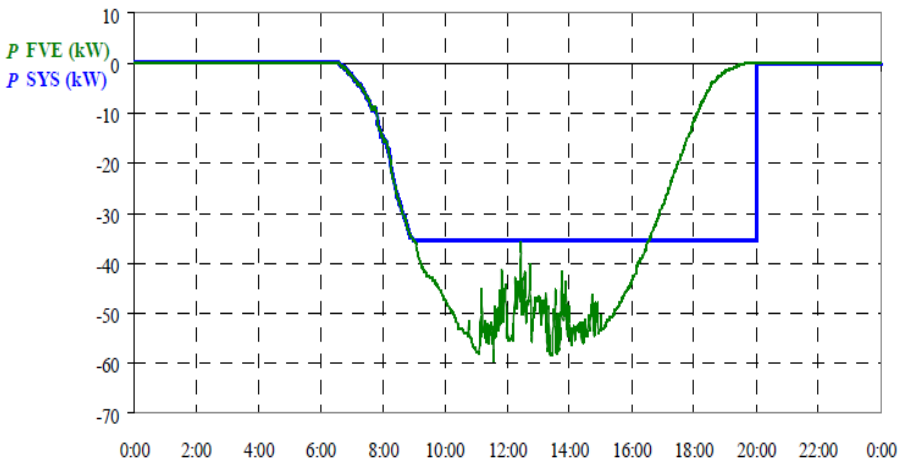


Fig.6 energy accumulation

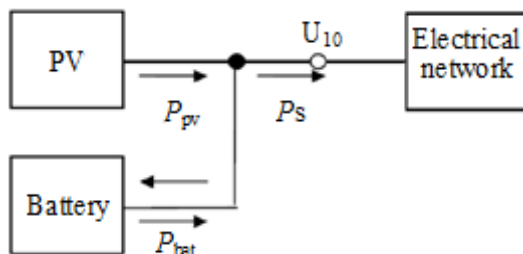


Fig.7 connection FVE with the accumulation

The main objective of the energy accumulation is a reduction of negative impacts caused by operation FVE on the distribution network. Energy produced in excess of levels is stored in batteries and then it covers the supply drops of FVE. The remaining part of the energy is used to extend the power supply to the network.

4 Conclusion

The basic options of the energy accumulation in batteries for the use in the distribution system are described in this article. This solves the problem of negative effects on the distribution system, mainly the voltage change in the connection FVE. The application itself in the accumulation system is after the design phase and in the stage of production and construction. The calculated and devised parameters of the accumulation system can be verified after installation and commissioning of the system. The information obtained from the accumulating system was also used to improve the hybrid island grid on VŠB-TUO.

Acknowledgment

The article was created by the project number SP2012/53

References

1. Provozovatelé distribučních soustav: *Pravidla pro paralelní provoz zdrojů se sítí provozovatele distribuční soustavy*. 2012, PPDS, příloha č.4.
2. Vramba J.: *Zpětné vlivy obnovitelných zdrojů na distribuční soustavu*, Diplomová práce. VŠB-TU Ostrava, 2011.
3. Ing. Jakub Vramba, doc. Ing. Stanislav Mišák, Ph.D., Ing. Jindřich Stuchlý, *Akumulace energie v bateriích pro aplikaci v distribuční soustavě*, sborník EPE 2012, Ostrava: VSB - Technical University of Ostrava, 2012.
4. Ing. Jakub Vramba, Ing. Jindřich Stuchlý, *Negativní zpětné vlivy fotovoltaické elektrárny na distribuční soustavu* EPE 2012, Ostrava: VSB - Technical University of Ostrava, 2012.

Heating with Heat Pumps

Petr Zach

Department of Electrical Power Engineering, FEECS,
VŠB – Technical University of Ostrava, 17. listopadu 15, 708 33 Ostrava – Poruba
petr.zach@vsb.cz

Abstract. The article deals with building heating Assembly Hall at VSB - Technical University of Ostrava. The Assembly Hall is fitted with warm-water floor heating and hot-air system. The source of heat comprises 10 heat pumps with the total output of 700 kW. The source of low-potential heat is represented by a system of 110 boreholes to the depth of 140 m each. Auxiliary heat source is then formed by a calorifier room of the central heat supply system.

Keywords. Heating, heat pumps, geothermal energy.

1 Introduction

The paper deals with heating in large-capacity buildings. An example of a large-capacity building heating system is the Assembly Hall building at the VSB – Technical University of Ostrava. Then Assembly Hall heating comprises three systems; the warm-water floor heating, radiators and the hot-air system.

2 Description of Heating Assembly Hall Building

The Assembly Hall and Information Technologies Centre building is heated by means of geothermal heat pumps. The source of low-potential heat is boreholes. Heat pumps supply 82-85% of heat to the building in an average year. Bivalent, i.e. auxiliary, heat source is a calorifier room within the central heating system. The total built-up area is 3,917 m². The source of heat is formed by 10 heat pumps manufactured by the IVT company of Sweden with the total output of 700 kW using the system of 110 boreholes to the depth of 140 m each. These boreholes are situated in the parking area at Assembly Hall and library buildings of the VSB – TUO. Internal fittings in these boreholes include four-pipe pattern arranged in two loops of PE piping of DN 32 mm type provided with a special connecting base. These boreholes have been installed with approximately 70,000 m of polyethylene pipe. Boreholes have been injected with cement-concrete mixture. The primary circuit is filled with antifree heat-carrying liquid amounting to the total volume of 18000 litres. The system of 110 boreholes is concentrated into five collection shafts, which means 22 boreholes per 1 shaft. Every

shaft is also provided with a separate pipe with its independent circulation pump. The heat loss of Assembly Hall equals to 1,200 kW at the outside temperature of -15 °C. The heating system comprises floor heating, radiators and air-conditioning. Individual heating systems have been designed for low-temperature gradient. Production of domestic hot water is provided by means of plate exchanger in hot water accumulation tanks.



Fig. 1. Heat Pumps - 10 units



Fig. 2. Circulation Pumps in Primary Circuit

Table 1. Output parameters of heat pump in accordance with EN255

Temperature (°C)	Heating output (kW)	Electric input (kW)	Heating factor (-)
0/35	67,8	16,7	4,06
0/50	69,8	22,3	3,13

3 Evaluation of Data Measured

Heat pumps are controlled by the ProCop Monitor software. The software ensures automatic monitoring of all values within 10 minute intervals and their continuous storing into database. The ProCop Monitor monitoring and visualisation system is distributed by Siemens company in the Czech Republic under Visonik Alfa trade name. The data used for evaluation has been obtained over heating season from 2011/2012. Heating season subject to evaluation, i.e. the period from 2011 till 2012, began on 1st October and ended on 30th April each year. Table 2 shows evaluation of the course of heating seasons with energy supplied by heat pumps, energy supplied into air-conditioning – hot-air heating, energy supplied into the central heating system – floor heating and radiators, energy consumed by heat pumps and outside temperature details. Further details include the heating factor calculated over individual heating seasons. Heating factor is the essential parameter of a heat pump and it is calculated as the ratio of heat produced and electric power consumed.

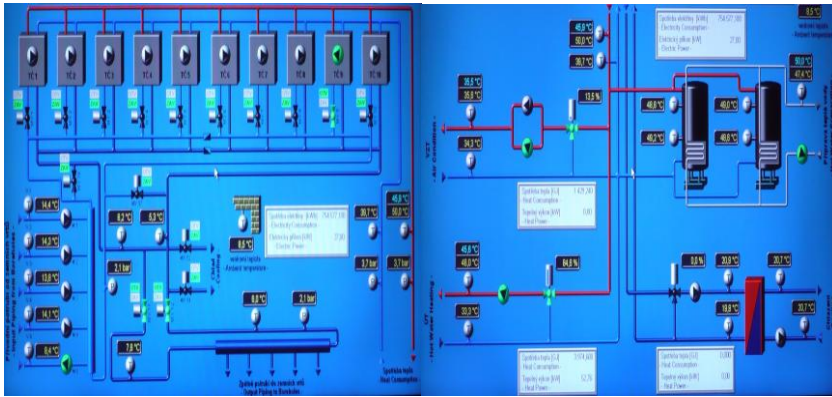


Fig. 3. Heat pumps connection diagram

Fig. 4. Connection diagram for energy supplied from heat pumps

Table 2. Energy supplied and consumed within heating season

Heating season	2011-2012
Energy supplied by heat pumps (GJ)	1445,97
Energy supplied into air-conditioning (GJ)	305,84
Energy supplied into central heating (GJ)	1140,12
Energy consumed by heat pumps (kWh)	143178,50
Average outside temperature (°C)	4,15
Heat pumps heating factor (-)	2,81

3.1 Evaluation of Energy Produced

Graph 1 shows the course of energy produced by heat pumps in heating season. This energy is supplied into the central heating and air-conditioning systems by heat pumps. The Assembly Hall heating is provided rather by central heating system than the air-conditioning setup. That is due to the fact that floor heating operates with water of lower temperature provided by heat pumps. If the output temperature is lower, heat pumps work with higher heating factor.

3.2 Evaluation of Energy Consumed

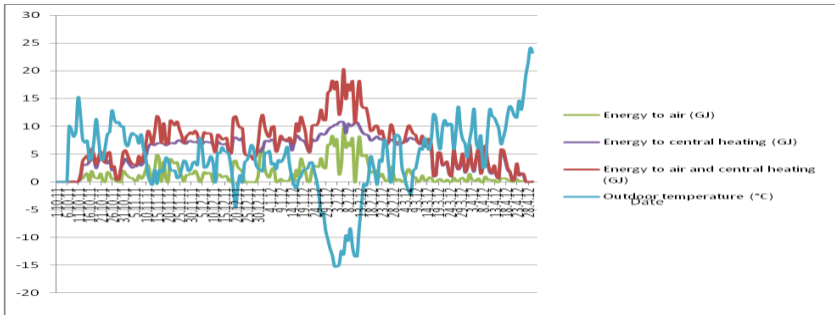
Graph 2 shows the course of energy consumed by heat pumps in heating season. The volume of energy consumed is given by sum of energy required to drive the compressor of heat pumps, circulation pumps in the primary circuit and power supply to the control.

3.3 Heating Factor Evaluation

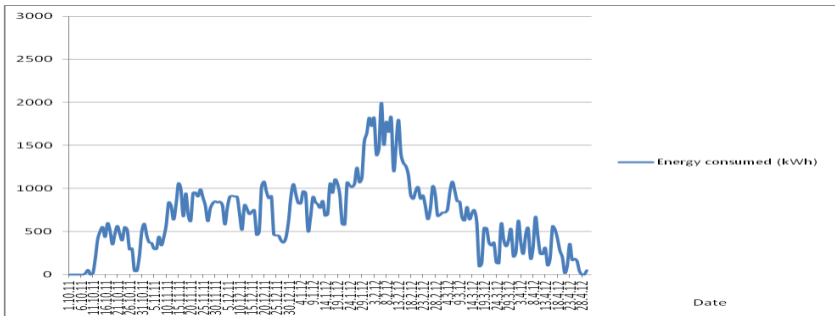
Graph 3 shows the course of heating factor of heat pumps in heating season. This graph helps to determine the dependency of heating factor on the outside temperature. The heating factor experiences a slight drop with positive values of outside temperature and that is caused by initiation of heat pumps and circulation pumps. When the outside temperature reaches negative values, the heating factor is balanced, which means that heat pumps have enough of primary low-potential energy from boreholes.

3.4 Temperature Course Evaluation

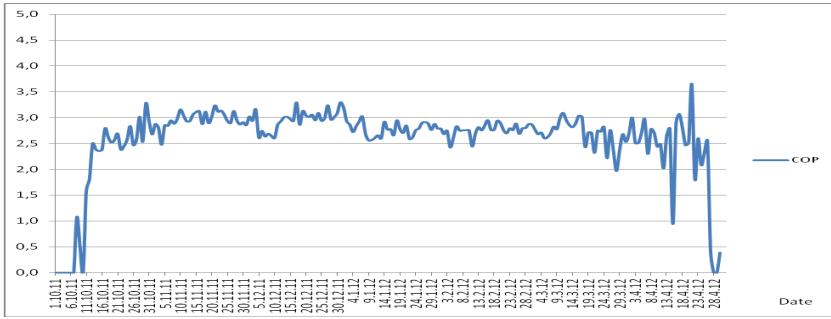
Graph 4 shows the course of temperature within particular circuits of boreholes, input temperature of heating water and outside temperature within heating season. Heating in the Assembly Hall is ensured by means of low-potential heat with the system of 110 boreholes. These boreholes are grouped into 5 circuits, which means there are 22 boreholes per circuit. When the heat is being drawn from any of these circuits, the temperature inside boreholes will drop after a certain period. Such exploited circuit will be disengaged, allowing boreholes to restore their internal temperature, while another circuit will be used. Each circuit will be utilised for the period of 7 days.



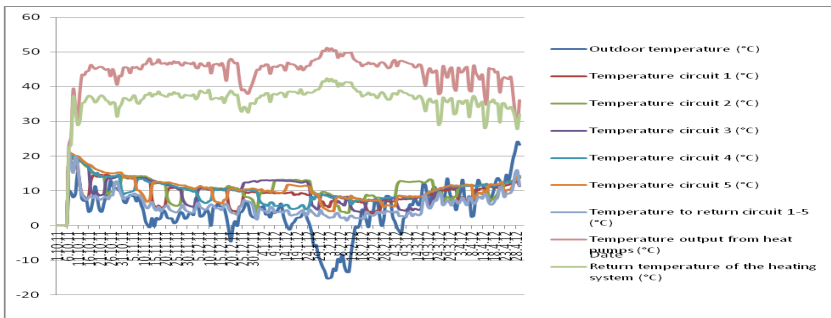
Graph 1. Course of energy produced by heat pumps in the 2011/2012 heating season



Graph 2. Course of energy consumed by heat pumps in the 2011/2012 heating season



Graph 3. Course of heating factor of heat pumps in the 2011/2012 heating season



Graph 4. Course of temperature within individual borehole circuits in the 2011/2012 heating season

4 Conclusion

Heating of large-capacity buildings can be achieved successfully by means of heat pumps. Heat pumps supply up to triple the volume of heat energy compared to the electric power they draw from mains. Heating with heat pumps is set for fully automatic operation with performance control and the option for manual control depending on specific use of the Assembly Hall building. Data obtained by measurement on heat pumps refer to heating season 2011/2012. The data is used for evaluation of course of heating season with respect to the total volume of energy supplied by heat pumps, energy supplied into the air-conditioning system, energy supplied into the central heating, energy consumed by heat pumps and outside temperature. Further details include the calculated heating factor in heating season.

Acknowledgment

This work was supported by the Czech Science Foundation (102/09/1842), by the Ministry of Education, Youth and Sports of the Czech Republic (SP2012/188) and by the project ENET (Research and Development for Innovations Operational Programme (CZ.1.05/2.1.00/03.0069)).

References

1. Hradílek, Z., Zach, P.: Heat pumps, renewable source of energy for Aulum at VŠB - TU Ostrava. *EPE 2010*. Brno, 2010. ISBN 978-80-214-4094-4.
2. Zach, P.: Heat pumps, renewable source of energy for Aulum at VŠB - TU Ostrava - Evaluation of the heating factor. *WOFEX 2010*. Ostrava, 2010. ISBN 978-80-248-2276-1.
3. Hradílek, Z., Zach, P.: Heat pumps, renewable source of energy for Aulum at VŠB - TU Ostrava - Analysis of histograms of heating factor. *ELEN 2010*. Praha, 2010. ISBN 978-80-254-8089-2.
4. Hradílek, Z., Zach, P.: Heat pumps, renewable source of energy for Aulum at VŠB - TU Ostrava - Evaluation of the heating factor. *ELNET 2010*. Ostrava, 2010. ISBN 978-80-248-2349-2.
5. Zach, P.: Heat pumps, renewable source of energy for Aulum at VŠB - TU Ostrava - Evaluation of the heating season. *11.WORKSHOP 2011*. Ostrava, 2011. ISBN 978-80-248-2378-2.
6. Hradílek, Z., Zach, P.: Heat pumps, renewable source of energy for Aulum at VŠB - TU Ostrava - Evaluation of the heating season. *EPE 2011*. Dlouhé Stráně, 2011. ISBN 978-80-248-2393-5.
7. Zach, P.: Heat pumps for heating Aula at VŠB - TU Ostrava - Evaluation of this year's heating season. *WOFEX 2011*. Ostrava, 2011. ISBN 978-80-248-2449-9.
8. Hradílek, Z., Zach, P.: Heat pumps for heating Aula at VŠB - TU Ostrava. *ELNET 2011*. Ostrava, 2011. ISBN 978-80-248-2510-6.
9. Hradílek, Z., Zach, P.: Energy Issues in Heating of Large Buildings. *EPE 2012*. Brno, 2012. ISBN 978-80-214-4514-7.

Data Collection System for Application Artificial Neural Networks in Controlled Drives

Pavel Bílek

Department of Electronics, FEECS,
VŠB – Technical University of Ostrava, 17. listopadu 15, 708 33 Ostrava – Poruba
pavel.bilek@vsb.cz

Abstract. In this paper, there is a description of Data collection system for application Artificial neural networks in controlled drive. It used Digital Signal Controller TMS320F28335 and external interface (external static RAM module).

1 Introduction

The data collection system is important for data collection and training of artificial neural networks.

2 Application Artificial Neural Networks in Controlled Drives

Artificial neural networks have many advantageous properties for application in modern electric controlled drives. This is mainly a property of approximate unknown system behavior with the required accuracy, learning ability according to set patterns, resistance to noise and distortion and does not need a mathematical description of the behavior of an unknown system. The prices of signal controllers is reduced, on the other hand the performance is increased. It is possible to apply artificial neural networks in large scale.

2.1 DC drive control structure

Block scheme of the drive is shown in Fig. 1. Power section is composed of DC to DC converter a DC motor. An armature current is controlled by current controller. A speed controller provides the speed control.

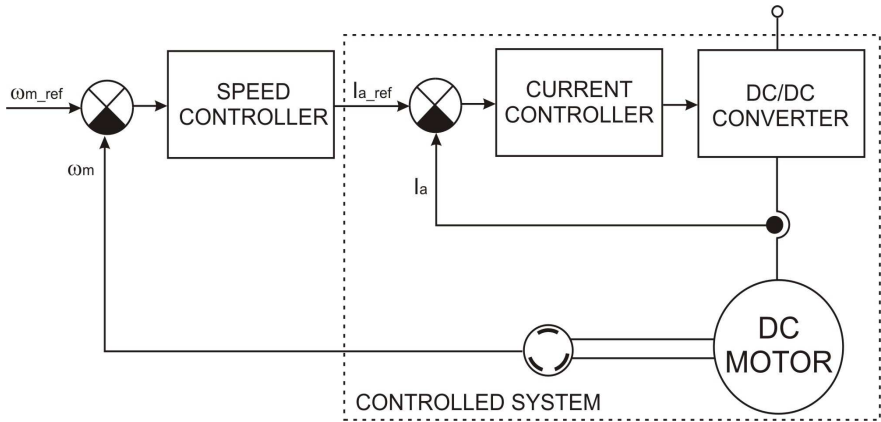


Fig. 1. Block scheme of DC drive.

2.2 Control with conventional PID controller

Conventional PID controller is used as the speed controller. It can be described as follows:

$$i_{a_ref} = K_p (\omega_{m_ref} - \omega_m) + K_i \int (\omega_{m_ref} - \omega_m) dt + K_d \frac{d}{dt} (\omega_{m_ref} - \omega_m) \quad (1)$$

where i_{a_ref} is the reference value of the torque producing current (armature current), ω_{m_ref} and ω_m are the reference and actual value of the rotor angular speed, K_p is the proportional gain, K_i is the integral gain, and K_d is the derivative gain.

2.3 Sensorless control using Artificial neural networks

The speed control requires a feedback signal which is obtained by the speed sensors such as digital shaft position encoder. These sensor is source of trouble. The main reasons for the development of sensorless drives are: reduction of hardware complexity and cost, increasing mechanical robustness, reliability.

Removing speed sensors from a control structure of electrical drive leads to so-called sensorless drive, which naturally requires other sensors for the monitoring of currents and voltages.

To realize the speed estimator [1], it is necessary to determine the appropriate structure of the neural network with appropriate input variables, which will implement the views defined by the following equation:

$$\omega_{m(k)} = \mathbf{f}[i_{a(k)}, i_{a(k-1)}, u_{a(k)}, u_{a(k-1)}, \mathbf{w}] \quad (2)$$

It has been designed three layer feedforward 4-22-1 ANN (see Fig.2) with following inputs $i_a(k)$, $i_a(k-1)$, $u_a(k)$, $u_a(k-1)$, (armature current and voltage of the DC motor) and output $\omega_m(k)$ (mechanical speed).

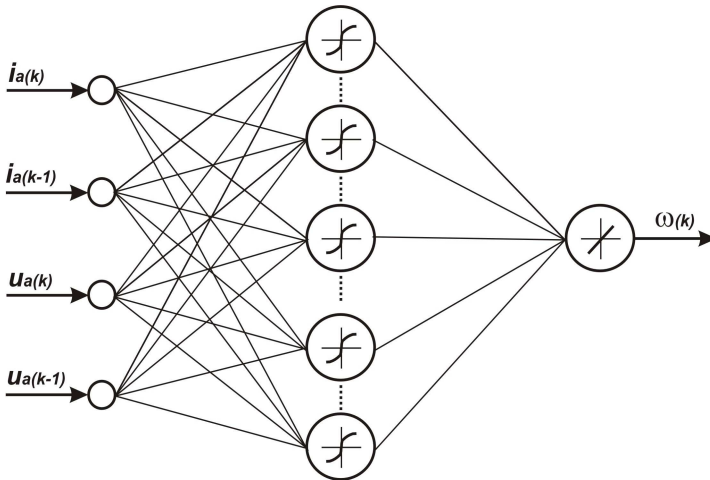


Fig. 2. Artificial neural network speed estimator.

3. Data collection for application Artificial neural network in Controlled drives

Figure 2 shows that we need monitoring the quantities which enter into the artificial neural network. It is important for neural network training and implementation to the sensorless control.

3.1 Experimental workplace with Data collection system

The Experimental workplace with data collection system block scheme is shown in Fig 3. The right part of block scheme is Active load unit, the left part is controlled DC drive.

The experimental workplace consist of DC motor and load unit (AC induction motor). Both motors are connected by common shaft. The position encoder is mounted too. The next level in this block scheme are two converters, two digital signal controllers and two control computers. There are common rectifier and DC link for both converters.

Data collection system is connected to left digital signal controller.

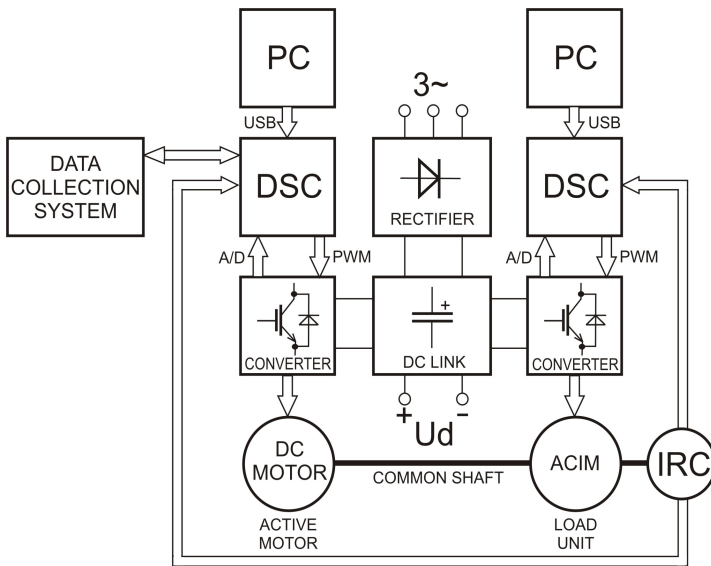


Fig. 3. Experimental workplace with Data collection system block scheme.

3.2 Data collection system

Data collection system is connected to Digital signal controller Texas Instrument TMS320F28335. In Fig.4 is block scheme of External interface connection [2].

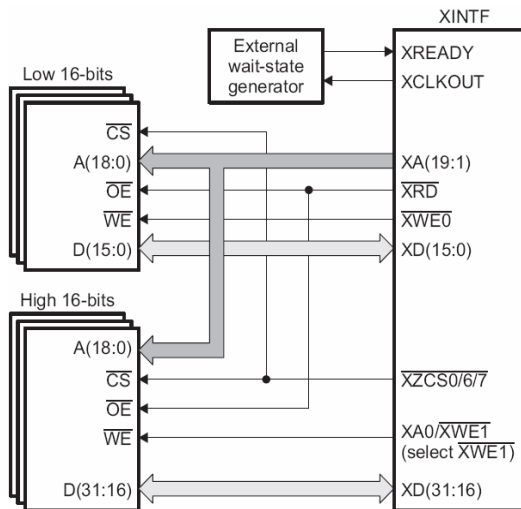


Fig. 4. External interface connection

On the left side there is two static RAM memories and on the right side there is Digital signal controller.

3.3 Practical realization of Data collection system

It was used two 1M word x 16bit low voltage static RAM (type r11v1616rsa). The whole system is build on a small printed circuit board-point (see Fig.5). There are 32-bit data bus, 20-bit address bus and control signals. The system is connected via the connector.

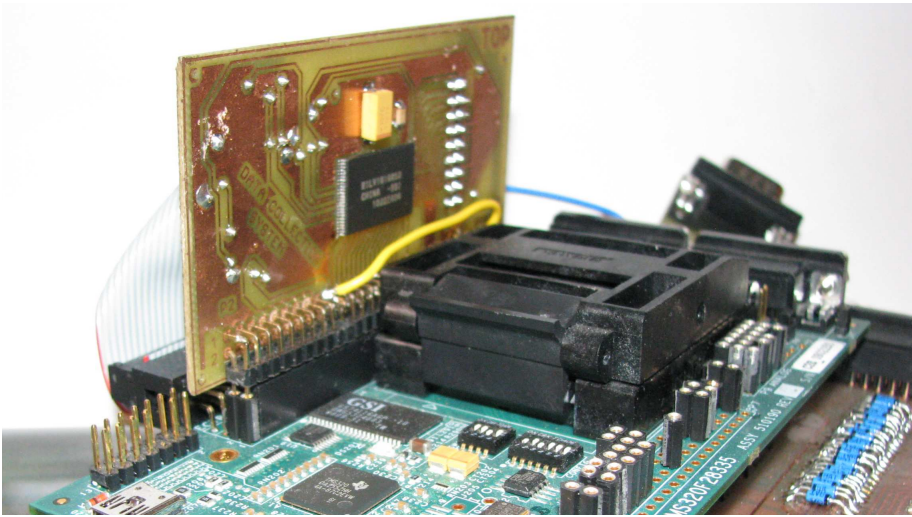


Fig. 5. Practical realization of Data collection system.

3.4 Software

It was written a utility for saving of data into memory. And then it was written the data reading and sending over the serial interface to the master computer.

The program for storing data in master computer will be generate. Neural networks will be trained.

4 Conclusion

In this article it was described the Data collection system for application Artificial neural networks in controled drives. There was suggested solutions with external interface (external RAM module).

5 Acknowledgment

In the paper there are the results of the project SP2012/85 which was supported by Student Grant Competition of VSB-Technical University of Ostrava. This research was supervised by Prof. Ing. Pavel Brandstetter, CSc.

References

1. Brandstetter, P.: A.C. Control Drivers, Modern Control Metod, VSB – Technical University of the Ostrava, 1999. ISBN 80-7078-668
2. Texax Instrument: TMS320F38335/28334/28332 Digital Signal Controllers (DSCs), Data manual, <http://www.ti.com/lit/ug/spru949d/spru949d.pdf>

Simulation of Sensorless Vector Control of Induction Motor using Kalman Filter by HIL Method

Marek Dobrovsky

Department of Electronics, FEECS,
VŠB – Technical University of Ostrava, 17. listopadu 15, 708 33 Ostrava – Poruba
marek.dobrovsky@vsb.cz

Abstract. This work deals with simulation of sensorless vector control of induction motor using Kalman filter by HIL method. The text in the first part deals with the description of vector control with the structure MRAS. The second part describes Kalman filter. The third part describes HIL. In the last section of this document are shown simulation results for changes engine speed from 0 to 30 rpm, respectively, from 30 to -30 rpm.

Keywords: Vector control, induction motor, magnetizing flux, torque, regulation, Kalman filter.

1 Observers using systems with reference model

MRAS observer structure with Kalman filter is shown in Figure 1. In this system, induction motor state variables are evaluated in the reference model based on the measured variables (stator voltages, stator currents). The reference model is independent of the speed and uses the voltage machine model. Adaptive model uses the current model of the machine and the mechanical angular speed of the machine is one of the input variables of this model. The difference between state variables is adaptive signal (AS) $\Phi(e)$, which is evaluated and minimized most often by the PI regulator in the block adaptation mechanism, which performs the estimate value of the mechanical angular velocity $\hat{\omega}_m$ and adapts adaptive model until the desired behavior. With feedback, the observer is able to limit the impact of changes in machine parameters to the accuracy of the calculation.

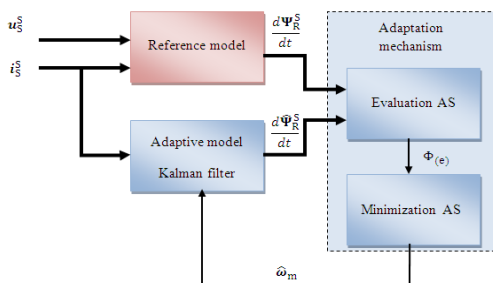


Fig. 1. MRAS with Kalman filter- basic scheme for the estimation of mechanical angular velocity.

1.1 Reference Frame MRAS

Reference frame MRAS (RF-MRAS) is the simplest variant of observers working on the principle of MRAS. For the estimation are used equations, which determine derivation of the rotor flux of machine.

1.2 Mathematical description RF-MRAS

The reference model of MRAS method is based on the application of voltage model with derivation of rotor flux, which is in the stator coordinate system described by the following equation:

$$\frac{d\Psi_R^S}{dt} = \frac{L_r}{L_m} \left[\mathbf{u}_S^S - R_S \mathbf{i}_S^S - \frac{L_s L_r - L_m^2}{L_r} \frac{d\mathbf{i}_S^S}{dt} \right] \quad (1)$$

This model requires, that equation (1) expands to the component form:

$$\frac{d\Psi_{R\alpha}}{dt} = \frac{L_r}{L_m} \left[u_{S\alpha} - R_S i_{S\alpha} - \frac{L_s L_r - L_m^2}{L_r} \frac{di_{S\alpha}}{dt} \right] \quad (2)$$

$$\frac{d\Psi_{R\beta}}{dt} = \frac{L_r}{L_m} \left[u_{S\beta} - R_S i_{S\beta} - \frac{L_s L_r - L_m^2}{L_r} \frac{di_{S\beta}}{dt} \right] \quad (3)$$

Adaptive model of MRAS method with Kalman filter is based on the application of current model with derivation of rotor flux, which is in the stator coordinate system described by the following equation (4), which depends on the mechanical angular velocity.

$$\frac{d\hat{\Psi}_R^S}{dt} = \left(\mathbf{j}\hat{\omega}_m - \frac{1}{T_R} \right) \hat{\Psi}_R^S + \frac{1}{T_R} L_m \mathbf{i}_S^S \quad (4)$$

Equation (4) can be written in component form:

$$\frac{d\hat{\Psi}_{R\alpha}}{dt} = -\frac{1}{T_R} \hat{\Psi}_{R\alpha} - \hat{\omega}_m \hat{\Psi}_{R\beta} + \frac{1}{T_R} L_m i_{S\alpha} \quad (5)$$

$$\frac{d\hat{\Psi}_{R\beta}}{dt} = -\frac{1}{T_R} \hat{\Psi}_{R\beta} + \hat{\omega}_m \hat{\Psi}_{R\alpha} + \frac{1}{T_R} L_m i_{S\beta} \quad (6)$$

The error signal entering to the controller is corresponding to the deviation of rotor fluxes and it is described by equation (7), after processing by PI controller, we get an estimate angular speed $\hat{\omega}_m$ on the output of adaptation algorithm - equation (8).

$$\Phi(e) = \frac{d\hat{\Psi}_R^S}{dt} \times \frac{d\Psi_R^S}{dt} = \frac{d\hat{\Psi}_{R\alpha}}{dt} \frac{d\Psi_{R\beta}}{dt} - \frac{d\hat{\Psi}_{R\beta}}{dt} \frac{d\Psi_{R\alpha}}{dt} \quad (7)$$

$$\hat{\omega}_m = K_1 \Phi(e) + K_2 \int_0^t \Phi(e) dt \quad (8)$$

Equation (7) corresponds to the opening angle of both vectors. The sign of the error signal $\Phi(e)$ then determines the type of request to change speed. Positive error

$\Phi(e) > 0$ requires increase of estimated speed and negative error $\Phi(e) < 0$ requires reduction.

2 Description of Kalman filter

Kalman filter is an adaptive filter used to model the states of discrete dynamic system. This technique was developed in the 60-ies to filter noise in electrical signals, but later found application in other areas. The advantage of this filter is its recursive structure, in which the coefficients in each step are adjusted on the basis of available information to provide the best estimate of future state. The new filter at every step of the filter correction arises from the previous step by the new incoming information without having to remember all previous values of input parameters. With the Kalman filter we can use the state representation, which allows us to create higher order systems working simultaneously as a system of mutually coupled systems of first order.

Method of calculation:

Equations of state and measurement equations:

$$z(t) = y(t) - H\tilde{x}(t) \quad \text{Improvement} = \text{measured value} - \text{prediction} \quad (9)$$

$$\hat{x}(t) = \tilde{x}(t) + K(t)z(t) \quad \text{Estimation of state} \quad (10)$$

$$\tilde{x}(t+T) = A\hat{x}(t) \quad \text{Prediction of state} \quad (11)$$

Kalman gain and error covariance equations:

$$K(t) = \tilde{P}(t)H^T(H\tilde{P}(t)H^T + R)^{-1} \quad \text{Kalman gain} \quad (12)$$

$$\hat{P}(t) = [I - K(t)H]\tilde{P}(t) \quad \text{Estimation of covariance matrix} \quad (13)$$

$$\tilde{P}(t+T) = A\hat{P}(t)A^T + Q \quad \text{Prediction covariance matrix} \quad (14)$$

3 Description of method HIL

Hardware in the Loop (HIL) simulation is a technique that is used in the development and testing of complex real-time systems. It is a tool that connects the hardware (controller) with a mathematical model (managed system) in a closed feedback loop. To simulate this method a real control system and a mathematical model is required. The mathematical model is used to configure the control system. The control system generates an actuator variable dependent on the control deviation, which is the

difference between desired and actual quantity. The Control variable enters the model, then output variable (actual value) gets off from the mathematical model, and then gets back in to the control system. This simulation works in real time. Results of this simulation approaches to reality, because the control system with sensors and actuators is implemented as close as it would be in real. To the fact that the results would match the reality, we need a sufficiently accurate mathematical model, on which simulation accuracy depends most. As soon as the control system is set up according to the requirements, a mathematical model can be replaced by the real system and the results can be compared.

Figure 2 is a general diagram of the simulation using method hardware in the loop. The meaning of values in this picture: $y(t)$... process value, $w(t)$... desired quantity, $e(t)$ the..control. error, $u(t)$... control variable $v(t)$... fault value, reg ... regulator.

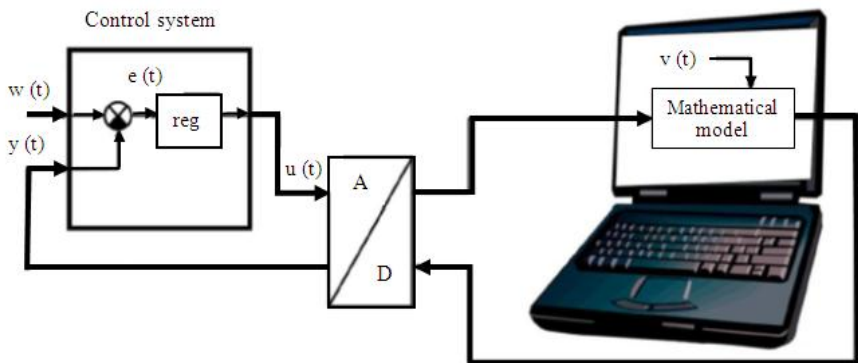


Fig. 2. Diagram of Hardware in the Loop Simulation.

4 Results of simulation sensorless vector control of induction motor using Kalman filter by HIL method

This section shows simulation results of sensorless vector control, which were recorded by program for setting control variables in LabVIEW environment. Control variable of magnetizing current was 4A and the desired speed was at first 30 rpm and then changed to -30 rpm.

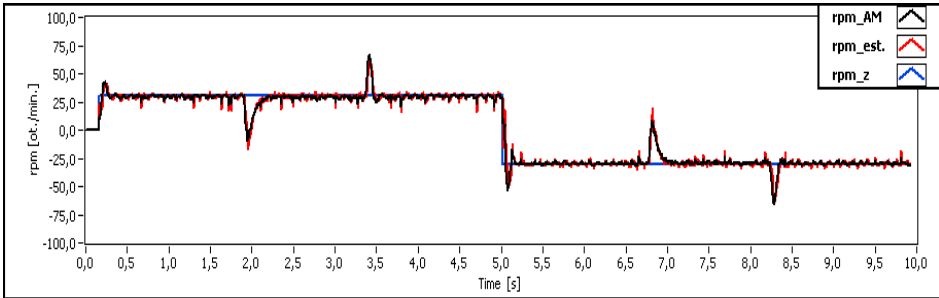


Fig.3. Change the engine speed [rpm] from 0rpm → 30rpm → -30rpm, the actual rpm (black), estimate rpm (red), desired rpm (blue).

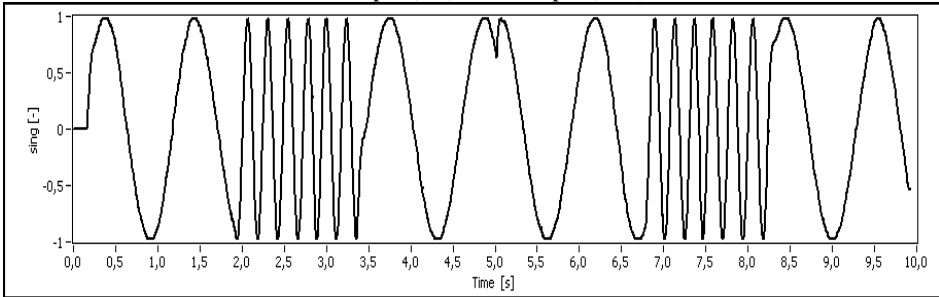


Fig.4. $\text{Sin}\gamma [-]$.

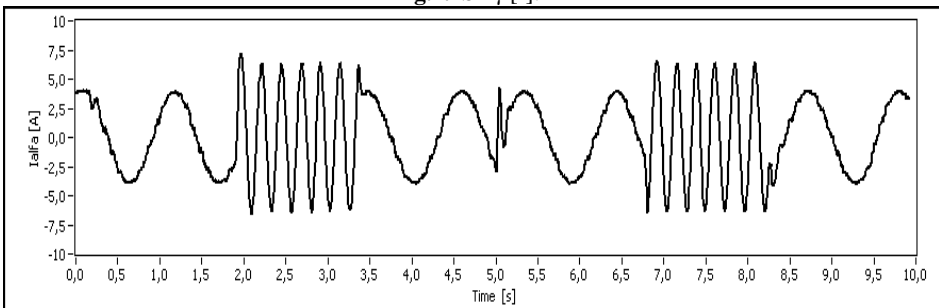


Fig.5. Stator current $i_{\alpha}[A]$.

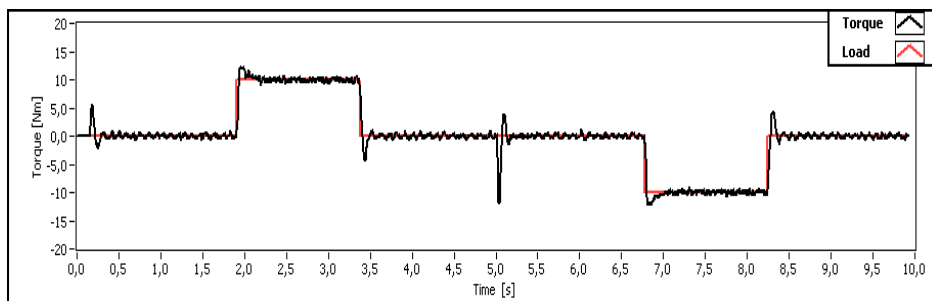


Fig. 6. The course of motor torque M_m [Nm], the electric motor torque (black), the load torque (red).

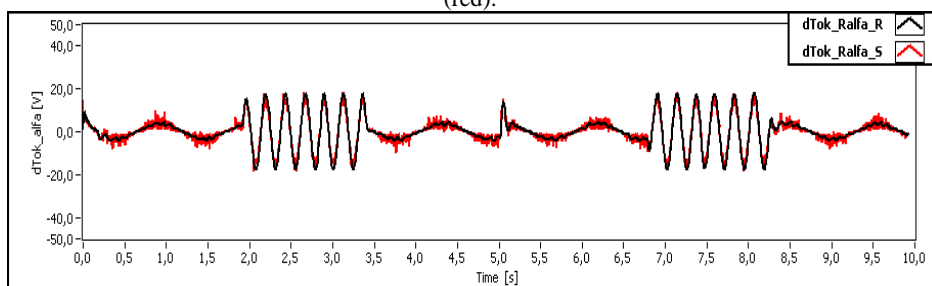


Fig. 7. The course of the flux derivative of the engine ψ_α [V], the derivative flux ψ_α from the current model (black), derivative ψ_α flux from the voltage model (red).

Acknowledgement

In the paper there are the results of the project SP2012/85 which was supported by Student Grant Competition of VSB-Technical University of Ostrava. This research was supervised by Prof. Ing. Pavel Brandstetter, CSc.

References

1. Brandštetter, P.: Střídavé regulační pohony – Moderní způsoby řízení, Ostrava: VŠB – TU Ostrava, 1999. ISBN 80-7078-668-X
2. Neborák, I.: Modelování a simulace elektrických regulovaných pohonů, Ostrava: VŠB-TU Ostrava, 2002.

Magnetic Properties of Core for Toroidal Transformers Made from Thin Low-loss Sheets and Thermal Influence on Resulting Transformer Idle Current

Aleš Folvarčný

Department of Electrical Power Engineering, FEECS,
VŠB – Technical University of Ostrava, 17. listopadu 15, 708 33 Ostrava – Poruba
ales.folvarcny@vsb.cz

Abstract: The paper presents the results of independent experimental analysis aimed at determining the magnetic properties of the selected type of toroidal transformer cores made from thin silicone alloyed sheets with a low loss number used in our case in the manufacture of toroidal transformers for higher class audio power amplifiers. Another part of the paper deals with the results of the experimental analysis aimed at determining the effect of temperature on size and type parameters of the current loading of small toroidal and conventional transformers. The aim of this measure was to assess the effect of temperature and voltage values at no load current of the selected type of toroidal and conventional transformers put in a climatic chamber. Furthermore, our attention was drawn to the observations of the effect of temperature and magnetic saturation on voltage transformer cores and to approximate formulation of magnetic properties of metal core type transformers in the form of BH hysteresis characteristics.

The samples were analysed and the waveforms U_{10} , I_{10} , U_{20} were measured and recorded. The measured values were then used for calculation of additional quantities of toroidal transformers (magnetic flux density, magnetic field intensity) that specify the magnetic properties of the measured samples. Finally, the measured results of both the toroidal and conventional transformers were compared.

The temporal analyses of saturation of cores are the outcome of extensive and time-consuming measurements and registration of signals in no-load state for various levels of supply voltage. The measurements were based on common knowledge of the properties of soft ferromagnetic materials.

Keywords: Toroid transformer, idly current, BH characteristics, climatic chamber, temperature.

1 Introduction

The aim of this exploratory analysis was to assess the effect of temperature and voltage values of the selected type of toroidal and conventional transformers under no load condition, i.e. for no-load current. The influences of temperature and voltage values of magnetic toroidal transformers were then described and theoretical findings were verified.

The samples were analysed and waveforms U_{10} , I_{10} , U_{20} were measured and recorded. The measured values were then calculated for other quantities of the toroidal transformer characterizing the magnetic properties of measured samples (magnetic flux density, magnetic field intensity).

The final part deals with the implementation of the comparison of the measured results for the toroidal and current transformers.

During actual measurements, the knowledge of ferromagnetic properties of soft magnetic materials used for production of transformer cores was employed.

2 General and brief notes to the given issue

An idle transformer is characterized best by its idle current. The size and shape of the current describes substantially the resulting properties of design, structural and magnetic characteristics of the transformer core material. In the known geometric dimensions and parameters of the transformer windings, the timing of this current together with the induced voltage signal can then be used for the analysis of magnetic parameters and ratios of magnetic core transformer. Such an analysis can then be used both for determination of the magnetic properties of the metal core and for the control analysis of the resulting saturation and losses as a result of the design and construction of the transformer.

3 Experimental part

In all, 4 toroid transformer samples supplied by Talema s.r.o. were used for measurements.

These transformers were intended for power audio-amplifiers in higher classes.

These transformers were placed in climatic chamber Vötsch 4018 for measurement.

Following samples were used for measurement:

- 92 902 - P1S4 CD 5x, supply voltage 230V (small transformer)
- 92 166 - P2 S6 DGR 1053/3, supply voltage 230V (middle-size transformer).

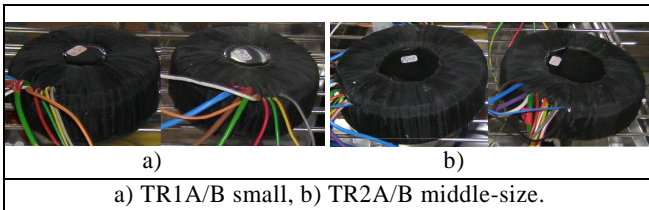


Fig. 1. Example of individual samples

The cores were made of the same material and with the same production technology. But they had different final technological finish. The core transformer 1A was subject to a thermal finish and varnished, the other cores are not treated for final production.



Fig. 2. Example of measured core samples 1A/1B

Both of these cores were winding of electrical sheet made by ORB Steel Cogent, type M111 with a thickness of 0.30 mm, max. loss of 1.11 W/kg.

The following samples were used for further measurement:

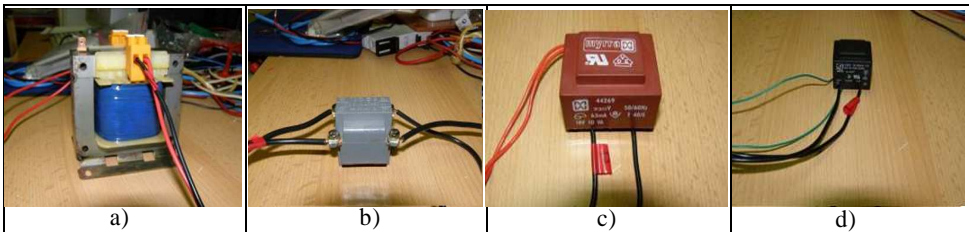


Fig. 3. Example of individual samples

a) TR1-230/24V;160VA, b) TR2-230/24V;22VA, c) TR3-230/18V;10VA, d) TR4-230/15V;3VA

This is the standard employment of transformers for various applications. The objective of these measurements on the transformers is, in particular, from the current value of nothing. Subsequently, these values are compared with the results measured on toroidal transformers designed for power audio amplifiers of a higher class.

Design and preparation of the workplace

To analyse the effect of temperature on the idle current of selected transformer types, the measuring workplace has been prepared; refer to the block diagram in Fig.4

The transformers put in climatic chamber had primary and secondary windings brought out to the terminal placed outside the climatic chamber. The individual windings are successively connected to the measuring site, where the required quantities were registered.

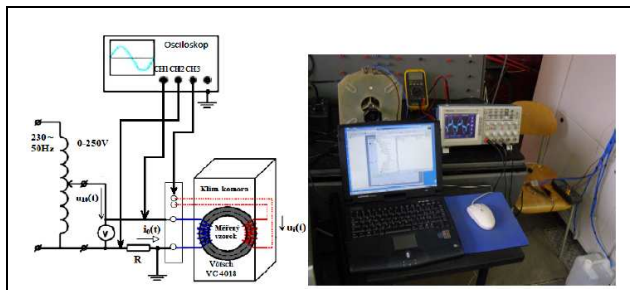


Fig. 4. Example of workplace

- Measuring resistor had a value of 1Ω .

The power for analysed samples was supplied by an autotransformer and the value of voltage for each type of transformer was adjusted in the range from 50 to 250 V. The individual toroidal transformers were put into the Vötsch VC 4018 climatic chamber.

The climatic chamber was always set to the required temperature before start of each measurement. The temperature set points for the climatic chamber: -40°C , -35°C , -30°C , -20°C , -10°C , 0°C , 10°C , 20°C , 30°C , 40°C , 50°C , 60°C , 70°C , 80°C , 90°C , 100°C and 120°C .

After reaching the desired temperature in the chamber, the measured transformers were left at standstill for half an hour so as to reach the temperature stability of the measured transformers and all of their volumes.

The records of the idle current signal and the induced primary voltage were performed using a Tektronix digital oscilloscope with GPIB communication interface and PC.

WaveStar v.2.4 was used to convert the readings into a text format and these were then imported into Microsoft Excel to be processed further.

4 Measurement results

Table 1. Samples of resulting U_{10} , I_{10} , U_{20}

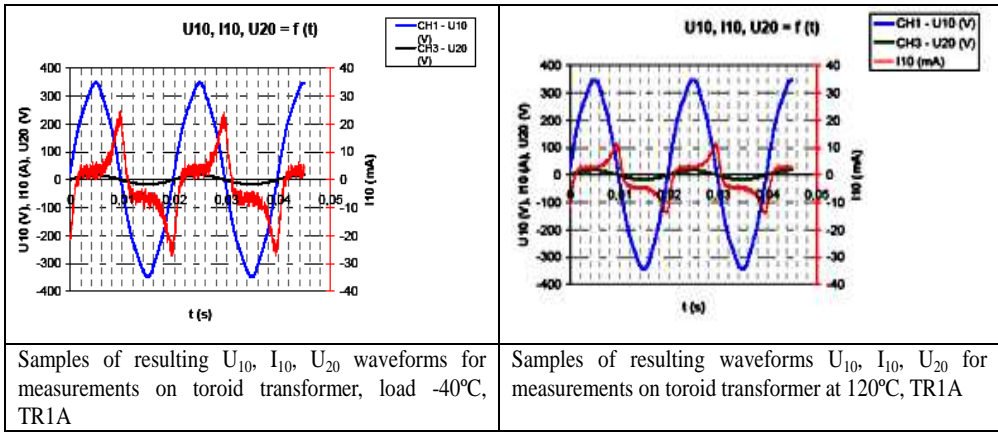


Table 2. Samples of resulting U_{10} , I_{10} , U_{20}

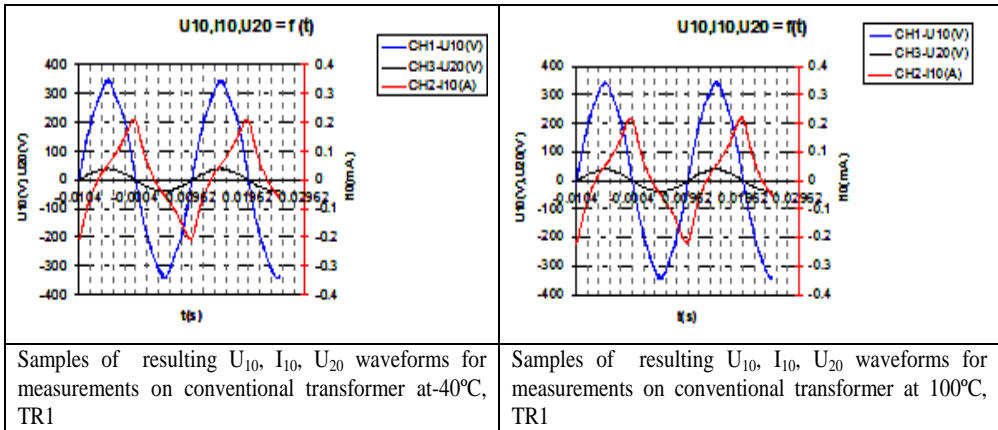
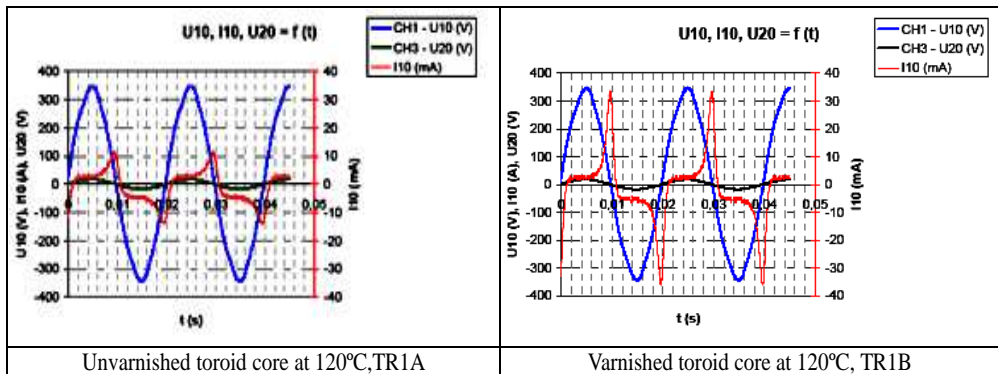


Table 3. Samples of resulting U_{10} , I_{10} , U_{20}



5 Conclusion

From the measured results of the analysed samples results that the current load value in the range of set temperature range -40°C to 120°C is lower temperature in growing, whilst this effect on conventional transformers was almost imperceptible.

The measured results of the analysed samples indicate that the value of idle current of toroidal transformers in the range of set temperatures -40°C to 120°C decreased whereas this effect was almost imperceptible in conventional transformers.

The magnetization of toroidal transformers made from very thin metal sheets with a high maximum permeability value decreased with increasing temperature, the hysteresis loop narrowed down proportionally along with the losses ensuing from it. This phenomenon can only be explained by a more profound description of the magnetization processes and magnetostrictive effects which was omitted for the need of this paper.

Besides, it is evident from the measured results that the toroidal transformer denoted as Tr1A showed much smaller value than the sample 1B whereas both of them were made from the same material and with the same dimensions. The resulting difference in behaviour of otherwise identical transformers is given by intentionally different surface finish of the transformer cores. The magnetic core of sample 1A was unvarnished and thermally unhardened while the transformer core 1B was varnished and thermally hardened. The varnishing and hardening processes result in introduction of stress within the core and in enlargement of the transversal air gaps among individual layers of the transformer-core laminations and in deterioration of magnetic properties of all cores, making the idle current to rise.

Change of the transformer winding resistance by changing temperature has no effect on the resulting transformer idling current, because of insignificant value of the winding resistance with regard to high value of the inductive reactance.

As next it is obvious that the effect of temperature on the magnetic properties of the core is negligible with the normal quality of metal sheets. For very thin sheets of toroidal cores is the temperature effect significant due to their high permeability. At low temperatures magnetic properties of sheets turn to deteriorative, the current idling is increasing and at the same time the vibration and noise go up.

References:

1. Folvarčný A.: Magnetic properties types core for toroidal transformers, Journal of Electrical Engineering. Bratislava, 2010.
2. Smolka K.: Typové toroidní transformátory-experimentální analýza elektromagnetických poměrů, při různých provozních stavech, Diplomová práce. VŠB-TU Ostrava, 2008.
3. Draxler K., Kaspar P., Ripka P.: Magnetické prvky a měření, ČVUT Praha, 1999.

Publications:

1. Folvarčný A., Marek M.: Experimentální analýza vlivu teploty na parametry proudu naprázdno typových toroidních transformátorů, porovnání s konvenčními typy transformátorů, Scientific Journal TRILOBIT 2010, Zlín 2010.
2. Folvarčný A.: Magnetic properties of types of core for toroidal transformers made from thin low-loss sheets and thermal influence on resulting transformer idle current, Journal of Electrical engineering, Slovakia 2010. ISSN 1335-3632.

Vector Control of AC Drives Using Fractional Order Controllers

Jiří Friedrich

Department of Electronics, FEECS,
VŠB – Technical University of Ostrava, 17. listopadu 15, 708 33 Ostrava – Poruba
jiri.friedrich@vsb.cz

Abstract. The so called vector control of AC drives is nowadays commonly used method with relatively very good dynamics and accuracy. Both this parameters are in case of standard vector control limited by the character of PI or PID controllers. Latest research was only focused on small improvements of this method, especially on so-called sensorless drives. Heretofore little notice was taken of fractional calculus application, which pushes forward the boundary of accessible accuracy and dynamics of the controlled process. It was caused, among others, by problems with practical realization because the approximation processes brings considerable computing demands. Until now the research was focused first of all on the application in the area of DC drives, but only few contributions deal with the application in the control structure of AC drives. Thus, the main aim of this paper is to present the simulation results of vector control of an AC drive using above mentioned fractional order controllers and analyze the suitability of its use.

1 Introduction

Standard elements of industrial control applications are proportional-integral-derivative (PID) controllers. The main benefit of using those types of controllers is the simplicity of design, because there are lots of suitable and very easy methods of design. The accuracy of this way controlled process is for major applications sufficient, however there are situations demanding better settling time respectively percentage overshoot. As an example it can be used a technological process working at low or almost zero speed.

2 Fractional order controllers

It was mathematically shown, that generalization and extending of the integer order PID to the plane is possible. To this purpose it is used the so-called theory of fraction-order calculus. The process of fractional integration and differentiation can be mathematical described in several manners. But mostly used is besides the Grünwald-Letnikov definition the so-called Riemann-Liouville definition. It is given as (1)

$$D^{-\alpha} f(t) = \frac{1}{\Gamma(\alpha)} \int_0^t (t - \tau)^{\alpha-1} f(\tau) d\tau \tag{1}$$

and for engineering praxis useable Laplace transform is shown in (2) as it is described e.g. in [1] - [4].

$$L\{D^{-\alpha} f(t)\} = s^{-\alpha} F(s) \tag{2}$$

In the similar way it is possible to obtain a definition of fraction-order derivative, expression in Laplace domain can be found in [3].

If we go back to controllers, application of the mentioned theory causes following change of PID frequency response. Equation (4) represents the standard PID and equation (5) the fractional-order PID.

$$G(s) = K_p + T_i s^{-1} + T_d s \tag{4}$$

$$G(s) = K_p + T_i s^{-\lambda} + T_d s^{\delta} \tag{5}$$

It is obvious from the frequency responses that the integer order PID requires designing of three parameters and fractional order PID five parameters. This expansion enables more flexibility to controller design, as it was desired.

On the one hand there are the mentioned benefits, but on the other hand it is necessary to mention, that this may also cause some problems. Firstly, standard design methods cannot solve this easily. Therefore it is necessary to use another one, e.g. particle swarm optimization technique. The next problem is selection of suitable FO operator approximation.

3 Simulation results

The described FO-PID was simulated by MATLAB-SIMULINK on a vector controlled AC drive with the induction motor. The controllers of quantities in control structure of AC drive with vector control were adjusted accordance with the parameters of the induction motor (type P 112 M04).

Parameters of the fractional-order PID were set in this way:

$$K_p = 1, T_i = 3.5 \text{ and } \lambda = 0.01, T_d = 0 \text{ and } \delta = 0$$

selected approximation and expansion: crone resp. cfe

This adjustment of parameters means that in fact only fractional order PI controller was simulated. This approach was chosen due to high computing demands of FO-PID in case of practical realization, which should be in future carried out.

Simulation was realized in three speed areas to sustain appropriate behavior in large speed range. In each situation was although monitored the demanded current time course, which is de facto the output variable from speed controller. Simulation results, representing the above mentioned, are shown in fig. 1. – 6.

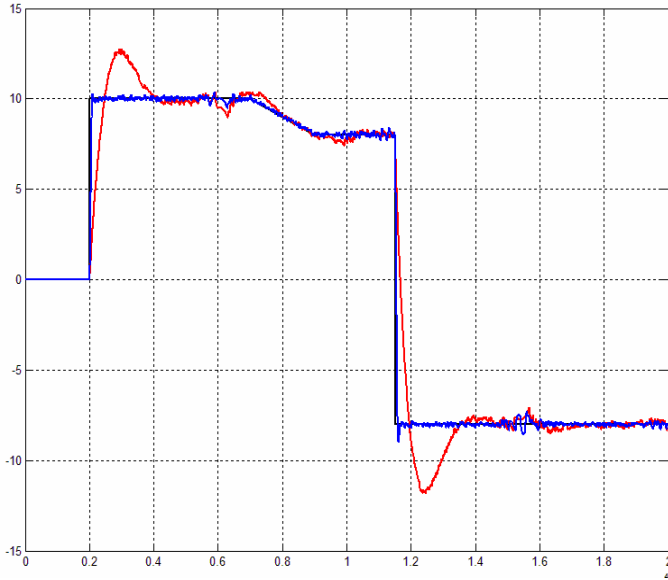


Fig. 1. Reference speed (black), standard controlled speed (red) and speed controlled using FO PI (blue) [rpm], area of very low speed. Time axis [s].

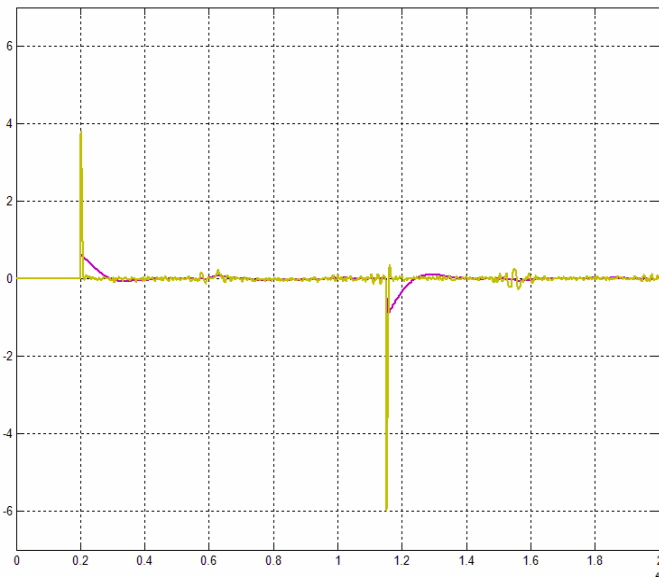


Fig. 2. Comparison of demanded current (area of very low speed). Standard vector control (violet), vector control using FO PI (yellow), [A]. Time axis [s]

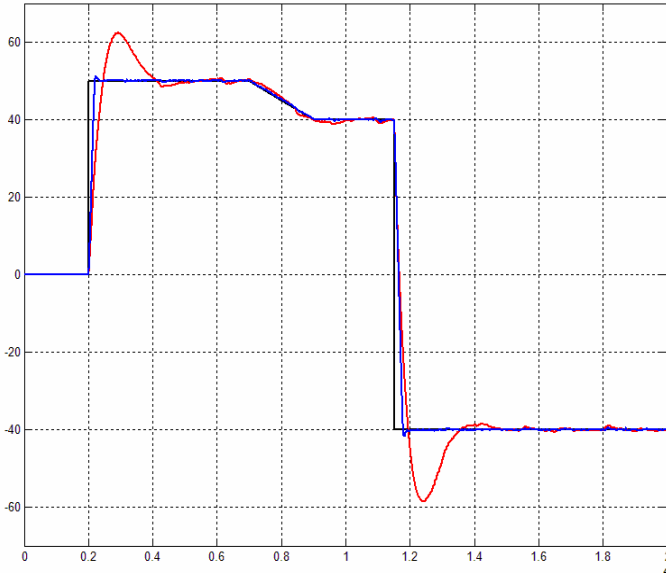


Fig. 3. Reference speed (black), standard controlled speed (red) and speed controlled using FO PI (blue) [rpm], area of low speed. Time axis [s]

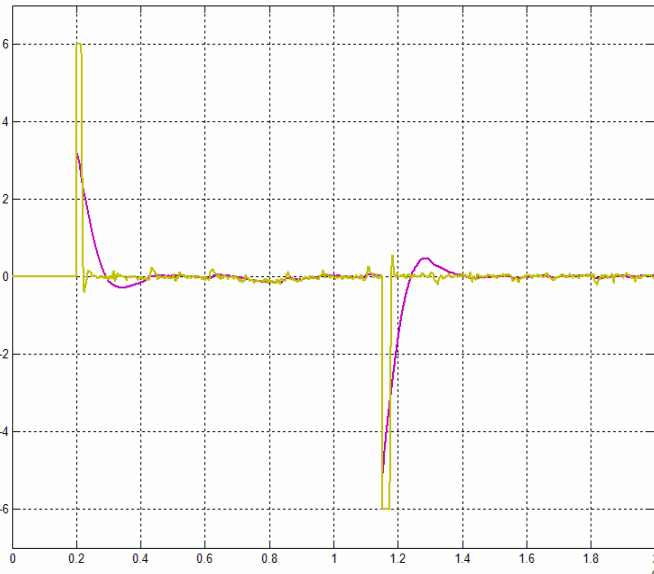


Fig. 4. Comparison of demanded current (area of low speed). Standard vector control (violet), vector control using FO PI (yellow), [A]. Time axis [s]

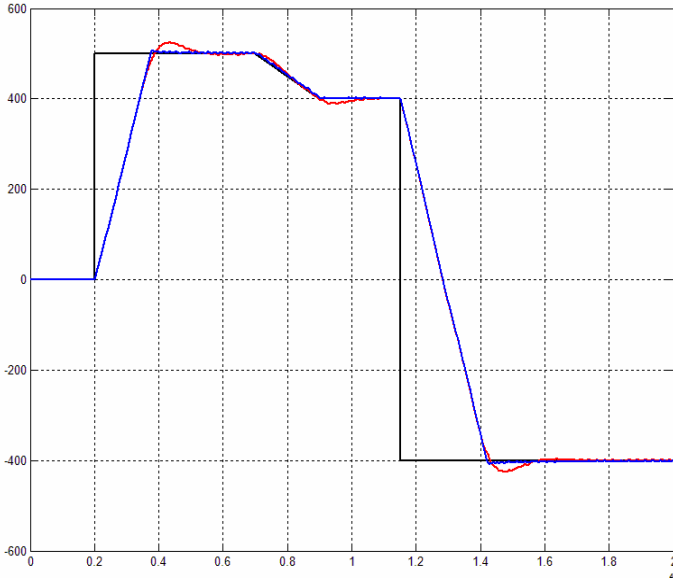


Fig. 5. Reference speed (black), standard controlled speed (red) and speed controlled using FO PI (blue) [rpm], area of normal speed. Time axis [s]

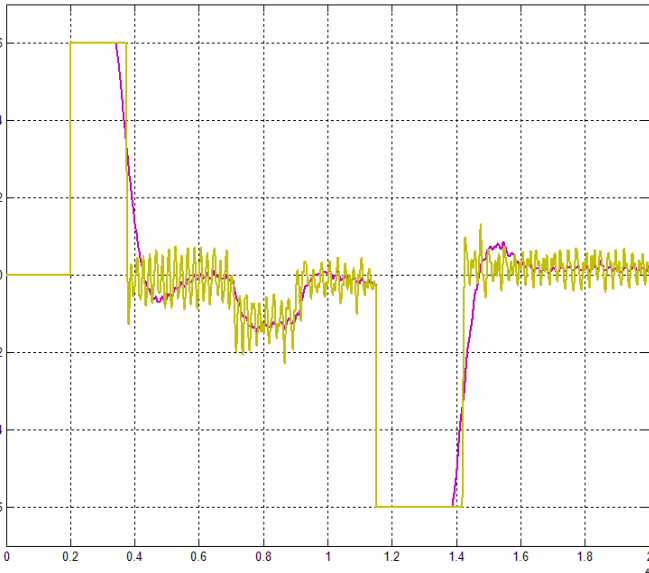


Fig. 6. Comparison of demanded current (area of normal speed). Standard vector control (violet), vector control using FO PI (yellow), [A]. Time axis [s]

Conclusions

The aim of this research was to analyze the possibility of modern fractional order controller application in the structure of vector controlled induction motor. It is obvious from the above presented simulation results that the application of fractional order controllers brings new quality and pushes forward the boundary of accessible accuracy and dynamics of the control process. The only disadvantage is considerable computing demand on the control system.

Simulation results fig. 1., 3., and 5. show that FO controllers can be used in wide range of speeds and already the use of simplified variant (FOPI) brings great improvement of speed control course, especially in area of low and very low speeds, which is in conformity with assumptions mentioned in literature. Fig. 2., 4., and 6. represent the fact, that during the control process is more appropriate used the maximum value of demanded current with positive impact on the time of regulation.

Acknowledgement

In the paper there are the results of the project SP2012/85 which was supported by Student Grant Competition of VSB - Technical University of Ostrava. This research was supervised by Prof. Ing. Pavel Brandštetter, CSc.

References

1. Press, W.H., Teukolsky, S.A., Vetterling, W. T., Flannery, B. P.: Numerical Recipes in C. The Art of Scientific Computing, 2nd edition, Cambridge University Press (1992).
2. Carlson, G.E., Halijak C.A.: Approximation of fractional capacitors $(1/s)^{1/n}$ by a regular Newton process. IRE Transactions on Circuit Theory, CT-11, No. 2 (1964), 210-213.
3. Podlubny, I.: Fractional-order systems and $PI^{\lambda}D^{\delta}$ controllers. IEEE Trans. On Automatic Control, vol.44, no. 1, (1999) 208-213
4. Petráš, I.: Fractional-order feedback control of a DC motor. Journal of Electrical Engineering, vol. 60, no. 3, 2009, 117-128

Computational Simulation of Electromagnetic and Electrostatic Lenses Used in Electron Microscopes

Regina Holčáková

Department of Electrical Power Engineering, FEECS,
VŠB – Technical University of Ostrava, 17. listopadu 15, 708 33 Ostrava – Poruba
regina.holcakova@vsb.cz

Abstract. The paper deals with simulation of electromagnetic and electrostatic field distribution in the real type lenses used in electron microscopes. The electromagnetic lenses were solved by finite element method using ANSYS software and electrostatic lenses were solved by finite difference method using SIMION software. This project and paper were created by financial support of state budget through the Ministry of Industry and Trade MPO-CR, project n. FR-TI1/334.

1 Introduction

The lenses are used to bend rays of electrons so they are deflected in a predictable way from their original paths. Although electron microscopes which employ electrostatic lenses have been made, most microscopes use electromagnetic lenses. There are several reasons. Electrostatic lenses are more sensitive to the quality of the vacuum and cleanliness of the components than are electromagnetic lenses. Some lens aberrations are more severe for electrostatic lenses compared to electromagnetic lenses. Electrostatic lenses require very powerful electrostatic fields which can lead for example to electrical breakdown. For this reason, electrostatic lenses cannot be made with focal lengths as short as magnetic lenses.

2 Electromagnetic and electrostatic lens

The electron beam is divergent after passing through the anode plate and must be refocused. The simplest type of electron lenses are electrostatic, which deflect beam electrons using electrically charged plates. While a charged particle is in an electric field, a force acts upon it. The faster the particle the smaller the accumulated impulse. Thus substantial lenses are required to deflect a high-voltage electron beam. Additionally, electrostatic lenses require a very clean high vacuum environment to prevent arcing across the plates.

At present, electrostatic lenses most commonly are used to deflect and focus ion beams in mass spectrometers. Microprobes and SEMs use magnetic lenses. Although electron lenses in principle behave the same as optical lenses, there are differences and the quality of electron lenses is not nearly as good as optical lenses in terms of aberrations.

The first magnetic electron lenses were developed by M. Knoll and E. Ruska in Germany in 1932. Their action is similar in principle to optical lenses, but electron lenses can be made only to converge, not diverge. Magnetic lenses consist of two circularly symmetric iron pole-pieces with copper windings with a hole in center through which beam passes. The two pole pieces are separated by "air-gap" where focusing actually takes place. The magnetic flux diverges along the electron beam axis.

2.1 Electromagnetic lens

Typical construction of the electromagnetic lens produces a strong field of short axial extent necessary for formation of images at high magnification. The specimen is placed within the magnetic field of the objective lens. Thus, any field introduced by contaminants in the specimen can distort the field of the lens. Note that this also means that part of the lens field is on the front side of the object and affects the electron beam before it passes through the object.

2.2 Electrostatic lens

A basic understanding of electrostatic lenses is important for two main reasons: the electron gun uses electrostatic lens action to form the primary beam source and it is quite common for a charge to develop on the non-conducting contamination which may accumulate on physical apertures and transform them into weak electrostatic lenses which can distort the electron image.

2.3 Lens defects

Electron lenses are not as good as optical lenses in terms of defects of focus, called aberrations. Aberrations are of two types. Spherical aberrations, in which the outer zones of a lens focus more strongly than inner zones, are most important in magnetic lenses. The result is that electrons along beam axis are deflected less than electrons passing through beam periphery, yielding more than one focal point. Chromatic aberrations, in which electrons of slightly different energies are focused differently, are relatively minor because the electron gun produces electrons with essentially uniform velocities. Spherical aberrations are minimized by placing a spray aperture in front of the magnetic lens, confining electrons to the center. This results in greatly reduced, but still acceptable, beam currents.

3 Computational simulation

Electromagnetic and electrostatic lenses shape the electron beam and focus it in the appropriate position of the observed sample. The required position of the electron beam is given by accurately setting electrostatic/electromagnetic field in electron path. The accurate determination of distribution of electrostatic/electromagnetic fields in the lens area using analytical computation is very complicated and sometimes practically impossible. However, with good knowledge of the actual electrostatic/electromagnetic field distribution of the lens, possible defects in the lenses can be discovered.

The electromagnetic lenses were solved by finite element method using ANSYS software and electrostatic lenses were solved by finite difference method using SIMION software. ANSYS Multiphysics software offers a comprehensive product solution for both multiphysics and single-physics analysis. The product includes 2D and 3D structural, thermal, fluid and both high- and low-frequency electromagnetic analysis. The product also contains solutions for both direct and sequentially coupled physics problems including direct coupled-field elements and the ANSYS multi-field solver. SIMION is suitable for a wide variety of systems involving 2D or 3D, static low-frequency (MHz) RF fields: from ion flight through simple electrostatic and magnetic lenses to particle guns to highly complex instruments, including time-of-flight, ion traps, quadrupoles, ICR cells, and other MS, ion source and detector optics.

3.1 Computational simulation of electromagnetic lens

Results of computational simulation describe the actual electromagnetic field distribution in the type electromagnetic lens with high accuracy. Another objective is to find critical points in the geometry, which could cause a defects of the lens. Electromagnetic field distribution was computed for 1 step of the excitation current corresponding to $NI=1000$ Ampere-turns (condenser lens) and $NI=2000$ Ampere-turns (objective lens).

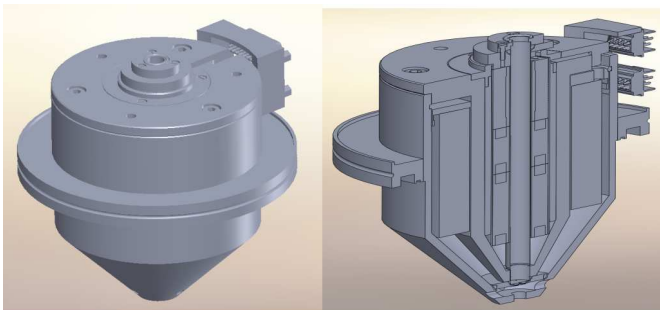
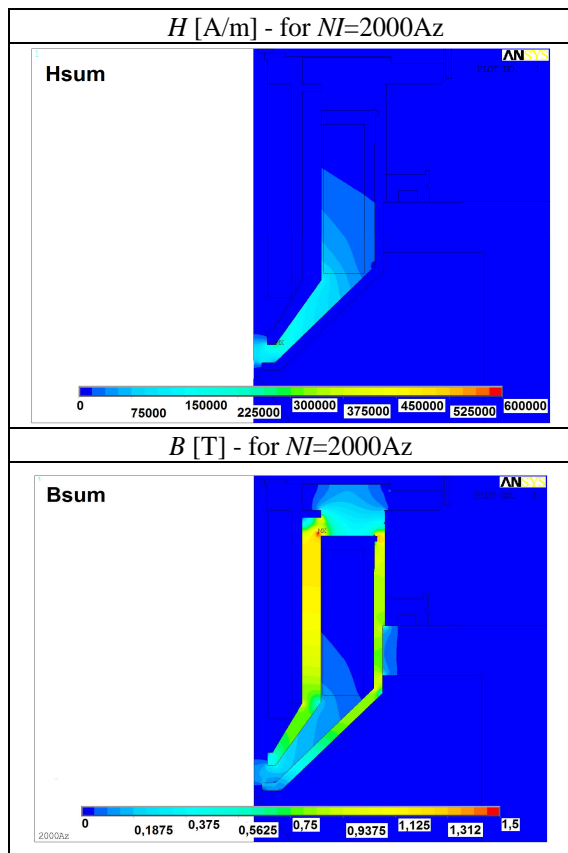


Fig. 1. Electromagnetic lens model

Tab. 1. Electromagnetic field distribution – examples of results

Magnetic intensity H_{sum} [A/m] and Flux density B_{sum} [T] for $NI=2000$ Az



3.2 Computational simulation of electrostatic lens

Results of computational simulation describe the actual electrostatic field distribution in the electrostatic lens system including 4 electrostatic lenses, grid and detector. Another objective is to compute electron beam trajectory, so-called time of flight analysis, for kinetic energy value $KE=10\text{eV}$. There was set 1000 trajectories with radius of circle distribution 1mm and for angles $\pm 1,2$.

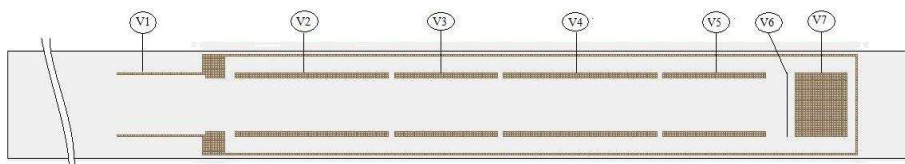
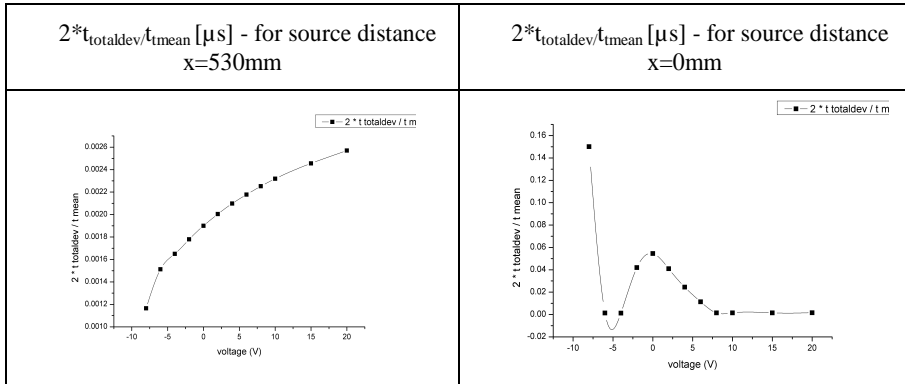


Fig. 2. Electrostatic lens system model

Tab. 2. Electrostatic lens system- time of flight analysis – resultsGaussian distribution $V_2=V_3=V_4 = -8, -6, -4, -2, 0, 2, 4, 6, 8, 10, 15, 20V$ 

4 Conclusion

The paper deals with partial results of the grant project focused on the innovative research of electron microscopes, which belongs to the category of worldwide high-tech technologies.

There was determined the electromagnetic/electrostatic field distribution in the lenses. Further, there were found the critical points in the lens, were designed modifications of the magnetic circuit and optimal configuration of electrodes in the electrostatic lens system.

In this respect, the results achieved in this way can be used for optimization of lenses or objectives and for another analyses.

References

1. J. H. Moore, C. C. Davis, M. A. Coplan: *Building scientific apparatus*, Addison-Wesley Publishing, 1983

Grants

1. MPO: FR-TI1/334-*Implementation of the innovation from the research of modern types chambers for electron microscopes in order to strengthen the position and competitive advantage of the Czech Republic on the world market*

Control Unit for Reversible Voltage Inverter

Michal Hromják

Department of Electronics, FEECS,
VŠB – Technical University of Ostrava, 17. listopadu 15, 708 33 Ostrava – Poruba
michal.hromjak@vsb.cz

Abstract. This paper describes the basic principle of chosen control method for reversible voltage inverter. This power converter creates the basic part of proposed power configuration in project ENET. The power configuration is designed to simulate model of Smart Grid. Next section deals with power converter control unit, which is based on digital signal processor TMS320F28335. The following is a brief description of used software development tools.

Keywords: DSP, Vector control, TMS320F28335

1 Introduction

Utilization of energy from renewable energy sources (RES) is still growing and it is increasingly important. The present energetic development is aimed into the incorporation of alternative and RES into the standard electrical grids. The renewable energy sources have different characteristics from traditional fossil energy sources. They are typically installed with a small capacity and large degree of decentralization. The technical solution of integration RES is building new intelligent type of electrical distribution system known as smart grids.

Next generation distribution system can be characterized as a transmission and distribution network capable of transmitting electric energy, which is derived as from large centralized MW sources, as well as from small units of up to several kW to the end customer with a high degree of management autonomy. Network monitors all the important qualitative and quantitative parameters of the transmitted energy and is able to automatically regulate the consumption and production of electricity.

Smart grid is the one of the main aims of project ENET. A part of this project deals problems of energy accumulation. The reversible power converter is needed to provide an efficient and reliable electric power flow between the accumulation units and the mains. The direction of electric power flow is determined by appropriate control method of converter. A more detailed description of the vector control method is given in the next section.

The control system of the inverter is provided by the DSP TMS320F28335. This processor disposes with high computational power and is therefore suitable for frequency converters control. The appropriate software environment with basic equipment containing I/O handling, control algorithms and communication routines has been created.

2 Vector control

In principle, the control method of power converter is derived from the vector control of AC machines. The basis of this method is the decomposition of the spatial current vector to the system of fixed α, β coordinates and subsequent transformation into a rotating d, q coordinates system. Coordinate system d, q rotates angular velocity equal to the frequency of mains.

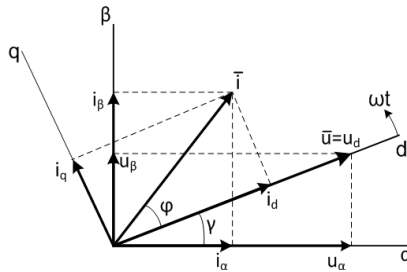


Fig. 1. Distribution of spatial current vector to the individual components

The output voltage of one phase of inverter can be expressed as:

$$\mathbf{U} = \mathbf{U}_S - \mathbf{I}_S(R_f + j\omega_S \cdot L_f). \quad (1)$$

The voltage vector and phase angle θ :

$$U = \sqrt{(U_S + I_S \cdot R_f)^2 + (I_S \cdot \omega \cdot L_f)^2}; \quad \theta = \arctg \frac{-I_S \cdot \omega \cdot L_f}{U_S - I_S \cdot R_f}. \quad (2)$$

For solving actual values the transformation in two-phase system is necessary:

$$\mathbf{u}^S = \mathbf{u}_S^S - R_f \cdot \mathbf{i}_S^S - j\omega \cdot L_f \frac{d\mathbf{i}_S^S}{dt}. \quad (3)$$

Rotating the vector-oriented system [d, q] and the subsequent adjustment we get the following equation, which describes the behavior of inverter in system of rotating coordinates:

$$L_f \frac{d(i_d)}{dt} = u_{sd} - i_d \cdot R_f + \omega \cdot L_f \cdot i_q - u_d. \quad (4)$$

$$L_f \frac{d(i_q)}{dt} = u_{sq} - i_q \cdot R_f + \omega \cdot L_f \cdot i_d - u_q. \quad (5)$$

As follows from equations (4) and (5) there is a mutual linkage between the two components. It can be easily removed by using the following equations:

$$u_d = -u_d^* + \omega \cdot L_f \cdot i_q + u_{sd}. \quad (6)$$

$$u_d = -u_q^* + \omega \cdot L_f \cdot i_d + u_{sq}. \quad (7)$$

After removing mutual linkage the transfer of inverter is:

$$L_f \frac{d(i_d)}{dt} = -i_d \cdot R_f + u_d^*. \quad (8)$$

$$L_f \frac{d(i_q)}{dt} = -i_q \cdot R_f + u_q^* \tag{9}$$

The regulatory structure of vector control allows independent control of both current components. The value of oriented angle Θ is determined on the basis of the measured waveform of line voltages, which are transformed into two-phase orthogonal coordinate system $[\alpha, \beta]$ with Clark's transformation:

$$\begin{bmatrix} u_\alpha \\ u_\beta \end{bmatrix} = \frac{2}{3} \begin{bmatrix} 1 & -\frac{1}{2} & -\frac{1}{2} \\ 0 & \frac{\sqrt{3}}{2} & -\frac{\sqrt{3}}{2} \end{bmatrix} \cdot \begin{bmatrix} u_a \\ u_b \\ u_c \end{bmatrix} \tag{10}$$

The value of oriented angle (or rather $\sin\Theta$ a $\cos\Theta$) is evaluated by using a vector analyzer VA block:

$$\sin\theta = \frac{u_{s\beta}}{u_s}, \quad \cos\theta = \frac{u_{s\alpha}}{u_s}, \quad \text{kde } u_s = \sqrt{u_{s\alpha}^2 + u_{s\beta}^2} \tag{11}$$

The currents flowing through the chokes and windings of transformer are transformed to d, q system in the block of vector rotation by using Park's transformation:

$$\begin{bmatrix} u_d \\ u_q \end{bmatrix} = \begin{bmatrix} \cos(\theta) & \sin(\theta) \\ -\sin(\theta) & \cos(\theta) \end{bmatrix} \cdot \begin{bmatrix} u_\alpha \\ u_\beta \end{bmatrix} \tag{12}$$

The values of these currents are compared with desired values in the PI current controllers R_{iu} . The output component from block BZV is added to the desired voltage values from PI regulators (u_{d*} , u_{q*}) for cancellation mutual linkage. After that come reverse vector rotation (from d, q to α, β coordinate system) and transformation back into the three-phase system. The control voltages u_a, u_b and u_c are implemented in PWM modulator, which produces the switching pulses for the IGBT transistors.

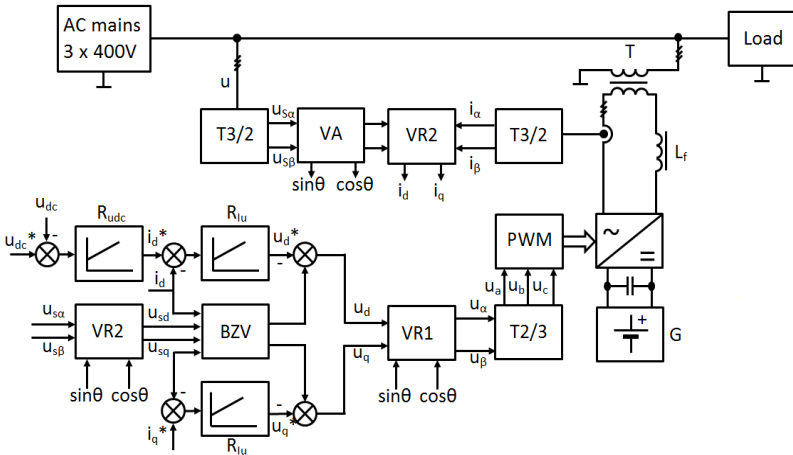


Fig. 2. Proposed control structure of power converter

3 Control Unit of the Converter

The control system of power converter is based on Digital signal processor TMS320F28335 by Texas Instruments. This processor provides sufficient computing power (150MMACS, 300 MFLOPS) and has a wide range of on-chip peripherals. There is also very useful possibility of debugging the system in real time by JTAG interface. The control system consists of three main printed circuit boards, which can be called: control board, digital board and analogue board. A short description of each part of the control system and their features are introduced.

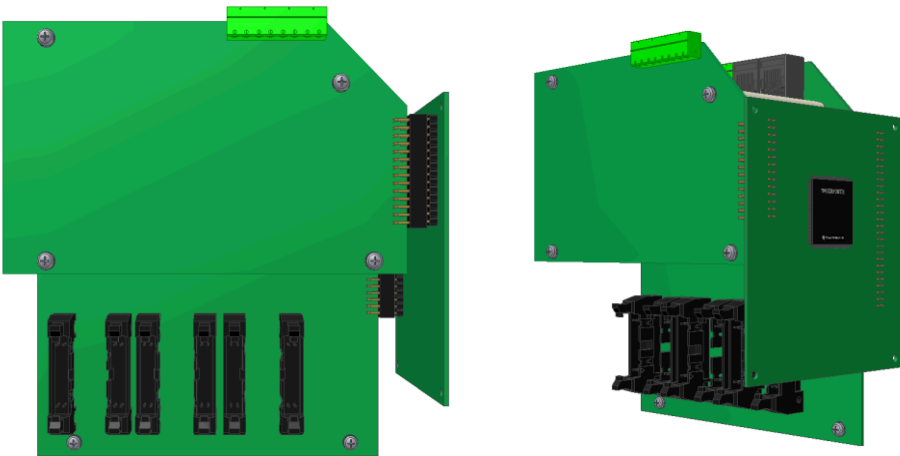


Fig. 3. CAD model of control system

Control board:

- DSP TMS320F28335
- Processor voltage regulator (3.3V)
- Serial port to USB converter
- Four-channel unipolar D/A converter
- 256k x 16 SRAM memory

Digital board:

- Power supplies for DSP and other circuits
- Signal power adaptation circuit between the processor's PWM modulator and IGBT driver
- Single-chip controller for measuring the IGBT temperature and flow rate of the cooling fluid
- Communication interface 1 x RS-485
- Possibility of external PWM retiming
- Complex failure management system – for error detecting and blocking of the inverter

Analogue board:

- 16 analog inputs for D/A converter with possible voltage range from -5 V to 5 V
- Amplifier for the output signals of the D/A converter with possible voltage range from -10 V to 10 V

The control and digital boards are both designed as a four-layer PCB due to the size and the large number of placed components. Power supply of whole control system is ensured from external source 24V. Switching converters which are placed on digital board transform this voltage to required voltage levels. Power supply for the analog board is isolated from other supply branches in order to prevent the spread of noise generated during operation of digital circuits.

5 Application Development Tools

A simple user interface in LabVIEW was created because of the need to enter values of input variables, visualize measured values, indicate possible fault conditions and other functions. The interface contains a number of control elements, which can control for example start and PWM pulses blocking, erasure flag errors from IGBT drivers, change the scale of displayed signals, etc. Connection between computer and control system is provided via a serial line.

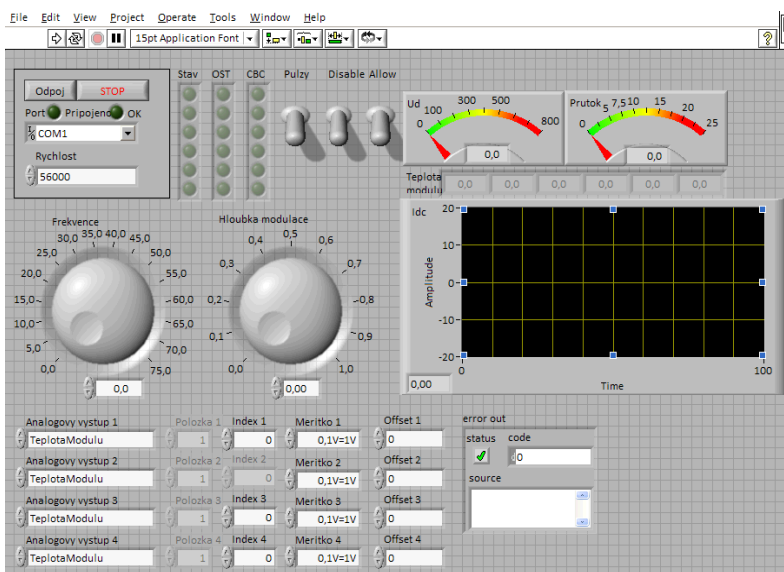


Fig. 4. Example of user interface designed for testing converters

For creating control algorithms the Code Composer Studio (CCS) is used. This application is designed for the development and implementation algorithms for the Texas Instrument DSP. CCS has a lot of features which simply allow to developing many applications. Very useful are supported libraries, header files and peripheral examples for new users. The code can be used as a basis for development platform and new user can quickly experiment with different peripherals. Well-arranged bit field and register-file oriented structure approach is used for accessing to registers.

6 Conclusion

This paper shows basic information about proposed control unit for reversible voltage inverter and its application range. The following is a basic description of chosen vector control method, which ensures possibility to operate the inverter in desired modes. The last part of this paper describes application development tools, which are necessary for creating and debugging control algorithms and for communicating with user. The control algorithm was implemented in the control unit and the power converter was tested in laboratory conditions. The next stage will be focused on testing the converter in industrial conditions and improving the control and user's software.

References

1. Vaculik, P., Havel, A., Tvrdon, M., Hromjak, M.: The Design and Construction of a Reversible Voltage Inverter Prototype. In International Scientific Conference EPE 2012, Brno, Faculty of Electrical Engineering a Communication, Department of Electrical Power Engineering, 2012, vol. 13., ISBN 978-80-214-4514-7.
2. Malinowski, M.: Sensorless Control Strategies for Three - Phase PWM Rectifiers, Ph.D. Thesis, Warsaw University of Technology, Poland, 2001.
3. Texas Instruments, TMS320F28335 Manual [online]. Av. from: <<http://focus.ti.com>>.
4. Fukuda, S. Ito, T.: Modeling and control of PWM voltage source rectifier with a buck-boost characteristic in its output. Industry Applications Conference, 1999. Thirty-Fourth IAS Annual Meeting. Conference Record of the 1999 IEEE, Phoenix, AZ, ISBN 0-7803-5589

Acknowledgments

This article has been supported by SGS SP2012/126 - Reversible converters for accumulation of electric energy and by ENET – Energy Units for Utilization of non Traditional Energy Sources.

Sensorless Control Simulation of Switched Reluctance Motor Using HIL Method

Petr Krňa

Department of Electronics, FEECS,
VŠB – Technical University of Ostrava, 17. listopadu 15, 708 33 Ostrava – Poruba
petr.krna@vsb.cz

Abstract. This work deals with sensorless control simulation of Switched reluctance motor using Hardware in the loop method. Sensorless control principle in this work is based on internal simulation model, which is controlled by sensors. This model with its parameters is very similar to the external motor in which the control pulses are fed the same as the internal model. The whole system has feedback loop. If there are some unequal of feedback variables (i.e. phasing current) is adds or subtracts appropriate torque to internal model of switched reluctance motor, and it adapts to external conditions. Possibilities of using HIL are very wide. It applies wherever there is the practical testing of control systems capital intensive and time consuming, i.e. in aviation, military and other industries. This simulation method extends the classical simulation by the real control system and the simulation is close to the real world.

Keywords: SRM, HIL, magnetic flux, torque.

1 Introduction

Electrical drives with SRM are characterized especially by their simple construction, low price and high efficiency. In spite of these advantages of the SRM, and the rapidly developing semiconductor and microprocessor technique, the number of commercially produced products is still very low, and to this day there is no universal way of design of electrical drive with switched reluctance motor and its control for a wider area of applications. At present many scientist workplaces try to develop mentioned universal design way of SRM drives.

In the present, SRM are developed for their positive features and parameters. In the past, SRM using was not possible because of the power electronic components and sufficiently fast control systems. Their main advantages are:

- simply construction and robust,
- low machine inertia,
- high torque overload capacity,
- high efficiency over wide speed-range.

1.1 The simulation model of SRM

Figure 1 describes a block diagram of one phase SRM. Switched reluctance motor was assembled according to the mathematical model of engine which with its parameters close to the real engine of the SR90 from company Magma Physics. Each stage contains a three-dimensional function of torque characteristics derived from the actual magnetization characteristics of SR90, which can be seen in Figure 1.

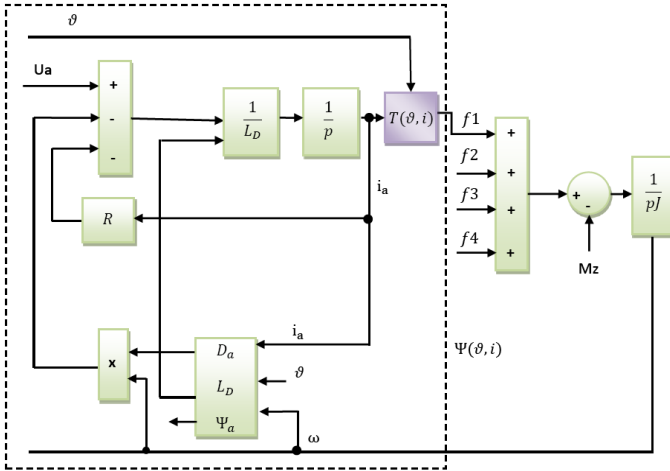


Fig. 1 Block diagram one phase of SRM

2 Hardware in the loop simulation

HIL method is used particularly in applications where is apply of real system expensive and time consuming. It's a case of complex systems in the automotive, aerospace, military, etc. The advantage of HIL simulation is real-time control using a real control system. The realistic of simulation results depends on how well is designed simulation model, which is represented by a computer model. In this work, it was created a computer model of switched reluctance motor 8/6 in Matlab-Simulink. The internal motor is represented by signal processor Freescale MC56F8037.

General block diagram of HIL test method is shown in Figure 2. Individual variables are: $y(t)$... process value, $w(t)$... reference value, $e(t)$... the error, $u(t)$... action variable, $v(t)$... fault value, reg ... regulator.

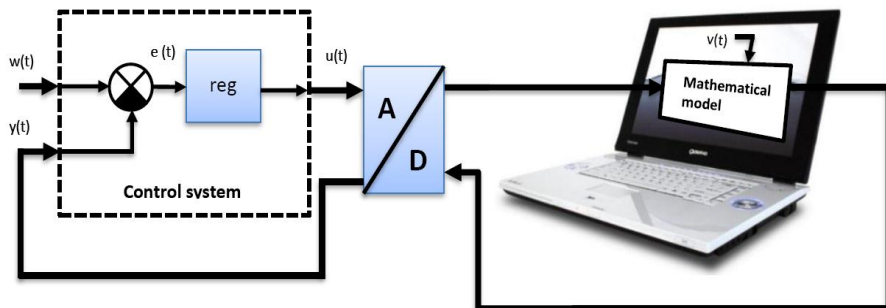


Fig. 2 Block diagram of Hardware in the Loop Simulation.

HIL testing method in this work was commissioned by the multifunction cards MF 624, which connects electronic devices and simulation system. The communication channel between the simulation model and control system is created by the A / D converters. Real control system is the signal processor Freescale MC56F8037.

3 Results of sensorless control SRM

Model of SRM was created in the program Matlab Simulink and it serves as a controlled engine in a closed loop HIL simulation. Input variables are pulses supplied from the signal processor to the model inverter, which controls the motor phases. Variables of engine output are fed to the processor where they are processed. The whole communication coincides between processor and multifunction card MF 624.

The results of sensorless control using HIL methods are in the following figures.

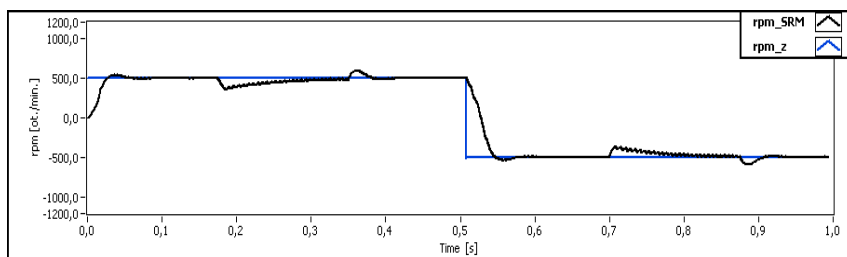


Fig. 3 Change the SRM speed [rpm] from 0/ 500/-500, The actual rpm (black points)

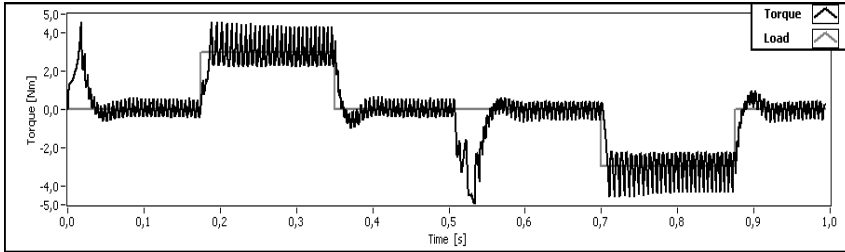


Fig. 4 Torque of SRM [Nm], torque of load (grey points)

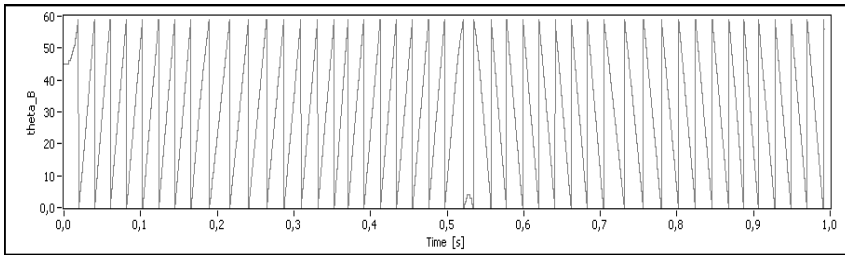


Fig. 5 Theta_B [°].

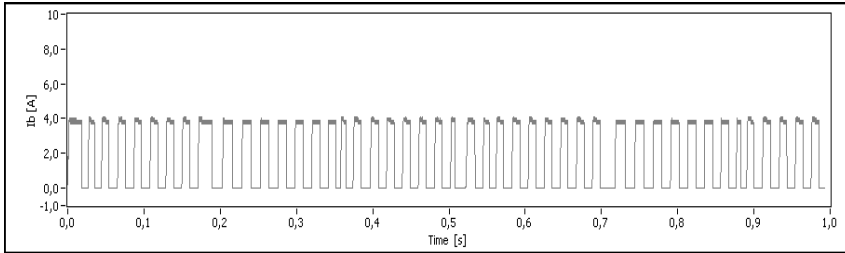


Fig. 6 Current of phase B [A]

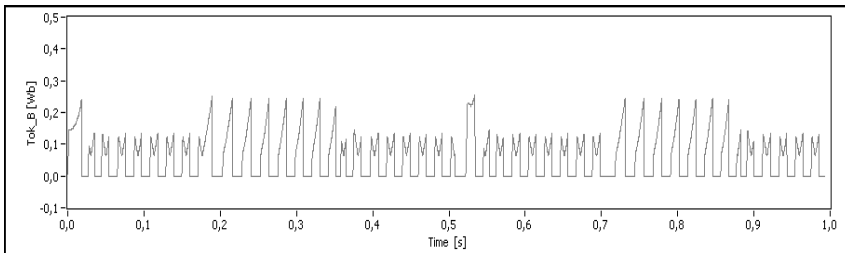


Fig. 7 Magnetic flux of phase B [Wb].

4 Conclusion

This article describes access of the sensorless control switched reluctance motor using HIL simulation. In this work is the control of SRM based on internal engine (engine in signal processor with position sensor), which has the same parameters as the real motor (simulated model in matlab). Circuit parameters (i.e. phase currents) were measured from external motor and they were compared with the parameters of internal engine. If there are some unequal of feedback current is adds or subtracts appropriate torque to internal model of switched reluctance motor, and it adapts to external conditions. Simulation results show a good adaptation of the simulation model engine. The resulting waveforms were sent in the program Labview from company National Instrument.

Acknowledgement

In the paper there are the results of the project SP2011/107 and SP2012/85 which were supported by Student Grant Competition of VSB-Technical University of Ostrava. This research was supervised by Prof. Ing. Pavel Brandstetter, CSc.

References

1. Brandštetter, P.: AC variable speed drives - Modern methods of management, Ostrava: VŠB - TU Ostrava, 1999. ISBN 80-7078-668-X
2. TJE Miller, Electronic control of switched reluctance machines. UK: Newness, 2001.
3. T. Miller, Switched reluctance motors and their control. Oxford, UK: Magna Physics . Publishing/Clarendon Press, 1993

Dynamic Voltage Restorer

Lukáš Odlevák

Department of Electronics, FEECS,
VŠB – Technical University of Ostrava, 17. listopadu 15, 708 33 Ostrava – Poruba
lukas.odlevak@vsb.cz

Abstract. The dynamic voltage restorer (DVR) is a series connected device which injects a set of three-phase AC output voltages in series, and in synchronism with the distribution voltages. The DVR employs solid-state switching devices in a pulse-width modulated (PWM) inverter to vary the amplitude and the phase angle of the injected voltages, thus allowing control of the real and reactive power exchange between the distribution system and the load. Energy storage is useful as a source of real power. Otherwise only reactive power could be absorbed or injected, and voltage sags to unity and near unity power factor loads could not be fully compensated.

1 Introduction

Power quality problems have received increasing attention in recent years because of the significant economic impacts they can impinge on industrial customers. One method to enhance supply quality is based on the use of series custom power-compensation technique, an example of which is the DVR. The device is shown to be particularly suitable for mitigating the undesirable impacts of the most common power-quality disturbances known as voltage sags. Essentially, a DVR functions by injecting a voltage component in series with the load voltage so that the load-side voltage is maintained to its nominal level during a voltage disturbance.

Voltage perturbation in the form of sag and swell exists in power systems where generally, voltage sag is defined as a decrease in voltage magnitude of between 0.1 to 0.9pu and a voltage swell is that of over 1.1pu. Presently, most studies on series compensation are focused on applying the technique in mitigating the effects of voltage sags. The main reason is because during voltage sag, there is a decrease in power delivered to loads. Through the actions of protective devices, some of these loads are often automatically disconnected from the supply system. The interruption in supply results in loss of production to customers. Hence, there is considerable interest in finding ways to mitigate the effects of the sags. [1], [2]

2 Power Circuit of DVR

The basic elements in a DVR are illustrated in Fig. 1, with a DVR in series with the supply and load.

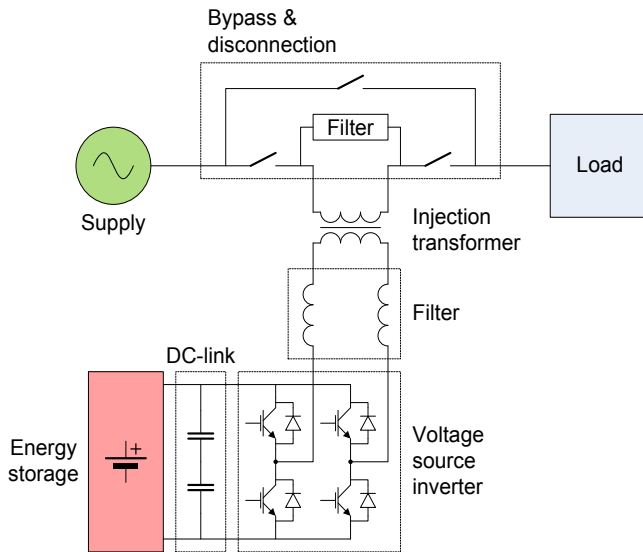


Fig. 1. Power Circuit of a DVR

The power circuit of the DVR can be divided into five parts [3], [4]:

- *Converter:*
The converter type is a voltage source inverter (VSI), which pulse width modulates (PWM) the DC from the DC-link to AC-voltages injected into the system.
- *Injection transformer:*
Injection transformer ensures galvanic isolation and simplifies the converter topology and protection equipment.
- *Passive filter:*
The passive filter is inserted to reduce the switching harmonics generated by the PWM-VSI. The filtering scheme in a DVR can be placed either on the system-side or the inverter-side of the series injection transformer. Moreover, the leakage reactance of the transformer is also used to aid the filtering characteristic.
- *Energy storage:*
Energy storage is required to provide real power to the load when large voltage sags take place. Examples of energy storage are lead-acid batteries, fly-wheel, superconducting magnetic energy storage (SMES), etc.
- *Bypass equipment:*
During faults and service, a bypass path for the load current has to be ensured.

3 Control Method

The two main control methods applied to DVR's are the open loop control and the closed loop control. Closed loop control has the potential of the best performance, but changes in the load leads to a varying system model and the voltage controller must be designed with caution. Open loop load voltage control is often used and combined with feed forward compensation of the voltage drop caused by the line filter and the injection transformer. In this paper closed loop control is used.

Space vector control has been applied to the DVR, hence the ABC voltages have been transformed into a space vector representation:

$$\begin{bmatrix} U_\alpha \\ U_\beta \end{bmatrix} = \frac{2}{3} \begin{bmatrix} 1 & -\frac{1}{2} & -\frac{1}{2} \\ 0 & \frac{\sqrt{3}}{2} & -\frac{\sqrt{3}}{2} \end{bmatrix} \begin{bmatrix} U_A \\ U_B \\ U_C \end{bmatrix} \quad (1)$$

Then the space vector is transformed into a rotating dq reference frame:

$$\begin{bmatrix} U_d \\ U_q \end{bmatrix} = \begin{bmatrix} \cos(\theta) & \sin(\theta) \\ -\sin(\theta) & \cos(\theta) \end{bmatrix} \begin{bmatrix} U_\alpha \\ U_\beta \end{bmatrix} \quad (2)$$

Three basic compensation strategies for a DVR can be stated as [3]:

- *Pre-sag compensation:*
The supply voltage is continuously tracked and the load voltage is compensated to the pre-sag condition. The method gives a nearly undisturbed load voltage.
- *In-phase compensation:*
The generated DVR voltage is always in phase with the measured supply voltage regardless of the load current and the pre-sag voltage.
- *Energy optimized compensation:*
To fully utilize the energy storage, information about the load current is used to minimize the depletion of the energy storage.

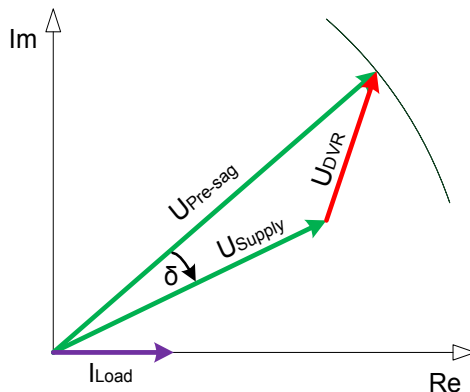


Fig. 2. Pre-sag compensation

4 Simulation

The DVR has been simulated using MATLAB/Simulink with SimPowerSystems software [5]. The balanced 70% voltage sag and related waveforms are shown in Fig. 4. The missing voltages are injected by the DVR from the lead-acid battery.

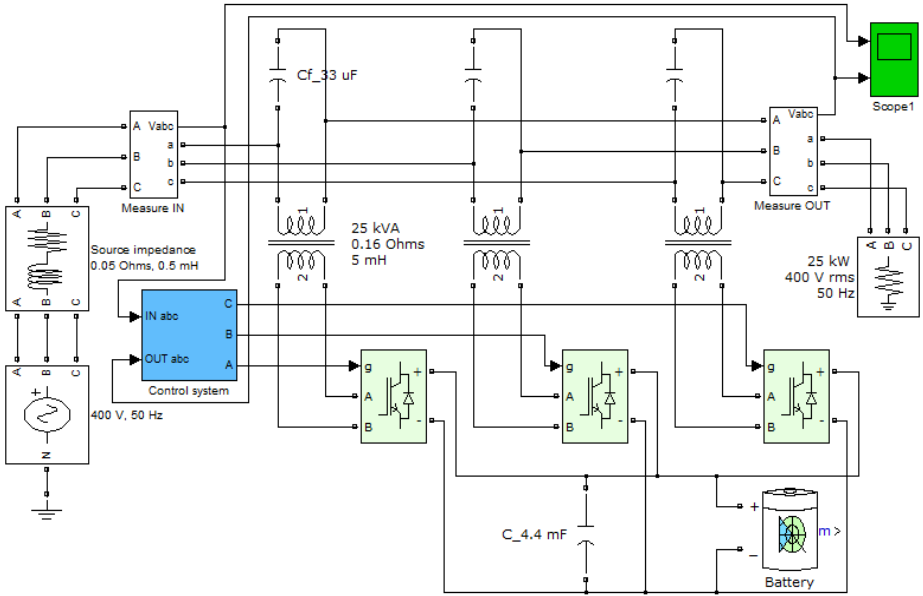


Fig. 3. Simulation model of DVR in MATLAB/Simulink

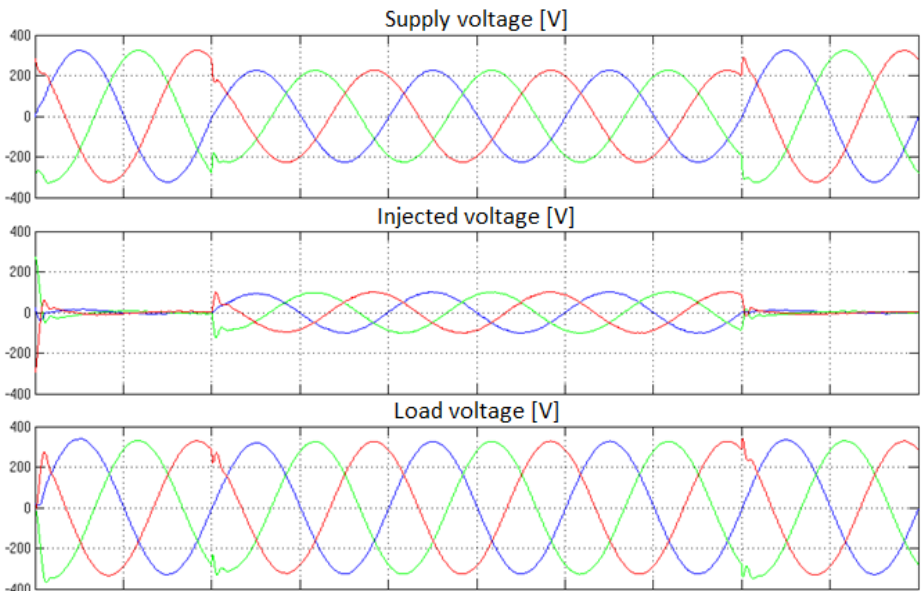


Fig. 4. Simulated 70% voltage sag in time interval of 0.02 – 0.08s

5 Conclusion

The DVR is generally considered as an effective device to compensate sensitive loads from externally disturbances. Voltage sag is a significant disturbance, which may lead to tripping and high cost to sensitive customers. In this paper power circuit of a DVR has been presented, followed by chosen space vector control method. The simulation model containing a power circuit together with a control system has been designed and implemented in MATLAB/Simulink.

Acknowledgement

This article has been supported by the project ENET – CZ.1.05/2.1.00/03.0069: Energy Units for Utilization of non-Traditional Energy Sources.

References

1. Ramachandaramurthy, V.K., Fitzer, Ch., Arulampalam, A., Zhan, C., Barnes, M., Jenkins, N.: *Control of a Battery Supported Dynamic Voltage Restorer*. IEE Proceedings, Vol. 149, No. 5, pp. 533-542, September 2002.
2. Choi, S.S., Li, J.D., Vilathgamuwa, D.M.: *A Generalized Voltage Compensation Strategy for Mitigating the Impacts of Voltage Sags/Swells*. IEEE Transactions on Power Delivery, Vol. 20, No. 3, pp. 2289-2297, July 2005.
3. Nielsen, J.G.: *Design and Control of a Dynamic Voltage Restorer*. PhD Thesis, Aalborg University, Institute of Energy Technology, Denmark, 2002, ISBN 87-89179-42-0.
4. Zhan, Ch., Ramachandaramurthy, V.K., Arulampalam, A., Fitzer, Ch., Kromlidis, S.: *Dynamic Voltage Restorer Based on Voltage-Space-Vector PWM Control*. IEEE Transactions on Industry Applications, Vol. 37, No. 6, pp. 1855-1863, December 2001.
5. The MathWorks, Inc.: *SimPowerSystems™ User's Guide*. USA, September 2011.

Design of Synchronous Machine with Permanent Magnets Using FEM

Ladislav Slíva

Department of Electrical Power Engineering, FEECS,
VŠB – Technical University of Ostrava, 17. listopadu 15, 708 33 Ostrava – Poruba
ladislav.sliva@vsb.cz

Abstract. This article follows on the issue of identification of selected parameters of synchronous machine with permanent magnets. After analyzing and creating SMPM FEM model is one of the options presented shape optimization, i.e., optimal shape design of an interior permanent magnet synchronous motor.

1 Introduction

Electrical machinery belongs to a group demanding disciplines of electrical engineering and are known are more than 100 years. Their theory was first written sometime around 1910 and so far the only rare exceptions, has not changed. Calculation methods are more precise, as well as calculations of cooling, ventilation calculations, mechanical calculations, and even machine parts. Using quality materials (particularly insulation), the performance of machines increase.

Not only at home but also abroad with both universities and private companies engaged in the improvement of various electric machines, especially the modern ones. In modern electric machine can be regarded as a synchronous machine with permanent magnet. Its use in practice gradually expanded and applied to the various electrical drives (trams, electric locomotives, etc.), among others, has a significant role in wind power as a synchronous generator with permanent magnet.

Before you start any engine optimization, you first need to understand its behavior in various configurations, and then find a possible way of optimizing. Can not only optimize the efficiency, which is very popular, but also as torque ripple or induced voltage. Very useful tool for optimization of electrical machines are used principally programs based on finite element method (FEM). Used as the 2D version, and the 3D version.

The actual work is concerned with optimization of synchronous machine with PM. In the first year of study I did identify the parameters of the replacement scheme (calculations, measurements, FEM) and also used the magnetostatic analysis in programming environments Ansys Workbench for the analysis of 3D magnetic circuit. Now follows the work already optimized geometry of the rotor itself.

2 Synchronous Machine with Permanent Magnets

Permanent-magnet synchronous motors (PMSM) have higher torque to weight ratio as compared to other AC motors. There are different rotor topologies that divide into two basic types, i.e., Exterior Permanent Magnet motors (EPM) and Interior Permanent Magnet motors (IPM). Surface mounted Permanent magnet synchronous motor (SPMSM) and inset permanent magnet motor, belong to former and buried or interior type permanent magnet synchronous motor (IPMSM) and flux concentration or spoke type permanent magnet synchronous motor, belong to the latter. Because of the mechanical and electromagnetic properties of each type, different topologies have different advantages and disadvantages used in high speed applications. They have different control strategies and there is usually torques, speed, angular position and current-control loops in the control system. [1], [2]

Interior permanent magnet synchronous motor, has many advantages over other permanent magnet synchronous motors. It has usually larger quadrature axis magnetizing reactance than direct axis magnetizing reactance. These unequal inductances in different axes, enable the motor to have both the properties of SPMSM and synchronous reluctance motor (SynchRel).

Instantaneous torque of a brushless permanentmagnet motor has two components, a constant or useful average torque and a pulsating torque which causes torque ripple. There are three sources of torque pulsations. The first is field harmonic torque due to non-ideal distribution of flux density in the airgap, i.e., nonsinusoidal in the PMSM . The second is due to the cogging torque or detent torque caused by the slotted structure of the armature and the rotor permanent magnet flux. The third is reluctance torque, produced due to unequal permeances of the d and q axis. This torque is produced by the self inductance variations of phase windings when the magnetic circuits of direct and quadrature axis are unbalanced. In IPM synchronous motor, the effective airgap length on the d axis is large so the variation of the daxis magnetizing inductance, due to magnetic saturation, is minimal. For the q axis, there is an inverse condition, i.e., the effective airgap length on the q axis is small and therefore the saturation effects are significant (Fig. 1). [2]

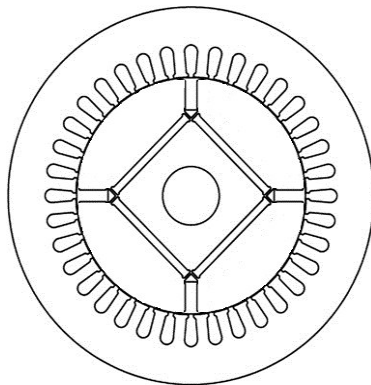


Fig. 1. Cross-section of synchronous machines with PM on the axis d and q

3 Design of Interior Permanent Magnet Synchronous Machine

Proposed method present a shape design optimization method to reduce cogging torque of an IPM synchronous motor using the continuum finite elements sensitivity analysis combined with FEM. It is used the finite element nodes on the rotor outer surface as control points and used the B spline curves to relate design variables vector and control points vector to each other. There is only a slight difference between initial shape and final shape of rotor outer surface. [2]

The proposed optimal design method in this part is industrially applicable to the rotor and motor drive operation is considered too. The optimal shape is evaluated at different load conditions which shows good improvement in all loading conditions. Electrical circuits' equations of different stator windings and rotor mechanical motion equations are coupled to magnetic field equations, to obtain a comprehensive model for the IPM motor drive. The optimal shape design is obtained based on addition of three circled type holes that are drilled in the rotor iron.

To reduce the pulsation torque, which consists of cogging torque and torque ripples, it is necessary to redistribute the flux in rotor. For flux pattern optimization, it needs to change the iron and air combination in a practical approach. In this research, small holes have been drilled in the flux path at rotor surface (Fig. 2). The place and radius of these holes are found to minimize the torque pulsations. [3], [4]

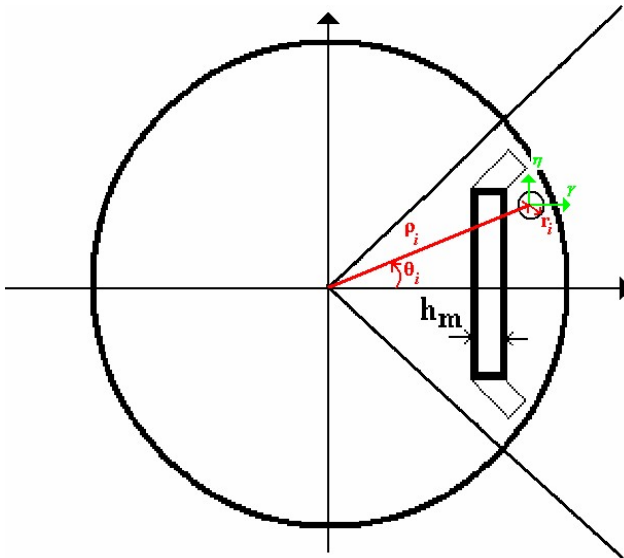


Fig. 2. The model used to optimize the IPM synchronous machine

A first order optimization method is used and this constrained problem is translated into an unconstrained one using penalty functions. Each iteration is composed of subiterations that include search direction and gradient (derivatives).

The d-q components of the reference currents that were calculated according to the method described in section 2, are used for estimation of phase currents. So the reference currents, $i^*(t)_A$, $i^*(t)_B$ and $i^*(t)_C$ will be applied to the FEM model, according to Fig. 3. [4]

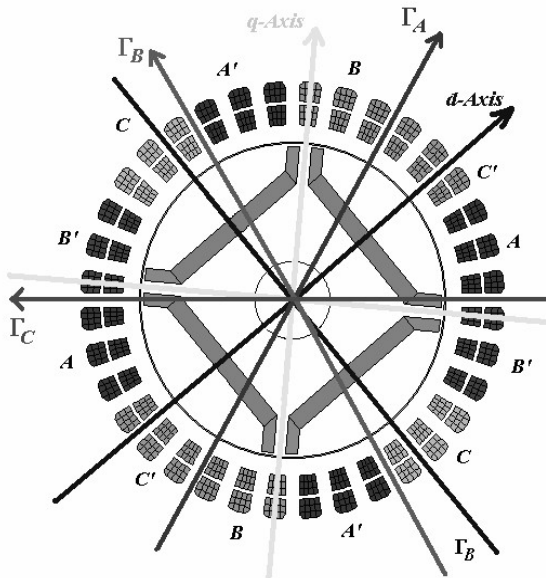


Fig. 3. Cross section of the IPM synchronous motor based on different phase mmf axes

Fig. 4 shows equipotential lines for the magnetic vector potential solutions at a time obtained by time stepped FEM. Fig. 5 presents different wave forms of motor torque, corresponding to different rotor shapes, for the operational point A. Fig. 6 shows the spectrum of curves shown in Fig. 5. In this Fig., curve 1 is the motor torque and the rotor has no holes, curve 2 presents the output torque of motor when three equal area circles are created on the rotor and curve 3 shows the rotor torque when three optimized circles are drilled into the rotor. [4]

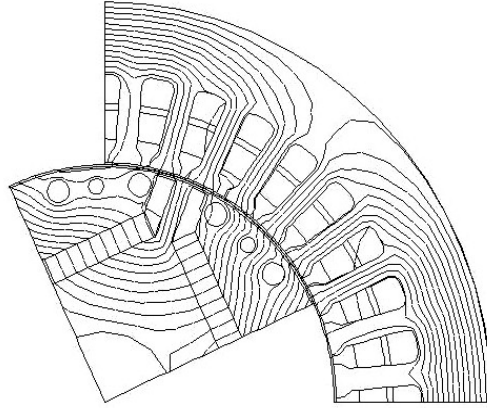


Fig. 4. Equipotential lines: flux distribution (full load condition) at time $t=0.556$ S, after creating optimal circular holes

It can be seen that there is a valuable improvement both in performance index, torque pulsations and saliency ratio. This new shape of the rotor with optimized holes, has the advantage of increasing the maximum speed for the field weakening region from almost 1.83 p.u. to 1.96 p.u. above the base speed. Optimal shape design of rotor has large effect on reduction of torque pulsations of IPM synchronous motor. [4]

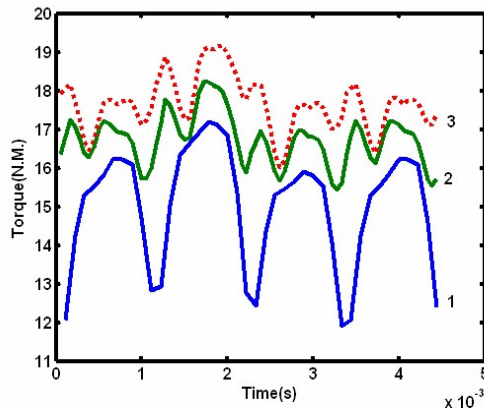


Fig. 5. Comparison of electromagnetic torque calculated by FEM for different rotor structures: no holes on the rotor, curve 2: same holes on the rotor and curve 3: optimized holes on the rotor

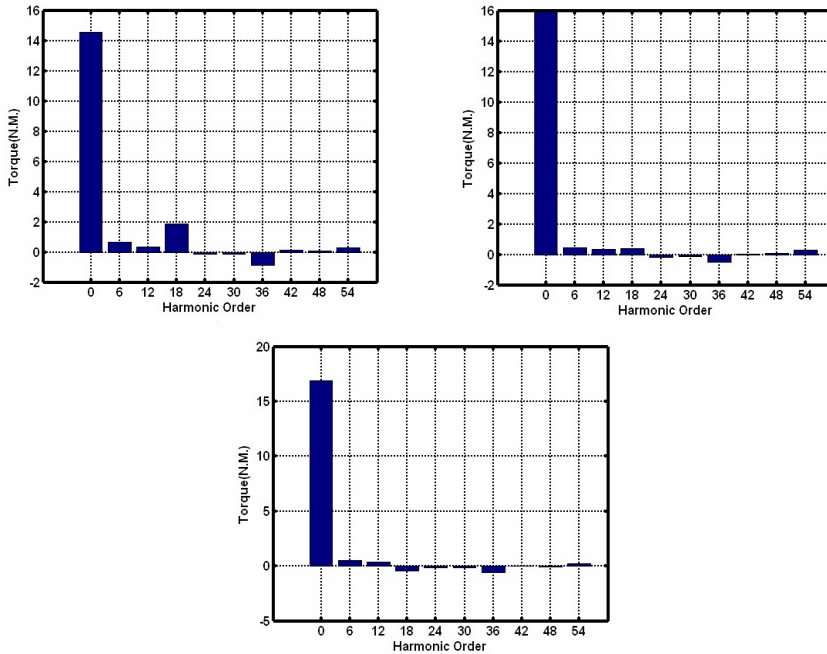


Fig. 6. Spectrum of three curves shown in Fig.5, curve 1: no holes on the rotor, curve 2: same holes on the rotor and curve 3: optimized holes on the rotor

4 Conclusion

Optimization has been carried out by drilling internal circular holes of optimal radius in the flux path at rotor surface. The torque curves of the optimized motor show lower pulsating torque and higher average torque. Another advantage is that the field weakening region has been extended for optimized motor. Although the shape optimization is done at nominal operation point, the performance evaluation of optimized motor at other operation conditions shows improvement too. The new shapes are easily applicable in the factory by drilling the holes of different radius at predetermined positions.

References

- 1 Hrabovcová, V., Rafajdus, P., Franko, M., Hudák P.: *Measurements and modeling of electric machines*. 2nd. ed., Zilina, 2009, ISBN 978-80-8070-924-2.
- 2 Gieras, F.J., Wing, M.: *Permanent magnet motor technology*. 2nd ed., Dekker, 2002, ISBN: 0-8247-0739-7.
- 3 Pyrhonen, J.; Jokinen, T.; Hrabovcová, V.: *Design of Rotating Electrical Machines*. 1st ed., John Wiley & Sons Ltd., 2008, ISBN: 978-0-470-69516-6.
- 4 Ruzojic, B. ; Zarko, D.; Ban, D.: *Interior permanent-magnet motor for ship propulsion, design and testing*, Power Electronics and Applications. 2009. EPE 09. ISBN: 978-1-4244-4432-8.

Second Order Low-Pass and High-Pass Filter Designs Using Method of Synthetic Immittance Elements

Lukas Klein

Department of Electronics, FEECS,
VŠB – Technical University of Ostrava, 17. listopadu 15, 708 33 Ostrava – Poruba
lukas.klein@vsb.cz

Abstract. The paper briefly describes the basics of frequency filter design method using synthetic immittance elements with current conveyors. An introduction of paper explains the advantages and also disadvantages of using this method. Other chapters briefly introduce a design process of simple second order low-pass and high-pass filter. A theory of current conveyors is discussed too, because they are the basic building blocs of proposed synthetic element and also active frequency filters. Finally, the particular solutions of low-pass and high-pass filters are given and verified by OrCAD PSpice simulations.

1 Introduction

Current conveyor can be considered well-known active element. However, this electronic building block is still waiting for its user expansion since 1968 [1]. Currently, new applications using current conveyors were proposed [2]. Current conveyors are applied not only in the basic electronic circuits, but also in more comprehensive circuit structures. One of the many areas of electronics, where current conveyors can be successfully used, are active frequency filters [3].

Current conveyors can be described as modern active elements. They have three types of terminals. Terminals labeled X represent current inputs and simultaneously voltage outputs with positive or negative transfer of voltage from terminal Y, terminals Y are voltage inputs. Terminals Z represent current outputs with positive or negative transfer of current from terminal X [1]. Schematic symbol of current conveyor is shown in Fig. 1. The advantages of current conveyor include low voltage supply, wide frequency range, improved noise immunity [2]. The main disadvantage of current conveyors is their low commercially availability. Current conveyors are also used for realization of synthetic immittance elements of higher orders as this paper describes. Synthetic immittance elements [4] are comprised of serial or parallel circuitries of elementary dipoles of D type or E type. There are four types of synthetic immittance elements. Synthetic elements DS and DP are serial respectively parallel circuitry of D type elementary dipoles and synthetic elements ES and EP are serial respectively parallel circuitry of E type elementary dipoles [4].

All above-mentioned theoretical knowledge was used to realize basic applications of frequency filters – second order low-pass and high-pass.

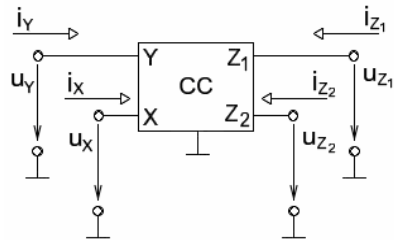


Fig. 1. Schematic symbol of four-port current conveyor

2 Synthetic Immittance Elements Design

Synthetic immittance element design process starts by the general circuit network proposition. This circuitry consists of nine passive elements (admittances) and one general four-port current conveyor (GCC). Necessary number of admittances to realize the synthetic element is three. Therefore all remaining admittances are removed [3]. Selection of appropriate admittances is random. Then particular values of general four-port current conveyor coefficients a , b , c_{11} , c_{22} are added. These coefficients can take discrete values $a = \{-1; 1\}$, $b = \{-1; 0; 1\}$, $c = \{-1; 1\}$ [2]. Suitable passive elements type choice is then final step to propose synthetic immittance element solution.

There were found several circuit structures suitable for synthetic immittance elements realization. Particular solution of one of them is presented in following text. Particular solution of circuit suitable for realization of synthetic immittance element of DP or EP type is shown in Fig. 2.

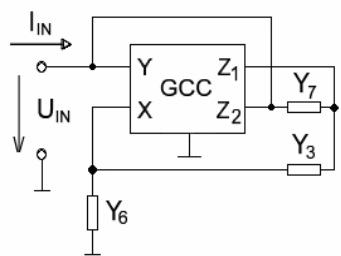


Fig. 2. General circuit structure suitable for implementation of synthetic immittance element

This circuitry consists of three selected admittances and one GCC. General input admittance of the circuit solution has form:

$$Y_{IN} = \frac{Y_3 Y_7 - Y_3 Y_7 a + Y_3 Y_7 b - Y_3 Y_7 ab + Y_3 Y_7 c_{11} - Y_3 Y_7 a c_{11} + Y_3 Y_7 c_{22} - Y_3 Y_7 a c_{22} - Y_3 Y_7 ab - Y_3 Y_7 a c_{22} - Y_6 Y_7 ab - Y_6 Y_7 a c_{11} - Y_6 Y_7 a c_{22}}{Y_3 ab + Y_3 c_{11} + Y_7} \tag{1}$$

This equation has suitable form for following implementation of DP or EP type synthetic element [3]. Another step is substitution of current coefficients which define particular type of current conveyor. There were chosen coefficients $a= 1, b= 0, c_{11}= -1, c_{22}= -1$, which define non-inverting negative four-port current conveyor CCII-/- [2]. This modification affects and simplifies input admittance of circuit. Changed equation then has form:

$$Y_{IN} = \frac{Y_6 Y_3}{Y_7} + 2Y_6 \tag{2}$$

Final step in the synthetic element design process is suitable choice of passive elements (resistors, capacitors) and their substitution on the places of general admittances [4]. Resulting circuitry of second order synthetic immittance element of DP type is shown in Fig. 3.

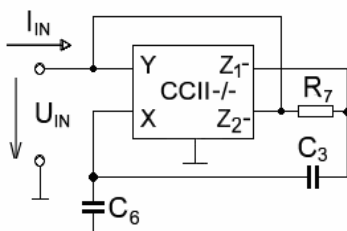


Fig. 3. Second order synthetic immittance element of DP type

Characteristic input admittance is defined by equation of form:

$$Y_{IN} = p^2 R_7 C_3 C_6 + 2p C_6 \tag{3}$$

3 Frequency Filters with Synthetic Immittance Elements

Second order low-pass is shown in Fig. 4. This solution of frequency filter use synthetic element shown in Fig. 3 in its circuit structure. Low-pass filter was created by substitution of synthetic element into the general structure of voltage divider. There was added also first order passive low-pass into the structure of second order active low-pass because of shaping of amplitude frequency response at higher frequencies.

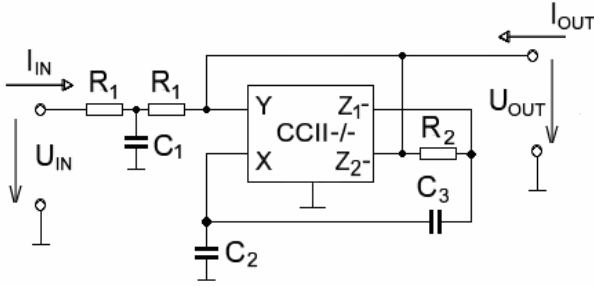


Fig. 4. Second order low-pass filter with synthetic immittance element

Transfer function of resulting circuit structure of second order low-pass filter is described by equation:

$$K_U(p) = \frac{1}{p^3 2R_1 R_2 C_1 C_2 C_3 + 2p^2 (R_1 R_3 C_2 C_3 + 2R_1 C_1 C_2) + p(4R_1 C_2 + R_1 C_1) + 1} \quad (4)$$

From the transfer function then can be derived the design formulas of passive elements of active filter. These formulas have forms:

$$R_1 = \frac{c_{21}}{4\omega_0 C_2}, \quad R_2 = \frac{2c_{22}}{\omega_0 c_{21} C_3} \quad (5a,b)$$

There was chosen Butterworth approximation and cut-off frequency 1MHz for the filter. Coefficients of second order Butterworth approximation take the values $c_{21}=1.4142$ and $c_{22}=1$. There were calculated the following values of passive elements: $C_1=270\text{pF}$, $C_2=100\text{pF}$, $C_3=100\text{pF}$, $R_1=560\Omega$ and $R_2=2.2\text{k}\Omega$.

Second order high-pass filter was also proposed. Circuitry of high-pass solution is shown in Fig. 5.

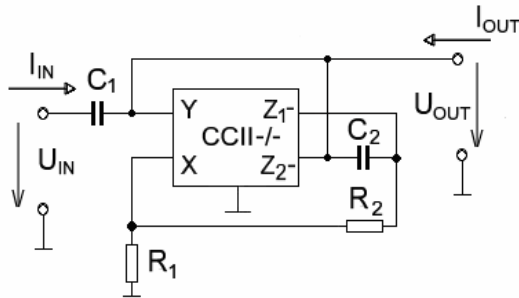


Fig. 5. Second order high-pass filter with synthetic immittance element

In this case, there were again chosen Butterworth approximation and cut-off frequency 1MHz. Design formulas are based on transfer function of frequency filter. Transfer function has form:

$$K_U(p) = \frac{p^2 R_1 R_2 C_1 C_2}{p^2 R_1 R_2 C_1 C_2 + 2pR_2 C_2 + 1} \tag{6}$$

Design formulas of passive elements then have forms:

$$R_2 = \frac{c_{21}}{2\omega_0 C_2} , R_1 = \frac{2c_{22}}{\omega_0 c_{21} C_1} \tag{7a,b}$$

Second order high-pass has the resulting values of passive elements $C_1=100\text{pF}$, $C_2=100\text{pF}$, $R_1=1.1\text{k}\Omega$ and $R_2=2.2\text{k}\Omega$.

The frequency responses of second order low-pass and high-pass express the dependence of filter gain or phase vs. changing frequency. The final amplitude and phase frequency responses were simulated using PSpice. There was used Monte Carlo simulation to proof the influence of passive elements tolerance in to the amplitude and phase frequency responses. The resulting amplitude and phase frequency responses of low-pass are shown in Fig. 6. Amplitude and phase frequency responses of high-pass are shown in Fig. 7.

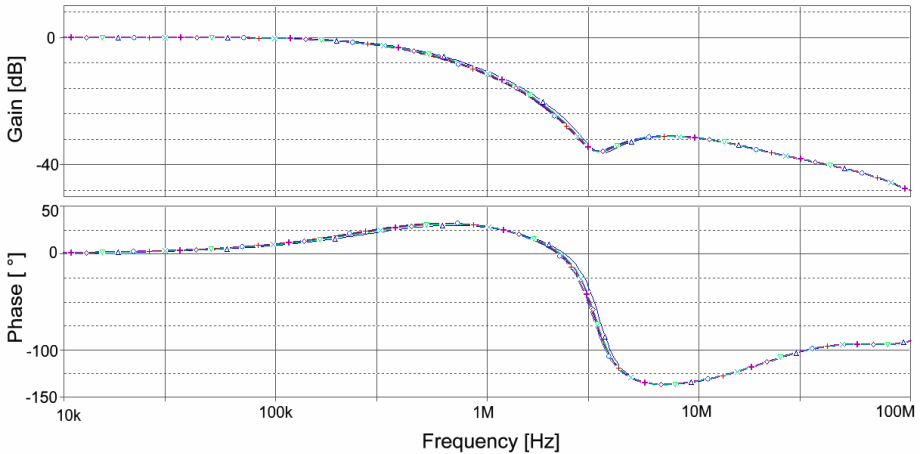


Fig. 6. Amplitude and phase frequency response of second order low-pass filter

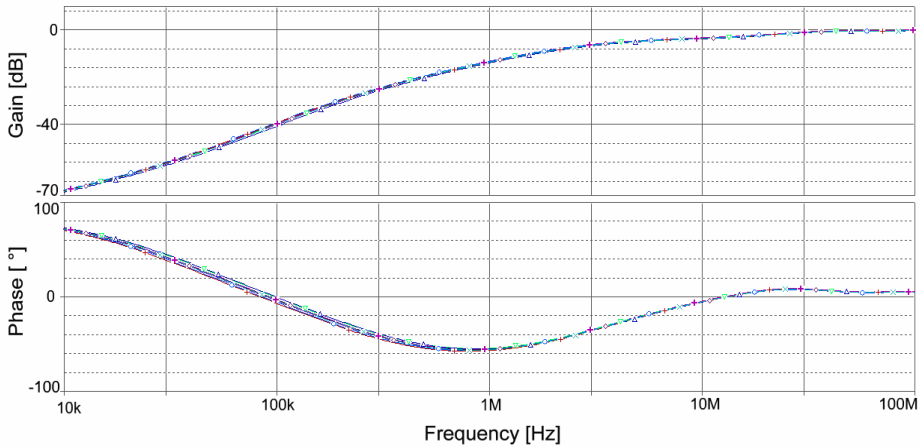


Fig. 7. Amplitude and phase frequency response of second order high-pass filter

4 Conclusion

Resulting characteristics show, that the use of synthetic immittance elements with current conveyors is possible in the circuit structures of frequency filters and brings certain advantages. The main advantage is the possible use at higher frequencies. The theoretical design method is not very complicated.

On the other side, final results also present issues, which can occur in the design. Passive low-pass in the circuit of second order active low-pass can change the position of cut-off frequency. The main disadvantage is commercial unavailability of current conveyors. Despite these facts, synthetic immittance elements with current conveyors appear very perspective.

References

1. Smith, K.C., Sedra, A.: A second generation current conveyor and its applications. *IEEE Transactions on Circuit Theory*. Vol. 17. (1970) 132–134, ISSN 0018-9324
2. Brandstetter, P., Klein, L.: The Applications of non-inverting positive second generation current conveyor as a commercially available versatile active element. *ICSES'10*. (1970) 157–160, ISBN 978-1-4244-5307-8
3. Koton, J., Vrba, K.: Generalized methods for frequency filters design. *Elektrorevue* [online]. Available at WWW: <http://www.elektrorevue.cz>. Brno (2008)
4. Sponar, R., Vrba, K.: Synthetic dipole elements with higher-order immittances in frequency filters with current conveyors. *Elektrorevue* [online]. Available at WWW: <http://www.elektrorevue.cz/clanky/04013/index.html>. Brno (2004)

Analysis of FFT Algorithms for DSP Texas Instruments

Josef Opluštil

Department of Electronics, FEECS,
VŠB – Technical University of Ostrava, 17. listopadu 15, 708 33 Ostrava – Poruba
josef.oplustil@vsb.cz

Abstract. This paper deals with analysis of several FFT algorithms and analyses speed and efficiency of these algorithms for using in DSP TMS320F28335 made by Texas Instruments. Result of this paper is the table which contains time demands of these algorithms. Analysis is focused especially to small length of data.

Keywords: DFT, FFT, Radix2, Radix4, DIT, DIF, DSP, Texas Instruments.

1 Introduction

Calculation of frequency spectrum is important part of frequency converters, power active filters and regulation algorithms. It is good to know the frequency spectrum to check whether converter works properly, because it is important to provide output waveform which is most similar to harmonic waveform with fundamental frequency. If we want to connect our converter to power grid this is very important thing. Nowadays the most of converters use digital signal processors (DSP) to control the converter and pulse width modulation to obtain the output waveform. Some types of DSPs are designed especially for this purpose. They are including AD converters, PWM modules, timers and peripheral circuits on one chip and we don't need to add any other circuits.

DSPs, which can be currently used, have speed of hundreds MFLOPs and their AD converters can operate on frequency of hundreds MHz. Speed of AD converters is not so important because the speed which can react the load is limited and depends on its power. Higher power means lower frequency.

2 Basic methods

2.1 Discrete Fourier Transformation (DFT)

Discrete fourier transformation serves to conversion of input digital signal from time domain to frequency domain. This conversion is described by following expression.

$$X_k = \sum_{n=0}^{N-1} x_n \cdot e^{-i \cdot 2\pi \frac{k}{N} n} \quad (1)$$

X_k is array of components of frequency spectrum, x_n is array of input samples and N is number of input samples. For calculation of this equation in DSP we need to modify it. DSP can't calculate with complex number so we have to divide this equation by Euler's formula to real and imaginary part and then compute each part separately.

$$\begin{aligned} X_k &= \sum_{n=0}^{N-1} x_n \cdot e^{-i \cdot 2\pi \frac{k}{N} n} = \\ &= \sum_{n=0}^{N-1} x_n \cdot \cos\left(2\pi \frac{k}{N} \cdot n\right) + x_n \sin\left(2\pi \frac{k}{N} \cdot n\right) \end{aligned} \quad (2)$$

$$X_{kRe} = \sum_{n=0}^{N-1} x_n \cdot \sin\left(2\pi \frac{k}{N} \cdot n\right) \quad (3)$$

$$X_{kim} = \sum_{n=0}^{N-1} x_n \cdot \cos\left(2\pi \frac{k}{N} \cdot n\right) \quad (4)$$

Results of these equations are two arrays of real and imaginary components for individual frequencies. Calculation of sine and cosine can be performed by lookup table or any other way but lookup table is the fastest way.

In this method we don't need to calculate whole equations in every step but we can calculate part of it ahead. We can calculate $2\pi \frac{k}{N}$ for every k and we can use this result n times.

Also we can use the fact that frequency spectrum is symmetrical for real signals and we need to calculate only one half of spectrum. We can simply improve efficiency of this algorithm by this way.

3 Fast Fourier transform (FFT)

The FFT algorithms are based on division of input or output components to smaller parts for which we calculate DFTs separately and then we put the results together. The most common methods divide the components to two or four parts. If we divide input samples it is called Decimation in Time (DIT) and if we divide the output samples it is called Decimation in Frequency (DIF).

3.1 Decimation in time Radix 2

For calculation of classical DFT we need N^2 multiplications. The principal of acceleration in this method lies in division the input samples to odd and even samples and now we can calculate two DFTs for them. Now we need only $2(N/2)^2$ multiplications. The original equation is divided like this:

$$X(k) = \sum_{n=0}^{\frac{N}{2}-1} x(2n) \cdot e^{-i \cdot 4\pi \frac{k}{N} n} + \sum_{n=0}^{\frac{N}{2}-1} x(2n + 1) \cdot e^{-i \cdot 4\pi \frac{k}{N} (n+1)} \tag{5}$$

This equation can be further rearranged to:

$$X(k) = \sum_{n=0}^{\frac{N}{2}-1} x(2n) \cdot e^{-i \cdot 4\pi \frac{k}{N} n} + e^{-i \cdot 2\pi \frac{k}{N}} \cdot \sum_{n=0}^{\frac{N}{2}-1} x(2n + 1) \cdot e^{-i \cdot 4\pi \frac{k}{N} n} \tag{6}$$

We can divide this equation to odd and even components more and more until we get only 2 components and we achieve only $N \cdot \log_2 N$ multiplications. Expression $e^{-\frac{i \cdot 2\pi}{N}}$ is called Twiddle factor and it is representing vector rotation. It can be marked W_N .

3.2 Decimation in frequency Radix 2

In DIF algorithm we are not dividing the input samples as in DIT but we are calculating the odd and even output samples. The basic equation for this adjustment looks like below.

$$X_r = \sum_{n=0}^{N-1} \left(x(n) + W_2^r \cdot x\left(n + \frac{N}{2}\right) \right) W_N^{rn} \tag{7}$$

As r we substitute $2k$ for even components and $2k+1$ for odd components so we obtain equations for even and odd components like this:

$$X(2k) = \sum_{n=0}^{\frac{N}{2}-1} \left(x(n) + x\left(n + \frac{N}{2}\right) \right) W_N^{\frac{kn}{2}} \tag{8}$$

$$X(2k + 1) = \sum_{n=0}^{\frac{N}{2}-1} \left(\left(x(n) - x\left(n + \frac{N}{2}\right) \right) W_N^n \right) \cdot W_N^{\frac{kn}{2}} \tag{9}$$

We can divide components until we get only two components and demands of this calculation are the same as in previous case.

3.3 Decimation in time Radix 4

With radix 4 we proceed same way as in radix 2 but we are dividing the input sequence to four parts. We can do this division until we get four groups with four components. We can rewrite the original equation to this form:

$$\begin{aligned}
 X(k) = & \sum_{n=0}^{\frac{N}{4}-1} x(4n) \cdot e^{-\left(i \frac{2\pi(4n)k}{N}\right)} + \sum_{n=0}^{\frac{N}{4}-1} x(4n+1) \cdot e^{-\left(i \frac{2\pi(4n+1)k}{N}\right)} + \\
 & + \sum_{n=0}^{\frac{N}{4}-1} x(4n+2) \cdot e^{-\left(i \frac{2\pi(4n+2)k}{N}\right)} + \sum_{n=0}^{\frac{N}{4}-1} x(4n+3) \cdot e^{-\left(i \frac{2\pi(4n+3)k}{N}\right)} \quad (9)
 \end{aligned}$$

If we use twiddle factor instead of expression $e^{-\frac{i \cdot 2\pi}{N}}$ we can write:

$$\begin{aligned}
 X(k) = & \sum_{n=0}^{\frac{N}{4}-1} x(4n) \cdot W_N^{2nk} + W_N^k \sum_{n=0}^{\frac{N}{4}-1} x(4n+1) \cdot W_N^{2nk} + \\
 & + W_N^{2k} \sum_{n=0}^{\frac{N}{4}-1} x(4n+2) \cdot W_N^{2nk} + W_N^{3k} \sum_{n=0}^{\frac{N}{4}-1} x(4n+3) \cdot W_N^{2nk} \quad (10)
 \end{aligned}$$

3.4 Decimation in frequency Radix 4

This algorithm is similar to radix 2 again and it can look like this:

$$X_r = \sum_{n=0}^{N-1} \left(x(n) + W_4^r \cdot x\left(n + \frac{N}{4}\right) + W_4^{2r} \cdot x\left(n + \frac{N}{2}\right) + W_4^{3r} \cdot x\left(n + \frac{3N}{4}\right) \right) W_N^{rn} \quad (11)$$

As r we now substitute 4k, 4k+1, 4k+2, 4k+3 and we obtain following equations:

$$X_{4k} = \sum_{n=0}^{\frac{N}{4}-1} \left(\left(X_n + X_{n+\frac{N}{2}} \right) + \left(X_{n+\frac{N}{4}} + X_{n+\frac{3N}{4}} \right) \right) \cdot W_N^{kn} \quad (12)$$

$$X_{4k+1} = \sum_{n=0}^{\frac{N}{4}-1} \left((X_n + X_{n+\frac{N}{2}}) - i(X_{n+\frac{N}{4}} + X_{n+\frac{3N}{4}}) \right) \cdot W_N^n \cdot W_{\frac{N}{4}}^{kn} \tag{13}$$

$$X_{4k+2} = \sum_{n=0}^{\frac{N}{4}-1} \left((X_n + X_{n+\frac{N}{2}}) - (X_{n+\frac{N}{4}} + X_{n+\frac{3N}{4}}) \right) \cdot W_N^{2n} \cdot W_{\frac{N}{4}}^{kn} \tag{14}$$

$$X_{4k+3} = \sum_{n=0}^{\frac{N}{4}-1} \left((X_n + X_{n+\frac{N}{2}}) + i(X_{n+\frac{N}{4}} + X_{n+\frac{3N}{4}}) \right) \cdot W_N^{3n} \cdot W_{\frac{N}{4}}^{kn} \tag{15}$$

4 Results

Time demands of described algorithms were obtained with help of mathematical software Matlab. From these results we can determine the best algorithm according to the number of input samples. For fully comparison there is also computation time of Matlab function FFT.

Table 1. Time demands of algorithms

N	Time (µs)					
	DFT	Radix2DIT	RADIX2DIF	RADIX4DIT	RADIX4DIF	Matlab
8	88	551	911	505	616	63
16	182	552	858	508	629	62
32	381	613	885	643	1347	67
64	1275	746	1419	634	1371	73
128	4428	1078	2432	1385	4048	87
256	14986	1857	4199	1434	4230	90
512	60187	4218	8664	5480	18134	122
1024	222617	7610	19295	5602	17418	256
2048	913630	14944	45753	22234	84306	281

Because the radix 2 and radix 4 algorithms can compute frequency spectrum only from input arrays with size 2^N and 4^N , respectively, all of these algorithms were modified to compute with any length of input data. This modification lies in widening of input samples by zeros.

5 Conclusion

From the results it is obvious that for small length of data it is better to use classical DFT algorithm and for more than 128 samples it is better to use some of the fast algorithms. In the table 1, there are differences between time demands of DIT and DIF algorithms. From assumption that both of these algorithms should have the same time demands, there is reason to believe that Matlab isn't a good tool to provide reliable results. It is possible that Matlab is using some optimization which can influence the results. For another research it will be better to use some other testing method but for quick view it is sufficient.

In cases when we need to compute only a few components of frequency spectrum there is classical DFT algorithm a best possible solution. In case of power electronics we need to know only some primary components, mostly it is 5 or 7 components and none of the fast algorithms is usable because the computation of 5 components is less demanding than computation of whole spectrum with some FFT algorithm.

References

1. HORÁK, David. *Diskrétní transformace* [online]. 2012. vyd. [cit. 2012-07-17]. Dostupné z: http://mi21.vsb.cz/sites/mi21.vsb.cz/files/unit/diskretni_transformace.pdf
2. MATUSIAK, Robert. Implementing Fast Fourier Transforms of Real/Valued Sequences With the TMS320 DSP Platform. [online]. 2001 [cit. 2012-07-17]. Dostupné z: <http://www.ti.com/lit/an/spra291/spra291.pdf>

Simulations of the Frequency Converter

Josef Opluštil and Roman Šprlák

Department of Electronics, FEECS,
VŠB – Technical University of Ostrava, 17. listopadu 15, 708 33 Ostrava – Poruba
{josef.oplustil, roman.sprlak}@vsb.cz

Abstract. The aim of this article is to present function and structure of the frequency converter. There are some important parts of converters described and there is microcontroller equipment mentioned as well. At the end of this article there are simulation schemes of frequency converter for two types of simulation software – Matlab and PSpice

Keywords: Frequency converter, microcontroller system, simulations, Matlab, PSpice.

1 Introduction

The article deals with analysis of frequency converter and its parts. Frequency converter converts voltage of the utility system to voltage with other parameters. This can help to optimal driving of AC motors.

Changing of the frequency of supply voltage is the best method to control the speed of the asynchronous motor. It is also convenient to vary the magnitude of the voltage due to appropriate magnetization of the motor.

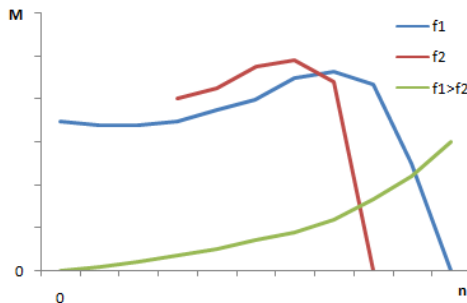


Fig. 1. Torque characteristic of the asynchronous motor

Frequency to voltage ratio leads to torque variations. Therefore, the speed of asynchronous motor varies too. Figure 1 shows the torque characteristic of the asynchro-

nous motor for two frequencies to voltage ratios. With this kind of control, there is no efficiency decrease. [1]

2. Main parts of frequency converter

First part of the frequency converter is rectifier. It can be controlled or non-controlled rectifier. There are two basic types of frequency converters according to DC circuit. Voltage DC circuit uses capacitor to store the energy and current DC circuit uses inductor to store the energy. Energy stored in the DC circuit is converted by the transistor or thyristor bridge to alternating voltage or current at the output. On figure 2 there are block diagrams of two basic types of frequency converters.

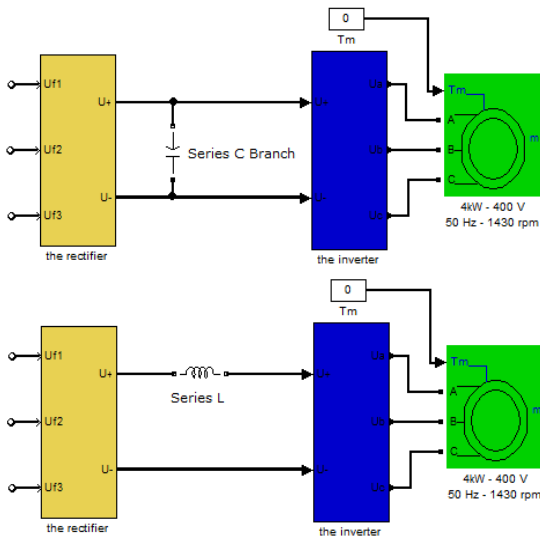


Fig. 2. Block diagrams of frequency converters

2.1 Voltage fed converter

Currently, the most used converters are like on figure 2.a). At the input there is uncontrolled rectifier which is the most economic option. DC link consists from capacitor of large capacity. It can be considered like the load for rectifier and the power source for the output bridge. Switches of the bridge consist from MOS-FETs or IGBTs and from GTOs for the largest powers. [1-2]

2.2 Current fed converter

Basic scheme of the current fed converter is shown on figure 2.b). DC link consists from large inductor which makes the current smooth. The rectifier is usually full controlled. The inverter works with PWM or with rectangular control and uses thyristors. [1-2]

3. Control circuits for frequency converter

So far we spoke about power electronic parts but for the correct function of the converter we need control circuits too. Nowadays, the most converters are controlled by processors. DSPs are the most used to this purpose. These processors are specially made to control the electrical drives. They have AD converters, inputs for sensors and communication circuits so we can connect voltage sensors, current sensors, rotation sensors, display, terminal and lots of other.

4. Design of the frequency converter

Practically, we have 2 possibilities how to design the frequency converter. First one is numerical and second one is simulation.

4.1 Numerical design

To design the frequency converter we have to know the type of the converter. This type depends on desired power of the converter and utilization. From required power we chose types of switches and we calculate their current and power dissipation. Next we calculate DC link according to desired ripple of DC voltage or current. All of these depend on switching frequency and other parameters and we have to look into datasheets for them.

Problem of this method is if we want to change anyone of parameters we need to calculate everything again.

4.2 Simulation design

First step is similar to numerical design – we need to choose the type of the converter. Next we have to draw the simulation scheme. We can draw simplified one or we can draw complete circuits of converter. This isn't necessary if we want to know only a few things from simulation.

To perform the simulation we have plenty possibilities. We chose two most used software – Matlab and PSpice.

5 Simulations

5.1 Simulation in PSpice

PSpice is part of the OrCad software. To perform this simulation OrCad 16.2 was used. All versions of this software are similar but latest version has some improvements in algorithms and precision of calculations.

To perform the analysis we need to draw the simulation circuits first. If we don't want to know exactly all of the values in frequency converter we can use simplified simulation scheme. Simplification lies in substitution of some circuits simpler ones. For example if we don't need to know behavior of the transistor as a switch we can replace him by ideal switch. And we can do more simplifications like this.

On figure 3 there is simplified simulation scheme of the voltage fed frequency converter. This simulation scheme was performed to obtain the output waveforms during PWM modulation.

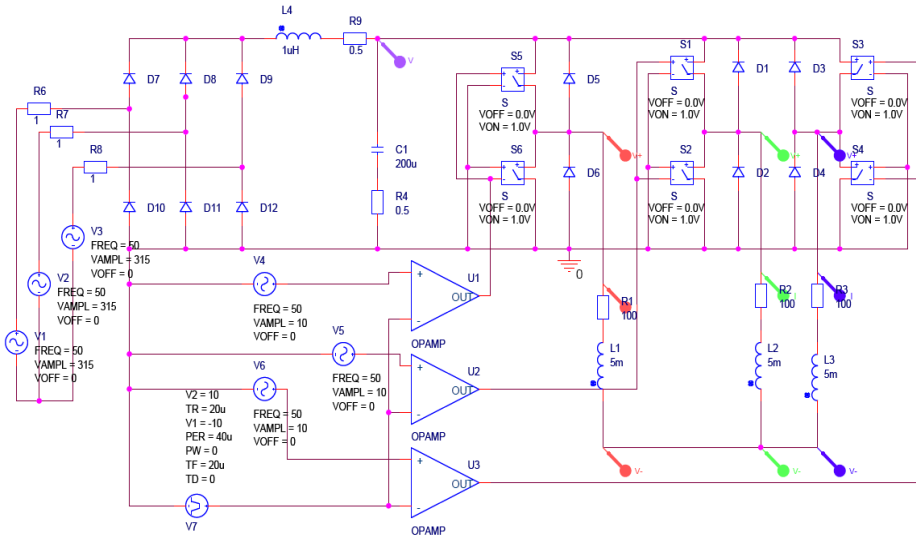


Fig. 3. PSpice simulation scheme

All of the parts used in this simulation were ideal and we added some more parts to achieve the similarity with real ones. This can't be necessary because the PSpice has large library with models of real parts but this is only simplified simulation scheme where we don't need to know all of variables.

In this software we can perform several types of analysis. The most used is Time domain analysis. By this analysis we can watch changes of values depending on time. We can obtain values from simulation by adding the probes to our simulation scheme. There are voltages, current and power probes in PSpice and we can do mathematical operation with these values in addition.

Typical result from time domain simulation shows figure 4.

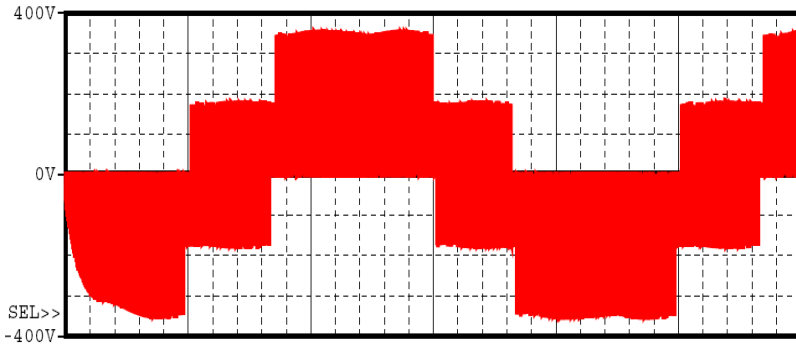


Fig. 4.Results from simulation in PSpice

On the simulation results we can see on figure 4. All of the results correspond to hypothetical waveforms.

5.2 Simulation in Matlab

For electric simulations in Matlab there is the part called Simulink. In this software we can draw simulation schemes by using block diagrams. One big advantage of the Matlab is that we can add some functions to our simulation scheme which can be described only by mathematical expression or conditions like – IF, WHILE, FOR etc. On figure 5 there is simulation scheme of voltage fed frequency converter.

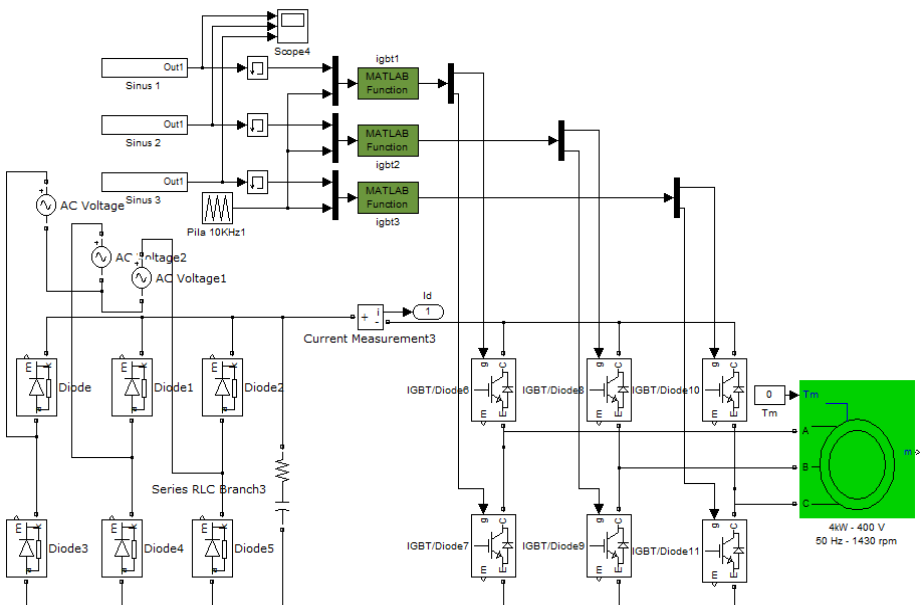


Fig. 5.Matlab simulation scheme

To watch the variables we can use tools called Scope and we can see results in time domain like in PSpice software. Results from simulation can look like below.

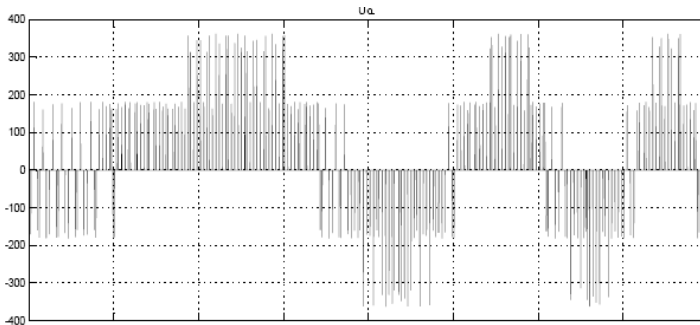


Fig. 6. Matlab simulation results

Another big advantage of Matlab, against the PSpice, is that matlab has whole function blocks like asynchronous motor, synchronous motor etc. in libraries.

7. Conclusion

The aim of this paper was to present the opportunities how to perform the electrical analysis. Principals of simulations in two most common programs are described here briefly. As next, there is simple description of the frequency converter and its parts and possibility of its utilization.

References

1. Brandštetter, P., Střídavéregulačnípohony – Modernízpůsobyrřízení, Ostrava 1999
2. Grinberg, R.,Advanced DC link capacitor technology application for a stiff voltage-source inverter, Vehicle Power and Propulsion, 2005 IEEE Conference, Moscow Power Eng. Inst., Russia ,0-7803-9280-8.
3. Grinberg, R.,Advanced DC link capacitor technology application for a stiff voltage-source inverter, Vehicle Power and Propulsion, 2005 IEEE Conference, Moscow Power Eng. Inst., Russia ,0-7803-9280-9.
4. Chlebis, P., Havel, A., Vaculik, P., Pfof, Z.: Modern Instruments for increasing the Efficiency of the Energy Transfer in Electric Vehicles, 14th EPE-PEMC 2010.

Thermal Field of Heat Sink

Roman Šprlák

Department of Electronics, FEECS,
VŠB – Technical University of Ostrava, 17. listopadu 15, 708 33 Ostrava – Poruba
roman.sprlak@vsb.cz

Abstract. Aim on this paper is an analysis of the water heat sink which is commonly used for cooling in frequency converters with high lost power modules. Therefore, it was created the 3D models of heat sinks. These models were used for thermal simulations with constant power dissipation. From obtained results it was proposed the construction modification of heat sinks. Next simulation of thermal field was created with modification of the heat sink. At the end of this paper there is evaluation of all thermal simulations performed on the heat sinks.

Keywords. heat sink, thermal field, simulation.

1 Introduction

Two different types of cooling are used in frequency converters. First type is represented by a large passive heat sink with fan. This configuration is commonly use in frequency converters which have low power dissipation in modules and their size isn't limited. Second type of cooling is represented by water heat sink. In these heat sinks flows cooling liquid that ensures conduction of thermal energy.

Thermal simulation with heat sink WP16 from the company Semikron was created for this paper. The power dissipation during this simulation was constant. From results of simulation the new structural design of heat sink WP16 was created. Next thermal simulation was performed with the new 3D model created from adjustment of heat sink WP16.

For thermal simulation we must set the initial conditions and other properties which are necessary to create simulations.

2 Heat Transfer Theory

The analysis of the heat transfer combines three basic physical principles: conduction, convection, and radiation. Conduction is a form of heat transfer typical for solids. The heat transfer characteristic is described by Fourier partial differential equation (Fourier PDE) which is explained further in the text below. The Fourier PDE is solved for initial and boundary conditions corresponding to the particular physical problem. [2-3]

According to three basic methods of heat transfer the boundary conditions of Fourier PDE are usually divided into three basic types:

1. The boundary condition of the first kind is usually given by the temperature $T=T(x, y, z, t)$ of a surface.
2. The boundary condition of the second kind is given from a source of density of the heat flow rate $q=q(x,y,z,t)$ at the surface of the body.
3. The boundary condition of the third kind is defined by given ambient temperature. It has the form $Q = \alpha T_A - T_S$, where q is the density of heat flow rate [Wm^{-2}], α is the heat transfer coefficient [$Wm^{-2}K^{-1}$], T_A is the ambient temperature [K], T_S is the temperature of solid surface [K]. [2-3]

3 The 3D Model

The 3D model was created with help of web page www.semikron.com. There is placed the datasheet of heat sink WP16. Model was created in 3D CAD software where the material properties were defined. Then the model was converted through exchange SAT format (SAT is the most common exchange format for 3D models) into the multi-physics software. The thermal simulations were created in multi-physics software by using the finite element method.

Length of the heat sinks was 640 mm. There is the standard heat sink WP16 with IGBT modules on figure 1. On figure 2. there is the experimental heat sink based on WP16. This model was composed from three materials with different thermal capacity. The main part was created from heat sink WP16. The copper plate was added to this part under the IGBT modules. On borders of heat sink the aluminum plate was added. [4-5]

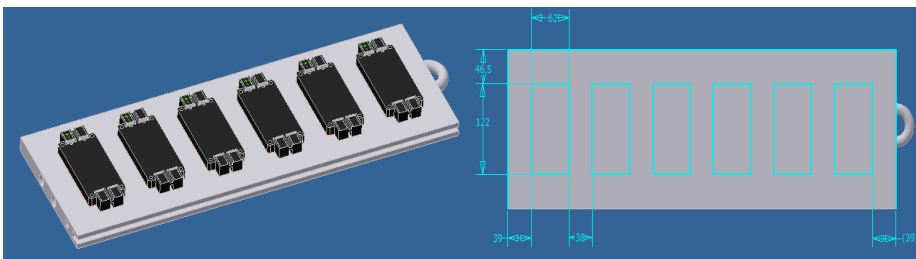


Fig. 1. Heat sink WP16 with IGBT modules.

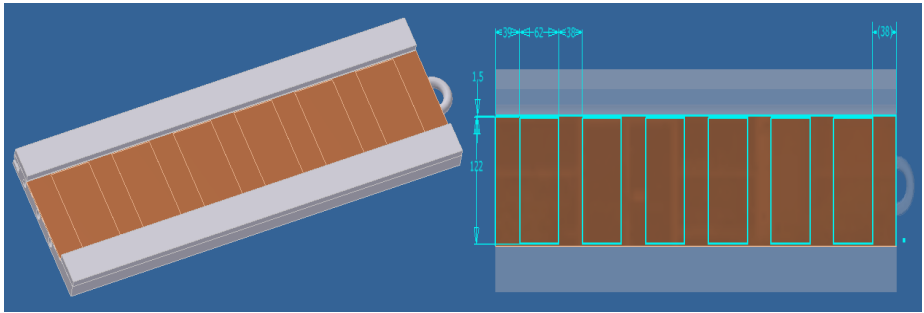


Fig. 2. Experimental heat sink WP16 without modules.

4 Simulation Results

The analysis was performed to analyze thermal behavior of water cooling without IGBT modules. The IGBT modules were replaced by areas with constant load. Power dissipation was set to 700 W per area. Water with temperature 25°C was used as a cooling medium. There is no environment considered for simulations. This fact simulates the most negative scenario where all of dissipation must be accumulated in heat sink or taken away by water. Initial temperature of heat sink was set 25°C. [4-5]

The first simulation is performed for heat sink with dimensions 640x215x20 mm.

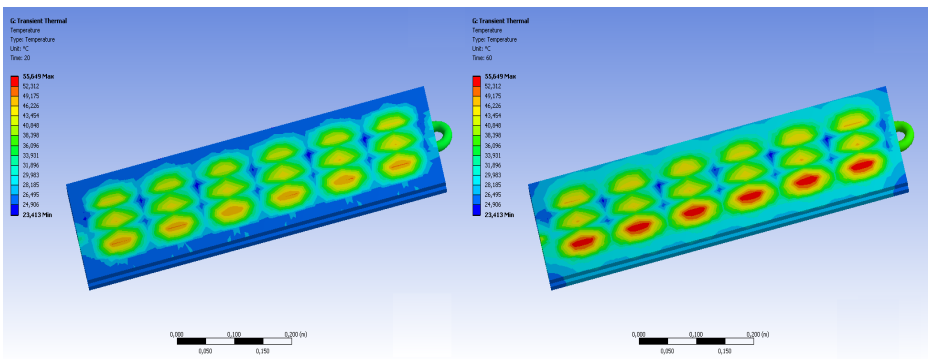


Fig. 3. Thermal field of heat sink.

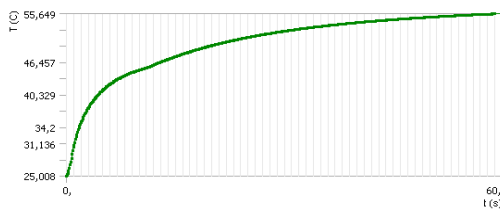


Fig. 4. Graph of temperature of heat sink in time 60 seconds.

The second simulation is performed for experimental heat sink with dimensions 640x225x26 mm.

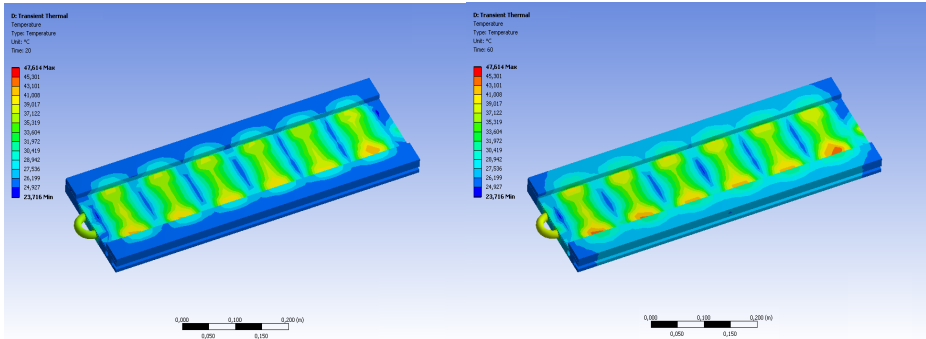


Fig. 5. Thermal field of experimental heat sink.

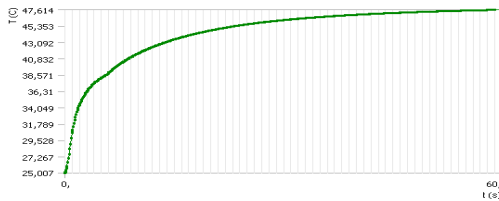


Fig. 6. Graph of temperature of experimental heat sink in time 60 seconds

5 Dynamic simulation

These simulations were performed from dynamic loss power in time. Time of simulation was set to 60 second. Water with temperature 25°C was used as a cooling medium. Initial temperature of heat sink was set to 25°C.

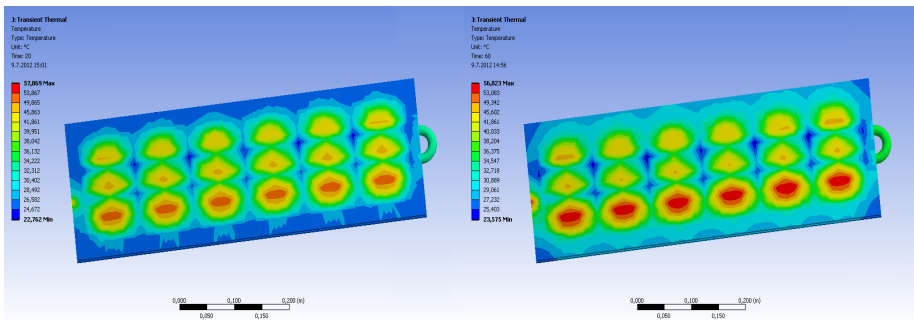


Fig. 7. Thermal field of the heat sink.

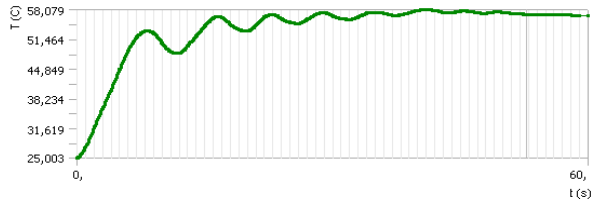


Fig. 8. Graph of temperature of the heat sink in time 60 seconds.

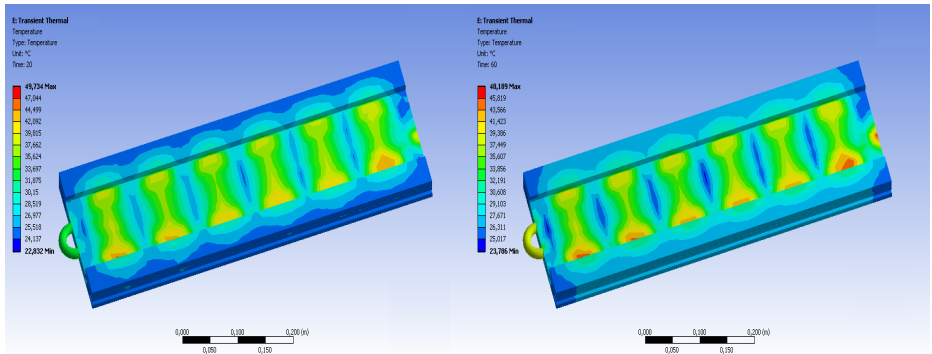


Fig. 9. Thermal field of experimental heat sink.

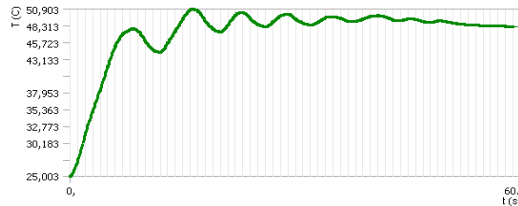


Fig. 10. Graph of temperature of the heat sink in time 60 seconds.

6 Evaluation of the Results

Previous figures show the thermal results of heat sinks. Maximal temperature of the standard heat sink WP16 was 55.649 °C. In this case steady value of temperature was not achieved. This problem is shown in figure 4. Figure 5 shows the thermal field of the experimental heat sink. Maximal temperature of this heat sink was 47.614 °C. In this situation the temperature reached the steady state. With experimental model of heat sink the maximal temperature was lower by 8 °C. This difference may be important for overloading of the heat sink.

7 Conclusion

The aim of this paper was comparison of standard heat sink WP16 with the experimental adjustment of this heat sink. The thermal analyses of these 3D models were performed. The experimental model has dimensions 640x215x26 mm and it is larger than the standard model about 6mm in height.

Experimental model was composed from three materials of different thermal capacity. The main part represents the standard heat sink WP16. The area with dimensions 640x130x5 mm was milled out. In this area was placed by the copper plate with size of milled out area. On borders of the heat sink there were placed aluminum boards with size 640x40x6 mm.

The experimental model achieved lower temperature than standard model of heat sink WP16. In this case we can say that experimental model of heat sink is better overloading or faulty operation.

References

1. Jaluria Y., Torrance K.E.: Computational Heat Transfer. Taylor and Francis, New York, 2003, ISBN 1-56932-477-5.
2. Madeci E., Guven I.: The Fienite Element Method and Applications in Engineer-ing Using ANSYS. Springer, New York, 2006, ISBN 0-387-28289-0.
3. Machacek Z., R. Hajovsky, S. Ozana, J. Krnavek: Experiments of Thermal Fields of Sensors Supported by Digital Image Processing, Ajaccio, France June 25-27, 2008, ISBN: 978-1-4244-2504-44.
4. Chlebis, P., Havel, A., Vaculik, P., Pfof, Z.: Modern Instruments for increasing the Efficiency of the Energy Transfer in Electric Vehicles, 14th EPE-PEMC 2010 International Power Electronics and Motion Control Conference, September 6-8, Ohrid, Republic of Macedonia 2010, vol. 14., p. 89-93, ISBN 978-1-4244-7854-5
5. Chlebis, P., Dudek, J.: Comparison of Power Losses and Quality of Output Vol-tage from Different Types of Inverters. In 35th Annual IEEE Power Electronics Specialists Conference, Aachen, Germany, 2004, VOLS 1-6, pp. 3120-3126, ISBN 0-7803-8399-0.

Design and Construction Power Converter with the Aid of 3D CAD System

Martin Tvrdoň

Department of Electronics, FEECS,
VŠB – Technical University of Ostrava, 17. listopadu 15, 708 33 Ostrava – Poruba
martin.tvrdon@vsb.cz

Abstract. This paper describes the design and construction of new series of power converters with liquid cooling system. This power series is created for ENET – Energy Units for Utilization of non Traditional Energy Sources. First power converter is determined for stationary battery system use, the second one is used as an inverter/rectifier for a small solar plant system and the last power inverter is used as a fast charger for electric vehicles.

Key words. Power inverter, design, 3D CAD, fast charger.

1 Introduction

The present energetic development is oriented into the considerable incorporation of alternative and renewable energy sources into the standard electrical grids in an effort to build very efficient, economic and reliable smart grids. This approach produces series of technical problems, which have to be solved. One of the most actual ones is the electric energy accumulation. Let the solar plant systems, a fast charger station for electric vehicles and many others examples. To satisfy an efficient and economic functioning of such station, the energy surplus has to be stored into the batteries and extracted back when necessary. It is also necessary to ensure sufficient battery power for fast charging of the electric vehicle's traction batteries. These power inverters are needed to provide an efficient and reliable electric power flow between the accumulation units and others devices. These one are gradually crated prototype. These power inverters will be introduced one by one in the following chapters on this paper.

2 Reversible voltage inverter

Arises in the project ENET storage system for which it is necessary to create a 3-phase voltage inverter with two-way flow of energy. This inverter has in relation to the electrical grid several important functions. These functions are the link between energy storage batteries and electric grid, correction element electric grid, backup

power for the position in the island's regime seized power operation and a few other less important functions.

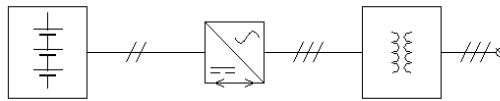


Fig. 1. Circuit topology in which is located the converter.

Due to the required converter functions and its inclusion in the traffic that is sized to the specified output type is selected, the inverter output to about 70 kW. The proposal indicates that the conveter power losses are the order of several kilowatts. Voltage level on the DC side ranges from 380 to 450 V. On the electric grid side converter is connected to the system 230 V. The drive is designed around the current 180 A.

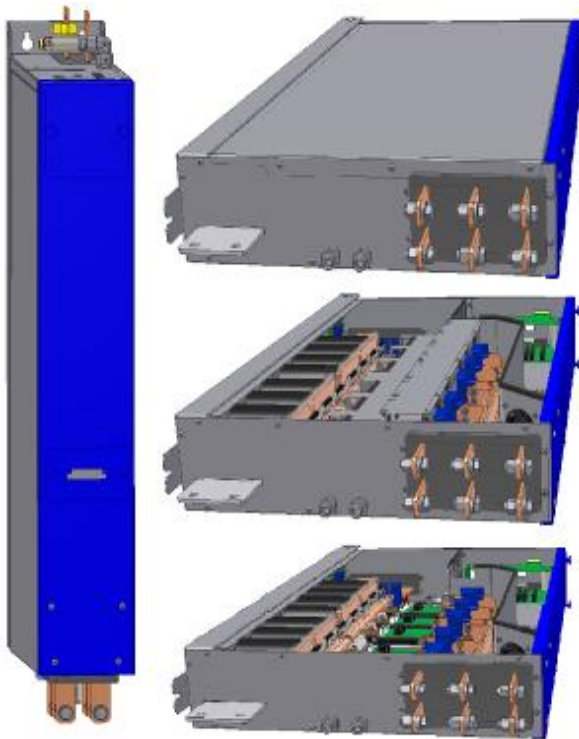


Fig. 2. Sample design solutions the reversible voltage inverter. The first appearance of the inverter is shown in the basic position. On the other illustrations, there are several views inside the inverter.

Looking at the power circuit of the converter is a 3-phase units consist of IGBT modules. These modules are assembled system bus. The DC circuit capacitor bank is located. This capacitor is designed for rapid exchange of energy in function of the

converter. For power loss listed above would not be appropriate to use an air cooling system. The inverter is cooled by a liquid cooling system.

The converter is controlled by a control system invented by directly for many of these converters with the digital signal processor TMS 320F28335. This control system has many inputs for measurement in the circuit in real time. Furthermore, the 6 PWM outputs and analog outputs are used for service purposes.

3 Power inverter for the solar plans

Nowadays, when there are a lot of solar power plants with time-average power inefficient operation when sufficient electrical energy, the idea that excess energy to accumulate. From this idea in turn requires the storage system with energy storage in the hundreds of kVA. Such a system is situated in a shipping container with an easy to install in the desired position, which would include a set of batteries for the accumulation of excess electric power and support equipment for the operation of the system.

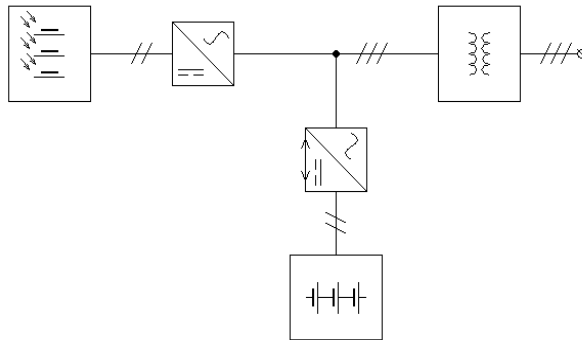


Fig. 3. Circuit topology in which is located the converter.

For the function of the storage system is necessary to use the power converter for converting AC power to DC for battery charging, and vice versa for converting DC power to AC to supply energy to the electric grid. This converter is placed between the electric grid and the battery pack, see Figure 3.

The inverter is designed as the AC connection between electric grid and storage batteries. When there is an energy surplus in the electric grid, the energy produced by the solar power plant will be stored in battery storage. By contrast, in a time when solar power does not produce electricity or produces very little and by the grid is a requirement for delivery, the energy is pumped from a storage battery to the grid. This operation creates demand for a 3-phase pulse rectifier and a 3-phase pulse inverter. Due to the topology of these converters can use the same equipment that will work in the rectifier and inverter.

Power converter will be operated on AC power supply with the parameters of 3 x 400 V 50 Hz, and storage batteries with a capacity of 600 kVA. Due to the optimal utilization of the inverter is required to type 60 kW. The connected battery will have a

nominal voltage of 800 V at full battery voltage reaches approximately 1000 V. This value will be rated for the inverter voltage. The inverter will be operated in a closed air-conditioned container. To ensure adequate dissipation of heat generated during operation of the inverter will be used in water cooling system.



Fig. 4. Sample design solutions the power inverter for the solar plans. The first appearance of the inverter is shown in the basic position. On the other illustrations, there are several views inside the inverter.

The inverter is designed as a 3-phase bridge converter. DC converter circuit is equipped with a capacitor bank made up of DC link capacitors - cylindrical cases. The 3-phase bridge is assembled of IGBT insulated modules.

4 Fast charger for electric vehicles

Nowadays is a growing field of electromobility. For its further development is necessary to build a network of charging stations. The project ENET thus creates development fast charging stations for electric vehicles.

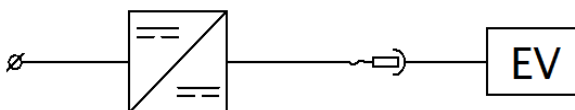


Fig. 4. Circuit topology in which is located the converter.

The concept of this converter is very similar to the previous case. But it is a 3-phase DC / DC converter. Power converter is set to 70 kW. This performance is chosen to maximize the possibility of charging electric vehicles. The voltage of this inverter is the input of about 400 V DC. Charging the battery voltage must always be lower than the voltage source. Compared with the previous inverter is reduced capacitor bank.

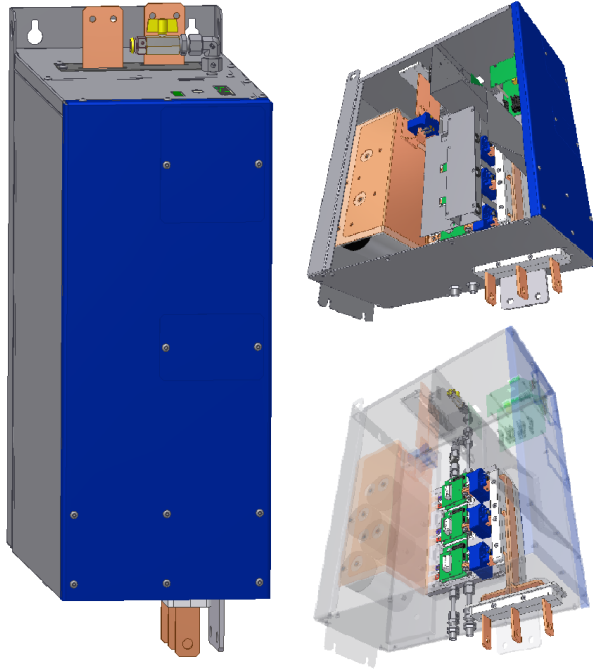


Fig. 6. Sample design solutions the fast charger for electric vehicles. The first appearance of the inverter is shown in the basic position. On the other illustrations, there are several views inside the inverter.

The converters are used again as switching components the IGBT insulated modules. Sensors of voltage and current are distributed in circuit for linking to control algorithms. To control is again used control system, which is developed by the Department. The control system is equipped with a digital signal processor TMS 320F28335.

5 Conclusion

This paper presented the design and construction of water cooled series of power converters for renewable energy plants or smart grid systems targeted on the electric energy accumulation. The reversible voltage inverter is fully operational in these days and the future work will be focused on the control algorithms optimization in order to

enhance the efficiency of the inverter. The power converter for solar plans and the fast charger are fully designed and produced documentation. The future work will be focused on realization prototypes and their testing.

Acknowledgements

The research described in this paper was supported by these projects:

- SGS project SP2012/126 - Reversible Converters for Electric Energy Accumulation.
- ENET – Energy Units for Utilization of non Traditional Energy Sources

This research was supervised by prof. Ing. Petr Chlebiš, CSc. and Ing. Petr Vaculík, Ph.D. from Department of Electronics, VSB - TU Ostrava.

References

1. Chlebis, P., Dudek, J.: Comparison of Power Losses and Quality of Output Voltage from Different Types of Inverters. In 35th Annual IEEE Power Electronics Specialists Conference, Aachen, Germany, 2004, VOLS 1-6, pp. 3120-3126, ISBN 0-7803-8399-0.
2. Vaculík, P., Havel, A., Tvrdoň, M., Hromják, M.: The Design and Construction of a Reversible Voltage Inverter Prototype, 13th International Scientific Conference Electric Power Engineering 2012, May 23 – 25, Brno, Czech Republic, str.: 1059-1062, 2012, ISBN 978-80-214-4514-7.
3. Chlebis, P., Havel, A., Vaculík, P., Pfof, Z.: Modern Instruments for increasing the Efficiency of the Energy Transfer in Electric Vehicles, 14th EPE-PEMC 2010 International Power Electronics and Motion Control Conference, September 6-8, Ohrid, Republic of Macedonia 2010, vol. 14., p. 89-93, ISBN 978-1-4244-7854-5

Nonparametric Predictive Inference as an Alternative to the Kaplan-Meier Estimator in Survival Analysis

Kateřina Janurová

Department of Applied Mathematics, FEECS,
VŠB – Technical University of Ostrava, 17. listopadu 15, 708 33 Ostrava – Poruba
katerina.janurova@vsb.cz

Abstract. Survival analysis is a set of methods for the analysis of time to event data, typically consisting of observed event times and right-censoring times. This type of data may arise from various situations: the survival times of patients in medical trials, the lifetimes of machine components in industrial reliability, studies of recidivism or the duration of periods of unemployment in duration modeling. The possible fields of applications are therefore medicine, engineering, economics, sociology, demography and science. In this article are compared two nonparametric approaches used in survival analysis: well known and widely used Kaplan-Meier estimator of survival function on one side and relatively new nonparametric predictive inference on the other.

Keywords: survival analysis, right-censored medical survival data, Kaplan-Meier estimator, nonparametric predictive inference (NPI)

1 Introduction

In this paper is presented relatively new method for statistical inference, nonparametric predictive inference - NPI, which uses lower and upper probabilities, denoted by $\bar{P}(A)$ and $\underline{P}(A)$ respectively, with $0 \leq \bar{P}(A) \leq \underline{P}(A) \leq 1$, for quantifying uncertainty. It basically differs from the Kaplan-Meier estimator of survival function because it provides model of predictive survival function instead of the estimation of population survival function. NPI is based on Berliner and Hill method for nonparametric survival analysis [3], which depends on Hill's assumption $A_{(n)}$ for prediction of probabilities for one (or more) future values, on the basis of n prior observations. The results are demonstrated via example in context of medical survival data of patients after colorectal surgery and compared with traditional Kaplan – Meier estimator of survival function.

2 Nonparametric predictive inference

2.1 Hill's assumption - $A_{(n)}$

Assumption $A_{(n)}$ was presented by Hill in 1968 for deriving predictive probabilities for a future observation in the case of extremely vague prior knowledge about characteristics of the underlying source of the observation [4]. Assumption is defined on the principle of exchangeability of random quantities, which states that if we have n ordered random quantities $x_{(1)} < x_{(2)} < \dots < x_{(n)}$, then probability of the rank of the next random quantity X_{n+1} is uniformly distributed over the values 1 to $n + 1$ ($P(X_{n+1} \in (x_i, x_{i+1})) = 1/(n+1)$), for $i = 0, \dots, n$, where $x_{(0)} = 0$ and $x_{(n+1)} = \infty$). Random quantity X_{n+1} can represent the time of death of one future patient in medical trials.

The following definition provides notation for probability mass assigned to intervals without any further restrictions on the spread within the intervals.

Definition (*M*-function). A partial specification of a probability distribution for a real-valued random quantity X can be provided via probability masses assigned to intervals, without any further restriction on the spread of the probability mass within each interval. A probability mass assigned, in such a way, to an interval (a, b) is denoted by $M_X(a, b)$, and referred to as *M*-function value for X on (a, b) .

It is clear that sum of all *M*-function values for X on all intervals is equal to one and each *M*-function value should be in $[0, 1]$. The predictive probabilities according to $A_{(n)}$ are then specified by $M_{X_{n+1}}(x_i, x_{i+1}) = 1/(n+1)$ for $i = 0, \dots, n$.

2.2 Imprecise probabilities

For a subinterval (a, b) of $(0, \infty)$ is the lower probability for event $X_{n+1} \in (a, b)$ derived, via principle used in [1], by summing only the probability masses, that necessarily must be in (a, b) , so by summing all *M*-function values for X_{n+1} on intervals which fall completely within (a, b) .

$$\underline{P}(X_{n+1} \in (a, b)) = \sum_{(x_{(i)}, x_{(i+1)}) \subset (a, b)} M_{X_{n+1}}(x_{(i)}, x_{(i+1)}). \tag{1}$$

The upper probability for this event is derived by summing all probability masses that can be in (a, b) , so by summing all *M*-function values for X_{n+1} on intervals which have non-empty intersection with (a, b) .

$$\overline{P}(X_{n+1} \in (a, b)) = \sum_{(x_{(i)}, x_{(i+1)}) \cap (a, b) \neq \emptyset} M_{X_{n+1}}(x_{(i)}, x_{(i+1)}). \tag{2}$$

Example 1. Suppose that we have $n = 6$ observations which create 7 intervals, assumption $A_{(n)}$ implies that the next observation X_7 will fall in any of these intervals with probability $1/7$, then $\underline{P}(X_7 \in (a, b)) = 1/7$, as shown Fig. 1 a) and

$\bar{P}(X_7 \in (a, b)) = 3/7$, Fig. 1 b), imprecision is difference between lower and upper probabilities $\bar{P} - P = 2/7$.

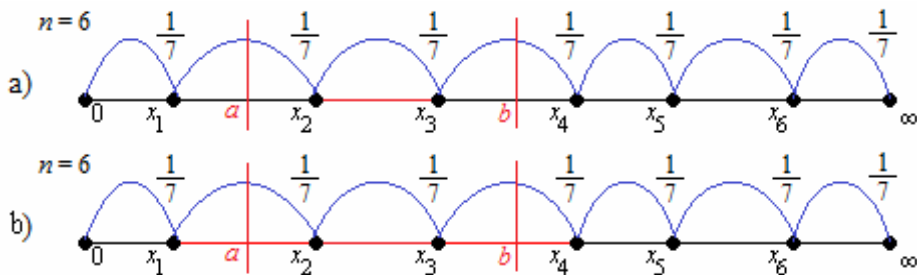


Fig. 1. Lower and upper probabilities for the event that $X_7 \in (a, b)$

2.3 Right-censoring assumption –rc- $A_{(n)}$

Assuming now that we may obtain from the experiment among n independent observations $m \leq n$ observed number of death $t_{(1)} < t_{(2)} < \dots < t_{(m)}$ and $p (= n-m)$ right-censored observations $c_{(1)} < c_{(2)} < \dots < c_{(p)}$ and that in the sample no ties have occurred (treatment of ties is discussed by Coolen and Yan [2]). Let $t_{(0)} = 0$ and $t_{(m+1)} = \infty$. Assumption $A_{(n)}$ can not deal directly with right censored observations therefore it is not appropriate for using in survival analysis, as a result Coolen and Yan presented in 2004 a generalization of $A_{(n)}$ called right-censoring or rc- $A_{(n)}$. Contrary to $A_{(n)}$ rc- $A_{(n)}$ requires one extra assumption that, at the censored time, the residual lifetime of right-censored patient is exchangeable with the residual lifetimes of all other patients still at risk of dying [5]. The probability distribution for the next observation T_{n+1} is then partially specified by rc- $A_{(n)}$ by following M -function values:

$$M_i^T = M_{T_{n+1}}(t_{(i)}, t_{(i+1)}) = \frac{1}{n+1} \prod_{\{r:c_r < t_{(i)}\}} \frac{\tilde{n}_{c_{(r)}} + 1}{\tilde{n}_{c_{(r)}}}, \tag{3}$$

$$M_{i,k}^T = M_{T_{n+1}}(c_k^i, t_{(i+1)}) = \frac{1}{(n+1)\tilde{n}_{c_k^i}} \prod_{\{r:c_r < c_k^i\}} \frac{\tilde{n}_{c_{(r)}} + 1}{\tilde{n}_{c_{(r)}}}, \tag{4}$$

where $i = 0, 1, \dots, m$ and $k = 1, 2, \dots, l_i$ and $\tilde{n}_{c_{(r)}}$ is the number of individuals in the risk set just prior to time $c_{(r)}$. The rc- $A_{(n)}$ is illustrated on the following example.

Example 2. Suppose once again that we have $n = 6$ observations, but now two of these observations are right-censored at times c_1 and c_2 , so we have four observed times of death of patients. At first, shown in Fig. 2 a), are assigned the probability masses for the intervals created by the four times of deaths equally to $1/7$ and also a probability mass $1/7$ spreading over the intervals (c_1, ∞) and (c_2, ∞) , because what we know is, without any other assumption, that survival time of these patients is beyond their censored value. As a next step, the probability mass assigned to the first censored observation c_1 is divided equally to the intervals to the right of c_1 , including

the interval (c_2, ∞) , see Fig. 2b). As a result we have accumulated probability mass $1/7 + 1/28 = 5/28$ assigned to the intervals (x_3, x_4) , (x_4, ∞) and (c_2, ∞) , see Fig. 2 c). This process is repeated for the censored observation c_2 , the probability mass assigned to this observation is divided equally to the intervals to the right of c_2 , see Fig. 2 d). Now we have a total probability mass assigned to interval (x_4, ∞) $5/28 + 5/56 = 15/56$ and $5/56$ to (c_2, x_4) , see Fig. 2 e). This process can be understood in the way of the redistribute-to-the-right algorithm of Efron [6] for calculating the Kaplan-Meier estimator of survival function.

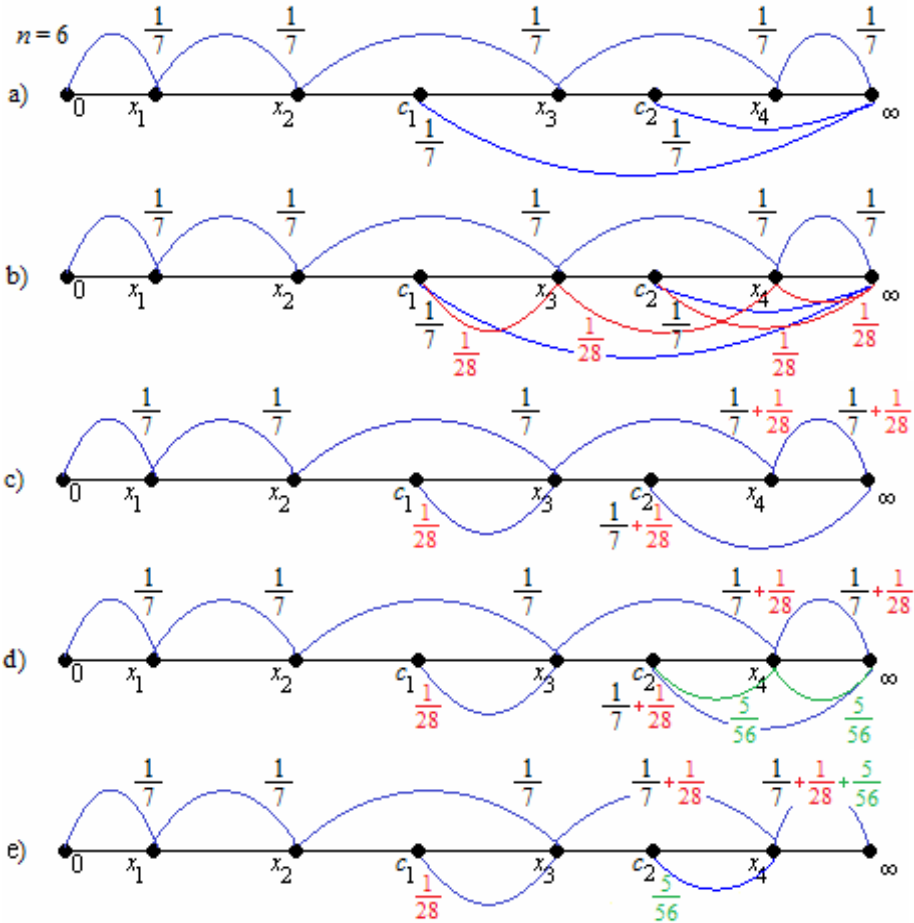


Fig. 2. Right-censored $A_{(7)}$ with two censored observations

2.4 Lower and upper survival functions

When we applied survival analysis on medical data, we want to describe how long the patients live, rather than how quickly they die. That is the reason, why we concentrate in medicine on estimation of survival function. It represents the probability that the survival time of patient is greater than some specified time t , denoted $S(t) = P(T > t)$.

The lower and upper survival functions for T_{n+1} are derived by using $rc-A_{(n)}$ as follows:

$$\underline{S}_{T_{n+1}}(t) = \underline{P}(T_{n+1} > t) \text{ for } t \geq 0, \tag{5}$$

$$\bar{S}_{T_{n+1}}(t) = \bar{P}(T_{n+1} > t) \text{ for } t \geq 0. \tag{6}$$

3 Comparison of NPI and Kaplan-Meier estimator

Data from about 850 patients who underwent colectomy at the University Hospital of Ostrava during the years 2001-2010 were used to construct the lower and upper survival functions based on nonparametric predictive inference as well as the Kaplan-Meier estimator of survival function see Fig. 3.

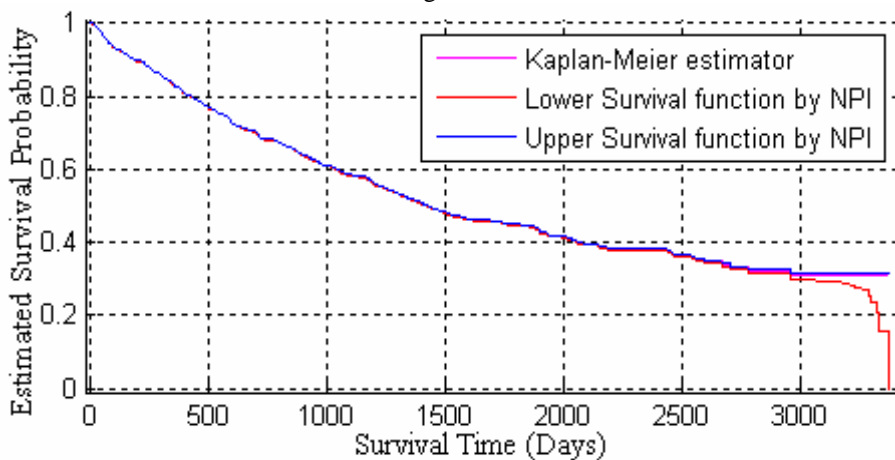


Fig. 3. Comparison of survival functions based on NPI and Kaplan-Meier estimator

All, the lower and the upper, survival functions based on NPI and Kaplan-Meier estimator of survival function are decreasing step-functions, which start in one. They are constant between observed times, the upper survival function based on NPI and Kaplan-Meier survival function decrease only at each event time (but censoring has influence on the amount of decrease), while the lower survival function based on NPI decreases at each observed time (events + censored times), as a consequence the difference between upper and lower survival functions based on NPI increases at each observed censored time till the next event time. In interval probability theory, this difference is often inversely related to the amount of information on which such bounds are based, so censoring may be considered as loss of information. Clearly the upper survival function based on NPI is on $[0, t_1)$ equal to one and on $[t_m, \infty)$ is positive constant, while the lower survival function based on NPI is zero beyond the largest observation. Kaplan-Meier survival function is on the other hand zero beyond the largest observation only if the last observed time is the time of death.

4 Conclusion

Real medical survival data including right-censored observations were elaborated and evaluated by the use of two nonparametric approaches. Despite the difference in approaches between NPI and Kaplan-Meier method, NPI provides model of predictive survival function instead of the estimation of population survival function, all curves practically coincide (apart from the last part of these curves – 3000 days and after). That is due to a large number of evaluated observations.

The main advantage of NPI approach is in the way of dealing with censoring times. Unlike the Kaplan-Meier estimator of survival function, the NPI lower survival function decreases at each observation, so also at censored observations, which provides more information about all observed events, especially if the largest observation is censoring time.

Results were presented on the PSAM 11 & ESREL 2012 Conference (11th International Probabilistic Safety Assessment and Management Conference and The Annual European Safety and Reliability Conference, Helsinki, 2012).

Acknowledgement

This work was funded by grant SGS SP2012/108 VŠB-TU Ostrava.

References

1. Yan K.J. Nonparametric predictive inference with right-censored data. Ph.D. thesis, Durham University, Durham, UK, (2002). Available from www.npi-statistics.com.
2. Coolen F.P.A., Yan K.J. Nonparametric predictive inference with right-censored data. *Journal of Statistical Planning and Inference*, No. 126, (2004), pp. 25-54.
3. Berliner L.M., Hill B.M. Bayesian nonparametric survival analysis (with discussion). *Journal of the American Statistical Association*, No.83, (1988), pp.772-784.
4. Hill B.M. Posterior distribution of percentiles: Bayes' theorem for sampling from a population. *Journal of the American Statistical Association*, No. 63, (1968), pp. 677-691.
5. Maturi T. A. Nonparametric Predictive Inference for Multiple Comparisons. Ph.D. thesis, Durham University, Durham, UK, (2010). Available from www.npi-statistics.com.
6. Efron B. The two sample problem with censored data. *Proceedings of the Fifth Berkeley Symposium on Mathematical Statistics and Probability*, volume 4 New York: Prentice Hall, (1967), pp. 831-853.

Interdisciplinary Approach to Renewable Energy Storage Global Planning

Filipe Campos¹, Radim Hercík², Lili Nemeč³, and Alejandro Santana-Alonso⁴

¹Universidade do Minho, High-Assurance Software Laboratory
fcampos@di.uminho.pt

²Department of Cybernetics and Biomedical Engineering, FEECS,
VŠB – Technical University of Ostrava, 17. listopadu 15, 708 33 Ostrava – Poruba
radim.hercik@vsb.cz

³Maribor University, School of Media Communications, Slovenia
lili.nemec@uni-mb.si

⁴University of Vigo, School of Industrial Engineering, Spain
asantana@uvigo.es

Abstract. There are several financial, environmental and technical issues involved in and derived from worldwide energy production. Renewable Energies are considered a fair solution. But their intermittent and unpredictable nature requires another complementary solution, which is provided by Energy Storage (ES) Technologies. As their combined use enables a sustainable energy production with high power quality standards, and would lead to the prosecution of the smart grid paradigm. Therefore, the planning of such ES is a matter of utmost importance. Planning ES in power grids is a process where financial, technical, environmental, social, geopolitical, geographical and regulatory issues have to be taken into account. The definition of an interdisciplinary framework to plan the deployment of ES solutions in the power grid, with a special focus on the conjunction with Renewable Energy Systems (RES), is essential for the increasing adoption of such eco-friendly energy production systems.

1 Introduction

The current worldwide energy scenario shows escalating power consumption, rising pollution levels, increasing energy crisis, congestion of power grids and diminishing of traditional fossil-based energy resources. In order to alleviate these problems, Renewable Energy Systems (RESs) are considered as a key solution regarding the environmental aspects of these energy problems. They also provide diversity to the electrical grids. But the wide adoption of RESs is not enough, as it poses several technical and financial challenges when applied at large-scale. These are given by the fluctuating and non-fully predictable nature of RESs. An accepted solution is the combined use of RESs and new Energy Storage Technologies (ESTs). Therefore, both widespread adoption and efficient usage of RESs rely on EST [1,2,3].

The purpose of this paper is to explore the background of the optimal use of natural resources by the Energy Market Governance (EMG)¹. This paper analyzes some of the

existing tools for sizing and choosing the most appropriate Energy Storage (ES) solution for power grids, with special focus on Renewable Energy Systems (RES), whilst considering a global interdisciplinary approach. ES technologies require an integration plan, where financial, technical, environmental, social, geopolitical, geographical and regulatory issues are taken into account. This paper explores energy storage technologies in Section 2, where efficient usage of RES technologies are investigated. In Section 3 regulations concerning the RES, important regulatory issues in different countries are presented. In Section 5, the planning of energy storage deployment explores the existing planning tools for energy storage. In Section 4 energy storage deployment and management, the paper presents social methods, which could be adopted by the proposed tool for selecting the right ES setup for each scenario, taking into consideration the existing RES capacity.

2 Energy Storage Technologies

RESs have been developed overtime and some of them have reached a high state of maturity [3]. However, the power delivery of RES is usually intermittent. The widespread use of these RES and their efficient use depends on EST. A successful ES strategy is important so that renewable energy can be stored when generation is higher than the demand and then deliver it on the opposite situation, which is usually called “renewable energy time-shifting”. It also must keep compliant with grid Power Quality (PQ) constraints. This combination of energy generation and storage technologies has many benefits: leads to a better reliability and stability of power grids, maximizes the renewable energy contribution, allows for a better demand and generation matching, reduces global power generation costs and environmental hazards, and helps to avoid power grid congestions and black-out risk. Therefore, its benefits are economic, environmental, technological and social, therefore, global. [4]

The different EST can be classified in three vast categories, mainly regarding the power discharge rate they can provide, and each is aimed to fulfill different needs. First category comprises short-term response ESTs, which provide high power in a very short amount of time. They are used to improve power quality, specially by stabilizing voltage during transients (from few seconds to minutes). That is the case of Uninterruptible Power Systems (UPS) and Power Quality Systems (PQS). The second encompass long-term response ESTs, which are used in power systems that may usually provide and absorb electrical energy for time periods ranging from some minutes to several hours. They are useful to help in frequency regulation and grid management. And finally, the third category include real long-term response ESTs (from many hours to days), which are used as a reservoir of energy to match energy demand and supply energy for longer periods of time and usually in a higher scale [4].

Regarding ES solutions, there are several proposed technologies, with different levels of maturity and sometimes aimed for solving different problems. These different technologies have many applications all along the energy chain, from generation, transmission and distribution, to end-user applications.

Pumped Hydro ES (PHES) is probably the most mature of the ESTs, as it is been used for load balancing for more than 80 years. In this technology potential energy is

stored in the form of water, pumping it from lower reservoirs to higher ones. PHES is classified as a real long-term EST because it stores big amounts of energy and can provide different quantities of power over several days [2].

Among the other best-known ESTs, there is Compressed Air ES (CAES). It is also capable of storing large amounts of energy, stored in form of compressed air, usually in underground sealed caves (natural or manmade).

Among the main technical criteria to be considered while evaluating the feasibility of a EST plant, the following can be mentioned: Type of application, storage capacity, feasibility, electrical efficiency, reliability, lifetime, energy density, response time, power density, environmental impact and power rating.

3 Regulations

Technical aspects are not the only thing in consideration while evaluating the viability of a ES plant and planning its deployment. Global Planning for ES of RES has to deal with a number of regulations. Each country or region may have specific energy, environmental and political laws and regulations and they may even overlap. These regulations may restrict or promote actions, technologies or investments.

Environment regulations can involve restrictions regarding actions over air, water, climate or waste. During planning it is necessary to consider the political limitations and advantages. Among them we find insurance requirements, property ownership regimes or liability considerations. The planning process can interfere with other elements of government policy such as tax credit, liability limit or financial arrangements. Also, the political prospects of regulation can have an important role, as it is important to consider future regulatory rules in investments planning.

It is important to realize that power grid in Europe was not originally designed to transfer power across countries or regions. The majority of the power grid was designed as a national or regional network. During the design process of these networks, issues like the differences in voltage, phase, or network load, were not taken into account. Interconnection and the opening of the electricity market has led to a rise in load and demands on the transmission network. This interconnection still faces some serious deficiencies. The increasing market demand for energy consumption and the integration of RES like photo-voltaic or wind power plants, causes sudden fluctuations that can result in network failure [5].

Regulations usually affect the way energy is produced and injected in the grid. Open energy market can't fully predict the network, specially in the case where energy is transported over long distances, for example, from northern to southern Europe. Currently, there is an insufficient number of cross-over connections, which would allow to fully compensate local overload. The technologies to enhance stability and security networks are available, but they are not yet fully integrated into existing networks. These new ES technologies have significantly lower environmental impact, smaller footprints and are extremely flexible in their operation [5,6].

The situation is slightly different in the U.S. as its power grid is a complex electrical power network. It is known that the network is sensitive to weather changes, and

threats to its stability are mainly storms, which can damage various parts of the network or fully decommission it. Changes made in the U.S. have reduced its network's operating costs and increased flexibility in the provision of electricity distribution. However, this means that the ability of a network to deal with power shortages and blackouts was reduced. A blackout is a significant power outage that interrupts the supply of a large area [4].

4 Energy Storage Deployment and Management

The planning process must also take into account a number of restrictive criteria, which are not always related to technical limitations of the grid, but also to other factors such as political, environmental or social perspectives.

In the deployment and management of technologies for planning the ES for RESs, some methods that could be used in planning and final exploitation of the product are presented in this paper. This chapter is focused on methods that have already been used in similar cases of energy deployment and on other methods that could also be taken into account for this purpose.

The framework of socio-political evaluation of energy deployment is a combined qualitative and quantitative analytic model with requires interdisciplinary research on factors influencing energy technology deployment. The framework presents three research methods, which are policy review and analysis, media analysis and the last one with focus groups and structured interviews with key stakeholders. Within these research methods some guidelines for consideration are set for energy technology deployment [7].

In the part of social area, important considerations are set, such as perception of technology by key actors, public trust, detection of risks and benefits, historical usage of land and impact on social groups. A research, which explores the barriers for renewable energy penetration divides the barriers into more categories: market failure/imperfection, market distortions, economic and financial, institutional, technical, social, cultural and behavioral. Within this research, the barriers that are set for social, cultural and behavioral category are reliability of the product, consumers acceptance of the product and social acceptance of RES [8].

The management of technologies is also considered in the ES planning point of view. When an EMG accepts a decision of researching the possibilities of accepting new technologies, they go through a decision making process. It is important that all the basic steps of decision making process are understood. Within the process, the key actors for approving the new technology normally identify the purpose of the decision, gather information on new technologies and its benefits [9].

In the deployment of technologies, important social factors should be taken into account when planning the ES for RES. These factors include consumers acceptance of the product, public trust, detection of risks and benefits, historical usage of land, reliability of the product and social acceptance of RES. Also knowing the important steps of how the key actors will accept the decision of changing or adding a new technology into their market is important and we explored.

5 Energy Storage Deployment Planning Tools

Regarding the decision making process on the usage of RES, the combined operation with ES systems is one of the most important trends to ensure the correct operation of the grid, during the current transition from fossil fuel to renewable power generation. In order to assess the most appropriate ES technology or combination of technologies for each scenario, planning tools are needed. They should translate the multicriteria recommendations into simplistic financial information which must be comprehensible to decisionmakers so they are able to select the solution that best fits their needs [10].

Currently, there are several computer tools to assist on the analysis of the integration of RES and ES in power grids. However, there is no ideal tool that covers all the aspects that should be considered for this kind of integration. Also, the notion of such an ideal planning tool depends on the objectives for a specific scenario, as well as on the considered energy-sectors, technologies, time parameters, tool availability and previous studies [8].

The majority of the analyzed tools consider annual results in a long-term scenario, as RETScreen and MesapPlaNet. There is one tool that just considers hourly results throughout the simulation of one year, whereas others can use both approaches. Some of these tools can be used for optimizing operating costs or investments in new technologies and stations [10,11].

In terms of currently planned research projects, attention should go to the American Energy Storage Program which, supported by the Department of Energy, aims to develop, until 2015, ES deployment planning tools that are sufficiently generic in order to model various storage technologies, but still realistic and verified by a standards body.

6 Conclusions

Energy Storage (ES) has become the enabler for continuously growing and widespread adoption of Renewable Energy Systems (RES), in order to increase distributed and environmentally sustainable energy production. As energy utilities rely more and more on distributed energy production from renewable sources, there is the need for the introduction of technologies that minimize the impact of the intermittent nature of these sources. This is a key opportunity for different ES technologies to be applied in scenarios according to technical conditions, like application purposes, grid scale, or existing RES, but also taking into account financial, environmental, social, geopolitical, geographical and regulatory issues. With this intention, we propose the development of a tool to assess the deployment of ES technologies in any given country, taking into consideration the mentioned issues in order to determine the viability of the investment, and to select an appropriate ES setup for each scenario.

Such planning tool would be a useful resource for vendors to rapidly plan a solution that appropriately fulfills in each case all its potential customer needs. But it would also be an interesting tool for any EMG, helping in the process of modifying and enhancing regulations by measuring their potential impact on markets, evaluating different alternatives.

Acknowledgements

We would like to thank all people involved in organizing the ICCES Erasmus IP 2012 in Porto, as well as the people from EFACEC.

References

1. Barin, A., Canha, L., da Rosa Abaide, A., and Magnago, K. (2009a). Selection of storage energy technologies in a power quality scenario - the ahp and the fuzzy logic. In *Industrial Electronics, 2009. IECON '09. 35th Annual Conference of IEEE*, pages 3615–3620.
2. Masaud, T., Lee, K., and Sen, P. (2010). An overview of energy storage technologies in electric power systems: What is the future? In *North American Power Symposium (NAPS), 2010*, pages 1–6.
3. Roberts, B. (2009). Capturing grid power. *Power and Energy Magazine, IEEE*, 7(4):32–41.
4. Massoud Amin, J. S. (2008). The electric power grid: Title today and tomorrow title. *MRS Bulletin*, 33(April):339
5. Treichel, K. (2009). The european power grid - the need for regulatory changes and advanced technology. *Europe*, 3:3.
6. Saphores, J., Gravel, E., and Bernard, J. (2004). Regulation and investment under uncertainty: An application to power grid interconnection. *Journal of Regulatory Economics*, 25(2):169–186.
7. Stephens, J., Wilson, E., and Peterson, T. (2008). Sociopolitical evaluation of energy deployment (speed): An integrated research framework analyzing energy technology deployment. *Technological Forecasting and Social Change*, 75(8):1224–1246.
8. Painuly, J. (2001). Barriers to renewable energy penetration; a framework for analysis. *Renewable Energy*, 24(1):73–89.
9. Huitt, W. (1992). Problem solving and decision making: Consideration of individual differences using the myers-briggs type indicator. *Journal of Psychological Type*, 24:33–44.
10. Barin, A., Canha, L., Magnago, K., da Rosa Abaide, A., and Wottrich, B. (2009b). Multi-criteria decision making for management of storage energy technologies on renewable hybrid systems - the analytic hierarchy process and the fuzzy logic. In *Energy Market, 2009. EEM 2009. 6th International Conference on the European*, pages 1–6.
11. Krajacic, G., Duić, N., and Carvalho, M. D. G. (2009). H2res, energy planning tool for island energy systems - the case of the island of mljet. *International Journal of Hydrogen Energy*, 34(16):7015–7026.

Topology of Fuel Cell Laboratory Pilot Extension

Kristýna Friedrischková and Bohumil Horák

Department of Cybernetics and Biomedical Engineering, FEECS,
VŠB – Technical University of Ostrava, 17. listopadu 15, 708 33 Ostrava – Poruba
{kristyna.friedrischkova, bohumil.horak}@vsb.cz

Abstract. Reducing fossil fuel demand and higher environmental performance makes the energy sector. This article is devoted to the description of the wider framework of the extension of the pilot system topology Labs fuel cells to meet the dissertation topic related to energy management and operational optimization of energy systems of the future family house.

Keywords: hydrogen, fuel cells, renewable energy, energy independence, the island mode, network mode, hybrid mode, optimization, energy management, expert systems, machine learning, a pilot system.

1 Introduction

The worldwide energy demand is covered by 90 % fossil fuels. The excessive usage of fossil energy sources has two main problems. The known energy reserves of fossil fuels are going to its limits. This will lead in a middle term and long term to increased prices. The global very inhomogeneous distributed deposits of oil reserves constitute a very high exposure for politically motivated conflicts.

If renewable energy sources will be used more excessive e.g. solar radiation, wind energy and cogeneration, energy accumulators need to be installed to balance non-isochronic or conflictive profiles of energy tender and energy demand.

Inside these energy supply systems the conversion of renewable energies, storage and consumption must be balanced. The energy balance (seasonal or long-term) of stochastic input and output need to be paid attention to.

In the field of energy storage hydrogen will play a vital role in future. It is able to be stored longterm, energy conversion is emission free and endangerment is not bigger than the other energy sources.

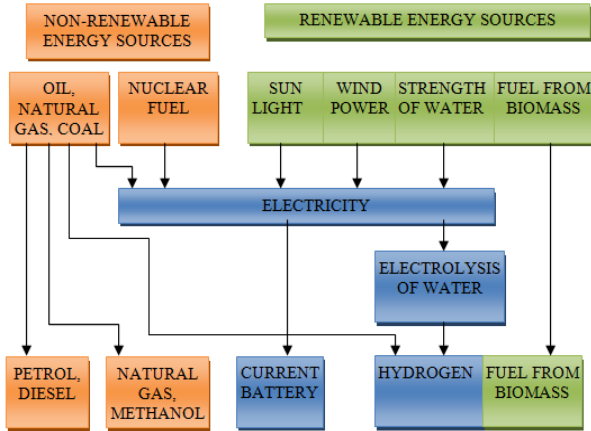


Fig. 1. Block diagram of the energy alternatives

Project initiation and development laboratory fuel cells and other activities related to trends in the promotion of renewable and unconventional energy sources and sustainable society.

Fuel Cell The laboratory was established in 2004. The laboratory collaborates with many of external commercial companies in the solution of technological and application problems associated with applications of fuel cells. Applied research is focused on the future use of technology and technical potential industrial Ostrava region along with the natural rich the Ostrava-Karvina coal basin and their use for energy production the processing of fuel cells.

2 Basic functions of a pilot system

Topology Labs fuel cells (abbreviation LFC) used technology is focused primarily on implementation of fuel cell technology (membrane systems for generating electricity and / or electrolytic decomposition of water) and other methods of energy storage (accumulation of electrical energy between the production and accumulation of hydrogen).

The pilot technological system with the support of other progressive elements allows produce electricity by using solar photovoltaic system. It allows the electricity accumulated in the installed station batteries and / or deliver to the public grid.

PEM electrolyzer, which is powered from the station batteries and / or the public grid produces hydrogen from demineralized water and stores it in metalhydridových or standard pressure containers. This system allows produce and deliver into the public grid electricity from the stored hydrogen fuel cell system and DC / AC inverters.

3 Extension of the pilot system

Extension the topology LFC is initiated research and development-oriented team in recent years and the interest the commercial sector about the results of research and development of LFC and cooperation with the commercial sector.

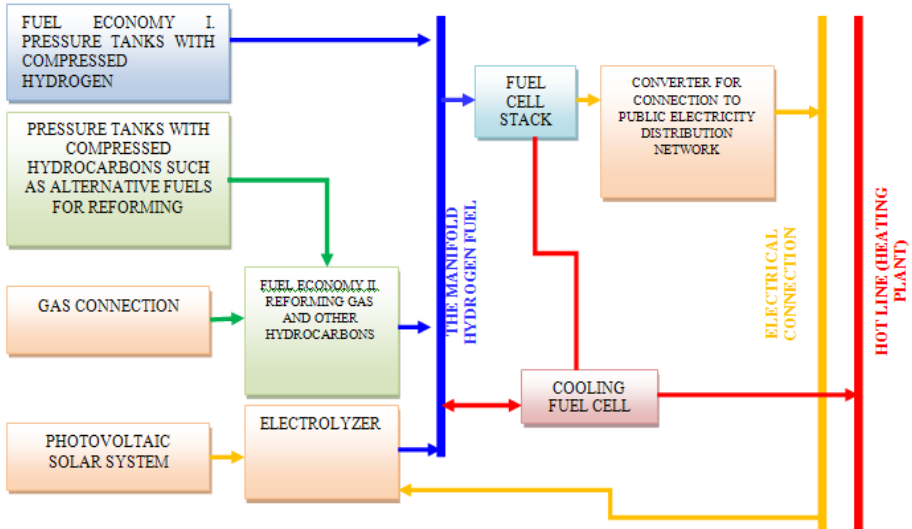


Fig. 2. Conceptual design of the system

The current topology of requires an extension in the areas of energy resources and topology optimization sources and storage systems and management of energy flows. The main objectives of energy independence is a pilot system modeling needs a family house and maximize energy profits and increase investments.

Major will use small wind turbines, which will be complement the renewable energy system generating electricity. The use of small wind turbines in a pilot system based on a philosophical view of the timing of the possibility of using wind energy at a time when the sun is off or in the reduced intensity of solar radiation.

Another planned source of energy is combined production electrical energy and heat micro cogeneration unit (the MCU). Development alternatives MCU are MCU with internal combustion piston engine and internal combustion engine with a circular piston. A third alternative is the implementation of the MCU system with high temperature fuel cell. Implementation of the MCU is tendentious:

1. It is long and still unrealized intention of implementing a solid oxide fuel cell (SOFC the) fuel cell system in a pilot LFC.
2. This technology is a global trend for the majority of heat and electricity generation as a secondary process. It increases the energy efficiency of the final system.
3. This is based on the secondary results a team of research projects from previous years.
4. Research, development and commercial team partners have expressed interest and suggested support for the continuation plan in the future.

The optimization topology sources and storage systems associated with the implementation and testing of modern photovoltaic solar systems and the unavailability of commercial converters for island technology with voltage storage systems of hundreds of volts. At the same time expected future integration the electric car to the family home at the level of the appliance electrical energy in the mode power charging and storage system as an extension of electricity.

Management of energy flows expected knowledge of the energy needs of the family house specified in the expert system with the implementation of machine learning. We can drive energy source, energy storage and consumption when is the criteria independence of the pilot system to operate in island mode or as to maximize financial gain system working in network mode.

3.1 Micro-cogeneration unit

Micro-cogeneration unit (the MCU) is system consists of an internal combustion engine - generator power energy or high-temperature fuel cell. At the present is commercially available technologies prefer solutions with combustion engine for mass production of components such MCU. MCU with high-temperature fuel cell is an excellent source of today a number of strengths in the future.



Fig. 3. The prototype developed by MCU team and the Technical University of Ostrava and ISOTRA

3.2 Photovoltaic solar system

Existing solar photovoltaic system LFC can deliver high-energy 2kW to the system in the island system with battery electrical energy with a voltage of 48V and 75Ah capacity.

For the purpose of energy-independent family house is necessary to meet its needs in the period when the sun is off or in the period with limited or no sunlight. About meet the energy demands during these periods is responsible a small wind turbine system and / or accumulation of electrical energy system. In exceptional cases, micro-cogeneration unit or a public grid.

Extension the solar photovoltaic system into several systems optimized capacity and chemical battery voltage electrical energy and the use of the principles photovoltaic cells using of solar radiation and diffuse solar radiation with extended-spectrum. This solution can seem like a solution to reduce the risk of failure of this energy source.

3.3 Accumulation of power system

Modified energy storage system uses the existing dual potential for accumulation. Accumulation through the production and storage of hydrogen gas by electrolysis of water and the accumulation of electrical energy to the station batteries. In addition, attention is paid to a station with battery accumulation of chemical energy as follows:

1. Choice of technology accumulation of chemical energy.
2. Selecting the optimal size of the storage system with chemical batteries and electric power distribution into groups (the "Bank").
3. Technology and algorithms, control of the charge and discharge process and strategy of charging and discharging of the individual "bank" of batteries in the context of the needs of the proposed family house.
4. Implementation of expanding storage systems (electric, electric hand tools, electric lawn mower, etc.) to support the optimization of energy flows.

3.3 Energy management, expert system, preparation and data collection

In order to ensure energy independence and optimize the properties of the system according of the selected criteria system must be strategically managed. A good management system can be based on information from the expert system, implemented multi-agent systems with machine learning.

To meet the expert system knowledge and implementation of energy management in the extended pilot system is necessary to create database links and decision rules based on knowledge of the energy needs of a family house (the FH) in a real environment. At the same time in the operation phase of the expert system must implement an algorithm to optimize properties of the system according to selected criteria and additional database expert system - necessary to implement machine learning algorithm.

To obtain the real data must be done long-term measurements of various physical quantities and the record in a time sequence. They measured the following tasks:

1. Measurement of solar radiation, air temperature and wind speed and direction versus time during the days of the year.
2. Measurement of heat in the family house in relation to time during the day and week and time of year in the calendar year.
3. Measurement of power consumption in the family house depending on the time during the day and week and time of year in the calendar year.

5 Conclusion

The use of hydrogen as a fuel (fig.1), it is not possible for various reasons. The main advantage of hydrogen is clean and closed cycle energy conversion. This process can be understood as energy storage. In the production of hydrogen by electrolysis is necessary to use only renewable energy sources.

The current implementation allows the development of projects related to themes of renewable and alternative energy sources at the University of Ostrava. Induced tight inter-faculty collaboration. It stimulates the development of cooperation and cooperation between universities in the workplace not only CR but also other research, development and commercial European and global workplace.

Organizational and technical background allows to realize a long-term teaching and presentation activities in fuel cells, electrolytic hydrogen production and distribution and storage of energy. The issue may be the general public and those interested in technical issues of renewable energy sources to learn more of the open days organized by the LFC, organized seminars, workshops and innovative website.

With this latest technology designed popularize issues related to renewable and alternative energy sources are doing to help further the visibility of high school, studying technical fields but also help inform the public about energy sources, effects on the environment in connection with their drawings and renewable sources of energy without tendentious and political influences.

6 Acknowledgment

Text above article was prepared as part of the IGA in 2012 sp2012/182 “Control of technological systems with alternate energy sources for independent sustainable development of complex systems”.

References

1. Friedrischková, K., Horák, B., Kazárik, J., Minařík, D.: Kaipán VoltAge and his serial hybridization, International Hydrogen and Fuel Cell Conference Birmingham, UK, 2012.
2. Friedrischková, K., Horák, B. Měřicí soustava pro sledování chybových artefaktů fotovoltaických solárních článků metodou elektroluminiscence, Trojanovice 2011, ISBN 978-80-214-4297-9
3. Minařík, D. a kol.: Projekt ENET – Hybridní energetický systém s technologiemi pro akumulaci elektrické energie, Workshop Perspektivní projekty vývoje řídicích a senzorických technologií 2012, Trojanovice, 2012, ISBN 978-80-214-4527-7

Testing of Dynamic Behavior of PMU and the Results of the Basic Tests

Marek Horinek and Petr Bilik

Department of Cybernetics and Biomedical Engineering, FEECS,
VŠB – Technical University of Ostrava, 17. listopadu 15, 708 33 Ostrava – Poruba
{marek.horinek, petr.bilik}@vsb.cz

Abstract. The PMU (Phasor Measurement Unit) is used for accurate measurement of synchronous phasor of voltages and currents. Based on synchronous phasor continuous measurement at the different location of distribution network is possible prevent fault which can cause blackout. Synchronous phasor measurement is described in IEEE C37.118-2005 standard. The IEEE C37.118-2005 is primarily focused on communication with the PMU and precision of the measurement at steady state. PMU manufacturers declare compliance with IEEE C37.118-2005, which doesn't mean correct behaviour of the PMU for dynamic changes in the power network. The new standard for the PMU is currently developing. This standard should contain both the issues included in IEEE C37.118-2005 and description of PMU testing in connection with dynamic changes in power network. This article deals with the implementation of tests for testing the dynamic properties of PMU. These tests are conducted by tester, which was designed and implemented based on virtual instrumentation. The results of several tests of commercial PMUs are presented in the article

1 Introduction

One of the requirements imposed on the distribution network of the electrical network is especially the safety and reliability of electrical energy supplies. At present, the issue of preventive measures how to stop from failure states in the distribution network, which may be the source of large power cuts in the electrical energy system, is often discussed. The importance of this issue is growing with the increasing number of dispersed sources of electrical energy from renewable resources (solar and wind power plants).

One of the steps dealing with this issue is implementation of a monitoring system of wide power networks WAMS (Wide Area Monitoring System). On the basis of monitoring, regulatory measures in the distribution network, that can positively influence the stability of the network, can be carried out. The system of monitoring of wide networks uses Phasor Measurement Units (PMU) [2] for the measurement of the parameters of the network.

The function PMU is defined by standard IEEE C37.118-2005. This standard describes the basic properties of PMU units and, especially the communication with these units. Nowadays, a new standard is coming to existence. This standard should contain both the matters defined in IEEE C37.118-2005 and the issue of testing of phasor measurement units. This article deals with implementation of tests for testing of dynamic properties of units for measurement of synchronous phasors. The tests are performed by means of the use of a tester working on the basis of virtual instrumentation. Virtual instrumentation provides flexibility of change of the required tester behaviour on the basis of current needs of the user.

2 The Issue of PMU Testing

Error evaluation of PMU measurement should be performed on the basis of so called total vector error (TVE). The computation of this error is carried out by means of the following relation:

$$TVE = \sqrt{\frac{(X_r(n) - X_r)^2 + (X_i(n) - X_i)^2}{X_r^2 + X_i^2}} \quad (\%) \tag{1}$$

where $X_r(n)$ and $X_i(n)$ are the measured values and X_r and X_i are the theoretical values at the moments of measurement. On the basis of the above stated relation, it is obvious that TVE is defined between theoretically derived values of vectors of synchronous phasors and the measured values. The standard defines two levels of accuracy at steady state – 0 and 1. The levels differ in the extent of changes of the reference conditions, where the PMU must reach the accuracy of 1%. The survey of tested qualities and their extent for compliance with the 1% accuracy of TVE (Total Vector Error) for individual levels are indicated in Table 1 [1]. At the end of the article, results of several tests that were performed in accordance with IEEE C37.118-2005 will be presented.

Table 1. Admissible limits of errors TVE for sustaining the level 0 and 1

Measured quality	Ref. condition	Level 0		Level 1	
		Extent of measurement	TVE[%]	Extent of measurement	TVE[%]
frequency	$f_{nominal}$	$\pm 0,5$ Hz	1	± 5 Hz	1
amplitude	$A_{nominal}$ 100%	80 % to 120 %	1	10 % to 120 %	1
phase	0 rad	$\pm \pi$ rad	1	$\pm \pi$ rad	1
harmonic distortion	<0,2% (THD)	1% of each harmonic to 50 harm.	1	10% of each harmonic to 50 harm.	1

3 The Testing Workplace

Since 2010, development of a workplace dealing with the issue of testing of phasor measurement units has been taking place in the Department of Cybernetics and Bio-medical Engineering of VŠB – Technical University in Ostrava. At the first stage, the hardware concept of the tester was designed which was subsequently put into effect.

3.1 The Hardware platform of the Tester

The tester is built on the concept of virtual instrumentation. The hardware consists predominantly of components by the company National Instruments. The decision to choose this concept was made on the basis of the long-time experience gained by the staff of our department in the area of virtual instrumentation.

The core of the testing workplace is the system NI PXI that is supplemented with the card of analogue outputs NI PXI-6733 and the card for time synchronization NI PXI-6682. Next, it contains a GPS signal receiver that is used for the time synchronization of the generated signal and time synchronization of other devices participating in the test, including the tested PMU. The synchronization signal is transferred to the devices by means of the protocol IRIG-B. The analogue output (AO) is equipped with a 16bit converter for each analogue output. The maximum sampling frequency for the analogue module used is 1,000,000 samples/s.

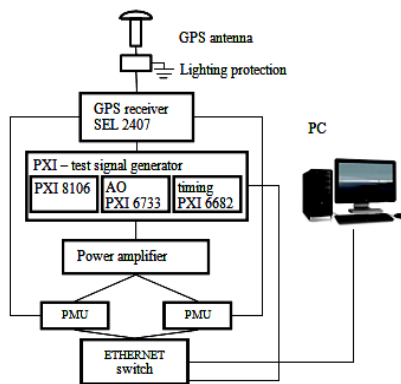


Fig. 1. The PMU tester block diagram

Two amplifiers DEXON DAP1500 are used for amplification of the analogue signal from the AO card. By means of these amplifiers, the output signal is amplified to a level which is suitable for excitation of analogue signals of the tested devices. The tester enables to generate 3 voltage signals.

3.2 The Software for Generation of Test Signals

The software application of the tester is created in the graphical programming language LabView by the company National Instruments. The application consists of several parts:

- editor of the course of the test signal,
- calibrator – measurement frequency amplitude and phase characteristics of the amplifiers used,
- the main user menu.

The editor for creation of the test signal allows creating of various courses of signals for the testing of phasor measurement units. The signal can be created either by a simple course with constant parameters (amplitude, frequency and phase) depending on the time, or it is possible to create a signal with variable parameters in time, see Figure 2. This enables a change of parameters that can come to existence in a real electrical network.

The application also performs computation of the theoretical values of the amplitude, frequency and phase of the generated signal. The individual courses of the signals can be stored in configuration files and, on their basis, it is then possible to display the testing signal in the main user menu of the application or, possibly, on the basis of the configuration file of the given signal, its generation is carried out.

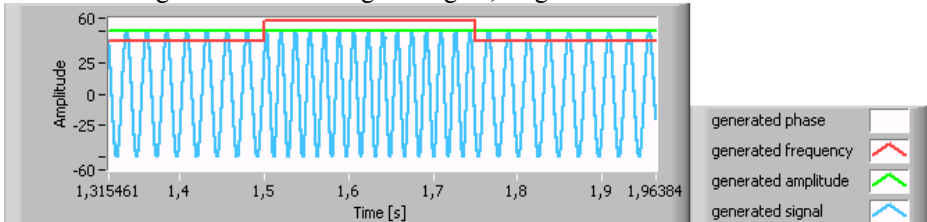


Fig. 2. An example of a change of the generated signal frequency

3.3 The Testing Process

With respect to the fact that classical audio amplifiers are used for the amplification of the signals for excitement of the input circuits of the tested devices, it is necessary to deal with certain problems concerning the amplified signal frequency dependence. After the measurement of the amplitude and phase frequency characteristics of the amplifiers used, nonlinearity of the amplifiers was found out in the range of low frequencies.

On the basis of the above stated facts, correction of the amplitude and the phase depending on the required frequency is performed when each signal is generated. The correction of the amplitude and the phase of the individual harmonic components contained in the signal are performed in the time domain.

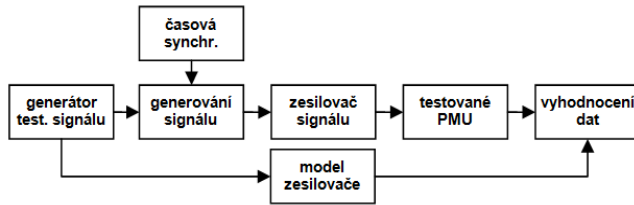


Fig. 3. Testing algorithm of PMU

Figure 3 shows the algorithm that is used for the testing of individual devices for the phasors measurement. It is evidenced from this figure that the course of the signal for the testing is both brought to the analogue output of the card and it at the same time passes through the block that represents the transmission function of the amplifier used. The discretized form of the transmission function obtained by identification is defined by the following relation:

$$H(z) = \frac{-1,718z^2 + 3,513z - 1,796}{z^2 - 1,907z + 0,907} \quad (2)$$

The theoretically computed course of the signal passes through the model of the amplifier; the data evaluation follows. The evaluation is carried out by comparison of the data that were obtained from the tested PMU and the value of the amplitude, frequency and phase of the generated signal after it passes through the model of the amplifier. The goal of the model is to simulate frequency dependence of the real amplifier on the theoretically computed course of the signal.

3.4 Results of the Partial Tests

The results of one of the tests that describes the behaviour the phasor measurement unit at steady state, i.e. when there are no dynamic changes of the measured parameters (the magnitude of the amplitude, the frequency and the phase), are shown in Figure 4, and Figure 5. The test is performed in compliance with IEEE C37.118-2005, see Table 1. Two devices SEL 351A by the American manufacturer SEL (Schweitzer Engineering Laboratories) were tested.

Parameters of the signal used for the test:

- amplitude 55 V
- frequency 49,5 Hz
- phase 0°

The individual courses in the below stated figures represent the dependence of the given quality (amplitude, frequency, or phase) on time. Each graph shows the course of the generated quality and the qualities that were obtained from the tested devices.

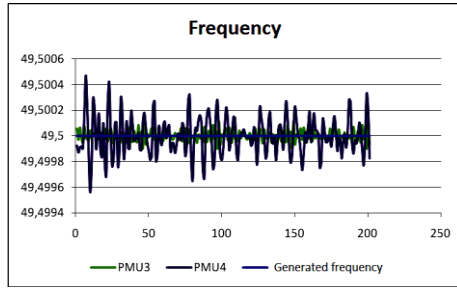


Fig. 4. Courses of the measured + generated frequency

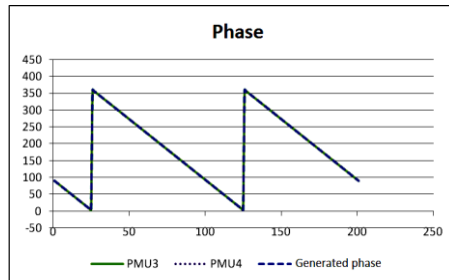


Fig. 5. Courses of the measured + generated phase

4 Conclusion

The development of the tester, both from the point of view of the hardware and the software application for creation of tested signals, still continues. Another goal we set is to carry out adjustments of the hardware part mediating amplification of the output signal. Steps are taken in order to improve frequency properties of the amplifiers in the range of low frequencies, which should result in improvement of accuracy of the generated signal. Furthermore, the arrival of a new standard dealing with the issue of testing of properties of phasor measurement units, on whose basis possible changes in the methodology of testing will be made, is expected.

The tests that have been prepared enable to carry out the verification of compliance of the properties of the tested PMUs with the requirements of the basic norm IEEE C37.118, the compliance of the properties with other requirements of the end user and, especially the properties of the tested PMUs at the occurrence of various perturbative factors that may occur in the real network.

In the following research, algorithms for testing of the PMU behavior for more elaborate conditions will be developed. Multiple repetitions and the following statistic evaluation are integral parts of the tests.

References

1. IEEE C37.118. *IEEE Standard for synchro phasors for Power Systems*. [s.l.]: IEEE Power Engineering Society, 21.10.2005. 65 s. Accessible from WWW: <<http://ieeexplore.ieee.org/stamp/stamp.jsp?tp=&arnumber=1611105>>.
2. Židek, J.; Šíma, J.; Hrudka, G. Testování vlastností jednotek měření fázorů (*Testing of properties of phasor measurement units*). Conference ČK Cired 2010, 2010. Tábor.
3. *Amplifiers DEXON* [online]. 2011 [cit. 2012-03-02]. DEXON DAP1500. Accessible from WWW: <<http://www.dexon.cz/data/popisy/27039.pdf>>.
4. National Instruments: NI LabVIEW System Identification Toolkit. [online]. [cit. 2012-03-13]. Accessible from: <<http://sine.ni.com/nips/cds/view/p/lang/en/nid/209045>>.

Built-in Smartphone Accelerometer Motion Pattern Recognition Using Wavelet Transform

Jakub Jirka and Michal Prauzek

Department of Cybernetics and Biomedical Engineering, FEECS,
VŠB – Technical University of Ostrava, 17. listopadu 15, 708 33 Ostrava – Poruba
{jakub.jirka1, michal.prauzek}@vsb.cz

Abstract. This paper is concerned with motion pattern recognition using built-in accelerometers inside of modern mobile devices - smartphones. More and more people are using these devices nowadays without using its full potential for user motion recognition and evaluation. As accelerometer magnitude level comparison is not sufficient for motion pattern recognition Morlet wavelet based recognition algorithm is introduced and tested as well as its device implementation is described and tested. Set of basic motion patterns walking, running and shaking with the device is tested and evaluated.

1 Introduction

Smartphone devices are spreading more and more in this society [1] and these devices themselves contain one of the most sophisticated sensors able to detect user motion in the three dimensional space we are living in. This motion is always connected to the real world context and represented by numeric values in the smartphone. This context can represent normal physiological everyday motion pattern as walking, running, driving or it can also represent pathological motion pattern as for example epileptic seizures or fall. All of this information is vital either for person's circadian rhythms [2] in case of physiological motion patterns or dangerous situation evaluation in case of pathological motion patterns.

This paper is concerned with context data extraction from device's accelerometer sensor and motion pattern recognition. Device used in this paper is Google Nexus S with built-in accelerometer ST Microelectronics - LIS331DLH capable of measuring acceleration $\pm 8g$ on 16bit ADC. Thus accelerometer gives sensitivity of 3,9mg/digit. Sampling frequency of this accelerometer varies from 23-26Hz in the normal setting but can go up to 50Hz in case of necessity.

Simple value threshold is not sufficient for motion pattern recognition as some of the movements like running shaking and fast walking have all similar amplitude. Thus time and frequency domain analysis is required. Based on the nature of accelerometer signal which is rather unpredictable and non-periodical, fast Fourier transform had been skipped and wavelet transform was used to classify different events.

2 Measurement

2.1 Accelerometer data acquisition and data dimension reduction

Dataset acquired from device was expressed by time series of three independent streams of data points from accelerometer axis X, Y, Z. This data express user acceleration in all direction. In most cases and use scenarios accelerometer data amplitude independent on direction is required. Thus in order of data dimension reduction and process simplification modulus of these three dimension values is calculated according to (2.1) as an absolute value of three axial data from the accelerometer.

$$Z_{ACC} = \sqrt{X^2 + Y^2 + Z^2} \quad (1)$$

Data retrieved from the device's accelerometer have frequency that varies between 23-26Hz which is sufficient for the most of the applications. Device is capable of frequency 50Hz in fastest setting. Three axial accelerometer is a very sensitive device capable of measuring acceleration $\pm 8g$ on 16bit ADC, accelerometer giving final sensitivity of 3,9mg/digit.

2.2 Motion patterns

Data measured by the device can be classified into motion patterns. These motion patterns described in this paper represents walking, running and shaking. The major attention is paid to the difference between running and shaking as it is same in the amplitude but different in time distribution as we can see on the figures (**Fig. 1**) and (**Fig. 12**). Walking and running is different in amplitude and thus not interesting for another processing in time or frequency domain.

This application is trying to put into context following activities (movement, shaking, pathological movements), thus this application is trying to create following equation motion pattern which is equivalent to contextual user action (movement). This request for real time processing gives a new request for minimal delay between data's input data analysis and output

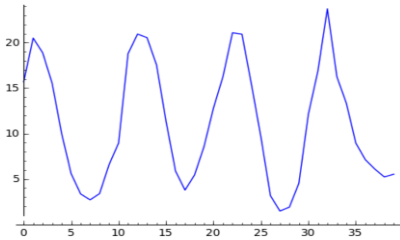


Fig. 1. Accel. running modulus values

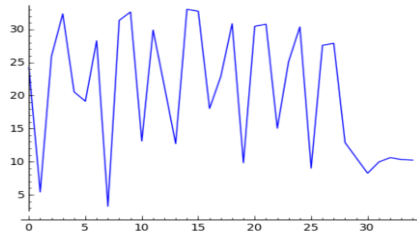


Fig. 2. Accel. shaking modulus values

2.3 Wavelet analysis

Thanks to furrier transform limitations for non-periodical signals wavelet analysis is used for accelerometer signal analysis and followed classification. Wavelet is a time limited signal (wavelet + window) that interfere with components of analyzed signals. Wavelet is specifically designed for classification of specific components and convolution of this wavelet and input signal is used to extract motion pattern information from the signal [6]. Convolution represents how strongly the components of wavelet presented in analyzed accelerometer signal are. Parameters and thus wavelet shape can be changed in time. Morlet wavelet had been selected as a mother wavelet.

Morlet wavelet is a sinus signal modulated by Gaussian window function of probability distribution and is defined by equation (2) in real numbers domain [3].

$$\Psi_{\sigma}(t) = c_{\sigma} \pi^{-\frac{1}{4}} e^{-\frac{1}{2}t^2} (\cos(\sigma t) - \kappa_{\sigma}) \tag{2}$$

σ defines change in a time-frequency properties of wavelet. Lesser the value better the time resolution for the cost of frequency resolution. In this application $\sigma=5$ is used shown on figure (

Fig. 3).

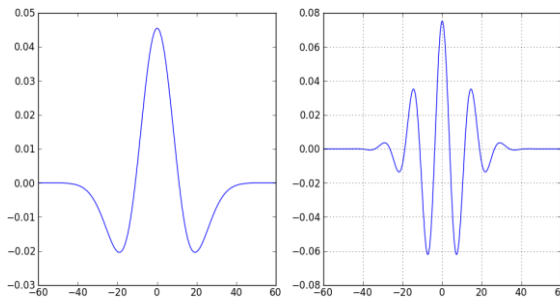


Fig. 3. Morlet wavelet with $\sigma = 1$ on left and $\sigma=5$ on right

Wavelet analysis performed on input signal is defined with equation (3) as convolution of input signal with given wavelet and implemented by fast wavelet transformation performing convolution of FIR filters bank. Filters in filter bank are created by the wavelet property change. Fast wavelet transform is using downsampling of mother wavelet samples changing its central frequency. Downsampling to the half number of samples gives twice the central frequency of original wavelet.

$$\omega[n] = \sum_{-\infty}^{+\infty} X[m]f[n - m] \tag{3}$$

2.4 Wavelet algorithm implementation for accelerometer data analysis and motion pattern extraction

Implemented application is using cascade of low pass H(scaling) and high pass G(wavelet) filters created as a quadrature mirrored filters [6] of scaled mother wavelet. Used scaled versions of mother wavelet are described in table (Table 1). Mother wavelet is defined from -2 to 2 with default step between samples 0,0125 displayed in figure (

Fig. 3).

Table 2. Scaled wavelets table that forms the filter bank

Wavelet ID	Time step between samples
w1	0,0125
w2	0,0250
w3	0,05
w4	0,1
w5	0,2
w6	0,4
w7	0,5

Scaled Morlet wavelet is applied to the input signal as described in chapter (2.3). Output signal power is calculated according to the following equation (4).

$$p_n[k] = \frac{1}{N} \sqrt{\sum_{k-N+1}^k w_n[k]^2} \tag{4}$$

3 Wavelet algorithm testing results

At first graph of signal that represents running is displayed in figure (Fig. 1). This signal's wavelet analysis is displayed in figure (Fig. 4). This figure and all others that

follow this result contains input data in a first subplot wavelet results in the second subplot and signal power spectrum in the third subplot.

Running test results

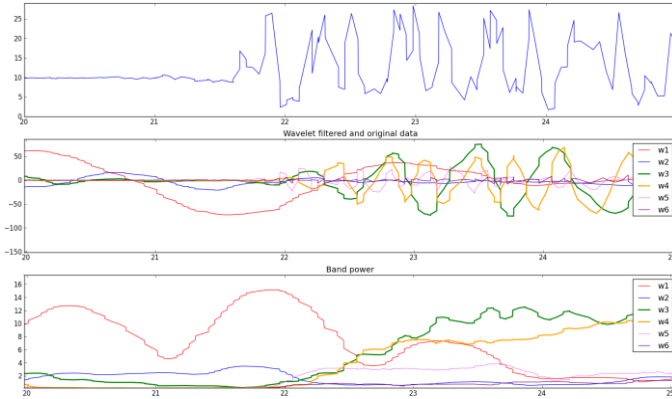


Fig. 4. Running action wavelet analysis with highlighted w3 and w4

Shaking test results

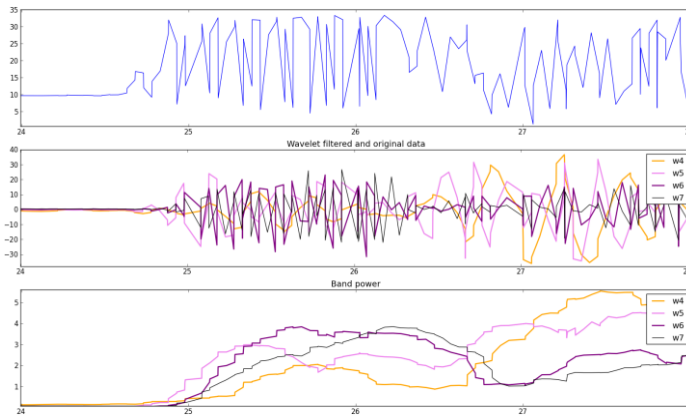


Fig. 5. Shaking action wavelet analysis with highlighted w4, w5 and w7

As expected energy of shaking had moved to higher frequency band and most time and frequency expressing wavelet is wavelet w6 (**Fig. 5**) that has step between samples 0,5 which gives us 8 samples in scaled wavelet from -2 to 2. This means at sampling frequency 25Hz that shaking was at frequency 3,125Hz. From this we can clearly extract the information about shaking from accelerometer signal.

Test and results evaluation

Algorithm motion pattern extraction capability and correct classification had been tested in number of cases using three devices with built in accelerometers running android operating system. These devices are, Samsung Nexus S, Motorola Razr, LG Optimus One. Each motion pattern was tested 8 times always with different user. Tested parameters were motion pattern extraction success rate with other variables of device type and device placement.

Device implementation notes

Motion pattern extraction and detection algorithm was implemented in Java and C programming languages into smartphone device running on Android platform. Performance hungry sections of application code were implemented in C programming language using NDK (Native Development Toolkit). These sections of code includes fast wavelet transform algorithm that renders into series of FIR filter bank convolutions.

Conclusion

This article proposes a solution to the motion pattern extraction and classification by the means of wavelet analysis method. Fast wavelet analysis forming a filter bank of quadrature mirrored low pass (approximation coefficients) and high pass (detail coefficients) is used to extract and identify motion pattern like walking, running or shaking.

Algorithm introduced and used in this paper is only the base algorithm for more sophisticated algorithm used for the classification of spastic epileptic seizures detection algorithm.

Project publications

This project results has been accepted to be presented on SOCO 2012 conference.

References

1. M. Brownlow. "Smartphone statistics and market share", Email marketing reports, June 2010
2. A. Cagnacci, J. A. Elliott, S. S. Yen. "Melatonin: a major regulator of the circadian rhythm of core temperature in humans", *The Journal of Clinical Endocrinology & Metabolism* August 1, 1992 vol. 75 no. 2. P447-452. University of California-San Diego, 1992
3. P. Barralon, N. Vuillerme, N. Noury. "Walk Detection With a Kinematic Sensor: Frequency and Wavelet Comparison ", *Proceedings of the 28th IEEE EMBS Annual International Conference*, New York City, USA, Aug 30-Sept 3, 2006
4. P. Goupillaud, A. Grossman, J. Morlet. "Cycle-Octave and Related Transforms in Seismic Signal Analysis", *Geophysical Research Letters*, 1984

5. S. Mallat. A Wavelet Tour of Signal Processing. 2nd ed. Academic Press, 1999. P. 5, 257.
6. K. Schneider, M. Farge. “Wavelets: Mathematical Theory”, Encyclopedia of Mathematical Physics, 2006. P426 – 438.
7. J. Vrána. „Quadrature mirror filter banks with sigma delta modulators“, Doctoral thesis, VUT-Brno, 2007

Handheld Vital Function Monitoring Device

Jan Kijonka and Marek Penhaker

Department of Cybernetics and Biomedical Engineering, FEECS,
VŠB – Technical University of Ostrava, 17. listopadu 15, 708 33 Ostrava – Poruba
jan.kijonka@vsb.cz

Abstract. The paper deals with the hardware design of a mobile unit for vital function data monitoring. General purposes of the device are measurement, visualization, data storing, viewing and wireless transmission of the measured data to create a part of a home-care system. The device is built-in a small handheld package powered by a single cell battery and equipped by a user communication interface, ECG, accelerometer, temperature, wireless Zigbee transceiver, audio DAC, charger, fuel gauge and real-time clock modules, all controlled by a low-cost and low-power AVR 8-bit RISC architecture microcontroller. Zigbee wireless provides a connection with some medical equipment, as external pulse oximeters, thermometers, accelerometers, scales, passive infrared sensors (PIR sensors), chest heart rate meters and other devices including the base station of the home-care system.

1 Introduction

The most important features in today's patient monitors are mobility, ease of use and patient data transfer between other medical devices. The mobility is achieved by miniaturizing and integrating of these electronic circuits that serves as the main components of the medical devices. Many functions can be integrated on a single chip with several analog inputs and one serial or parallel digital communication output interface. For example, the analog front ends with capability of ECG, EMG, EEG and other biosignals measurements integrated on a single chip, including high resolution delta-sigma analog-to-digital converters (ADCs) with built-in programmable gain amplifiers (PGAs). They incorporate all of features commonly required in medical ECG and EEG applications. The high level of integration reduces also the power and overall cost of whole measurement system. The inner circuit allows many configurations accessible through the digital communication interface.

Ease of use can be achieved with wide spectrum of user interface possibilities. Today, ever-increasing usage of touch screens enables a comfortable user menu browsing and data entering without physical keypad usage, which again cuts down the device space requirements and gives more space for large display, that can be installed over whole device surface.

The patient data transfer needs to be possible across wireless or serial communication like USB, RS232.

Two most used wireless communication standards for medical application are ZigBee and Bluetooth. More and more medical devices especially in patient monitoring and home healthcare can benefit from low energy wireless technologies. ZigBee is simple reliable, low cost and low power standard, that can be used to monitor patients with ZigBee sensors in homecare or in hospital area application.

Bluetooth low energy solutions are designed for low cost, low power and short range connectivity. The technology enables direct communication to cellular phones, laptops and other devices like sports and fitness watches, GPS.

Patient monitoring and biosignals data transferring is important feature of discussed devices, but often one poses more requirements, as real-time measured data analysis and remote health care problems signaling. In this case, the control unit and its correct selection is necessary for reaching the required features of the whole system. The key requirements are the low power consumption and system versatility.

2 Materials and Methods

The main idea of the project was to design a low cost simple handheld vital function monitoring device, embedded in a mobile phone case, using the original LCD, keypad and speaker, and powered by the original single cell Li-Ion battery. Another requirement was short development of the application. It was reached by selection of simple, already well-proven control unit for the project.

The requirements for monitored vital functions:

- ECG Einthoven and Goldberg leads measurement using the 4 limb electrodes RA, LA, LL, RL, with right leg drive (RLD) and hardware pacemaker detection.
- Two temperature sensors for internal and external temperature measurements with a possibility of body temperature measurement and a capability of storing the measured values.
- Two 3-axis accelerometers for internal and external static and dynamic acceleration measurements. Motion, position and activity detections, additional possibilities (pedometer, epileptic fit detection).
- Wireless ZigBee communication for data transreceiving and remote home care monitoring
- PPG biosignal measurement, body weight, location and events data monitoring and storage from external sensors and devices via ZigBee.
- Time waveform trends of measured biosignal data
- Real time clock, date, time and alarm settings
- Emergency call button

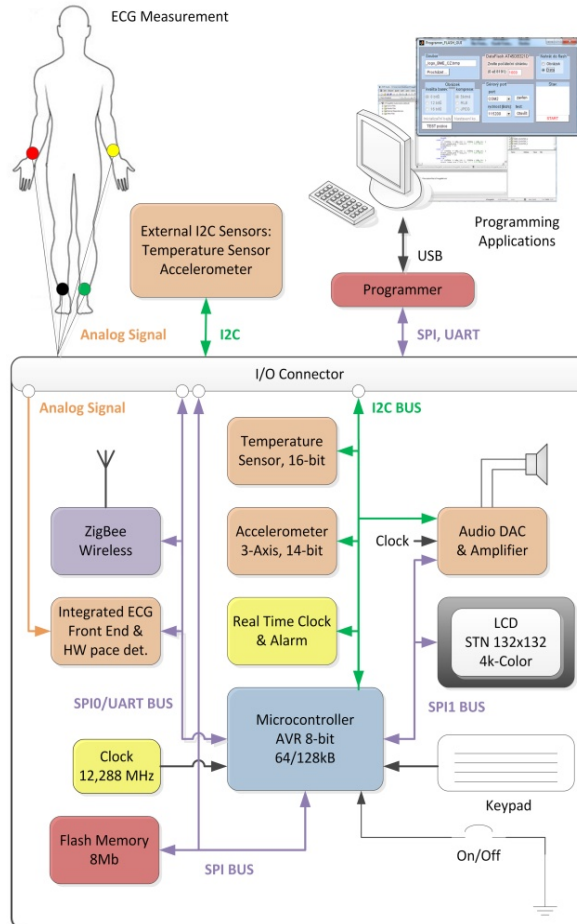


Fig. 1. Vital function monitoring system; block diagram of the device

Microcontroller. As the device's microcontroller was chosen an 8-bit AVR architecture based chip with 64 or 128kB of programmable flash memory and 4 or 16kB SRAM. The current consumption is only 3,5mA in active mode and 0,1 μ A in power down mode. The crystal frequency clock of 12,288MHz was chosen to deliver clock also to the Audio DAC clock input. The design of the device has brought the following requirements for the communication interfaces: one serial peripheral interface (SPI), two universal serial asynchronous / synchronous receiver and transmitter (USART), capable to operate in SPI mode and one inter-integrated circuit (I2C) interface.

ECG. The ECG analog front end has eight differential inputs for maximum of 12-lead ECG measurement with resolution of 24-bit on 2400mV range. It operates at data rates from 250SPS to 32kSPS, allowing the implementation of software PACE detection. The ECG analog front end enables also the lead off detection. The application

doesn't use all the 12 leads, so the remaining inputs are used for augmented leads hardware measurement and for the test square signal. The hardware pace detection is provided by the analog output of the device and a simple circuit with feedback connected to one of the device general purpose inputs. The output from the analog front end is the all digital SPI.

Accelerometer. Accelerometry provides the three-axis, 14-bit accelerometer, with programmable selectable sensitivity of $\pm 2/\pm 4$ or $\pm 8g$ and frequency range up to 800Hz. The built-in feature allows automatic static orientation detection (portrait/landscape, up/down, left/right, back/front) position identification. Next feature - motion detection - can be used for human body movement detection or for entering the device power saving mode. The dynamic accelerometry is utilized for activity level measurement, and provides many additional usage possibilities as pedometry and sleep disturbances analysis. It can be also used in sport disciplines for motion trajectory and stroke strength analysis.

Thermometer. The temperature sensor measures with the accuracy of $\pm 0,2^{\circ}C$ in the range from $-10^{\circ}C$ to $+85^{\circ}C$ with 16-bit resolution. In external mounting it is acceptable for approximate body temperature measurement too. More accurate results can be achieved by calibrating the sensor.

Memory. For the data storage serves the 8Mbit flash memory with its own SPI interface to perform continuous reading/writing operation without additional addressing the memory. This SPI is available also on the I/O connector of the device for the microcontroller in-system programming (ISP) mode.

Audio DAC. The device also implements an audio DAC for sounds and speech reproduction and for the alarm clock. However, the sounds cannot be used continuously with waveform rendering, for example for beat beeps, due to absence of direct memory access (DMA). The μC is not able to handle several interrupts at once.

User Interface. The user interface consists of mobile phone keypad pushbuttons and a super-twisted nematic (STN) liquid crystal display (LCD) with 132x132 pixels resolution and 4k colors. The user interface graphic a simple several level user menu with color icons associated with some function or function group.

ZigBee. The ZigBee wireless solution is connected to the SPI0 together with the ECG module to subsequently transmission the ECG data stream. The SPI0 is also connected to the I/O connector. Like that it serves for programming the flash memory in UART mode.

Power Management. All the used circuits are designed for the voltage from 2,7 to 3,3V. However, the microcontroller clock frequency is purposely chosen higher, to achieve the higher computing power. So, for keeping stability of the application, there are used the 3,0V low drop out voltage (LDO) regulators. When the battery is fully discharged, the voltage falls just to the 3V threshold, the drop out voltage is only 40mV at 250mA. Therefore, it is not necessary to use the non-effective step-up converters. The device has 3 LDOs. The LDO1 is a low noise (filtered) power, supplying the ECG analog front end. The LDO2 is always enabled, even if the device is in power-down mode. In power down mode (the device is powered off), the current consumption is only 0,4 μA for μC power-down mode and 0,3 μA for the real-time clock,

which holds the date, time and alarm in active mode. The device is activated again by power on/off pushbutton (fig. 1), connected to an interruptible μC input. The LDO3 is a power supply for another external devices (memory, ZigBee, Thermometer, Accelerometer, Audio DAC, LCD), this voltage is also accessible on the device's I/O connector.

The device has a fuel gauge to determine the full charged and remaining capacity, time to discharge, actual voltage, current of the battery and other fuel gauge parameters. These parameters are available in the device user menu.

For the backlight there is a DC-DC converter controlled by PWM signal. The backlight has the most current consumption of whole system. So this is reasonable to set the backlighting to the minimal necessary level and turn it off when it is not necessary.

3 User Interface

The main menu window offers these three possibilities:

- Monitoring (monitoring of a real-time biosignals data measurement; signals with the constant sampling period)
- Time Trends (records of one shot measured values from some meters or slower varying signals – one second period or more)
- Settings

Monitoring Section. In the monitoring section, only the PPG is not possible to measure directly by the device. This biosignal is measured by an external PPG device. In the occurrence of the measurement, the user is advised by a short message displayed on the LCD.

Each monitored signal can be recorded. The number and total length of the records is limited by built-in memory size. For typical sampling frequency of 250SPS, this is possible to record about 30 minutes of 3 leads ECG to the usable space in the flash memory.

There are several options for waveform signals imaging for ECG, PPG and accelerometry. The ECG waveform imaging speed is adjustable to 10 or 25 or 50mm/s. On the screen it can be displayed one signal or the screen can be splitted to 2 or 3 parts to show up to 3 signals simultaneously. The same applies for PPG and accelerometry X, Y and Z signals. The user can set data rates, sensors sensitivities or others in appropriate setting sections.

Time Trends Section. The time trends section is usable for the long term data browsing and analyzing. For example, the human body temperature or physical activity can be measured directly by the device. Data of the internal and external thermometers and accelerometers can be stored to make time trends.

The blood pressure, body weight and location data are accessible only via ZigBee. The body scales, sphygmomanometers, PIR sensors and other medical devices

can be arranged on the monitored area.

Settings. The last main menu section is devoted to appropriate function settings or reviewing.

3.1 Biometric Data Storage and Broadcasting

The biometric data as the blood pressure, body weight or internal and external temperature can be stored automatically, or with a selectable time period to the flash memory. For these one shot and long term data storage, there is allocated a fixed size of the flash memory of the array data type. When the maximum index in the array is reached, the index returns back to the beginning of the array, so the oldest values are re-written by newer ones.

The data from the ECG and ACC modules and all the data with a constant sampling period are stored as a data stream. The data stream has defined opcodes for differentiate signals from one to another. At the beginning of each record is the header, each record is finished by a stop opcode.

For transmitting the records via Zigbee, there is the similar system of the data streaming, but without headers and stop opcodes.

The user can select the period for internal and external temperature storage, or the data storage of selectable data can be disabled.

4 Conclusion

The work deals with the handheld vital function monitoring device hardware designing and description of the selected implementation. Using highly integrated circuits, it is possible to design a small device with integrated analog front end 12-leads ECG, accelerometry and temperature measurements with the popular wireless ZigBee interface.

References

1. Farahani, S. *ZigBee Wireless Networks and Transceivers*, Newnes, 2008.
2. Havlík, J., Uhlíř, J., Horčík, Z. *Human Body Motions Classifications*, In IFMBE Proceedings EMBEC 2008, [CD-ROM], Berlin: Springer, 2008, ISBN 978-3-540-89207-6.

An Approach to Knowledge Adaptation of Regulator in PID Control with PLC Implementation

Jiri Kocian and Jiri Koziorek

Department of Cybernetics and Biomedical Engineering, FEECS,
VŠB – Technical University of Ostrava, 17. listopadu 15, 708 33 Ostrava – Poruba
{jiri.kocian1, jiri.koziorek}@vsb.cz

Abstract. The paper sums up research and development of fuzzy approach applied for adaptation of parameters of classical PID controllers. It introduces its implementation on programmable logic controllers S7 300/400. It also shows the concept of supervisor – an expert system that handles the above mentioned adaptation. Control performance monitoring, setting the model of the regulated system, its verification, the process of identification and subsequent adaptation of PID controller parameters are discussed.

1 Introduction

On the field of fuzzy expert systems that perform monitoring and adaptation of conventional controllers a lot of publications has been released [e.g. 1, 2, 3]. Most of them focus on problematic of fuzzy supervisors at a higher control level; evaluating responses to a step change of set-point and based on gained data they adapt the controller parameters according predefined fuzzy rules.

In several contributions we described different self-tuning techniques on PLC background and control systems with self-tuning methods design [4, 5, 6, 7].

In following articles, we have focused on the theoretical background and practical implementation of fuzzy-based control systems. We proposed and presented function blocks for fuzzy regulator [8], PID regulator [10], fuzzy expert system [9], statistical evaluation of regulation and control performance monitoring [11] and identification of regulated systems [15, 16]. Then we proposed complex system for knowledge adaptation of regulator in PID control with PLC implementation [11, 13]. Besides this we described application of modeling and simulation techniques for technology units in industrial control which we need for our complex system [12, 14].

Chapter 2 introduces concept of knowledge adaptation of PID controller based on evaluation of quality of control.

Chapter 3 contains brief introduction of our results in area of implementation of system for knowledge adaptation.

2 The concept of the knowledge adaptation of PID regulator

Above the basic control loop containing PID controller and regulated plant there is Supervisor – expert knowledge system. Detailed structure of the feedback control loop with Supervisor is shown on Fig. 1.

Supervisor also contains further particular functionalities, such as:

- Monitoring of quality of control. Regarding practical operation, the knowledge system will be implemented for evaluation of quality of control based on measured data in online mode.

- Determination of the model of regulated plant if quality of control becomes worse. In this case there comes an analysis resulting in finding out if this is caused by the fact that dynamics of the regulated plant is changed in current time point and current operating point. If the knowledge system detects such situation, it launches identification experiment which based on measured data determines local model of regulated plant or model of control circuit.

- Control of identification experiment.

- Synthesis of the controller based on identified model, resulting in adaptation of the parameters of PID controllers either by knowledge or classical methods.

Evaluation of criteria of control quality and determination of controller constants will be carried out by use of knowledge approaches, e.i. by fuzzy logic. In order to perform the identification experiment a white noise signal has been chosen. Model of controlled plant will be determined in the form of SOPDT (second-order plus dead time) by use of appropriate optimization algorithm.

All the algorithms mentioned above will be implemented at the lowest control level, within programmable controller.

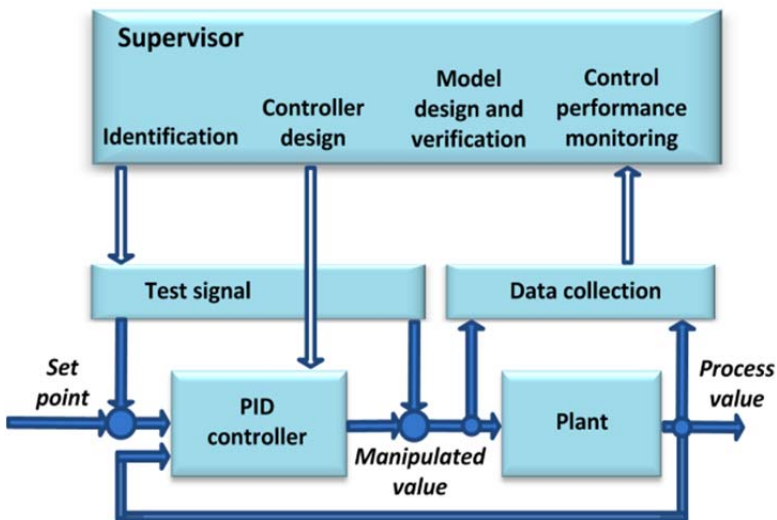


Fig. 1. The concept of adaptation of PID controller.

We have implemented several function blocks for control performance monitoring function and for identification. For regulated system identification we use ARX procedures.

For practical experiments we used the simulated closed loop with PID controller and controlled systems to make simulated controlled systems outputs.

Implemented functions *ArxIdent* (Leas square method with exponential forgetting) and *RecArxIdent* (Recursive least square method with exponential forgetting) are used to determine controlled system models. All functions are directly implemented to the PLC so no connections to higher levels of the control systems are needed.

Example of implemented functions for identification of controlled system is on fig. 2. Detailed description of AR, information of implementation and practical results are in [16].

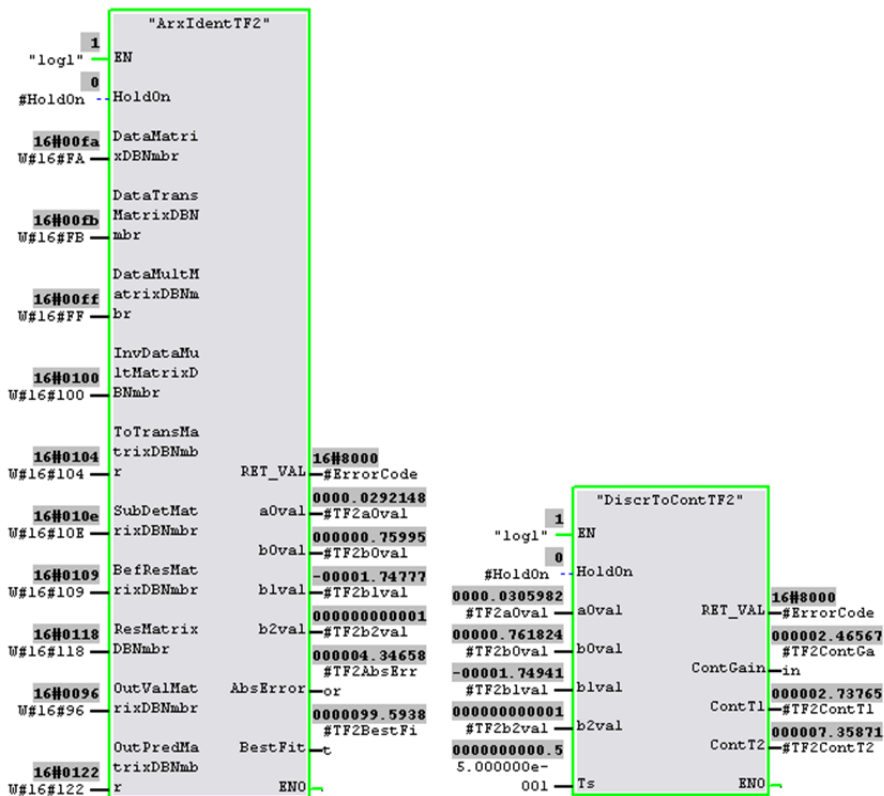


Fig. 2. Example of implemented functions for identification.

3 Practical results

In area of practical results we have implemented number of function blocks and functions for PID controlling, control performance monitoring (Fig. 3). Detailed descrip-

tion, implementation details and practical results are in references [4, 5, 6, 7, 8, 9, 10, 11, 12, 13, 14, 15, 16].

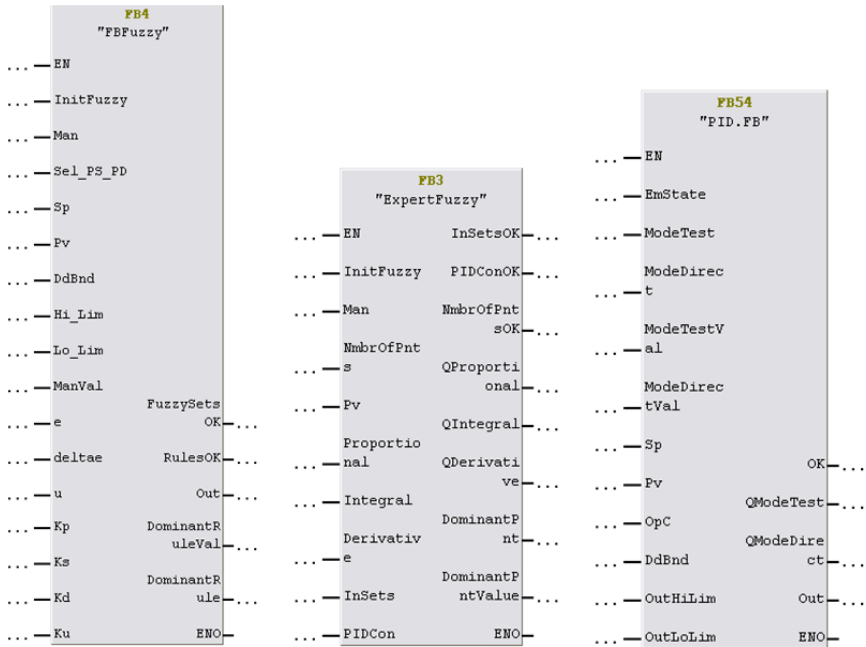


Fig. 3. Implementation of some functions and function blocks.

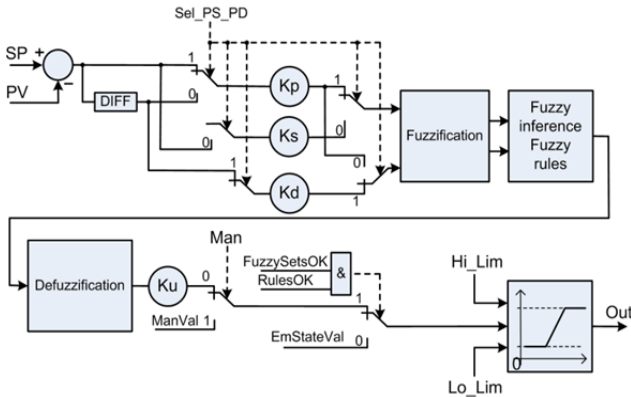


Fig. 4. The block scheme of the implemented fuzzy regulator.

4 Conclusion

In this contribution we present the approach to knowledge adaptation of regulator in PID control with PLC implementation and its individual components. The usage of controlled systems model design by ARX procedures with PLC implementation and other function blocks and functions are presented. These functions will be used in a complex fuzzy knowledge adaptation mechanism for PID regulator control.

The following work at the research area according the concept of the knowledge adaptation of PID regulator will include

- Design and tuning of on-line knowledge system for adaptation of parameters of PID controllers according identified models.
- Testing the concept of the adaptation mechanism on the real plant in the industry.

Acknowledgements

Research and development during my PhD. studies have been supported by several projects of Student Grant System, FRVS grant system, VSB-TU Ostrava and also by the company of Ingeteam a.s. Ostrava.

References

- [1] AYDOGMUS, Z.: Implementation of a fuzzy-based level control using SCADA. In Expert Systems with Applications. Volume 36, Issue 3 Part 2, April 2009, Pages 6593-6597. ISSN: 09574174.
- [2] BABUSKA, R., DAMEN, M., R., HELLINGA, C., MAARLEVELD, H.: Intelligent adaptive control of bioreactors. In Journal of Intelligent Manufacturing. Vol. 14, Num. 2, p. 255-265, DOI: 10.1023/A:10229637/16905.
- [3] VAN NAUTA LEMKE, H., R., WANG DE-ZHAO: Fuzzy PID Supervisor. In Decision and Control, 1985. Proceedings of the 24th IEEE Conference. DOI: 10.1109/CDC.1985.268559.
- [4] KOCIAN, J., KOZIOREK, J.. Self-Tuning Techniques on PLC Background and Control Systems with Self Tuning Methods Design. Advances in Electrical and Electronic Engineering. 2010, Vol. 8, No. 2, p. 40-47. ISSN 1804-3119.
- [5] KOCIAN, J., KOZIOREK, J.. An Outline of Advanced Process Control and Self Tuning Techniques on PLC Background. In ETFA 2010: Proceedings of IEEE International Conference on Emerging Technologies and Factory Automation, Bilbao, Spain, September 13 - 16, 2010. ISBN 978-1-4244-6849-2.

- [6] KOCIAN, J., KOZIOREK, J.. An Outline of Advanced Regulation Techniques on PLC Background and Control Systems with Self Tuning Methods Design. In PDES 2010: Proceedings of 10th IFAC International Workshop on Programmable Devices and Embedded Systems, Psczyna, Poland, October 06 – 08, 2010, p. 143-148. Psczyna, Poland.
- [7] MARTEN, T., TYSER, J., AXMAN, D., KOCIAN, J. Možnosti modelování a simulace výrobních technologických procesů v průmyslu. In Modelování procesů 2010: Proceedings of 1st Workshop on Simulation of Processes, Jihlava, Czech Republic, October 21, 2010, p. 66-82. ISBN 978-80-87035-32-0.
- [8] KOCIAN, J., KOZIOREK, J., POKORNY, M.. Implementation of Fuzzy Logic Control Based on PLC. In ETFA 2011: Proceedings of IEEE International Conference on Emerging Technologies and Factory Automation, Toulouse, France, September 5 - 9, 2011. ISBN 978-1-4577-0016-3.
- [9] KOCIAN, J., KOZIOREK, J., POKORNY, M.. An Approach to PLC-Based Fuzzy Expert System in PID Control. In ICDIPC 2011: Proceedings of International Conference on Digital Information Processing and Communications, Ostrava, Czech Republic, July 7 - 9, 2011.
- [10] KOCIAN, J., KOZIOREK, J., POKORNY, M.. An Approach to PLC-Based Fuzzy Control. In IDAACS 2011: Proceedings of Intelligent Data Acquisition and Advanced Computing Systems: Technology and Applications, Prague, Czech Republic, September 15 - 17, 2011, p. 322-327. ISBN: 978-1-4577-1424-5.
- [11] KOCIAN, J., OZANA, S., KOZIOREK, J.. Fuzzy Knowledge Adaptation Mechanism for PID Controllers Implemented in PLC S7-300/400. In 3CA 2011: Proceedings of International Conference on Computer, Communication, Control and Automation, Zhuhai, China. November 19 - 20, 2011.
- [12] KOCIAN, J., TUTSCH, M., OZANA, S., KOZIOREK, J.. Application of Modeling and Simulation Techniques for Technology Units in Industrial Control. In 3CA 2011: Proceedings of International Conference on Computer, Communication, Control and Automation, Zhuhai, China. November 19 - 20, 2011.
- [13] KOCIAN, J., OZANA, S., KOZIOREK, J.. The Concept of Knowledge Adaptation of PID Controller with PLC Implementation. In ICACTE 2011: Proceedings of 4th International Conference on Advanced Computer Theory and Engineering, Dubai, UAE. December 28 - 30, 2011.
- [14] KOCIAN, J., TUTSCH, M., OZANA, S., KOZIOREK, J.. Modeling and Simulation of Controlled Systems and Technologies in Industrial Control. In ICACTE 2011: Proceedings of 4th International Conference on Advanced Computer Theory and Engineering, Dubai, UAE. December 28 - 30, 2011.
- [15] KOCIAN, J., OZANA, S., POKORNY, M., KOZIOREK, J.. Optimization of Fuzzy Regulator Parameters by Genetic Algorithm. In TCP 2011: Proceedings of International Conference on Technical Computing Prague, Prague, Czech Republic. October 8, 2011.
- [16] KOCIAN, J., KOZIOREK, J., OZANA, S.. An Approach to Identification Procedures for PID Control with PLC Implementation. IEEE International Conference on Emerging Technologies and Factory Automation, ETFA 2012, Krakow, Poland.

Energy Storage Utilizing Hydro Pump and Battery Technologies

Jaromír Konecny¹, Simon Holmbacka², Dorotea Bueno Silva³,
Roman Chvalek¹, and Amer Kareem Al Fatlawi⁴

¹VŠB-TU of Ostrava, Ostrava - Czech rep.

{jarek.konecny, roman.chvalek}@gmail.com

²Abo Akademi Univ., Turku – Finland, sholmbac@abo.fi

³Univ. of Minho, Guimaraes – Portugal, doroteab@uol.com.br

⁴Newcastle Univ., Newcastle – UK, amer.kareem@ncl.ac.uk

Abstract. Renewable energy sources rapidly gain popularity in the Europe together with the technology to utilize these sources efficiently. Fluctuations in the power output depending on meteorologist reasons are a usual forecast when using renewable energy sources such as wind, wave or solar power plants. Optimization and further development of these techniques is an ongoing issue to improve the infrastructure of renewable energy sources. This proposal investigates improvements the temporary energy storage techniques hydro pump in combination with renewable energy sources for off-grid locations. This proposal is a base for recognizing state-of-the-art solutions, create an environment suitable for technical improvement and apply novel solutions to either retrofit existing systems or new constructions. We propose a marketing model for optimizing size-to-market of an energy storage facility. With the innovations proposed we expect improvement in the energy storage sector beneficial for financial marketing, sustainability and technical efficiency.

1 Introduction

Power fluctuations and uneven energy production in relations to consumption are the major reasons for temporary energy storage systems. These occurrences are most clearly visible when using renewable energy sources, since these types of energy sources rely on unstable and fairly unpredictable factors such as weather conditions. For these reasons, hydro pump [2] and battery [1] storage has been used for several decades, and is continuously being improved.

An applicable real-life system should provide the necessary capacity for the customers during all parts of the day. It should prove safety and stability both for personnel and the end users. The power system should also be environmentally sustainable, but still have a financial budget reasonable for investors and financiers. The aforementioned parameters usually conflict each other, which means that compromises must be made with respect to requirements stated by many partners. This problem of optimization often shows in marketing as the investors demand payback for their investments. This area of research has proven to clearly show room for improvement – a reason for why initiative has been taken, from our part, to move closer towards efficient integration of renewable energy sources with energy storage,

better utilization of new technologies such as the smart grid and decreasing use of fossil fuel-based energy sources.

In this proposal novel methods are applied for improving the already existing techniques in the area of temporary energy storage in off-grid locations such as small islands. As mentioned, several parameters are of major importance when creating a globally beneficial system. With modern techniques such as smart grid [4] new doors open for improving the storage system; making it easier to accommodate to renewable energy sources and more tightly integrate to the power grid. By combining state-of-the-art technologies, mutual benefits for multiple partners have a common potential to increase. For this reason investigation has been initiated for fabricating a hybrid between hydro pump energy storage and battery storage. This conjunction of technologies will provide possibilities for using the huge energy capacity of hydro pump storage, while still maintaining the fast response time of the battery to adapt to changes in power demands. Other properties of both technologies such as reliability and flexibility create a common product with advantages over currently existing competitors.

Locations not connected to the main grid show different objectives for the energy ecosystem. Main objectives of the energy provider are not necessarily energy export and economical profit as the situation on the mainland. The major obstacle is instead to, with a limited power supply, deliver energy to the whole community during any environmental circumstances. Our focus in this project is on the lastly mentioned areas; a field of research opens to improvements and innovations.

2 State-of-the-art

In order to reconcile our propositions with the current technologies, we must consider the state-of-the-art development and currently positioned products on the market. This section gives an overview of energy storage techniques applied hydro pump energy storage. After this introductory briefing, Section 3 presents a proposal beyond state-of-the-art for improving the energy storage techniques.

Pumped Hydro Storage (PHS) is already a well-developed technology on the market, and it is a part of the renewable energy sources and its ecosystem. The main parts of a PHS (Fig. 1) is two water reservoirs, tunnels that convey water from one reservoir to another, a reversible pump/turbine, transformers, and transmission connection.

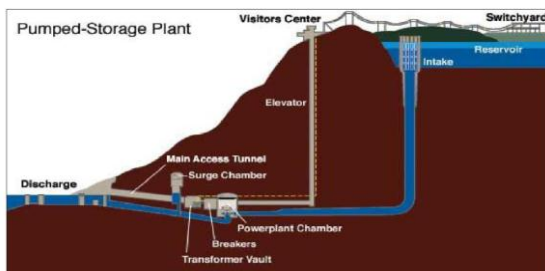


Fig. 1 Structure of a hydro pump energy storage system.

Pumped-storage is a type of hydroelectric power generation used by certain power plants for load balancing. The method stores energy in the form of water, pumped from a lower elevation reservoir to a higher elevation. Low-cost off-peak electric power is used to run the pumps. During periods of high electrical demand, the stored water is released through turbines to produce electric power. Although the losses of the pumping process makes the plant a net consumer of energy overall, the system increases the revenue by selling more electricity during periods of peak demand (when electricity prices are highest). Pumped storage is the largest-capacity form of grid energy storage now available. The amount of stored electricity is proportional to the product of the volume of water storage in upper lake and the height between the reservoirs. [3]

3 Dual-tube system

The main advantage of the hydro power plant in isolated off-grid locations is to utilize the renewable energy sources and eliminate the dependency of conventional energy sources. For increased efficiency of the hydro pump storage, our innovation is to add one extra tube and divide the plant into two parts shown in Figure 2. The first part is responsible for pumping the water up as the storage is charging. The energy source for this action comes directly from the renewable energy sources. During discharge, the water falls down through a separate generator to produce stable energy. This construction makes the whole storage function as big buffer capable of circulating water continuously during day and night. It has therefore a faster response time for charge and discharge compared to a conventional single tube system. Furthermore, it helps to overcome blackout of renewable sources because of the large energy capacity of the hydro pump storage. However, the hydro pump with an extra pipe needs a strategy position; it requires two large lakes or reservoirs and wind farm or PV panels close to the pumped hydro because of transport losses. It also requires the additional infrastructure and equipment for constructing the suggested strategy.

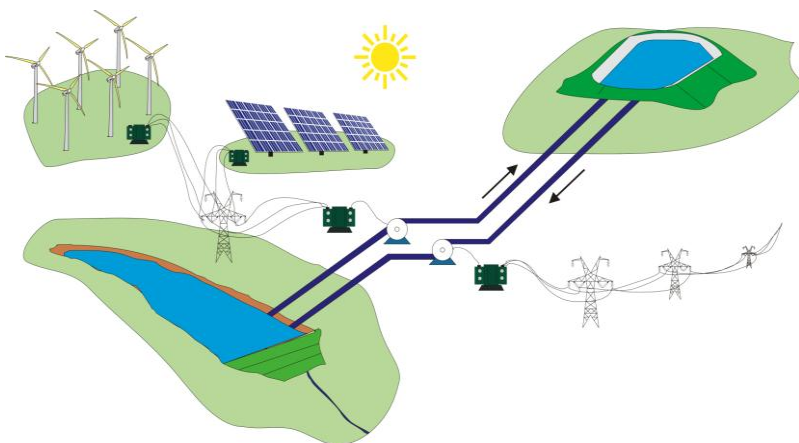


Fig. 2 Structure of a hydro pump energy storage system with multiple pipes.

3.1 Small islands and off-grid system

As described, our main target for the energy storage innovations is the off-grid installations on for example small islands. In the off-grid scenario, install capacity of the RES (PV and wind) has to be equal to or more than the average grid consumption in the isolated location. In practice, the energy sources require a slight overdimension in order to cover the power peaks, which occur during low wind or weak sun. On the other hand, the excess energy is used for pumping water up and storing the potential energy for turbine/generator. For e.g. small islands it is of importance to store excess energy for later usage during peak conditions.

In our scenario (Fig. 3), the grid is continuously powered from wind farms since the wind power generation is not directly controlled by time of day. In contrast, the power from PV panels grows continuously from the beginning of the day to charge the batteries, which are used to cover potential fluctuations in the system (flexibility, faster response, maintain power quality). If there is a lack of wind energy (and no suitable energy from PV), the turbine/generator is supplied by water previously pumped up to the reservoir and is supplied to the grid. As power from PV panels reach the required value, the energy is directly used to supply the grid and support the wind farm in energy generation. The turbine/generator can be switched off as the energy sources reach the required value. Excess of the energy can always be used for charging the batteries (if they are not fully charged). If the batteries are fully charged, the control system starts the motor and pumps the water back up to the reservoir. At the same time, the PV panels (and wind farm) supply the grid and in case of excess of energy pump the water up. During night, the grid is initially powered from the batteries, and when the battery charge reaches a lower limit the generator/turbine is started. At this state, the grid is powered by the hydro storage generator until the RES become available again.

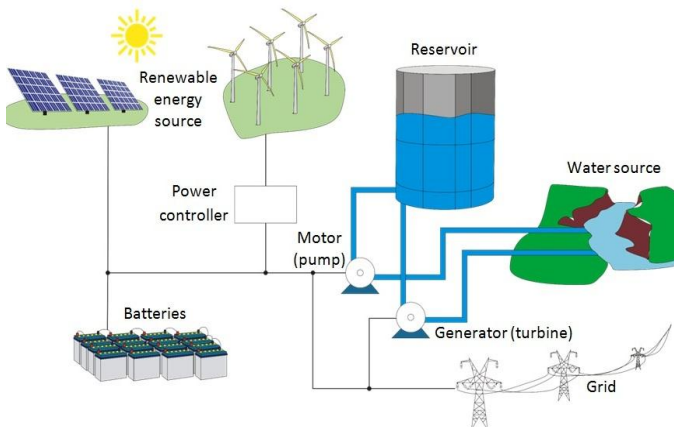


Fig. 3 Overview of the small-island off-grid system.

The main benefits of the system are the possible usage of renewable energy continuously, and the accumulation of excess energy useful as the output of the RES

diminishes. Secondly, the system provides independence from conventional power plants to decrease the CO_x emissions. Also, the excess of renewable energy can be used in water desalination or charging the batteries in electric cars, which could also be turned into a possible part of future Smart Grid.

4 Cost issues

Financial benefits and investments are a deciding factor when building an energy storage system. Naturally the financial investment must provide an as efficient system as possible in order for the investors to benefit from the construction. Financial details for four different constructions of hydro pump energy storages is listed in [5]; the ranges for different sizes of facilities in this example is listed from \$7,500,000 to \$23,500,000 depending on the size, location etc. for the facility.

Constructing a PHES, including dams, has high capital expenditures and a long construction time. If an existing hydro plant is extended to also be a PHS, the investment per installed MW is significantly lower and the construction time between 2 and 3 years. The PHS facilities are dependent on local geography and currently have capacities up to 1 MW. In addition to large variations in capacities PHS has also other characteristics regarding such as the discharge time, which is ranging from several hours to a few days.

The importance from this observation is to clarify the meaning of different parameters when constructing a hydro pump energy storage system. Moreover, an energy storage site can output power as the primary energy sources are not delivering their full potential. This means that the dimensions of the energy sources can be limited to only the necessary dimensions for certain weather conditions, and thus result in a diminished pricing range.

This section lists the most vital points used to motivate a certain configuration of energy storage system.

5 Conclusion

In this proposal, new innovative ideas are presented in order to extend and improve the hydro pump and battery storage for storing renewable energy in off-grid locations. The general outlook of our innovative design is the hybrid combination of both technologies, which extends the end product with the strength of both sides. Apart from this starting point, we go deeper into the technologies themselves, and propose specific technical solutions for communities located on small islands.

Battery technologies have been compared with the hydro pump storage as the first step towards constructing hybrid storage. We have recognized the fast response time and flexibility of battery storage – a property useful for fast load leveling and rapid deployment. Moreover, the, slow-to-build, but massive energy amount in hydro pump storage is essential to a sufficiently large energy potential for the renewable energy sources.

For marketing reasons, we simulate the energy consumption and production for a given region to determine required storage capacity and throughput. Simulation is a fast and cheap way to estimate the dimensions of a construction without producing the construction itself. Initial results show that a simulation framework could have the potential to, quickly and simple, suggest essential input parameters to a storage site with the assumption that production/usage parameters are given. Initially, we intend to utilize the simulation framework for off-grid constructions since – with its simple layout – off-grid locations are a desired starting point for starting our marketing. With this document as the foundation for our project, we hope to establish a functional and efficient ecosystem with renewable energy sources and energy storage.

Acknowledgements

We would like to acknowledge and extend our gratitude to EFACEC and especially Alberto Bernardo, Nuno Delgado and Nuno Silva for their important input to this work. Furthermore we would like to thank our supportive professors Stepan Ozana, Tatjana Welzer and Peter Larsen for the encouragement and support during the time of the project. Finally we like to send a special acknowledgement to Prof. Joao Fernandes who organized this cooperation opportunity.

References

- [1] Bayar, T. (2011). Batteries for energy storage: New developments promise grid flexibility and stability.
<http://www.renewableenergyworld.com/rea/news/article/2011/08/batteries-for-energy-storage-new-developments-promise-grid-flexibility-and-stability>.
http://storagealliance.org/presentations/CESA_OIR_Storage_Project_Examples.pdf.
- [2] Connolly, D. (2010). A review of energy storage technologies for the integration of fluctuating renewable energy. Master's thesis, University of Limerick.
- [3] Levine, J. G. (2007). Pumped hydroelectric energy storage and spatial diversity of wind resources as methods of improving utilization of renewable energy sources. Master's thesis, Michigan Technological University.
- [4] Vittal, V. (2009). U.s. energy infrastructure investment: Large-scale integrated smart grid solutions with high penetration of renewable resources, dispersed generation, and customer participation. Technical report.
- [5] Yanity, B., Johnson, G., and Hermanson, J. (2009). Energy storage review. Technical report, Alaska Energy Authority

The Application for Hybrid Power System Data Evaluation

Jakub Mañas

Department of Cybernetics and Biomedical Engineering, FEECS,
VŠB – Technical University of Ostrava, 17. listopadu 15, 708 33 Ostrava – Poruba
jakub.manas@vsb.cz

Abstract. In conference EPE 2011, the monitoring system to measure and visualize the performance parameters of the hybrid power system was presented. In this year we would like to present data analysis results computed by developed application. The application reads the measurement data (it has been acquired for last nine months) from the monitoring system. This data is transformed to power flows in the individual branches, equipment effectiveness and performance parameters in the graphs. The application is currently used for hybrid power system review. The paper describes achieved results and needs for further improvements of such solution.

Keywords: Hybrid Monitoring System, Data Analysis, SW

1 Introduction

A hybrid power system consisting of two photovoltaic and two wind power stations came to existence last year at VŠB-TU Ostrava. As its behavior has to be monitored, the need for measurement and visualization at the hybrid system arose. The article describing the monitoring system was presented at Conference EPE 2011 and its brief summary is found in Part 2. Now, the hybrid system has been in operation (March 2012) for nearly a year (9 months) and a lot of valuable data have been collected since then. Therefore, the application for evaluation of the measured data, which this article wants to cover, has been created.

2 The hybrid power system by VŠB-TU Ostrava

The hybrid power system consists of two photovoltaic and two wind power stations that together charge the accumulator battery. The battery is also used for the feed of two lamps of the public lighting. The block diagram of the system is in Fig. 1.

The hybrid system uses two photovoltaic panels of whose performance is 130 W (FV1) and 200 W (FV2). The transmission of the energy from the FV panels to the batteries is controlled by the regulator (REG). The wind power station VT1 uses for the conversion of wind energy to electrical energy a 200 W generator with a built-in regulator of charging, so the regulator can be connected directly to the batteries.

At VT2 is, on the other hand, used a 200 W synchronous 3f generator, whose performance is transferred to the battery via the rectifier and the regulator (the block with the diode, see Fig. 1). The appliances in the system are represented by two lamps

of the public lighting (VO1 and VO2). VO1 is an LED lamp with the input of 40 W and VO2 is a sodium-vapour lamp with the input of 50 W. Both lamps are operated with the voltage of 230 VAC, which is supplied there by the DC/AC converter. The battery consists of NiCad accumulators and its resulting capacity is 340 Ah at the nominal voltage of 12 VDC. [1]

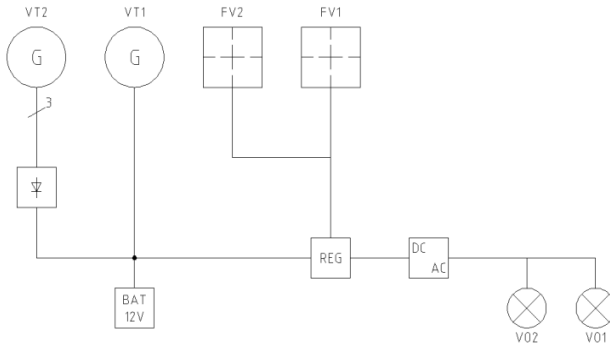


Fig. 1. The block diagram of a hybrid power system [1]

3 The monitoring system of the hybrid power system

The monitoring system is built on the HW platform NI CompactRIO. The voltage and currents in all branches of the circuit are measured, except for the appliances (the input of VO1 and VO2 is measured together). The individual measuring points are shown in Fig. 2. The monitoring system does not take any electrical energy from the batteries of the hybrid power system; its feeding is dealt with separately and provides uninterrupted operation (UPS). [1]

All the measuring HW is located in the existing outdoor distribution box where there is the whole electrical equipment of the hybrid power system. This box provides protection against weather conditions, but it is not thermally insulated. This places increased demands on the operating temperature of each component. [1]

All the components are placed on a metal structure located in the box. The dimensions of the free internal space of the box must be taken into consideration when choosing the components and the layout design. [1]

The measured data are stored in text files (daily records).

The current measured data are visualized on the website by means of a web server (Fig. 3), which is operated on a remote PC. The data are also backed up on the PC and can be downloaded by authorized users with the help of the FTP access.

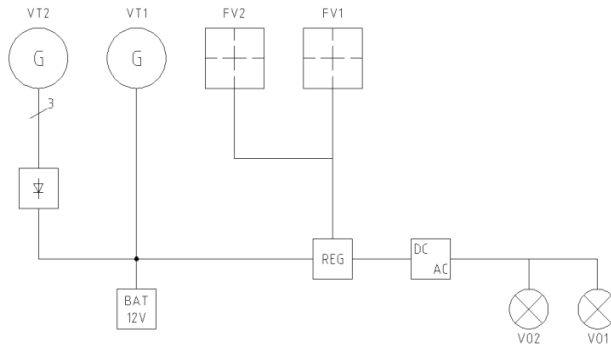


Fig. 2. The block diagram of the measured system and the measuring points [1]

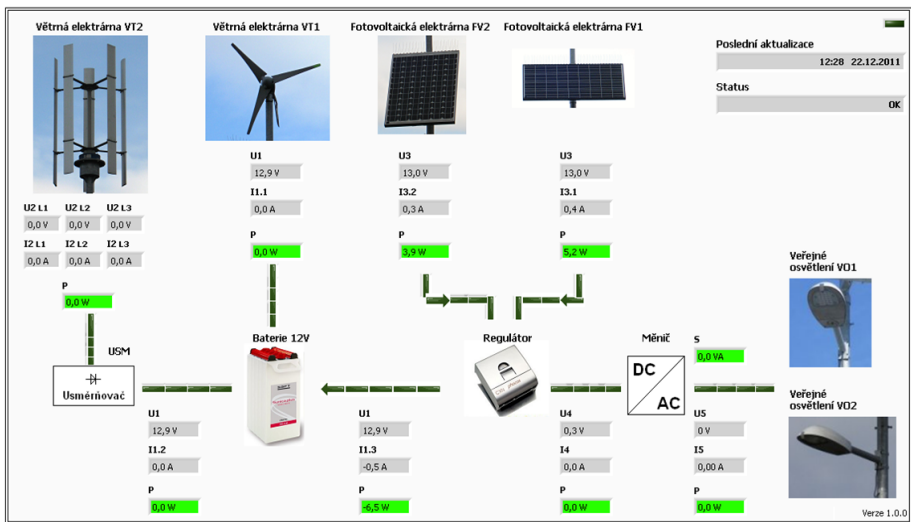


Fig. 3. Visualization of the measured data with the help of the web interface

4 Application for evaluation of the measured data

The developed application for evaluation of the measured data (application) enables graphical display of the measured and computed data (performance streams, component efficiency). The users can specify the accurate time period (the minimum resolution is 1 day) or they can choose from the menu “The last 3 days”, “The last week”, ..., “The last year” (Fig. 4). The application enables to display up to 4 parameters in the graph at the same time, when each parameter has its own vertical axis with its scaling.

The application then processes these data statistically so that the data are divided into certain time parts so that the total number of samples to the graph was approximately a thousand for each course of the parameter. The algorithm of searching for the

minimum and maximum value of the parameter and their display together with their time in the correct order is the reduction of the data.

If the sought-after parameter is not found in the measuring files and is not located in other files, this day is filled in the data with an invalid value that is not displayed in the graph.

The displayed data can be exported in the form of a picture, MS Excel table, text file and TDMS file (for data processing in the application NI DIAdem). [2]

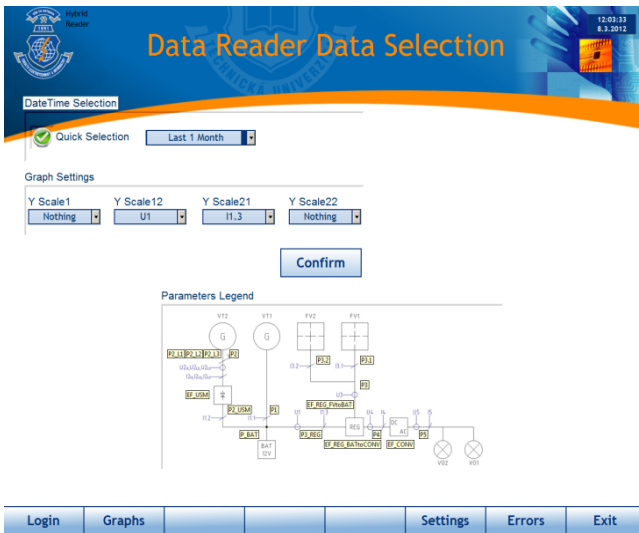


Fig. 4. GUI of the application created for the evaluated data selection

5 Examples of the measured data in the graphic form

For the illustration purposes, the results are shown in the graphic form. It is necessary to point out that the application serves for evaluation of the current state of the hybrid system and for its optimization, so it is necessary to take the displayed results with a pinch of salt.

So as something was not displayed in the optimum scale in the graphs, the courses for only one day are shown here.

Fig. 5 shows charging of the battery from photovoltaic panels. Parameter “P3” is the performance supplied to the regulator, “P3_REG” is the performance supplied from the regulator, “EF_REG_FVtoBAT” is the efficiency of the regulator (from the photovoltaic panels to the battery). The efficiency is calculated for performance greater than 10 W (user-configurable value), therefore efficiency waveform is not continuous.

Fig. 6 and Fig. 7 show the discharging of the battery into the lights (VO1 and VO2). In Fig. 6, there is parameter “P3_REG”, i.e. the performance supplied from the battery to the regulator. Parameter “P4” is the performance flowing from the regulator to the DC/AC converter and “EF_REG_BATtoCONV” is the efficiency of the

regulator (from the battery to the converter). Fig. 7 shows parameter “P5”, i.e. the performance consumed in the lights, “EF_CONV” is the efficiency of the converter and “U1” is the voltage at the battery. In the time of approximately 6/7/ 2011 2:15, the regulator evaluated that the voltage at the battery is low and stopped its discharging.

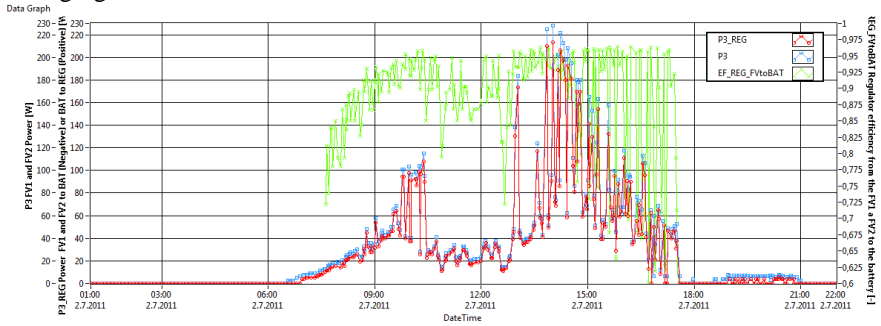


Fig. 5. An example of the application output (charging of the battery from photovoltaic panels)

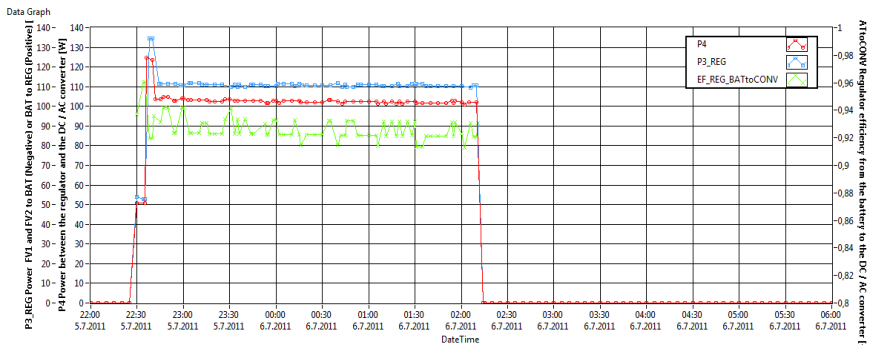


Fig. 6. An example of the application output (discharging of the battery into the lights)

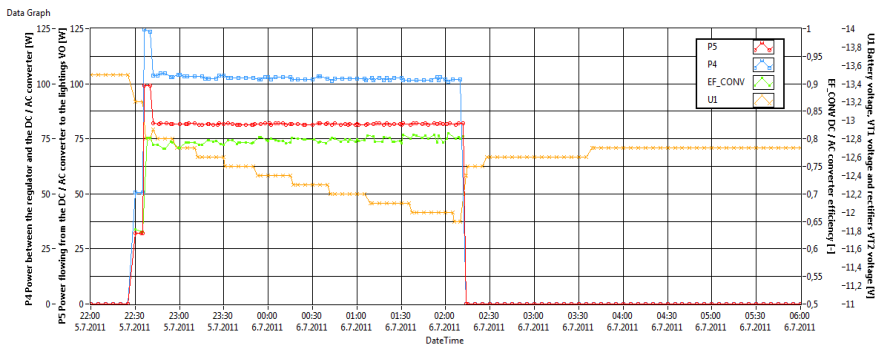


Fig. 7. An example of the application output (discharging of the battery into the lights)

6 Conclusion

The goal of this article was to describe the developed application for evaluation of the measured data from the hybrid power system consisting of two photovoltaic and two wind power stations.

The application allows an easier and more efficient analysis of phenomena in the hybrid system at VŠB-TU Ostrava. When the application NI DIAdem for the analysis of the measured data is used, the compilation of measurement protocols will be faster as well. These significant time savings enable the users to concentrate their time and energy on substantial issues during the research of the hybrid system.

The application uses the concept of virtual instrumentation, so it is expandable according to the future requirements without the need of higher time sources.

Acknowledgment

This report was prepared thanks to financial support of the project SGS no. SP2012/144 VŠB-TU Ostrava, FEI.

References

1. KVAPIL, Jakub; BILÍK, Petr; MIŠÁK, Stanislav: *Monitoring system of the hybrid power system* (Monitorovací systém hybridního napájecího systému). In Proceeding of the 12th International Scientific Conference Electric Power Engineering 2011. Kouty nad Desnou : VSB- Technical University of Ostrava, 2011. s. 1-3. ISBN 978-80-248-2393-5.
2. *National Instruments - Test and Measurement* [online]. 2010 [cit. 2012-05-03]. Dostupné z WWW: www.ni.com.

The Concept of Application for Intelligent Building Management on a “SaaS” Platform

Petr Pětvaldský and Petr Bilík

Department of Cybernetics and Biomedical Engineering, FEECS,
VŠB – Technical University of Ostrava, 17. listopadu 15, 708 33 Ostrava – Poruba
{petr.petvaldsky, petr.bilik }@vsb.cz

Abstract. The new concept of software systems solutions based on Web services is becoming more popular in information technology. The concept of „SaaS“ provides cost savings and eliminates the need for installation and operation of software on the user side. Especially for end-users this concept brings significant benefits. In engineering software applications it offers the possibility to use this concept for wide layer of users. One industry that is undergoing a dynamic expansion is the area of building management systems. Implementation of applications based on a "SaaS" can bring distinct advantages against common software solutions.

1 “SaaS” platform

With an increase in transmission capacity of the Internet in recent years, outsourcing of information systems in the new form of rent hosted applications developed. SaaS (Software as a service) is called the software that is provided as a service to customers. Customers connect via the Internet to this service and software applications are usually hosted on a server which is managed by provider.

This software outsourcing approach provides significant benefits for both customers and providers. For customers it is particularly eliminating installation and operation of applications on their own equipment, which reduces software costs, increased speed of deployment, the possibility of using the software on different devices without the need to transfer stored data, and especially the possibility to use applications on different platforms such as computers, tablets, mobile phones and various types of consumer electronics, which are equipped with a web browser (televisions, etc.).

From the perspective of providers the benefit is removal of software license sales (avoiding pirated copy, sales in regular payments) and the possibility to obtain immediate feedback from users (better adaptation to customer needs, planning to upgrade, technical support).

Software built on the concept of SaaS is nowadays being increasingly used in business applications. As an example we can mention Google Documents (document

management), DropBox (data storage), Salesforce (CRM systems), Google Talk, Skype, etc. (communication services).

Opponents of this approach point out that the concept of providing software as a service represents a potential security risk. Many people wish to have their own data under the control. In recent times the level of security and server backups of providers of these services is, however, at a far higher level than the customers themselves use. [5]

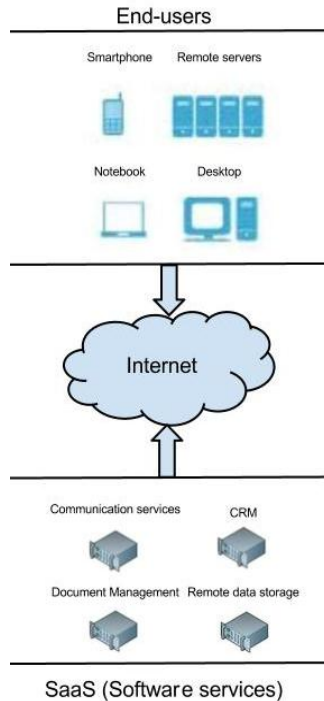


Fig. 1. The concept of SaaS

2 Integration with systems for building management

Connection of network structures for building management can now be basically divided into two parts. The primary (low level) part consists of sensors, actuators and controls (buttons, regulatory elements) that are usually connected by cable systems built on a standard (KNX, EIB, etc). The secondary part can be called the part of a higher level, which consists of control components (touch screens, control panels) that communicate via an interface such as Ethernet, RS-232, RS-485, etc. [1]

From a technical point of view to communicate with applications running on the principle of Web services any network router is sufficient for internet connection. It may be a part of the control system, or you can use a home router which is connected to the control system.

Another possibility is that the communication with the web application will be provided by your computer (or tablet), which is permanently connected to the control system and connected to the Internet. Nowadays intelligent systems for building management are often equipped with the data router to be connected to the Internet.

Manufacturers of these control systems usually offer web interfaces for monitoring the measured values and switching actuators.

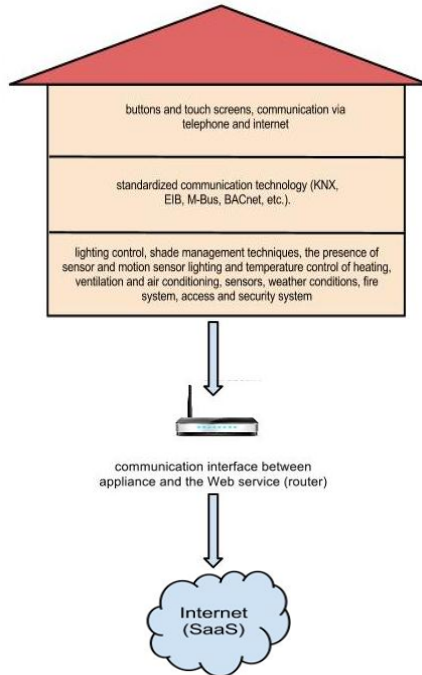


Fig. 2. Integration of systems for building management

This concept, however, does not only aim to create an application for a proprietary solution to household management control but a modular application for a wide variety of technologies and equipment.

The degree of automation in the lives of ordinary people is growing. Therefore, the ordinary users will surely demand applications that can integrate systems from different manufacturers and that allow to control and monitor by a single application not only a household control system but also car controllers or controllers of public facilities (such as monitoring of the progress and consumption during charging at public stations for electric vehicles).

3 The benefits of the concept of "SaaS"

In the future rapid development in many technical areas can be expected: consumer electronics, energy networks on the principle of smart grids, electric mobility, web

technologies and social networks. All of these areas can benefit from the above proposed system concept. The Internet is already a common part of televisions. In the near future it will certainly become a part of the smart meters of consumption and automobiles.

With the growing number of technologies that we use in everyday life also the time we spend with managing and setting these technologies is growing. Only the integration of all these technologies will bring satisfaction. Web-based applications services offer wide varieties of expansion and benefits. Some of them are described below.

4 Distributed measurement and control, centralized data management

As it has been already said, the intended application concept is not a proprietary solution, which is already being widely offered by various manufacturers of automation systems, but it will be a universal application that enables to control systems of different manufacturers and, more importantly, systems in different places.

This is useful not only for ordinary users (capability to manage an apartment, office, cottage, etc.) but also for more complex entities (such as office buildings). Hence the core will be one application on a remote server and users will be the only application access from any terminal equipment (control panel, computer, mobile phone, TV, etc.), thus eliminating the need for storing and managing data at the measurement point.

Another advantage is the access to current data from anywhere on the Internet. Today technical solutions for safe operation of such applications are available in a large scale. For example, large software companies such as Google, Amazon and Microsoft provide "cloud services" that are an excellent solution for applications with large data consumption and are able to differentiate high demands on computing power at different times. [2]

An advantage may also be possible mass processing of measured anonymous data for statistical evaluation of consumer behavior (e.g. temporal patterns of electricity consumption).

5 Multilevel administration

Thanks to the single data repository on a remote server a multi-level administration for more complex units can be created. Using the definition of different access rights in a central data repository application will allow each user to display just the data needed.

For illustration we can take an office building as an example. An ordinary employee, in the interface of his application, will be able to monitor and adjust the optimum environment in his office. One level higher there can be the owner of a com-

pany that hires a number of offices in an office complex. He will be able to monitor aggregate consumption and attendance at all his offices.

Next level will be the building manager, who will be able to monitor and evaluate consumption throughout the building, control security systems and administer technical support of common space in the office building. The setting of access rights and administration possibilities is highly variable, and therefore needs to be set so that all of the parties involved were satisfied, especially the service provider.

6 Possibilities of implementation of web services

Many popular Web services provide the application programming interface (API) for the purpose of interconnection or integration with other web applications or services. Many of these APIs can also use applications described in this article. Several web services and examples of usage for illustration:

- Google Maps API – can be used to locate the user, e.g. for switching heating schemas when approaching to the place of residence.
- Google Mail, Calendar API - automatic (and collective) alert for users to certain conditions, for example the alarm thresholds of consumption, planned inspections of appliances
- Logging into the application using a Google ID, Facebook ID.

Indeed, a wide variety of web services from which you can freely benefit is nowadays available on the internet. The advantage of Web applications is that it is a constantly living system that can be continually supplemented at any time, depending on user preferences.

Over the last few years social networks such as Facebook, Google+ and Twitter have gained great popularity and are already used in many branches. For many people they are a part of everyday life. Their importance will certainly continue to grow and the connection with everyday used services, such as household remote control, will become a necessity. [2]

7 Integration in other applications in the form of a "widget"

With the growing number of applications, which are used today (e-mail client, profiles at social networks, systems for project planning etc.), it becomes very difficult to monitor all the necessary applications simultaneously. Therefore, it is becoming the standard to allow the user to monitor current events, for example in this case, the state of the security system, current consumption etc., in a simplified form of the so-called "widget". This "widget" can then be integrated directly in the operating system of your computer, mobile phone, tablet, etc. The system automatically notifies predefined events and allows tracking the desired values. [6]

8 Conclusion

This article is an introductory summary of options for creating a web application prototype for automated management system on the "SaaS". As mentioned above, the applications working on the principle of services have recently quickly found their place in social and administrative are of information technology. It is only a matter of time when this solution will find wide application in technical fields, especially automation.

Infrastructure to move the abovementioned concept and its general extension offers many enhancements that are in current conditions, rather the music of the future. As an example we can mention the possibility of purchasing energy commodities from different suppliers, depending on the price currently offered, or the automatic setup of required rating schemas, air conditioning and lighting after coming to work, home or the car through wireless communication with a mobile phone and using GPS tracking location.

References

1. MERZ, Hermann, Thomas HANSEMANN a Christof HÜBNER. *Automatizované systémy budov: sdělovací systémy KNX/EIB, LON a BACnet*. 1. vyd. Praha: Grada, 2008, 261 s. ISBN 978-802-4723-679.
2. Software as a Service. In: *Wikipedia: the free encyclo-pedia* [online]. San Francisco (CA): Wikimedia Foun-dation, 2001-2012 [cit. 2012-01-25]. http://cs.wikipedia.org/wiki/Software_as_a_Service
3. GRUMAN, Galen. The Truth About Software as a Service (SaaS). In: [Http://www.cio.com](http://www.cio.com) [online]. 21. 5. 2007 [cit. 2012-02-02]. http://www.cio.com/article/109706/The_Truth_About_Software_as_a_Service_SaaS
4. West LA Corporate Office. The Truth About Software as a Service (SaaS). In: [Http://www.itstrategists.com](http://www.itstrategists.com) [online]. [cit. 2012-02-05]. <http://www.itstrategists.com/Cloud-Computing.aspx>
5. MATHER, Tim, Subra KUMARASWAMY a Shahed LATIF. *Cloud Security and Privacy: An Enterprise Per-spective on Risks and Compliance*. Cambridge: O'Reil-ly Media, 2009. ISBN 978-0-596-80750-4.
6. HATCH, Ralph. *SaaS architecture, adoption and monetization of SaaS projects: using best practice service strategy, service design, service transition, service operation and continual service improvement processes*. Brisbane, Australia: The Art of Service Pty, Ltd, 2008. ISBN 978-192-1523-144.
7. CHOU, Timothy Chen Kuang. *The end of software: finding security, flexibility, and profit in the on demand future*. Indianapolis, Ind.: Sams, c2005, 170 s. ISBN 06-723-2698-1.
8. BENIOFF, Marc R a Carlye ADLER. *Behind the cloud: the untold story of how Salesforce.com went from idea to billion-dollar company--and revolutionized an indus-try*. 1st ed. San Francisco, CA: Jossey-Bass, c2009, 278 s. ISBN 04-705-2116-3.
9. *New frontiers in information and software as services: service and application design challenges in the cloud*. 1st ed. New York: Springer, 2011. ISBN 36-421-9293-9.

PMU Data Stream Generator for Testing of Transmission Properties in PMU Virtual Networks

Pavel Řepka and Petr Bilík

KatedraKybernetikyBiomedIngEN
{pavel.repka, petr.bilik}@vsb.cz

Abstract. Increasing demands for quality and reliability of electrical supply with rising complexity of electrical networks put emphasis on possibility to monitor and foresee behavior of these networks. One of the main aims of this monitoring is to prevent events that may cause failure or even damages of the transmission network or the user side. This is the reason why units for synchrophasor measurements getting increased attention these days. Main function of PMU units is to measure and report the network status in predefined locations. PMU features in terms of evaluation and reporting describe the standard IEEE C37.188. As well as measurement, very important part is also a data transfer to higher systems. This article describes standard IEEE C37.118 in terms of data frames transfer and structure of these frames between PMU and PDC systems. Part of this work also describes PMUGen software which simulate PMU data stream and enables to study transmission in PMU networks. This software is developed in graphical environment LabVIEW. This software enables creation of virtual PMU units without using of any special hardware and will be used as a tool for teaching students interested in this field.

1 Introduction

Electrical energy has nowadays become a prime commodity without which a modern human being cannot even imagine a good-quality life. As the customers' requirements concerning quality, accessibility and stability of electrical energy supplies increase, the requirements concerning the transmission system itself increase as well. In the last few years this area has undergone considerable changes that influence the electricity network significantly. One of these changes is the rapid coming of renewable resources of electrical energy, which are by its nature unevenly spread across the transmission network, and their contribution depends especially on many factors that cannot be influenced by the humans. Another big change was the deregulation of the market that enabled more companies to enter this area of business, which consequently caused increased competition in this area. However, with this competition the pressure to reduce the costs heightens, which partly restricts the development of these networks that are working on the limits of their capacities these days. Last but not least, the permanently increasing demand for electrical energy, which despite all

efforts cannot be reduced, plays an important role here. These are the main reasons why the transmission networks are becoming much more complex currently and it is much more difficult to monitor and control them, which leads to a higher probability of occurrence of faults. Therefore, the need to focus more on the monitoring of the state of the electricity network arises, which will subsequently enable to prevent or, possibly, detect such faults and unwanted states and to take the necessary measures on time.

2 Measurement of phasors

The impulse to accelerate the development and the deployment of systems for monitoring of transmission networks originated due to several enormous electricity blackouts in USA and Europe in 2003. At that time, the technique of measurement of synchrophasors came into focus. The first standard dealing with this issue is IEEE 1344 from 1995, which was revised substantially in 2005 to form standard IEEE C37.118 [1]. The second version of this standard IEEE C37.118.2 [2] was issued in December 2011.

In order to find out the state and the behavior of the transmission network, it is necessary to compare the measured phasors from various places, but at the same time, especially their dynamic behavior in time. Therefore, it is necessary to assign the phasors measured at certain points of the network an accurate time mark according to a common time base, which was achieved by means of the GPS system. Besides other information, the GPS system also emits the PPS signal with the frequency of 1Hz with high accuracy (the standard deviation does not exceed 1 μ s). This was the beginning of devices called PMU that measure electric signals in defined points of the electrical network. These signals are then reported in the form of phasors indicated with an absolute time mark [3].

In this case, phasor is a vector expressing the amplitude and the phase shift of the sinusoidal signal at a particular time. According to standard IEEE C37.118 [1], the phase shift is related to the reference cosine signal on the nominal frequency of the network synchronized with the time base inferred from the GPS. The magnitude of the phasor is set as an RMS value. The principle of inference of the phasor is found in (1). The signal that at the time of the entry of the PPS signal corresponds with the cosine signal (the maximum value of amplitude in $t=0$), has the phase angle $\varphi=0^\circ$, and the signal that at the time of the entry of the PPS changes its polarity from negative to positive (i.e. the signal corresponding with the sine function), has the phase angle $\varphi=-90^\circ$ [1].

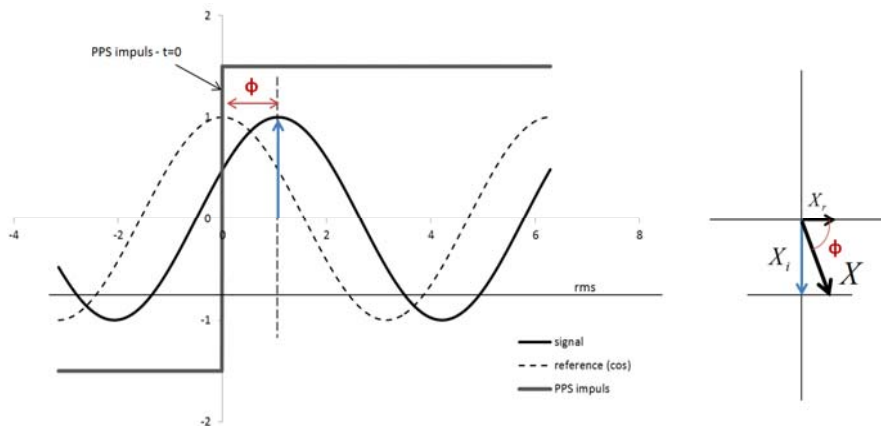


Fig. 1. Principle of inference of the phasor measured signal

Phasor (vector) is defined as follows [4]:

$$X = X_r + jX_i$$

$$X = (X_m/\sqrt{2})e^{j\varphi}$$

3 Architecture PMU Network

The PMU units are located in important points of the network from which their results are sent, via certain transmission paths, to the superior systems. These superior systems are indicated as PDC. The PDC system is able to receive the data streams transmitted by the PMU units, process, assess and save these data and also to transfer them to other systems. The data stream between the PMU and PDC units is defined by a standard developed for measurement and transfer of synchrophasors, these days most often according to IEEE C37.118 in the version from 2005 (1). The PDC output is widely configurable and can also be defined according to standard IEEE C37.118, which enables data transfer within PDC systems themselves as well. Another important function of some PMU units is their ability to be connected to multiple superior systems, thus sending them different information. These properties enable creation of a very complex network when certain data are routed do other PDC units which then treat them in different ways, transfer them between each other, etc. This way, it is possible to transfer information about voltage and currents to another PDC than for example information about frequencies of measured signals.

The connection between the PMU units and the PDC systems, or possibly between PDC systems themselves, was in the past carried out via telephone lines of telecommunication operators. However, at present, this communication is being transferred to IP networks that are very accessible and their support is widely spread. Nevertheless, a

question concerning the use of the rented circuits, VPN networks and other possibilities for ensuring greater safety and stability of transfers arises here.

The superior system mostly receives data from more subordinate units, over which it subsequently performs operations (analyses, mathematical operations, backing up, etc.). Hence, it is important that these data should be available in a certain moment; otherwise they will not be included in the subsequent processing. A critical emphasis on the time of the data transfer from the source to the target unit or system, which should be as little as possible, results from this. The requirement for high reliability of such connections is obvious.

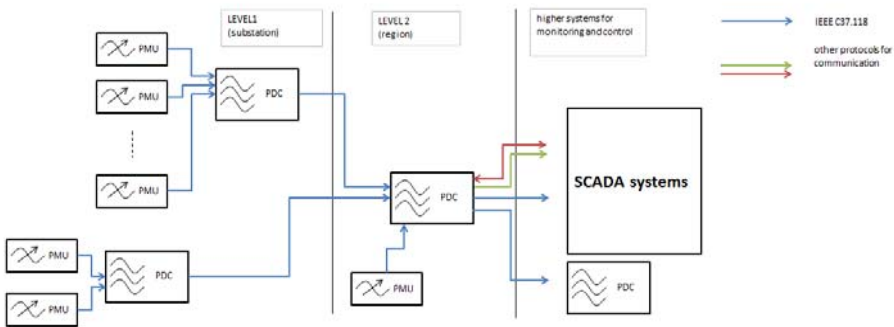


Fig. 2. Scheme of connection of PMU units

The PDC system then processes the received data and transfers them to the superior SCADA systems that monitor (WAM), control (WAC) and protect (WAP) the monitored networks. The monitoring of the synchrophasors enables these SCADA systems a dynamic look on the observed network. The previous monitoring systems were, due to their low transfer speeds and asynchronicity, very static and they detected short-term states and events in the transmission network with difficulties. PMUs thus enabled expansion of possibilities of control and monitoring systems. [5].

4. Conclusion

This article focuses on measurement of synchrophasors from the perspective of creation and transmission of data frames between the PMU and PDC systems according to standard IEEE C37.118. It also contains an introduction to the techniques of synchrophasors measurement, which is necessary for the subsequent comprehension of close connections when creating and transferring the data frames to superior systems. There is also a description of the principle of the created software called PMUGen that is used for generation of the PMU data stream according to the preset criteria. The software was created for the ones who are interested in penetration into the area of

synchrophasors measurement, especially for tests on various kinds of transmission media.

The software also enables work with PDC systems without the necessity to possess a physical PMU unit, which is convenient especially in the teaching process. The software PMUGen is continually developing and other functions are supposed to be added. The students themselves will be able to take part in this process within their semester works. When developing the software, we also take into account clearness and lucidity so that the pre-programmed code served as a teaching aid. In the following versions of the software, it is planned to extend the possibility of configuration and addition of some functions, e.g. sending of analogue and digital signals, upgrade to version 2 of standard IEEE C37.118, etc. it is also planned to transfer this software to the system CompactRIO by the company National Instruments, where it will be possible to achieve, by means of the GPS module, synchronization of the time base with by the PPS signal.

References

1. IEEE Standard for Synchrophasors for Power Systems (IEEE Std C37.118 -2005)
2. IEEE Standard for Synchrophasors for Power Systems (IEEE Std C37.118.2 -2011)
3. PMU simulation and application for power system stability monitoring, H. Karig, B.Cvorovic, C. Mycock, D. Tholomier, R. Mai
4. Phasor measurement units: functionality and applications, D. Tholomier, H. Kang, B. Cvorovic, AREVA T&D(CAN), AREVA T&D (UK)
5. Testing of Phasor Measurement Units, F. Steihauser. T. Schossig, A. Apostolov, Fellow, IEEE

Statistical Evaluation of Compression Methods for Storing Binary Image into Memory of Microprocessor

Roman Slabý

Department of Cybernetics and Biomedical Engineering, FEECS,
VŠB – Technical University of Ostrava, 17. listopadu 15, 708 33 Ostrava – Poruba
roman.slaby@vsb.cz

Abstract. This article deals with the assessment of the success rates of selected binary image compression algorithms, used as models of correlation functions of OCR algorithms. The success rate is assessed using the basic characteristics of exploratory statistics. Compression algorithms are used to reduce the data stream, allowing less demand on hardware equipment.

1 Introduction

They are increasingly placed greater demands on the resolution of image sensors. This result in higher memory requirements at present. Most of the cognitive systems of alphanumeric characters used to decode the numbers, the OCR algorithm. The output of this algorithm is already recognized the value of each character. One method of OCR algorithm is correlation, indicating the degree of similarity found with defined character patterns. Usually patterns are made up of a binary matrix of points representing the digital form of the search character. Recognition systems based on low power microcontrollers which do not provide enough space to store large amounts of data. For this reason, it is necessary to compress the various patterns to achieve what the lowest data stream. [1]

2 Compression methods

Data compression is a special procedure for storing or transporting data, whose task is to reduce the data stream. All compression methods are based on the fact that normally used methods of data representation are designed to allow easy manipulation of data, regardless of the fact that in some parts of the data often repeated. The consequence is that data needed to store often enjoy more space than is absolutely necessary. Compression is a method of encoding, which reduces the space required to store the data by eliminating repetitive occurrences. [2], [3]

2.1 Compression method 1

This is lossless compression method used for compressing binary patterns. The principle of this method consists in encoding information using a single byte, where the upper 7 bits represent the number of repeated occurrences. The principle of this method is shown in Fig. 1.

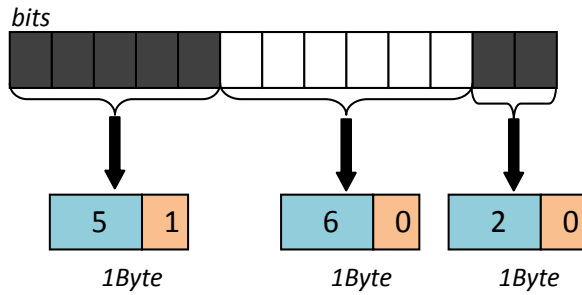


Fig. 1. Principles of Method 1

2.2 Compression method 2

Method number two is based on the same principle as compression method one except that this method contains the starting byte and the sequence of data bytes. The start byte contains information on the value of the initial element of the original pattern and data bytes contain information on the frequency of individual occurrences.

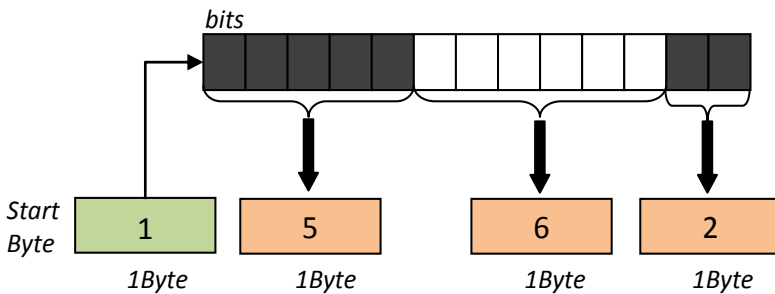


Fig. 2. Principles of Method 2

3 Exploratory data analysis

It is a summary of the methods used for data exploration and the search for hypotheses. Selective files represent the number of bytes required to encode each pattern. Digital representation of alphanumeric characters is shown in Fig 3.

0 1 2 3 4 5 6 7 8 9

Fig. 3. Patterns

Measurement was realized by specially developed user's application. This application was developed in C#. Intuitive user interface allows you to set the basic parameters and to display the encoded data stream. The numbers of encoded bytes constituting the sampling, the individual patterns were then recorded in the table shown below.

Table 1. The number of encoded bytes from described compression methods for image digits patterns storing

NO.	Method 1	Method 2
	N_1 [B]	N_2 [B]
1	158	114
2	107	98
3	133	96
4	154	122
5	145	102
6	126	112
7	157	138
8	132	88
9	167	132
10	144	112

Itself statistical evaluation was carried out using Statgraphics software tool. This tool allows for easy data manipulation and actual evaluation of sampling. Basic statistical parameters compared compression methods are shown in Table 2

Table 2. Table of basic statistical parameters

NO.	Method 1	Method 2
Count	10,0	10,0
Average	142,3	111,4
Median	144,5	112,0
Variance	324,9	256,0
Standard deviation	18,0	16,0
Minimum	107,0	88,0
Maximum	167,0	138,0
Range	60,0	50,0

3.1 Assessment of normality

Determination of the null hypothesis H_0 , the data comes from a normal distribution
 Determination of the alternative hypothesis H_A , the data not come from normal distribution

Statgraphics software tool did not generate χ^2 test of goodness, because of the low number of observations identified in the file. In order to assess normality was used Kolmogorov - Smirnov test under which it was found that for method 1, was determined as p-value 0.987 and for Method 2 p-value was determined as 0.992. It follows that the null hypothesis is not rejected at the 0.05 level of significance for either compression method, and therefore can be said that both samples come from normal distribution. Kolmogorov-Smirnov test statistics can be seen on the chart, which compares the actual and theoretical distribution function. [4], [5]

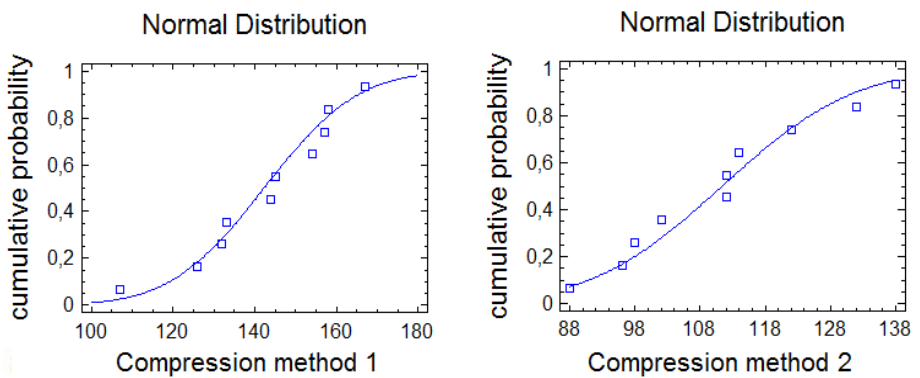


Fig. 4. Kolmogorov-Smirnov test statistics for compression compression method 1 and method 2

3.2 Assessment of homoskedasticity

Independence is found on the parameter assessment. First, it is necessary to establish null and the alternative hypothesis.

$$H_0 : s_1 = s_2 \tag{1}$$

$$H_A : s_1 > s_2 \tag{2}$$

The value p-value equals 0.364. It follows that, do not reject the null hypothesis at significance level 0.05.

3.3 Student's t-test

This test is used in statistics to verify the results of the first measurement of the sample differ significantly from the results of the second sample. Student's t-test can only be used for sampling, from a normal distribution. [4]

Determination of null and alternative hypotheses:

$$H_0 : \bar{x}_1 = \bar{x}_2 \quad (3)$$

$$H_A : \bar{x}_1 > \bar{x}_2 \quad (4)$$

P-value = 0,000372284

The chosen significance level 0.05 can be stated that refuse consent for the null hypothesis in favor of alternative hypotheses. And then we can say that the mean values between methods 1 and 2 there is a statistically significant difference.

4 Conclusion

In recognition systems with limited memory space is necessary to choose the most appropriate compression algorithm to reduce the data stream. To assess the suitability described algorithms to take advantage of statistical methods. Assessment of normality revealed that both samples come from normal distribution. Based on this finding could compare test hypotheses about the mean value and the comparison of two sampling, related to compression methods that led to Student's t-test. Based on a comparison Student's t-test can be argued that Method 2 is, in terms of stream efficient than Method 1 is suitable for use in systems with limited memory space.

References

1. Machacek Z., Hercik R., Slaby R. Smart user adaptive system for intelligent object recognizing // Studies in Computational Intelligence – Berlin Heidelberg, 2011. – No. 351. – P.197–206.
2. Salomon D.: A Guide to Data Compression Methods. – Springer, 2002. – 304 p.
3. Salomon D.: A Concise Introduction to Data Compression. – Springer, 2008. – 314 p.
4. Briš, R.: Exploratorní analýza proměnných. Ostrava. Skriptum VŠB-TOU
5. Pokorný, M., Hájovský, R.: Statistické výpočty v Matlabu Statistics toolbox. Ostrava, Skriptum. VŠB-TUO, 2010

Wireless System for Biotelemetry

Martin Stankus

Department of Cybernetics and Biomedical Engineering, FEECS,
VŠB – Technical University of Ostrava, 17. listopadu 15, 708 33 Ostrava – Poruba
`martin.stankus@vsb.cz`

Abstract. Wireless applications are of growing importance today. This paper deals with implementation of wireless communication into a biomedical system including presentation of acquired experience. There are many biomedical applications with prospect of implementation of wireless communication. IEEE 802.11 wireless module WISMC01 by Laird is one of commercially available wireless solutions. Module provides various communication interfaces and inputs - RS232, analog to digital converters and digital GPIO pins among others. Module supports proprietarial scripting language for user defined scripts. Various aspects of hardware and software development and wireless security are discussed in this paper.

1 Introduction

Wireless networks based on IEEE 802.11 standard are very popular today. These networks are capable of deployment in many embedded applications including biomedical applications. Nevertheless biomedical embedded systems are often designed as deep embedded systems lacking resources required for implementation of IEEE 802.11 based network. Moreover, existing applications are often built using simple communication interfaces (like RS232) and without possibility to easily interface advanced communication solutions, and therefore biomedical wireless solution should be of stand-alone design and capable of integration into existing systems. Usage of IEEE 802.11 wireless network in embedded system is, however, not without certain trade-offs. IEEE 802.11 network benefits from high data rates, wide spatial coverage, easy roaming and proven security mechanisms. Fundamental disadvantage of said networks is somehow high power consumption. Although there are specialized low-power biomedical wireless solutions (mainly from IEEE 802.15 family of PANs), usage of IEEE 802.11 solution seems to be viable at least in some biomedical embedded systems. This paper is aimed at description of experience with such a wireless solution.

2 Wireless module

IEEE 802.11 Wireless module WISMC01 by Laird is integrated solution for implementation of IEEE 802.11b/g wireless lan client. Module is designed around ARM7 CPU equipped with WLAN interface, RAM and Flash memory. Module

is connected to client system using 40-pin miniature connector made by Hirose. This connector is used to provide wireless module with power and to interface module to application. Module provides application with RS232 compatible asynchronous serial interface (speed up to 921600 Baud), 12 GPIO lines, and two 10-bit ADCs. Module is powered by 5V power supply. Albeit IEEE 802.11 power save modes are supported, power consumption is usually in range of 1.25W to 2.5W. Power consumption makes device rather unsuitable for highly mobile applications. Cooling of module is passive. Module's maximal transmit power is 13 dBm in IEEE 802.11g mode. Equipped onboard aerial has gain of 2 dBi. It's possible to connect external aerial via provided connector. Communication with module is implemented using asynchronous interface. Module provides application with AT command set for management. It's possible to directly run user application written in UWScript scripting language so that module can be used in pure stand-alone configuration.

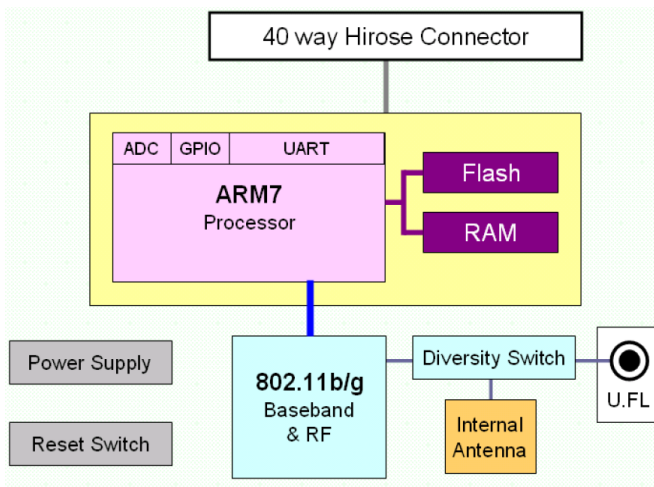


Fig. 1. Architecture of WISMC01 module

3 Development support

Development of actual wireless biomedical system cannot be done without suitable hardware and software development tools. Wireless module itself has to be used with adequate development board. Development board should be flexible enough to allow easy development and at the same time cheap enough to allow limited field deployment. We opted for in-house designed development board as we found no board with properties suitable for our needs. Wireless module itself is powered by 5V power rail. Module's digital inputs and outputs are 3.3V based. Need for interfacing of these I/Os by external circuitry makes presence of

3.3V power rail necessary. Both power rails are powered by appropriate LDOs. No specific power sequencing is necessary. Development board is equipped with two internal connectors, namely GPIO and ADC connectors. Module's 12 GPIO lines are connected to GPIO connector. Two ADC inputs are connected to ADC connector. Both power rails are available on each connector together with sufficient number of ground connections. Wired communication with application is supposed to be achieved using RS232 interface. RS232 interface is DTE (male) wired and is implemented with well-known MAX3232 level shifter. Development board is implemented on two layer PCB. Signal integrity is not of special concern as signal paths are rather short. PCB layout can be seen in figure 2.

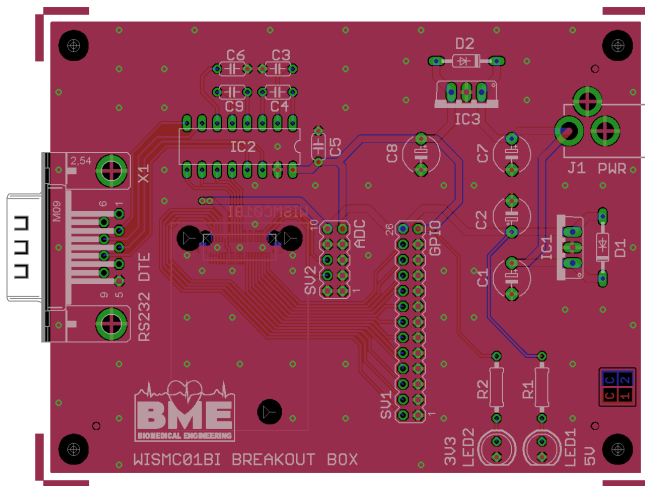


Fig. 2. PCB layout

4 Software development

Software development is performed using scripting language named UWscript. UWscript is proprietary procedural language with build-in support for module's specific hardware. Scripts are stored in onboard non-volatile flash memory controlled by simple filesystem. Size of this memory is 128 kB. After start-up, module begins to execute default script. Purpose of this default build-in script is to perform platform specific initialization of the module. After this event, specific script provided by user is loaded from non-volatile memory and executed. This step can be bypassed by setting module's specific GPIO or by not providing specific auto-run script. Module subsequently enters interactive mode which can be used to load script into non-volatile memory, run saved script or perform other management tasks. Non-volatile memory and script management is

achieved by simple set of AT commands available in interactive mode. Functionality of WISMC01 module after start-up described by state diagram can be seen in figure 3.

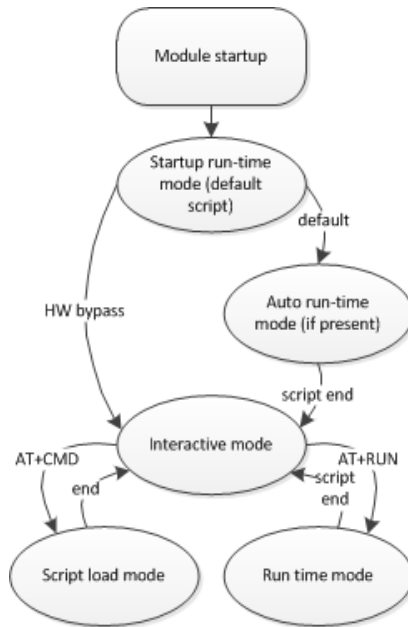


Fig. 3. Functional states of the module

Module implements HTTP server. Developer can design web pages written HTML language that can interact with scripts. CGI scripts are unfortunately not supported. HTML files share 128 kB of non-volatile memory space with user scripts. UWscript provide access to BSD-like TCP and UDP sockets. Module can act as both TCP/UDP client and server. Socket IO operations can not only be natively used by scripts, but can be redirected to RS232 port as well. Module can act as pure network processor this way with client device implementing the rest of functionality. Simple debugging is supported by breakpoints. Breakpoint execution makes script to temporarily exit non-interactive mode and enter interactive mode, therefore developer is able to examine status of executed script. Profiling is not supported. Software development is not facilitated by specialised development software. Scripts can be written in any text editor. The only tool provided by vendor is terminal emulator named UWterminal. This tool provides access to WISMC01 module via RS232 connection. Any terminal emulator can be used but UWterminal is adapted for easy upload of scripts. Sample screenshot of UWterminal window can be seen in figure 4. Note that UWterminal is MS Windows based. Solution for other operating systems is not provided by Laird.

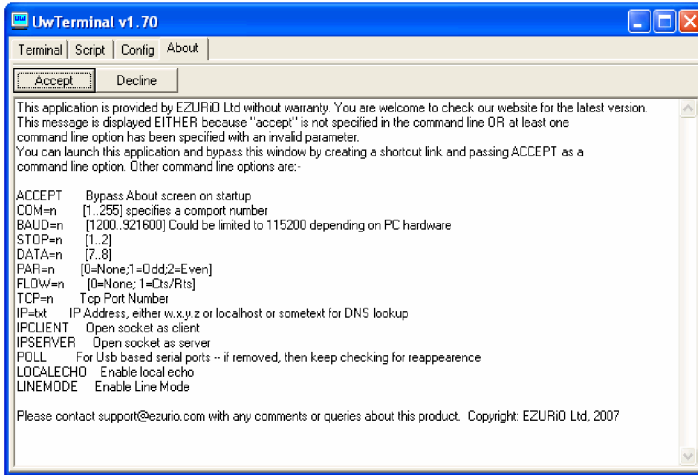


Fig. 4. UWterminal window

5 Wireless security

Security of wireless data transmission in biomedical application is crucial. WISMC01 module supports WPA2-Personal authentication utilizing strong AES-based CCMP encryption. Although module's documentation states that WPA2-Enterprise is supported, we were not able to make it work. We suppose the lack of WPA2-Enterprise support to be inappropriate as deployment of strong authentication and authorization mechanism (EAP-TLS or PEAP) makes network security substantially more manageable. WPA2-Enterprise makes exclusion of compromised devices possible. This is not possible with plain WPA2-Personal. Module lacks support for Cisco Compatible Extensions (CCX). Version 5 of Cisco Compatible Extensions defines Management Frame Protection (MFP). Management Frame Protection describes methods for protection against certain types of DoS attacks by authentication of IEEE 802.11 management frames using Message Integrity Check (MIC) sequence. Another method for Management Frame Protection is described by IEEE 802.11w standard. Unfortunately neither CCXv5 or IEEE 802.11w is supported by WISMC01.

6 Development experience

We decided to evaluate WISMC01 module in real biomedical application. Our application of choice was one channel electrocardiograph (ECG) device. Selected electrocardiograph device integrates anti-alias filter and is protected against potential noise generated by digital circuits. This makes this particular analog circuit well suited for connection to WISMC01 module. WISMC01 was for purpose of this experiment used as stand-alone device without anything connected to RS232 port. UWscript scripting language turned out to be powerful and

straightforward. We used UWscript language to design simple application implementing all required software functionality. Any software engineer with basic knowledge of BSD sockets and procedural programming should have no difficulty in mastering UWscript. Asynchronous events (like timer expiration) are implemented as callbacks. UWscript has no prospect of processes or threads. This prevents possibility of race condition and removes need for synchronization API calls. Operational behaviour of the module was very satisfactory. IEEE 802.11 roaming between particular access points worked well and without connection drops. Module is guaranteed to achieve steady data rate of 921 kbps (this is roughly corresponding to 921600 Bd of asynchronous interface). Transfer speed required by electrocardiograph is well under limit as we used sampling frequency of 512 Hz. The only significant disadvantage of WISMC01 module we found is considerable power consumption, in bursts as high as 2.5W.

7 Conclusions

We have proven that IEEE 802.11 based wireless network is viable communication technology for biomedical applications although there are possibilities for security improvements. Software development support is simple but sufficient. Evaluated module Laird WISMC01 is carefully designed and is generally performing well. The biggest obstacle is significant power consumption that makes IEEE 802.11 based technology in the form of WISMC01 module less suitable for highly portable biomedical applications.

8 Acknowledgements

The work and the contribution were supported by the projects: Ministry of Education of the Czech Republic under project 1M0567 Centre of applied electronics, student grant agency SP 2012/75 User adaptive system II and TACR TA01010632 SCADA system for control and measurement of process in real time.

References

1. Milenkovic, A., Otto, C., Jovanov, E. Wireless sensor networks for personal health monitoring: Issues and an implementation. *Computer communications - Elsevier*, 2006 - No. 29 - P.2521-2533.
2. Tan, K.S., Hinberg, I. Effects of a wireless local area network (LAN) system, a telemetry system, and electrosurgical devices on medical devices in a hospital environment. *Biomedical instrumentation technology - Association for the Advancement of Medical Instrumentation*, 2000 - No. 34 - P.115-118.
3. Dolgov, A.B., Zane, R. Low-power wireless medical sensor platform - *Engineering in Medicine and Biology Society*, 2006. EMBS'06. 28th Annual International Conference of the IEEE, 2006 - P.2067-2070.
4. Jovanov, E., Milenkovic, A., Otto, C., De Groen, P.C. A wireless body area network of intelligent motion sensors for computer assisted physical rehabilitation. *Journal of neuroengineering and rehabilitation - BioMed Central Ltd*, 2005 - No. 2.

Methodology for Assessing Efficiency of a Photovoltaic Plant

Michal Tutsch

Department of Cybernetics and Biomedical Engineering, FEECS,
VŠB – Technical University of Ostrava, 17. listopadu 15, 708 33 Ostrava – Poruba
michal.tutsch@vsb.cz

Abstract. The paper deals with the methodology for assessing the production of a solar photovoltaic (PV) power plant. According to a number of newly installed plants, such as in the Czech Republic, it is a very topical issue. Operational quality of a solar power is given to early detection of possible failures of individual components. This can be achieved only by constantly monitoring the status of the plant and their proper evaluation. The first part of this paper is centered on architecture of own developed monitoring system, including four stages. It is described some designing this monitoring system, based on data mining, automatic detection of failures, and software evaluation of measured data. In the second part, behavior of energy delivery and production efficiency is discussed in connection with an efficiency of PV panels, their temperature, momentary value of actual irradiance, and total efficiency of the PV power plant. The proposed procedures are validated in operation and maintenance of solar power with the performance 350 kW (peak value), built at campus of VŠB – Technical University of Ostrava.

1 Introduction

The paper deals with some methodology for assessing the production of solar photovoltaic power plant. Operational quality of a solar power is given to early detection of possible failures of individual components. This can be achieved only by constantly monitoring the status of the plant and their proper evaluation.

It is described design of whole data acquisition system based on data mining and automatic detection of failures and follow-up evaluation of data.

According to a number of newly installed plants, such as in the Czech Republic, it is a very topical issue. The proposed procedures are validated in operation and maintenance of solar power with the performance 350 kW (peak value) built in campus of VŠB – Technical University of Ostrava (also VŠB-TUO).

Quality of service of a solar power plant and thus yield ultimately is subjected to proper monitoring and servicing components. The whole system control status of the plant should be finalized with periodic balance of power production and calculation of the efficiency of power plants. The data should be compared with the data guaranteed by component manufacturers and also with those of the energy audit. In case of

different results, it should be approached to more accurate ways to verify the status of components, such as power testing of panels or inverters in the test room.

In general, the immediate production of solar plant is directly proportional to solar radiation incident at any given moment on the PV (photovoltaic) panels. Solar radiation is transformed in panels to electrical energy and interlinked in strings to inverters, where it is transformed from a DC voltage to AC one. Inverters are usually the closest device to the panels, which provide information in regular time samples not only on production. In real operation, the actual amount of solar radiation incident on the individual panels influenced by rapidly changing weather during the day, month, year and function of plant components.

The comparison of selected monthly summary exposure in individual years may not coincide with each other and thus do not correspond with the long-term average values reported irradiance in the energy audit. On the other hand, we can assume that the ultimate total production from the plant, which is dependent on the sunshine with a little variation, will be equal to the audit and also in view of decreasing effectiveness of panels over the years. [1]

Some proper evaluation of production can be only done by continuous monitoring values, which consist of recorded data of all inverters and monitoring equipment including measuring devices. Then it must be carried out by filtering the data (taking into account the operational status of the device, etc). The advantage is that VŠB-TUO has got own solar power plant and now we are developing own monitoring own SCADA system, which is mainly intended for purposes of monitoring solar power plants.

2 Architecture of Monitoring System

The project itself aims to design a comprehensive monitoring system of solar power plant, which consists of an optimal hardware solution and a software one. The system will automatically collect data; in case of failures or underproduction, it will alert technicians. It will analyze and calculate the effectiveness of PV plant and its changes over the long term. In future, we assume the system will evaluate alerts fully autonomously.

3 Development of Monitoring System

For the purposes of design of methods to evaluate plant efficiency, we have developed monitoring system based on real-time measurement by dataloggers, PLCs (Programmable Logical Controller) and other sensors and devices. All data acquisition devices are connected to the Ethernet, so real-time data are transferred and sent into SQL database. This database can be easily accessed by some client application, developed in MS Visual Studio and written in C# programming language. This application is also used to detect segment faults in the system of the plant, communication errors as well as differences in generated power among inverters.

Based on our assumption, we found necessary to measure at least these variables of the plant to determine proper plant features, whereas they could be electrical or non-electrical, thus:

- electrical power of the inverters (W),
- electrical current in string boxes (A),
- momentary delivery measured by a electricity meter (kWh),
- irradiance ($\text{W}\cdot\text{m}^{-2}$),
- temperatures of the PV panels and ambient ($^{\circ}\text{C}$),
- network quality parameters measured by a Q-meter.

Based on the irradiance measurement, we can predicate production and retroactively compare the actual electricity supply corresponding to the expected production. Irradiance conditions of the plant can dramatically change during the day, especially when it is variable cloudiness. In this case, the analysis must be much more sophisticated. Naturally, next issue is to synchronize sample time among devices due to comparing measured data at the same time moment.

Collecting the data from the device is as follows, whereas all inverters provide data about:

- current performance,
- daily and the total power supplies,
- AC/DC currents and voltages,
- states of the inverters – their fault states and some error reports.

These data values are provided via RS-485 bus, through which the datalogger accesses these values. After their transfer and conversion into a suitable format, data are stored into SQL database. Another device used in monitoring system is a PLC, whereas:

- it monitors some signals from a circuit breaker to detect some power plant's disconnection or short circuit,
- the signals from temperature sensors and irradiance sensor are connected to the PLC, which also communicates via RS-485 with a network analyzer,
- data are sent at precise moments into the database, when events like the dropping of the circuit breaker are sent immediately to be evaluated as soon as possible and malfunction fixed. [2]

4 Measured and Analyzed Data

Our monitoring system already collects data for a few months and the first analyses have just been done.

Initially, we chose a day with optimal irradiance, i. e. there were no clouds. In this day, we compared the total supply of real power plants with expected energy output. This expected supply calculation approach depends on these factors, such as a total irradiance, flat panels, panels and efficiency – see (1) in a simplified form (at specified conditions).

$$E_{est.} = 3600 \cdot S \cdot \prod_{j=1}^N \eta_j \cdot \int_{t_0}^{t_c} i_{r(act.)}(\tau) \cdot d\tau . \tag{1}$$

Where

- $E_{est.}$ estimated energy supply of PV plant (W · h),
- $i_{r(act.)}(t)$ momentary value of irradiance (W · m⁻²),
- S total area of PV panels (m²),
- η_j j th efficiency component (-),
- t_c stop calculation time (s),
- t_0 start calculation time (s).

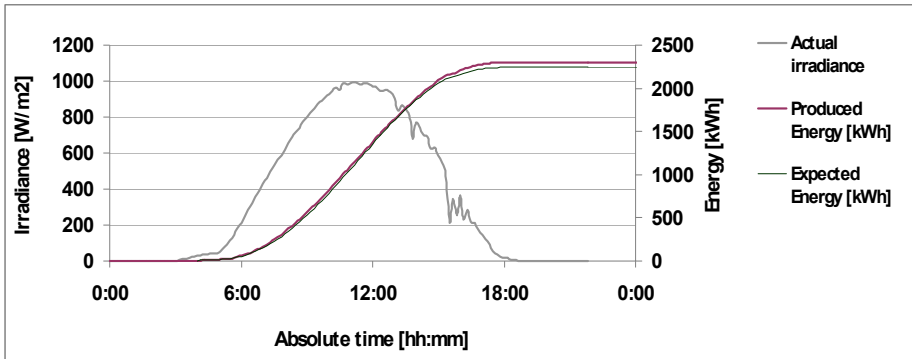


Fig. 1. Comparison of power plant supplies – real energy supply (Produced Energy curve) and estimated energy supply (Expected Energy curve), the third curve (Actual Irradiance curve) is focused on the momentary value of irradiance; all the characteristics are dependent on absolute time (at 24-hour measurement period)

Equation (1) is valid only at constant efficiency values of components, whereas operating points of them and PV panel temperature are not considered and discussed.

For example, let us consider these values, thus:

- at an irradiance value of 1000 W · m⁻² and an ambient temperature of 25 °C, the PV efficiency equals to 13.8 % [3],
- at the maximum power of 15 kW, the inverter efficiency equals to 98 % [4].

Some differences between real and expected energy outputs are shown in Fig. 1 (see graphs). It is evident that the real supply and the calculated ideal one vary by 2.5 % (neglecting the error of measurement about 1 % of energy). [5]

To calculate the percentage efficiency of electricity production from solar energy (the percentage of amount of sunlight energy which is converted into electricity), we use the following ratio – see (2a) and (2b):

$$\eta_{plant} = \frac{E_{real.}}{E_{est.}} \quad (2)$$

And (in percent)

$$\eta_{plant(\%)} = \eta_{plant} \cdot 100 = \frac{E_{real.}}{E_{est.}} \cdot 100 \quad (3)$$

Where

$E_{est.}$ estimated energy supply of PV plant (W · h),

$E_{real.}$ real energy supply of PV plant (W · h),

η_{plant} total efficiency of PV plant (-),

$\eta_{plant(\%)}$ total efficiency of PV plant (%).

The course of the production efficiency is shown in Figure 2.

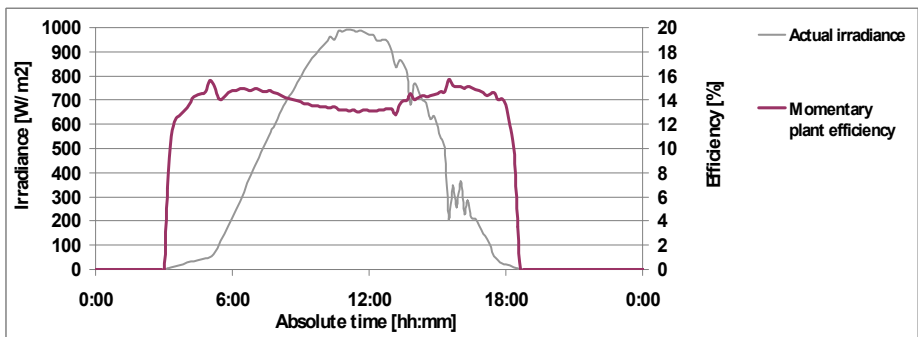


Fig. 2. Production efficiency (Momentary Plant Efficiency curve) versus power plant irradiation (Actual Irradiance curve); both characteristics are dependent on absolute time (at 24-hour measurement period)

5 Conclusion

This paper brought some presentation of designing the monitoring system of solar photovoltaic power plant. It presents two areas – at first development of hardware for monitoring system, second area is the software for analyzing efficiency of each part of solar power plant. The presented solution is widely applicable in industry, because it is implemented on commonly available hardware and it extends features of existing facilities for monitoring and analysis of data.

Acknowledgements

This paper was supported by the project SP2012/111, named “Data Acquisition and Processing from Large Distributed Systems II”, of Student Grant Agency (VŠB – Technical University of Ostrava).

References

1. Blaesser G.: PV System Measurements and Monitoring, the European Experience // Solar Energy Mater Solar Cells. – Elsevier, 1997. – Vol. 47, Issue 1-4. – P. 167-176.
2. Machacek Z., Srovnal V.: Automated System for Data Measuring and Analyses from Embedded Systems // 2005 Proceedings of 7th WSEAS International Conference on Automatic Control, Modeling and Simulation. – WSEAS, 2005. – P. 43-48.
3. BP Solar. 225 W Photovoltaic Module BP 3225T // [Online]. Available at: <<https://na3.salesforce.com/sfc/p/3000000001pz9EhQCWjbfLvIqQX6uil1DWTCFqw=>>. – 2 p.
4. Danfoss Solar Inverters A/S. TripleLynx Inverter Range // [Online]. Available at: <http://www.danfoss.com/NR/rdonlyres/0/DanfossTripleLynxGB_TLX006.pdf>.
5. Vergura S., Acciani G., Amoroso V.: Patrono G. E., Vacca F. Descriptive and Inferential Statistics for Supervising and Monitoring the Operation of PV Plants // IEEE Transactions on Industrial Electronics. – IEEE Xplore, 2009. – Vol. 56, Issue 11. – P. 4456-4464.
6. Forero N., Hernández J., Gordillo G.: Development of a Monitoring System for a PV Solar Plant // Energy Conversion and Management. – Elsevier, 2006. – Vol. 47, Issue 15-16. – P. 2329-2336.
7. Tutsch, M., Vojcinak, P., Koziorek, J.: Metodika vyhodnocování účinnosti FV elektrárny, In Proceedings of the 13th International Scientific Conference EPE2012, 23.-25.5.2012, Brno, Czech Republic, str. 511 – 515, ISBN 978-80-214-4514-7
8. Tutsch, M., Vojcinak, P.: METHODOLOGY FOR ASSESSING EFFICIENCY OF PHOTOVOLTAIC POWER PLANT, Workshop Perspektivní projekty vývoje řídicích a senzorických technologií, 27.-29. Června 2011, Trojanovice, ČR, vydání 1., Brno : Vysoké učení technické v Brně, Fakulta elektrotechniky a komunikačních technologií, 2011, str. 202-208, ISBN 978-80-214-4297-9
9. Tutsch, M., Vojcinak, P., Koziorek, J., Skrepek, M., Using Automated Evaluation of Efficiency for Photovoltaic Power Plant, In Proceedings of 16th IEEE International Conference on Emerging Technologies and Factory Automation, ETFA 2011, 5-9 September 2011, Toulouse, France
10. Kašík, V., Tutsch, M.: Simulation and Measurement of Axle Counter With FPGA. In: Technical Computing Prague 2011, 19th Annual Conference Proceedings. Prague, Czech Republic, 2011. ISBN 978-80-7080-794-1
11. Kocian, J., Tutsch, M., Ozana, S., Koziorek, J., Application of Modeling and Simulation Techniques for Technology Units in Industrial Control, 2011 International Conference on Computer, Communication, Control and Automation, 3CA 2011 - Zhuhai, China, November 19-20, 2011
12. KOCIAN, J., TUTSCH, M., OZANA, S., KOZIOREK, J.. Modeling and Simulation of Controlled Systems and Technologies in Industrial Control. In ICACTE 2011: Proceedings of 4th International Conference on Advanced Computer Theory and Engineering, Dubai, UAE. December 28 - 30, 2011

Improving the Quality of Hospital Care by Using RFID Technology

Lucie Valová

Department of Cybernetics and Biomedical Engineering, FEECS,
VŠB – Technical University of Ostrava, 17. listopadu 15, 708 33 Ostrava – Poruba
lucie.valova@vsb.cz

Abstract. This article presents possibilities of using RFID technology in hospital care. The barriers of implementation new technologies are analyzed in the aspect of hospital management, staff and technical conditions. Below, there are described possibilities of improving health care with RF identification and benefits for all participants. There is shown advantages against bar codes, which is commonly used in hospitals at present. RFID eases work for medical staff and provides safer care for patients. At emergency income is important to know patient's condition, treatment and his location in emergency area. These can be performed by RFID.

1 Introduction

Continuous strain on increasing work productivity efficiency in health care leads to implement automated technology also in fields, which have been still human's domain.

Health care is a line of business with large potential for using RFID for identification and locating objects and peoples. In several hospitals abroad are already in use passive RFID wristband for hospitalized patient's identification. In Europe, it is Asklepios Klinik Bamberk in Hamburg, which is also nicknamed as "Hospital of Future". In Slovakia, there is a commercial hospital Medissimo in Bratislava. In our country, there is only particular use of RFID, like e. g. in Masaryk Memorial Cancer Institute in Brno.

2 The barriers of RFID implementation

2.1 Distrust of hospital management, that investment into RFID technology is returned in few years.

This is the first and principal assumption for creating a "high-tech hospital". Big amount of capital investment is needed in the infrastructure. Today, when hospitals contend with lack of money, improvements are focused to medical devices and other equipments for direct care. Supporting technologies stay behind and may be implement only if some funds left.

The management's thinking isn't complex already in the initial part of planning. Expensive medical devices often can't be use with all their functions without supporting technologies, so they aren't able to bring their whole added value.

As an example, we can point to commonly available diagnostic device in hospital such digital X-ray. Doctor usually read the X-ray in his PC. If he needs to talk with the patient, he has to go to patient's bed with printed X-ray and thoughts in his mind. In case, that doctor has a tablet computer and hospital has wi-fi connection, he still has to go to patient's bed, but he can see the X-ray in his tablet, he can zoom it in or out as he needs, talks with patient and writes notes at the same time, without missing something important before he reaches his desk.

Return on investment can be shown on blood-tracking study from Blood Center in Wisconsin from 2009. "For blood center, which drawing about 250,000 transfusions annually, would typically recoup their expense of installing an RFID blood-tracking system within 3.9 years. This is based on estimate that technology, including handheld or desktop readers, tags and software, would cost about \$744,000 to acquire and install, and would provide a savings of \$827,000 over a five-year period. Savings would be the result of fewer man-hours spent tracking the movements of blood products and a reduction in wastage resulting from blood products that had expired before they could be located and used. Another benefit is the increased safety that would be created by better ensuring patients get the correct blood products." [1]

2.2 The willingness of staff to work with modern technologies

The staff shall themselves want to use new technologies, or they will "throwing obstacles in the way" during implementation. They must not be ordered, but explained. RAND Europe study about requirements and options for RFID in health care published in 2009 has a typical example. [2] The Dutch government supported this technology a lot. A hospital in Amsterdam was chosen for pilot project. Technology was introduced in multiple different activities within the hospital, but there was great resistance from personnel who had the impression that they will be monitored and the project failed.

2.3 Technological background

The cornerstone of this technology is a communication infrastructure. Wi-fi is commonly used in hospitals, but somewhere in medical environment is using wi-fi prohibited in terms of possible interactions with medical devices.

For the implementation of RFID in hospitals should also take into account the possibility of mounting hardware for the technology in existing buildings. From a structural point of view may be a problem at key points such as doors, elevators, etc.

Regarding the identification technologies most of healthcare facilities using linear barcodes. They satisfy the fundamental conditions of identification, but have at least two disadvantages – must be visible for reading and data are static. Some medical facilities have already using 2D code, which can hold more data, but other properties have the same as linear barcodes. Both of these identifiers have one common advantage, they are relatively cheap.

3 Emerging methods of identification using RFID

Compared to the already mentioned barcodes, RFID has several indisputable advantages:

- No need to have direct line of sight between label and reader
- Possibility to write additional data
- Possibility of tracing the object or people in periodic time interval
- Possibility of monitoring the environment in which the object is located
- Possibility to simultaneously read multiple tags
- Can be read from a distance

RFID - Radio Frequency Identification - is a method of identification using radio waves. Objects can be identified not only in the key points of the supply chain, but they can be monitored in real-time and also record the value of the environment. An object that is identified is provided with the tag. This device consists of a chip and antenna and battery in case of active tag. It may take the form of stickers, plastic cards, key chains, etc. The reader, or interrogator, is device for communicate with the tag. Readers are handheld, mobile or stationary. The principle of technology is as follows: reader transmits electromagnetic waves to its surroundings. If the tag, working on the same frequency, is in the range of the reader, waves activate tag's control circuit and tag's identification is sand in the form of the modulated signal back to the reader. The system also includes middleware, where data adopted by the reader is processed and then transmits to the follow-up information system. [3]

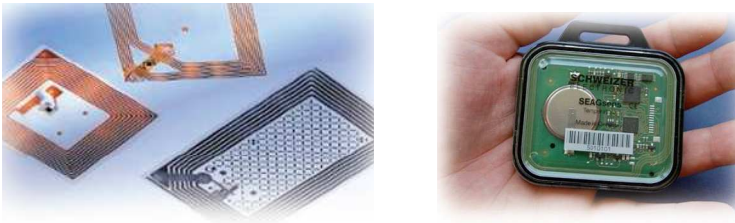


Fig. 1 Passive and active tags

RFID works on the following frequencies:

- 125 to 135 kHz
- 13,56 MHz
- 865 to 928 MHz
- 2,4 GHz

3.1 RFID in hospital care

To identify hospitalized patients are using wristbands with passive RFID chip. To the wristbands with a unique identification number can be written more information about the patient such as name, age, diagnosis. The advantage of this identification is as

compared to using barcode to read the patient's wristband without direct line of sight, e.g. when the wristband is under the covers or under the body. This will, among other things, increase patient's comfort, there is not necessary to wake him up or to manipulate him.

This identification also helps to prevent errors in medication because of patient confusion (another room, another bed because of disorientation) or because of errors in drug administration with a similar name or just the reasons that nurses have too many patients to care for.

Active tags are suitable for locating of selected groups of patients: patients with Alzheimer's disease, pediatric patients, patients from psychiatric wards, infectious patients...

Nurses have a PDA with RFID reader. They can make records of activities such temperature measurement just at the bedside. Every nurse have in the PDA the list of all patients, she is caring for, their diagnosis, medications, time to next control, etc. Doctors are equipped with tablet computers, where the records can be written also directly at the patient's bedside. This may be useful also during regular ward. Today, nurse reads patient's data during ward from paper records. If doctor change the cure, nurse notices it to the papers and this changes are later transcribed into hospital information system. Here is space for making mistakes. Papers could be swapped, matches could be bad read during rewriting. Staffing by this techniques helps to avoid such errors and changes in records appear in the system immediately.

Hospitals are working with expensive medical devices and often inefficient, since it is not always clear where some of the portable device is located. Devices marked with RFID can not only locate, but also track where, how often and by whom they are used.



Fig. 2 Identification of RFID wristband, RFID-Enabled pocket PC

3.2 RFID in the emergency income

Specific workplace in hospital is emergency, where patients, often in jeopardy of life are treated. Emergency in hospitals similar as University Hospital of Ostrava treats an average of about 40 heavily traumatized patients per month. Therefore, it might seem deployment of RFID technology, whose implementation is considerable financial resources, as extras. Large hospitals must cope with the onslaught of mass accident, as was the case of a tram collision on line number 5 or railway accident in Studénka, when it is necessary to care for many patients in a short time. The identification using RFID may be helpful. However, even during standard operation, emergency solves more cases at a time, especially the wounded from a car accident.

Before the patient is transported by ambulance to the hospital, basic information about him, his health condition and first aid treatment, are communicated to emergency income. At present, the information is communicated by the phone and later during the patient’s intake is handed over as a paper records. Therefore the patient could be equipped with RFID wristband already in the ambulance and all the necessary data for identification and treatment would have been recorded in the wristband, and would also determine the priority treatment. This saves time for emergency personnel, which now needs to rewrite patient’s data into the hospital information system.

The key points on emergency department will hold stationary reader and patient movement will be monitored on-line. Staff will be equipped with handheld readers in the form of a PDA. In the case of mass accidents will reduce the risk of substitution of patients by identifying wristband. Also situations when patient is long time without care may trigger alarm. Collecting data of the patient movements in emergency department areas is also important for feedback control.

RFID tags will also be equipped with devices allowing to monitor their usage and to use them more effectively. This is also applied to cord blood, which are available for emergency department and are stored directly on their premises. Cord blood will also have a temperature sensor to monitor the quality of blood. It may be situations when there are treating severely injured patient the blood bag is removed from the refrigerator, but for some reason it is not used and is returned back into the fridge without anyone noticing how long it was outside. If this is repeated several times, it may cause that blood is no longer suitable for use, and information system in cooperation with RFID would warn.

All information about the patient during treatment on emergency department will be on-line transferred to the hospital information system. A doctor or nurse would use "hot keys" for notifying the department where the patient will be sent. This department can prepare in advance, because the data about incoming patient will already be in the information system.

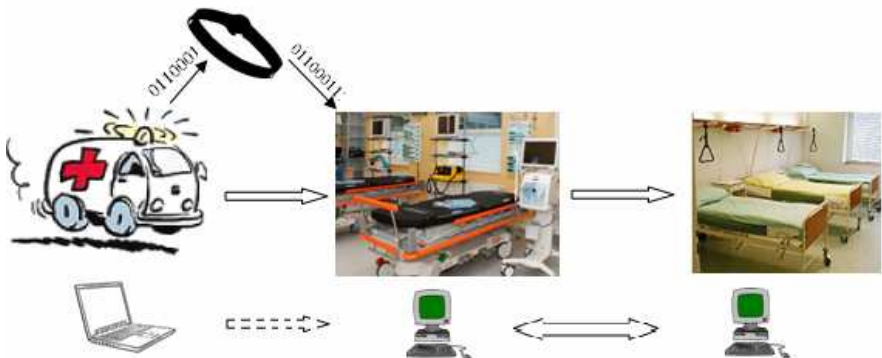


Fig. 3 If the information system of the ambulance is not connected with hospital information system, one possibility to transfer important data for rapid patient identification is using RFID wristband.

Conclusion

The implementing of RFID technology as a means of identification in hospital for more efficient services needs to be addressed for all activities ongoing in the facility, from the identification of surgical instruments to identify the bedding.

When using RF identification, personnel will be forced to follow the established way of organizing work, which today do not always follow, because as it stands now is very time consuming ineffective and thus leads to making errors.

Benefit that arises by introducing RFID in hospital, in terms of economic efficiency will be utilization of staff performance, instrumentation and medical supplies and reducing errors caused by human factor. Management will also gain better statistical reports for further managing of the hospital. For patients there will be more comfortable and safer care. Staff will be less burdened with administrative tasks, and instead will be able to pay its original mission, care for the patient.

References

1. <http://www.rfidjournal.com/article/view/5356>
2. Vilamovska, A.-M.; Hatziandreu, E.; Schindler, H., R.; Van Oranje-Nassau, C.; De Vries, H.; Krapels, J., RAND EUROPE: STUDY ON THE REQUIREMENTS AND OPTION FOR RADIO FREQUENCY IDENTIFICATION IN HEALTHCARE, RAND Corporation, 2009
3. <http://www.rfidportal.cz>

Measurement of Thermal Boreholes with Programmable Logical Controller of B&R and Sensors with Interface of 1-Wire

Tomas Vavrla and Jiri Koziorek

Department of Cybernetics and Biomedical Engineering, FEECS,
VŠB – Technical University of Ostrava, 17. listopadu 15, 708 33 Ostrava – Poruba
{tomas.vavrla, jiri.koziorek}@vsb.cz

Abstract. The paper sums up research and development of measuring system for measurement of temperature profiles of thermal boreholes. The work includes the development libraries for application interface of 1-Wire, implementation of the measuring system with programmable logical controller of B&R X20 and realization of autonomous database server for saving the measured data and fault diagnosis.

1 Introduction

Today, mankind is beginning to recognize the issue of finding alternative sources of energy, because fossil fuel era is coming to end. Geothermal energy is one of many possible types of energy for the acquisition of clean energy. The term “Geothermal energy” can be defined in a broader sense as heat in the Earth’s core and mantle. It is used in the form of thermal energy for residential heating or for electricity generation in geothermal power plants. The use of this energy is indeed simple at first glance, but the technical solution is difficult, because the hot water extracted from itself borehole contains many minerals and thereby clog technological devices [1].

Two experimental works (the experimental polygons) are in the vicinity VSB – TUO. They deal with the issue of geothermal energy (temperature changes of the rock massif) [1, 2, 3]:

- The Big Research Polygon (BRP),
- The Small Research Polygon (SRP).

Other experimental work is located in the place of the firma Green Gas.

The installed measuring systems both polygons realizes getting some information about the behavior of heterogeneous earth and heat pumps. The information obtained is used for mathematical modeling and simulation of heat exchange (between the earth and the heat pump) and the prediction of system behavior in the future [1, 2, 3].

The work follows the previous published work. The work realizes two basic parts:

- Realization of the measuring system by using the Micro LAN network – This part is devoted chapters 2 and 3,
- Realization of the database server for saving data – This part is devoted chapter 4.

Communication is introduced in order to limit the number of wires in the borehole. Direct use of sensors (the analog sensors) for every sensor requires at least two wires. Number of wires in the communication (the digital or the analog sensors with communication interface) with a higher number of sensors remains the same.

2 Micro LAN

This is a simple and inexpensive network technology for automation. It is defined in norm IEEE 1451.4. It uses 1-Wire protocol, therefore the 1-Wire bus. Components are devices and equipment with 1-Wire interface and block 64 to 128 bits identification number (8 bits => CRC, 48 bits => serial number and 8 bits => device type „family code“) [1].

8-BIT CRC		48-BIT SERIAL NUMBER				8-BIT FAMILY CODE (28h)	
MSB		LSB	MSB	LSB	MSB		LSB

Fig. 1. Identification number of the sensor Dallas “Maxim” DS18B20 [1].

Identification number can uniquely identify the device on the network. Device containing these two parts is declared by the manufacturer as standard Micro LAN. Other parts of the network may be different adapters and controllers [1].

3 The system with the Micro LAN network

Basic of measuring system (The Small Polygon and Green Gas) is programmable logic controller. The programmable logic controller is based on X20 architecture the Austrian manufacturer Bernecker & Rainer. For this reason, the system with Micro LAN controlled by a programmable logic controller B&R X20. In order to programmable logic controller control and communicate with the network contains 1-Wire Micro LAN network converter communications. This converter converts the 1-Wire communications on the serial communications (RS232). Superior system PLC consists of desktop computer with HMI/SCADA applications (visualization using VNC) and the database system. Block diagram of the system with Micro LAN network is show in Figure 2. The complete system has the following features [1]:

- Temperature measurement using accurate and reliable sensors 1-Wire,
- Control of Micro LAN communication using serial link,
- The obtained temperature data are saved in FLASH memory card and database system,

- Data transmission through integrated Ethernet interface,
- The Direct FTP access to the PLC,
- Control system with Micro LAN network and data visualisation using HMI/SCADA application (visualization using VNC).

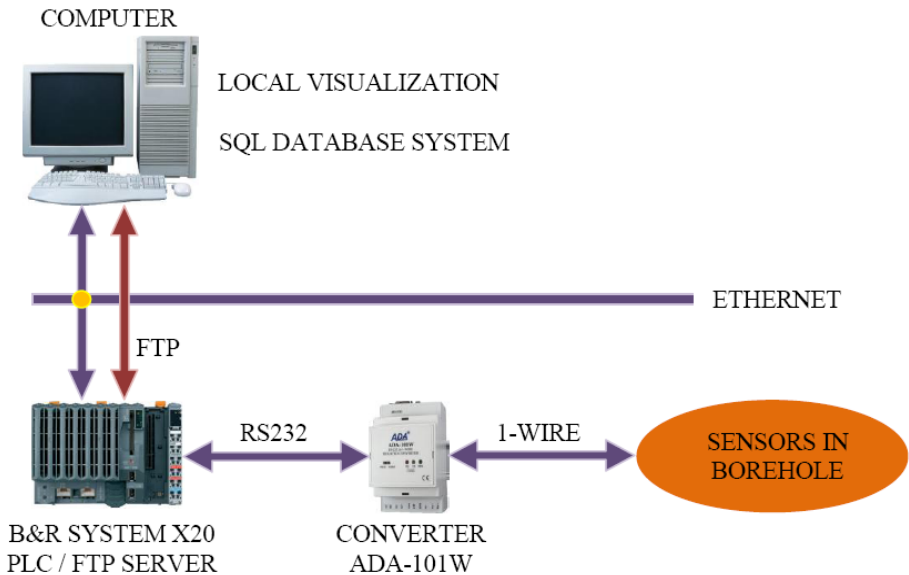


Fig. 2. Block diagram of system with Micro LAN network [1].

System with Micro LAN network has in term of software programmable logic controller two parts. The first part performs network control (network management). The second part performs the evaluation of measured data. Based on evaluation of data are send over Ethernet to the desktop computer or saved to file on the FLASH card. The file can be read or downloaded at any time as programmable logic controller working as an FTP server. So if the PLC stops working for some reason, the obtained data are always available on the FLASH card and on the FTP. In addition, the FLASH card saves configuration file with line spacing and file errors [1].

Evaluation of data carried out on the end of the communication. This means that initially will be communication between the programmable logic controller and sensors. The data extract is evaluated after the end of communication obtained using comparing the identification number sensor with the table identification numbers. Table identification numbers are created in advance based on the position sensors in the borehole. We get comparing specific information about the position sensors in the borehole and it still appropriate temperature [1].

As already mentioned in the preceding paragraph, are the most important part of communication and its control. For this purpose was developed the universal library of the functions using ANSI C. The library is dependent on the support serial communication (RS232). This library can be used in any programmable logic controller Ber-

necker & Rainer with support for serial communication. The library consists of three blocks of elementary functions. And it:

- **The function for handling serial port PLC** – It contains the elementary functions for working with the serial port. E.g.: Functions for opening and closing the serial port. etc.,
- **The utilities** – It contains the auxiliary functions. They are: function for implementation delay; functions for realization of the CRC calculation and function realization conversion format the identification number into human readable form. The most important functions are here function for calculating the CRC (Influence communication). Using function of calculating CRC are detected the errors.,
- **The function for communicating with 1-Wire network** – This is the most important block of the elementary functions. Elementary functions for realization of communication uses the functions for handle the serial port.

Combining the elementary functions (from the third block “Function for communication with 1-Wire network”) is realizes communication between the programmable logic controller and the 1-Wire sensors [1].

4 The autonomous system for acquisition of data and diagnostic of errors

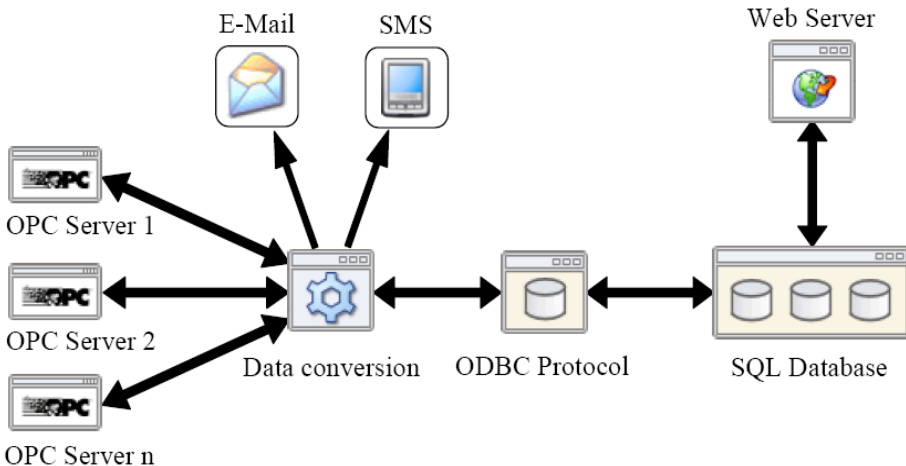


Fig. 3. The principle of data acquisition and fault diagnosis.

The result is the autonomous database server system saves data from connected devices. The system includes of testing errors. Errors are tested for individual communi-

cations. Based on the detected error is send an SMS message or e-mail system administrator. Message contains the detected error and requests its removal.

Core of the system is a computer with architecture designed for server application. The device provides data to the system connect using Ethernet and OPC protocol. An important part of the transfer protocols. It is the transfer of communication OPC and ODBC. During this conversion errors may occur, therefore the system includes means for the detection errors. The acquired data is saved in a SQL database.

Part of the system is web visualization (the SCADA application). Based on the web visualization accuse individual data (Errors = E-mail, data = SQL) in the form of tables and graphs.

Export do CSV | Export do arku | Aktualizovat

Export dat do CSV souboru

1) Vyberte tabulky pro export

Malý polygon - VEC

Název	Popis tabulky
vec	VEC - AMRci vrt
vec1	VEC - Technologicky vrt
vec2	VEC - Technologicky vrt
vec3	VEC - AMRci vrt
vec4	VEC - AMRci vrt
vec5	VEC - AMRci vrt
vec6	VEC - AMRci vrt
vec7	VEC - AMRci vrt
vec8	VEC - AMRci vrt
vec9	VEC - AMRci vrt
vec10	VEC - AMRci vrt
vec11	VEC - AMRci vrt
vec12	VEC - AMRci vrt
vec13	VEC - AMRci vrt
vec14	VEC - AMRci vrt
vec15	VEC - AMRci vrt
vec16	VEC - AMRci vrt
vec17	VEC - AMRci vrt
vec18	VEC - AMRci vrt
vec19	VEC - AMRci vrt
vec20	VEC - AMRci vrt
vec21	VEC - AMRci vrt
vec22	VEC - AMRci vrt
vec23	VEC - AMRci vrt
vec24	VEC - AMRci vrt
vec25	VEC - AMRci vrt
vec26	VEC - AMRci vrt
vec27	VEC - AMRci vrt
vec28	VEC - AMRci vrt
vec29	VEC - AMRci vrt
vec30	VEC - AMRci vrt
vec31	VEC - AMRci vrt
vec32	VEC - AMRci vrt
vec33	VEC - AMRci vrt
vec34	VEC - AMRci vrt
vec35	VEC - AMRci vrt
vec36	VEC - AMRci vrt
vec37	VEC - AMRci vrt
vec38	VEC - AMRci vrt
vec39	VEC - AMRci vrt
vec40	VEC - AMRci vrt
vec41	VEC - AMRci vrt
vec42	VEC - AMRci vrt
vec43	VEC - AMRci vrt
vec44	VEC - AMRci vrt
vec45	VEC - AMRci vrt
vec46	VEC - AMRci vrt
vec47	VEC - AMRci vrt
vec48	VEC - AMRci vrt
vec49	VEC - AMRci vrt
vec50	VEC - AMRci vrt
vec51	VEC - AMRci vrt
vec52	VEC - AMRci vrt
vec53	VEC - AMRci vrt
vec54	VEC - AMRci vrt
vec55	VEC - AMRci vrt
vec56	VEC - AMRci vrt
vec57	VEC - AMRci vrt
vec58	VEC - AMRci vrt
vec59	VEC - AMRci vrt
vec60	VEC - AMRci vrt
vec61	VEC - AMRci vrt
vec62	VEC - AMRci vrt
vec63	VEC - AMRci vrt
vec64	VEC - AMRci vrt
vec65	VEC - AMRci vrt
vec66	VEC - AMRci vrt
vec67	VEC - AMRci vrt
vec68	VEC - AMRci vrt
vec69	VEC - AMRci vrt
vec70	VEC - AMRci vrt
vec71	VEC - AMRci vrt
vec72	VEC - AMRci vrt
vec73	VEC - AMRci vrt
vec74	VEC - AMRci vrt
vec75	VEC - AMRci vrt
vec76	VEC - AMRci vrt
vec77	VEC - AMRci vrt
vec78	VEC - AMRci vrt
vec79	VEC - AMRci vrt
vec80	VEC - AMRci vrt
vec81	VEC - AMRci vrt
vec82	VEC - AMRci vrt
vec83	VEC - AMRci vrt
vec84	VEC - AMRci vrt
vec85	VEC - AMRci vrt
vec86	VEC - AMRci vrt
vec87	VEC - AMRci vrt
vec88	VEC - AMRci vrt
vec89	VEC - AMRci vrt
vec90	VEC - AMRci vrt
vec91	VEC - AMRci vrt
vec92	VEC - AMRci vrt
vec93	VEC - AMRci vrt
vec94	VEC - AMRci vrt
vec95	VEC - AMRci vrt
vec96	VEC - AMRci vrt
vec97	VEC - AMRci vrt
vec98	VEC - AMRci vrt
vec99	VEC - AMRci vrt
vec100	VEC - AMRci vrt

Velký polygon - NA

Název	Popis tabulky
na1	NA - Monitorovací vrt
na2	NA - Monitorovací vrt
na3	NA - Monitorovací vrt
na4	NA - Monitorovací vrt
na5	NA - Monitorovací vrt
na71	NA - Technologicky vrt
na72	NA - Technologicky vrt
na73	NA - Technologicky vrt
na74	NA - Technologicky vrt
na75	NA - Technologicky vrt
na76	NA - Technologicky vrt
na77	NA - Technologicky vrt
na78	NA - Technologicky vrt
na79	NA - Technologicky vrt
na80	NA - Technologicky vrt
na81	NA - Technologicky vrt
na82	NA - Technologicky vrt
na83	NA - Technologicky vrt
na84	NA - Technologicky vrt
na85	NA - Technologicky vrt
na86	NA - Technologicky vrt
na87	NA - Technologicky vrt
na88	NA - Technologicky vrt

Green Gas

Název	Popis tabulky	GreenGas - Technologická data
gg_control	GreenGas - Technologická data	
gg_05	GreenGas - Technologicky vrt	
gg_06	GreenGas - Technologicky vrt	
gg_07	GreenGas - Technologicky vrt	
gg_08	GreenGas - Technologicky vrt	
gg_09	GreenGas - Technologicky vrt	
gg_10	GreenGas - Technologicky vrt	
gg_11	GreenGas - Technologicky vrt	
gg_12	GreenGas - Technologicky vrt	
gg_13	GreenGas - Technologicky vrt	
gg_14	GreenGas - Technologicky vrt	
gg_15	GreenGas - Technologicky vrt	
gg_16	GreenGas - Technologicky vrt	
gg_17	GreenGas - Monitorovací vrt	
gg_18	GreenGas - Monitorovací vrt	
gg_19	GreenGas - Monitorovací vrt	
gg_20	GreenGas - Monitorovací vrt	
gg_21	GreenGas - Monitorovací vrt	
gg_22	GreenGas - Monitorovací vrt	
gg_23	GreenGas - Monitorovací vrt	
gg_24	GreenGas - Monitorovací vrt	
gg_25	GreenGas - Monitorovací vrt	

2) Zvolte formát exportu

3) Zvolte interval mezi aktualizacemi

25

Vytvořit CSV

Fig. 4. Example Web visualization.

Currently, this autonomous system is connected with Small Research Polygon, Big Research Polygon and the measuring device from Green Gas.

4 Conclusion

Based on this work was developed measuring system and autonomous system for data acquisition. Both systems were created on several communication protocols (ODBC, OPC, Ethernet, RS232 and Micro LAN).

The principle of measuring system is a library and communication converter that controls all measurement. Order to the library could be used in other applications of measurement and control is universal. It is limited to the use of programmable logic controller Bernecker & Rainer with supports serial communication.

The principle of autonomous system is data transfer “data conversion”. It is possible for him connect many data sources (using OPC). The system is therefore universal. The final autonomous system has been registered as a function pattern (106/08-12-2011_F).

Acknowledgements

This paper was supported by the project SP2012/111, named “Data Acquisition and Processing from Large Distributed Systems II“, of Student Grand System (VSB – Technical University of Ostrava).

References

- [1] VAVRLA, T., KOZIOREK, J.. Temperature Measurement in Boreholes by Programmable Logical Controller B&R and Temperature Sensors 1-Wire. In PDES 2012: Proceedings of 11th IFAC/IEEE International Conference on Programmable Devices and Embedded Systems, Brno, Czech Republic, May 23 – 25, 2012, p. 358 – 363.
- [2] HAJOVSKY, R., KOZIOREK, J.. Using PAC System for Temperature Monitoring. In ICSE 2009: Proceedings on 20th International Conference on Systems Engineering, Coventry University, Coventry, United Kingdom of Great Britain and Northern Ireland, 2009, p. 195 – 200.
- [3] KOZIOREK, J., HORAK, B., HAJOVSKY, R., BUJOK, P.. Measurement of Thermal Conditions in Rock Massif. In PDES 2009: Proceedings on 9th IFAC Workshop on Programmable Devices and Embedded Systems, VSB – TUO, Ostrava, Czech Republic, p. 230 – 235.

Implantation System for the Real Usage as the Educational Support

Karel Vlach, Jakub Jirka, Viktor Michna, and Radka Pustková

Department of Cybernetics and Biomedical Engineering, FEECS,
VŠB – Technical University of Ostrava, 17. listopadu 15, 708 33 Ostrava – Poruba
{karel.vlach, jakub.jirka1, viktor.michna, radka.pustkova}@vsb.cz

Abstract. The teaching of technical parts in medicine is as important as the humanitarian nowadays. Students of biomedical engineering represent the future of non-medical hospital employees who also directly contribute to the quality of health care. The aim of this paper is the presentation of methods used for teaching students at VSB-Technical University of Ostrava. Students are introduced to tasks with real time data capturing and processing from the vital signs monitor (DASH or EAGLE) to ImplantSys application implementing communication protocol for data transfer. Students are able to measure, process and evaluate data sets from ECG, pulse oxymetry, blood pressure, etc. Several lessons in two courses that combine technical and medical practice are preparing. The lessons are focused on the whole process of medical data acquisition and designing the software which allows that.

1 Introduction – The Whole System

System being developed is designed for the purposes of archiving, measuring, analyzing, storing and synchronizing. It can be used as the informational support for pacing team at cardio operation rooms. When it is used there it will significantly improve the workflow of the team by tasks automation.

The system is designed as the interconnection between several parts used by the medical personnel. Interconnection of these parts is maintained by the software application named ImplantSys. This application serves as the database management system of patients with the ability to store their information. It can receive some of the patient's data directly from the hospital information system (HIS). It can communicate with the vital signs monitor and thus allows for processing of the received signals. It's able to import data from implant control system and therefore auto-fill some of the required fields in the form. It allows exporting of the operational reports to the national pacemaker registry. And it can be used for filling the form with results after the required patient pacemaker's checks. All of these main features divide the system into the several components which are described in the next chapter. It is also possible to use every of these components of the system as standalone application.

Physical interconnection of the new system is shown in Fig. 1. There are four sources of data that the new developed system has to combine for the most effective

workflow of the operational team. The hospital's HIS which contains patient's administration data, DASH (or EAGLE) vital signs monitor used mainly for measuring electrocardiogram (ECG), implant control system ICS3000 mainly used for measuring intra-cardiac electrogram (IEMG) and programming the pacemaker, and the REPACE central registry of pacemakers.

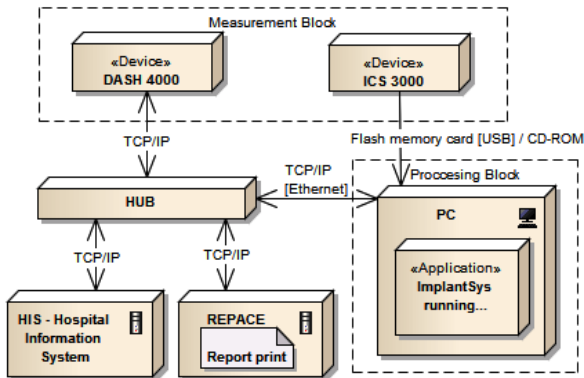


Fig. 1. Physical interconnection architecture

The ImplantSys application is running on the PC in the block of processing. There is a HUB that connects HIS, DASH and REPACE via an Ethernet interface. The ICS3000 does not support online connection in real-time. Therefore the data from the ICS3000 is transferred via one of the supported media (USB flash drive or CD) in PDF or XML format. Communication with the REPACE registry is via the internet.

2 Database of Patients

There are important data in HIS which needs to be imported to the ImplantSys. Such data includes patient's name, birthdate, gender, weight, height, diagnosis, address, insurance and other relevant information. This will help the physician to automatically fill in the form of the report and prevent them from making a typo mistake. The data can be also inserted manually. The user can add, edit or delete the records and sees all the records in the sortable table as shown in Fig. 2. Therefore the application can be used as a patients management system – database.

The name of the compatible HIS is CLINICOM. CLINICOM is a robust hospital information system with a modular design and an object-relational database Caché from the InterSystems company [1]. It is used by several hospitals in Czech Republic [2]. Communication between the ImplantSys and the CLINICOM database is solved by the interface implemented as a dynamic-link library in C#. This interface contains several methods for getting the relevant data from the database to the ImplantSys application. The form for the report creation is filled in with the information and can then be edited. Relevant data is picked from the database by a method in which the personal identification number serves as the primary key for selection. If there is

more than one record associated with the patient another key for selection is used. Date/time is the secondary key.

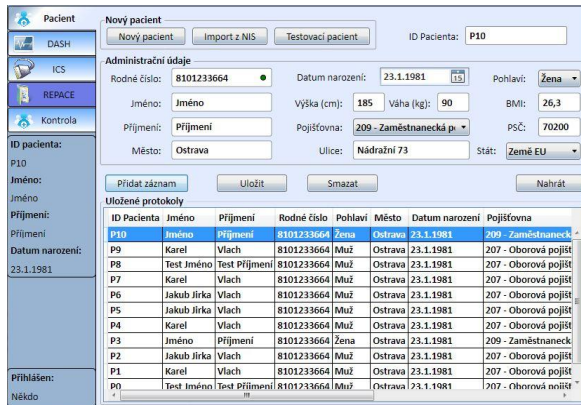


Fig. 2. ImplantSys screen with management of patients

The application can be also used for managing results of pacemaker’s checks. These mandatory checks are periodically performed on the patients that wear the pacemaker.

3 Communication with DASH Devices

There are several devices that use DASH communication protocol. These are vital signs monitors named DASH and EAGLE of various series. The protocol was programmed in the C# language to be used in the .NET framework.

For long-term remote monitoring by the application, it was necessary to create a driver that allows a reliable connection to the DASH devices in real-time. The ImplantSys uses advanced design technology with regard to the real-time data processing [3]. Based on the described specification, the driver for patient monitor DASH was developed in the .NET framework [4].

There could be created many ECG recordings for every patient in the ImplantSys as shown in Fig. 3. The user can see in real-time the graph, exact size, actual length and filename where the data are saved. It is possible to select the leads to show, add comment, take screenshots, zoom, etc. User can also load and show or delete existing recordings. Every record can be automatically compressed with GZip technology to reduce the amount of bytes which every file has.

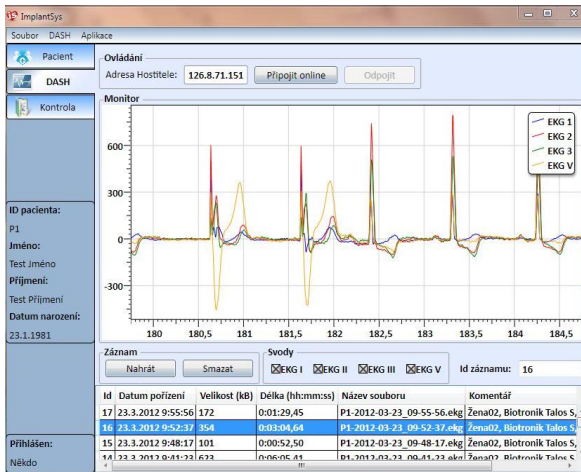


Fig. 3. ImplantSys screen with patient's ECG records

4 ICS3000 File Import

Biotronik ICS3000 serves as a mobile implant control system that helps surgeons to fully control an implanted pacemaker. Also it is used for the measurement of electrical parameters and as the external pacemaker. As for the measured electrical variables, there are, for example IEMG, voltage threshold, impedance of the electrodes and others.

In order to integrate the ICS3000 device and the patient's data into the ImplantSys application, an interface component needs to be implemented. First there is a need for converting the exported file in pdf format to the xml format and then parsing the data into the ImplantSys.

5 REPACE Synchronization

REPACE is the name of the nationwide central registry developed by the Institute of Biostatistics and Analyses at the Faculty of Medicine and the Faculty of Science of the Masaryk University, Brno, Czech Republic. This registry contains reports from the implantations of pacemakers and other relevant operations such as re-implantations.

Reports contain information about the operation such as patient's data, implanted devices, electrodes, complications, measured data and the names of the operational personnel. All this data is inserted via the screen with forms in ImplantSys as shown in Fig. 4.

The screenshot displays the ImplantSys application interface. At the top, there are navigation buttons: 'Informace o pacientovi', 'Přidat formulář', and 'Smazat formulář'. Below this is a table of patient records with columns for 'Id', 'int ID', 'Vytvořeno', 'Centrum (c_id)', 'Naposledy upraveno', and 'Naposledy změnil'. A 'Nový pacient' dialog box is open, showing a form for entering patient data. The form includes fields for 'ID pacienta' (P1), 'Datum narození' (23.1.1981), 'Pohlaví' (Muž), 'Výška (cm)' (185), 'Váha (kg)' (90), and 'BMI' (26.3). There are also checkboxes for 'Oběhová zástava', 'Synkopa', 'Presynkopa', 'Palpitace', 'Bradykardie', 'ICHS bez IM', 'ICHS stav po IM', 'Chlopenní vada aortální', 'Chlopenní vada mitrální', and 'Chlopenní vada jiné'.

Fig. 4. ImplantSys screen with REPACE forms

Most of this data ImplantSys can obtain automatically – from the CLINICOM, DASH device and ICS3000. An option to export the data to the REPACE is another one of the developed main features. The implementation lies in .NET interface which enables creation of XML file with patient's data. This file is then sent to the REPACE system online where it is imported to the ORACLE database running under the REPACE.

6 Educational Benefits

The described system will be used as an educational support for the students of the two programs: Biomedical Technician and Biomedical Engineering on VŠB – Technical University of Ostrava. The students will receive knowledge from the both technical and medical fields. The main benefit of this is that they will be in direct touch with the system, its parts and components. This is considerably more inspiring and motivating than teaching them only the theory. It is the real example of what they can achieve, what they can create with knowledge from the studies.

The students will deepen their skills of programming, informatics and signal processing. There are several lessons prepared for them in two courses. The name of the first one is Monitoring and Control Systems. This course is more aimed at the programming skills and informatics. The second one is named Biological Signals Processing and it's more focused on the processing of the received signal from the DASH devices and on the medical knowledge.

They will learn about hardware interfaces used for connections in the system. This includes knowledge about technologies like Ethernet, HUB, TCP/IP.

From the programming skills they will familiarize with more difficult programming methods, real examples used in the ImplantSys application and try to solve some similar problems on their own. The main programming languages to teach are the .NET C# and Matlab.

The processing of the biological signals is another field of study prepared for the students. They will learn how to obtain signals from the human body and how to process this signal to receive some information from it. Thanks to the connection between the DASH devices and the ImplantSys students can acquire various biological parameters as the ECG, blood saturation, blood pressure, temperature, etc. These signals are then available for the mathematical processing via the Matlab environment or in the .NET.

7 Conclusion

The ImplantSys is very helpful as it connects four sources of information and combines it into one framework where the user – the physician/student – can effectively work with it in the modern GUI (Graphical User Interface).

Every part of the system can be used alone for developing other applications. For example there can be a simple application used in ambulances car to store important vital signs during patient transfer where the DASH is used. This data can later be used for analysis. There is also the possibility of using the concepts of the ImplantSys for making ECG, SpO₂, and blood pressure classifiers with neuro-fuzzy or other methods approach. Also getting data from devices that are DASH communication protocol compatible (vital signs monitors) allows for usage as the central where every device and its data can be visualized, stored and prepared for the next processing step. Other applications can be developed with the ICS300 dynamic library or the REPACE interface anywhere it is needed.

Due to the fact that the system is oriented on the real problems and its solutions it has high impact on the inspiration and motivation of the students. They will see the practical solutions of some part of the biomedical engineering problems. Learn how to implement these principles and deepens their knowledge from the fields both technical and medical.

References

1. CompuGroup. *CareCenter G3 NIS CLINICOM* [online]. c2010, [cit. 2011-30-03]. <http://www.compugroup.cz/underwood/download/files/cc_g3_cz_cg_newdesign_v01.pdf>
2. SMS spol s.r.o.. *Reference SMS system implementation* [online]. c2005, [cit. 2011-30-03]. <<http://test.nlogv.cz/smsbrno/public/reference.html>>
3. CERNOHORSKY, Jindrich – KOZIOREK, Jiri – HRUDKA, Gustav. The examples of implementation of two specialized case tools as extensions of a general framework. In *IECON 2006 – 32nd Annual Conference on IEEE Industrial Electronics 2006*. New York: IEEE, 2006. Vols 1-11., pp. 4909-4914. (ISSN: 1553-572X, ISBN: 978-1-4244-0135-2).
4. MICHNA, Viktor – BABUSIAK, Branko. *Zobrazování a analýza EKG z pacientského monitoru DASH. Mezinárodní konference Technical Computing Prague 2009*. HUMUSOFT s.r.o., 2009. pp. 72. (ISBN 978-80-7080-733-0). <<http://www.humusoft.cz/akce/matlab09/sbornik/>>

Using Improved Methodology for Detailed Investigating and Evaluating the Results of In-situ Thermal Response Test Experiments

Petr Vojčínák

Department of Cybernetics and Biomedical Engineering, FEECS,
VŠB – Technical University of Ostrava, 17. listopadu 15, 708 33 Ostrava – Poruba
petr.vojcinak@vsb.cz

Abstract. Geothermal resources are economically used for parts of geothermal energy, whereas its resources are utilized nowadays and specified via a number of boreholes, and geophysical and geochemical data. In case of potential geological localities, the resources could be used, but relevant data have not been acquired to evaluate them quantitatively. So this paper deals with some usage of a full-scale *in-situ* TRT experiment's framework for detailed determining temperature conditions inside borehole heat exchangers, namely at considering some blocks including information on geological and geographical conditions, automatized measurements of undisturbed/disturbed temperature profiles, and acquired TRT data evaluations. Using some sophisticated software of EED 3.0, it is also possible to realize some additional data evaluation, related to a simulation and/or design of consumption and temperature conditions at a planned long-term operation of heat pumps.

Keywords: Borehole, Borehole heat exchanger (BHE), EED software application, Fourier partial differential equation, Heat pump (HP), Heat transfer, ILS/FLS model, Mathematical modelling, Rock massif, Thermal conductivity, Thermal resistance, TRT experiment.

1 Introduction

1.1 Features of Thermal Response Test (TRT)

Thermal response test (TRT abbreviation) or geothermal response test (GRT or GeRT abbreviation) is a field method, how to investigate some thermo-physical properties of a BHE, which is drilled into a soft/hard rock massif, and its surroundings. The BHE typically contains one or more loops (PE pipes; e. g. types of a single U-tube with one pair of pipes or one collector circuit, or a double U-tube with two pairs of pipes or two collector circuits), where a heat carrier fluid is pumped into the collector circuit at a constant rate (typically a constant mass-flow, M_f , in $\text{kg}\cdot\text{s}^{-1}$). This fluid – in case of our TRT experiments, water is usually used – may be heated by a TRT device's heater at a constant injected heating power (Q ; in W), whereas quantities of an inlet fluid temperature (T_{fIN} ; in K or °C), an outlet fluid temperature (T_{fOUT} ; in K or °C), a

volume-flow (Q_V ; in $\text{m}^3\cdot\text{s}^{-1}$), a pressure (p ; in Pa), and other electric and/or non-electric ones are measured and logged continuously [2].

The U-tube look/loops, through which the heat carrier fluid circulated, is/are inserted inside the borehole to the same depth as the BHE, planned for a site. To provide a constant heat flux (q , in $\text{W}\cdot\text{m}^{-2}$) to the ground, a fluid flow rate (also the mass-flow) inside the loop/loops, and a temperature difference between the inlet and outlet fluid temperatures must be constant during a TRT experiment. [2]

For determining some essential ground thermal properties – typically a thermal conductivity (λ ; in $\text{W}\cdot\text{m}^{-1}\cdot\text{K}^{-1}$ or $\text{W}\cdot\text{m}^{-1}\cdot^\circ\text{C}^{-1}$) and a thermal borehole resistance (R_B ; in $\text{K}\cdot\text{m}\cdot\text{W}^{-1}$ or $^\circ\text{C}\cdot\text{m}\cdot\text{W}^{-1}$) – from output TRT data [2], different kinds of analytical and numerical methods have been developed yet. The BHE, which consists of two pipes or one collector circuit, separated by a filling material (also a borehole grout), can be modelled as a heat source in the form of a line (line-source theory; ILS/FLS model by Carslaw and Jaeger, 1959) or a cylinder (cylinder-source theory; ICS/FCS model by Ingresoll et al., 1954) [2].

In case of determining the thermal conductivity (λ) of the rock massif, it is very important parameter affecting a borehole depth (h_B ; in m). Well, if we have some research polygon (also a group of BHEs in this case), then we usually determine an average value of the thermal conductivity inside drilled rocks. Nowadays, there are two field methods (or approaches), which enable to determine a value of this parameter, thus [3]:

- laboratory methods (*ex-situ* methods) – it is required to realize so-called borehole inventing to get some rock samples for their detailed analysis,
- measurement methods (*in-situ* methods) – they are realized inside a fully-equipped borehole, whereas in Europe, we talk about the TRT (Thermal Response Test) experiments; in the USA, we talk about the FTCT (Formation Thermal Conductivity Testing) experiments.

A standard TRT experiment is based on acquiring the data, used for design and model processing of some larger BHE field (e. g. a research polygon with one or more BHEs). Using the TRT experiment, it is also possible to evaluate a technical integrity of these BHEs. In case of a conventional TRT experiment's evaluation approach, based on the line-source theory, it is required long-term test durations (t_{test} ; in s), typically taking 48 hours or 72 hours, to obtain some quasi-steady state (which is time-independent) conditions. In case of applying the cylinder-source theory, a precision of the evaluation is enhanced and the test durations are reduced, because unsteady state (which is time-dependent) is evaluated. [2, 3]

2 Realized TRT Experiments in 2011 and 2012

2.1 Results of Realized TRT Experiments

Our TRT device (produced by UBeG GmbH & Co. KG, Wetzlar – Nauborn, Germany) is able to carry out some analysis and evaluation of the essential properties of the rock massif and to measure its thermal response, too. This device is often used

not only for other research activities, but also for realizing the TRT experiments at specific localities [2] in the Czech Republic, see Table 1 for their summarization. [1]

Table 1. Summarizing input parameters (a timestamp of realizing our TRT experiments, and a number of tested BHEs and their configuration) and output parameters (average values of the thermal conductivity and the thermal resistance, and an undisturbed thermodynamical temperature).

Locality Name	Input/ouput TRT Parameters					
	Month and Year of Realization	Number of Tested BHEs	BHE Config.	$\lambda_{(AVG)}$	$R_{B(AVG)}$	T_0
				$W \cdot m^{-1} \cdot K^{-1}$	$K \cdot m \cdot W^{-1}$	K
ID1	03/2011	1	2-U	5.670	0.042	285.29
ID2	07/2011	16	2-U	-----	-----	-----
ID3	09/2011	1	2-U	3.905	0.060	280.33
ID4	11/2011	1	2-U	2.020	0.137	283.73
ID5	04/2012	1	2-U	2.605	0.079	285.09
ID6	05/2012	1	2-U	3.895	0.034	279.90
ID7	05/2012	1	1-U	3.415	-----	-----

1-U – single U-tube, 2-U – double U-tube

3 Example of the TRT Experiment at the ID6 Locality

This TRT experiment was realized from 11th May 2012 till 14th May 2012, whereas this locality is located about 1300 meters above the sea level. Considering this level and geological position of this locality, there are very harsh climate conditions here, thus:

- monthly average temperature in May 4.8 °C,
- annual average temperature 0.9 °C,
- annual rainfall 1231 mm.

At measuring the undisturbed temperature profile (see Fig. 2a), a 143 m measurement cable with Pt1000/A sensors was used along a BHE depth of 120 m. After acquiring the TRT data, the disturbed temperature profiles (see Fig. 2b) were measured by the Pt1000/A, and Dallas DS18B20 sensors.

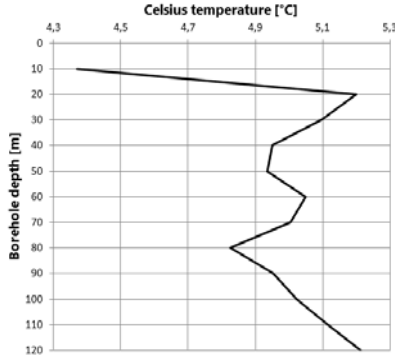


Fig. 2a. The ID6 locality: 2D graph of the undisturbed temperature profile along the BHE depth of 120 m (measured on 11th May 2012; Pt1000/A sensors).

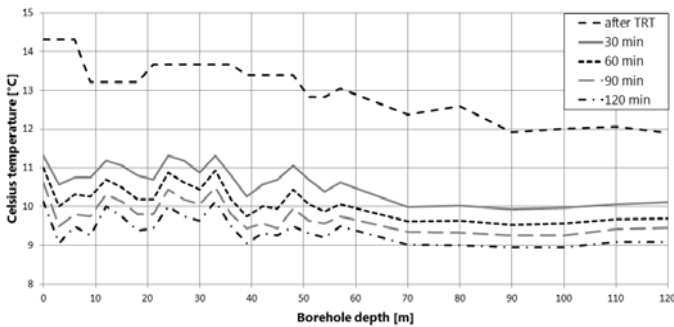


Fig. 2b. The ID6 locality: 2D graph of the disturbed temperature profiles along the BHE depth of 120 m (measured on 14th May 2012; sensors of Pt1000/A and DS18B20; a 30-minute measurement period).

Nowadays, the temperature profiles are measured by the DS18B20 sensors only, namely inside a backward pipe (preferred choice; see T_{fOUT} in Table 2) or inside a forward pipe (see T_{fIN} in Table 2), to reduce a paper logging and to prefer some automatized process of data acquisition, their analysis, and presentation.

A purpose of this TRT experiment is focused on measuring some temperature (generally physical) parameters inside the rock massif at this locality, where some BHE polygon with installing heat pumps is also planned:

- at the first level of data evaluation (by GeRT-CAL) – average values of desired quantities, such as the thermal conductivity (λ), the (internal) thermal borehole resistance (R_B), and the undisturbed temperature ($T_0 \equiv T_{ug}$; measured at the beginning of the TRT), are experimentally estimated or determined,
- at the second level of data evaluation (by EED 3.16) – the data from the first level and data sets (i. e. the additional information sources) are used for a simulation of a heat consumption inside the planned BHE polygon, namely for a 25-year operation period; this process enables to evaluate feasibility

and management of 17 BHEs, drilled inside a specific rock massif, at specific climate conditions.

Table 2. Summarizing selected input and output parameters, which are available at a TRT print-out (see the left table columns) and summarizing other exactly calculated parameters for this TRT experiment (see the right table columns). [4]

Parameter	Value	Unit	Parameter	Value	Unit
h_B	120	m	$\alpha_{(AVG)}$	$1.6928 \cdot 10^{-6}$	$\text{m}^2 \cdot \text{s}^{-1}$
r_B	$75 \cdot 10^{-3}$	m	$\lambda_{(AVG)}$	3.8936	$\text{W} \cdot \text{m}^{-1} \cdot \text{K}^{-1}$
Q	7658	W	$\lambda_{eff.}$	3.3412	$\text{W} \cdot \text{m}^{-1} \cdot \text{K}^{-1}$
$\rho \cdot c_p$	$2.3 \cdot 10^6$	$\text{J} \cdot \text{m}^{-3} \cdot \text{K}^{-1}$	$R_{Beff.}$	0.2993	$\text{K} \cdot \text{m} \cdot \text{W}^{-1}$
t_{test}	245998	s	Q_l	0.8492	$\text{m} \cdot \text{s}^{-1}$
	68.33	hours	Re	27012.33	1
T_0	279.90	K	T_{fIN}	286.56	K
	6.75	°C		13.41	°C
$t_{b(AVG)}$	4.615	hours	$T_{f(AVG)}$	285.22	K
$\lambda_{(AVG)}$	3.895	$\text{W} \cdot \text{m}^{-1} \cdot \text{K}^{-1}$		283.89	K
$R_{B(AVG)}$	0.034	$\text{K} \cdot \text{m} \cdot \text{W}^{-1}$	T_{fOUT}	10.74	°C

Re – the Reynolds number

For creating an EED – it is an abbreviation for the Energy Earth Designer – simulation, we must define several data sets of these input parameters, e. g. [4]:

- parameters of a ground – $\lambda_{(AVG)}$, $\rho \cdot c_p$, a value for the annual average temperature (valid for this locality), and an average value of a heat flux (typically $0.060 \text{ W} \cdot \text{m}^{-2}$),
- parameters of a borehole – r_B , h_B , a prescribed configuration (108 is for “17:3:8 U-configuration”; 17 boreholes, double U-tube, collector dimensions), a value of the thermal conductivity of a grout, a value of the thermal resistance at a U-tube/grout interface,
- parameters of other thermal resistances – $R_{B(AVG)}$, and a value of the thermal resistance at a fluid/rock interface,
- parameters of the anti-freeze fluid – density, specific heat capacity, viscosity, freezing point, volume-flow per one borehole, etc.,
- nominal values of building consumptions – annual ones of a prepared hot service water (HSW) and heating with their season power factors, and a monthly energy profile for the prescribed operation period of 25 years.

Finally, this EED simulation generates some tables and 2D graphs including these output parameters, e. g. [4]:

- calculated values of a monthly heat consumption from the borehole,
- calculated average values of anti-freeze temperatures at the end of a month – e. g. during the 25th year of the operation period, a minimal average fluid temperature is equalled to minus 16.88 °C (256.27 K; at the end of December) and a maximal average fluid temperature is equalled to minus 11.97 °C (261.18 K; at the end of August).

4 Conclusion

The first part of this paper is centred on a general description of the TRT approach, based on the ILS/FLS model and the *in-situ* method in this case, and the summarization of all the localities (their specific names have not been mentioned due to commercial obligations), where the TRT experiments have been realized by our TRT device of UBeG. The measurement management, mainly including the basic conception of the framework for these TRT experiments, is also introduced.

The second part of this paper is centred on the practical example of the TRT experiment, realized at the ID6 locality. This example demonstrates using two-level data evaluation – the first level (i. e. using measured/calculated results focused on the temperature profiles, the TRT experiment, information on the geological assessment, the geological profile, or some geological description of a locality), and the second level (i. e. using the additional data evaluation by the EED, related to the prescribed conditions) – to carry out the detailed analysis. For this locality, it is predicted the rock massif will be continuously frozen at the total annual heat energy consumption of 624 MWh (i. e. 357.12 MWh for the HSW and 266.88 MWh for heating).

Acknowledgement

This work is supported by the project SP2012/111, named “Data Acquisition and Processing from Large Distributed Systems”, of Student Grant System (VŠB – Technical University of Ostrava) and by the project TA01020932, named “Using Geothermal Energy for Renewable Energy Sources Systems Including Verification of Energy Accumulation”, of Technology Agency of the Czech Republic.

This research is supervised by doc. Ing. Jiří Koziorek, Ph.D.

References

1. P. Vojčínák, R. Hájovský, J. Koziorek, “Using Measurement, Data Analysis and Modelling for Research Borehole Polygons”, In IDAACS 2011: Proceedings of the 6th IEEE International Conference, Prague (CZ), 2011, pp. 2 – 9.
2. P. Vojčínák, R. Hájovský, J. Koziorek, “Using ILS Mathematical Model and Measurements for Detailed Evaluating Results of Thermal Response Tests”, In ICCAS 2012: Proceedings of the 12th International Conference, Jeju Island (KR), 2012.
3. P. Vojčínák, R. Hájovský, J. Koziorek, “Using TRT for Determining the Essential Parameters of Rock Massif”, In PDES 2012: Proceedings of the 11th IEEE/IFAC International Conference, Brno (CZ), 2012.
4. P. Vojčínák, P. Pospíšil, R. Hájovský, J. Koziorek, “Using Improved Methodology for Investigating Results of Thermal Response Test Experiments”, In HTE 2012: Proceedings of the 10th WSEAS International Conference, Istanbul (TR), 2012.

The Computer Based Vectorcardiography Monitoring System with Driven Right Leg Circuit

Michal Vozda, Barbora Hrvolova, Jana Krohova,
Maros Smondrk, and Marek Penhaker

Department of Cybernetics and Biomedical Engineering, FEECS,
VŠB – Technical University of Ostrava, 17. listopadu 15, 708 33 Ostrava – Poruba
{michal.vozda, barbora.hrvolova, jana.krohova,
maros.smondrk, marek.penkaker}@vsb.cz

Abstract. The vectorcardiography (VCG) represents the cardiac electric field by vectors and provides morphological interpretation of the cardiac electrical field. The main objective of this paper has been to describe our VCG device that has been determined for scientific research and for the clinical diagnosis of heart diseases. We have designed the hardware as a small portable device and the software that measures data saved in a raw form accessible for further processing. The main contribution is in the new way of common mode reduction (driven right leg circuit). The designed device has a great potential thanks to the new methods of data interpretation, the automatic signal evaluation and the small procurement price.

Keywords: Vectorcardiography, Frank's leads, Driven right leg circuit

1 Introduction

Recently, a great progress in the medication of cardiovascular illnesses has been observed. A fast and accurate diagnosis of these illnesses could reduce the number of sudden deaths. The Electrocardiography (ECG) is the most common diagnostic method, but the results are usually difficult to interpret. The ECG includes the vectorcardiography (VCG) that provides a better morphological interpretation of the cardiac electric field.

In 1913, Einthoven, Fahr and de Waart wanted to represent the cardiac electric field by vectors that have sense, magnitude and direction. Since then, the development of VCG has gone in different directions. The VCG presents several types of lead systems, for example, Frank, McFee-Parungao, and SVEC III. These lead systems differ by the number of electrodes and by spatial sensitivity properties. The most common VCG method is the Frank's reference vectorcardiography system created by Ernst Frank in 1954. This system uses seven special located electrodes. Location of the electrodes ensures measurement independence from the heart position and body size of the examined.

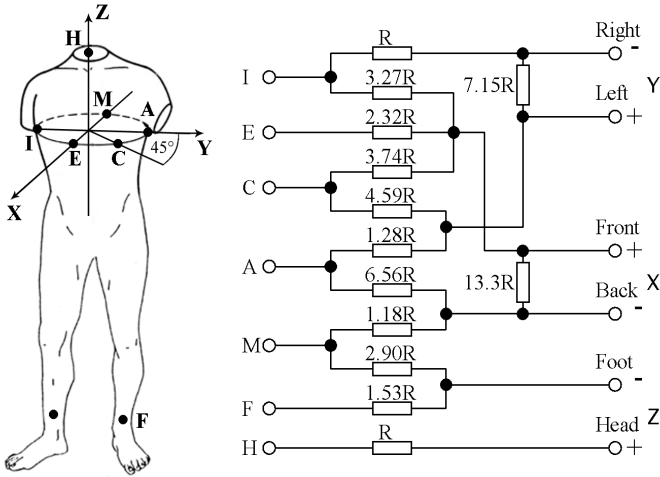


Fig. 1. The lead matrix of the Frank VCG system. The transverse plane contains the electrode E - on the front side, M - in the middle of the dorsal side, I - on the right side under the armpit, A - on the left side under the armpit. The electrode C makes an angle of 45 degrees between the electrodes E and A. The electrode H is placed on the back of the neck. The electrode F can be found on the left leg, between the knee and ankle [1-3].

Five electrodes are placed on the same transverse plane (Fig. 1). The placement of the electrodes allows to record cardiac heart activity in the three orthogonal planes x, y, and z [1, 2]. A resistor network compensates the unbalanced heart location and provides the same impedance value in every amplifier lead. The great advantage of this system is orthonormality that provides equal voltage levels of the measured X, Y, and Z leads [1].

2 Problem definition

The commercially available VCGs are designed as closed systems. The specialized software of these VCGs can provide only predefined diagnostics. The data are preprocessed without the possibility of the signal postprocessing. VCGs are often combined with conventional 12-channel ECG. The orthogonal leads can be computed from six precordial and two limb leads, or these systems display only the monocardioagrams. The price of these devices can exceed the costs of common ECGs. The advantages of these devices are the complexity, functionality and the automatic diagnostics. These medical diagnostic devices are assigned to the ambulant examination of patients.

Our proposed device differs from the commercially available VCGs; our system provides the output data in a raw form that can be postprocessed. Data from the VCG are filtered within the range between 0.5 Hz and 150 Hz. We have developed the software in the LabVIEW software environment that can

insert data into a database. The VCG has a better diagnostic value than the conventional ECG. Our system has been designed to expand the application of the VCG in the diagnosis of heart diseases, for example, the localization of myocardial infarction, the left anterior fascicular block and the left septal fascicular block. The VCG can also be used in the evaluation of electrically inactive areas [4].

3 The suggested Measurement Vectorcardiography Unit

The concept of the Frank’s corrected orthogonal lead system is well known [3]. The designed device consists of the Frank’s lead system, a driven right leg circuit, a resistor network, instrumentation amplifiers, filters, and a data acquisition unit (Fig. 2).

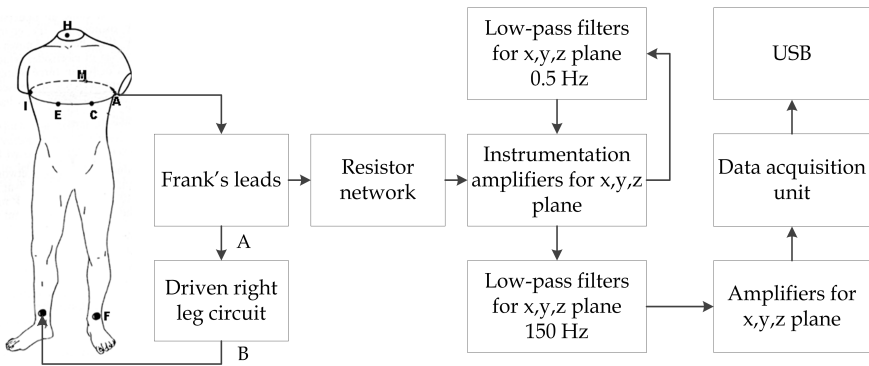


Fig. 2. Block diagram of the functional vectorcardiograph unit

In general, the amplitude of the signals measured from the body surface takes values within the range of hundreds of μV to tens of mV . These signals are usually affected by man-made interference. There are four ways in which the electromagnetic field interferes with the measured biological signals. The interference paths are magnetic induction, the displacement current induced into the leads, the displacement current induced into the patient causing interference voltage between the two recording electrodes, and the displacement current induced into the patient causing interference voltage between the recording electrodes and the amplifier common, i.e. common mode voltage (Fig. 3), [5].

The solutions of these four interferences are as follows. The use of mutually twisted wires reduces the interference generated by the magnetic induction. The induced current in the E_1 and E_2 leads can be minimized by shielded wires that reduce the capacity of capacitors C_{p1} and C_{p2} . Careful electrode positioning avoids recording of the voltage caused by displacement currents flowing through the body impedance [7]. The common mode voltage of the electrodes can be removed using grounding or the driven right leg circuit. In ideal conditions, the

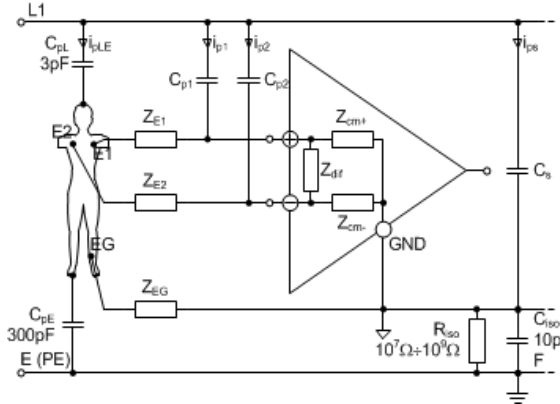


Fig. 3. Interference paths in biosignal measurements from the body surface [6]

common mode voltage is suppressed for the amplifier with a very large common mode rejection ratio (CMRR). In practice, voltage is indirectly manifested due to the unequal impedance of the leads as interfered differential voltage. It can be calculated by the following expression [5]

$$v_i = v_c \left(\frac{1}{CMMR} + \frac{Z_d}{Z_c} \right) \quad (1)$$

where v_i is the interfered differential voltage, v_c is the common mode voltage, Z_d is the difference of the impedance between two electrodes, and Z_c is the common mode impedance. CMRR is a parameter of the differential amplifier that represents the ratio of the power of differential gain over the common mode gain. It is usually measured in positive decibels, for real circuits within the range 60 to 120 dB [5].

As it is not possible to provide the same impedance on all leads, the value of the common mode voltage v_c has to be reduced. In our device, we have used the driven right leg circuit (an electrode on the patient's right leg) that is usually used for the conventional ECG. It provides a connection between the patient and a common amplifier in order to minimize the common mode voltage [8]. The signals of the individual leads are averaged, inverted and amplified. The conduction of a signal modulated in this way to the patient provides noise reduction (Fig. 4).

In the measurement of biological signals, there are more kinds of the common mode noise such as low frequency differential signals. They are located in the frequency range below 0.5 Hz and mainly produced by moving artefacts, electrodes polarizing voltage, impedance changes due to breathing, etc. The High Pass Filter (HPF) can reduce these artefacts. In our device, we use the Low Pass Filter (LPF) connected, in the feedback loop, to the instrumentation amplifier. Low frequencies can be thus simply removed. Other interferences are electrical activity produced by skeletal muscles, noise components, higher harmonic frequencies,

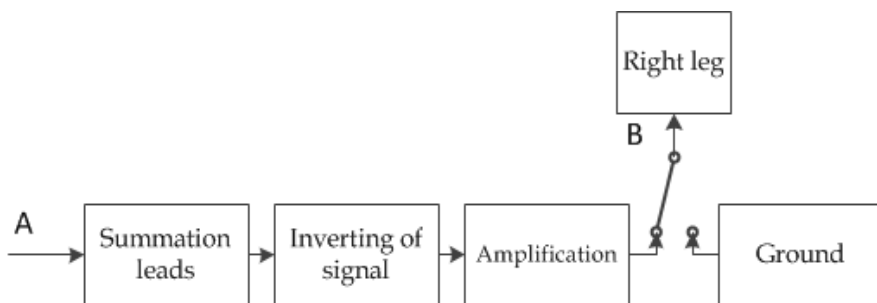


Fig. 4. Block diagram of the functional driven right leg circuit

etc. The upper cut-off frequency equal to 150 Hz is considered as optimal for the purpose of ECG diagnostics. The last part of our device is the data acquisition unit (DAU). The DAU consists of a 16 bit microcontroller (MCU). The MCU reads data from an analogue to digital converter (ADC) via a serial peripheral interface. We used the analogue to digital converter with a sampling frequency of 2 kHz and 12 bit resolution. The acquired data were formatted into a data packet and sent to a workstation by USB for the subsequent processing and evaluation. The device is powered by a USB source voltage of 5 V. The patient is electrically connected to the voltage source (driven by the right leg circuit) and it is thus necessary to ensure the safety of the equipment. It means that the device has been designed in such a way that the requirements on medical devices are satisfied. One of these conditions is the galvanic isolation of the circuits connected to the patient from other electronic circuits. In our device, a galvanic isolation of the power supply and a signal bus between the ADC and the MCU buses has been made.

4 Device Implementation and Data Interpretation

The VCG was constructed as a small portable device (15×8 cm) powered by USB. The analogue and digital parts have been on separated printed circuit boards. These parts have separated grounds which are connected only in one point in the circuit. The device has been inserted into a plastic box with external outlet leads, a USB connector, and LED. The LED indicates that the device is in recording mode. The whole device is shown in Fig. 5 A.

The output signals represent the orthogonal planes x, y, and z. These signals can be displayed in different views (1D, 2D and 3D) (Fig. 5 B). The one-dimensional view of the signals does not provide new information about the heart activity. The 3D view performs the heart vector movement. The diagnostic importance has the representation of dependencies between the individual planes (the 2D and 3D view). The heart electrical activity (atrial depolarization, ventricular depolarization, atrial repolarization and ventricular repolarization) is represented there by loops. The changes of its shapes can provide information about potential pathology.

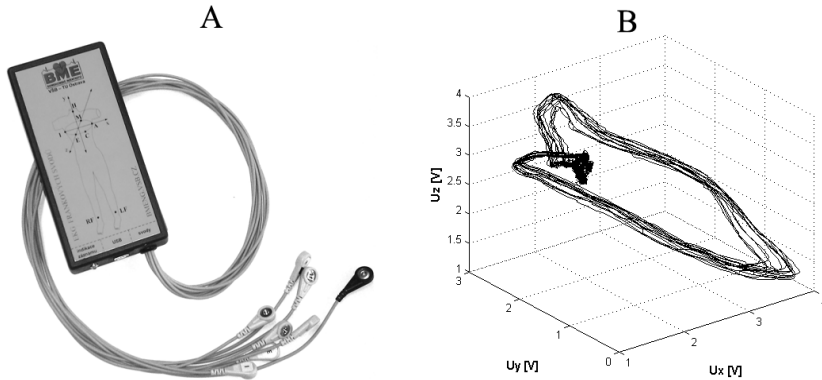


Fig. 5. A - VCG hardware realization with outlet external leads, B - 3D view of 10 measured heart cycles

5 Conclusions

The objective of this work has been to propose, implement and test VCG for scientific research, the clinical diagnosis of heart diseases and for education. We proposed both hardware and software parts of this equipment. We see the main contribution in the new way of common mode reduction. Measured data saved in raw form are easily readable and accessible for further processing. The great potential of our designed device is seen in the new methods of interpretation and automatic signal evaluation. Our device is more affordable than the vectorcardiographs with computed data interpretation.

References

1. Malmivuo J., Plonsey R.: Bioelectromagnetism - principles and applications of bioelectric and biomagnetic fields. New York: Oxford University Press (1995) 482–483
2. Burch G.E.: The history of vectorcardiography. Medical History No.5. (1985) 103–131
3. Frank E.: An Accurate, Clinically practical system for spatial vectorcardiography. Circulation - Vol. 13. - No. 5. (1956) 737–749
4. Prez Riera A. R., Uchida A. H., Filho C. F., Meneghini A., Ferreira C., Schapacknik E., Dubner S., Moffa P.: Significance of vectorcardiogram in the cardiologic diagnosis of the 21st Century. Clin. Cardiol. - Vol. 30. - No.7. (2007) 319–323
5. Winter B. B., Webster J. G.: Reduction of Interference Due to Common Mode Voltage in Biopotential Amplifiers. IEEE Transactions on Biomedical Engineering - Vol.BME 30. - No.1. (1983) 58–62
6. Penhaker M., Imramovsky M., Tiefenbach P., Kobza F.: Medical diagnostics instruments - learning texts. VSB-TU Ostrava (2004) 98–99
7. Huhta J. C., Webster J. G.: 60-Hz Interference in Electrocardiography. IEEE Transactions on Biomedical Engineering - Vol.BME 20. - No.2. (1973) 91–101
8. Winter B. B., Webster J. G.: Driven-right-leg circuit design. IEEE Transactions on Biomedical Engineering - Vol.BME 30. - No.1. (1983) 62–66

Index-based N-gram Extraction from Large Document Collections

Václav Bašniar

Department of Computer Science, FEECS,
VŠB – Technical University of Ostrava, 17. listopadu 15, 708 33 Ostrava – Poruba
vaclav.basniar@vsb.cz

Abstract. N-grams are applied in some applications searching in text documents, especially in cases when one must work with phrases, e.g. in plagiarism detection. N-gram is a sequence of n terms (or generally tokens) from a document. We get a set of n-grams by moving a floating window from the begin to the end of the document. During the extraction we must remove duplicate n-grams and we must store additional values to each n-gram type, e.g. n-gram type frequency for each document and so on, it depends on a query model used. Previous works utilize a sorting algorithm to compute the n-gram frequency. These approaches must handle a high number of the same n-grams resulting in high time and space overhead. In this paper, we show an index-based method to the n-gram extraction for large collections. This method utilizes common data structures like B⁺-tree and Hash table. We show the scalability of our method by presenting experiments with the gigabytes collection.

Keywords: n-grams, n-gram extraction, basic indexing structures, document n-gram matrix

1 Introduction

N-grams are applied in applications searching in text documents, especially in cases when one must work with phrases, e.g. in the case of plagiarism detection [5, 16, 12, 3, 17] (more general co-derived documents [4]) or language detection [2, 14] systems. N-gram is a sequence of n tokens (e.g. words) in a document and we get a set of n-grams by moving a floating window from the begin to the end of the document. Although, we can distinguish various types of tokens (see [5]), in this article, we consider only n-grams of terms.

During the extraction we must remove duplicate n-grams and compute the frequency of the n-gram types (count of types occurrences). Additionally, other values are stored together with n-gram type and frequency, e.g. n-gram unique number, but it is document and query model dependent. In Figure 1, we see a common architecture of an n-gram extraction framework.

This work was described a framework introduced in [10, 1] In this article, we show a time and space efficient method for the n-gram extraction; we do not consider various methods of document parsing, term pre-processing, and n-gram building and pre-processing. We show that we can use data structures well

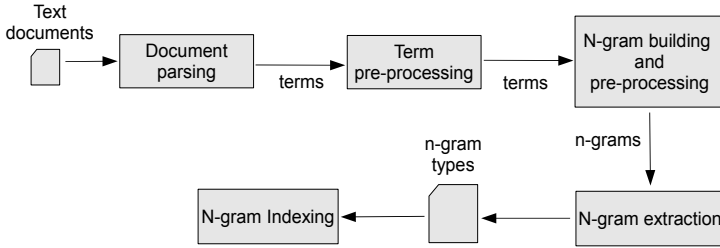


Fig. 1. A common architecture of an n-gram extraction framework

known in the area of database management systems [7] and physical database design [11] for this purpose. In this way, we utilize the same data structures for the n-gram indexing and the n-gram extraction. Additionally, we show a high scalability of our method; it is usable for large document collections including up-to 10^9 n-grams regardless the amount of the main memory.

In this paper we introduce the building of index of n-grams for collections of documents and for each document in the collections. Moreover we present some of the statistic results of the n-gram extraction and their possible application.

Example: Let us consider the following sentence:

”The array includes these items, the list includes these items as well.”

We distinguish the following sets and values for 3-grams:

- 3-grams ($N_n = 10$): The array includes, array includes these, includes these items, these items the, items the list, the list includes, list includes these, includes these items, these items as, items as well
- 3-gram types with frequency ($T_n = 9$): The array includes (1), array includes these (1), includes these items (2), these items the (1), items the list (1), the list includes (1), list includes these (1), these items as (1), items as well (1)
- $T_3^{uniq} = 8$, $T_3^{dup} = 1$

2 Related Work

In previous works, authors often apply sorting n-grams to compute the frequency of n-gram types. In [9], authors introduce a method based on a suffix array. It is implemented by a sequence of pointers, each of which points to a corpus token (e.g., a term, a character, etc.) in the real corpus and stands, virtually, for the sequence of tokens from the token to the end of the corpus. There is another class of approaches [4, 12, 16] assuming that only duplicate n-gram types are needed after the documents collection analysis.

We should see that the phase removing unique n-grams proposed in [4, 12, 16] is not always possible to use. Let us suppose a case when we want to detect if an article is a plagiarism of an article from an indexed collection. In this case,

the unique n-gram types can strongly characterize documents, therefore it is not possible to remove unique n-gram types.

It is clear that these sorting-based methods must handle many same n-grams to compute frequencies of n-gram types. In [8] authors describes their tool that uses the B⁺-Trees for indexing the large n-gram corpora like Web1T 5-gram Corpus. In [6] inventor introduces data structure called ternary search tree (TST) and its usage to index n-grams in large documents corpora. In the next section, we introduce a method using common data structures to omit handling of duplicate n-grams and allowing us to build an index for fast future inserts of documents and plagiarism detection.

3 Index-Based N-gram Extraction

For the collection we model the n-gram type as a tuple $\langle \mathbf{ngram}, \mathbf{id}, \mathbf{frequency} \rangle$, where **ngram** is the key. A common technique is that n-gram includes ids of terms instead of terms. For the n-gram extraction we need a data structure providing the following methods:

- Insert(in ngram) – it inserts the n-gram if the n-gram type does not exist in the index, if this n-gram type exists in the index, the frequency is incremented. Additionally it returns id of the n-gram.
- Find(in ngram, out frequency, out id) – it returns true together with **frequency** and **id** if the n-gram type is stored in the index, otherwise it returns false.

We also want a vector of n-grams for each document in a collection. In this case we don't need the tuple as it is used for the whole collection. The tuple we need is modeled as $\langle \mathbf{id}, \mathbf{frequency} \rangle$, where **id** is the key and has unique value in the collection's scope and **frequency** is frequency of n-gram type occurrence in the document. We can retrieve the n-gram ids from the collection index. Data structure for the document index needs following method:

- Insert(in ngramId) – it inserts the id of an n-gram if the id does not exist in the index, if the id already exists in the index, the frequency is incremented.

We utilize two common data structures B⁺-tree and Hash table.

4 Experimental Results

In our experiments¹, we have used four collections: iDoc, PAN Plagiarism Corpus 2010 (in this document referenced as a PAN Plagiarism Corpus) [13], LA Times and WebTREC [15]. Collection iDoc contains thesis works made by VSB - Technical University of Ostrava students in 2010. We do not apply any pre-processing techniques to terms and n-grams; the parser ignores only tags in XML and HTML files. In Table 1, we see statistics of the test collections.

¹ The experiments were executed on an Intel Xeon X5670@2.93GHz, 2.0 MB L2 cache per one core; 96GB of the main memory; Windows 2008 Server.

Table 1. Test collections and terms statistics

Collection	#Documents	Collection size [MB]	#Terms	#Term types
iDoc	4,198	423	62,486,207	485,577
PAN Plagiarism Corpus	11,147	1,685	298,672,883	1,512,783
WebTrec	1,231,686	15,505	1,193,207,677	3,157,449
LATimes	131,896	475	68,790,087	329,052

The statistics of 4-grams extraction for the test collections and average documents shows that the test collections' unique n-gram types can form approximately 74–91% of all 4-gram types and 93–99% of 4-gram types in average document respectively. Moreover with increasing n the portion of unique n-gram types increases too. We can tell that unique n-gram types can strongly characterize each document in corpus and it would make the identification or comparison of the document harder if the unique n-gram types or the n-gram types with low frequencies are omitted.

Using the statistic results we can define the document n-gram matrix for querying. The document n-gram matrix can be formed from vectors of n-grams extracted from each document and can be used for document and n-gram search.

5 Conclusion

In this paper, we introduced the index-based method to the n-gram extraction. This method utilizes common data structures like B⁺-tree and Hash table. We stated a theoretical model and experimental results with the gigabytes data collections confirmed this theoretical model. Moreover from statistic results we can determine that the vectors of n-grams extracted from each document in collection can form a document n-gram matrix.

6 Projects and Publications

Václav Bašniar is a member of team solving the grant of GAČR, Czech Republic, No. GAP202/10/0573 and the grant of SGS No. SP2012/132, Detekce plagiovaných dokumentů (řešitel: Ing. Radim Bača, Ph.D.). He is co-author of one submitted journal article [1].

Own References

1. M. Krátký, R. Bača, D. Bednář, J. Walder, J. Dvorský, P. Chovanec, and V. Bašniar. Index-Based N-gram Extraction from Large Document Collections. *Submitted in Journal of Digital Information Management*, 2012.

Other References

2. B. Ahmed, S.-H. Cha, and C. Tappert. Language identification from text using n-gram based cumulative frequency addition. In *Proceedings of CSIS 2004, Pace University, May 7th, 2004*.
3. A. Barrón-Cedeño and P. Rosso. On automatic plagiarism detection based on n-grams comparison. In *Proceedings of the 31th European Conference on IR Research on Advances in Information Retrieval, ECIR '09*, pages 696–700, Berlin, Heidelberg, 2009. Springer-Verlag.
4. Y. Bernstein and J. Zobel. A scalable system for identifying co-derivative documents. In A. Apostolico and M. Melucci, editors, *String Processing and Information Retrieval*, volume 3246 of *Lecture Notes in Computer Science*, pages 1–11. Springer Berlin / Heidelberg, 2004.
5. S. Brin, J. Davis, and H. García-Molina. Copy detection mechanisms for digital documents. In *Proceedings of the 1995 ACM SIGMOD international conference on Management of data, SIGMOD '95*, pages 398–409, New York, NY, USA, 1995. ACM.
6. M. Flor. Systems and Methods for Optimizing Very Large N-Gram Collections for Speed and Memory, 2011.
7. H. Garcia-Molina, J. Ullman, and J. Widom. *Database Systems: The Complete Book*. Prentice Hall, 2nd edition, 2008.
8. R. M. H. Ceylan. An Efficient Indexer for Large N-Gram Corpora. In *Proceedings of the 49th Annual Meeting of the Association for Computational Linguistics: Human Language Technologies, ACL-HLT 2011, System Demonstrations*, 2011.
9. C. Kit and Y. Wilks. The Virtual Corpus Approach to Deriving N-gram Statistics from Large Scale Corpora. In *Proceedings of 1998 International Conference on Chinese Information Processing (1998)*, pages 223–229, 1998.
10. M. Krátký, R. Bača, D. Bednář, J. Walder, J. Dvorský, and P. Chovanec. Index-Based N-gram Extraction from Large Document Collections. In *Sixth International Conference on Digital Information Management (ICDIM)*, 2011.
11. S. S. Lightstone, T. J. Teorey, and T. Nadeau. *Physical Database Design: the Database Professional's Guide*. Morgan Kaufmann, 2007.
12. J. Pomikálek and P. Rychlý. Detecting Co-Derivative Documents in Large Text Collections. In *Proceedings of the Sixth International Language Resources and Evaluation (LREC'08). Marrakech, Morocco*, pages 132–135. European Language Resources Association (ELRA), 2008.
13. M. Potthast, B. Stein, A. Barrón-Cedeño, and P. Rosso. An Evaluation Framework for Plagiarism Detection. In *Proceedings of the 23rd International Conference on Computational Linguistics (COLING 2010)*, Beijing, China, Aug. 2010. Association for Computational Linguistics.
14. I. Suzuki, Y. Mikami, A. Ohsato, and Y. Chubachi. A language and character set determination method based on n-gram statistics. *ACM Transactions on Asian Language Information Processing (TALIP)*, 1:269–278, September 2002.
15. TREC Web Corpus. .GOV, http://ir.dcs.gla.ac.uk/test_collections/govinfo.html, 2009.
16. Z. Češka, I. Hanák, and R. Tesař. Teraman: A tool for n-gram extraction from large datasets. In *Intelligent Computer Communication and Processing, 2007 IEEE International Conference on*, pages 209–216, 2007.
17. W. Zhang, L. Yang, X. Sun, and Y. Liu. A copy detection method for chinese text by character based n-gram. *JCIT: Journal of Convergence Information Technolog*, 6:277–282, March 2011.

Processing of Range Query Using SIMD and GPU

Pavel Bednář

Department of Computer Science, FEECS,
VŠB – Technical University of Ostrava, 17. listopadu 15, 708 33 Ostrava – Poruba
pavel.bednar@vsb.cz

Abstract. Onedimensional or multidimensional range query is one of the most important query of physical implementation of DBMS. The number of compared items (of a data structure) can be enormous especially for lower selectivity of the range query. The number of compare operations increases for more complex items (or tuples) with the longer length, e.g. words stored in a B-tree. Due to the possibly high number of compare operations executed during the range query processing, we can take into account hardware devices providing a parallel task computation like CPU's SIMD or GPU. In this paper, we show the performance and scalability of sequential, index, CPU's SIMD, and GPU variants of the range query algorithm. These results make possible a future integration of these computation devices into a DBMS kernel.

Keywords: range query processing, multidimensional range query, GPU, CUDA, SSE, SIMD, rtree

1 Introduction

Range query (or range scan) [11] is one of the most important query of physical implementation of DBMS [9]. There are two basic variants: onedimensional and multidimensional range query. DBMS often utilize two types of data structures (and algorithms) supporting these range queries.

Onedimensional range query is often implemented in a data structure like a B-tree [2] and it can be processed in an execution plan of the following SQL statement: `SELECT * FROM T WHERE ql1 ≤ T.atr1 ≤ qh1`. Multidimensional range query is often implemented by multidimensional data structures, e.g. n -dimensional B-tree [5], R-tree [7] or R*-tree [3] and it can be processed for the following SQL statement: `SELECT * FROM T WHERE ql1 ≤ T.atr1 ≤ qh1 AND ... AND qln ≤ T.atrn ≤ qhn`. In other words, this query retrieves all tuples of an n -dimensional space matched by an n -dimensional query rectangle.

Due to the possibly high number of compare operations executed during the range query processing, we can take into account hardware devices providing a parallel task computation like CPU's SIMD or GPU [8].

In generally, there are no significant differences between one and multidimensional range queries; both range queries must compare individual values of a tuple. We aim our effort to the multidimensional range query in this work summarizing our article [1].

2 Multidimensional Range Query Processing

In the case of the multidimensional range query, we have two primitive operations: *IsInRectangle*, returning true if a tuple is in the query rectangle, and *IsIntersected*, returning true if a rectangle (or MBR – minimal bounding rectangle) intersects the query rectangle. These operations are used in both sequential as well R-tree range query implementations. Since, in our experiments, we test only point data, we invoke only the *IsInRectangle* operations for the sequence scan. Both these operations must perform two compare operations for each dimension. However, in [4], we show that it is not necessary to check all dimensions in the case of the conventional implementation and it is the reason why the SIMD implementation is not always successful.

2.1 Range Query Processing Using CPU’s SIMD

In [4], we depicted the SIMD variants of operations *IsIntersected* and *IsInRectangle*. These SIMD implementations work correctly only if the space dimension n is a multiple of *PackCount* (the number of values fit in one SIMD register, $PackCount = 4$ for SSE and 32 bit-length values). We introduce the new SIMD *IsInRectangle* algorithm handling tuples of any space dimension.

We proposed some additional optimizations. Loading the query rectangle into the SIMD registers can be excluded from each function invocation when $n \leq PackCount$ (when we do not store the query rectangle in more than two registers); the values are loaded at the beginning of the range query. Moreover, these functions can process multiple tuples at once. For example, if $PackCount = 4$ and $n = 2$ we can compare two couples of tuples at once. This optimization is more usable in the case of AVX with 8×32 bit-length registers, where we are able to compare up-to four couples of 2D, three 3D or two 4D tuples at once.

Although the SIMD algorithms cause less branch misspredictions than conventional operations [8], in [4], we show that it improves the performance at most $2\times$. In Section 3, we put forward that our new implementation is only little bit faster than the original SIMD algorithms. However, the improvement of the new implementation is up-to $6\times$ when we utilize the proposed optimizations and AVX.

2.2 Range Query Processing using GPU

Our GPU range query algorithm is written in C++ and CUDA SDK for the compute capability 2.0 and higher [10]. In the area of GPU algorithms, a common technique is to arrange data for needs of the GPU algorithm. Since we suppose common row-oriented DBMS, input data are unchanged in the form of n-tuples. We do not consider another tuple arrangement, e.g. column-oriented [12].

3 Experimental Results

In our experiments, we compare the performance of range query processing using sequential and index algorithms. In the case of the sequential scan, we compare

three variants: conventional, CPU’s SIMD (SSE), and GPU. In the case of the R-tree, we compare two variants: conventional and SSE.

All SSE experiments have been executed with aligned memory access without software prefetching since data structures are organized as blocks to be scanned without random accesses. All data structures have been implemented in C++ and compiled for x86 a x64 by Microsoft C++¹. The difference between both platforms is relatively low (approximately 10%); therefore, we ignore it. Since we want to compare only the main-memory run in all cases; we ignore disk I/O costs.

In our test, we utilized 5 real collections. We tested the performance for 40 range queries for each data collection divided to 4 query groups according to the selectivity. All range queries were 10× repeatedly executed and results have been averaged for one query. The time of adding tuples into a result set has not been measured, since it is the same for all algorithms.

Table 1. Test Data Collections

Collections (Dimension)	XML (8)	CARS (4)	TIGER (2)	WORDS (3)	STOCK (11)
#Tuples	15,884,160	3,318,583	5,889,786	483,450,157	19,610,499
Domain	Integer	Float	Integer	Integer	Float
Tuple Size [B]	32	16	8	12	44
Size [MB]	349	106	112	7,720	997

In [4], we showed that successfulness of the SSE implementation depends on the number of cycles which executes the conventional *IsInRectangle* or *IsIntersected* algorithms; we call it the number of cycles (or #Cycles, see the penultimate column of Table 2). If #Cycles is close to the space dimension (it arises especially in the case of the low selectivity), we obtain at most a 2× improvement of the query processing time (see Table 2). There are two exceptions. In the case of TIGER and WORDS, a query rectangle is loaded into the xmm registers before the whole query is executed. Moreover, in the case of TIGER, we process two tuples by one packed instruction. Together with other technical improvements of our new algorithms, we obtain up-to 4× lower processing time. In the case of AVX, we can process more tuples at once compared to SSE. As result, in Table 3, we see up-to the 6× improvement compared to the conventional algorithm. Moreover, the minimal improvement is 5×, whereas in Table 2, we see that the SIMD implementation can be slower in case we can not apply any optimization.

In Table 2, we see that the R-tree is particularly successful² in the case of low-selectivity queries, on the other hand, results of our GPU algorithm are

¹ <http://msdn.microsoft.com/visualc>

² The experiments were executed on an Intel Core i5-P2450 3.2Ghz, 6.0 MB L2 cache; 8GB of DDR3; Windows 7 SP1.

Table 2. Results of various range query implementations

Collection (Dimension)	Query Group	Result Size	Time [s]				IsInRectangle	IsInRectangle
			Conventional	SSE	GPU	R*-tree	Avg. #Cycles	Calls
XML (8)	1	1.0	0.128	0.173	0.081	0.0000	1.058	15,884,160
	2	591.4	0.155	0.191	0.081	0.0002	1.374	
	3	38,668.4	0.204	0.200	0.081	0.0130	2.005	
	4	417,003.0	0.415	0.228	0.081	0.1046	4.718	
TIGER (2)	1	1.0	0.066	0.014	0.010	0.0000	1.000	5,889,786
	2	510.6	0.065	0.014	0.010	0.0009	1.002	
	3	40,992.1	0.067	0.014	0.010	0.0021	1.079	
	4	856,908.4	0.080	0.017	0.010	0.0291	1.445	
WORDS (3)	1.	1.0	6.562	2.271	1.075	0.0024	1.000	483,450,157
	2.	528.1	3.970	2.265	1.064	0.0804	1.114	
	3.	23,922.5	4.814	2.279	1.077	0.1794	1.429	
	4.	475,487.9	5.558	2.274	1.071	0.3384	1.709	
STOCKS (11)	1.	1.0	0.199	0.216	0.086	0.0001	1.414	19,610,499
	2.	519.6	0.206	0.215	0.086	0.0028	1.500	
	3.	32,538.1	0.264	0.231	0.086	0.0355	2.105	
	4.	977,986.0	0.477	0.293	0.086	1.0235	3.822	

approximately the same for all query selectivities. However, we must keep in mind that the R-tree processes less operations than the sequence-based approaches. Results of the R-tree with SSE are not depicted for deficit of space, we state that the query processing time of the R-tree with SSE is at most $2 \times$ lower compared to the R-tree without SSE. The GPU variant³ is up-to $8 \times$ more efficient than the conventional sequential algorithm; however, this table includes only the kernel processing time with the maximal buffer size (see Table 4).

Table 3. Query Statistics for float AVX implementation

Collection (Dimension)	Query Group	Result Size	Time [s]		IsInRectangle	IsInRectangle
			Conventional	AVX	Avg. Cycle	Calls
CARS (4)	1	1.0	0.0314	0.0064	1.00008	3,360,277
	2	484.0	0.0326	0.0066	1.02825	
	3	62,077.9	0.0371	0.0064	1.25278	
	4	1,159,228.0	0.0541	0.0075	2.25448	

In Table 4, we put forward detail results of GPU over the WORDS data collection. In this table, we show results for various buffer sizes, which is the size of data transfered and searched on a GPU in one step. The kernel column includes only the query processing time. H->D and D->H (H means host, D means device) include the transfer time of data on a GPU and the transfer time of an output from the GPU. Lower buffer sizes correspond to a naive integration of GPU in a DBMS kernel: if we need a range query computation over a block (mostly 8 kB in size), this block is transfered on a GPU and the range query is

³ The experiments were executed on nVidia GeForce 550Ti with 1GB of DDR5 (Memory speed 4,104 Mhz), 4 SM, 48 cores/SM.

executed. As result, we obtain all processing times very long. In the case of the large buffer size, the time of computation is the same as the data transfer time.

Table 4. Query Statistics for GPU

Collection (Dimension)	Buffer Size [B]	Query Group	Result Size [s]	Time [s]			Total Time [s]
				Kernel	H->D	D->H	
WORDS (3)	8,168	1	1.0	212.878	23.134	16.366	252.378
		2	528.1	212.731	19.623	16.165	248.519
		3	23,922.5	212.900	19.459	16.503	248.862
		4	475,487.9	212.871	24.067	16.746	253.684
	635,278,860	1	1.0	1.075	0.870	0.075	2.019
		2	528.1	1.064	0.870	0.075	2.008
		3	23,922.5	1.077	0.869	0.074	2.020
		4	475,487.9	1.071	0.869	0.074	2.014

4 Conclusion

In this article, we compared the convention, SSE, and GPU variants of range query algorithms. Conventional and SSE implementations are utilized in the case of sequential as well as the R-tree variants. We summary the results. (1) For a lower space dimension, when we can use pre-loading of the query rectangle and process more tuples at once, an improvement of the sequential SSE variant is up-to $6\times$. On the other hand, if it is not possible to utilize these optimizations, the improvement is relatively low. (2) The results of GPU show the fast range query computation (up-to $8\times$ faster than the conventional sequential algorithm). However, GPU does not provide any significant improvement when we consider the data transfer time. In contrast, this issue is not, for example, reported by articles related to using GPU to metric searching [6], the reason is that a distance computation is much more expensive than the cost of both primitive range query operations. Moreover, other GPU devices must be tested, since the improvement of the GPU algorithm compared to the sequential SSE algorithm is only up-to $3\times$. (3) Due to the GPU performance, the GPU algorithms can be used in indices, e.g. in the R-tree. However, our experiments with sequence-based approaches show that we can not use a naive method with a transfer and searching of single pages (see results with the 8kB buffer size).

As result, an integration into a DBMS kernel is not so straightforward and we must solve mainly these issues in our future work: the data transfer time must be effaced in the live cycle of DBMS and we must forward only low-selectivity range queries on a GPU because the number of compare operations increases for indices like B-tree or R-tree in this case.

5 Projects and Publications

Pavel Bednář is a member of team solving the grant of GAČR, Czech Republic, No. GAP202/10/0573. Pavel Bednář is a co-author of article [1].

Own References

1. P. Bednář, M. Krátký, P. Gajdoš, and P. Chovanec. Processing of Range Query Using SIMD and GPU. In *Proceedings of GID 2012 (GPUs in Databases), ADBIS 2012. To appear in AISC, Springer, 2012.*

Other References

2. R. Bayer and E. McCreight. Organization and Maintenance of Large Ordered Indexes. *Acta Informatica*, 3(1):173–189, 1972.
3. N. Beckmann, H.-P. Kriegel, R. Schneider, and B. Seeger. The R*-Tree: An Efficient and Robust Access Method for Points and Rectangles. In *Proceedings of the ACM International Conference on Management of Data (SIGMOD 1990)*, 1990.
4. P. Chovanec and M. Krátký. Processing of Multidimensional Range Query Using SIMD Instructions. In *Informatics Engineering and Information Science*, volume 254. Springer, 2011.
5. M. Freeston. A General Solution of the n -dimensional B-tree Problem. In *Proceedings of the ACM International Conference on Management of Data (SIGMOD 1995)*. ACM Press, 1995.
6. V. Garcia, E. Debreuve, and M. Barlaud. Fast k Nearest Neighbor Search using GPU. In *Computer Vision and Pattern Recognition Workshops*, pages 1–6. IEEE Computer Society, 2008.
7. A. Guttman. R-Trees: A Dynamic Index Structure for Spatial Searching. In *Proceedings of the ACM International Conference on Management of Data (SIGMOD 1984)*, pages 47–57. ACM Press, June 1984.
8. J. L. Hennessy and D. A. Patterson. *Computer Architecture: A Quantitative Approach*. Morgan Kaufmann, 4th edition, 2006.
9. S. S. Lightstone, T. J. Teorey, and T. Nadeau. *Physical Database Design: the Database Professional's Guide*. Morgan Kaufmann, 2007.
10. nVIDIA. Cuda Programming Guide, 2012.
11. H. Samet. *Foundations of Multidimensional and Metric Data Structures*. Morgan Kaufmann, 2006.
12. M. Stonebraker, D. Abadi, A. Batkin, X. Chen, M. Cherniack, M. Ferreira, E. Lau, A. Lin, and S. Madden. C-store: A Column Oriented DBMS. In *Proceedings of the International Conference on Very Large Data Bases, VLDB'05*, 2005.

Parking Lot Detection System Based on the Heat Transfer

Radovan Fusek, Karel Mozdřeň, and Milan Šurkala

Department of Computer Science, FEECS,
VŠB – Technical University of Ostrava, 17. listopadu 15, 708 33 Ostrava – Poruba
{radovan.fusek.st, karel.mozdren, milan.surkala}@vsb.cz

Abstract. In this paper, we introduce a new parking lot occupation detection approach based on the heat transfer. In our approach, the heat transfer is applied into each parking place separately. We obtain a specific shape of transfer heat for each parking space. On the basis of this shape, we decide about the occupancy. In the other words, the occupied and empty places have different responses to the heat. Our algorithm detects each obstacle (humans, bicycles, motorbikes, etc.), not only the cars and we show its properties on the real parking lots in our experiments.

1 Introduction

Parking space detection has become an interesting challenge in recent years. The information about parking lot occupancy can be very useful especially for drivers who need to find the free parking spaces. The numbers of free parking spaces can be determined by human or intelligent unsupervised system. Unsupervised system is a more sophisticated solution. This system can automatically provide the information about the number of free (occupied) parking spaces or evaluate parking availability at different times. Many methods have been developed for solving this problem (e.g. [8, 3, 4]). We use the camera system and the heat transfer for the occupancy detection in our method. Heat transfer is simulated by the diffusion equation. In recent years, many methods have been developed for edge detection and image filtering using diffusion equation (e.g. [1, 2, 5–7, 9]). In the next sections, we describe our approach and we show some results.

2 Algorithm and Experiments

In the first step, we acquire the image from the camera. The location of our camera is on the roof above the parking lot (Fig. 1(a)). A Sample image obtained from this camera is shown in Fig. 1(b).

In the second step, we obtain the coordinates of the parking spaces. Each parking space is defined by four coordinates. The coordinates were obtained from the map in Fig. 1(c).

After receiving the coordinates, we can acquire images for each parking space separately. These images are normalized. Normalization includes an important

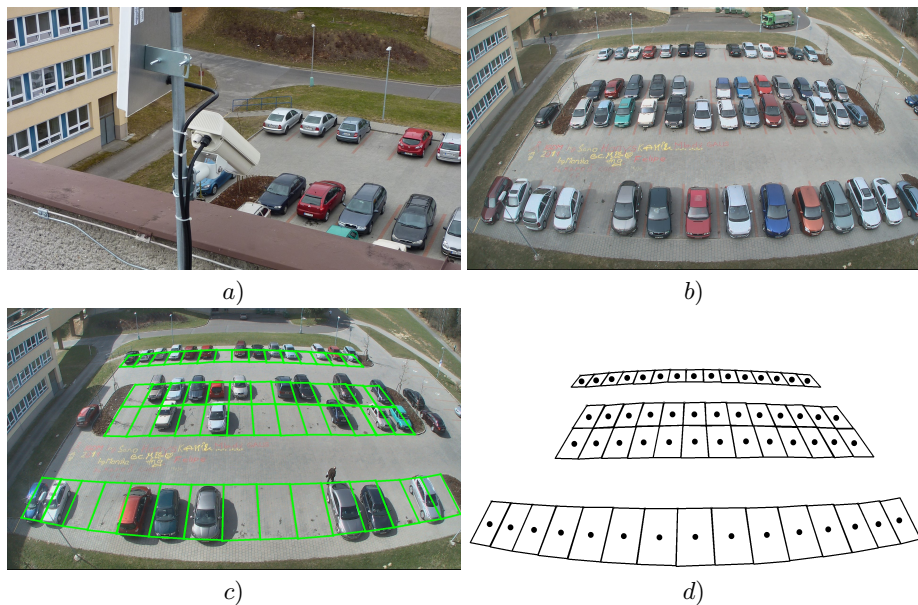


Fig. 1. Images illustrating the basic steps of our approach: a) the location of our camera b) the image from the camera c) the map of parking spaces d) the black spots represent manually inserted heat sources.

preprocessing steps: a perspective transformation and size normalization of each frame.

We use normalized images as an input to the heat transfer and we define the heat sources. The location of the heat sources is in the middle of each parking space (Fig. 1(d)). The heat is mathematically described by the diffusion equation

$$\frac{\partial I}{\partial t} = \text{div}(c \cdot \nabla I), \tag{1}$$

where I is input signal, div is divergence operator, ∇ is a gradient and c is a diffusion coefficient.

An important advantage of diffusion is that it respects the edges in image and is not prone to noise. In other words, diffusion respects the strength of edges in the image because the heat transfer has a variable transfer speed. The strength of edges in image defines the speed of heat transfer. The stronger the edge is, the slower is the heat transfer. Therefore, the edges in the images are not blurred. After discretization of previous equation (the scheme for the heat simulation after the discretization is shown in Fig. 2.), the heat transfer is calculated using the following equation

$$I_{i,j}^{t+1} = I_{i,j}^t + \lambda(c_N \cdot \nabla_N I + c_S \cdot \nabla_S I + c_E \cdot \nabla_E I + c_W \cdot \nabla_W I)_{i,j}^t \tag{2}$$

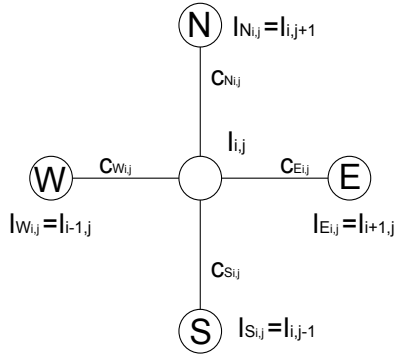


Fig. 2. One node of a grid (brightness value $I_{i,j}$), its four neighbors (I_N, I_S, I_E, I_W) and conductivity coefficient (heat transfer speed) c to the arcs.

where $\lambda \leq \frac{1}{N}$ (N is number of neighbors), $I_{i,j}$ is brightness value, the ∇ symbol represents differences in directions (north, south, east, west). For instance: $\nabla_E I_{i,j} = I_{i,j+1} - I_{i,j}$. The heat transfer speed is computed as

$$c = g(\|E\|), \tag{3}$$

where E is an edge estimate. In our case, the edge estimate E is defined as gradient of the image. The function $g(\cdot)$ has the following form

$$g(\nabla I) = \frac{1}{1 + \left(\frac{\|\nabla I\|}{K}\right)^2}, \tag{4}$$

where K is a constant number representing the sensitivity to the edges.

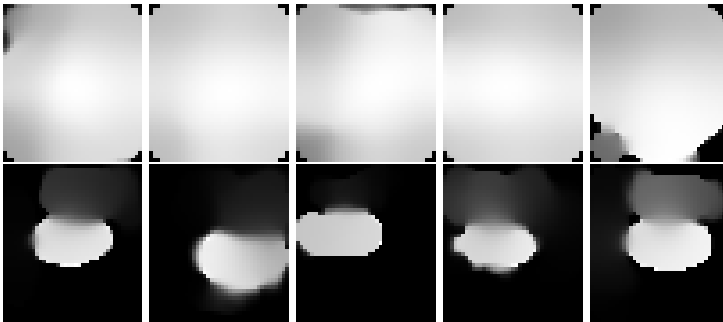


Fig. 3. Responses to the heat transfer. These images represent temperature values after 400 iteration. The first row represents empty places, the second row represents occupied places in the parking.



Fig. 4. Detection results of our approach. Green dots represent free parking places. Red dots represent occupied parking places.

Example of the heat transfer after 400 iterations (time necessary for the heat transfer from the source) is shown in in Fig. 3. In our case, the obstacle creates to the parking place a thermal insulator that avoid heat propagation. According to these results, we can decide about the occupancy of parking spaces. Decision-making is based on the amount of the heat transferred in the individual parking spaces. Detection results of our approach is shown in Fig. 4.

3 Conclusion

In this paper, we presented the approach for parking lot occupation based on the diffusion equation and the video camera system. First, we obtain the images for each parking space then these images are used for heat transfer. In fact, starting place for the heat transfer is located into the middle of each parking space. For future work, we plan try another solution to the locate starting places to achieve better results. We tested our approach on real images and we proved that using

our suggested solution with heat transfer can be used for parking lot occupation problem without user intervention with satisfactory results.

4 Acknowledgments

This work was supported by the SGS in VSB – Technical University of Ostrava, Czech Republic, under the grant No. SP2012/58.

References

1. Luis Alvarez, Pierre-Louis Lions, and Jean-Michel Morel. Image selective smoothing and edge detection by nonlinear diffusion. ii. *SIAM J. Numer. Anal.*, 29(3):845–866, June 1992.
2. Francine Catté, Pierre-Louis Lions, Jean-Michel Morel, and Tomeu Coll. Image selective smoothing and edge detection by nonlinear diffusion. *SIAM J. Numer. Anal.*, 29(1):182–193, February 1992.
3. Chang-Hsing Lee, Ming-Gang Wen, Chin-Chuan Han, and Da-Cheng Kou. An automatic monitoring approach for unsupervised parking lots in outdoors. In *Security Technology, 2005. CCST '05. 39th Annual 2005 International Carnahan Conference on*, pages 271–274, oct. 2005.
4. I. Masaki. Machine-vision systems for intelligent transportation systems. *Intelligent Systems and their Applications, IEEE*, 13(6):24–31, nov/dec 1998.
5. P. Perona and J. Malik. Scale-space and edge detection using anisotropic diffusion. *IEEE Trans. Pattern Anal. Mach. Intell.*, 12:629–639, July 1990.
6. G. Sapiro and D.L. Ringach. Anisotropic diffusion of multivalued images with applications to color filtering. *Image Processing, IEEE Transactions on*, 5(11):1582–1586, nov 1996.
7. D. Tschumperle and R. Deriche. Vector-valued image regularization with pdes: a common framework for different applications. *Pattern Analysis and Machine Intelligence, IEEE Transactions on*, 27(4):506–517, april 2005.
8. Xiaoguang Wang and A.R. Hanson. Parking lot analysis and visualization from aerial images. In *Applications of Computer Vision, 1998. WACV '98. Proceedings., Fourth IEEE Workshop on*, pages 36–41, oct 1998.
9. Juyong Zhang, Jianmin Zheng, and Jianfei Cai. A diffusion approach to seeded image segmentation. In *Computer Vision and Pattern Recognition (CVPR), 2010 IEEE Conference on*, pages 2125–2132, june 2010.

Detection of Vehicles on Parking Lots from Multiple Images via Graph Cuts

Michael Holuša

Department of Computer Science, FEECS,
VŠB – Technical University of Ostrava, 17. listopadu 15, 708 33 Ostrava – Poruba
`michael.holusa.st@vsb.cz`

Abstract. In this paper, we present a new method for detecting vehicles on parking lots from multiple images. Unlike the general stereo-reconstruction methods, we propose a method for specific scenes only, which is motivated by the known fact that, in special circumstances, a specialised method will probably perform better than a general one. The theoretical model of the scene expects that all vehicles have roofs placed in a certain height over the scene base plane. The method is based on minimisation of an energy function. The function that has been found useful for the model is presented. For minimisation, the graph cuts technique is used, which is modified by an iterative process in which the original edge weights are changed on the basis of the residual graph.

1 Introduction

The problem of parking lot occupancy detection is well-studied in the case of detection from a single image [6], but there are still challenges to solve, such as the shadow effects, car occlusions or the luminance variations. Solving the problem from multiple images may overcome some of these difficulties. Many general methods that find the depth map from multiple images exist [1, 2], but they do not usually give the best possible results for all scenes and images, and they need not be acceptable in real-time applications. Therefore, we decided to develop a new method that takes into account the specific conditions of the mentioned problem. The theoretical model of the scene expects that roofs of the vehicles are placed in the approximately same height over the base plane. The goal is to detect the vehicles and the base plane from a pair of stereo images.

The proposed method is based on minimisation of the energy function introduced in the paper. For minimisation, the graph cut technique, which was introduced in [4], is utilised in an iterative way, when the residual capacities of edges are used to modify the capacities in the original graph.

In the following section the construction of the energy function for our model is described. The results are presented in Section 3, section 4 is a conclusion.

2 The New Method

Firstly, we focus on the geometric transformation between the stereo images without considering occlusions. We suppose that we have two images of a scene

taken from different positions. We use the notation u_L and u_R for the brightness function of the left and the right image, respectively. Due to the pinhole model, the images are connected by a projective transformation that is supposed to be known. Say that, in the left image, we see a certain point whose position is x (its brightness is $u_L(x)$). In the right image, the position of the corresponding point is denoted by $\pi_{LTR}(x)$ in the case of top (roof) point, or $\pi_{LBR}(x)$ if it is a bottom (base plane) point. A similar transformation also works in the opposite direction. From the geometrical point of view, the point seen at $\pi_{LTR}(x)$ in the right image need not necessarily be only the top point that is seen at x in the left image, but at the same place, a bottom point can also be seen whose position in the left image is $\pi_{RBL}(\pi_{LTR}(x)) \equiv \pi_{LTB}(x)$. Similarly, the point at $\pi_{LBR}(x)$ in the right image need not only be the bottom point in the left image, but it can also be a top point seen at $\pi_{RTL}(\pi_{LBR}(x)) \equiv \pi_{LBT}(x)$. See Fig. 1 for graphical explanation.

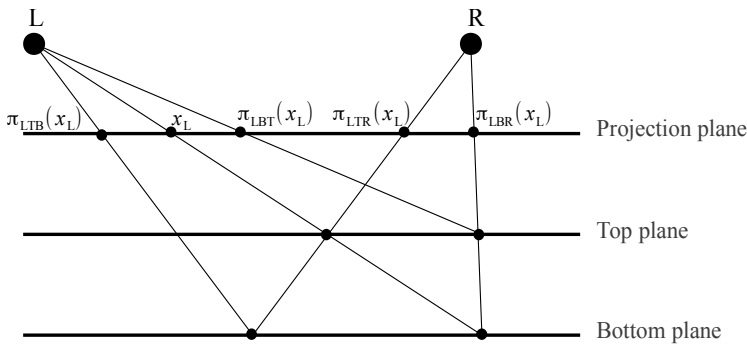


Fig. 1. Projective transformation between the images (without occlusions): a top point seen at x_L in the left image should also be seen at $\pi_{LTR}(x_L)$ in the right image; similarly, a bottom point at x_L should be seen at $\pi_{LBR}(x_L)$. The point at the position of $\pi_{LTR}(x_L)$ in the right image need not necessarily be only the top point seen at x_L ; at the same place the bottom point can also be seen whose projection in the left image is at $\pi_{LTB}(x_L)$, and vice versa.

For determining the membership of x from the left image to the set of either top or bottom points, we define the function, denoted by $\varphi(x)$. The function is of the form

$$\varphi(x) = [u_R(\pi_{LBR}(x)) - u_R(\pi_{LTR}(x))] - [u_L(x) - u_L(\pi_{LTB}(x))]. \quad (1)$$

The way how the function works is illustrated in Fig. 2 that depicts the situation if the base plane and the particular vehicles have constant brightness and if the vehicle is brighter than the base plane. Under these assumptions, $\varphi(x)$ indicates whether the points are the top points (indicated by negative values of $\varphi(x)$) or bottom (base plane) points (positive values) or whether the membership cannot be decided (zero values).

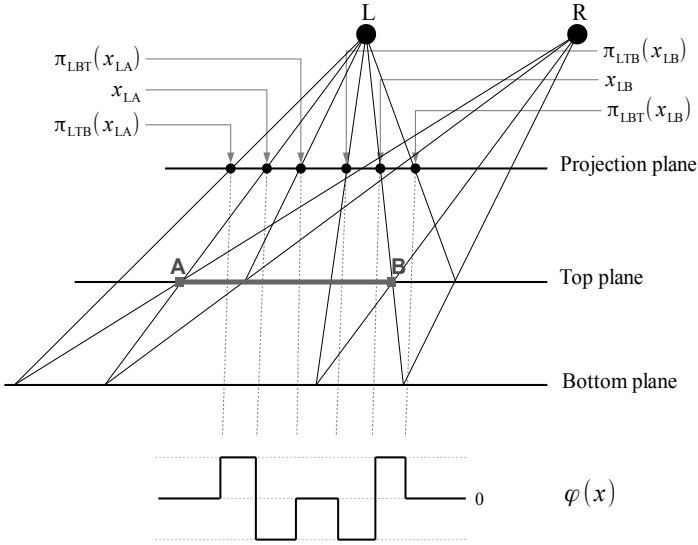


Fig. 2. The graphic explanation of Eq. (1) for the image in which the base plane has a constant brightness of b_B and the car has the brightness of b_T . We suppose that $b_T > b_B$ and we introduce $b_T - b_B = \delta b$. The function $\varphi(x)$ takes the value of $+\delta b$ in the neighbourhood of car, the value of $-\delta b$ inside the car, and the value of zero otherwise; the nonzero values only appear in the neighbourhood of car boundary.

2.1 Energy Function

Let P be a set of all image pixels, and let L be a set of possible labels. A problem is to assign a label $l \in L$ to each pixel $p \in P$.

A graph $G = (V, E)$ consists of a set of vertices V and a set of edges E . The set V contains all nodes from P and two additional terminal nodes t, b representing the top and the bottom layer, respectively. The set E contains two types of edges: t -links connect all non-terminal nodes with both terminals, and n -links connect the neighboring non-terminal nodes. The graph-cut algorithm minimizes an energy function that can be written in the form of

$$E(l) = \sum_{p \in P} D_p(l_p) + \alpha \sum_{(p,q) \in E} V_{p,q}(l_p, l_q), \quad (2)$$

where l_p, l_q stand for the labeling of p and q , respectively. Since the second part $V_{p,q}(l_p, l_q)$, called the smoothness term, which penalizes the discontinuity of labeling between the neighboring pixels (n -links), is realised in an usual way [5], we focus only on the first part, the data term $D_p(l_p)$, which sets individual penalties for assigning a label l to a pixel p (t -links). The weight parameter α sets a relative importance of the smoothness term versus the data term. A detailed description of the graph cut technique can be found in [3–5].

The construction of the data term is described in the following paragraphs. Our new term is based on evaluating the mismatches between the stereo images.

Data term For the data term, we use the function $\varphi(p)$ (p stands for a point) that is able, on the basis of the stereo images, to give the information about the expected membership of particular points either to the top or to the bottom layer. Since the values of $\varphi(p)$ vary between positive and negative values, we transform the values into the interval $\langle 0, 1 \rangle$. It is done by the function

$$F_\varphi(p) = \frac{1}{1 + e^{\eta\varphi(p)+4\xi}}, \quad (3)$$

whose value can be regarded as a probability $P(p \in T)$. The η parameter sets the slope of the function and its value is chosen in dependence on the brightness range. The ξ parameter is used to decrease the probability of the membership to the top layer. The values of $\varphi(p) = 0$ are mapped to $F_\varphi(p) = 0.5 - \xi$. This initial preferring the background instead of cars reduces the false car detections.

Since the $F_\varphi(p)$ is only able to reliably detect the parts of the cars and the back plane near the car boundaries, the remaining work should be done by the smoothness term in Eq. (2). However, the smoothness term itself is not always capable to do all the work sufficiently. It may sometimes happen that the parts of one car are not merged together or less significant cars are not detected at all.

Due to this fact, we support the term (3) by an additional process that can increase the reduced probability back and distinguishing between the inner vehicle areas and the background. For this purpose, we analysed the results of the data from the residual graph that remains after performing the max-flow algorithm. The obtained data are used to modify the weights of the t -links in the original graph. A new graph cut is carried out afterwards, which makes the method iterative.

Let G_{res} be the residual graph. The residual capacity of the t -link (p, b) connecting p with b (the terminal corresponding to the base plane) is denoted by $w_r(p, b)$. From its value, we can see, how “far” the edge was from saturating. If the value of $w_r(p, b)$ is low, the edge was almost saturated, the detection was weak, and a certain chance exists that the point should belong to the top layer instead to the base plane as was detected.

We have observed that the t -links with low residual weights are situated mainly around the areas convincingly detected as a vehicle by a high value of $F_\varphi(p)$. It is caused by a high flow from the top terminal that is transported mainly to these vehicle points and then through the neighboring points inside the car roof. The flow to the points outside is eliminated by a low capacity of the edges connecting the points with a higher brightness difference, which occurs between the car and the background. These fact explains why the inner car areas have lower residual capacities $w_r(p, b)$ than the background. We modify the weights of edges in the original graph by increasing the probability of being a point in top layer. According to the properties of the residual graph, these probabilities are more increased in the inner car areas. The maximum increase of probability is set to ξ , defined in Eq. (3), which compensates for previously preferring the background instead of vehicle.

The probability of the event that, in the $(k + 1)$ -st iteration, a point will become a top point, providing that in the k -th iteration it was marked as a

bottom point is set to the following value

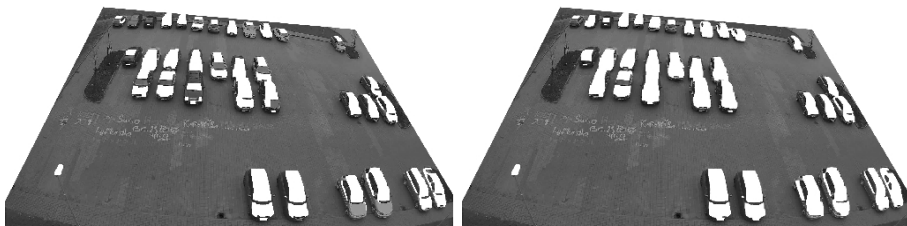
$$F_{\text{res}}^k(p) = P(p \in T^{k+1} | p \in B^k) = \xi e^{-\frac{w_r^k(p,b)}{2\sigma}}. \tag{4}$$

The move in the opposite direction is not possible since it is assumed that once a point is marked as a top point, it is done correctly.

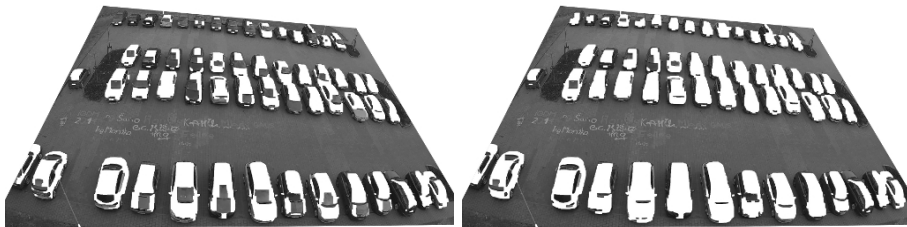
We may now sum up that after introducing the correcting mechanism, the function expressing the capacity for the k -th iteration of the edge connecting p with the top terminal can be formulated as

$$F^k(p) = \min(F_\varphi(p) + F_{\text{res}}^{k-1}(p), 1). \tag{5}$$

In the first iteration, $F_{\text{res}}^0(p) = 0$ for all $p \in P$. Finally, the weights of the t -links are set as $F^k(p)$ and $1 - F^k(p)$ for the weights of the edges connecting p with the top and the bottom terminal, respectively, in the k -th iteration. For solving the max-flow, the algorithm from [4] was used. Once the max-flow is found, the weights of the t -links are changed according to the values from the residual graph. The next iterations then follow until no change in cut is done (according to our experience, two or three iterations are sufficient).



(a) Example 1: 1st & 2nd iteration



(b) Example 2: 1st & 2nd iteration

Fig. 3. Results of our method and a comparison of the results after one and two iterations; the left column contains the results after single graph cut with data term set according to Eq. (3); the right column is after second iteration using Eq. (5)

3 Results

In this section, we describe the experiments with our method. The images are provided by a pair of uncalibrated cameras; the lens distortion is not compensated. The transformations $\pi_{LTR}(x_L)$, $\pi_{LBR}(x_L)$, $\pi_{LTB}(x_L)$, and $\pi_{LBT}(x_L)$ have been chosen to be two-value functions that have the form of bicubic polynomials whose coefficients were found by the least squares method from two sets of calibrating points that were determined manually. The first set of calibrating points contained selected corresponding points lying on the ground of parking lot; the second set contained selected corresponding points on the car roofs.

Fig. 3 contains the results from two parking lot situations. Both situations contain the result after one and two iterations, i.e., without and with the F_{res} term. The second iteration marks more pixels, which belong to a vehicle, correctly as top points, some vehicles are detected only after the second iteration.

The computational time of the method is about 3 seconds for the image resolution 960×540 and about 10 seconds for 1920×1080 after 2 iterations.

4 Conclusion

We have proposed a new method for detecting vehicles on parking lots using the graph cuts with a new data term of energy function. The term is constructed on the basis of evaluation of mismatches between the images. The additional part of this term, which utilizes data from the residual graph, is proposed to reach more accurate results. The method assumes that cars have similar height and that the transformation between both images is known. Therefore, it is not usable for general stereo reconstruction problems. According to the experiments, the method provides fast and promising results if the input conditions are fulfilled.

This work is a part of the paper that has been published in the conference proceedings at the 8th International Symposium on Visual Computing.

References

1. Kolmogorov, V., Zabih, R.: Multi-camera Scene Reconstruction via Graph Cuts. In: Heyden, A., Sparr, G., Nielsen, M., Johansen, P. (eds.) ECCV 2002. LNCS, vol. 2352, pp. 82–96. Springer, Heidelberg (2002)
2. Sun, J., Zheng, N.N., Shum, H.Y.: Stereo matching using belief propagation. *IEEE Trans. Pattern Anal. Mach. Intell.* 25, 787–800 (2003)
3. Kolmogorov, V., Zabih, R.: What energy functions can be minimized via graph cuts. *IEEE Trans. on Pattern Analysis and Machine Intelligence* 26, 65–81 (2004)
4. Boykov, Y., Kolmogorov, V.: An experimental comparison of min-cut/max-flow algorithms for energy minimization in vision. *IEEE Trans. on Pattern Analysis and Machine Intelligence* 26, 359–374 (2001)
5. Boykov, Y., Funka-Lea, G.: Graph cuts and efficient n-d image segmentation. *Int. J. Comput. Vision* 70, 109–131 (2006)
6. Huang, C., Wang, S.J.: A hierarchical bayesian generation framework for vacant parking space detection. *IEEE Trans. Circuit Syst. Video Techn.* 20, 1770–1785 (2010)

Knowledge-base Approach to Software-process Development

Michal Košinár

Department of Computer Science, FEECS,
VŠB – Technical University of Ostrava, 17. listopadu 15, 708 33 Ostrava – Poruba
michal.kosinar@vsb.cz

Abstract. Software products in companies are a substantial part of their production and a necessary condition of their business success. However, there is still a problem of software proper specification and verification. We propose a formal specification method for software processes based on Transparent Intensional Logic, TIL. This method is logic-oriented, because logical specification within a rich formal framework makes it possible to explicitly define process resources as well as process logic. Moreover, our novel contribution consists in integrating a knowledge-based method with process dynamic modeling.

1. Introduction

Process modeling is usually driven by a specific goal. The goal has to be defined prior to the modeling process in order to vote for a proper process calibration. Yet regardless of a particular process development objective, we need a general method of a software-process development. In this paper we introduce a knowledge-base and ontology driven method that meets application desiderata specified as follows:

- Iterative, step-by-step development and refinement of the initial model;
- Integration and sharing; independently of a particular modeling approach we should be able to share a common ontology and conceptual system, detect concept duplicates and unify terminology

Our background formal framework is Transparent Intensional Logic (TIL for short) and its computational variant, the TIL-Script programming language. Using TIL as a universal and at the same time powerful logical system makes it possible to specify system elements (be it elements of an ontology and knowledge base of a process) in a unique way.

2. Software-process development

Business processes represent the core of a company behavior. They define activities which companies perform to meet their customers needs. As for the definition of a business process, we quote from Workflow Management Coalition: “Business process is a set of one or more linked procedures or activities which collectively realize a business objective or policy goal, normally within the structure defining functional roles and relationships.” A software process is also a kind of business process; it comes with its development and maintenance phases. In the development phase we aim at risk and cost reduction [1]. This phase can be divided into activities of different kind, as they are defined by the process life-cycle engineering [2]. The process life-cycle spiral includes these activities: Meta-modeling; Modeling, Analysis; Simulation; Redesign; Visualization; Prototyping, walk-through and performance support; Administration; Integration, etc. For details on particular activities, see, for instance [2].

3. Knowledge based approach to process modeling

Based on the summary of approaches described in [13], the knowledge-based approach has been chosen as a primary tool for capturing and dealing with software process for SPI purposes. The selected approach was mainly inspected as a tool for process simulation but it is strong enough to be used during the whole process lifecycle. It also deals with problems and goals defined in the introduction:

- Iterativeness; mentioned by Redesign and Evolution
- Transformation; support in principle; it is defined by mappings between different domains
- Integration of other methodologies; mapping or transformation can be defined between different approaches.

4. State-of-the-art of knowledge-based approach

A well-defined meta-model of a software process for the knowledge-based approach is described in [11] where the authors define a unified resource model (URM) for integrating types of objects appearing in models of the software process. The URM consists of resource classes and relations between different types of resources. The type of a resource can be a developed system, a document (or more generally an artifact), a development tool, a particular software process and others. This meta-model defines the generic model that consists of three objects: resource, simple-resource,

aggregate-resource; and relations among these classes: is-a-subclass; has-member-resource, has-neighbors, has-resource-specs. This generic model is specialized into five specific models for a developed software system, document, agent, tool and process model. In every model, object types are specified – Resource becomes Tool, Simple-resource becomes Program and aggregate-resource becomes Toolkit in the tool model. Additional relations among resources from different models have also been added.

The previous approach was based on the platform for AI and knowledge representation named Knowledgecraft [14]. Currently this platform is not available anymore.

5. State-of-the-art of knowledge-based approach

The current mainstream for knowledge representation and its use consists in the applications of semantic webs [15] and multi-agent systems.

The concept of ontology-based modeling in process modeling and simulation has been applied in [16], where a model represented by ontology is transformed into a description for JSIM simulation system. The ontology approach offers basic functions of abstraction for modeling. The generalization is represented by the relation “super-class” between sets. The conceptualization is represented by sets and individuals. The aggregation is not directly supported but it could be represented by object property as a relation whole-part (“whole” object has a property of “part” type).

Our background theory for analysis, design and building the semantic annotation of a software process is Transparent Intensional Logic (TIL). It is a higher-order system primarily designed for the logical analysis of natural language.

Due to its rich and transparent procedural semantics, all the semantically salient features can be explicitly represented by the language of TIL constructions. It includes explicit intensionalisation and temporalisation, as well as a hyper-intensional level of algorithmically structured procedures (known as TIL constructions) which are of a particular importance in the logic of attitudes, epistemic logic and the area of knowledge representation and acquisition.

The standard modeling tools for ontologies is OWL [17]. However, it has some disadvantages; in particular using OWL we cannot define a multi-level classification, i.e. a class of classes, etc. (see [4]). Multilevel classification is also important during the use of meta-model based OMG specifications [18,19]. For these reasons we prefer specification in TIL and we developed an OWL – TIL transformation.

6. Meta-model creation

A creation of the software process meta-model is defined in [19]. This paper provides a clear overview of the problem. Different approaches and methodologies are considered – including the OMG business process definition meta-model (for more details see [20]). The authors suggested a simple mechanism for the integration of multiple meta-models into simple cores with possible flexible extension for the purpose of further modeling. Five metamodels from different viewpoints are identified: activity, product, decision, context and strategy; The integrating part is a process domain meta-model [19]. These meta-models are defined by MOF – Meta-Object Facility that is the language used for “meta-model” creation; MOF is defined in a “meta-metamodel” level. Activity and process domain metamodel [19].

Before modeling, these meta-models are combined into one that contains selected subclasses of every part. The selection is based on the demands placed on the process. We have created a separate ontology for every part of the meta-model. These ontologies are defined in the TIL-Script programming language (the computational variant of TIL). Classes from particular parts of the meta-model are represented by ontology classes, while associations are represented by object properties and inheritance is represented by sub-classing.

7. Conclusion and future works

The superstructure of the direct ontology definition will be created in the future. Our vision is to provide a graphical editor. The editor will provide a view of a selected part of the model. There is also a planned feature for the simple creation of typical model constructs.

Methodology creation is another important issue. A full overview of modeling constructions or patterns will be arranged for the purpose of process modeling. For every construction, a corresponding implementation in TIL-Script and/or OWL will be defined. The methodology will solve the problem of when to use individuals for modeling and when to use subclasses.

The created model is not the goal itself. It is necessary to utilize its possibilities. Transformations for various simulation approaches will be defined. A process enactment is similar to the process simulation and it is planned to be developed. Apart from simulation or enactment, various analyses could also be used.

Compared to TIL, the modeling possibility of OWL and other approaches based on FOL are limited. For example, it does not support the multilevel classification.

8. Recent publications and awards

1. Košinár, M., Kohut, O.: Applying Statistical Methods in Knowledge Management of a Multi-agent System. *Organon F*, XVII, n.2, SAV Bratislava, 2010.
2. Košinár, M., Kohut, O.: Methods in Knowledge Management of a Knowledge Based Multi-agent System, In *GIS Ostrava 2010*, Faculty of electrical engineering and computer science, VŠB - Technical University of Ostrava, 2010, Editors: Lucie Hrubá, Michal Podhoranyi, Adrian Kapias, ISBN 978-80-248-2171-9
3. Košinár, M., Štolfa, S., Kožusznik, J.: Využití znalostí a ontologií v softwarových procesech, In Pavel Smrž (Ed.) *Znalosti 2010*, Vysoká škola ekonomická v Praze, Fakulta managementu, 2010, ISBN 978-80-245-1636-3
4. Košinár, M., Štolfa, S., Kožusznik, J.: Knowledge Support for Software Processes, To appear in *ENASE 2010*, Athens, Greece
5. Duží, M., Košinár, M., Kožusznik, J., Štolfa, S.: Knowledge-base approach to software-process development based on TIL; In *Proceedings of the 22nd European-Japanese Conference on Information Modeling and Knowledge Bases*; Editors: Yasushi Kiyoki, Takehiro Tokuda; 2012, Prague
6. Kožusznik, J., Štolfa, S., Košinár, M., Duží, M., Číhalová, M., Vondrák, I.: Know How and Know What for Software Processes. In *Journal Communications in Computer and Information Science*. 2011
7. Košinár, M.: Formal Methods in Software Process Modeling. In *Proceedings of the Wofex 2011 umphrey WS (1995) A Discipline for Software Engineering*. Addison-Wesley Professional.

Author was Grand aided student of Municipality of Ostrava, Czech Republic in academic year 2010/2011 and 2011/2012.

References

1. Humphrey WS (1995) *A Discipline for Software Engineering*. Addison-Wesley Professional.
2. Scacchi W, Mi P (1997) *Process Life Cycle Engineering: A Knowledge-Based Approach and Environment*. *Intelligent Systems in Accounting, Finance, and Management* 6:83--107-183--107.
3. Smith JM, Smith DCP (1977) Database abstractions: aggregation and generalization. *ACM Trans Database Syst* 2 (2):105-133. doi:10.1145/320544.320546
4. Machado EP, Caetano Traina J, Araujo MRB (2000) Classification Abstraction: An Intrinsic Element in Database Systems. Paper presented at the *Proceedings of the First International Conference on Advances in Information Systems*,
5. Vergidis K, Tiwari A, Majeed B (2008) *Business Process Analysis and Optimization: Beyond Reengineering*. *Systems, Man, and Cybernetics, Part C: Applications and Reviews*, *IEEE Transactions on* 38 (1):69-82.
6. Raffo DM (1996) Modeling software processes quantitatively and assessing the impact of potential process changes on process performance. Ph.D. thesis, Carnegie Mellon University.
7. Brooks FP (1987) No Silver Bullet - Essence and Accidents of Software Engineering (reprinted form *information processing* 86, 1986). *Computer* 20 (4):10-19.

8. Curtis B, Kellner MI, Over J (1992) Process modeling. *Commun ACM* 35 (9):75-90.
9. Garg PK, Scacchi W (1989) ISHYS: Designing an Intelligent Software Hypertext System. *IEEE Expert: Intelligent Systems and Their Applications* 4 (3):52-63.
10. Mi P, Scacchi W (1990) A Knowledge-Based Environment for Modeling and Simulating Software Engineering Processes. *IEEE Trans on Knowl and Data Eng* 2 (3):283-294. doi:10.1109/69.60792
11. Mi P, Scacchi W (1996) A meta-model for formulating knowledge-based models of software development. *Decis Support Syst* 17 (4):313-330. doi:[http://dx.doi.org/10.1016/0167-9236\(96\)00007-3](http://dx.doi.org/10.1016/0167-9236(96)00007-3)
12. Madachy RJ (2008) *Software Process Dynamics*. 2nd edn. Wiley-IEEE Press.
13. Scacchi W (1999) Experience with software process simulation and modeling. *Journal of Systems and Software* 46 (2-3):183-192.
14. Laurent J-P, Ayel J, Thome F, Ziebelin D (1984) Comparative Evaluation of Three Expert System Development Tools: Kee, Knowledge Craft, Art. *The Knowledge Engineering Review* 1 (04):18-29. doi:doi:10.1017/S0269888900000631
15. Allemang D, Hendler J (2008) *Semantic Web for the Working Ontologist: Effective Modeling in RDFS and OWL*. Morgan Kaufmann.
16. Silver GA, Lacy LW, Miller JA (2006) Ontology based representations of simulation models following the process interaction world view. Paper presented at the Proceedings of the 38th conference on Winter simulation, Monterey, California,
17. W3C (2009) OWL 2 Web Ontology Language. <http://www.w3.org/TR/owl2-overview/>.
18. Object Management Group(OMG) (2010) *OMG Unified Modeling Language(OMG UML), Infrastructure, Version 2.3*.
19. Hug C, Front A, Rieu D, Henderson-Sellers B (2009) A method to build information systems engineering process metamodels. *Journal of Systems and Software* 82 (10):1730-1742. doi:10.1016/j.jss.2009.05.020
20. Object Management Group(OMG) (2008) *Business Process Definition MetaModel (BPDM),Version 1.0*.

Using Prolog to Detect Resource Conflict in Processes Modelled using EPC

Jakub Macek

Department of Computer Science, FEECS,
VŠB – Technical University of Ostrava, 17. listopadu 15, 708 33 Ostrava – Poruba
`jakub.macek1@vsb.cz`

Abstract. Event-driven Process Chain (EPC) diagram notation is one of the few well known process modelling notations that are used by businesses today. While this notation has its flaws, it is very flexible and its basic semantics is clear. In this paper I present a method of transformation of EPC diagrams into a Prolog knowledge base and propose an approach of detection of conflicts of resources between process instances.

Keywords: Prolog, Event-driven Process Chain, EPC, verification, conflict of resources, business modelling

1 Introduction

Event-driven Process Chain (EPC) diagram notation is one of the few well known process modelling notations that are used by businesses today. While this notation has its flaws, it is very flexible and its basic semantics is clear. In this paper I present a method of transformation of EPC diagrams into a Prolog knowledge base and propose an approach of detection of conflicts of resources between process instances.

In this paper I focus on so called "human resources", namely worker roles participating in process' activities. Therefore there is only one available of resource (as in one Adam, one Bert, ...). While similar approach can be devised for quantifiable resources such as money or water, the time required for the computation would be significantly greater.

The detection of conflict requires a four step preparation of a Prolog knowledge base. This process is described in the following sections:

1. EPC diagram transformation
2. State-of-the-world formalization
3. EPC semantics
4. Conflict detection rules

2 EPC diagram transformation

2.1 EPC notation description

EPC is a diagram notation developed by Wilhelm-August Scheer for business modelling with the focus on control flow. A given process is represented as a sequence of *events* that describe the current state of the process and *activities* (or *functions*) that serve as transitions between the events. Events and activities can be either connected directly or through one or more *connectors*.

The AND connector represents parallel execution and the XOR connector represents decision, usually based on a result of immediately preceding activity. The OR connector is not as widely used as the XOR connector, mostly due to its unclear non-local semantics[1]. In addition to these basic elements, the EPC notation makes it also possible to model additional information, such as resources associated with activities.

2.2 EPC diagram formal definition

Although EPC originally doesn't have a formal definition, I have extended the generally accepted definition from [1]:

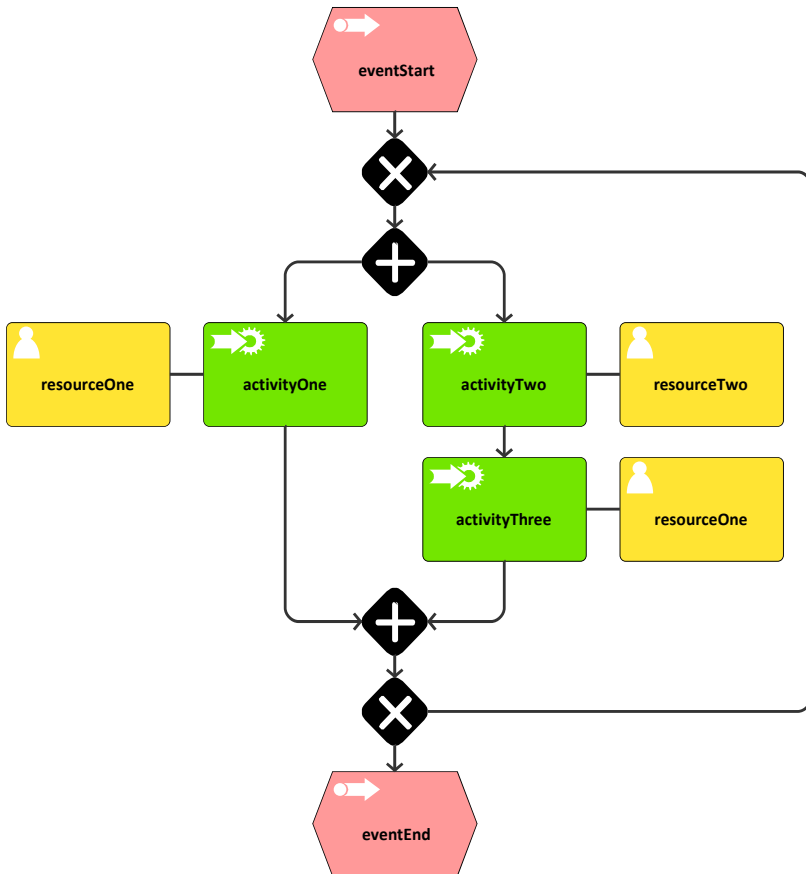
Definition 1 (EPC diagram). *An EPC process diagram $P = (E, F, C, l, A, s, R, p)$ consists of four pairwise disjoint sets of events E , functions (or activities) F , connectors C and resources R , a mapping $l : C \rightarrow \{and, xor, or\}$, a binary relation of arcs $A \subseteq (E \cup F \cup C) \times (E \cup F \cup C)$, a mapping $s : (E \cup F \cup C \cup A) \rightarrow \mathbb{N}$ and a mapping $p : F \rightarrow 2^R$ such that*

- $E \neq \emptyset$
- sets E, F, C, A, R are finite
- set N is called a set of nodes of the diagram and $N = E \cup F \cup C$
- mapping l assigns a type to a connector
- mapping s assigns to each element of the diagram (member of any of the sets E, F, C, A, R) a unique natural number (for the purpose of ordering)
- mapping p assigns to each function a set of participating resources
- there is exactly one starting event $e_{start} \in E : [\forall n \in N : (n, e_{start}) \notin A]$
- there is exactly one ending event $e_{end} \in E : [\forall n \in N : (e_{end}, n) \notin A]$
- there are incoming and outgoing arcs for other nodes: $\forall n \in N : [\exists k, m \in N : (((n, m) \in A) \vee (n = e_{end})) \wedge (((k, n) \in A) \vee (n = \{e_{start}\})))]$

2.3 Transformation

As an example, a simple diagram with all mentioned elements is used. The nodes are directly defined using predicates for the respective sets in the definition. The arcs are defined using different predicates depending the semantics of the flow between the arcs start-point and end-point.

Fig. 1. Example EPC diagram used in this paper



```

process(proOne).
activity(actOne).
activity(actTwo).
activity(actThree).
event(eveStart).
event(eveEnd).
xorSplit(xorS0ne). xorJoin(xorJ0ne).
andSplit(andS0ne). andJoin(andJ0ne).
activityRes(actOne,res0ne).
activityRes(actTwo,resTwo).
activityRes(actThree, resOne).
processStart(proOne,eveStart).
processEnd(proOne,eveEnd).
  
```

```

directFlow(eveStart,xorJOne).
directFlow(xorJOne,andSOne).
andSplitFlow(andSOne,actOne,0).
andSplitFlow(andSOne,actTwo,1).
andSplitFlowCardinality(andSOne,2).
andJoinFlow(actOne,andJOne,0).
andJoinFlow(actThree,andJOne,1).
directFlow(actTwo,actThree).
andJoinFlowCardinality(andJOne,2).
directFlow(andJOne,xorSOne).
xorSplitFlow(xorSOne,xorJOne,0).
xorSplitFlow(xorSOne,eveEnd,1).
xorSplitFlowCardinality(xorSOne,2).

```

3 State-of-the-world formalization

The state-of-the-world is essentially represented by three sets of facts for every process instance. First the process instance is assigned a specific process model and start time. Then all resource roles for this instance are filled and finally any available decisions are defined as branch choices of XOR connectors.

In this case, two process instances `proOne_1` and `proOne_2` are defined, 1 time unit apart. The first argument of `branchChoice` predicate is time to allow for different decisions in loops - in this case the decision is set to be the same for every pass.

```

proInst(proOne_1,proOne).
proInstStart(0,proOne_1).
resInst(proOne_1,resOne,resOne_1).
resInst(proOne_1,resTwo,resTwo_1).
branchChoice(_,proOne_1,xorSOne,1).

```

```

proInst(proOne_2,proOne).
proInstStart(1,proOne_2).
resInst(proOne_2,resOne,resOne_1).
resInst(proOne_2,resTwo,resTwo_1).
branchChoice(_,proOne_2,xorSOne,1).

```

4 EPC semantics

For the purpose of this paper, the following rules adequately represent the semantics of direct flow and the semantics of AND and XOR connectors. The predicate `act` recursively defines whether a node is active. The AND connector is the most complex, since it requires synchronization for which the predicates `actJP` (AND

join point branch is active) and `actJPA11` (all AND join point branches are active) are used.

To shorten the code, the following abbreviations are used: T - time, TB - time before (in previous step), P - process (model), PI - process instance, JP - join point, BP - branch point, B - branch (number).

```
act(T,PI,X) :- proInstStart(T,PI),proInst(PI,P),processStart(P,X).
act(T,PI,X) :- T > 0,TB is T - 1,act(TB,PI,Y),directFlow(Y,X),!.
act(T,PI,X) :- T > 0,TB is T - 1,act(TB,PI,Y),andSplitFlow(Y,X,_).
```

```
actJP(T,PI,JP,B) :- T > 0,act(T,PI,Y),andJoinFlow(Y,JP,B).
actJP(T,PI,JP,B) :- T > 0,TB is T - 1,actJP(TB,PI,JP,B),
    not(actJPA11(TB,PI,JP)).
actJPA11(T,PI,JP) :- andJoinFlowCardinality(JP,2),
    actJP(T,PI,JP,0),actJP(T,PI,JP,1).
act(T,PI,JP) :- T > 0,TB is T - 1,actJPA11(TB,PI,JP).
```

```
act(T,PI,X) :- T > 0,TB is T - 1,act(TB,PI,BP),
    xorSplitFlow(BP,X,B),branchChoice(TB,PI,BP,B).
```

5 Conflict detection rules

Using the previously defined `act` predicate, the conflict detection is now straightforward. A resource instance is used at a given time if it is assigned to an activity that is active in any process instance.

A simple rule of resource conflict can be then defined as a resource instance being used in two different process instances at the same time.

Few additional abbreviations are used in this code fragment: R - resource (role), RI - resource instance, A - activity.

```
used(T,PI,RI,A) :- activityRes(A,R),resInst(PI,R,RI),act(T,PI,A).
conflict(T,RI) :- used(T,PI1,RI,A1),used(T,PI2,RI,A2),not(PI1=PI2),
    write(RI),write(T),write(PI1),write(A1),write(PI2),write(A2),nl.
```

From a practical standpoint it is preferable to discover all conflicts up to a given time point (the limiting aspect is usually the availability of decisions as most processes are fully planned only up to a point). Following predicate `conflictMaxT` achieves this goal.

```
conflict(T) :- resInst(_,_,RI),conflict(T,RI).
conflictMaxT(0) :- fail.
conflictMaxT(T) :- T > 0,resInst(_,_,RI),conflict(T,RI).
conflictMaxT(T) :- T > 0,TB is T - 1,conflictMaxT(TB).
```

6 Conclusion

In this paper, I have described a straightforward method of transformation of business process model from an EPC diagram into Prolog knowledge base. Furthermore I have presented an approach that can be successfully used to detect an impending conflict of resources in a given set of process instances. This approach can be further improved to simulate the consequences of undetermined decisions by extending the `branchChoice` predicate. This is however best done targeting specific decision points on case-by-case basis due to the computation complexity.

Acknowledgements This research has been supported by the Grant Agency of the Czech Republic, projects 401/09/H007 ‘Logical Foundations of Semantics’ and 401/10/0792 ‘Temporal aspects of knowledge and information’, and also by the internal grant agency of VSB-TU of Ostrava - SP2012/26 ‘An utilization of artificial intelligence in knowledge mining from software processes’.

References

1. van der Aalst, WMP: *Formalization and verification of event-driven process chains*. In INFORMATION AND SOFTWARE TECHNOLOGY. ELSEVIER SCIENCE BV, NETHERLANDS. 1999. 639-650. ISSN 0950-5849
2. Mendling, J., van der Aalst, WMP: *Formalization and verification of EPCs with OR-joins based on state and context*. In Advanced Information Systems Engineering, Proceedings. Ed. Krogstie, J., Opdahl, A., Sindre, G. SPRINGER-VERLAG BERLIN. 2007. ISBN 978-3-540-72987-7
3. Gruhn, V., Laue, R.: *Detecting Common Errors in Event-Driven Process Chains by Label Analysis*. In Enterprise Modelling and Information Systems Architecture. 2011. 315.

Deductive Reasoning in High-order Logic

Marek Menšík, Lukáš Vích, and Luboš Chupáč

Department of Computer Science, FEECS,
VŠB – Technical University of Ostrava, 17. listopadu 15, 708 33 Ostrava – Poruba
{marek.mensik, lukas.vich.st, lubos.chupac.st}@vsb.cz

Abstract. The goal of this paper is to introduce Transparent Intensional Logic (TIL) as a logical framework apt for the logical analysis and deductive reasoning in natural language. TIL operates with a single procedural semantics for all kinds of logical-semantic context. There is a many uncertainties in the natural language. Some kinds of logical systems just cannot analyze natural language so smoothly. So there is rising a new question: Is deduction in such that logical system really adequate? What if the meaning of some sentence is not so clear? For that reasons we introduce TIL as a very strong system for analyzing sentences of natural language. It's not a target to say which meaning of sentence is that adequate analysis. Instead of that, TIL will offer sort of analysis and after that, it depends only on our opinion, which meaning is that correct.

1 Introduction

TIL makes it possible to build an inference machine that in principle neither over-infers (which yields paradoxes) nor under-infers (which leads to the lack of knowledge). However, there are two problems connected with TIL deduction system. First, since the system is hyper-intensional, which means that the meaning of an expression is a construction specified by the analyzed expression, rather than the product of the construction denoted by the expression, we must strictly distinguish between constructions and their products. This amounts for distinguishing a context in which a construction is used to produce an entity (if any), and the hyper-intensional context in which the construction itself is only mentioned as an object of predication. And if the construction is used, we must distinguish the context in which it is used intensionally and the context in which it is used extensionally. If the former, then the so constructed function is an object of predication; and if the latter, the value of the constructed function is an object of predication. Only then we can specify rules of deduction for extensional, intensional as well as hyper-intensional context. The second problem is partiality. The primitive notion of TIL is function rather than relation. And it is a strong fact that we need to work with properly partial functions, i.e. functions that are undefined at some arguments. The problem crops up when a properly partial function is applied to an argument at which the function does not return any value. Traditional formal lambda-calculi avoid this problem by simply excluding non-denoting terms as meaningless. Yet, this is not a quite right solution for the semantics of natural language.

Though, for instance, the present King of France does not exist (the office is vacant) this does not mean that the term ‘King of France’ is meaningless. If it were, we could not reasonably and truly assert that the King of France does not exist.

2 An introduction to TIL

TIL is an overarching semantic theory for all sorts of discourse, whether colloquial, scientific, mathematical or logical. The theory is a procedural one, according to which sense is an abstract, pre-linguistic procedure detailing what. Operations to apply to what procedural constituents to arrive at the product (if any) of the procedure. Such procedures are rigorously defined as TIL *constructions*. The semantics is entirely anti-contextual and compositional and it is, to the best of our knowledge, the only one that deals with all kinds of context (whether extensional, intensional or hyperintensional) in a uniform, extensional way. Thus the sense of a sentence is an algorithmically structured *construction* of the proposition denoted by the sentence. The denoted proposition is a flat, or unstructured, mapping with domain in a logical space of possible worlds. Our motive for working ‘top-down’ has to do with anti-contextualism: any given unambiguous term or expression (even one involving indexicals or anaphoric pronouns) expresses the same construction as its sense whatever sort of context the term or expression is embedded within. And the meaning of an expression determines the respective denoted entity (if any), but not vice versa. The denoted entities are (possibly 0-ary) functions understood as set-theoretical mappings. Thus we strictly distinguish between a procedure (construction) and its product (here, a constructed function), and between a function and its value.

Intuitively, construction C is a *procedure* (a generalised algorithm). Constructions are *structured* in the following way. Each construction C consists of sub-instructions (constituents), each of which needs to be executed when executing C . Thus a specification of a construction is a specification of an instruction on how to proceed in order to obtain the output entity given some input entities.

There are two kinds of constructions, atomic and compound (molecular). Atomic constructions (*Variables* and *Trivializations*) do not contain any other constituent but themselves; they specify objects (of any type) on which compound constructions operate. The *variables* x, y, p, q, \dots , construct objects dependently on a valuation; they v -construct. The *Trivialisation* of an object X (of any type, even a construction), in symbols 0X , constructs simply X without the mediation of any other construction. *Compound* constructions, which consist of other constituents as well, are *Composition* and *Closure*. *Composition* [$F A_1 \dots A_n$] is the operation of functional application. It v -constructs the value of the function f (*valuation-*, or v -, -constructed by F) at a tuple-argument A (v -constructed by A_1, \dots, A_n), if the function f is defined at A , otherwise the Composition is *v -improper*, i.e., it *fails* to v -construct anything.¹ *Closure* [$\lambda x_1 \dots x_n X$] spells out the instruction to v -construct a function by abstracting over the values of the variables x_1, \dots, x_n in the ordinary manner of the λ -calculus. Finally, higher-

¹ We treat functions as partial mappings, i.e., set-theoretical objects, unlike the *constructions* of functions.

order constructions can be used twice over as constituents of composite constructions. This is achieved by a fifth construction called *Double Execution*, 2X , that behaves as follows: If X v -constructs a construction X' , and X' v -constructs an entity Y , then 2X v -constructs Y ; otherwise 2X is v -improper, failing as it does to v -construct anything.

TIL constructions, as well as the entities they construct, all receive a type. The formal ontology of TIL is bi-dimensional; one dimension is made up of constructions, the other dimension encompasses non-constructions. On the ground level of the type hierarchy, there are non-constructional entities unstructured from the algorithmic point of view belonging to a *type of order 1*. Given a so-called *epistemic (or objectual) base* of *atomic types* (\mathbf{o} -truth values, \mathbf{t} -individuals, $\mathbf{\tau}$ -time moments / real numbers, $\mathbf{\omega}$ -possible worlds), the induction rule for forming functional types is applied: where $\alpha, \beta_1, \dots, \beta_n$ are types of order 1, the set of partial mappings from $\beta_1 \times \dots \times \beta_n$ to α , denoted ' $(\alpha \beta_1 \dots \beta_n)$ ', is a type of order 1 as well.² Constructions that construct entities of order 1 are *constructions of order 1*. They belong to a *type of order 2*, denoted '*₁'. The type *₁ together with atomic types of order 1 serves as a base for the induction rule: any collection of partial mappings, type $(\alpha \beta_1 \dots \beta_n)$, involving *₁ in their domain or range is a *type of order 2*. Constructions belonging to a type *₂ that identify entities of order 1 or 2, and partial mappings involving such constructions, belong to a *type of order 3*. And so on *ad infinitum*.

2.1 Three kinds of context

As mentioned above, constructions are full-fledged objects that can be not only used to construct an object (if any) but also serve themselves as input/output objects on which other constructions (of a higher-order) operate. This is so, because expressions of natural language, when used in a communicative act, can be used in three different ways³.

1. Hyperintensional context: the sort of context in which a construction is not used to v -construct an object. Instead, the construction itself is an argument of another function; the construction is just mentioned. Examples: Consider the sentence "Charles is solving the equation $1 + x = 3$ ". When Charles is looking for the solution of ' $1 + x = 3$ ', he is not looking for the number 2. And though the solution of ' $1 + x = 3$ ' is the same as, e.g., of ' $6 - x = 4$ ', it does not follow that Charles is solving the latter equation. Thus the meaning of the solution of ' $1 + x = 3$ ' is only mentioned here. It is predicated of this very meaning that Charles is striving to find the object constructed by this meaning. When evaluating the truth-conditions of this sentence, we do

² TIL is an open-ended system. The above epistemic base $\{\mathbf{o}, \mathbf{t}, \mathbf{\tau}, \mathbf{\omega}\}$ was chosen, because it is apt for natural-language analysis, but the choice of base depends on the area and language to be analysed. For instance, possible worlds and times are out of place in case of mathematics, and the base might consist of, e.g., \mathbf{o} and \mathbf{v} , where \mathbf{v} is the type of natural numbers.

³ An exact definition is out of the scope of this paper. For more details, see [3].

not solve the equation, it is Charlie’s matter. The expression, or rather its meaning, occurs here hyper-intensionally.

2. Intensional context : the sort of context in which a construction C is used to v-construct a function but not a particular value of the function, and C does not occur within another hyperintensional context. Example: “The President of Finland is selected for the period of six years”. The object of predication is the office of the president, that is the function of **type** ι_{τ_0} . The sentence predicates of this office (rather than of its contingent holder, if any) that it has the property of being eligible for the period of six years. The sentence is true even if the office is vacant; its truth is established by the Finnish constitution. Hence the meaning of ‘the President of Finland’ occurs here with *de dicto* supposition.

3. Extensional context : the sort of context in which a construction C of a function is used to construct a particular value of the function at a given argument, and C does not occur within another intensional or hyperintensional context. Example: “The President of Finland is the first female holder of the office”. Now the property of being the first female holder of the office is not predicated of the entire office, but of its present holder, i.e. the value of type ι of the function of type ι_{τ_0} . Hence the meaning of ‘the President of Finland’ occurs here extensionally, with *de re* supposition. To avoid a misconception, we want to stress that the specification of particular contexts in which a construction occurs, does not involve a reference shift or even a meaning shift, as Frege proposed⁴. Our analysis is anti-contextualistic. This is to say that the meaning of an unambiguous expression is the same in all the contexts.

Example 1 (hyper-intensional context): “Charles is solving the equation $1 + x = 3$ ”. When solving the equation, Charles wants to find out which set (here a singleton) is constructed by the Closure $\lambda x [^0=[^0+ ^0 1 x]^0 3]$. Thus he is related to the Closure itself rather than its product, a particular set. Otherwise the seeker would be immediately a finder and Charles’s solving would be a pointless activity. The analysis comes down to:

$$\lambda w \lambda t [^0 \text{Solve}_{wt} ^0 \text{Charles} ^0 [\lambda x [^0 = [^0 + ^0 1 x]^0 3]]] \tag{1}$$

Thus the following argument is invalid:

“Charles is solving the equation $1 + x = 3$ ”
“The solution of $1 + x = 3$ is equal to the solution of $6 - x = 4$ ”
 “Charles is solving the equation $6 - x = 4$ ”

This is revealed by the analysis:

$$\lambda w \lambda t [^0 \text{Solve}_{wt} ^0 \text{Charles} ^0 [\lambda x [^0 = [^0 + ^0 1 x]^0 3]]] \\
\lambda x [^0 = [^0 + ^0 1 x]^0 3] = \lambda y [^0 = [^0 - ^0 6 y]^0 4] \\
\lambda w \lambda t [^0 \text{Solve}_{wt} ^0 \text{Charles} ^0 [\lambda y [^0 = [^0 - ^0 6 y]^0 4]]]$$

⁴ For more details, see [4].

The construction $[\lambda x[{}^0= [{}^0+ {}^01 x]{}^03]]$ occurs in the first premise hyper-intensionally. On the other hand, the Trivialization ${}^0[\lambda x[{}^0= [{}^0+ {}^01 x]{}^03]]$ is a constituent used in (1) intensionally. It can never be ν -improper, and the following argument is valid:

$$\begin{array}{c} \text{“Charles is solving the equation } 1 + x = 3\text{”} \\ \lambda w \lambda t [{}^0 \text{Solve}_{wt} {}^0 \text{Charles } {}^0 [\lambda x [{}^0 = [{}^0 + {}^0 1 x]{}^0 3]]] \\ \text{“There is something Charles is solving”} \\ \lambda w \lambda t \exists c [{}^0 \text{Solve}_{wt} {}^0 \text{Charles } c] \end{array}$$

Proof. Let *Proper* / (o^*_n) be the class of constructions that are not ν -improper for any valuation ν . Then in any world w at any time t the following steps are truth-preserving:

$$\begin{array}{ll} [{}^0 \text{Solve}_{wt} {}^0 \text{Charles } {}^0 [\lambda x [{}^0 = [{}^0 + {}^0 1 x]{}^0 3]]] & \text{assumption} \\ \frac{[{}^0 \text{Proper}_{wt} {}^0 [\lambda x [{}^0 = [{}^0 + {}^0 1 x]{}^0 3]]]}{\exists c [{}^0 \text{Solve}_{wt} {}^0 \text{Charles } c]} & \begin{array}{l} \text{the rule of improperness} \\ \text{existential generalisation} \end{array} \end{array}$$

Example 2 (intensional context): “Charles wants to be The President of Finland”.

$$\lambda w \lambda t [{}^0 \text{Want_to_be}_{wt} {}^0 \text{Charles } \lambda w \lambda t [{}^0 \text{President_of}_{wt} {}^0 \text{Finland}]] \quad (2)$$

The Closure $\lambda w \lambda t [{}^0 \text{President_of}_{wt} {}^0 \text{Finland}]$ occurs intensionally, i.e. with de dicto supposition, because it is not used in (2) to ν -construct the holder of the office (particular individual, if any). Thus the following argument is invalid:

$$\begin{array}{c} \text{“Charles wants to be the President of Finland”} \\ \frac{\text{“The President of Finland is the first female holder of the office”}}{\text{“Charles wants to be the first female holder of the office”}} \end{array}$$

The analysis reveals the invalidity of the argument:

$$\begin{array}{c} \lambda w \lambda t [{}^0 \text{Want_to_be}_{wt} {}^0 \text{Charles } \lambda w \lambda t [{}^0 \text{President_of}_{wt} {}^0 \text{Finland}]] \\ \lambda w \lambda t [{}^0 = \lambda w \lambda t [{}^0 \text{President_of}_{wt} {}^0 \text{Finland}]_{wt}] \\ \frac{[{}^0 \text{First}_{wt} \lambda x [{}^0 \text{Female}_{wt} x] \wedge [{}^0 = x \lambda w \lambda t [{}^0 \text{President_of}_{wt} {}^0 \text{Finland}]_{wt}]]]}{\lambda w \lambda t [{}^0 \text{Want_to_be}_{wt} {}^0 \text{Charles} \\ \lambda w \lambda t [{}^0 \text{First}_{wt} \lambda x [{}^0 \text{Female}_{wt} x] \wedge [{}^0 = x \lambda w \lambda t [{}^0 \text{President_of}_{wt} {}^0 \text{Finland}]_{wt}]]]} \end{array}$$

Example 3 (extensional context): “The President of Finland is watching TV”. The analysis of this sentence comes down to the Closure.

$$\lambda w \lambda t [{}^0 \text{Watch}_{wt} \lambda w \lambda t [{}^0 \text{President_of}_{wt} {}^0 \text{Finland}]_{wt} {}^0 \text{TV}] \quad (3)$$

The meaning of ‘the President of Finland’ occurs with de re supposition in (3), i.e. extensionally. Thus we can apply the extensional rules that are also known as two

principles de re. They are the *Principle of existential presupposition* and the *Substitutivity of co-referential expressions*. The following arguments are valid:

Argument 1:

“The President of Finland is watching TV”
“The President of Finland exists”

$$\frac{\lambda w \lambda t [{}^0 \text{Watch}_{wt} \lambda w \lambda t [{}^0 \text{President_of}_{wt} {}^0 \text{Finland}]_{wt} {}^0 \text{TV}]}{\lambda w \lambda t [{}^0 \text{Exist}_{wt} \lambda w \lambda t [{}^0 \text{President_of}_{wt} {}^0 \text{Finland}]]}$$

Argument 2:

“The President of Finland is watching TV”
“The President of Finland is Tarja Halonen”
“Tarja Halonen is watching TV”

$$\frac{\lambda w \lambda t [{}^0 \text{Watch}_{wt} \lambda w \lambda t [{}^0 \text{President_of}_{wt} {}^0 \text{Finland}]_{wt} {}^0 \text{TV}]}{\frac{\lambda w \lambda t [{}^0 \text{President_of}_{wt} {}^0 \text{Finland}]_{wt} {}^0 \text{Halonen}}{\lambda w \lambda t [{}^0 \text{Watch}_{wt} {}^0 \text{Halonen} {}^0 \text{TV}]}}$$

Conclusion

In this paper we described basic principles of TIL. Also we advocated for TIL with its expressive procedural semantics, because this is the way how distinguish between the three kinds of context: extensional, intensional and hyperintensional. TIL operates on all the three levels of abstraction smoothly, in an extensional way. It can be usefull if we are looking for solution of adequate analysis of some expression meaning for which the pure extensionally logics frameworks has just not necessary facilities.

References

1. Menšík, M., Číhalová, M., Vích, L.: Dedukce v multi-agentních systémech za pomoci logiky vyšších řádů. In *Kognice a umělý život XII*, 2012, ISBN 978-80-86742-34-2.
2. Duží, M., Menšík, M., Číhalová, M., Ciprich, N., Frydrych, T.,: Deductive reasoning using TIL.. In *RASLAN'09, Recent Advances in Slavonic Natural Langure Processing*. Ed. Sojka, P., Horák, A. Brno: Masarykova universita. 2009. 25-38. ISBN 978-80-210-5048-8
3. Duží, M., Jespersen B., Materna P.: *Procedural Semantics for Hyperintensional Logic; Foundations and Applications of Transparent Intensional Logic*. Series Logic, Epistemology and the Unity of Science. Springer, Berlin, 2010, ISBN 978-90-481-8811-6.
4. Frege G., Über Sinn und Bedeutung, *Zeitschrift für Philosophie und philosophische Kritik*, vol. 100, pp. 25-50, 1892.

Mean Shift and Anisotropic Diffusion

Karel Mozdřeň, Radovan Fusek, and Milan Šurkala

Department of Computer Science, FEECS,
VŠB – Technical University of Ostrava, 17. listopadu 15, 708 33 Ostrava – Poruba
{karel.mozdren, radovan.fusek.st, milan.surkala.st}@vsb.cz

Abstract. Mean Shift is considered as a good segmentation method. Recently, some interesting modifications were presented. These methods use different kinds of kernels, and some also change its shape or the size during the computation to achieve better segmentation results. In this paper, we provide reader with notes about our recent development of anisotropic diffusion mean shift. It is inspired by anisotropic diffusion and medoid shift. We use anisotropic diffusion to measure the similarity of data points. The differences of temperatures of corresponding points are used instead of Euclidean distance metrics in mean shift. First, we introduce the reader into mean-shift methods, then we describe anisotropic diffusion and its application in our approach. In the final part of our paper, we show the experiments with image segmentation and filtering.

1 Introduction

Image segmentation is a process in which an image is portioned into multiple segments. Mean Shift (MS) [1–5] is very popular segmentation method family. Unfortunately, it suffers from some weaknesses, such as scattered segmentation lines or may have problems to process discontinuous edges.

In the paper [6] by Carreira-Perpinan, the gaussian blurring mean shift (GBMS) method is presented. The author developed this method from blurring mean shift (BMS) presented by Fukunaga and Hostetler [1]. Comaniciu et al. [7] describe how to adaptively change the bandwidth of the kernel to achieve better segmentation results by computing suitable kernel sizes. Another interesting MS modification is a Medoidshift by Sheikh et al. [5], which uses original data to find new position for the shifted points.

In our paper, we present a new approach to measure the similarity of data points based on natural laws of diffusion. First, we describe the basic mean-shift methods in Section 2, anisotropic diffusion in Section 3; its application in our approach in detail in Section 4. Furthermore, we show some experimental results, and discuss advantages and disadvantages of our approach in Section 5.

2 Mean Shift

MS is based on moving the image points (pixels) towards an attractor using a mean-shift vector that points to the highest local density. This is done iteratively

until all points converge. The points that converge to the same attractor belong to the same segment. To compute the MS, we have to know the kernel density estimation. Let us consider a dataset $\{x_i\}_{i=1}^N \subset R^D$ and kernel density estimate

$$p(x) = \frac{1}{N} \sum_{i=1}^N K \left(\left\| \frac{x - x_i}{\sigma} \right\|^2 \right), \quad (1)$$

where N is a number of points in the dataset, x is an actual point we are computing the density for, x_i represents the points in computation, K is a density kernel function, and σ is a bandwidth. This function assigns a weight to each neighboring point x_i . The most popular is the Gaussian kernel and it has the form $K(\tau) = \exp^{-\frac{1}{2}\tau}$. If we want to move a point towards its attractor, we have to find the function $x^{(t+1)} = f(x^{(t)})$, which computes a new position $x^{(t+1)}$ from the old position $x^{(t)}$. This is derived from stationary point equation $\nabla p(x) = 0$. Therefore, the position of the point in the next iteration can be computed as

$$f(x) = \sum_{i=1}^N \frac{K' \left(\left\| \frac{x - x_i}{\sigma} \right\|^2 \right)}{\sum_{i'=1}^N K' \left(\left\| \frac{x - x_{i'}}{\sigma} \right\|^2 \right)} x_{i'}. \quad (2)$$

A problem with segmentation emerges when we are trying to segment object with discontinuous edges. Let us consider an example of such a image: a circle drawn with discontinuous line (Fig. 1a). In this case, we expect the circle as a separate segment, but MS algorithms create segments that do not respect discontinuous lines (Fig. 1b). We have developed a method, that is able to deal with this problem using combination of anisotropic diffusion and mean shift.

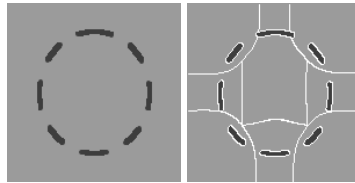


Fig. 1. Left image: source image for the segmentation; Right image: example of the segmentation by classical MS.

3 Anisotropic Diffusion

Diffusion is widely used in image processing for image smoothing and noise removal. In its basic forms, it is diffusion and is represented by partial differential equation (PDE) as $\delta I / \delta t = c \Delta I$, where t is a time parameter, c is a conductivity coefficient, and Δ denotes the Laplace operator.

Perona-Malik [8] proposed a method known as anisotropic diffusion or Perona-Malik diffusion. Their idea was to drive the conductivity by the magnitude of the gradient in the image. For this they introduced stopping function $g(\cdot)$. It slows down the diffusion process along the edges. Diffusion equation modification using the stopping function has the following form

$$\frac{\delta I}{\delta t} = \text{div} [g(\|\nabla I\|) \nabla I], \quad (3)$$

where $g(\cdot)$ is a stopping function for diffusion, and it is driven by the image gradient magnitude $\|\nabla I\|$. This function must be nonnegative and for $g(x) \rightarrow 0 : x \rightarrow \infty$. In this case, for big gradient magnitude the diffusion slows down or stops entirely. That makes the edges in the image barriers. The most popular stopping function has the following form

$$g(\|\nabla I\|) = \frac{1}{1 + \left(\frac{\|\nabla I\|}{\lambda}\right)^2}. \quad (4)$$

In this function, the parameter λ is used to set the sensitivity to the edges. Discrete iterative scheme for anisotropic diffusion has the following form

$$I_s^{t+1} = I_s^t + \frac{1}{|\eta_s|} \sum_{p \in \eta_s} g(\|\nabla I_{s,p}\|) \nabla I_{s,p}, \quad (5)$$

where s is the position of the pixel in discrete 2D grid (image), t is the discrete time step, I_s^t is discretely sampled image, η_s represents a set of the neighboring pixels, and $|\eta_s|$ is number of neighbors. Gradient of the image ∇I should not be confused with ∇I , which is a temperature difference denoted as $\nabla I_{s,p} = I_p - I_s$, $p \in \eta_s$. For color images, the maximal value over image gradients in all color channels can be used.

4 Anisotropic Diffusion and Mean Shift

The MS algorithm is used with many different kernels like Gaussian, Epanechnikov, uniform and many others. The problem is that it uses the same kernel shape and size for the whole segmentation process. In [7] the authors presented the method called variable bandwidth mean shift (VBMS) to adapt kernel radius according to the knowledge of the data. This method leads to better image and video segmentation. In our case, we present an idea of anisotropic diffusion mean shift (ADMS), which changes the view on distance measure by application of the Anisotropic Diffusion in Mean-Shift.

Inspired by VBMS, we developed MS with the anisotropic diffusion. It is based on the idea of heat spread across the image from a specific point. It would spread mainly to points with similar properties. It means that points near to themselves are transferring more heat than points with greater distance. This brings the idea to use anisotropic diffusion to compute adequate weight for each data point, based on a new similarity measure for mean shift.

When we give a point heat impulse and let it spread over all data points in the neighborhood, then all the near points get some heat. We are iteratively transferring the heat over all data points, and in the end, all the points transitively near to the starting point get the most heat. We can deduce from this idea that points with the most heat are nearer to starting point than points with less heat. We use this instead of the Euclidean metrics for mean shift and point density estimate then have following form

$$p(x) = \frac{1}{N} \sum_{i=1}^N K \left(\frac{d(x, x_i, t, \lambda)}{\sigma} \right), \quad (6)$$

where $d(x, x_i, t, \lambda)$ is a function that gives us nonnegative difference of the temperatures between points x and x_i at time t . The temperature is defined by the simulation of anisotropic diffusion in dataset, where the temperature at time t_0 (iteration 0) for point x is set to 1 and all other data points have temperature set to 0. The λ defines sensitivity to edges. At time t (iteration t) the temperature is distributed over all data points, and we acquired desired values. In this case, bandwidth σ is constraining the temperature difference.

To compute the difference we have to define a distribution function representing the heat distribution over all data points. We denote this function as D . The impulse at time $t = 0$ at point x is set to 1 and we solve the anisotropic diffusion PDE driven by the gradient magnitude of the original image. It has the following form

$$\frac{\delta D}{\delta t} = \text{div} [g(\|\nabla I\|) \nabla D]. \quad (7)$$

The heat difference is computed as $d(x, x_i, t) = |D(x, t) - D(x_i, t)|$, where x and x_i are the points we compute the difference for, and impulse is set at point x . The equation to compute position of the point in the next MS iteration has the following form

$$f(x) = \sum_{i=1}^N \frac{K' \left(\frac{d(x, x_i, t, \lambda)}{\sigma} \right) x_i}{\sum_{i'=1}^N K' \left(\frac{d(x, x_{i'}, t, \lambda)}{\sigma} \right)}. \quad (8)$$

The problem we have been solving was the point movement in each MS iteration. It does not move along the image manifold but it is floating in space. This results in re-computation of anisotropic diffusion for each point in each iteration, and it is very computationally expensive. Our solution to this problem is inspired by medoidshift algorithm by Sheikh et al. [5].

Medoidshift behaves the same as MS, but additionally it approximates the shifted point by the nearest point from the original data points set. This requests to compute the shifts for all points only in one iteration. Then the points are replaced by its modes and the process repeats until the movement of points stops. Inspired by this algorithm we compute anisotropic diffusion for impulse in each point in the image before we start the MS itself. After we shift the point, we find the nearest point we have values computed for, and use it for another shift. The example of the image segmented by MS with anisotropic diffusion can

be seen in Fig. 2. In contrast with the segmentation by MS with the Gaussian kernel, the anisotropic diffusion makes the circle as a separate segment. More images can be seen in Experiments section 5 in Fig. 3.

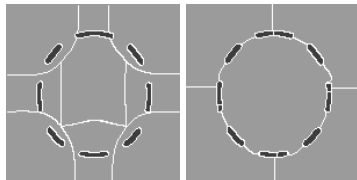


Fig. 2. Example of the image segmented by blurring MS with diffusion.

5 Experiments

In this section, we provide the reader with the results of the image segmentation using MS with the anisotropic diffusion. There are practically two parameters in our method. The first one is the sensitivity to the edges λ , and the second one is the number of iterations for kernel computation t . Setting the sensitivity to edges too high results in many segments in the final segmentation, and setting it too low ignores the details. On the other hand, if the number of iterations is set too high, it takes very long time to compute. The more iterations used, the bigger part of the image is taken in account for the computation. If a high sensitivity to edges is combined with the big number of iterations, then the heat eventually finds the way across the noise, and determines the real edges in the image. The iterations can be set to 500 for most cases, but the sensitivity has to be set according to desired filtering ability and it varies for each image. We recommend to set λ on the scale from 10 to 20. We prepared some example segmentations of the images obtained from The Berkeley Segmentation Dataset [9] provided also with the human made segmentations as a suggestive measure in Fig. 3.

6 Conclusion

We presented a Mean-Shift algorithm with the anisotropic diffusion. The motivation for our work was that the anisotropic diffusion used in segmentation gives the algorithm ability to include global segmentation properties into the calculation, unlike from locally based kernels estimations. The diffusion has a positive influence on segmentation of images with discontinuous contours. We experimentally tested its use in segmentation and filtration. Moreover, we compared our results with manual segmentations obtained from The Berkeley Segmentation Dataset.

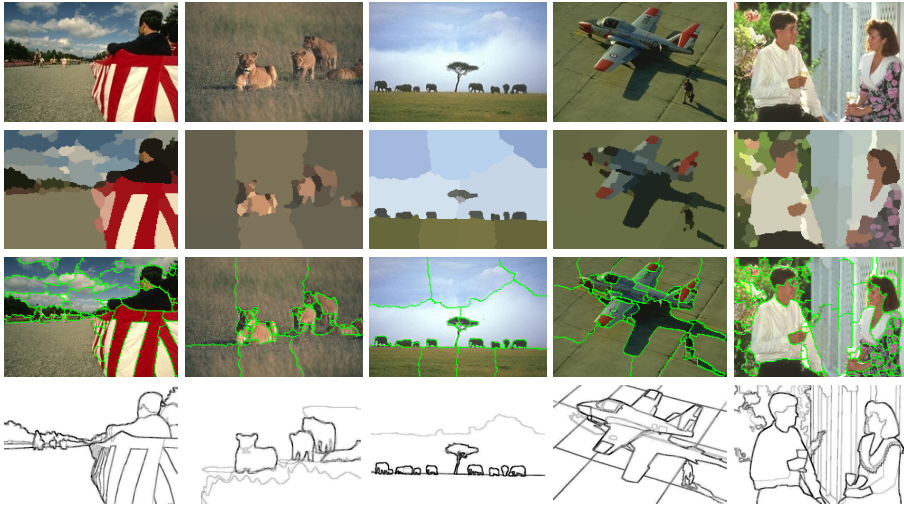


Fig. 3. First row: Original images, Second row: Filtering, Third row: Segmentations, Forth row: human made segmentations.

References

1. Fukunaga, K., Hostetler, L.: The estimation of the gradient of a density function, with applications in pattern recognition. *IEEE Transactions on Information Theory* **21** (1975) 32–40
2. Cheng, Y.: Mean shift, mode seeking, and clustering. *Pattern Analysis and Machine Intelligence, IEEE Transactions on* **17** (1995) 790–799
3. Carreira-Perpinan, M.: Mode-finding for mixtures of gaussian distributions. *Pattern Analysis and Machine Intelligence, IEEE Transactions on* **22** (2000) 1318–1323
4. Comaniciu, D., Meer, P.: Mean shift: a robust approach toward feature space analysis. *Pattern Analysis and Machine Intelligence, IEEE Transactions on* **24** (2002) 603–619
5. Sheikh, Y., Khan, E., Kanade, T.: Mode-seeking by medoidshifts. In: *Computer Vision, 2007. ICCV 2007. IEEE 11th International Conference on.* (2007) 1–8
6. Carreira-Perpiñán, M.: Fast nonparametric clustering with Gaussian blurring mean-shift. In: *Proceedings of the 23rd international conference on Machine learning. ICML '06, New York, NY, USA, ACM* (2006) 153–160
7. Comaniciu, D., Ramesh, V., Meer, P.: The variable bandwidth mean shift and data-driven scale selection. In: *Computer Vision, 2001. ICCV 2001. Proceedings. Eighth IEEE International Conference on. Volume 1.* (2001) 438–445 vol.1
8. Perona, P., Malik, J.: Scale-space and edge detection using anisotropic diffusion. *IEEE Trans. Pattern Anal. Mach. Intell.* **12** (1990) 629–639
9. Martin, D., Fowlkes, C., Tal, D., Malik, J.: A database of human segmented natural images and its application to evaluating segmentation algorithms and measuring ecological statistics. In: *Proc. 8th Int'l Conf. Computer Vision. Volume 2.* (2001) 416–423

Image Segmentation Utilizing Multiple Mean – Shift Executions

Milan Šurkala, Karel Mozdreň, and Radovan Fusek

Department of Computer Science, FEECS,
VŠB – Technical University of Ostrava, 17. listopadu 15, 708 33 Ostrava – Poruba
{milan.surkala.st, karel.mozdren, radovan.fusek.st}@vsb.cz

Abstract. Image segmentation is one of many image processing methods. Various segmentation methods exist, each has its own drawbacks and advantages. Mean shift is relatively slow but very precise method that is still widely developed. We present a new method called Layered Mean Shift that utilizes multiple mean-shift executions with different bandwidths and picks up the most significant segment boundaries. This method effectively reduces the over-segmentation problem even with very small kernels. Slightly better speed is the next advantage.

Keywords: mean-shift, segmentation, filtration, acceleration, layered

1 Introduction

The mean shift algorithm (MS) was firstly presented in 1975 by Fukunaga and Hostetler [6]. It is quite successful statistical tool that can be used for searching segments in various data sets. In this article, we focus on digital images and, therefore, our data sets are composed of pixels in images. MS has very nice filtration and segmentation abilities but suffers from an insufficient speed and occasionally over-segmentation (depends on the size of the kernel). Because of that, many faster method were presented in recent years.

The algorithm uses Parzen window technique to estimate the density of data points. According to the computed estimate, data point is shifted. This computation is iteratively repeated until the shift is smaller than a preset threshold or even zero. In such a case, convergence is achieved and the point is assigned to an attractor (place of the point convergence). Many attractors can emerge in digital images. Each of them forms the segment and covers pixels with similar properties in spatial and range (luminance) domain. There are two main approaches in the mean-shift method. Blurring Mean Shift (BMS) [6], [1] shifts the original data points and the data set is slightly blurred after each iteration. Classical Mean Shift (MS) [2], [3], [4] maintains two data sets. The first data set is the original one and the second data set is formed by the computed (shifted) data.

2 Layered Mean Shift

Let $X = \{x_i\}_{i=1}^n \subset R^d$ be a dataset of n points in the d -dimensional space. We can define *kernel density estimator* as

$$p(x) = \frac{1}{n\sigma^d} \sum_{i=1}^n K\left(\frac{x-x_i}{\sigma}\right), \quad (1)$$

where x is a processed pixel and x_i are the pixels in a neighbourhood given by the bandwidth parameter σ . In digital images, two types of bandwidth are used. The spatial bandwidth σ_s limits the size of kernel in x and y axis, the range bandwidth σ_r limits the luminance or color difference. The fraction at the beginning of the equation is a normalization term. The function $K(x)$ is a kernel function that weighs the contribution of pixels in the computation. If a truncated kernel is used (Epanechnikov, uniform), all pixels not belonging to a hypersphere given by both σ parameters are neglected. If we use broad infinite kernel (Gaussian), the bandwidth parameters only adjust the contribution of pixels. In both cases, the values of parameters influence the size of final segments in the image. In Eq. (2), the Epanechnikov kernel is presented.

$$K(x) = \begin{cases} 1 - x^2, & \text{if } \|x\| \leq 1 \\ 0, & \text{otherwise} \end{cases} \quad (2)$$

The resulting mean-shift vector is given by the Eq. (2). It is the difference between the former position of point x and the mean of all pixels x_i in the neighbourhood of pixel x that have fallen inside the searching window (kernel). As already stated, computation ends when this difference is very small or zero. It means that the point x converged to the local position of the highest density of data points. The only difference between MS and BMS in this equation is using processed pixels x in BMS instead of the original position x_{orig} in MS. In this paper, BMS is used.

$$m_{\sigma,k}(x) = \frac{\sum_{i=1}^n x_i k\left(\left\|\frac{x-x_i}{\sigma}\right\|^2\right)}{\sum_{i=1}^n k\left(\left\|\frac{x-x_i}{\sigma}\right\|^2\right)} - x \quad (3)$$

The spatial bandwidth parameter used with broad kernels influences size of segments but the computational speed is not affected very much. On the other hand, smaller bandwidth can dramatically improve the speed of algorithm with truncated kernels. This phenomenon is used in our algorithm. In Fig. 1, small and large bandwidth is compared. It is obvious that small bandwidth improves the speed (only 13 seconds) but suffers from heavy over-segmentation. Large bandwidth lowers the over-segmentation problem but it is still present. Moreover, the speed has been significantly reduced (377 seconds). Variable bandwidth approaches are widely studied in recent years [3], [5], [8] in order to achieve better results and use larger kernels only in such places, where it is really needed.

The goal is to develop such a method that does not lead to enormous over-segmentation and concurrently achieves low computational times. Our approach

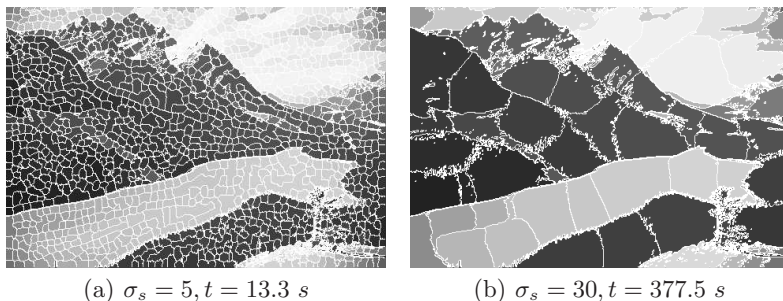


Fig. 1. Segmentation output and computational times with different spatial bandwidths.

uses multiple executions of mean-shift segmentation, each with different spatial bandwidth. We use especially lower values of the bandwidth. If more computations with different settings are processed, they would create the same segment boundaries in the same places and over-segmentation artifacts will be placed randomly.

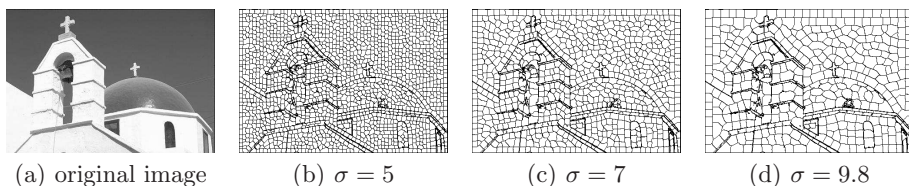


Fig. 2. Phases of the LMS method. Original image is in the first column. Images with different bandwidths are shown in next three figures.

Such segmentations are shown in Fig 2. We use images from the Berkeley Image Database [7]. Boundaries and details of the church are clearly presented in all three segmentation results. In the next step, we have to determine which segments should be grouped and which should be separated. We use very simple and effective method. All pairs of pixels in the image are picked up and we count the number of segmentations in which they were in the same segment. If the number is higher than a preset threshold, they are grouped into one large final segment. The threshold should be lower than the number of segmentations but not very significantly. If we stack only 3 segmentations, two positive correspondences to the same segments are the ideal threshold. Even if more segmentations are stacked (for example 7-15), the ideal threshold is one or maximally two less. It was observed that we do not need to test correspondence with all pairs in the image but only the pairs with the distance smaller than maximal σ_s in the last segmentation is sufficient. Such an acceleration significantly improves the speed

of algorithm and makes the merging stage as insignificant in the final computational time. Some post-processing that is merging very small segments is needed (for example, we eliminate all the segments that are smaller than $1/5000$ of an image area).

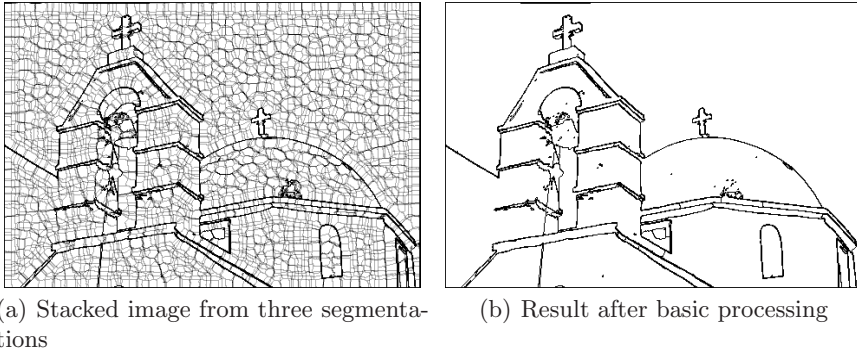


Fig. 3. Stacked segmentation and result of merging the segments.

3 Experiments

This section is going to present some experimental results with our LMS algorithm. Because we use BMS as its base algorithm, we can denote it as LBMS. LMS abbreviation was used to denote the whole family of layered mean-shift algorithms.

Table 1. The numbers of segments (seg) and speed (t[s]) depending on algorithm

image	BMS		LBMS	
	t[s]	seg	t[s]	seg
church	158.1 s	274	58.7 s	114
mountains	158.1 s	238	56.2 s	85
airplane	185.0 s	145	168.6 s	27

In Fig. 4, results with three different images are presented. All BMS segmentations used $\sigma_s = 20$ whereas LBMS results are created with significantly smaller spatial bandwidth (first segmentations use only $\sigma_s = 4$ and in the following stages, bandwidths were slightly enlarged - for example, values of 5.6 and 7.8 were used in the second and third stacked segmentation with the images of church and mountains). We can clearly see that even with such small bandwidths, over-segmentation is not presented. Table 1 shows the computational

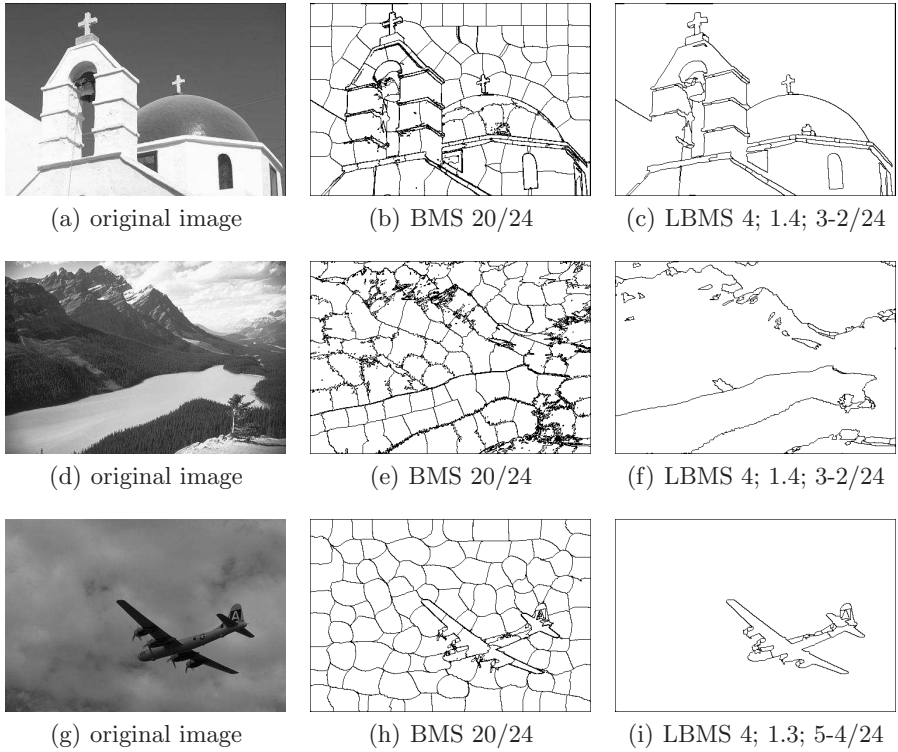


Fig. 4. Segmentations carried out with BMS and LBMS. Range bandwidth σ_r is the number after the slash. In BMS, the number before the slash is the spatial sigma σ_s . The first number in the LBMS notation denote σ_s in the first segmentation and the second number is the spatial bandwidth multiplier. The notation 3 – 2 denotes that 3 segmentations were processed and pixels that were at least twice in the same segmentation have been grouped.

times. They are similar if we use larger number of stacked segmentations but significantly lower if we use only three of them. Our algorithm not only decreases over-segmentation problem, it also improves the speed.

4 Conclusion

Layered mean-shift methods proved to be very effective way for elimination of the over-segmentation problem. They can also improve the speed in some cases and they emphasize the most significant segments and their boundaries. The only problem is in a proper adjustment of the parameters that can change the result more than in classical mean-shift methods. Because of that, hierarchical version of the algorithm is in development. It should not create small segments that have to be eliminated and it can not suffer from another merging problems (slightly varying lines between stacked segmentations). We expect even better speed than in LMS and LBMS.

References

1. Carreira-Perpiñán, M.: Fast nonparametric clustering with Gaussian blurring mean-shift. In: Proceedings of the 23rd international conference on Machine learning. pp. 153–160. ICML '06, ACM, New York, NY, USA (2006)
2. Cheng, Y.: Mean shift, mode seeking, and clustering. *IEEE Transactions on Pattern Analysis and Machine Intelligence* 17, 790–799 (1995)
3. Comaniciu, D., Meer, P.: Mean shift analysis and applications. *Computer Vision, 1999. The Proceedings of the Seventh IEEE International Conference on* 2, 1197–1203 vol.2 (1999)
4. Comaniciu, D., Meer, P.: Mean shift: a robust approach toward feature space analysis. *IEEE Transactions on Pattern Analysis and Machine Intelligence* 24(5), 603–619 (May 2002)
5. Comaniciu, D., Ramesh, V., Meer, P.: The variable bandwidth mean shift and data-driven scale selection. *Computer Vision, IEEE International Conference on* 1, 438 (2001)
6. Fukunaga, K., Hostetler, L.: The estimation of the gradient of a density function, with applications in pattern recognition. *IEEE Transactions on Information Theory* 21(1), 32–40 (January 1975)
7. Martin, D., Fowlkes, C., Tal, D., Malik, J.: A database of human segmented natural images and its application to evaluating segmentation algorithms and measuring ecological statistics. In: *Proc. 8th Int'l Conf. Computer Vision*. vol. 2, pp. 416–423 (2001)
8. Zhao, Q., Yang, Z., Tao, H., Liu, W.: Evolving mean shift with adaptive bandwidth: A fast and noise robust approach. In: *ACCV (1)'09*. pp. 258–268 (2009)

Application of Edge-magic Total Labelings

Ondrej Grunt

Department of Applied Mathematics, FEECS,
VŠB – Technical University of Ostrava, 17. listopadu 15, 708 33 Ostrava – Poruba
ondrej.grunt@vsb.cz

Abstract. Operating with high-dimensional sparse matrices is not possible without their proper structure manipulation and effective storage with minimal time intensity. In this article, we investigate the possibility of using generalized edge-magic labeling form with lifted requirements, yet without time intensity increased, for sparse matrix storage. In this paper we present generalized edge-magic labeling of $P_m \square P_n$ (for every integer m, n where m is odd) graph. We also compared time intensity results of derived generalized edge-magic storage form with other known forms of sparse matrix storage.

Keywords: Graph labeling; Edge-magic total labeling; Super edge-magic total labeling; Generalized edge-magic total labeling; Sparse matrix; Sparse matrix storing; Edge-magic labeling storing form;

1 Introduction

Many real-world problems take a form of some kind of net, represented by an incidence matrix of an undirected graph with corresponding number of vertices and edges. In higher dimensions, the incidence matrix will be populated primarily with zero values, effectively becoming a sparse matrix. Because operations with high-dimensional sparse matrices using dense matrix algorithms consume large amounts of memory, if are not unfeasible at all, numerous storing algorithms are applied. The goal of this work was to find new approach to sparse matrix storing specifically for graph-represented spare matrices based on magic labeling from graph theory.

Edge-magic labeling algorithm was compared to other known storage methods (namely *ijv*, *compressed row* and *compressed column*) in [3]. However, despite the fact that operations with sparse matrix using edge-magic labeling storage method had lower or equal time intensity, algorithm could not find edge-magic labeling for graphs of 30 or more vertices. In the conclusion, author proposed defining a construction of edge-magic labeling for graphs representing high-dimension spare matrices.

In the first part of this article, generalized edge-magic total labeling (GEMT) is introduced and its construction is defined. In the second part, sparse matrix storing using GEMT is explained. In the last part, results of time intensity comparison between GEMT method and other known storage forms are discussed.

2 GEMT labeling

As computer-based computation of magic labeling was unable to find correct labeling for graphs $P_m \square P_n$, for every integer m, n where m is odd, representing high-dimension sparse matrices, we assumed, that the generalization is the best approach to find magic labeling for these graphs. However, we had to lift some requirements, the most notable difference from EMT definition being that we left some label values unused.

For its similarity with $P_m \square P_n$ graphs, we chose to generalize SEMT labeling of generalized prism $C_m \square P_n$ given in [2]. Vertex label values are given by the following equation :

$$f(v_{i,j}) = \begin{cases} \frac{i+(2j-2)m+1}{2} & \text{for } i \text{ odd, } j \text{ odd} \\ \frac{i+(2j-1)m+1}{2} & \text{for } i \text{ even, } j \text{ odd} \\ \frac{i+(2j-1)m}{2} & \text{for } i \text{ odd, } j \text{ even} \\ \frac{i+(2j-2)m}{2} & \text{for } i \text{ even, } j \text{ even} \end{cases}, \tag{1}$$

where $i = 1, 2, \dots, m$ and $j = 1, 2, \dots, n$.

Before we proceed further, we need to compute magic constant. As we know exact number of vertices and their corresponding label values, we can find two incident vertices with the lowest sum of label values. Then, we add combined number of vertices and edges in our graph, which gives us the highest possible label value in our generalized prism graph.

$$k = \frac{6mn - m + 3}{2}, \tag{2}$$

As our goal is to find magic labeling for $P_m \square P_n$ graph, we need to transform generalized prism into rectangular mesh, thus getting our representation of spare matrix. Our solution is very simple : we make straight cut through all edges between two rows of vertices. It is worth noting that we don't lose any of the vertices, their assigned label values (see figure 1 for example) or the value of a magic constant, however we lose number of label values corresponding to the number of cut edges.

With known magic constant and label value of each vertex, it is now simple to get label values for all edges in the graph from the following equation given by edge-magic labeling property :

$$g(v_{i_1j_1}v_{i_2j_2}) = k - f(v_{i_1j_1}) - f(v_{i_2j_2}), \tag{3}$$

We can now formulize GEMT definition as follows:

Definition 1. GEMT - Generalized Edge-Magic Total Labeling of a graph G is an injective projection λ of union of sets $V(G) \cup E(G)$ onto integers

$$1, 2, \dots, v + e + d,$$

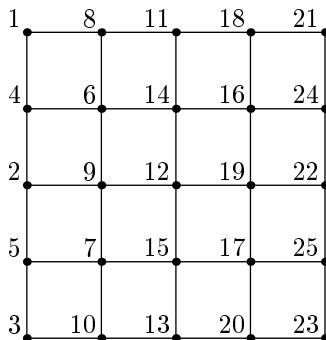


Fig. 1. Vertex labeling of $P_5 \square P_5$.

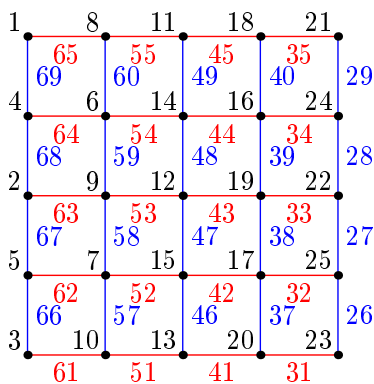


Fig. 2. Vertice and edge labeling of $P_5 \square P_5$.

where $v = |V(G)|, e = |E(G)|$ and d is a small natural number corresponding to number of unused label values (edges cut), and there exists integer k satisfying

$$\lambda(x) + \lambda(xy) + \lambda(y) = k.$$

Integer k is called the magic constant. Members of set $V(G)$ are assigned lowest possible integers from sequence $1, 2, \dots, v$ by projection λ .

Proof of GEMt definition is presented in [1]. Example of GEMT labeled graph can be seen in figure 2.

3 GEMT storage

For effective use of GEMT storage method on sparse matrix, we have to hold several values, namely value of magic constant, number of rows and columns of vertices in graph $P_m \square P_n$ ¹. In addition, array containing nonzero values $h[]$ and incidence array $s[][2]$ are used and stored.

¹ As we stated before, number of rows m must be odd integer

3.1 GEMT Storing

In the first step, we arrange all edges by its label values in ascending order, then we fill incidence array $s[][2]$ with their endpoint vertices, or, in case of the labeled vertices, we place the vertex twice in the incidence array. As we noted before, our generalization of magic labeling led to some label values left unused, we have then option to leave corresponding rows in incidence matrix blank or substitute endpoint vertices with verbal commentary.

Nonzero value in sparse matrix is represented by an edge in used graph, therefore we have to assign each nonzero value to corresponding edge in order to create array of nonzero values $h[]$. As we already constructed incidence array, this task is simple, as we already know the order in which all values will be sorted in array $h[]$. As lone vertices cannot refer to nonzero value in sparse matrix, their corresponding label values are not used, this also means, that the nonzero values array will be smaller in size than the incidence matrix. Edges assigned to an unused label value cannot be left out, instead they are stored as representing zero value in sparse matrix.

Last, vertices array $w[]$ is made, consisting of label values of each vertex sorted by according index in used graph. This array is not stored, as it is simply constructed using information from the incidence array.

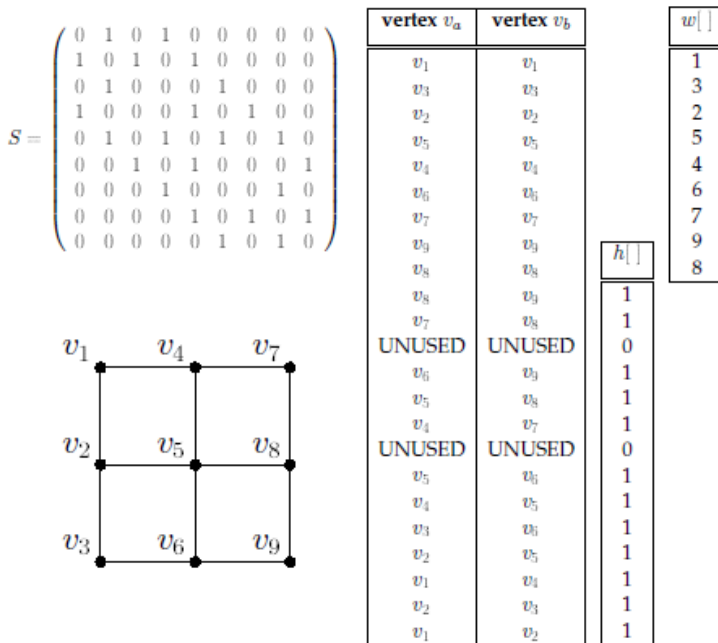


Fig. 3. GEMT storing of sparse matrix S with corresponding graph and arrays.

3.2 GEMT Retrieving

Let S be sparse matrix stored using GEMT method and let s_{xy} be element of that matrix. In the first step, we denote label values of both the ending vertices of given element/graph edge from vertices array $w[]$. Then we can compute label value of the graph edge, as we know the magic constant.

$$\lambda(v_x v_y) = k - (\lambda(v_x) + \lambda(v_y)).$$

Received label value then points to row in the incidence matrix, if given value exceeds array size, points to an unused label value or points to vertex, s_{xy} is zero element of sparse matrix. In other case, we inspect stored pair of endpoint vertices and compare them with vertices given by s_{xy} . If both set of vertices are not equal, then again s_{xy} is zero element. For retrieving value from nonzero values array, we take label value of s_{xy} from incidence array and decrease it by number of vertices present in graph, that way we get row index of $h[]$ for s_{xy} .

$$s_{xy} = h[\lambda(v_x v_y) - mn].$$

4 Results

GEMT labeling and storing algorithm was realized using C++ programming language and compared to other known storage methods.² Three sparse matrix operations (retrieving all sparse matrix element, right matrix-vector multiplication and left vector-matrix multiplication) were tested for each storage method and their time intensity was measured (example seen in Table 1). More results and insight in the GEMT storage algorithm are available in [1].

Size of graph G	Storage form	$\vec{v}A$	$A\vec{v}$	Retrieving all elements s_{xy}
121×121	ijv	0,0046254	0,0047729	132,19
	compr. col.	0,0011133	0,0016691	19,824
	GEMT	0,0014948	0,0014766	14,8
145×140	ijv	0,0061747	0,0061984	232
	compr. col.	0,0018167	0,0025357	32,745
	GEMT	0,0020898	0,0020188	26,553
151×151	ijv	0,0075019	0,0073986	381,298
	compr. col.	0,0012613	0,0019205	41,828
	GEMT	0,0015772	0,0015342	38,283

Table 1. Time intensity results of sparse matrix operations.

The lowest time intensity of reconstructing sparse matrix by retrieving all its elements was achieved by using GEMT storing method, followed by compressed

² ijv method and compressed column method were chosen for this testing.

column method, which was only slightly slower. Last tested method, *ijv*, lasted almost ten times as long as GEMT method.

The lowest time intensity of left vector-matrix multiplication was achieved by using compressed column storage method, GEMT followed with slight increase in time intensity while *ijv* method needed significantly longer time to process operation.

The lowest time intensity of right vector-matrix multiplication was achieved by using GEMT storing method, second being compressed column method with minimal delay, followed by *ijv* method, which took almost four times more to finish the task.

Operation time intensity was measured for sparse matrixes represented by $P_m \square P_n$ graphs of maximum size $m, n = 151$.

5 Conclusion

In this work, GEMT labeling for $P_m \square P_n$ graphs, based on the generalized SEMT labeling for $C_m \square P_n$ graph was defined and its construction described. Sparse matrix storage method was derived and successfully implemented, its time intensity was compared with other known forms of sparse matrix storing.

Through experiments, GEMT storing method achieved lower or equal time intensity compared to compressed column method, while significantly faster than *ijv* method. However, use of GEMT method is limited, as not every sparse matrix take form of incidence matrix, and thus being represented by GEMT labeled graph. Also, any structural changes can severely limit repeatable use of GEMT storage method, as it is very sensitive on the structure of the sparse matrix.

References

1. O. Grunt, *Application of edge-magic total labelings*, diplomova prace, VSB-TUO (2011).
2. R.M. Figueroa-Centeno, R. Ichishima, F.A. Muntaner-Batle, *The place of super edge-magic labelings among other classes of labelings*, Discrete Mathematics 231 (2001) 153 – 168.
3. L. Srubarova, *Aplikace magických ohodnocení grafu*, diplomova prace, VSB-TUO (2010).

Parallel Implementation of Domain Decomposition Solvers

Václav Hapla^{1,2}, Michal Merta^{1,2}, and David Horák^{1,2}

¹Department of Applied Mathematics, FEECS,
VŠB – Technical University of Ostrava, 17. listopadu 15, 708 33 Ostrava – Poruba
² Centre of Excellence IT4Innovations,
VŠB – Technical University of Ostrava, 17. listopadu 15, 708 33 Ostrava – Poruba
{`vaclav.hapla`, `michal.merta`, `david.horak`}@vsb.cz

Abstract. In this paper we present two implementations of Total-FETI domain decomposition method based on PETSc and Trilinos software frameworks. We briefly describe their implementations, compare efficiencies of the codes and present the latest results of numerical benchmarks.

1 Introduction

Domain decomposition methods are very suitable for parallel solution of elliptic partial differential equations arising from many technical problems. These methods are based on the “divide and conquer” strategy. Using the FETI-1 method the spatial domain is decomposed into non-overlapping subdomains and the continuity of the solution among subdomains is enforced by Lagrange multipliers. Efficiency of the FETI-1 method was further improved by introducing special orthogonal projectors and preconditioners.

Total-FETI (TFETI) by Dostal et al. [3] simplifies the inversion of stiffness matrices of subdomains by using Lagrange multipliers not only for gluing the subdomains along the auxiliary interfaces, but also to enforce the Dirichlet boundary conditions.

The most difficult part - solution of subdomain problems - may be carried out in parallel without any coordination and data transfers, so that high parallel scalability is enjoyed. The increasing number of subdomains decreases the subdomain problem size resulting in shorter time for subdomain stiffness matrix factorizations and subsequently forward and backward substitutions during stable pseudoinverse application. On the other hand, assuming fixed discretization parameter, the dual dimension and coarse problem size increase with increasing number of subdomains which results in longer time for all dual vector operations and orthogonal projectors application. The coarse problem couples all the subdomains computations which complicates implementation on massively parallel distributed memory systems. One of the possible solution of this bottleneck using the parallel sparse direct solver MUMPS is presented in this article.

2 TFETI

Let us consider linear elasticity problem in 2D or 3D. To apply the FETI-1 based domain decomposition let us partition domain Ω into N_s subdomains Ω^s and denote by K^s , f^s and u^s the subdomain stiffness matrix, the subdomain load vector and the subdomain displacement vector, respectively. B^s is a matrix with entries -1, 0, 1 describing the subdomain gluing. The finite element discretization with appropriate node numbering results in the QP problem

$$\min \frac{1}{2} u^T K u - u^T f \quad \text{s.t.} \quad B u = 0. \tag{1}$$

Contrary to the original FETI-1 method where the boundary subdomains inherit the Dirichlet conditions from the original problem, in TFETI [3] all subdomains are kept floating. The Dirichlet data are enforced by adding the appropriate rows into the constraint matrix B . Using this approach all subdomain stiffness matrices have the same rank and the basis of their kernel is known a-priori. This basis forms a block-diagonal matrix R .

Let us apply the duality theory to (1) and let us establish the following notation

$$F = B K^\dagger B^T, \quad G = R^T B^T, \quad d = B K^\dagger f, \quad e = R^T f,$$

where K^\dagger denotes a generalized inverse matrix satisfying $K K^\dagger K = K$. Our minimization problem reads

$$\min \frac{1}{2} \lambda^T F \lambda - \lambda^T d \quad \text{s.t.} \quad G \lambda = e. \tag{2}$$

Further the equality constraints $G \lambda = e$ can be homogenized to $G \lambda = 0$ by splitting λ into $\mu + \tilde{\lambda}$ where $\tilde{\lambda}$ satisfies $G \tilde{\lambda} = e$ (e.g. $\tilde{\lambda} = G^T (G G^T)^{-1} e$) which implies $\mu \in \text{Ker } G$. We then substitute $\lambda = \mu + \tilde{\lambda}$, omit terms without μ , minimize over μ and then add $\tilde{\lambda}$ to μ .

Finally, the equality constraints $G \lambda = 0$ can be enforced by the projector $P = I - Q$ onto the null space of G , where $Q = G^T (G G^T)^{-1} G$ is the projector onto the image space of G^T ($\text{Im } Q = \text{Im } G^T$ and $\text{Im } P = \text{Ker } G$). It holds that $P \mu = \mu$ because $\mu \in \text{Ker } G$, so the final problem reads

$$P F \mu = P (d - F \tilde{\lambda}). \tag{3}$$

Problem (3) may be solved effectively by a generic CG algorithm. The proof of the classical estimate $\kappa(P F P | \text{Im } P) \leq C \frac{H}{h}$ of the spectral condition number κ of $P F P$ on the range of P by the ratio of the decomposition parameter H and the discretization parameter h which was published by Farhat, Mandel and Roux remains valid for TFETI.

Parallelization of FETI/TFETI can be implemented using SPMD technique – distributing matrix portions among processing units. This makes the algorithms almost the same for sequential and parallel case; only data structure implementation differs. Most of computations (subdomains problems) to be performed are

purely local and therefore parallelizable without any data transfers. However, if we want to accelerate also dual actions, some communication is needed due to primal-dual transition.

Distribution of primal matrices is quite straightforward as every subblock reflects a subdomain. But the bottleneck of the TFETI method is the application of the projector Q . The action time and level of communication depend first of all on G matrix distribution and implementation of the coarse problem solution.

3 Implementation using PETSc and Trilinos

PETSc (Portable, Extensible Toolkit for Scientific computation), developed by Argonne National Laboratory, is “a suite of data structures and routines for the scalable parallel solution of scientific applications modeled by partial differential equations” [9]. Features include sequential/parallel vectors and matrices with dense as well as several sparse storage formats which can be easily and efficiently assembled, scalable parallel preconditioners, Krylov subspace methods for solution of linear systems, parallel Newton-based nonlinear solvers and parallel timestepping ODE solvers. It is coded primarily in C language and is usable from C, C++, Fortran 77/90, and Python codes. Current version is 3.2.

In our codes we use mainly matrix (`Mat`) subclass `mpiaij` (default parallel sparse matrix with compressed row storage) and vector (`Vec`) subclass `mpi` (default parallel vector) and PETSc utility routines (`Petsc`) for I/O, command-line options etc. Part of our most current design is use of `Mat` subclass `composite` – a linear operator class representing the implicit (not assembled) sum (or product) of one or more matrices (linear operators). The main advantage is that we can use built-in generic KSPCG solver with the Hessian *PPF* as a system matrix.

Trilinos [10] is a collection of relatively independent packages developed by Sandia National Laboratories. It provides a tool kit for basic linear algebra operations (both serial and parallel), direct and iterative solvers to linear systems, PDE discretization utilities, mesh generation tools and many other features. Its main advantages are object oriented design, high modularity and use of modern features of C++ language such as templating. These features contribute to high programming effectiveness without compromising computational effectiveness. In comparison with PETSc it seems that Trilinos acts more as an object-oriented software framework encouraging external extensions. It is currently at version 10.12

In our codes we use the `Epetra` as well as `Tpetra` packages as bases for linear algebra computations. They provide users with distributed dense vectors and matrices as well as sparse matrices in compressed row format (`Epetra_CrsMatrix`, `Tpetra::CrsMatrix`), distributed vectors/multivectors etc. The `Epetra` package is now well-established and tested, however it is slowly becoming obsolete as it supports only 32-bit data type. For this reason we use `Epetra` mainly for testing purposes and the main TFETI library is coded in fully templated `Tpetra`. As an object-oriented wrapper to common sequential and parallel direct linear systems solvers (such as SuperLUDist, UMFPACK, PARDISO etc.) we use the

Table 1. Performance of the Total FETI implementation for varying decomposition and discretization for the first benchmark

Number of subdom.	1	4	16	64	256	1024
Number of cores	1	4	16	64	256	1024
Primal dimension	31,752	127,008	508,032	2,032,128	8,128,512	32,514,048
Dual dimension	252	1,512	7,056	30,240	124,992	508,032
Kernel dimension	3	12	48	192	768	3072
PETSc						
K factorization	5.2	5.2	5.2	5.2	5.2	5.2
CG time	1.14	2.66	4.16	4.74	4.92	5.84
- of which Q act.	1.98e-3	1.08e-2	3.45e-2	1.39e-1	3.03e-1	1.26e+0
CG iterations	33	68	94	105	105	102
Time per iteration	3.46e-2	3.92e-2	4.42e-2	4.52e-2	4.69e-2	5.73e-2
Total time	6.5	8.0	10.1	10.9	11.2	13.7
Trilinos						
K factorization	2.5	2.5	2.5	2.5	2.5	2.5
CG time	1.39	3.01	4.80	6.25	10.31	28.05
- of which Q act.	1.50e-3	1.68e-2	5.98e-2	2.74e-1	3.26e-0	1.41e+1
CG iterations	34	63	96	105	105	102
Time per iteration	4.48e-2	4.76e-2	5.00e-2	5.95e-2	9.81e-2	2.75e-1
Total time	5.8	8.2	11.6	12	19	60

Amesos package. We have also developed a collection of quadratic programming algorithms for a solution of constrained minimization problems to be used as internal solvers of TFETI method for both linear and contact problems. This collection can be used as an independent optimization package.

4 Numerical experiments

The implementations were tested for 2D linear elasticity problem - see Figure 1. Recently [1], we suggested several ways of handling the matrix G and subsequent coarse problem $GG^T x = b$ solution. The variant used for the presented benchmark was: G distributed across the dual dimension, GG^T sequential, $GG^T x = b$ solved using LU factorization. We used no FETI preconditioning. The results are depicted in Table 1.

The solution of the coarse problem is one of the main bottlenecks of TFETI method. To overcome this bottleneck we have recently implemented its solution using parallel multifrontal direct sparse solver MUMPS. This enables us to effectively solve very large problems on thousands of processors. The results of the benchmark implemented in PETSc are depicted in Table 2.

Benchmarks were run on *HECToR* supercomputer at EPCC in Edinburgh [11]. The current main HECToR facility is the phase 3. This was used for our experiments. It is a Cray XE6 system offering a total of 2816 computing nodes, each with two 16-core AMD Opteron 2.3GHz Interlagos processors giving a total

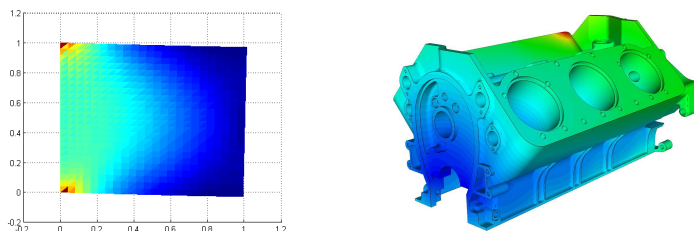


Fig. 1. Geometry of the first (left) and the second (right) benchmark

of 90,112 cores. Theoretical peak performance is around 800 Tflops. Each 16-core processor shares 16Gb of memory.

5 Conclusion

We have presented our parallel implementations of TFETI based solvers. At this moment the implementation in PETSc is capable of solving larger problems thanks to the usage of MUMPS solver for the solution of the coarse problem. One of the goals for future is its usage also in the Trilinos implementation.

Table 2. Performance of the Total FETI implementation for varying decomposition and discretization for the second benchmark

Number of subdom.	102	1024	5012
Number of cores	102	1024	5012
Primal dimension	2,520,240	2,839,734	98,214,558
Dual dimension	152,826	472,320	13,395,882
Kernel dimension	612	6,048	30,072
PETSc			
K factorization	114	1.2	134
CG time	42.7	10.0	217
- of which Q act.	3.5	5.6	180
CG iterations	221	169	176
Time per iteration	0.19	0.06	1.23
Total time	158.0	12.1	356

Acknowledgements

This paper has been elaborated in the framework of the project SPOMECH - Creating a multidisciplinary R&D team for reliable solution of mechanical problems, reg. no.

CZ.1.07/2.3.00/20.0070 supported by Operational Programme 'Education for competitiveness' funded by Structural Funds of the European Union and state budget of the Czech Republic.

The research has also been supported by the HPC-Europa programme funded under the European Commission Research Infrastructures activity of the Structuring the European Research Area programme (contract No. RII3-CT-2003-506079). The machine used for benchmarking is HECToR [11] in the UK which is part of the PRACE HPC ecosystem.

References

1. Hapla, V. and Horak, D.: "TFETI coarse space projectors parallelization strategies", to appear in proceedings of PPAM 2011, Springer LNCS series
2. Kozubek, T., Vondrak, V., Mensik, M., Horak, D., Dostal, Z., Hapla, V., Kabelikova, P., Cermak, M.: "Total FETI domain decomposition method and its massively parallel implementation", *Advances in Engineering Software*, submitted
3. Dostal, Z., Horak, D. and Kucera, R.: "Total FETI – an easier implementable variant of the FETI method for numerical solution of elliptic PDE", *Commun. in Numerical Methods in Engineering* 22, 2006, 1155-1162.
4. Farhat, C., Roux, F.-X., "An unconventional domain decomposition method for an efficient parallel solution of large-scale finite element systems", *SIAM Journal on Scientific Computing* 13, 1992; 379-396
5. Farhat, C., Mandel, J., Roux, F.-X., "Optimal convergence properties of the FETI domain decomposition method", *Comput. Methods Appl. Mech. Eng.* 115, 1994; 365–385.
6. Dostal, Z., Kozubek, T., Brzobohaty, T., Markopoulos, A., Vondrak, V., Horyl, P.: "Theoretically supported scalable TFETI algorithm for the solution of multibody 3D contact problems with friction", *Computer Methods in Applied Mechanics and Engineering*, 2011.
7. Dostal, Z., Kozubek, T.: "An optimal algorithm and superrelaxation for minimization of a quadratic function subject to separable convex constraints with applications", *Mathematical Programming*, 2011.
8. Dostal, Z., Kozubek, T., Brzobohaty, T., Markopoulos, A., Vondrak, V., Horyl, P.: "Theoretically supported scalable TFETI algorithm for the solution of multibody 3D contact problems with friction", *Computer Methods in Applied Mechanics and Engineering*, accepted 2011.
9. "PETSc Web page, 2011". <http://www.mcs.anl.gov/petsc>
10. "The Trilinos Project web page, 2011". <http://trilinos.sandia.gov/>
11. "HECToR Home Page", <http://www.hector.ac.uk/>
12. "Total-FETI Massively Parallel Implementation Research Group", <http://spomech.vsb.cz/feti/>

Numerical Solution of Stokes – Brinkman Equations Using the Mixed Finite Element Method

Martin Hasal and Pavel Burda

Department of Applied Mathematics, FEECS,
VŠB – Technical University of Ostrava, 17. listopadu 15, 708 33 Ostrava – Poruba
`martin.hasal@vsb.cz`, `pavel.burda@fs.cvut.cz`

Abstract There exist several ways how to model flow in porous media with fractures. One approach is to use Stokes-Brinkman equations. The base of this approach will be shown in this paper. These equations allow to model fluid flow in porous media such as rock as well as free flow regions (fractures, caves) in a single system of differential equations. For numerical simulations it is used mixed finite element method with Taylor-Hoods Elements. The numerical experiments are presented at the last part of the paper.

Key words: porous media, fracture, Darcy's equation, Stokes' equation, Stokes-Brinkman equation

1 Introduction

Naturally fractured porous media in geology are characterized by a wide range of length scales. The presence of fractures and caves at multiple scales is shown in Figure 1. These domains can be described, at each individual scale, as an ensemble of porous media, with well defined properties (porosity and permeability) and free flow region. It is straightforward, that the main problem is the co-existence of porous and free flow regions, typically at several scales. The next problem is probably existence fractures and long range caves which can form various types of connected networks which change the effective permeability of the media by orders of magnitudes. The fill (gravel, sand etc.) and presence of damage at the interface between porous media and caves or free flow regions presents another important problem in real simulations. Typically, porous media with fracture is described using both Stokes' and Darcy's equations. Stokes' equations represent Stokes's flow. Darcy's equation describes the flow of a fluid through a porous medium. Stokes-Brinkman equations can reduced Stokes or Darcy equations by appropriate choice of the parameters, in other words Stokes-Brinkman equations allow to represent porous media such as rock as well as free flow regions (fractures, caves) in a single system of differential equations.

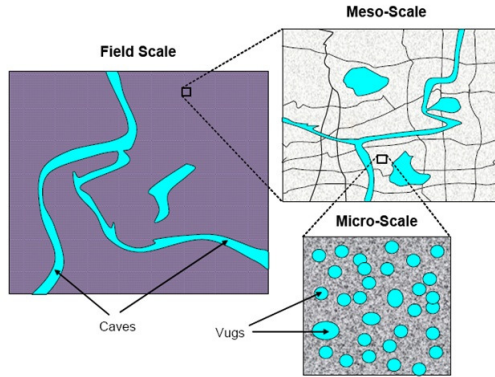


Figure 1. Conceptual model of a fractured and free flow regions at multiple scales, from [2]

2 Mathematical model

In this paper, we consider the following model equations on a bounded, connected, and polygonal domain $\Omega \subset \mathbb{R}^n$, where $n = 2, 3$. Next we denote free flow domain Ω_f (vugs, caves, fractures) and porous part Ω_p (effective media with certain permeability and porosity). In the problems of fluid flow two physical variables are needed, where one depends on the other. The first one is velocity \mathbf{u} (vector), which represent the actual physical velocity of the fluid in the free flow domains Ω_f , but in the porous domains Ω_p represents the Darcy (or averaged) velocity. The second one variable is pressure p (scalar). External forces denotes the \mathbf{f} (vector), for example gravitation, centrifugal force etc.

2.1 Stokes-Brinkman model

The Stokes-Brinkman equation for a single phase flow in a porous/free flow media is written as follows

$$\begin{aligned} \nu \mathbf{K}^{-1} \mathbf{u} + \nabla p - \nu^* \Delta \mathbf{u} &= \mathbf{f} && \text{in } \Omega, && (1) \\ \nabla \cdot \mathbf{u} &= 0 && \text{in } \Omega, && (2) \end{aligned}$$

where ν^* is the effective viscosity and ν - the physical viscosity is a material constant that defines the fluid under consideration (e.g., water, oil, etc.) and in this paper it is a uniform constant in the entire domain Ω . \mathbf{K} is a permeability tensor, which in Ω_p is equal to the Darcy permeability of the porous media. In [3] is shown, that Stokes-Brinkman equation with the choice $\nu^* = \nu$ in the porous region is very close to the solution of coupled Stokes and Darcy's equations.

The advantage of Stokes-Brinkman model is usage of uniform equations for porous and free flow domains. Boundary conditions between these two domains are represented by \mathbf{K} . This approach makes it possible to model heterogeneous material. Moreover, by a numerical point of view, it is easier to solve a monolithic system such as Stokes-Brinkman, in contrast to a coupled Darcy-Stokes system

which requires an additional iterative scheme. Also, near the interface, Stokes-Brinkman equations allow us to avoid the typical grid refinement issues necessary for solving the interface between Darcy and Stokes region. Disadvantage of this approach is usage of Taylor-Hood’s element for all domain, in other words, big load for memory.

3 Weak formulation of Stokes-Brinkman equations

From weak formulation stems from of the Stokes-Brinkman equation system (1) and (2). Then the problem is Find $\mathbf{u} \in \mathbf{H}_E^1$ and $p \in L^2(\Omega)$ such that

$$\mu^* \int_{\Omega} \nabla \mathbf{u} : \nabla \mathbf{v} + \mu \int_{\Omega} \mathbf{u} G \mathbf{v} - \int_{\Omega} p \nabla \cdot \mathbf{v} = \int_{\Omega_N} \mathbf{s} \cdot \mathbf{v} \quad \forall \mathbf{v} \in \mathbf{H}_{E_0}^1, \tag{3}$$

$$\int_{\Omega} q \nabla \cdot \mathbf{u} = 0 \quad \forall q \in L_2(\Omega). \tag{4}$$

where $\mathbf{K}^{-1} = G$ and for all \mathbf{v} and q from suitably chosen spaces of test functions. Equations (3) and (4) together with the boundary condition (7) lead to the following velocity solution and test spaces

$$\mathbf{H}_E^1 := \{ \mathbf{u} \in H^1(\Omega)^n \mid \mathbf{u} = \mathbf{w} \text{ na } \partial\Omega_D \}, \tag{5}$$

$$\mathbf{H}_{E_0}^1 := \{ \mathbf{v} \in H^1(\Omega)^n \mid \mathbf{v} = \mathbf{0} \text{ na } \partial\Omega_D \}, \tag{6}$$

Recall that, $\partial\Omega = \partial\Omega_D \cup \partial\Omega_N$, given by

$$\mathbf{u} = \mathbf{w} \text{ on } \partial\Omega_D, \quad \frac{\partial \mathbf{u}}{\partial n} - \mathbf{n} p = \mathbf{s} \text{ on } \partial\Omega_N, \tag{7}$$

where \mathbf{n} is the outward-pointing normal to the boundary, and $\partial \mathbf{u} / \partial n$ denotes the directional derivative in the normal direction. More information can be found in [4].

4 Approximation using mixed finite elements

From theory of finite element method [1], we replace the spaces $\mathbf{H}_{E_0}^1$ and $L^2(\Omega)$, theirs finite dimensional subspaces $\mathbf{X}_0^h \subset \mathbf{H}_{E_0}^1$ a $M^h \subset L_2(\Omega)$. Specifically, given a velocity solution space \mathbf{X}_E^h , the discrete problem is find: $\mathbf{u} \in \mathbf{X}_E^h$ and $p \in M^h$ such that

$$\nu^* \int_{\Omega} \nabla \mathbf{u} : \nabla \mathbf{v} + \nu \int_{\Omega} \mathbf{u} G \mathbf{v} - \int_{\Omega} p \nabla \cdot \mathbf{v} = \int_{\Omega_N} \mathbf{s} \cdot \mathbf{v} \quad \forall \mathbf{v} \in \mathbf{X}_0^h, \tag{8}$$

$$\int_{\Omega} q \nabla \cdot \mathbf{u} = 0 \quad \forall q \in M^h. \tag{9}$$

Note, $\mathbf{u} \in \mathbf{X}_E^h$ here is another, then $\mathbf{u} \in \mathbf{H}_E^1$ above this section. $\mathbf{u} \in \mathbf{H}_E^1$ is the rigorous solving, but $\mathbf{u} \in \mathbf{X}_E^h$ is the exact solution only in nodes of discretization

and between this nodes approximation is used. The difference between these solutions develops the theory of errors etc. For us it is just good to remember that, there is a difference between these rates. The same applies to the pressure.

From theory of the Galerkin finite element method, we need a finite n - dimensional vector space of test functions $\{\phi_1, \phi_2, \dots, \phi_n\}$, which create a convenient basis above introduced spaces. We extend this basis set by defining additional functions $\{\phi_{n+1}, \phi_{n+2}, \dots, \phi_{n+n_\partial}\}$, so that the function $\sum_{j=n+1}^{n+n_\partial} \mathbf{u}_j \phi_j$ interpolates the boundary data \mathbf{w} on $\partial\Omega_D$. And so

$$\mathbf{u}_h = \sum_{j=1}^{n_u} u_j \phi_j + \sum_{j=n_u+1}^{n_u+n_\partial} u_j \phi_j, \tag{10}$$

where $\{\phi_j\}$ is vector of basis functions (for velocity) and $\sum_{j=1}^{n_u} u_j \phi_j \in \mathbf{X}_0^h$. Introducing a set of scalar (pressure) basis functions $\{\psi_j\}$, and setting

$$p_h = \sum_{k=1}^{n_p} p_k \psi_k, \tag{11}$$

we find that the discrete formulation (8) and (9) can be expressed as a system of linear equations

$$\begin{bmatrix} \mathbf{A} & B^T \\ B & 0 \end{bmatrix} \begin{bmatrix} \mathbf{u} \\ \mathbf{p} \end{bmatrix} = \begin{bmatrix} \mathbf{f} \\ \mathbf{g} \end{bmatrix}. \tag{12}$$

The entries are given by

$$\mathbf{A} = [a_{ij}], \quad a_{ij} = \nu^* \int_{\Omega} \nabla \phi_i : \nabla \phi_j + \nu \int_{\Omega} \phi_i G \phi_j, \tag{13}$$

$$B = [b_{kj}], \quad b_{kj} = - \int_{\Omega} \psi_k \nabla \cdot \phi_j, \tag{14}$$

for $i, j = 1, \dots, n_u$ and $k = 1, \dots, n_p$. The entries of the right-hand side vector are

$$\mathbf{f} = [\mathbf{f}_i], \quad \mathbf{f}_i = \int_{\partial\Omega_N} \mathbf{s} \cdot \phi_i - \sum_{j=n_u+1}^{n_u+n_\partial} u_j \nu^* \int_{\Omega} \nabla \phi_i : \nabla \phi_j, \tag{15}$$

$$\mathbf{g} = [\mathbf{g}_k], \quad \mathbf{g}_k = \sum_{j=n_u+1}^{n_u+n_\partial} u_j \int_{\Omega} \psi_k \nabla \cdot \phi_j, \tag{16}$$

and the solution \mathbf{u}_h a p_h obtained by substituting the solution vectors $\mathbf{u} \in \mathbb{R}^{n_u}$ a $p_h \in \mathbb{R}^{n_p}$ into (10) and (11) is the **mixed finite element solution**.

4.1 Stable rectangular elements $\mathbf{Q}_2 - \mathbf{Q}_1$

Only a few words about $\mathbf{Q}_2 - \mathbf{Q}_1$ ¹ elements, these elements confirm the discrete Ladyzhenskaya-Babuška-Breezi² condition, therefore *stable* elements. A

¹ Often referred to in the literature as the TaylorHood elements and TaylorHood method.

² Often referred to in the literature as (LBB) or inf-sup condition.

rectangular elements because in this article is considered only regular network is considered (Figure 4.1)

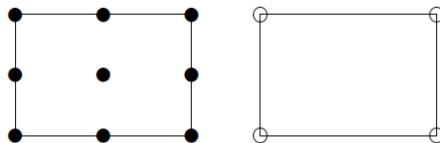


Figure 2. $Q_2 - Q_1$ element (• two velocity components, ◦ pressure).

5 Numerical results - Numerical Solution in 2D

All numerical tests was provided in MATLAB enviroment (R2011a, 64bit), from meshing to drawing picture of solution. **Example 1** is depicted in Figure 3, together with fluid and porous parameters. The solution of the Example 1 is depict in Figure 4.

The solution of **Example 2** is depicted in Figure 7, and has the same parameters as the first example. The difference between the Examples 1 is in two free fluid regions. First rectangular free fluid region is on coordinate $\langle 0.2, 0.4 \rangle \times \langle 0.2, 0.4 \rangle$ and the second region is on coordinate $\langle -0.2, -0.4 \rangle \times \langle -0.2, -0.4 \rangle$.

In the **Example 3** permeability tensor is set up in agreement with Figure 6. The solution is depicted in Figure 7.

6 Discussion and Summary

In this paper was considered the Stokes-Brinkaman equation as model for flows in porous media. Mixed finite element method was used to solve isolated free flow region in porous region. It was shown, that the Stokes-Brinkaman equation allows the simulation in a sense of natural flow. In this paper was consider example, where the permeability tensor was set up in agreement with CT scan of rock. The results of this paper was compared with [3] and their results have very similar output.

7 Acknowledgments

Author would like to thank prof. Pavel Burda and prof. Radim Blaheta for valuable discussion and comments.

References

1. ELMAN, H. C. - SILVESTER, D. J. - WATHEN, A. J. *Finite elements and fast iterative solvers: with applications in incompressible fluid dynamics*. Numerical Mathematics and Scientific Computation, Oxford University Press, New York, 1994.

2. P. POPOV, Y. EFENDIEV, G. QIN, Multiscale Modeling and Simulations of Flows in Naturally Fractured Karst Reservoirs, *Global Science Preprint*.
3. P. POPOV, L. BI, Y. EFENDIEV, R. E. ERVING, G. QIN, Multi-physics and multi-scale methods for modeling fluid flow through naturally-fractured vuggy carbonate reservoirs, *SPE International*. SPE 105378
4. X. XIE, J. XU, G. XUE, Uniformly-stable finite element method for Darcy-Stokes-Brinkman models, *Journal of Computational Mathematics*, Vol.26, No.3, 2008, 437455.
5. M. KROTKIEWSKI, I. S. LIGAARDEN, K-A. LIE, D. W. SCHMID, On the Importance of the Stokes-Brinkman Equations for Computing Effective Permeability in Carbonate Karst Reservoirs, *Global Science Preprint*.

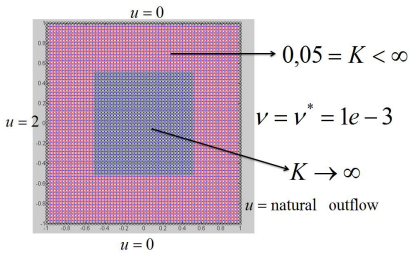


Figure 3. Domain distribution and material properties of Example.1

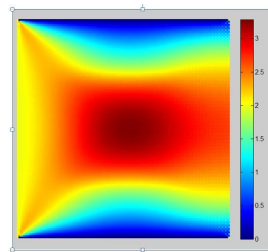


Figure 4. Absolute value of velocity at each element of the mesh from Example.1

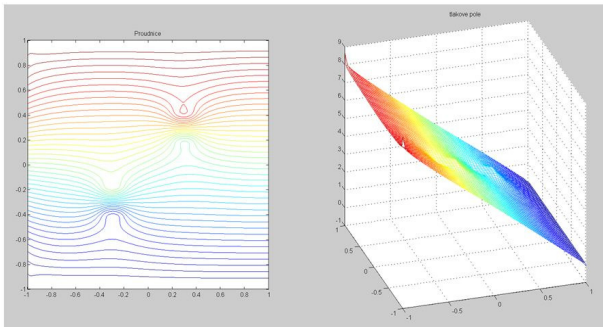


Figure 5. Streamlines and pressure field for Example.2

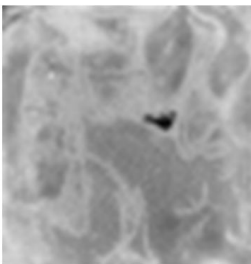


Figure 6. CT scan of rock

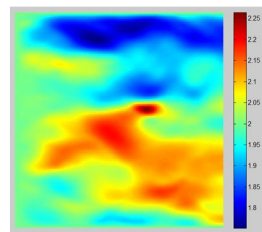


Figure 7. Absolute value of velocity at each element of the mesh from Example.4

Preconditioning for Block Matrices and Applications

Rostislav Hrtus, Radim Blaheta, and Petr Byczanski

Department of Applied Mathematics, FEECS,
VŠB – Technical University of Ostrava, 17. listopadu 15, 708 33 Ostrava – Poruba
Institute of Geonics of the Academy of Sciences of the Czech Republic, Ostrava,
Studentská 1768, 708 00 Ostrava – Poruba
{hrtus, blaheta, byczanski}@ugn.cas.cz

Abstract. The paper concerns testing of preconditioners for block matrices arising in poroelasticity as well as discussion about their implementation in C++ with the usage of Trilinos library.

1 Introduction

The motivation for solving poroelasticity problems is the modelling of porous media behaviour in geo-applications or bio-engineering, cf. e.g. [7] and [2]. Since the model couples the flow with mechanics, we obtain block structured system of equations.

In this paper, we firstly describe the problem of poroelasticity leading to block saddle point structured matrices, which we want to precondition in some specific and effective way. Secondly we discuss the implementation of selected preconditioners including effective implementation using Trilinos library and provide some numerical results for a model problem.

2 Poroelasticity

We consider flow in deformable porous elastic media and describe poroelasticity as a coupled model of elasticity and single phase Darcy flow. Then we focus on solving large linear systems which are obtained from discretization of poroelasticity problems. Our model problem also consider possible heterogeneity in permeability of the porous material.

Note that we assume that the porous space is fully saturated by fluid and that the fluid is of a constant temperature. Porous material is of elastic type. Laminar flow follows from the Darcy model.

We solve an elasticity problem

$$- \operatorname{div} \underline{\sigma} = F,$$

where σ is the stress tensor and F represents density of forces. In the case of isotropic elasticity and pore pressure p , we get modified Navier–Lamé elasticity equations.

$$-\operatorname{div}(\mu(\nabla u + \nabla^T u)) - \nabla(\lambda \operatorname{div} u) + \nabla(c_{up}p) = F, \tag{1}$$

where u are displacements, p pressures and c_{up} is a constant dependent on the bulk modulus expressing contribution of pressures into displacements.

We couple the above equation (1) with the Darcy flow in the following form

$$\begin{cases} K^{-1}v - \nabla p = 0 \\ \frac{\partial \zeta}{\partial t} - \operatorname{div}(v) = S \\ \zeta = c_{pu} \operatorname{tr}(\epsilon) + c_{pp}p = c_{pu} \operatorname{div}(u) + c_{pp}p \end{cases}, \tag{2}$$

where K is the symmetric hydraulic conductivity tensor, v are the fluid velocities (fluxes). ζ is measure of fluid content (ratio of fluid volume per unit volume of the porous material), S denotes the fluid source/sink, c_{pu} and c_{pp} are positive constants, ϵ are deformations.

The poroelasticity problem can be formulated in terms of u, v, p and discretized using standard linear finite elements for elasticity, lowest order Raviart–Thomas elements for flow and the backward Euler method in time. In the time discretization steps, it provides the FE system in the following block form

$$\mathcal{A} \begin{pmatrix} u \\ v \\ p \end{pmatrix} = \begin{pmatrix} A & B_{up}^T \\ & M & B_{vp}^T \\ B_{up} & B_{vp} & -D \end{pmatrix} \begin{pmatrix} u \\ v \\ p \end{pmatrix} = \begin{pmatrix} F \\ 0 \\ -S \end{pmatrix}, \tag{3}$$

The details can be found in [2]. Note that, we assume that \mathcal{A} is symmetric, regular, indefinite, A, M and D are symmetric and positive definite, D is diagonal.

The system (3) can be solved iteratively with a suitable preconditioner. There are various types of preconditioners (Jacobi etc.), but here we introduce preconditioners based on the block structure of the linear system (3). We use partial elimination of variables for constructing Schur complement. Important question is which variable do we want to eliminate within the Schur complement.

The first type of preconditioners is diagonal preconditioner P_{1D} introduced and analyzed in [6] and its triangular variant P_{1T} , see [1]. These preconditioners have the following form

$$P_{1D} = \begin{pmatrix} A & & \\ & M & \\ & & S1 \end{pmatrix}, \quad P_{1T} = \begin{pmatrix} A & B_{up}^T \\ & M & B_{vp}^T \\ & & S1 \end{pmatrix}. \tag{4}$$

where $S1 = D + B_{vp}(\operatorname{diag}(M))^{-1}B_{vp}^T$ is a negative Schur complement with respect to fluxes. This $S1$ is an approximate Schur complement to the exact negative Schur complement $S = D + B_{vp}(M)^{-1}B_{vp}^T + B_{up}(A)^{-1}B_{up}^T$.

Another choice is to use different preconditioner based on elimination of pressures instead. This gives us inexpensive computation of the Schur complement,

as it would be seen further and we do not make any approximation of Schur complement beside inexact solution of the Schur complement systems. The papers [2] and [5] introduce block diagonal preconditioner and it's triangular variant

$$P_{2D} = \begin{pmatrix} S_{11} & S_{21} & \\ S_{12} & S_{22} & \\ & & -D \end{pmatrix}, \quad P_{2T} = \begin{pmatrix} S_{11} & S_{21} & B_{up} \\ S_{12} & S_{22} & B_{vp} \\ & & -D \end{pmatrix}, \quad (5)$$

where the Schur complements have in the both cases the following form

$$S_2 = \begin{pmatrix} S_{11} & S_{21} \\ S_{12} & S_{22} \end{pmatrix} = \begin{pmatrix} A & \\ & M \end{pmatrix} + \begin{pmatrix} B_{up}^T D^{-1} B_{up} & B_{up}^T D^{-1} B_{vp} \\ B_{vp}^T D^{-1} B_{up} & B_{vp}^T D^{-1} B_{vp} \end{pmatrix} \quad (6)$$

We can use those preconditioners directly, but it could be expensive. We precondition the Schur complement part S_2 to solve linear system from P_{2D} or P_{2T} more efficiently by CG with the preconditioners $P_{P_{2a}}$ or $P_{P_{2b}}$ defined in the following way

$$P_{2a} = \begin{pmatrix} A & \\ & M \end{pmatrix} \quad P_{2b} = P_{2a} + \begin{pmatrix} B_{up}^T D^{-1} B_{up} & \\ & B_{vp}^T D^{-1} B_{vp} \end{pmatrix}. \quad (7)$$

3 Model problem

As in [2] we consider an academic poroelasticity problem in the domain $\Omega = \langle 0, 1 \rangle \times \langle 0, 1 \rangle$, see Fig. (1). The material properties are hypothetic here. The elastic part uses homogenized properties given by the elastic modulus $E = 10$ and Poisson's ratio $\nu = 0.25$ in the whole domain Ω . The flow part assumes possible heterogeneity with the permeability coefficient k , which has a random character. We shall assume that, for all $x \in \Omega$, the quantity

$$z(x) = \log k(x)$$

has a normal distribution with the mean value $\mu = 0$ and variance $\tilde{\sigma}$. This stochastic microstructure problem enables us to investigate the robustness of iterative methods with respect to oscillations in the PDE's coefficient.

$$\begin{array}{ccc} \sigma \cdot \underline{\nu} = 0, & & \\ \underline{\nu} \cdot \underline{\nu} = 0 & & \\ \underline{u} \cdot \underline{\nu} = 0, \sigma_t = 0 & \square_{\Omega} & \underline{u} \cdot \underline{\nu} = 0, \sigma_t = 0 \\ p = 1 & & p = 0 \\ \sigma \cdot \underline{\nu} = 0, & & \\ \underline{\nu} \cdot \underline{\nu} = 0 & & \end{array}$$

Fig. 1. A unit square domain Ω and boundary conditions.

The elastic part uses zero volume force F and boundary conditions with zero pressure $\underline{\sigma} \cdot \underline{\nu}$ on one face of the boundary and zero normal displacement plus zero tangential stresses $\underline{\sigma}_t = 0$ on the rest of the boundary $\partial\Omega$. The flow part uses zero volume source S and the boundary conditions $p = 1$ on the left boundary $\{x : x_2 = 0\}$, $p = 0$ on the right boundary $\{x : x_2 = 1\}$ and zero normal flux $\underline{v} \cdot \underline{\nu} = 0$ on the rest of the boundary $\partial\Omega$.

The elastic part is discretized by the finite element method on a regular grid Ω_h created by a division of Ω into $1/h^2$ small congruent squares and subsequent division of the squares into triangles. Then, the linear Courant elements are used. The flow part is discretized by a mixed finite element method on the same triangular grid with the lowest order Thomas-Raviart finite elements.

It is also possible to use a 3D variant of this model problem.

4 Implementation of P_{2D} and P_{2T} preconditioners

The general scheme for implementation of the preconditioners P_{2D} and P_{2T} has three levels with different iterations.

1. *level of outer iterations.* We solve the system (3) with the block matrix by flexible GMRES [9]. Within each iteration we apply (inexactly) P_{2D} or P_{2T} as a right preconditioner.
2. *intermediate level.* The application of the right preconditioner P_{2D} or P_{2T} in each flexible GMRES iteration means to solve the system $P_{2D}z = v$ or $P_{2T}z = v$, respectively, see [9]. As D is diagonal, this solution reduces in both cases to the solution of system $S_2\bar{z} = \bar{v}_0$. There \bar{v} , \bar{z} denote vectors created by the first two blocks of v , z , $\bar{v}_0 = \bar{v}$ for P_{2D} , whereas \bar{v}_0 contains a modification of \bar{v} for P_{2T} . The system $S_2\bar{z} = \bar{v}_0$, with S_2 described in (6), is solved by inner iterations with accuracy ε_1 . The big advantage is that the matrix S_2 has not to be formed explicitly, only matrix by vector multiplication with S_2 described in (6) has to be implemented. Flexible variant of GMRES on level 1, allows even a very crude solution of the system with S_2 , see Tab. 1. As S_2 is symmetric and positive definite, we can use the CG method or better its flexible variants (e.g. [3] and the references therein) for inner iteration. Within each inner iteration, we apply a left preconditioner.
3. *innermost level.* The application of the preconditioners P_{2a} or P_{2b} from (7) requires the solution of two systems. Note that both these systems are again symmetric and positive definite. For P_{2a} , we have two systems with already assembled matrices, but the efficiency of P_{2a} is low. For application of P_{2b} preconditioner, we have not assembled the matrices (matrix free implementation) if we again solve these systems iteratively, now with an inner-inner iterative method accuracy ε_2 . But there is a further discussed question how to get an efficient preconditioner for the inner-inner iterations.

The above computing scheme was used for development of a test code in MATLAB. It uses FGMRES in the outer iterations and standard CG with P_{2b}

preconditioner for inner iterations. In the innermost level, we assembly the diagonal systems for P_{2b} and solve them either directly (using the backslash solver) or by application of an inner-inner CG method with incomplete Choleski factorization preconditioners. The performance of such method applied to the described model problem, namely numbers of outer and inner iterations, can be seen in Table 1.

Table 1. Numbers of iterations for solving the model problem with accuracy $\varepsilon = 10^{-6}$. Columns 2D and 2T provide numbers of outer iterations for P2D and P2T preconditioners, columns (ii) provide total sums of the corresponding inner iterations. The rows correspond to heterogeneity with variance $\bar{\sigma} = 0, 1, 2$.

$\bar{\sigma}$	preconditioner $\varepsilon_1 = 10^{-6}$				preconditioner $\varepsilon_1 = 10^{-4}$				preconditioner $\varepsilon_1 = 10^{-2}$			
	2D	ii	2T	ii	2D	ii	2T	ii	2D	ii	2T	ii
0	8	784	2	200	8	557	4	908	11	413	6	179
1	8	1265	2	324	8	892	4	411	11	667	6	329
2	8	1706	3	641	8	491	4	565	11	834	6	423

Note that the blocks in P_{2b} are solved by the inner-inner preconditioned CG iterations with accuracy $\varepsilon_2 = 10^{-6}$. Here we use the incomplete Choleski preconditioner defined by drop tolerance 0.0005 and diagonal compensation by 10^{-5} for the elasticity block and $5 \cdot 10^{-4}$ for the second block corresponding to fluxes. We can see relatively small numbers of outer iterations (2 outer iterations for exact P_{2D} are confirmed by the theory). We can see that the dependency on the inner accuracy ε_1 is not too high, which favourite to use a lower accuracy ε_1 in computations. Note that more numerical experiments are planned and will be reported elsewhere.

To solve large scale 3D problems, we attempt to implement the above scheme with the aid of C++ and Trilinos library. This way of implementation is supported by a collaboration with P. Arbenz and E. Turan from ETH Zurich with a possibility to use their code PorFE, which implements 3D poroelasticity with preconditioners P_{1D} , P_{1T} , see [1].

PorFE implements the blocks of the matrix (3) as follows:

- the elasticity matrix A is implemented with 3×3 blocks as a Epetra_RowMatrix,
- the matrices M , B_{up} and B_{vp} are implemented as Epetra_CrsMatrix,
- the diagonal matrix D is implemented as Epetra_Vector.

This storage provides possibility to implement matrix by vector multiplication with \mathcal{A} in the outer iterations. The preconditioner is defined as an Epetra.Operator. For inner iterations the matrix by vector multiplication can be implemented with usage of the blocks stored as above. The remaining question

is how to implement solution of systems with matrices

$$A + B_{up}^T D^{-1} B_{up} \text{ and } M + B_{vp}^T D^{-1} B_{vp}. \quad (8)$$

The possible way is in simplification of the first matrix to A (some support for this and an alternative view can be found in [4]) and handling the second system similarly as for $S1$ in (4).

Trilinos provides us also parallelization, which we do not have to take care about during the implementation, but we have to take care about distribution of vectors and matrices in meaning of splitting data into as many parts as many processes we run.

5 Conclusions

In this paper we discussed the solution of poroelasticity problems with special block structured matrix preconditioners. We showed how to choose and implement such preconditioners based on Schur complements.

Acknowledgements

The reported work received funding from IT4Innovations Centre of Excellence, reg. no. CZ.1.05/1.1.00/02.0070 and SPOMECH, reg. no. CZ.1.07/2.3.00/20.0070 projects supported by Operational Programme Research and Development for Innovations funded by Structural Funds of the European Union and state budget of the Czech Republic. The collaboration with P. Arbenz and E. Turan from ETH Zurich is greatly acknowledged. A stay of the first author in Zurich was possible owing to project CZ.1.07/2.4.00/31.0035.

References

1. Arbenz, P., Turan, E.: Preconditioning for large scale micro finite element analysis of 3D poroelasticity. Conference PMAA 2012
2. Axelsson, O., Blaheta R., Byczanski P.: An efficient preconditioner for saddle point type matrices arising in poroelasticity problems, submitted (2012)
3. Blaheta R.: GPCG-generalized preconditioned CG method and its use with non-linear and non-symmetric displacement decomposition preconditioners. Numerical Linear Algebra with Applications, Volume 9, Issue 6-7, pages 527-550 (2002)
4. Blaheta R., Axelsson, O., Byczanski P., Hrtus R.: Block factorization based preconditioners with applications. GAMM Workshop on Applied and Numerical Linear Algebra, Liblice (2012)
5. Ferronato, M., Castelletto, N., Gambolati, G.: A fully coupled 3-D mixed finite element model of Biot consolidation. Journal of computational physics 229, 4813-4830, (2010)
6. Lipnikov, K.: Numerical Methods for the Biot Model in Poroelasticity. Ph. D. Thesis, University of Houston, (2002)
7. ParFE (<http://parfe.sourceforge.net>)
8. The Trilinos Project Home Page, <http://trilinos.sandia.gov/>
9. Saad, Y.: Iterative methods for sparse linear systems. SIAM Philadelphia, 2003

Hybrid Total FETI Method

Marta Jarošová¹, Tomáš Kozubek^{1,2},
Martin Menšík^{1,2}, and Alexandros Markopoulos¹

¹Centre of Excellence IT4Innovations

²Department of Applied Mathematics, FEECS,
VŠB – Technical University of Ostrava, 17. listopadu 15, 708 33 Ostrava – Poruba
{marta.jarosova, tomas.kozubek, martin.mensik,
alexandros.markopoulos}@vsb.cz

Abstract. We describe a hybrid FETI (Finite Element Tearing and Interconnecting) method based on our variant of the FETI type domain decomposition method called Total FETI. In our approach a small number of neighboring subdomains is aggregated into the clusters, which results into the smaller coarse problem. To solve the original problem Total FETI method is applied twice: to the clusters and then to the subdomains in each cluster. This approach simplifies implementation of hybrid FETI methods and enables to extend parallelization of the original problem up to tens of thousands of cores due to the coarse space reduction and thus less memory requirements. The performance is demonstrated on a linear elasticity benchmark.

1 Introduction

The goal of this paper is to describe a hybrid FETI method based on our variant of the FETI type domain decomposition method called Total FETI [5].

The original FETI algorithm, where only the favorable distribution of the spectrum of the dual Schur complement matrix [2] was considered, was efficient only for a small number of subdomains. So it was later extended by introducing a natural coarse problem [3, 4], whose solution was implemented by auxiliary projectors so that the resulting algorithm became in a sense optimal [3, 4].

In Total FETI method [5] also the Dirichlet boundary conditions are enforced by Lagrange multipliers. Hence all subdomain stiffness matrices are singular with à-priori known kernels which is a great advantage in the numerical solution. With known kernel basis we can regularize effectively the stiffness matrix [6] and use any standard Cholesky type decomposition method for nonsingular matrices.

Even if, there are several efficient coarse problem parallelization strategies [7], still there are size limitations of the coarse problem. So several hybrid (multilevel) methods were proposed [9]. The key idea is to aggregate small number of neighboring subdomains into the clusters, which naturally results into the smaller coarse problem. In our Hybrid Total FETI, the aggregation of subdomains into

the clusters is enforced again by Lagrange multipliers. Thus Total FETI method is used on both cluster and subdomain levels. This approach simplifies implementation of hybrid FETI methods and enables to extend parallelization of the original problem up to tens of thousands of cores due to less memory requirements. This is positive effect of reducing the coarse space. The negative one is getting worse convergence rate comparing with the original TFETI.

2 Hybrid Total FETI

Let us consider the problem of linear elasticity. To apply H-TFETI approach to solve the problem, we first of all tear the body from the part of the boundary with the Dirichlet boundary condition as in Total FETI approach. Then we decompose the body into the clusters and the clusters into the subdomains. Finally, we introduce new “gluing” conditions on the subdomain interfaces to ensure the continuity of the solution and on the boundaries with imposed Dirichlet data.

Let domain Ω be decomposed into N_c relatively large non-overlapping clusters of the diameter H_c and let each cluster be decomposed into N_s all floating non-overlapping subdomains of diameter H_s . The total number of subdomains is then $N = N_c \times N_s$. To ensure the continuity of the displacements and of their normal derivatives across the interface we have to introduce so called gluing conditions.

The resulting quadratic programming (QP) problem reads as

$$\min_{\mathbf{u}} \frac{1}{2} \mathbf{u}^\top \mathbf{K} \mathbf{u} - \mathbf{f}^\top \mathbf{u} \quad \text{subject to} \quad \mathbf{B} \mathbf{u} = \mathbf{c}, \tag{1}$$

where

$$\mathbf{K} = \begin{bmatrix} \mathbf{K}^1 & & & \\ & \mathbf{K}^2 & & \\ & & \ddots & \\ & & & \mathbf{K}^N \end{bmatrix} \tag{2}$$

denotes a symmetric positive semidefinite stiffness matrix of order n , \mathbf{B} denotes an $m \times n$ full rank constraint matrix, $\mathbf{f} \in \mathbb{R}^n$ is a load vector, and $\mathbf{c} \in \mathbb{R}^m$ is a constraint vector.

The fact that the blocks \mathbf{K}^i corresponding to Ω^i are positive semidefinite sparse matrices with kernel bases known a-priori enables us to regularize each block and then decompose it efficiently using the standard (sparse) Cholesky factorization for non-singular matrices [14]. The load vector \mathbf{f} describes the nodal forces arising from the volume forces and/or some other imposed traction.

The matrix $\mathbf{B} = [\mathbf{B}_g^\top, \mathbf{B}_D^\top]^\top \in \mathbb{R}^{m \times n}$ also called jump operator and the vector $\mathbf{c} = [\mathbf{o}^\top, \mathbf{c}_D^\top]^\top$ enforce the continuity at the interface variables and the Dirichlet data. Typically m , number of Lagrange multipliers, is much smaller than n , number of degrees of freedom. The matrix \mathbf{B} is constructed using values $\{-1, 0, 1\}$ in such a way, that the values of the solution \mathbf{u} associated with more than one subdomain coincide when $\mathbf{B}_g \mathbf{u} = \mathbf{o}$ and the values of the solution \mathbf{u} on

the boundary with the Dirichlet condition satisfy $\mathbf{B}_D \mathbf{u} = \mathbf{c}_D$. Let us note that \mathbf{B} can be directly assembled to have orthonormal rows by only special treating of the rows of \mathbf{B} corresponding to the nodes shared by more than two subdomains.

The problem (1) has the same structure as in standard Total FETI method and could be solved by this standard approach. However, to describe the H-TFETI method, we will consider the problem (1) in the form

$$\min \frac{1}{2} \mathbf{u}^\top \mathbf{K} \mathbf{u} - \mathbf{u}^\top \mathbf{f} \quad \text{subject to} \quad \begin{cases} \mathbf{B}_0 \mathbf{u} = \mathbf{c}_0 \\ \mathbf{B}_1 \mathbf{u} = \mathbf{c}_1 \end{cases}, \tag{3}$$

where the equality constraints are split up into two parts. The first part $\mathbf{B}_0 \mathbf{u} = \mathbf{c}_0 := \mathbf{o}$ consists of m_0 equalities enforcing the continuity in the subdomain corner nodes of each cluster, while $\mathbf{B}_1 \mathbf{u} = \mathbf{c}_1$ consists of m_1 equalities enforcing the continuity across the rest of the subdomain interfaces and the Dirichlet condition.

The KKT optimality conditions lead to the saddle point problem

$$\begin{bmatrix} \mathbf{K} & \mathbf{B}_0^\top & \mathbf{B}_1^\top \\ \mathbf{B}_0 & \mathbf{O} & \mathbf{O} \\ \mathbf{B}_1 & \mathbf{O} & \mathbf{O} \end{bmatrix} \begin{bmatrix} \mathbf{u} \\ \lambda_0 \\ \lambda_1 \end{bmatrix} = \begin{bmatrix} \mathbf{f} \\ \mathbf{c}_0 \\ \mathbf{c}_1 \end{bmatrix} \tag{4}$$

or

$$\begin{bmatrix} \tilde{\mathbf{K}} & \tilde{\mathbf{B}}^\top \\ \tilde{\mathbf{B}} & \mathbf{O} \end{bmatrix} \begin{bmatrix} \tilde{\mathbf{u}} \\ \tilde{\lambda} \end{bmatrix} = \begin{bmatrix} \tilde{\mathbf{f}} \\ \tilde{\mathbf{c}} \end{bmatrix}, \tag{5}$$

where $\tilde{\mathbf{K}}, \tilde{\mathbf{B}}, \tilde{\mathbf{u}}, \tilde{\lambda}, \tilde{\mathbf{f}}$, and $\tilde{\mathbf{c}}$ respect the block structure indicated in (4).

The first equation of the system (5) has a solution iff

$$\tilde{\mathbf{f}} - \tilde{\mathbf{B}}^\top \tilde{\lambda} \in \text{Im} \tilde{\mathbf{K}}, \tag{6}$$

which can be expressed more conveniently by means of a matrix $\tilde{\mathbf{R}}$ whose columns span the null space of $\tilde{\mathbf{K}}$ as

$$\tilde{\mathbf{R}}^\top (\tilde{\mathbf{f}} - \tilde{\mathbf{B}}^\top \tilde{\lambda}) = \mathbf{o}, \tag{7}$$

where

$$\tilde{\mathbf{R}} = \begin{bmatrix} \mathbf{R}_c^1 & & \\ & \ddots & \\ & & \mathbf{R}_c^{N_c} \\ \mathbf{O} & \mathbf{O} & \mathbf{O} \end{bmatrix} \quad \text{and} \quad \mathbf{R}_c^i = \begin{bmatrix} \mathbf{R}^{1,i} \\ \vdots \\ \mathbf{R}^{N_s,i} \end{bmatrix}, \tag{8}$$

with $\mathbf{R}^{p,i}$, $p = 1, \dots, N_s$ meaning the p th subdomain of the i th cluster. As the kernel bases of the subdomains are known à-priori, the blocks $\mathbf{R}^{p,i}$ may be assembled directly from the segments \mathbf{R}_k defined for the k th mesh node as follows

$$\mathbf{R}_k = \begin{bmatrix} 1 & 0 & -y_k \\ 0 & 1 & x_k \end{bmatrix} \text{ in 2D} \quad \text{and} \quad \mathbf{R}_k = \begin{bmatrix} 1 & 0 & 0 & 0 & -z_k & y_k \\ 0 & 1 & 0 & z_k & 0 & -x_k \\ 0 & 0 & 1 & -y_k & x_k & 0 \end{bmatrix} \text{ in 3D.} \tag{9}$$

In order to eliminate the primal variables $\tilde{\mathbf{u}}$ from the singular system given by the first equation in (5) we use a generalized inverse matrix $\tilde{\mathbf{K}}^+$ to $\tilde{\mathbf{K}}$ satisfying $\tilde{\mathbf{K}}\tilde{\mathbf{K}}^+\tilde{\mathbf{K}} = \tilde{\mathbf{K}}$. It may be easily verified that if $\tilde{\mathbf{u}}$ is a solution to the first equation of (5), then there exists a vector $\tilde{\boldsymbol{\alpha}}$ such that

$$\tilde{\mathbf{u}} = \tilde{\mathbf{K}}^+(\tilde{\mathbf{f}} - \tilde{\mathbf{B}}^\top \tilde{\boldsymbol{\lambda}}) + \tilde{\mathbf{R}}\tilde{\boldsymbol{\alpha}}. \tag{10}$$

Substituting (10) into the second equation of (5) and using (7), we get

$$\begin{bmatrix} \tilde{\mathbf{B}}\tilde{\mathbf{K}}^+\tilde{\mathbf{B}}^\top & -\tilde{\mathbf{B}}\tilde{\mathbf{R}} \\ -\tilde{\mathbf{R}}^\top \tilde{\mathbf{B}}^\top & \mathbf{O} \end{bmatrix} \begin{bmatrix} \tilde{\boldsymbol{\lambda}} \\ \tilde{\boldsymbol{\alpha}} \end{bmatrix} = \begin{bmatrix} \tilde{\mathbf{B}}\tilde{\mathbf{K}}^+\tilde{\mathbf{f}} - \tilde{\mathbf{c}} \\ -\tilde{\mathbf{R}}^\top \tilde{\mathbf{f}} \end{bmatrix}. \tag{11}$$

Let us introduce new notation

$$\begin{aligned} \tilde{\mathbf{F}} &= \tilde{\mathbf{B}}\tilde{\mathbf{K}}^+\tilde{\mathbf{B}}^\top, \quad \tilde{\mathbf{g}} = \tilde{\mathbf{B}}\tilde{\mathbf{K}}^+\tilde{\mathbf{f}} - \tilde{\mathbf{c}}, \\ \tilde{\mathbf{G}} &= -\tilde{\mathbf{R}}^\top \tilde{\mathbf{B}}^\top, \quad \tilde{\mathbf{e}} = -\tilde{\mathbf{R}}^\top \tilde{\mathbf{f}}, \end{aligned}$$

so that the system (11) reads as

$$\begin{bmatrix} \tilde{\mathbf{F}} & \tilde{\mathbf{G}}^\top \\ \tilde{\mathbf{G}} & \mathbf{O} \end{bmatrix} \begin{bmatrix} \tilde{\boldsymbol{\lambda}} \\ \tilde{\boldsymbol{\alpha}} \end{bmatrix} = \begin{bmatrix} \tilde{\mathbf{g}} \\ \tilde{\mathbf{e}} \end{bmatrix}. \tag{12}$$

As in standard TFETI we introduce orthogonal projector $\tilde{\mathbf{P}} = \mathbf{I} - \tilde{\mathbf{G}}^\top(\tilde{\mathbf{G}}\tilde{\mathbf{G}}^\top)^{-1}\tilde{\mathbf{G}}$ onto the kernel of $\tilde{\mathbf{G}}$. Applying $\tilde{\mathbf{P}}$ to (12) we get

$$\tilde{\mathbf{P}}\tilde{\mathbf{F}}\tilde{\boldsymbol{\lambda}} = \tilde{\mathbf{P}}\tilde{\mathbf{g}} \quad \text{subject to} \quad \tilde{\mathbf{G}}\tilde{\boldsymbol{\lambda}} = \tilde{\mathbf{e}} \tag{13}$$

and after homogenization of the constraints we get

$$\tilde{\mathbf{P}}\tilde{\mathbf{F}}\tilde{\boldsymbol{\lambda}}_{\text{Ker}} = \tilde{\mathbf{P}}(\tilde{\mathbf{g}} - \tilde{\mathbf{F}}\tilde{\boldsymbol{\lambda}}_{\text{Im}}) \quad \text{for} \quad \tilde{\boldsymbol{\lambda}}_{\text{Ker}} \in \text{Ker}\tilde{\mathbf{G}}, \tag{14}$$

where $\tilde{\boldsymbol{\lambda}}_{\text{Im}} = \tilde{\mathbf{G}}^\top(\tilde{\mathbf{G}}\tilde{\mathbf{G}}^\top)^{-1}\tilde{\mathbf{e}}$ and $\tilde{\boldsymbol{\lambda}} = \tilde{\boldsymbol{\lambda}}_{\text{Ker}} + \tilde{\boldsymbol{\lambda}}_{\text{Im}}$.

Lemma 1. *The matrix $\tilde{\mathbf{P}}\tilde{\mathbf{F}}$ is symmetric positive definite on $\text{Ker}\tilde{\mathbf{G}}$.*

Proof. Let $\boldsymbol{\mu} \in \text{Ker}\tilde{\mathbf{G}}$. Then $\mathbf{o} = \tilde{\mathbf{G}}\boldsymbol{\mu} = -\tilde{\mathbf{R}}^\top \tilde{\mathbf{B}}^\top \boldsymbol{\mu} = -\tilde{\mathbf{R}}^\top \mathbf{v}$, where $\mathbf{v} = \tilde{\mathbf{B}}^\top \boldsymbol{\mu}$. Hence $\mathbf{v} \in \text{Im}\tilde{\mathbf{B}}^\top \cap \text{Im}\tilde{\mathbf{K}}$. It is enough to show that $\sigma_{\min}(\tilde{\mathbf{P}}\tilde{\mathbf{F}}|_{\text{Ker}\tilde{\mathbf{G}}}) > 0$, where $\sigma_{\min}(\mathbf{X})$ denotes the smallest eigenvalue of \mathbf{X} . We get

$$\sigma_{\min}(\tilde{\mathbf{P}}\tilde{\mathbf{F}}|_{\text{Ker}\tilde{\mathbf{G}}}) = \min_{\substack{\boldsymbol{\mu} \in \text{Ker}\tilde{\mathbf{G}} \\ \boldsymbol{\mu} \neq \mathbf{o}}} \frac{\boldsymbol{\mu}^\top \tilde{\mathbf{P}}\tilde{\mathbf{F}}\boldsymbol{\mu}}{\boldsymbol{\mu}^\top \boldsymbol{\mu}} = \min_{\substack{\boldsymbol{\mu} \in \text{Ker}\tilde{\mathbf{G}} \\ \boldsymbol{\mu} \neq \mathbf{o}}} \frac{\boldsymbol{\mu}^\top \tilde{\mathbf{B}}\tilde{\mathbf{K}}^+\tilde{\mathbf{B}}^\top \boldsymbol{\mu}}{\boldsymbol{\mu}^\top \tilde{\mathbf{B}}\tilde{\mathbf{B}}^\top \boldsymbol{\mu}} \cdot \frac{\boldsymbol{\mu}^\top \tilde{\mathbf{B}}\tilde{\mathbf{B}}^\top \boldsymbol{\mu}}{\boldsymbol{\mu}^\top \boldsymbol{\mu}} \tag{15}$$

$$= \min_{\substack{\mathbf{v} \in \text{Im}\tilde{\mathbf{B}}^\top \cap \text{Im}\tilde{\mathbf{K}} \\ \mathbf{v} = \tilde{\mathbf{B}}^\top \boldsymbol{\mu}, \boldsymbol{\mu} \in \text{Ker}\tilde{\mathbf{G}}, \boldsymbol{\mu} \neq \mathbf{o}}} \frac{\mathbf{v}^\top \tilde{\mathbf{K}}^+ \mathbf{v}}{\mathbf{v}^\top \mathbf{v}} \cdot \frac{\boldsymbol{\mu}^\top \tilde{\mathbf{B}}\tilde{\mathbf{B}}^\top \boldsymbol{\mu}}{\boldsymbol{\mu}^\top \boldsymbol{\mu}} > 0 \tag{16}$$

using $\boldsymbol{\mu}^\top \tilde{\mathbf{P}}\tilde{\mathbf{F}}\boldsymbol{\mu} = \boldsymbol{\mu}^\top \tilde{\mathbf{F}}\boldsymbol{\mu}$ for $\boldsymbol{\mu} \in \text{Ker}\tilde{\mathbf{G}}$, $\tilde{\mathbf{B}}\tilde{\mathbf{B}}^\top = \mathbf{I}$, and the fact that $\mathbf{v}^\top \tilde{\mathbf{K}}^+ \mathbf{v}$ is independent of the choice of $\tilde{\mathbf{K}}^+$ iff $\mathbf{v} \in \text{Im}\tilde{\mathbf{K}}$. The symmetry is obvious. ■

Because of Lemma 1 the problem (14) may be solved efficiently by PCGP (Preconditioned Conjugate Gradient with Projectors) algorithm.

In every PCGP iteration we need to compute $\tilde{\mathbf{x}} = \tilde{\mathbf{K}}^+ \tilde{\mathbf{b}}$, where $\tilde{\mathbf{b}}$ is a given vector. To do this we solve the system

$$\tilde{\mathbf{K}}\tilde{\mathbf{x}} = \tilde{\mathbf{b}} \iff \begin{bmatrix} \mathbf{K} & \mathbf{B}_0^\top \\ \mathbf{B}_0 & \mathbf{O} \end{bmatrix} \begin{bmatrix} \mathbf{x}_0 \\ \boldsymbol{\mu}_0 \end{bmatrix} = \begin{bmatrix} \mathbf{b}_0 \\ \mathbf{d}_0 \end{bmatrix} \quad (17)$$

by a TFETI based solver again. Using

$$\mathbf{x}_0 = \mathbf{K}^+(\mathbf{b}_0 - \mathbf{B}_0^\top \boldsymbol{\mu}_0) + \mathbf{R}_0 \boldsymbol{\beta}_0, \quad (18)$$

and substituting it into the second equation in (17) we get

$$\begin{bmatrix} \mathbf{F}_0 & \mathbf{G}_0^\top \\ \mathbf{G}_0 & \mathbf{O} \end{bmatrix} \begin{bmatrix} \boldsymbol{\mu}_0 \\ \boldsymbol{\beta}_0 \end{bmatrix} = \begin{bmatrix} \mathbf{g}_0 \\ \mathbf{e}_0 \end{bmatrix}, \quad (19)$$

where

$$\begin{aligned} \mathbf{F}_0 &= \mathbf{B}_0 \mathbf{K}^+ \mathbf{B}_0^\top, \quad \mathbf{g}_0 = \mathbf{B}_0 \mathbf{K}^+ \mathbf{b}_0 - \mathbf{d}_0, \\ \mathbf{G}_0 &= -\mathbf{R}_0^\top \mathbf{B}_0^\top, \quad \mathbf{e}_0 = -\mathbf{R}_0^\top \mathbf{b}_0, \end{aligned}$$

and

$$\mathbf{R}_0 = \begin{bmatrix} \mathbf{R}^1 & & \\ & \ddots & \\ & & \mathbf{R}^N \end{bmatrix}, \quad N = N_c \times N_s. \quad (20)$$

We note that matrices \mathbf{R}^j , $j = 1, \dots, N$ in (20) are the same as $\mathbf{R}^{p,i}$, $p = 1, \dots, N_s$, $i = 1, \dots, N_c$ in (8) with $j = (i - 1) \cdot N_s + p$. To obtain full-rank matrix $\mathbf{G}_0 = -\mathbf{R}_0^\top \mathbf{B}_0^\top$ we introduce matrix $\bar{\mathbf{R}}_0$, which is obtained from \mathbf{R}_0 by deleting the block columns corresponding to the last subdomains of all clusters. Let $\bar{\mathbf{e}}_0 = -\bar{\mathbf{R}}_0^\top \mathbf{b}_0$.

Lemma 2. *Let $\mathbf{K}^+ := \mathbf{K}_\rho^{-1}$ be the symmetric positive definite generalized pseudo-inverse obtained by the regularization of \mathbf{K} introduced in [14]. Then the matrix \mathbf{F}_0 is symmetric positive definite on \mathbb{R}^{m_0} .*

Proof. The proof follows immediately from the full-rank of \mathbf{B}_0 and the positive definiteness of the matrix \mathbf{K}^+ . \blacksquare

Obviously using the above lemma and replacing \mathbf{G}_0 and \mathbf{e}_0 by $\bar{\mathbf{G}}_0$ and $\bar{\mathbf{e}}_0$ in (19) we get well defined saddle-point system which can be solved by PCGP again or because of its small size by a direct solver.

3 Numerical experiments

The proposed massively parallel HTFETI algorithm was implemented in C++ using PETSc library as a linear algebra backbone. The code was compiled by Cray compiler with a MPI library optimized for the architecture of the HEcTOR

supercomputer at EPCC in Edinburgh. For the main scalability benchmark we chose a simple 2D geometry. We modeled a square steel box fixed on the left side and deformed only by its own weight. The square was decomposed into the increasing number of subdomains with a constant number of nodes (121×121). These subdomains were organized into square clusters per 16. This hierarchy fitted the structure of the hardware - each computing node was formed by two 16-core AMD Opteron 2.3GHz Interlagos processors. All matrices and vectors related only to the clusters are stored directly on the node occupied by that cluster. Thanks to that all the operations inside the clusters were done in shared memory minimizing a communication overhead and the memory requirements are well distributed over the machine.

Table 1. Performance of the HTFETI implementation with the lumped preconditioner.

Subdomains	DOFs	Iter.	Init. [s]	Sol. [s]	Total [s]
400	11.712.800	115	50	46	96
1024	29.984.768	122	53	47	100
1936	56.689.952	122	53	50	103
4624	135.399.968	127	56	55	110
7744	226.759.808	127	65	61	126

The results match our original assumptions about the behaviour of the algorithm. We can notice substantially higher number of iterations in comparison with the results of the TFETI algorithm [7] applied to the similar benchmark. This is due to the reduced coarse space working as a preconditioner. The linear loss of efficiency with rising number of used cores was partly caused by the increasing number of iterations and partly by increasing hardware overhead. On the other hand a problem with such a number of subdomains would not be possible to solve on the same machine with original TFETI algorithm due to memory requirements on the master node.

4 Conclusions

Current state of implementation challenge us by multiple topics. We would like to increase its effectivity by using fast direct solvers in shared memory of clusters (such as Pardiso or MUMPS). Besides to that we are working on thorough numerical analysis of the algorithm and on the development of more efficient preconditioner.

5 Acknowledgments

This work was supported by the European Regional Development Fund in the IT4Innovations Centre of Excellence project (CZ.1.05/1.1.00/02.0070) and by

the project SPOMECH - Creating a multidisciplinary R&D team for reliable solution of mechanical problems, reg. no. CZ.1.07/2.3.00/20.0070 within Operational Programme 'Education for competitiveness' funded by Structural Funds of the European Union and state budget of the Czech Republic.

This paper is extract from original paper submitted to Eccomas 2012.

References

1. C. Farhat, F-X. Roux, "An unconventional domain decomposition method for an efficient parallel solution of large-scale finite element systems", *SIAM J. Sci. Stat. Comput.* 13: 379–396, 1992.
2. F-X. Roux, "Spectral analysis of interface operator", *Proceedings of the 5th Int. Symp. on Domain Decomposition Methods for Partial Differential Equations*, ed. D. E. Keyes et al., SIAM, Philadelphia 1992; 73–90.
3. C. Farhat, J. Mandel, F-X. Roux, "Optimal convergence properties of the FETI domain decomposition method", *Comput. Methods Appl. Mech. Eng.* 115, 1994; 365–385.
4. F-X. Roux, C. Farhat, "Parallel implementation of direct solution strategies for the coarse grid solvers in 2-level FETI method", *Contemporary Math.* 218, 1998; 158–173.
5. Z. Dostál, D. Horák, R. Kučera, "Total FETI - an easier implementable variant of the FETI method for numerical solution of elliptic PDE", *Communications in Numerical Methods in Engineering*, 22(2006), 12, pp. 1155-1162
6. Z. Dostál, T. Kozubek, A. Markopoulos, M. Mensik, "Cholesky decomposition and a generalized inverse of the stiffness matrix of a floating structure with known null space", *Applied Mathematics and Computation* 2011; **217**:6067–6077.
7. T. Kozubek, V. Vondrak, M. Mensik, D. Horak, Z. Dostal, V. Hapla, P. Kabelikova, M. Cermak, "Total FETI domain decomposition method and its massively parallel implementation", *Advances of Engeneering Software*, accepted
8. A. Klawonn, O. Rheinbach, "Highly scalable parallel domain decomposition methods with an application to biomechanics", *ZAMM*, 90, No. 1, pp.5-32, 2010
9. Jungho Lee: "A hybrid domain decomposition method and its applications to contact problems in mechanical engineering", PhD thesis, New York University, 2009.
10. A. Klawonn and O. Rheinbach, "A parallel implementation of Dual-Primal FETI methods for three dimensional linear elasticity using a transformation of basis", *SIAM J. Sci. Comput.*, 28(5):1886–1906, 2006
11. A. Klawonn and O. B. Widlund, "Dual-primal FETI methods for linear elasticity", *Communications on pure and applied mathematics*, 59(11):1523–1572, 2006
12. J. Li and O. B. Widlund, "FETI-DP, BDDC, and block Cholesky methods", *International journal for numerical methods in engineering*, 66:250–271, 2006
13. T. Brzobohaty, Z. Dostal, T. Kozubek, P. Kovar, and A. Markopoulos, (2011), Cholesky decomposition with fixing nodes to stable computation of a generalized inverse of the stiffness matrix of a floating structure. *Int. J. Numer. Meth. Engng.*, 88: 493509. doi: 10.1002/nme.3187
14. D. Horak, Z. Dostal, "Parallelization of the Total-FETI-1 Algorithm for Contact Problems using PETSc", in P. Ivanyi, B.H.V. Topping, (Editors), "Proceedings of the Second International Conference on Parallel, Distributed, Grid and Cloud Computing for Engineering", Civil-Comp Press, Stirlingshire, UK, Paper 1, 2011. doi:10.4203/ccp.95.1

Solution of Contact Problems with Level Set Based Conditions of Non-interpenetration

Petr Kotas

Department of Applied Mathematics, FEECS,
VŠB – Technical University of Ostrava, 17. listopadu 15, 708 33 Ostrava – Poruba
petr.kotas@vsb.cz

Abstract. Contact mechanics is an important part of the computational mechanics which deals with modelling of interfacial phenomena between bodies in mutual contact. Our work extends the framework for contact between elastic body and rigid obstacle presented by Krause and Mohr. We mainly focus on formulating physically admissible contact condition using the signed distance function computed via level set framework.

Keywords: level set, contact problems, elasticity

1 Introduction

Contact mechanics is an important part of the computational mechanics which deals with modelling of interfacial phenomena between bodies in mutual contact. Such problems may eventually occur in any complex mechanical system. Therefore the real world applications may range from a design of mechanical bearing to modelling of an artificial joint. One of the biggest problems from implementation point of view is the correct representation of a non-penetration condition and proper contact localization. In this work, we focus on the problem of contact between two elastic bodies using the level set method for an approximation of a gap function. The idea was originally presented by Krause and Mohr in [1] for a contact between an elastic body and a rigid foundation.

2 Contact problem between two deformable bodies

Our testing setup (shown in Figure 1) consists of a elastic body $\Omega \subset \mathbb{R}^2$ with Lipschitz boundary $\partial\Omega$ and a rigid obstacle $O \subset \mathbb{R}^2$. The boundary $\partial\Omega$ of the elastic body consists of three disjoint parts: the Dirichlet boundary Γ_D , the Neumann boundary Γ_N and contact boundary Γ_C .

In the following text, we denote deformations of elastic body by \mathbf{u} . The deformations are defined as a map $\mathbf{u} : \bar{\Omega} \rightarrow \mathbb{R}^2$ and are restricted by the rigid obstacle O . This non-penetration condition could only be enforced by allowing the deformations that fullfils the kinematic contact condition

$$\text{int}(\mathbf{u}(\Omega) \cap O) = \emptyset. \quad (1)$$

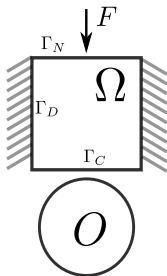


Fig. 1: Initial setup for rigid body contact problem.

Since this condition is not very suitable for direct computation, we introduce slightly different formulation based on a signed distance function $d_O : \mathbb{R}^2 \rightarrow \mathbb{R}$ as presented in [1]

$$d_O(\mathbf{x}) = \text{dist}(\mathbf{x}, O^C) - \text{dist}(\mathbf{x}, O), \tag{2}$$

where O^C is complement to the rigid the obstacle O . Taking into account contact zone Γ_C (defined earlier) the non-penetration condition is equivalent to

$$d_O(\mathbf{u}(\mathbf{x})) \leq 0, \forall \mathbf{x} \in \Gamma_C. \tag{3}$$

Also, we need to define potential energy of the examined system. This is done via energy functional

$$J(\mathbf{u}) := \frac{1}{2}a(\mathbf{u}, \mathbf{u}) - b(\mathbf{u}),$$

where the bilinear form

$$a(\mathbf{u}, \mathbf{v}) := \sum_{p=1}^2 \int_{\Omega^p} c_{ijkl}^p(\mathbf{u}^p) e_{kl}^p(\mathbf{v}^p) \, d\Omega, \quad e_{kl}^p := \frac{1}{2} \left(\frac{\partial u_k^p}{\partial x_l^p} + \frac{\partial u_l^p}{\partial x_k^p} \right)$$

represents the inner energy of the bodies and the linear form

$$b(\mathbf{u}) := \sum_{p=1}^2 \int_{\Omega^p} (\mathbf{g})^\top \mathbf{u}^p + \int_{\Gamma_N^p} (\mathbf{F}^p)^\top \mathbf{u}^p \, d\Gamma$$

represents the work of applied volume forces and tractions on the Neumann parts of the boundaries.

To summarize our problem, we need to solve constraint minimization problem

$$\begin{aligned} \min J(\mathbf{u}), & \quad \forall \mathbf{u} \in W^{1,p}(\Omega, \mathbb{R}^2), \\ \mathbf{u}(\mathbf{x}) = \hat{\mathbf{u}}(\mathbf{x}), & \quad \forall \mathbf{x} \in \Gamma_D, \\ d_O(\mathbf{u}(\mathbf{x})) \leq 0, & \quad \forall \mathbf{x} \in \Gamma_C, \end{aligned} \tag{4}$$

where the initial deformations are prescribed on Γ_D with given deformation $\hat{\mathbf{u}} \in W^{1,p}(\Omega, \mathbb{R}^2)$.

The accurate approximation of signed distance d_O could pose a tricky problem when working with complex concave geometries. One possible solution is to utilize level set framework and to compute signed distance based on interface motion, as will be described in the following text.

3 Level set methods

The level set method is relatively new method for modelling complex closed objects. It combines low-level volumetric representation, methods for deformable implicit surfaces and robust numerical schemes, providing powerful novelty approach for modelling shapes. In our work, we have used level set framework to overcome problems of patching two different finite element meshes as well as to allow computation of complex shapes. It is worth noting that we only work with closed interfaces and thus we always can determine interior and exterior of the body.

3.1 Signed distance

The accurate representation of the implicit function lies right in the heart of the level set framework. In the heart of the level set framework lies accurate representation of implicit function. As Osher stated in [2], the best choice is to use signed distance function (SDF) as the approximation to the implicit function. In this section, we use slightly different definition of SDF according to [2]

$$\phi(x) := \begin{cases} d(x, \partial\Omega) & \text{for } x \text{ outside of } \Omega \\ -d(x, \partial\Omega) & \text{for } x \text{ inside of } \Omega \end{cases}, \quad (5)$$

with

$$d(x, \partial\Omega) := \min(|x - x_{\partial\Omega}|),$$

where $d(x, y) \in \mathbb{R}$ is standard euclidean distance. Although equation (5) seems different from equation (3) it states the same property. Signed distance function is differentiable almost everywhere, which is important for computation of some geometrical properties like unit outward normal

$$N(x) = \frac{\nabla\phi}{|\nabla\phi|}, \quad (6)$$

and curvature

$$\kappa = \nabla \cdot N(x) \quad (7)$$

and for numerical schemes used in evolution solvers.

Figure 2 shows signed distance computed around the rectangular interface (gray contour). In this way, arbitrary front could be embedded in higher dimensional function $\phi(x)$. And this is exactly what we need to do when approximating the non-penetration condition in equation (4).

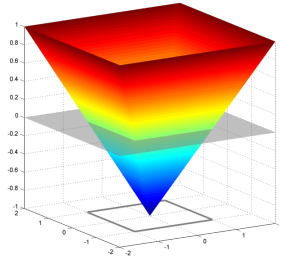


Fig. 2: Signed distance around square interface.

3.2 Fast marching

One of the possibilities to construct the signed distance function is to utilize fast marching method. Fast marching was first proposed by Sethian in his paper [3] where he described an efficient solver for Eikonal equation

$$F|\nabla\phi| = 1.$$

Solving Eikonal equation with the right choice of F satisfies the properties of signed distance function. One of the possibilities is to choose

$$F = \frac{1}{\max(dx, dy)}, \quad (8)$$

where dx, dy is resolution of cartesian grid.

In our work, we use Hassouna variant, multi-stencil fast marching method introduced in [4]. This method offers better accuracy than the original and its implementation is straightforward.

4 Algorithm

To solve problem (4), one has to compute approximation of the distance function $d_{\mathcal{O}}$. The key idea presented in [1], is to use signed distance as the approximation of a gap function between rigid obstacle and elastic body. The initial setup is shown in Figure 3. The second part of Figure 3 shows signed distance computed around the original rigid obstacle.

Huge benefits of rigid body is its static behaviour. This allows us to compute signed distance function only once in initialization phase and then utilize fast search methods to locate the distance. Simply speaking, the signed distance function around the rigid obstacle is computed only once in the initialization step and than referenced as a table mapping distance.

Our implementation uses bisection method [5] to localize coordinate in the distance matrix. And in case when coordinate is not available in precomputed distance matrix the bilinear interpolation is used to return the correct value.

As mentioned beforehand, we followed the method presented in [1]. However, our approach slightly differs in choice of a problem solver. Krause and Mohr used

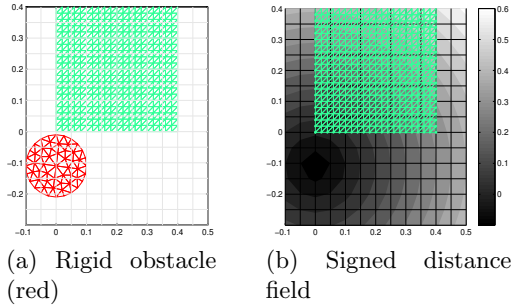


Fig. 3: A signed distance field computed around the rigid obstacle (circle).

their multigrid method [1] to solve the primal problem. Instead our algorithm uses the MPRGP algorithm, proposed by Dostál in [6] to solve the dual problem. Our version of Krauses algorithm is summarized in Algorithm 1 and it is worth noting that this is the only brief pseudocode. More detailed description of the dual problem methods can be found in Dostál's book [6].

The rest of the Algorithm 1 is best illustrated in attached videos. In each iteration the partial solution is computed with use of precomputed distance and gradient. Then the computed solution is added to the final solution and the termination condition is checked. This is known as a quasistatic approach to the contact problem and was previously described in [7].

As could be seen in attached videos the presented algorithm works well even for non-convex obstacles which was design purpose.

Algorithm 1 Algorithm for rigid body contact.

```

Initialize  $\phi, \nabla\phi, tol$ 
while  $\frac{\|\Delta u\|}{\|u\|} < tol$  do
    Solve :  $\Delta u \leftarrow \min \Delta u^T A \Delta u - b^T \Delta u,$ 
           subject to:  $B \Delta u + \phi(u) \leq 0$ 
     $u \leftarrow u + \Delta u$ 
end while
    
```

5 Further work

Here we conclude our work with final remarks on current work in progress. Currently, we are extending previously presented algorithm to support contact with multiple elastic bodies. Our actual algorithm wraps all colliding bodies with signed distance and uses it in further computation. Because of dynamic nature of the interface movement, we could not utilize the same approach as was originally intended. Instead we had to rebuild the level set in every iteration

to satisfy the increment in nodal displacement. The displacement increment of two colliding bodies is illustrated in Figure 4 with final stress and displacement shown in Figure 5.

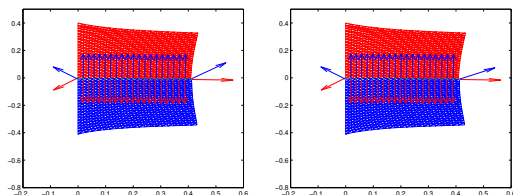


Fig. 4: Iteration progress of our proposed method.

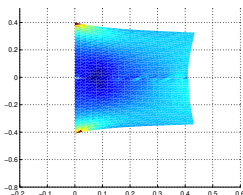


Fig. 5: Final stress and displacement for both bodies.

This version is still consuming a lot of CPU. Because of this we need to investigate further speedup possibilities. Further work contains: 1) implementing fast version of level set framework, 2) accelerate collision detection in dynamic problem, 3) find a way to reuse previously computed data.

References

1. Krause, R., Mohr, C.: Level set based multi-scale methods for large deformation contact problems. *Applied Numerical Mathematics* **61**(4) (2011) 428–442
2. Osher, S., Fedkiw, R.P.: *Level set methods and dynamic implicit surfaces*. Applied mathematical sciences. Springer (2003)
3. Sethian, J.: A Fast Marching Method for Monotonically Advancing Fronts. *Proceedings of National Academy of Sciences of the United States of America* **93**(4) (1996) 1591–1595
4. Hassouna, M.S., Farag, A.A.: MultiStencils Fast Marching Methods: A Highly Accurate Solution to the Eikonal Equation on Cartesian Domains. *IEEE Transactions on Pattern Analysis and Machine Intelligence* **29**(9) (2007) 1563–1574
5. Knuth, D.E.: *Art of Computer Programming, Volume 3: Sorting and Searching - Retrieval on Secondary Keys*. In Knuth, D.E., ed.: *Art of Computer Programming Volume 3 Sorting and Searching*. (1973)

6. Dostál, Z.: Optimal Quadratic Programming Algorithms. Volume 23 of Springer Optimization and Its Applications. Springer US (2009)
7. Wriggers, P.: Computational Contact Mechanics. John Wiley & Sons, Ltd (2002)

Improving the Probabilistic Prediction Model of the Phadiatop Test by Data Pre-processing

Pavĺína Kuráňová¹, Pavel Praks¹, and Zdeňka Hajduková²

¹Department of Applied Mathematics, FEECS,
VŠB – Technical University of Ostrava, 17. listopadu 15, 708 33 Ostrava – Poruba
pavlina.kuranova@vsb.cz

²University Hospital of Ostrava, Clinic of Occupational and Preventive Medicine,
17.listopadu 1790, Ostrava-Poruba, Czech Republic

Abstract. The Phadiatop test was developed for screening of allergic sensitization. As the Phadiatop test is not cheap, the aim of our research is to approximately predict results of the phadiatop test by a probabilistic model. Our database is based on patients who underwent examinations of the Phadiatop test at the Clinic of Occupation and Preventive Medicine, University Hospital of Ostrava, Ostrava, Czech Republic. The probabilistic prediction model has been verified on a consistent database of approximately 400 patients. Then, the second sensitivity analysis study has been performed and the prediction model has been finally simplified. As a result of the model simplification process, the final prediction model depends only on two independent variables (asthma and allergic rhinitis). The developed model is able to predict the approximate results of the Phadiatop test with 70% probability, which may represent a significant financial saving for the public health sector.

Keywords: Logistic regression, medical data, atopy, Phadiatop test.

1 Introduction

The atopy rate of inhabitants of the Czech Republic is increasing. Atopy could be understood as a personal or family predisposition to become, mostly in childhood or adolescence, hypersensitive to normal exposure of allergens, usually proteins. These individuals are more sensitive to typical symptoms of asthma, for example eczema. The Phadiatop test is used as a measure of atopy.

In the original prediction model that has been created for the Phadiatop test, we used two groups of variables, namely family and personal anamneses [4]. The results of the sensitivity analysis excluded the variables of family anamnesis. Thus the prediction model considers only four variables of the personal anamnesis [4-5].

According to disease severity, results of the Phadiatop test are divided into the six following groups: Groups 0 and I indicate none or weak form of atopy and the remaining groups (II, III, IV, V, VI) indicates increasing severe forms of the atopic symptoms. Knowledge of results of the Phadiatop test is very important especially for diagnosis of allergic dermatoses and also for the professional medical care of travelers [2], [3].

Information obtained from the personal anamneses questionnaires has been used for presence of asthma, allergic rhinitis, eczema or other forms of allergy (contact allergy, food allergy, and the other symptoms of an allergy). The personal anamnesis of each patient has been paired with results of the real Phadiatop test. Then, we created and verified a probabilistic classification model of patients into one of two groups of the Phadiatop test.

All mathematical operations are performed on the basis of those described in literature, see [1], [6]. All calculations were made in Matlab and Statgraphics software.

2 Problem Solution

The tested biomedical database is from the University Hospital of Ostrava, Department of Occupational and Preventive Medicine, Ostrava, the Czech Republic. The logistic regression technique is used in order to predict results of the Phadiatop test. The medical database contains Phadiatop test information and personal anamnesis of 1027 patients.

Patients in Group 0 have Phadiatop test 0 or I (no visible symptoms), so no treatment is necessary for these patients. The remaining patients with Phadiatop test II – VI are members of Group 1. For these patients, a medical treatment is necessary.

We have one dependent variable $Y=PhModel$, which depends on four independent variables: asthma, allergic rhinitis, eczema and others. Variable Y can be 0 or 1, according to the membership of a patient to Group 0-I or Group II-VI, respectively. Values of independent factors were obtained from medical experts. The expert severity scores are presented in Table 1. Here the category “Others” represents the score of various types of allergies (food allergies, etc). The independent variable of the logistic regression was obtained as a sum of these scores for each patient of the database.

Table 1. Expert severity scores for personal and family anamneses.

Factor	Asthma	Allergic rhinitis	Eczema	Others
Score	10	8	6	4

The logistic regression model has the form: $g(x) = \beta_0 + \beta_1 x_1 + \beta_2 x_2 + \beta_3 x_3 + \beta_4 x_4$,

where $\beta_i \in \mathfrak{R}, i = 0, 1, 2, 3, 4$ are logistic regression coefficients and vector x has four components: $x_1 = asthma$, $x_2 = allergic\ rhinitis$, $x_3 = eczema$, $x_4 = others$.

The dependence $\pi(x)$ on x has the form:

$$\pi(x) = \frac{e^{g(x)}}{1 + e^{g(x)}}. \tag{4}$$

Here $\pi(x)$ denotes the probability of occurrence of Phadiatop Group, i.e. $\pi(x) = PhModel$. Unknown coefficients $\beta_i, i = 0, 1, 2, 3, 4$ are determined by the maximum likelihood method. In our case, the maximum likelihood method for our logistic regression model can be expressed as

$$L(\beta) = \prod_{i=1}^n \pi(x_i)^{y_i} \cdot (1 - \pi(x_i))^{1-y_i}. \tag{5}$$

The estimation of regression parameters β is provided by maximization the logarithm of the maximum likelihood function, which can be expressed as:

$$\ln L(\beta) = \sum_{i=1}^n [y_i \cdot \ln \pi(x_i) + (1 - y_i) \cdot \ln(1 - \pi(x_i))]. \tag{6}$$

Now the logistic regression model can be used for predictions, whether the patient with given symptoms of atopy is a member of the selected Phadiatop group. The quality of a probabilistic prediction model can be characterized by terms: Sensitivity, Specificity, Positive and Negative Predictive Values [7].

4 Prediction results of the logistic model: full database

In the first step, we have tried to create a prediction model of the Phadiatop test by assuming all of the supplied data corresponding to 1 027 patients. Then, the developed model has been tested using the same data. We have obtained the following global prediction model:

$$\ln\left(\frac{PhModel}{1 - PhModel}\right) = -1.4856 + 0.1528 \cdot asthma + 0.3156 \cdot allergic\ rhinitis + 0.0765 \cdot ekzema + 0.1549 \cdot others \tag{7}$$

Our model has one dependent variable (PhModel) and four independent variables: asthma, allergic rhinitis, ekzema and others.

The prediction results of the global model (7) are summarized in Table 3. For example, there were 166 “true positive” patients with the positive Phadiatop test (PhTest=1) correctly recognized by the prediction model as PhModel=1. Similarly, there were 641 “true negative” patients, i.e. patients with negative Phadiatop test (PhTest=0) correctly recognized by the prediction model as PhModel=0.

Table 2. Prediction results of the logistic regression model: the global model, 1 027 patients.

		PhModel=1	PhModel=0
PhTest=1		166 (TP)	165 (FN)
PhTest=0		55 (FP)	641 (TN)
		Positive predictive value (PPV)	Negative predictive value (NPV)
Sensitivity (SE)	Specificity (SP)	0.75	0.80

A negative result from the Table 2 is very good at reassuring that a patient has no serious atopic syndrome, (NPV = 80%) and at this initial screen correctly identifies 92% of those who do not have the serious atopic syndrome (the specificity).

4 Prediction results of the logistic model: a reduced database

All of the incomplete filled records in the medical database belongs to patients with PhTest=0. In Section 4, these incomplete records have been replaced by zeros, because it had been expected that all positive allergic symptoms were stored in the database. In contrary to the previous section, this section brings prediction results of a case when all of the incomplete filled database records have been removed from the database. By this pre-processing process, i.e. by removing these incomplete filled records, the reduced database has had finally 376 records. For these records, we have created a novel prediction model - Model 2:

$$\ln\left(\frac{PhModel}{1-PhModel}\right) = -0.9765 + 0.1251 \cdot asthma + 0.2675 \cdot allergic\ rhinitis + 0.0113 \cdot ekzema + 0.0623 \cdot others \tag{8}$$

The prediction results of this model are presented in Table 3. For example, there have been observed 166 “true positive” patients. It means sick patients with PhTest = 1 has been correctly recognized by the prediction model as PhModel=1. Furthermore, the number of patients with a positive PhTest is 166+49=215.

Table 3. Prediction results of the regression model (8) for 376 patients.

		PhModel=1	PhModel=0
PhTest=1		166 (TP)	49 (FN)
PhTest=0		55 (FP)	106 (TN)
		Positive predictive value (PPV)	Negative predictive value (NPV)
Sensitivity (SE)	Specificity (SP)	0.75	0.68

As a result, a sensitivity of $166/215 = 77\%$ means that the model correctly recognizes 77 % actual positives – i.e. 77 % sick people are correctly recognized as being ill. The prediction model is also good at confirming the sick people (PPV = 75%).

The percentages of the model sensitivity indicate that the prediction outcome is a slightly better than the prediction outcome for the complete database of 1 027 patients: By removing incomplete filled records, only the fully relevant data is analyzed.

Let us also note, that although the database has been significantly reduced, results corresponding to the column “PhModel=1” of Table 2 and Table 3 are the same.

The prediction model of the reduced database (Model 2) has also been a subject of statistical tests; see Tables 4 and 5.

Table 4. Model 2: Analysis of deviance.

Source	Variance	Df	P-Value
Model	84.8205	4	0.0000
Residual	482.644	371	0.0207
Total (corr.)	513.464	375	

Table 5. Test of statistical significance for Model 2.

Factor	Chi-Square	Df	P-Value
Asthma	13.9485	1	0.0002
Allergic rhinitis	56.2333	1	0.0000
Ekzema	0.0356	1	0.8503
Others	0.6814	1	0.4091

Table 5 shows that the variables eczema and/or others are statistically insignificant and may be excluded from the prediction model. By excluding these statistically insignificant variables we obtain the following prediction model – Model 3:

$$\ln\left(\frac{PhModel}{1 - PhModel}\right) = -0.7927 + 0.1189 \cdot asthma + 0.2538 \cdot allergic\ rhinitis \tag{9}$$

Even this prediction model has been a subject of the accuracy testing for a patient inclusion in two Phadiatop groups. Based on these results we can conclude that the reduced model (Model 3) works exactly the same as in the case where we have four variables (Model 2).

6 Conclusion

The Phadiatop test is a powerful but an expensive technique developed for screening of allergic sensitization. For this reason we have constructed a probabilistic model, which evaluates data from a personal questionnaire obtained from patients with suspected allergic diseases. In the prediction model, just the personal history of patient’s allergic diseases is evaluated. Only asthma and allergic rhinitis seem to be significant factors for the Phadiatop prediction model, because all of the remaining attributes have been shown to be statistically insignificant and therefore these insignificant attributes have been removed from the prediction model. The prediction

model has interesting properties: the statistical testing over a real patient database indicates that 77% sick people have been correctly recognized as being ill. Thus, approximately only every fourth sick patient has been wrongly classified by the developed prediction model as being healthy.

In future research, we would like to cooperate with medical experts from the Clinic of Occupational and Preventive Medicine in order to minimize consequences of false positive and false negative predictions. Moreover, we would like to extend the prediction model in order to be able to predict more than two groups of the Phadiatop test.

Acknowledgement: This work was supported by the European Regional Development Fund in the IT4Innovations Centre of Excellence project (CZ.1.05/1.1.00/02.0070) and the FEECS VŠB – Technical University of Ostrava (Project No. SP2012/180).

This contribution is copyrighted by the Mendel 2012, 18th International Conference on Soft Computing, see the reference: Kuráňová P., Praks P., Hajduková Z.: Improving the Probabilistic Prediction Model of the Phadiatop Test by Data Pre-processing. In Mendel 2012: 18th International Conference on Soft Computing. Brno University of Technology, Brno, 2012, s. 500-504. ISSN 1803-3814. ISBN 978-80-214-4540-6

References

1. Hosmer, D.W. & Lemeshow S., *Applied Logistic Regression*. NewYork: Wiley-Interscience, 2000
2. Hajduková, Z. & Vantuchová, Y. & Klimková, P. & Makhoul, M. & Hromádka R., Atopy in patients with allergic contact dermatitis, *Jurnal of Czech Physicians: Occupational therapy*, No.2, 2009, pp. 69-73. In Czech.
<http://www.prolekare.cz/casopis-lekaru-ceskych-clanek?id=5780>
3. Hajduková, Z. & Pólová, J. & Kosek V., The importance of Atopy Investigation in the Department of Travel Medicine, *Allergies: Magazine for continuous education in allergy and clinical immunology*, No.2, 2005, pp. 106-109. in Czech.
http://www.tigis.cz/alergie/alergie_2_2005/obsah_f.htm
4. Kuráňová P., Hajduková Z. & Praks P., Logistic regression as a tool for atopy investigation, *Mendel- 16th International Conference on Soft Computing 2010*, pp.187-190.
5. Kuráňová P., The processing of the medical data with the use of logistic regression, *Reliability & Risk Analysis: Theory & Applications (R&RATA)*, Journal of international group on reliability, ISSN 1932-2321.
6. Rabasová M., Briš R. & Kuráňová P., Modified logistic regression as a tool for discrimination. *Reliability, Risk and Safety: Theory and Applications*. R. Briš, C. Guedes Soares, S. Martorell (eds.); Vol 3, 2010, pp.1967-1972
7. Mangrulkar Rajesh S., Gruber S., *Patients and Populations: Medical Decision-Making First Steps Towards Lifelong Learning*. University of Michigan, Retrieved 3 May 2012.
<http://open.umich.edu/sites/default/files/ml-patientspopulations-medicaldecisionmaking-syllabus-f08.pdf>.

Semi-Smooth Newton Method for 2D Contact Problems with Tresca and Coulomb Friction

Kristina Motyčková and Radek Kučera

Department of Applied Mathematics, FEECS,
VŠB – Technical University of Ostrava, 17. listopadu 15, 708 33 Ostrava – Poruba
{kristina.radkova.st, radek.kucera}@vsb.cz

Abstract The contribution deals with contact problems for two elastic bodies with friction. After the description of the problem we present its discretization based on linear or bilinear finite elements. The semi-smooth Newton method is used to find the solution. We present active sets algorithms. The non-symmetric and symmetric case is distinguished with using BiCGSTAB and CGM, respectively. Finally we will arrive at the globally convergent dual implementation of the algorithm.

Keywords: contact problems, semi-smooth Newton method, dual formulation

1 Introduction

Let us consider two homogeneous isotropic elastic bodies represented by bounded domains $\Omega^k \subset \mathbb{R}^2$ with sufficiently smooth boundaries $\partial\Omega^k$, $k = 1, 2$. Each boundary consists of three disjoint parts Γ_u^k , Γ_p^k , and Γ_c^k open in $\partial\Omega^k$ so that $\partial\Omega^k = \bar{\Gamma}_u^k \cup \bar{\Gamma}_p^k \cup \bar{\Gamma}_c^k$ and $\bar{\Gamma}_u^k \neq \emptyset$; The zero displacements are prescribed on Γ_u^k while surface tractions $\mathbf{p}^k \in (L^2(\Gamma_p^k))^2$ act on Γ_p^k . The bodies may get into contact on the *contact interface* given by Γ_c^1 and Γ_c^2 , where we consider three contact conditions: the non-penetration of bodies, the transmission of contact stresses, and the Coulomb friction law. Elastic properties of Ω^k are described by the Lamè constants $\lambda^k, \mu^k > 0$. Finally, assume the volume forces $\mathbf{f}^k \in (L^2(\Omega^k))^2$.

Our aim is to find an equilibrium state of Ω^1 and Ω^2 . By the solution of this problem we mean displacement vector fields $\mathbf{u}^k = (u_1^k, u_2^k)^\top$, $k = 1, 2$, satisfying the equilibrium equations and the Dirichlet and Neumann conditions.

To solve the contact problem with the Coulomb friction we use the method of successive approximations (fixed-point approach) and in each step we solve the problem with the Tresca friction (according to a predefined mapping).

The formulation of the contact problem with Coulomb friction results in an *implicit* variational inequality of the elliptic type. If we replace the slip bounds (of the Coulomb friction law) by an à-priori given positive function g defined on Γ_c^1 , we arrive at the contact problem with Tresca friction. This well known problem is represented by the variational inequality of the second type for which there is a unique solution (for an appropriate g).

2 Discrete problems

After the discretization of our problem we arrive at

$$\mathbf{K}\mathbf{u} - \mathbf{f} + \mathbf{N}^\top \boldsymbol{\lambda}_\nu + \mathbf{T}^\top \boldsymbol{\lambda}_t = \mathbf{0}, \tag{2.1}$$

$$\mathbf{N}\mathbf{u} - \mathbf{d} \leq \mathbf{0}, \boldsymbol{\lambda}_\nu \geq \mathbf{0}, \boldsymbol{\lambda}_\nu^\top (\mathbf{N}\mathbf{u} - \mathbf{d}) = \mathbf{0}, \tag{2.2}$$

$$\left. \begin{aligned} |\lambda_{t,i}| &\leq \mathcal{F}_i \lambda_{\nu,i} \\ |\lambda_{t,i}| &< \mathcal{F}_i \lambda_{\nu,i} \Rightarrow u_{t,i} = 0 \\ |\lambda_{t,i}| &= \mathcal{F}_i \lambda_{\nu,i} \Rightarrow \exists c_t \geq 0 : u_{t,i} = c_t \lambda_{t,i} \end{aligned} \right\} \quad i = 1, \dots, m. \tag{2.3}$$

We use two Lagrange multipliers $\boldsymbol{\lambda}_\nu, \boldsymbol{\lambda}_t \in \mathbb{R}^m$ that are the opposite of the discrete relative normal and tangential contact stresses, respectively. The stiffness matrix and the load vector are represented by \mathbf{K} and \mathbf{f} , respectively. Matrices \mathbf{N} and \mathbf{T} are associated with the contact nodes in normal and tangential direction, respectively. \mathcal{F} stands for the coefficient of the Coulomb friction. Our unknown vector of the nodal displacement is \mathbf{u} . As this is just short report we have omitted the corresponding dimensions.

In order to obtain the discrete contact problem with Tresca friction, we replace $\mathcal{F}_i \lambda_{\nu,i}$ in (2.3) by the entries g_i of $\mathbf{g} \in \mathbb{R}^m, \mathbf{g} \geq \mathbf{0}$.

Next we use the equivalent formulation of the previous problems as the systems of non-smooth equations. We introduce the projection mappings

$$\mathbf{P}_{\mathbb{R}_+^m} : \mathbb{R}^m \mapsto \mathbb{R}_+^m \quad \mathbf{P}_{\Lambda(\mathbf{r})} : \mathbb{R}^m \mapsto \Lambda(\mathbf{r})$$

with $\mathbb{R}_+^m := \{\boldsymbol{\mu} \in \mathbb{R}^m : \boldsymbol{\mu} \geq \mathbf{0}\}, \Lambda(\mathbf{r}) := \{\boldsymbol{\mu} \in \mathbb{R}^m : |\boldsymbol{\mu}| \leq \mathbf{r}\}$, respectively and $\mathbf{r} \in \mathbb{R}^m, \mathbf{r} \geq \mathbf{0}$. The definitions of the components of $\mathbf{P}_{\mathbb{R}_+^m}, \mathbf{P}_{\Lambda(\mathbf{r})}$ are based on the max-function in \mathbb{R}^1 :

$$(\mathbf{P}_{\mathbb{R}_+^m})_i(\boldsymbol{\mu}) = \max\{0, \mu_i\}, \tag{2.4}$$

$$(\mathbf{P}_{\Lambda(\mathbf{r})})_i(\boldsymbol{\mu}) = \max\{0, \mu_i + r_i\} - \max\{0, \mu_i - r_i\} - r_i. \tag{2.5}$$

Denote $\mathbf{y} := (\mathbf{u}^\top, \boldsymbol{\lambda}_\nu^\top, \boldsymbol{\lambda}_t^\top)^\top \in \mathbb{R}^{2n+2m}$ and consider a parameter $\rho > 0$. The discrete contact problem with Coulomb friction is equivalent to the equation

$$\mathbf{G}(\mathbf{y}) = \mathbf{0} \tag{2.6}$$

where $\mathbf{G} : \mathbb{R}^{2n+2m} \mapsto \mathbb{R}^{2n+2m}$ is defined by

$$\mathbf{G}(\mathbf{y}) := \begin{pmatrix} \mathbf{K}\mathbf{u} - \mathbf{f} + \mathbf{N}^\top \boldsymbol{\lambda}_\nu + \mathbf{T}^\top \boldsymbol{\lambda}_t \\ \boldsymbol{\lambda}_\nu - \mathbf{P}_{\mathbb{R}_+^m}(\boldsymbol{\lambda}_\nu + \rho(\mathbf{N}\mathbf{u} - \mathbf{d})) \\ \boldsymbol{\lambda}_t - \mathbf{P}_{\Lambda(\mathcal{F}\boldsymbol{\lambda}_\nu)}(\boldsymbol{\lambda}_t + \rho\mathbf{T}\mathbf{u}) \end{pmatrix}.$$

2.1 Algorithms

As we use the semi-smooth Newton method (SSNM) our algorithms are based on the following iterative scheme:

$$\mathbf{F}^o(\mathbf{y}^{(k-1)})\mathbf{y}^{(k)} = \mathbf{F}^o(\mathbf{y}^{(k-1)})\mathbf{y}^{(k-1)} - \mathbf{F}(\mathbf{y}^{(k-1)}), \quad k = 1, 2, \dots, \tag{2.7}$$

where $\mathbf{F} : \mathbb{R}^{2n+2m} \mapsto \mathbb{R}^{2n+2m}$ is slantly differentiable and $\mathbf{F}^o(\mathbf{y})$ is a slanting function to \mathbf{F} at $\mathbf{y} \in \mathbb{R}^{2n+2m}$. It is well known that sequence $\{\mathbf{y}^{(k)}\}$ generated by (2.7) converges superlinearly to the solution of $\mathbf{F}(\mathbf{y}) = \mathbf{0}$ when the initial iterate $\mathbf{y}^{(0)} \in \mathbb{R}^{2n+2m}$ is a sufficiently accurate approximation of the solution.

We will show an implementation of SSNM that is equivalent to an active set algorithm. Firstly, let us introduce notations. Let $\mathcal{M} = \{1, 2, \dots, m\}$ be the set of all indices and let $\mathbf{y} = (\mathbf{u}^\top, \boldsymbol{\lambda}_\nu^\top, \boldsymbol{\lambda}_t^\top)^\top \in \mathbb{R}^{2n+2m}$ be given. The active set $\mathcal{A}_\nu := \mathcal{A}_\nu(\mathbf{y})$ corresponding to the non-penetration condition is defined by

$$\mathcal{A}_\nu(\mathbf{y}) = \{i \in \mathcal{M} : \lambda_{\nu,i} + \rho(\mathbf{N}\mathbf{u} - \mathbf{d})_i > 0\}$$

and the respective inactive set is its complement $\mathcal{I}_\nu := \mathcal{I}_\nu(\mathbf{y}) = \mathcal{M} \setminus \mathcal{A}_\nu(\mathbf{y})$. For $S \subseteq \mathcal{M}$ we introduce the diagonal matrix

$$\mathbf{D}_S = \text{diag}(s_1, \dots, s_m) \in \mathbb{R}^{m \times m}, \quad s_i = \begin{cases} 1 & \text{for } i \in S, \\ 0 & \text{for } i \notin S. \end{cases}$$

Non-symmetric case. First we propose the algorithm for direct solving discrete contact problems with Coulomb friction. To this end we introduce two inactive sets $\mathcal{I}_t^+ := \mathcal{I}_t^+(\mathbf{y})$, $\mathcal{I}_t^- := \mathcal{I}_t^-(\mathbf{y})$ corresponding to the condition of Coulomb friction:

$$\begin{aligned} \mathcal{I}_t^+(\mathbf{y}) &= \{i \in \mathcal{M} : \lambda_{t,i} + \rho(\mathbf{T}\mathbf{u})_i > \mathcal{F}_i \lambda_{\nu,i}\}, \\ \mathcal{I}_t^-(\mathbf{y}) &= \{i \in \mathcal{M} : \lambda_{t,i} + \rho(\mathbf{T}\mathbf{u})_i < -\mathcal{F}_i \lambda_{\nu,i}\}. \end{aligned}$$

The respective active set is $\mathcal{A}_t := \mathcal{A}_t(\mathbf{y}) = \mathcal{M} \setminus (\mathcal{I}_t^+(\mathbf{y}) \cup \mathcal{I}_t^-(\mathbf{y}))$. After suitable adjustments we arrive at the following algorithm.

Algorithm ActiveSetCoulomb1

- (0) Set $k := 1$, $\rho > 0$, $\varepsilon_u > 0$, $\mathbf{u}^{(0)} \in \mathbb{R}^{2n}$, $\boldsymbol{\lambda}_\nu^{(0)}, \boldsymbol{\lambda}_t^{(0)} \in \mathbb{R}^m$.
- (1) Define the active and inactive sets at $\mathbf{y} = ((\mathbf{u}^{(k-1)})^\top, (\boldsymbol{\lambda}_\nu^{(k-1)})^\top, (\boldsymbol{\lambda}_t^{(k-1)})^\top)^\top$:

$$\mathcal{A}_\nu = \mathcal{A}_\nu(\mathbf{y}), \mathcal{I}_\nu = \mathcal{I}_\nu(\mathbf{y}), \mathcal{A}_t = \mathcal{A}_t(\mathbf{y}), \mathcal{I}_t^+ = \mathcal{I}_t^+(\mathbf{y}), \mathcal{I}_t^- = \mathcal{I}_t^-(\mathbf{y}).$$

- (2) Solve:

$$\begin{pmatrix} \mathbf{K} & \mathbf{N}^\top & \mathbf{T}^\top \\ \mathbf{D}_{\mathcal{A}_\nu} \mathbf{N} & \mathbf{D}_{\mathcal{I}_\nu} & \mathbf{0} \\ \mathbf{D}_{\mathcal{A}_t} \mathbf{T} & \mathcal{F}(\mathbf{D}_{\mathcal{I}_t^-} - \mathbf{D}_{\mathcal{I}_t^+}) & \mathbf{D}_{\mathcal{I}_t^+ \cup \mathcal{I}_t^-} \end{pmatrix} \begin{pmatrix} \mathbf{u}^{(k)} \\ \boldsymbol{\lambda}_\nu^{(k)} \\ \boldsymbol{\lambda}_t^{(k)} \end{pmatrix} = \begin{pmatrix} \mathbf{f} \\ \mathbf{D}_{\mathcal{A}_\nu} \mathbf{d} \\ \mathbf{0} \end{pmatrix}.$$

- (3) Set $\text{err}^{(k)} := \|\mathbf{u}^{(k)} - \mathbf{u}^{(k-1)}\| / \|\mathbf{u}^{(k)}\|$. If $\text{err}^{(k)} \leq \varepsilon_u$, return $\mathbf{u} := \mathbf{u}^{(k)}$, $\boldsymbol{\lambda}_\nu := \boldsymbol{\lambda}_\nu^{(k)}$, and $\boldsymbol{\lambda}_t := \boldsymbol{\lambda}_t^{(k)}$.

- (4) Set $k := k + 1$ and go to step (1).

As we deal in step (2) with non-symmetric matrices with generalized saddle-point structure we use BiCGSTAB.

Symmetric case. The only difference when we want to propose the algorithm for solving the discrete problem with Tresca friction is in the definition of inactive sets when $\mathcal{F}_i \lambda_{\nu,i}$ is substituted by g_i . The algorithm then differs only in the step (2). The matrix now can be made symmetric and we can use CGM. The algorithm stays the same and the step (2) is presented below.

Algorithm *ActiveSetTresca*

(2) Solve:

$$\begin{pmatrix} \mathbf{K} & \mathbf{N}_{\mathcal{A}_\nu}^\top & \mathbf{T}_{\mathcal{A}_t}^\top \\ \mathbf{N}_{\mathcal{A}_\nu} & \mathbf{0} & \mathbf{0} \\ \mathbf{T}_{\mathcal{A}_t} & \mathbf{0} & \mathbf{0} \end{pmatrix} \begin{pmatrix} \mathbf{u}^{(k)} \\ \lambda_{\nu, \mathcal{A}_\nu}^{(k)} \\ \lambda_{t, \mathcal{A}_t}^{(k)} \end{pmatrix} = \begin{pmatrix} \mathbf{f} - \mathbf{T}_{\mathcal{I}_t^+}^\top \mathbf{g}_{\mathcal{I}_t^+} + \mathbf{T}_{\mathcal{I}_t^-}^\top \mathbf{g}_{\mathcal{I}_t^-} \\ \mathbf{d}_{\mathcal{A}_\nu} \\ \mathbf{0} \end{pmatrix},$$

and set $\lambda_{\nu, \mathcal{I}_\nu}^{(k)} = \mathbf{0}$, $\lambda_{t, \mathcal{I}_t^+}^{(k)} = \mathbf{g}_{\mathcal{I}_t^+}$, $\lambda_{t, \mathcal{I}_t^-}^{(k)} = -\mathbf{g}_{\mathcal{I}_t^-}$.

In order to solve the discrete contact problem with Coulomb friction, one can use the algorithm *ActiveSetTresca* in each successive approximation. In order to achieve high computational efficiency, we prefer the inexact implementation in which one iteration of the algorithm *ActiveSetTresca* is performed. In other words, we modify the algorithmic scheme *ActiveSetTresca* so that we take $\mathbf{g} := \mathcal{F} \max\{\lambda_\nu^{(k-1)}, 0\}$ in the beginning of each iteration.

3 Implementation

In this section, we interpret each step (2) of algorithm *ActiveSetTresca* as the minimization of a strictly quadratic objective function in terms of λ , for that one can use the conjugate gradient method. We will arrive at the globally convergent dual implementation of the algorithm; see [3].

We start with notations.

$$\mathcal{A} = \{i \mid i \in \mathcal{A}_\nu\} \cup \{i + m \mid i \in \mathcal{A}_t\} \quad \text{and} \quad \mathcal{I} = \{1, 2, \dots, 2m\} \setminus \mathcal{A}.$$

Denote

$$\mathbf{B} = \begin{pmatrix} \mathbf{N} \\ \mathbf{T} \end{pmatrix}, \quad \mathbf{c} = \begin{pmatrix} \mathbf{d} \\ \mathbf{0} \end{pmatrix}, \quad \lambda = \begin{pmatrix} \lambda_\nu \\ \lambda_t \end{pmatrix},$$

and

$$q(\lambda) = \frac{1}{2} \lambda^\top \mathbf{A} \lambda - \lambda^\top \mathbf{b},$$

where $\mathbf{A} = \mathbf{B} \mathbf{K}^{-1} \mathbf{B}^\top$, $\mathbf{b} = \mathbf{B} \mathbf{K}^{-1} \mathbf{f} - \mathbf{c}$. Finally note that the gradient to q at λ reads as

$$\nabla q(\lambda) = \mathbf{A} \lambda - \mathbf{b}.$$

The linear system in step (2) of algorithm *ActiveSetTresca* reads as

$$\begin{pmatrix} \mathbf{K} & \mathbf{B}_\mathcal{A}^\top \\ \mathbf{B}_\mathcal{A} & \mathbf{0} \end{pmatrix} \begin{pmatrix} \mathbf{u}^{(k)} \\ \lambda_\mathcal{A}^{(k)} \end{pmatrix} = \begin{pmatrix} \hat{\mathbf{f}} \\ \mathbf{c}_\mathcal{A} \end{pmatrix}, \tag{3.8}$$

where $\widehat{\mathbf{f}} = \mathbf{f} - \mathbf{T}_{\mathcal{I}_t^+}^\top \mathbf{g}_{\mathcal{I}_t^+} + \mathbf{T}_{\mathcal{I}_t^-}^\top \mathbf{g}_{\mathcal{I}_t^-}$ and the remaining components of $\boldsymbol{\lambda}^{(k)}$ are given by

$$\boldsymbol{\lambda}_{\nu, \mathcal{I}_\nu}^{(k)} = \mathbf{0}, \quad \boldsymbol{\lambda}_{t, \mathcal{I}_t^+}^{(k)} = \mathbf{g}_{\mathcal{I}_t^+}, \quad \boldsymbol{\lambda}_{t, \mathcal{I}_t^-}^{(k)} = -\mathbf{g}_{\mathcal{I}_t^-}. \tag{3.9}$$

The following lemma interprets the solution.

Lemma 1. (i) Let $\mathcal{A} = \emptyset$. Then $\boldsymbol{\lambda}^{(k)}$ is fully determined by (3.9) and

$$\mathbf{u}^{(k)} = \mathbf{K}^{-1} \widehat{\mathbf{f}} = \mathbf{K}^{-1} (\mathbf{f} - \mathbf{B}^\top \boldsymbol{\lambda}^{(k)}).$$

(ii) Let $\mathcal{A} \neq \emptyset$. Then $\boldsymbol{\lambda}_{\mathcal{A}}^{(k)}$ is the minimizer to the problem

$$\min \frac{1}{2} \boldsymbol{\lambda}_{\mathcal{A}}^\top \mathbf{A}_{\mathcal{A}\mathcal{A}} \boldsymbol{\lambda}_{\mathcal{A}} - \boldsymbol{\lambda}_{\mathcal{A}}^\top \widehat{\mathbf{b}}_{\mathcal{A}}, \tag{3.10}$$

where $\widehat{\mathbf{b}}_{\mathcal{A}} = \mathbf{B}_{\mathcal{A}} \mathbf{K}^{-1} \widehat{\mathbf{f}} - \mathbf{c}_{\mathcal{A}}$. The remaining components of $\boldsymbol{\lambda}^{(k)}$ are given by (3.9) and

$$\mathbf{u}^{(k)} = \mathbf{K}^{-1} (\widehat{\mathbf{f}} - \mathbf{B}_{\mathcal{A}}^\top \boldsymbol{\lambda}_{\mathcal{A}}^{(k)}) = \mathbf{K}^{-1} (\mathbf{f} - \mathbf{B}^\top \boldsymbol{\lambda}^{(k)}).$$

In the next lemma, we show how to define the active and inactive sets without the knowledge of $\mathbf{u}^{(k)}$.

Lemma 2. Let $\boldsymbol{\lambda} = \boldsymbol{\lambda}^{(k)}$. It holds:

$$\begin{aligned} \mathcal{A}_\nu &= \{i \in \mathcal{M} : \lambda_{\nu,i} - \rho \nabla_i q(\boldsymbol{\lambda}) > 0\}, \\ \mathcal{I}_t^+ &= \{i \in \mathcal{M} : \lambda_{t,i} - \rho \nabla_{i+m} q(\boldsymbol{\lambda}) > g_i\}, \\ \mathcal{I}_t^- &= \{i \in \mathcal{M} : \lambda_{t,i} - \rho \nabla_{i+m} q(\boldsymbol{\lambda}) < -g_i\}. \end{aligned}$$

Finally, we show how to determine $\boldsymbol{\lambda}^{(k)}$ via the constrained minimization problem.

Lemma 3. Let $\mathcal{A} \neq \emptyset$. Then $\boldsymbol{\lambda}^{(k)}$ determined in step (2) of algorithm *ActiveSet-Tresca* is the minimizer of the problem:

$$\min q(\boldsymbol{\lambda}) \tag{3.11}$$

$$\text{subject to } \boldsymbol{\lambda}_{\nu, \mathcal{I}_\nu} = \mathbf{0}, \quad \boldsymbol{\lambda}_{t, \mathcal{I}_t^+} = \mathbf{g}_{\mathcal{I}_t^+}, \quad \boldsymbol{\lambda}_{t, \mathcal{I}_t^-} = -\mathbf{g}_{\mathcal{I}_t^-}. \tag{3.12}$$

Algorithm *ActiveSetTresca* (Dual Version: Implementation 1)

(0) Set $k := 1, \rho > 0, \varepsilon_\lambda > 0, \boldsymbol{\lambda}^{(0)} \in \mathbb{R}^{2m}$.

(1) Define the active and inactive sets at $\boldsymbol{\lambda} = \boldsymbol{\lambda}^{(k-1)}$:

$$\begin{aligned} \mathcal{A}_\nu &= \{i \in \mathcal{M} : \lambda_{\nu,i} - \rho \nabla_i q(\boldsymbol{\lambda}) > 0\}, \\ \mathcal{I}_t^+ &= \{i \in \mathcal{M} : \lambda_{t,i} - \rho \nabla_{i+m} q(\boldsymbol{\lambda}) > g_i\}, \\ \mathcal{I}_t^- &= \{i \in \mathcal{M} : \lambda_{t,i} - \rho \nabla_{i+m} q(\boldsymbol{\lambda}) < -g_i\}, \\ \mathcal{I}_\nu &= \mathcal{M} \setminus \mathcal{A}_\nu, \quad \mathcal{A}_t = \mathcal{M} \setminus (\mathcal{I}_t^+ \cup \mathcal{I}_t^-) \end{aligned}$$

and \mathcal{A}, \mathcal{I} .

(2) If $\mathcal{I} \neq \emptyset$, set $\boldsymbol{\lambda}_{\mathcal{I}}^{(k)}$ so that $\boldsymbol{\lambda}_{\nu, \mathcal{I}_\nu}^{(k)} = \mathbf{0}$, $\boldsymbol{\lambda}_{t, \mathcal{I}_t^+}^{(k)} = \mathbf{g}_{\mathcal{I}_t^+}$, $\boldsymbol{\lambda}_{t, \mathcal{I}_t^-}^{(k)} = -\mathbf{g}_{\mathcal{I}_t^-}$.
If $\mathcal{A} \neq \emptyset$, find

$$\boldsymbol{\lambda}_{\mathcal{A}}^{(k)} := \arg \min \frac{1}{2} \boldsymbol{\lambda}_{\mathcal{A}}^\top \mathbf{A}_{\mathcal{A}\mathcal{A}} \boldsymbol{\lambda}_{\mathcal{A}} - \boldsymbol{\lambda}_{\mathcal{A}}^\top \widehat{\mathbf{b}}_{\mathcal{A}}.$$

(3) Set $err^{(k)} := \|\boldsymbol{\lambda}^{(k)} - \boldsymbol{\lambda}^{(k-1)}\| / \|\boldsymbol{\lambda}^{(k)}\|$. If $err^{(k)} \leq \varepsilon_\lambda$, return

$$\mathbf{u} := \mathbf{K}^{-1}(\mathbf{f} - \mathbf{B}^\top \boldsymbol{\lambda}^{(k)}), \quad \boldsymbol{\lambda} := \boldsymbol{\lambda}^{(k)}$$

and stop.

(4) Set $k := k + 1$ and go to step (1).

At this moment we implement CGM in step (2) of this last algorithm. Some numerical experiments have been done.

References

1. Z. Dostál. *Optimal Quadratic Programming Algorithms, with Applications to Variational Inequalities*. Springer, 2008, New York, 1st ed.
2. G. H. Golub, C. F. Van Loan. *Matrix Computations*. The John Hopkins University Press, 1996, Baltimore, 3rd ed.
3. R. Kučera, K. Rádková. *An Experimental Study of the Semi-Smooth Newton Method for Solving 2D Contact Problems with Tresca and Coulomb Friction*, in preparation
4. J. Nocedal, S. J. Wright. *Numerical Optimization*. Springer, 2006, New York, 2nd ed.
5. K. Rádková. *Newton-like methods for nonlinear programming*. Master thesis, UP Olomouc, 2010.

The Polynomials in Barzilai-Borwein Algorithm

Lukáš Pospíšil

Department of Applied Mathematics, FEECS,
VŠB – Technical University of Ostrava, 17. listopadu 15, 708 33 Ostrava – Poruba
lukas.pospisil@vsb.cz

Abstract. This paper is a first step to deal with convergence of recently developed faster gradient descend method called Barzilai-Borwein algorithm. We try to establish our theory on polynomials in error analysis. This view can be also applied in other gradient descend methods.

Keywords: Barzilai-Borwein method, convergence, polynomials

1 Introduction

In this paper, we will introduce recently developed Barzilai-Borwein gradient method [2] for solving systems of linear equations

$$\mathbf{Ax} = \mathbf{b}, \quad \mathbf{A} \in \mathbb{R}^{n,n}, \mathbf{b} \in \mathbb{R}^n, \quad (1)$$

with symmetric, positive definite matrix \mathbf{A} , or equivalently the search for the minimum of the strictly convex quadratic function

$$f(\mathbf{x}) := \frac{1}{2} \langle \mathbf{Ax}, \mathbf{x} \rangle - \langle \mathbf{b}, \mathbf{x} \rangle. \quad (2)$$

Typical methods for solving this classical quadratic programming problem ((1) or (2)) are the well-known Steepest Descend method (SD) or the Conjugate Gradient method (CG), see e.g. [5].

In next pages, we will describe different choice of the step-size $\alpha_k \in \mathbb{R}$ in the line-search type algorithm

$$\mathbf{x}_{k+1} = \mathbf{x}_k + \alpha_k \mathbf{v}_k \quad (3)$$

with the gradient descend step-vector $\mathbf{v}_k := -\nabla f(\mathbf{x}_k) = \mathbf{b} - \mathbf{Ax}_k$.

This choice of the step-size rapidly decreases the number of iterations required for finding an approximation of the solution with the prescribed accuracy (see for example [1]).

2 Barzilai-Borwein algorithm

At first we consider the Newton method for solving one non-linear equation $g(\mathbf{x}) = 0$, $\mathbf{g} : \mathbb{R} \rightarrow \mathbb{R}$ with approximation of deriving $g'(\mathbf{x}_k)$ (also known as *secant method*) with iteration prescription

$$\mathbf{x}_{k+1} = \mathbf{x}_k - \frac{1}{g'(\mathbf{x}_k)}g(\mathbf{x}_k) \approx \mathbf{x}_k - \frac{\mathbf{x}_k - \mathbf{x}_{k-1}}{g(\mathbf{x}_k) - g(\mathbf{x}_{k-1})}g(\mathbf{x}_k). \quad (4)$$

If we denote $\mathbf{g}_k := g(\mathbf{x}_k) = \nabla f(\mathbf{x}_k)$ and

$$\alpha_k := \frac{\mathbf{x}_k - \mathbf{x}_{k-1}}{\mathbf{g}_k - \mathbf{g}_{k-1}}, \quad (5)$$

we can see the analogy between the formulas (3) and (4).

Using this formula, we manage to solve the equation $g(\mathbf{x}) = 0$, i.e. $\nabla f(\mathbf{x}) = \mathbf{Ax} - \mathbf{b} = 0$.

In more dimensional case, i.e. $g : \mathbb{R}^n \rightarrow \mathbb{R}^n$, there is a problem with evaluation of the coefficient $\alpha_k \in \mathbb{R}$ using (5). Instead of using (5), we assemble the equation (so-called *secant equation*)

$$\frac{1}{\alpha_k}(\mathbf{x}_k - \mathbf{x}_{k-1}) = \mathbf{g}_k - \mathbf{g}_{k-1} \quad (6)$$

and solve it in the least-squares sense

$$\frac{1}{\alpha_k} := \arg \min_{\beta \in \mathbb{R}} \|(\mathbf{x}_k - \mathbf{x}_{k-1})\beta - (\mathbf{g}_k - \mathbf{g}_{k-1})\|^2.$$

After denoting

$$\mathbf{s}_k := \mathbf{x}_k - \mathbf{x}_{k-1}, \quad \mathbf{y}_k := \mathbf{g}_k - \mathbf{g}_{k-1}$$

and some simplifications, we get the minimizing problem of strictly convex quadratic function

$$\frac{1}{\alpha_k} = \arg \min_{\beta \in \mathbb{R}} (\beta^2 \langle \mathbf{s}_k, \mathbf{s}_k \rangle - 2\beta \langle \mathbf{s}_k, \mathbf{y}_k \rangle + \langle \mathbf{y}_k, \mathbf{y}_k \rangle).$$

From the necessary conditions of a local minimum we get

$$\frac{1}{\alpha_k} = \frac{\langle \mathbf{s}_k, \mathbf{y}_k \rangle}{\langle \mathbf{s}_k, \mathbf{s}_k \rangle}. \quad (7)$$

The derivation of the algorithm is complete, but we can continue with adaption of equation (7). From line-search algorithm (3) one can see

$$\begin{aligned} \mathbf{y}_k &= \mathbf{g}_k - \mathbf{g}_{k-1} = (\mathbf{Ax}_k - \mathbf{b}) - (\mathbf{Ax}_{k-1} - \mathbf{b}) = \mathbf{As}_k \\ \mathbf{s}_k &= \mathbf{x}_k - \mathbf{x}_{k-1} = (\mathbf{x}_{k-1} - \alpha_k^{-1} \mathbf{g}_{k-1}) - \mathbf{x}_{k-1} = -\alpha_k^{-1} \mathbf{g}_{k-1} \end{aligned}$$

and after substitution into (7) we get

$$\alpha_k = \frac{\langle \mathbf{s}_k, \mathbf{s}_k \rangle}{\langle \mathbf{As}_k, \mathbf{s}_k \rangle} = \frac{\langle -\alpha_k^{-1} \mathbf{g}_{k-1}, -\alpha_k^{-1} \mathbf{g}_{k-1} \rangle}{\langle -\alpha_k^{-1} \mathbf{g}_{k-1}, -\alpha_k^{-1} \mathbf{Ag}_{k-1} \rangle} = \frac{\langle \mathbf{g}_{k-1}, \mathbf{g}_{k-1} \rangle}{\langle \mathbf{Ag}_{k-1}, \mathbf{g}_{k-1} \rangle}. \quad (8)$$

Final form of Barzilai-Borwein algorithm is (substitute (8) into (3))

$$\mathbf{x}_{k+1} = \mathbf{x}_k - \frac{\langle \mathbf{g}_{k-1}, \mathbf{g}_{k-1} \rangle}{\langle \mathbf{A}\mathbf{g}_{k-1}, \mathbf{g}_{k-1} \rangle} \mathbf{g}_k . \tag{9}$$

In conclusion we can state, that BB is like SD, but the step-size is computed using $g(\mathbf{x}_{k-1})$ instead of gradient in previous approximation $g(\mathbf{x}_k)$.

3 Polynomials in general Gradient Descend methods

Let us define absolute error in k -th iteration

$$\mathbf{e}_k := \mathbf{x}_k - \tilde{\mathbf{x}} .$$

Then after substitution (3) we get

$$\begin{aligned} \mathbf{e}_{k+1} &= \mathbf{x}_{k+1} - \tilde{\mathbf{x}} = \mathbf{x}_k - \alpha_k \mathbf{g}_k - \tilde{\mathbf{x}} \\ &= \mathbf{x}_k - \alpha_k (\mathbf{A}\mathbf{x}_k - \mathbf{A}\tilde{\mathbf{x}}) - \tilde{\mathbf{x}} = (\mathbf{I} - \alpha_k \mathbf{A})\mathbf{e}_k . \end{aligned} \tag{10}$$

If \mathbf{A} is symmetric positive definite matrix, there exists singular value decomposition $\mathbf{A} = \mathbf{U}^T \mathbf{D} \mathbf{U}$, where \mathbf{D} is a diagonal matrix with eigenvalues of \mathbf{A} on diagonal and \mathbf{U} is orthogonal matrix with appropriate eigenvectors. We can write system (1) in equivalent form

$$\mathbf{A}\mathbf{x} = \mathbf{b} \Rightarrow \mathbf{U}^T \mathbf{D} \mathbf{U} \mathbf{x} = \mathbf{b} \Rightarrow \mathbf{D} \mathbf{U} \mathbf{x} = \mathbf{U} \mathbf{b} \Rightarrow \mathbf{D} \tilde{\mathbf{x}} = \tilde{\mathbf{b}} .$$

So, in the following, we will consider \mathbf{A} as a diagonal matrix with positive eigenvalues on diagonal, i.e. $\mathbf{A} := \text{diag}(\lambda_1, \dots, \lambda_n)$.

Then every i -th component ($i \in \{1, \dots, n\}$) of vector \mathbf{e}_{k+1} given by (10) can be written in form

$$\{\mathbf{e}_{k+1}\}_i = (1 - \alpha_k \lambda_i) \{\mathbf{e}_k\}_i = \left[\prod_{j=0}^k (1 - \alpha_j \lambda_i) \right] \{\mathbf{e}_0\}_i . \tag{11}$$

If we define polynomial

$$p_k(\lambda) := \prod_{j=0}^k (1 - \alpha_j \lambda) , \tag{12}$$

then we can write equation (11) in form

$$\{\mathbf{e}_{k+1}\}_i = p_k(\lambda_i) \{\mathbf{e}_0\}_i . \tag{13}$$

The convergence of Gradient Descend method is equivalent to

$$\lim_{k \rightarrow \infty} \mathbf{x}_k = \tilde{\mathbf{x}} \Leftrightarrow \lim_{k \rightarrow \infty} \mathbf{e}_k = 0 \Leftrightarrow \forall i \in \{1, \dots, n\} : \lim_{k \rightarrow \infty} p_k(\lambda_i) = 0$$

The one way how to prove convergence is to show that the roots of $p_k(\lambda)$ (i.e. $1/\alpha_k$) converge to eigenvalues. For BB method this way was used in [3] and [4].

Let us consider Taylor expansion of $p_k(\lambda)$ in neighborhood of $1/\alpha_k$

$$p_k(\lambda) = p_k(1/\alpha_k) + \sum_{j=1}^{\infty} \frac{p_k^{(j)}(1/\alpha_k)}{j!} (\lambda - 1/\alpha_k)^j$$

and because $p_k(\lambda)$ is a polynomial of degree $k + 1$ and $1/\alpha_k$ is a root of $p_k(\lambda)$, we can simplify the last equation to

$$p_k(\lambda_i) = \sum_{j=1}^{k+1} \frac{p_k^{(j)}(1/\alpha_k)}{j!} (\lambda_i - 1/\alpha_k)^j .$$

From this, we can see that the value of $p_k(\lambda_i)$ (i.e. value of i -th component of error vector, see (13)) depends not only on distance between $1/\alpha_k$ and λ_i , but also on derivatives of p_k at root $1/\alpha_k$.

4 Numerical experiments

Let us consider simple diagonal matrix

$$\begin{aligned} \mathbf{A} &:= \text{diag} (0.2, 0.3, 1, 1.2, 1.25) , \\ \mathbf{b} &:= (1, 1, 1, 1, 1)^T , \\ \mathbf{x}_0 &:= (1, 1, 1, 1, 1)^T . \end{aligned}$$

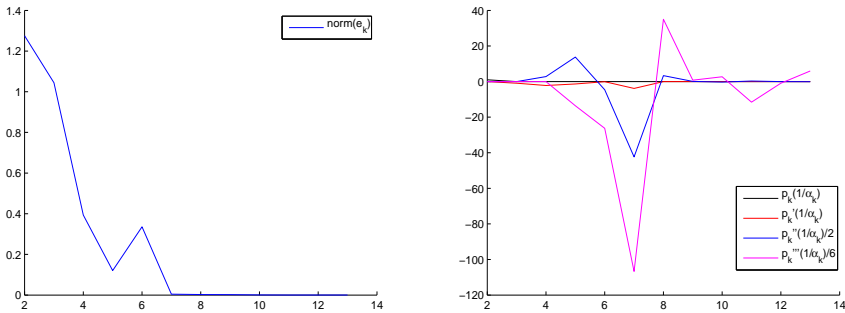


Fig. 1. Norm of absolute error in each iteration of BB for solving the first test problem (left). Values of derivatives of approximating polynomials in each iteration of BB for solving the first test problem (right).

Figure 1 (left) shows that norm of error in k -th iteration $\|e_k\|_2$ is not monotonically decreasing (like in SD or CG) - see also original paper of BB [2]. Values of polynomials $p_k(1/\alpha_k), p'_k(1/\alpha_k), p''_k(1/\alpha_k), p'''_k(1/\alpha_k)$ for every k -th iteration

are plotted in Figure 1 (right). This values are also nonmonotone. For computing these derivatives, we used numerical prescription

$$p_k^{(j)}(\lambda) = \frac{p_k^{(j-1)}(\lambda + d) - p_k^{(j-1)}(1/\alpha_k)}{d} .$$

For the next example, we take testing data

$$\begin{aligned} \mathbf{B} &:= \text{fivediag}(1, 1, 4, 1, 1) \in \mathbb{R}^{50,50} , \\ \mathbf{A} &:= \text{diag}(\sigma(\mathbf{B})) \in \mathbb{R}^{50,50} , \\ \mathbf{b} &:= (1, \dots, 1)^T \in \mathbb{R}^{50} , \\ \mathbf{x}_0 &:= (0, \dots, 0)^T \in \mathbb{R}^{50} . \end{aligned}$$

Values of polynomials $p_k(1/\alpha_k), p'_k(1/\alpha_k), p''_k(1/\alpha_k), p'''_k(1/\alpha_k)$ for this problem are shown in Figure 2.

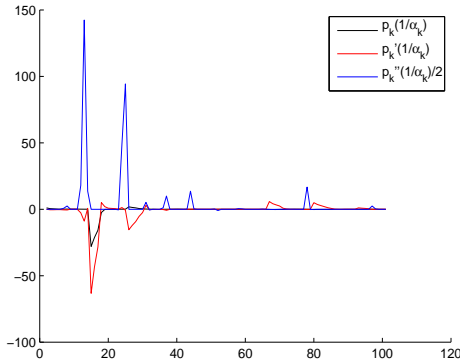


Fig. 2. Values of derivatives of approximating polynomials in each iteration of BB for solving the second test problem.

5 Conclusion

In this paper, we presented BB algorithm and tried to find another way how to prove its convergence. However, we exposed that BB algorithm is nonmonotone in derivations of error polynomials. In further work, we shall extend this theory.

6 Acknowledgements

This research has been supported by the grant GA CR 201/07/0294 and the Ministry of Education of the Czech Republic No. MSM6198910027. The author would like to express his thanks to Prof. RNDr. Zdeněk Dostál, DSc.

References

1. Pospíšil L., Menšík M.: *Faster Gradient Descent Methods*. SNA12, 2012.
2. Barzilai J., Borwein J. M.: *Two point step size gradient methods*. IMA Journal of Numerical Analysis, 8:141-148, 1988.
3. Raydan M.: *Convergence properties of the Barzilai and Borwein gradient method*. Rice University, 1991.
4. Dai Y.H., Liao L.Z.: *R-linear convergence of the Barzilai and Borwein gradient method*. The Institute of Mathematics and its Applications, 2002.
5. Vondrák V., Pospíšil L.: *Numerické metody 1*. syllabus (in czech), project MI21, <http://mi21.vsb.cz>, 2011.

Ant Colony Optimization for Traffic Routing on a Dynamic Network with Anti-Congestion Measures

Lukas Rapant

Department of Applied Mathematics, FEECS,
VŠB – Technical University of Ostrava, 17. listopadu 15, 708 33 Ostrava – Poruba
lukas.rapant@vsb.cz

Abstract. This article deals with traffic routing on a dynamic graph representing road network. It focuses on the selection of the fastest way in a traffic network. It assumes situation that at the beginning traffic network is empty and traffic comprises only of the cars released into the network. Strategy for optimization of routes for these cars is based on Ant colony optimization as it not only gives us tool for finding the fastest route but also a tool for representing indirect interaction between the cars.

Keywords: traffic routing, Ant colony optimization, dynamic graph

1 Introduction and problem statement

One of great optimization problems of today is how to deal with traffic fluency and congestions. However, we also have many tools to solve these problems. One of these tools are graph theory and Ant Colony Optimization (ACO). With these tools in mind, we can exactly define a problem. Let us have some traffic network and number of cars that have their start point and destination in this network. These cars can start their journey in various times of the day. Also note that in this basic scenario there are no other cars in the network in the beginning of the simulation. We want to find the fastest routes for all cars taking each others routes into consideration and therefore preventing congestions. This problem demands solution to two problems. The first one is how to represent dynamism in the traffic network since cars can depart and influence each other in various times. The second one is how to represent influence each car has on other cars.

1.1 Related works

Similar problems were addressed in many previous works. Tatomir and Rothkrantz [1] propose that dynamism and interaction can be introduced by direct communication of the navigation with the database and updating the database using

information obtained by individual cars. They are using basic ACO algorithms for the optimization. Similar approach to our is also used by Martinovic et al. in [2]. However they do not represent dynamism and use ACO only for individual cars. Bedi et al. [3] and Eyckelhof and Snoek [4] use ACO for traffic navigation of number of cars. However they offer a way to deal with congestions but not the exact way to prevent them. Many other approaches are presented in a survey made by Kwang Mong Sim and Weng Hong Sun [5]. They are however using much more complicated approaches and do not exactly deal with a dynamism in the network.

2 Problem Solution

Problem solution can be divided into two parts. In the first part ways how to represent dynamism in a traffic network will be shown and in the second one we will present modifications of ACO that take into account other cars.

2.1 Dynamic traffic network

Traffic network can be represented as a graph, where edges are representing roads, vertices crossroads and labels road lengths. This representation allows us to find the shortest path. This is, however, inaccurate as most of the time we are interested not in the shortest but in the fastest route. In static case these are identical but in dynamic system as traffic network we must separate these routes. For finding the fastest path we need to move into a time domain. Label then represents time it takes to traverse the edge. Difference between traffic density in peak hours with traffic density at midnight is huge so we need a model that will be able to represent dynamism of the network. This can be done by modeling the traffic network as a dynamic graph instead of static one. We define dynamic graph in definition 1 created in our previous work [7].

Definition 1. *Let us denote $G^*(V, E, t)$ to be dynamic graph where V is set of vertices, E is set of edges and t to be time. This graph has following properties:*

- *In each time t graph G^* can have different sets V and E .*
- *If graph G^* is weighted graph, it can have different $w(e, t) \forall e \in E$ in each time t .*

This approach allows us to precisely model every change of parameters of the traffic network in time. It is also desirable to mention that dynamism must not only be represented by changes of parameters of the graph in time but also in space. Maximum speed on a road is an example of dynamic parameter in space as there are various speed restrictions. We have developed Function method for representing both of the dynamisms.

This method deals with edge weight represented as functions describing time and space dynamism. Basic idea is that we recomputed edge weights to represent time it takes to traverse them in certain time. It is important to know in what

time we start to traverse the edge because in the dynamic graph parameters can change dynamically in time.

First we will define space dynamism. This can be simply defined by using integral calculus as

$$time = \int_0^l \frac{1}{v(s)} ds, \tag{1}$$

where v is function representing speed and l is a length of trajectory between A and B . It gives us method to compute time it takes to traverse some road when the speed is not constant. Time given by this equation is however still not influenced by other cars in the traffic network. This will be done by time-dependent function $\phi(t)$ which represents some form of delay caused by other traffic. In our case function $\varphi(t)$ is created by following equation

$$\varphi(t) = \frac{1}{\frac{(roadcap - traffic(t))}{roadcap}}, \tag{2}$$

where $roadcap$ is road capacity (in cars) and $traffic(t)$ is time-dependent function denoting number of cars on the road in each time t . Resulting function $\varphi(t)$ has its values between 1 (which represents empty road) and ∞ which represents absolutely congested road. This function $\varphi(t)$ then will be used as function denoting time increase caused by other traffic. However, this function is just an approximation. We have no data on actual traffic so it will be refined in the future as the data become available. Now only thing that remains is to compute final time it takes to traverse the road taking into account other traffic which is done by equation

$$time_{final} = \int_{t_0}^{t_0 + time} \varphi_{v(s)}(t) dt, \tag{3}$$

where t_0 is time we enter the road, $time$ is time we receive from equation (1) and $\varphi_{v(s)}(t)$ is a traffic delay function adapted for this particular road from equation (2). In case of car accident or congestion we will change value of the speed function $v(s)$ in place where accident happened to very small number so resulting integrals will yield number close to ∞ and the edge will not be traversable.

2.2 Ant colony optimization with negative pheromone

ACO is a class of algorithms based on behavior of colonies of ants. It was proposed by Dorigo in 1992 in his PhD thesis [6] and further developed by him and Maniezzo and Colorni. It is not a single algorithm with clear definition but entire spectrum of algorithms using the same principles. It is worthy to note that we are using here only basic variant. Exact description of these algorithms can be found in our previous work [7].

Now let us introduce our addition to basic ACO model. Let us say we will not have only positive pheromone, which is attracting ants but also a negative one which distracts them. Task of this pheromone is therefore not to make any edge more likely to be chosen by ant but to be less attractive. This can be used to model interaction between cars as cars are less likely to choose road with very high traffic density. It results in improvement of the length of their own route as well as those of other cars. There are many differences between positive and negative pheromone in our model. While level of positive pheromone is restarted after finding the fastest route for every car, negative pheromone evaporates only in real time of the model. Other difference is that it is updated after each car has found its fastest path and not inside the search for the fastest path. This pheromone is introduced into an ACO model as the third part of equation regarding probability of choosing an edge thus leading to equation

$$p_k(u, v) = \frac{[\delta(u, v)]^\alpha [\tau(u, v)]^\beta \left[\frac{roadcap(u, v)}{traffic_{(u, v)}(t)} \right]^\gamma}{\sum_{y \in N_u} [\delta(u, y)]^\alpha [\tau(u, y)]^\beta \left[\frac{roadcap(u, y)}{traffic_{(u, y)}(t)} \right]^\gamma}, \quad (4)$$

where $roadcap(u, v)$ is capacity of the edge (u, v) (in cars), $traffic_{(u, v)}(t)$ is number of cars on the edge (u, v) in time t and $\gamma > 0$ is coefficient of influence of the negative pheromone. The implementation of this approach will be presented in the next subsection.

2.3 Model implementation

Our model takes a traffic network as an oriented dynamic graph. Therefore every road (excluding one-way roads) is represented as two edges with opposite orientation. Every edge is labeled by two functions. Function (u, v) is obtained from real traffic network and represents real speed limit on a road. Function $traffic_{(u, v)}(t)$ is initially set as zero as there are no cars present in the network. However, as cars enter the network, the value of this time-dependent function will change according to the cars movements on the road. When one car in certain time drives the road, value of this function is set to be one, for two cars it is set to two and so on. As car leaves the edge value is lessened by one. This update is done after car is assigned its route and functions of edges it travels through are updated. The program run can be seen in following pseudocode.

Listing 1.1. Modified ACO pseudocode

```
function ACOGLOBAL(Traffic_network, number_of_ants, cars)
while (cars)
    pick_car(start, goal, time) // model receives request from car to provide
        the fastest route from start to goal starting in time t
    best_journey=Inf; // setting starting distance to infinity
    while(n!=number_of_ants) // algorithm termination by number of ants
        ant_journey=0;
        setAnt(start);
        while(goal_not_reached && applyProbabilityRule()!=0)
            // determining probabilities for neighboring
            edges using our equation with negative pheromone
        moveToChosenVertex();
```

```

        ant_journey=ant_journey+length(chosen_edge);
    end
    if length(ants_journey)<length(best_journey)
        best_journey=ants_journey; // saving best path
    end
    updatePheromones();
end
car_route=best_journey;
updateTrafficValues(car_route) // updating negative pheromone
end

```

We will be receiving the fastest route for each car in the traffic network as an output. These routes will be influenced by other cars in the network thanks to our dynamic approach to the graph and negative pheromone.

2.4 Real results

Usefulness of both our approaches has been assessed. Dynamic graph approach yields different time travels and even a different routes in a different times. More results concerning dynamic graph approach can be found in our previous work [7].

We have chosen to present functionality of our second improvement, ACO with negative pheromone, on simple traffic situation. Let us have dynamic traffic network like one on Fig.1. Functions $traffic_{(u,v)}(t)$ are set to zero and functions $v(s)$ are set according to the class of a road (the first class is the fastest, the third class is the slowest).

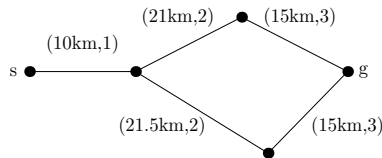


Fig. 1. Experimental traffic network (the first number in brackets is road length, the second number is road class)

We have chosen this situation of having two roughly equivalent roads because it demonstratively depicts benefits of our approach. Note that each edge represents both edges of an oriented graph. We are sending cars from vertex s to vertex g in interval of 5 seconds. The results of this experiment can be seen in Table 1. Parameters of ACO have been set as $\alpha = 1$, $\beta = 0.5$ and $\epsilon = 0.2$.

Times in the second and the third column represent average times it takes to drive from vertex s to g for all cars taking a trip (1000 in our case). Effectiveness of our approach slightly improves with growing γ . On the other hand as γ lowers, model approaches one without negative pheromone. However, it is not necessary to set γ higher than 10 as there is only very marginal difference. Please, note that the travel times are not exactly according to real times as we do not possess data for such calibration.

Table 1. Comparison of the results of ACO without and with negative pheromone.

Parameter γ	ACO without negative pheromone	ACO with negative pheromone
0.1	1.339 hour	1.3370 hour
1	1.3369 hour	1.3366 hour
2	1.3370 hour	1.3364 hour
10	1.3370 hour	1.3363 hour

3 Conclusion

In this article we have presented our approach to finding the fastest routes for a group of cars in a traffic network. Our approach has given slightly better results than basic one. Thanks to the dynamic graph approach these results are closer to the dynamic reality of the traffic.

4 Publications

This approach was not published yet but it will be published as part of bigger article concerning traffic navigation on a dynamic graph in a near future.

References

1. Tatominir B. and Rothkrantz L., Dynamic traffic routing using Ant Based Control, In *Proceedings of IEEE International Conference on Systems, Man and Cybernetics*, Hague, 2004, pp. 3970-3975.
2. Kromer P., Martinovic J., Radecky M., Tomis R. and Snasel V., Ant Colony Inspired Algorithm for Adaptive Traffic Routing, In *Proceedings of 2011 Third World Congress on Nature and Biologically Inspired Computing*, Hospedera del Colegio Fonsec a Salamanca, 2011, pp. 329-334.
3. Bedi P., Mediratta N., Dhand S., Sharma R. and Singhal A., Avoiding traffic jam using Ant Colony Optimization A novel approach, In *Proceedings of International Conference on Computational Intelligence and Multimedia Applications 2007*, Sivakasi, 2007, pp. 61-67.
4. Eyckelhof C. J., Snoek M., Ant Systems for a Dynamic TSP-Ants caught in a traffic jam, In *Ant Algorithms: Third International Workshop, ANTS 2002*, Brussels, 2002, pp. 88-99.
5. Kwang Mong Sim and Weng Hong Sun, Ant Colony Optimization for Routing and Load-Balancing: Survey and New Directions, *IEEE Transactions on systems, man, and cyberneticspart A: Systems and Humans*, Vol. 33, No. 5, 2003, pp. 560-572.
6. Dorigo M., *Optimization, Learning and Natural Algorithms*, PhD thesis, Dipartimento di Elettronica, Politecnico di Milano, 1992.
7. Rapant L., *Application of Dynamic Graphs for the Fastest Route Search in a Transport Network*, Diploma thesis, Department of Applied Mathematics, VSB-Technical University of Ostrava, 2011.

Parallel Mesh Multiplication for Petascale Systems

Aleš Ronovský, Pavla Kabelíková, and Vít Vondrák

Department of Applied Mathematics, FEECS,
VŠB – Technical University of Ostrava, 17. listopadu 15, 708 33 Ostrava – Poruba
{ales.ronovsky, pavla.kabelikova, vit.vondrak}@vsb.cz

Abstract. In this paper is described a new mesh multiplication package developed for Code_Saturne. The package implements parallel global refinement of hexahedral meshes for Code_Saturne to allow refining of existing meshes to more than 1 billion cells. This enables running Code_Saturne’s extremely large CFD simulations on PRACE Tier-0 systems. The effectiveness of the implemented multiplication algorithm is demonstrated on practical examples, which were carried out on CURIE system at CEA.

1 Introduction and Mesh Multiplication

Code_Saturne is a multi-purpose Computational Fluid Dynamics (CFD) software, which was originally designed for industrial applications and research activities in several fields related to energy production. Main aim of this project was to develop a parallel mesh multiplication package and integrate it to Code_Saturne to extend its capability to generate more than a billion cell meshes for petascale systems.

Mesh multiplication is the process of taking an existing mesh and changing its size, i.e. number and/or shape of the cells, to increase accuracy of the solution. In the case of Code_Saturne, we focused only on the multiplication of regular meshes, where the higher accuracy of the solution is attained refining each cell of the mesh. Since the main goal was to generate more than 1 billion cells meshes in 3D, we considered only meshes that contain hexahedral, tetrahedral, pyramidal and/or prismatic cells.

For an appropriate refinement, several methods are known to divide a single element in 2D as well as in 3D. We have used an approach, where each cell of the domain is divided into smaller cells using original cell vertices and midpoints on its edges. This ensures the global connectivity of vertices in the whole (global) refined mesh. The shape of the new mesh then depends on how the new midpoints are connected. The basic approaches are shown in Fig. 1. This type of refinement retains element types in case of hexahedral, tetrahedral and prismatic cells [1]. Therefore, this refinement produces smoother mesh of the same

types of cells. Refining of the pyramidal cell type in the same manner leads to the mesh with pyramidal and tetrahedral cells, i.e. hybrid mesh (but the global vertex connectivity of the mesh is still held).

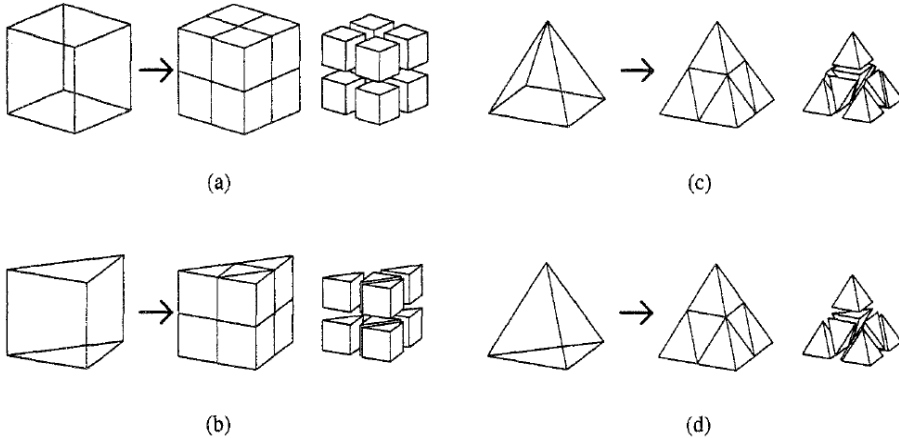


Fig. 1. 3D element refinement. (a) hexahedras, (b) prisms, (c) pyramids, (d) tetrahe-dras.

In the first step, we have implemented the refinement algorithm for hexahedral cells. Each hexahedral cell is refined into 8 smaller hexahedral cells by dividing in half along all axes (Fig. 1(a)). The step-by-step algorithm for hexahedral-type meshes refinement is described below:

Mesh refinement algorithm (hexahedral mesh):

1. Input: coarse mesh.
2. Create new vertex in the middle of each edge.
3. Create new vertex in the centre of each boundary face.
4. Refine all boundary faces (edge vertex connected to boundary face centre vertex).
5. Create new vertex in the centre of each inner face.
6. Refine all inner faces (edge vertex connected to inner face centre vertex).
7. Create new vertex in the middle of each cell.
8. Refine all cells (face centre vertexes connected to cell middle vertex).
9. Output: refined mesh.

2 Parallel Mesh Multiplication for Code_Saturne

The basic capabilities of Code_Saturne enable the handling of either incompressible or expandable flows with or without heat transfer and turbulence. Dedicated

modules are available for specific physics such as radiative heat transfer, combustion (gas, coal, heavy fuel oil, ...), magneto-hydrodynamics, compressible flows, two-phase flows (Euler- Lagrange approach with two-way coupling), or atmospheric flows. Code_Saturne is portable on all Linux and UNIX platforms tested so far (HP-UX, Solaris, Cray, IBM Blue Gene, Tru64, ...). It runs in parallel using MPI on distributed memory machines (clusters, Cray XT, IBM Blue Gene, ...). It is based on a co-located Finite Volume approach that accepts meshes with any type of cell (tetrahedral, hexahedral, prismatic, pyramidal, polyhedral, ...) and any type of grid structure (unstructured, block structured, hybrid, conforming or with hanging nodes, ...).

A mesh stored in Code_Saturne mesh_t format is used as a coarse mesh input to our parallel mesh multiplication routines (described in the previous section). This mesh is obtained during the Code_Saturne preprocessing and/or partitioning phase. If the mesh is not distributed yet, one of the inner partitioning routines of Code_Saturne is used to distribute it.

The process of mesh multiplication is then executed in parallel on distributed parts of the mesh, i.e. each parallel process takes care of its own part of the mesh, but the faces on the subdomain interface are shared with more processors. At this moment, it is guaranteed that the refined mesh does match on subdomain interfaces for hexahedral elements (and the other regular cell types are in progress).

3 Subdomain mesh refinement

In the Code_Saturne package, several mesh partitioning routines are implemented, as well as a possibility of using some of standard mesh partitioners like Metis, Zoltan, etc. In parallel environment, ParMetis package can be also used.

Since the Code_Saturne mesh_t structure handles only data structures of the mesh that is not sufficient for the efficient mesh refinement, it was necessary to extend the current mesh storage format by adding vertex-edge and edges-to-face information. Specifically, the second step of our algorithm “Create new vertex on each edge” requires indexation of edges, because the Code_Saturne mesh_t structure contains indexes just for faces, vertexes and cells. For cell refinement and the following indexation of new objects, we also needed to build the face-to-cell list, which was not included in original Code_Saturne structures.

The mesh refinement is executed in parallel on distributed parts of the mesh and it is done using local variables. During the final global re-indexation, special care has to be given to faces on the subdomain interfaces that are shared with other processors. Details will be described later. Very fine meshes can be obtained applying the implemented mesh multiplication algorithm recursively. If required, the next levels of refinement can be processed in the same way as

the first level.

Application of the parallel mesh multiplication on a distributed mesh duplicates some surface subdomain entities (vertices, edges and faces) in multiple processes. This implies reconfiguration of their global indexing. This task requires parallel communication between the neighbouring subdomains. Optimization of this intersubdomain communication uses the knowledge of adjacency of subdomains and some additional information like cells on boundaries and their neighbouring cells in neighbouring subdomains.

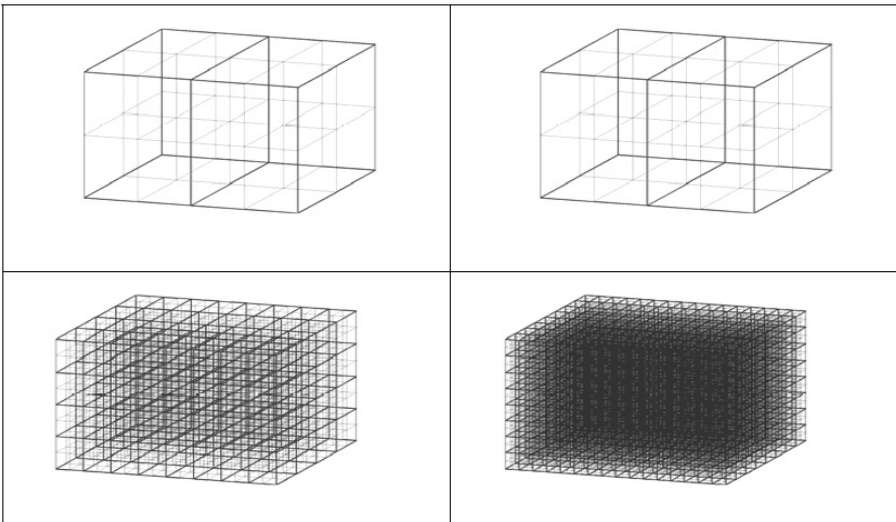


Fig. 2. Multilevel mesh refinement

4 Tests and results

Performance and scalability tests of the implemented parallel mesh multiplication package have been done on the CURIE cluster at CEA. The CURIE cluster has nodes with 16 CPU cores and 4GB of memory per core.

Test example

In this example, the mesh corresponds to a stratified flow in a T-junction. There are two inlets, a hot one in the main pipe and a cold one in the vertical nozzle. The volume flow rate is identical in both inlets. It is chosen small enough so that gravity effects are important with respect to inertia forces. Therefore, cold

water creeps backwards from the nozzle towards the elbow until the flow reaches a stable stratified state. The mesh used here contains 16320 elements. Again, we can use “arbitrary many” levels of refinement.

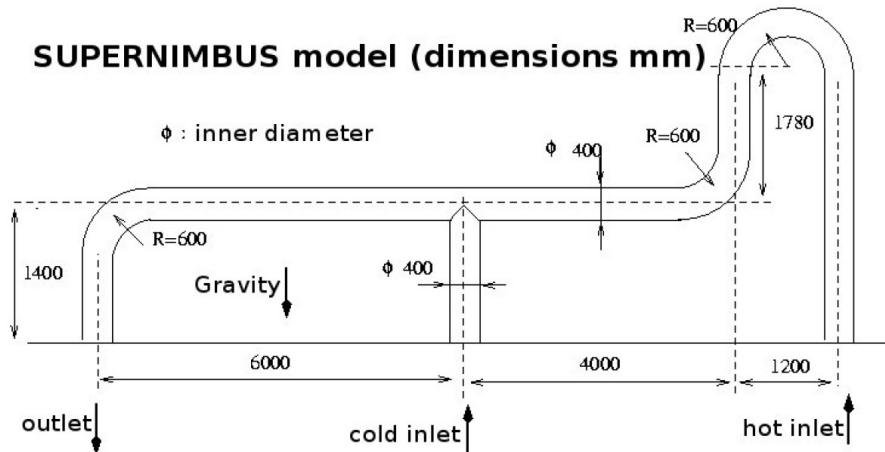


Fig. 3. Test example

Table 1 presents the scalability of the test example on the CURIE cluster. The times in the table show the pure time needed for the mesh refinement. The sixth level of refinement was carried out just on 128 cores because of the high memory requirements on a single core.

Table 1. Scalability of the test example on CURIE cluster.

Parameters of given mesh			Number of used cores					
Level of refinement	no. of cells	no. of vertices	32 cores		64 cores		128 cores	
			time [s]	vertices	time [s]	of vertices	time [s]	vertices
0	16320	18070	<0.1	850	<0.1	550	<0.1	280
3	8.4M	8.5M	<0.2	280k	<0.1	150k	<0.1	76k
4	66.8M	66M	1.5	2.2M	<1	1.1M	<1	600k
5	0.5B	0.5B	12	17M	6	8.6M	3.8	4.4M
6	4.3B	4.3B	-	-	-	-	28	34M

5 Conclusion

In our contribution to the Code_Saturne project, we have developed a new package for mesh multiplication for hexahedral meshes. This package has been in-

egrated into Code_Saturne and its functionality has been tested on several numerical examples on two types of clusters. The tests prove good parallel scalability of the presented solution. Using the CURIE cluster, we have obtained a refined mesh with more than 1 billion cells and vertices in less than 30 seconds. Future improvements of the optimization of the global indexation using other Code_Saturne internal structures and/or methods can lead to more effective computation of very fine meshes in smaller memory and communication requirements. In a future work, multiplication of other types of meshes has to be implemented to complete the full mesh multiplication functionality. While the multiplication of regular tetrahedral and prismatic meshes is straightforward and can be done very easily, the multiplication of pyramidal or hybrid meshes needs more effort.

6 Acknowledgements

This work was financially supported by the PRACE project funded in part by the EUs 7th Framework Programme (FP7/2007-2013) under grant agreement no. RI-211528 and FP7-261557. The work is achieved using the PRACE Research Infrastructure resources [CURIE, France].

References

1. M.L.Staten and N.L. Jones; Local refinement of three-dimensional finite element meshes, *Engineering with Computers* (1997), 13: 165- 174
2. Code_Saturne® : a Finite Volume Code for the Computation of Turbulent Incompressible Flows – Industrial Applications, Archambeau, F. Machitoua, N. and Sakiz, M (2004), *International Journal on Finite Volumes*, Vol. 1, 2004.
3. Developing Code_Saturne® for Computing at the Petascale, Y. Fournier, J. Bonelle, C. Moulinec, Z. Shang, A.G. Sunderland, J.C. Uribe, in *Press for Computers and Fluids Journal*, Special Edition 2011.
4. Development of a Two-velocities Hybrid RANS-LES Model and its Application to a Trailing Edge Flow. J. Uribe, N. Jarrin, R. Prosser, D. Laurence, *Journal of Flow Turbulence and Combustion* (DOI: 10.1007/s10494-010-9263-6), 2010.
5. A stress-strain lag eddy viscosity model for unsteady mean flow, A.J. Revell, S. Benhamadouche, T.J. Craft, D.R. Laurence, *Int. J. Heat Fluid Flow*, 2006.

Discrete-Time Markov Chains in Reliability Analysis

Pavel Skalny

Department of Applied Mathematics, FEECS,
VŠB – Technical University of Ostrava, 17. listopadu 15, 708 33 Ostrava – Poruba
pavel.skalny@vsb.cz

Abstract. The paper presents reliability analysis drawn up for an industrial firm. The aim of this paper is to estimate the probability of firm's failure to satisfy an order to its industrial partners. Discrete Markov chains To describe the issue a method of discrete time Markov chains was used. The method is suitable for many systems occurring in practice where we can easily distinguish various amount of states. The disadvantage of Markov chains is that the amount of computations usually increases rapidly with the amount of states. The Monte Carlo method was implemented to deal with the problem. Chebyshev's inequality was applied to estimate sufficient number of simulations.

1 Introduction

The reliability of production plays fundamental role in an industrial sphere. Nowadays the reliability of industry process is on a high level. It increases by improving the quality of each component or by redundancy of the production process. Even though it is the top reliability process, there is still a chance of system failing or system proceeding limitedly. In our case we analyse the process which has no redundancy. Thus the information about the probability of the systems failures for certain time period t is very valuable.

The research presented here, was motivated by the practical problem. Analysed company was asked what the probability of production failure was. Knowledge of risk, that the order won't be delivered in time, is important for the partner's firm to establish sufficient goods supplies. The extended version of this paper is presented in [1].

Our aim is to solve the problem by applying discrete time Markov chains (from now on we will understand Markov chain as a discrete time model) a well-known method of stochastic modelling. Nowadays "memoryless" method of Markov chains has various fields of application in physics, statistics, computer science etc. Markov chains were also effectively applied in stochastic and reliability modelling of industry process [2, 3]. The advantage of Markov chains is that calculations of its results are very easy in principle. On the other hand the amount of computations usually increases rapidly with amount of states and time.

Many numerical algorithms were developed to deal with the problem of high amount of computations [4-5]. Another way how to deal with the problem is to utilize simulations method. In this paper we have chosen the second approach, so well known Monte Carlo method was applied [7-8]. The simulation approach was used because even in our case study the amount of possibilities was too large to be solved analytically.

2.1. Markov Chains

Markov chain is a random process with a discrete time set $T \subset (\mathbb{N} \cup \{0\})$, which satisfies so called “Markov property”. The Markov property means that the future evolution of the system depends only on the current state of the system and not on its past history.

$$P\{X_{n+1} = x_{n+1} | X_0 = x_0, \dots, X_n = x_n\} = P\{X_{n+1} = x_{n+1} | X_n = x_n\}. \quad (1)$$

where:

X_1, \dots, X_n is a sequence of random variables. The index denotes concrete time $t \in T$

x_1, \dots, x_n is a sequence of states in concrete time $t \in T$

As a transition probability p_{ij} we regard probability, that the system changes from the state i to the state j .

$$p_{ij} = P\{X_{n+1} = i | X_n = j\}. \quad (2)$$

Matrix P , where p_{ij} is placed in row i and column j , for all admissible i and j is called transition probability matrix.

$$P = \begin{pmatrix} p_{11} & p_{12} & \dots & p_{1n} \\ p_{21} & p_{22} & \dots & p_{2n} \\ \vdots & \vdots & & \vdots \\ p_{m1} & p_{m2} & \dots & p_{mn} \end{pmatrix}. \quad (3)$$

Clearly all elements of the matrix P satisfy the following property:

$$\forall 1 \leq i \leq m : \sum_{j=1}^n p_{ij} = 1 \quad (4)$$

As $v(t)$ we denote vector of probabilities of all the states in the time $t \in T$. As $v(0)$ we denote an initial vector. Usually all its values are equal to zero except the i^{th} , which is equal to 1. It can be proved:

$$v(t) = v(0)P^t. \quad (5)$$

2.2. Monte Carlo Method

As F we denote a random variable, which presents the production of the factory within 8 hours. Let R denotes the desired production. In this chapter we will describe the estimation of a probability $p = P(F \geq R)$. The probability will be estimated by the Monte Carlo method.

Let's consider n independent simulations F_1, F_2, \dots, F_n . Let X be a binomial random variable, which represents an amount of successful simulations $X = |\{F_k: F_k \geq R\}|$. This random variable can be considered as a sum of n independent alternative random variables with parameter p . Let us recall formulas for an expected value and a variance:

$$E(X) = np, \quad D(X) = np(1 - p). \tag{6}$$

It follows immediately an expected value and a variance of a random variable $\frac{X}{n}$ from the formula (6):

$$E\left(\frac{X}{n}\right) = p, \quad D\left(\frac{X}{n}\right) = \frac{p(1 - p)}{n} \tag{7}$$

The random variable $\frac{X}{n}$ represents the mean success rate.

Let us remind, that for every finite $\varepsilon > 0$ and every random variable Y with a finite expected value $E(Y)$ and a finite variance $D(Y)$ satisfies the well-known Chebyshev's inequality:

$$P(|Y - E(Y)| < \varepsilon) \geq 1 - \frac{D(Y)}{\varepsilon^2} \tag{8}$$

Let us write $Y = \frac{X}{n}$. This implies:

$$P\left(\left|\frac{X}{n} - p\right| < \varepsilon\right) \geq 1 - \frac{p(1 - p)}{n\varepsilon^2} \tag{9}$$

Since $p(1 - p) \leq \frac{1}{4}$ and

$$P\left(p > \frac{X}{n} - \varepsilon\right) \geq P\left(\left|\frac{X}{n} - p\right| < \varepsilon\right).$$

We can write the lower estimate of the probability p :

$$P\left(p > \frac{X}{n} - \varepsilon\right) \geq 1 - \frac{1}{4n\varepsilon^2}. \tag{10}$$

Let us show an example. We choose $\varepsilon = 10^{-2}, n = 10^6$. Therefore:

$$p > 10^{-6}(X - 10^4). \tag{11}$$

The previous result is valuable in a significance level $1 - \alpha = 0.9975$.

Let us note, that correctness of the calculation mentioned above depends on an independency of simulations. Thus the quality of simulation depends on the quality of a pseudo random number generator. In our research we have used the generator from the MATLAB program.

2.3 Estimation of Input Probabilities

The firm, which our reliability analysis is made for, is a medium size company specialized in thin layer coating of hard materials. The company has requested not to

publish its name and not to publish important data of its production. Thus some information (for example production of certain machines) will be demonstrated as a relative variable.

Although the production process of the firm is much more sophisticated, only crucial part of the process will be analysed. We will calculate probabilities that the system fails or works under the condition that the rest of the process works properly.

The analysed part of a process consists of 4 machines, where each of them could work properly- state 1, or could be in failure -state 0. Since we have 4 machines we can distinguish $2^4 = 16$ different states. The huge data set (over three years) of fails and the length of repairs was granted for each machine.

We choose one hour interval as an appropriate period of each time step. The period of one hour was chosen, because it is approximately equal to the length of one coating process.

In the first data source, there was an information about the frequency of fails of each machine. The data were obtained from reports about the failure. We expect that the data of fails come from exponential distribution. Thus to estimate probability that the system fails during one hour we calculated the expected value as an average length of period fail- X :

$$p_f = \frac{1}{X}. \quad (12)$$

In the data about length of periods between two fails, there were few outlier measurements. These values increased the arithmetic mean of the variable X significantly. After the discussion with the production manager we removed the outlying measurements from the data.

In the second data source file, there was information about the length of repair time. Using the maximum likelihood method we estimated the probability p_r which says that a machine will be repaired within one hour:

$$p_r = \frac{\Delta R}{R} \quad (13)$$

where:

R is an amount of all repairs that were realized.

ΔR is an amount of all repairs that lasted less than one hour.

To calculate the transition probability matrix P we calculated probabilities p_f , p_r for each machine. The calculated probabilities for given machines a, b, c, d are presented in the table below.

Table 1 Calculated probabilities p_f and p_r

	a	b	c	d
p_f	0.01	0.006	0.004	0.003
p_r	0.36	0.36	0.4	0.375

In the second step we have to define all of 2^4 states. As a state 1 we understand the situation that all machines work properly. As a state 16 we understand the situation that all machines fail. Some states are presented in the table below, where 1 denotes the certain machine works and 0 denotes the certain machine is in a failure.

Table 2 Representation of states p_f and p_r

state	a	b	c	d
1	1	1	1	1
2	1	1	1	0
3	1	1	0	1
4	1	0	1	1
⋮	⋮	⋮	⋮	⋮
15	0	1	1	1
16	1	1	1	1

When we calculated the elements of probability transition matrix, we took into an account the change of states of certain machine. For example certain machine remains in the state 1 with the probability $1 - p_f$, change of the state from 1 to 0 is related to probability p_f . So the probability $p_{3,15}$ that the system changes from state 3 to the state 15 is equal to:

$$p_{3,15} = 0.0104 \cdot (1 - 0.0063) \cdot 0.36 \cdot (1 - 0.0031) = 0.0037.$$

Then we have to define the production of certain machines. As it was written before the production had to be presented as a relative variable. The table below presents the real values of power for every machine.

Table 3 Production of machines

	a	b	c	d
production	0.4	0.3	0.15	0.15

Now, using the previous table we can distinguish various levels of productions w_i for each state i . For example, according to the state 3:

$$w_3 = 1 \cdot 0.4 + 1 \cdot 0.3 + 0 \cdot 0.15 + 1 \cdot 0.15 = 0.85.$$

3. Results

In this chapter we will demonstrate the results of our application. We will present the outputs of the Monte Carlo method. In the table below, there are lower esti-

mates of probabilities $P(F \leq R)$ that the production F will be less than the given parameter R . Since we have realized one million simulations, our results are valuable in the significance level 0.9975 (See the formula (11)).

Table 4 Calculation of probability $P(F \leq R)$

R	8	7.6	7.2	6.4
$\hat{P}(F \geq R)$	0.8	0.89	0.93	0.98

4. Conclusion

In this paper we presented primeval reliability analysis of the industry firm. The analysis will be also processed as a report for the management of the firm. The probabilities of the failure will be also calculated for longer periods.

As we can see from the results in the previous chapter, probability the firm fails in delivering an order is quite little. We can expect that, if we would analyze the whole production process, the output probabilities of failure would be more pessimistic.

In the further research we want to analyze all the production process and develop a software application for collecting the input data and calculating the probabilities of failure and repair. Since the structure of the process can be viewed as an oriented cyclic graph we aim to apply the graph theory to principal decrease an amount of calculations.

References

1. Skalny P., Krajc B., Discrete-Time Markov Chains in Reliability Analysis-Case Study Soco 2012 (submitted)
2. Moura M. C. Semi Markov decision process for determining multiobjective optimal condition-based replacement policies, ESREL, 2000. -621 p.
3. Koutras M. V. On a Markov chain approach for the study of reliability structures, Journal of Applied Probability, 1999. -30 p.
4. Marek I. Algebraic Schwarz methods for the numerical solution of Markov chaos, Linear Algebra and its Applications, Prague 2004. -14 p.
5. Stewart W. Introduction to the Numerical Solution of Markov Chains, Princeton University Press, 1994. -538 p.
6. Dubi A. Monte Carlo Applications in Systems Engineering, Wiley, 2000. -266 p.
7. Bernd A. Berg. Markov Chain Monte Carlo Simulations and Their Statistical Analysis, Singapore, World Scientific, 2004. -67 p.
8. Beck J. L. Bayesian Updating of Structural Models and Reliability using Markov Chain Monte Carlo Simulation, Journal of Engineering Mechanics, 2001. -12 p.

Parallelization of MULTIDIS Code for Nonadiabatic Molecular Dynamics on European Supercomputers

Martin Stachon

Department of Applied Mathematics, FEECS,
VŠB – Technical University of Ostrava, 17. listopadu 15, 708 33 Ostrava – Poruba
`martin.stachon@vsb.cz`

Abstract. The famous Schrödinger equation discovered in the 1920's gives us complete formal understanding of matter on atomic level. However, solving the equation in its full form is impossible even today. Several approximations must be made to make the equation computationally treatable. One of these methods is diatomics-in-molecules, which is implemented in the package MULTIDYN, developed at University of Ostrava, the Institute of Geonics of the Academy of Sciences of the CR, and the VSB - Technical University of Ostrava in a close collaboration with the Heyrovsky Institute of Physical Chemistry, Prague, CR, and P. Sabatier University, Toulouse, FR. Simulating the dynamics of larger systems with MULTIDIS is computationally demanding and thus benefits greatly from parallelization, which is described in this article.

Keywords: parallel, molecular dynamics, non-diabatic, supercomputing

1 The DIM method

The MULTIDYN package focuses on the modeling of ionized rare gas clusters, because a reliable and computationally cheap interaction model with a sufficient number of excited states is available. This allows us to study various non-adiabatic phenomena like post-ionization fragmentation, photodissociation, and atom-cluster collisions.

Initial conditions (nuclear coordinates and velocities and electronic amplitudes) for the dynamics are generated using microcanonical Monte Carlo sampling. Because the initial conditions are independent, computation of their time evolution can be done in parallel.

The equations of motion for a system of classical nuclei surrounded by a cloud of electrons can be written within the mean-field approximation as coupled classical Hamilton equations for the nuclei,

$$\dot{q}_i = \frac{p_i}{m_i}, \quad (1)$$

$$\dot{p}_i = \langle \psi | - \frac{\partial \hat{H}}{\partial q_i} | \psi \rangle \quad (2)$$

and the time dependent Schrödinger equation for electrons

$$i\hbar \frac{\partial |\psi\rangle}{\partial t} = \hat{H} |\psi\rangle. \quad (3)$$

For solving the equations we need a reliable and computationally feasible electronic Hamiltonian. We use the DIM (*diatomics-in-molecules*) approach, where the electronic hamiltonian is written as a sum of diatomic and atomic contributions,

$$\hat{H} = \sum_{p=1}^{n-1} \sum_{q=p+1}^n \hat{H}_{pq} - (n-2) \sum_{p=1}^n \hat{H}_p, \quad (4)$$

where n denotes the number of atoms. The wavefunction basis set consists of $3n$ valence-bond Slater determinants and represents states with the positive charge localized on a particular atom in a valence p_m -orbital. After the electronic wavefunction is expanded against this basis set, the equations of motion become:

$$\dot{p}_i = - \sum_{\alpha, \beta, \gamma, \delta} \left[S_{\alpha\beta} S_{\gamma\delta} \frac{\partial \tilde{H}_{\beta\gamma}}{\partial q_i} + D_{\alpha\beta}^{(i)} S_{\gamma\delta} \tilde{H}_{\beta\gamma} + S_{\alpha\beta} D_{\delta\gamma}^{(i)*} \tilde{H}_{\beta\gamma} \right] a_{\alpha}^* a_{\delta}, \quad (5)$$

and

$$i\hbar \sum_{\beta} \dot{a}_{\beta} |\Phi_{\beta}\rangle + i\hbar \sum_{\beta, j} a_{\beta} \dot{q}_j \frac{\partial |\Phi_{\beta}\rangle}{\partial q_j} = \sum_{\beta} a_{\beta} \hat{H} |\Phi_{\beta}\rangle, \quad (6)$$

The model has been further extend by including the spin-orbit coupling using a semiempirical *atoms-in-molecules* scheme, which doubles the basis set, and the inclusion of three-body polarization forces of the induced dipole-induced dipole type. Recently a new approach for hybrid quantum-classical dynamics has been developed, which includes quantum decoherence by introducing periodic collapse of the electronic wave function. This is called the MFQ (mean field with quenching) method.

2 Decomposition

For parallelization, we used the most coarse decomposition of the simulation - compute each integration trajectory independently, with no inter-process communication involved. Implementation of this decomposition did not require too much changes to the existing sequential MULTIDIS code. However, this decomposition places a limit on maximal number of parallel processes able to be used in the simulation, which is the number of trajectories. To be able to use a larger number of parallel processes, a finer level of decomposition is planned for future work. Such a finer level decomposition must be made inside the computation of individual trajectories, in the computation of Hamiltonian matrix and its diagonalization.

3 Implementation

MULTIDIS program is written in FORTRAN90 and parallelization was implemented using standard MPI functions. A total of n parallel processes is launched on n CPU cores, with process ID 0 acting as master. The master process is responsible for reading input files, broadcasting configuration options and integration trajectories. The slaves processes receive the data and integrate the equations of motion. After the computation is finished, the trajectories are sent to the master process, which writes them to disk. In the static trajectory distribution scheme, the master process also computes the integration.

3.1 Sending and receiving trajectories

The inputs for trajectories and configuration data are complex data structures with many variables and arrays. Unfortunately, marshalling of complex data structures is not straightforward in MPI (unlike in more advanced middlewares, like CORBA). For transmission of data structures in MPI, there are basically three options :

- Transmit structure items separately, using individual `MPI_Send` and `MPI_Recv`. This results in many messages sent and considerable overhead.
- Creating custom data type for the structure, using `MPI_Type_struct` and send the structure as a whole. However, the declaration of such structure is a bit cumbersome and it cannot be used to transmit FORTRAN structures which contain pointers or arrays with variable length. This method was chosen for transmission of configuration options.
- Provide your own marshalling code using `MPI_Pack` and `MPI_Unpack`. This requires the most programming effort and thus is prone to errors, but it is the most flexible method. This method was chosen for transmission of trajectories.

3.2 Static vs. dynamic distribution of trajectories

Initially, the trajectories were distributed dynamically. Slave processes send a request for work to master, which in turn sends integration trajectory to be computed to the slave. After the slave finishes computation, it sends the result back to master and requests more work. This repeats until all trajectories are computed. The advantage of this distribution is that it can provide load balancing in case the computation time is different among processes. This system worked reasonably well on JUGENE and HERMIT computers, but failed to achieve parallel scalability on CURIE. It turned out that with large number of processes and fast CPU cores, the request-reply communication becomes a bottleneck.

Thus, we modified the system to use a static distribution. Each process is allocated a fixed number of trajectories it has to compute and the trajectories are sent using a single `MPI_Scatter`. After each slave computes its share, all results collected in one step using `MPI_Gather`. This scheme avoids extra communication and eliminates waiting times.

4 Results

Thanks to the PRACE Research Initiative, we were able to test the scalability of the code on the largest (Tier-0) European supercomputers : CURIE in France, HERMIT and JUGENE in Germany. Test problems were generated for clusters of Ar^{3+} , Ar^{6+} and Ar^{10+} with integration times 5 and 25ps. Some of the results are shown in Tables 1-3 and Fig. 1,2. We have managed to achieve a nearly-linear scaling for up to 16384 CPU cores.

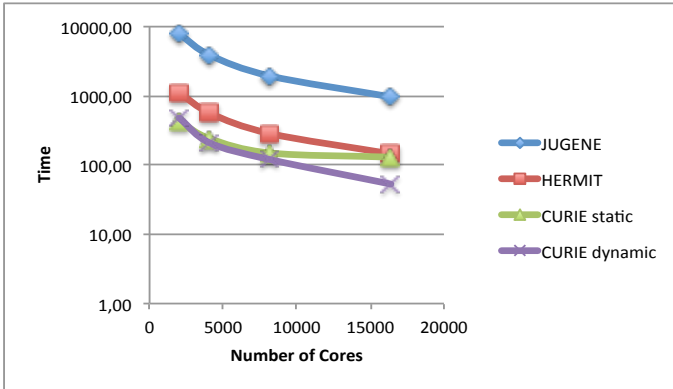


Fig. 1. Computation times on JUGENE, HERMIT and CURIE for Ar^{3+} , 25ps, fixed number of trajectories.

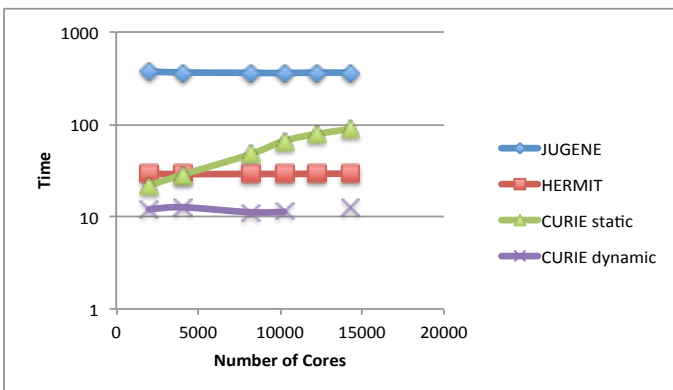


Fig. 2. Computation times on JUGENE, HERMIT and CURIE for Ar^{3+} , 5ps, number of trajectories equal to the number of processes.

Table 1. Computation times for Ar^{3+} , 5ps, fixed number of trajectories on JUGENE.

Number of CPU cores	Time [s]	Efficiency %
2048	1632,4	100,00
4096	826,08	98,80
8192	419,64	97,25
16384	215,11	94,86

Table 2. Computation times for Ar^{10+} , 25ps, fixed number of trajectories on HERMIT.

Number of CPU cores	Time [s]	Efficiency %
2048	9010,48	100,00
4096	4528,13	99,49
8192	2271,23	97,25
16384	1151,23	97,84

Table 3. Computation times for Ar^{6+} , 5ps, fixed number of trajectories on CURIE, comparing the static and dynamic trajectory distribution.

Number of CPU cores	Time dynamic [s]	Efficiency dynamic %	Time static [s]	Efficiency static %
2048	698,55	100,00	689,1	100,00
4096	391,8	89,15	344,55	99,83
8192	228,74	76,35	172,28	98,59
16384	183,28	47,64	86,14	86,67

5 Acknowledgements

Financial support by IT4Innovations Centre of Excellence project, reg.no. CZ.1.05/1.1.00/02.0070 supported by Operational Programme 'Research and Development for Innovations' funded by Structural Funds of the European Union and state budget of the Czech Republic.

We would like to thank the PRACE Research Initiative for granting computational resources in PRACE Preparatory Access Project PA0639.

References

1. MULTIDYN software, <http://moldyn.vsb.cz/multidyn>
2. D. Hrivnak, R. Kalus and F. X. Gadea, *Europhys. Lett.*, 71 (1), pp. 42–48 (2005)
3. I. Janecek, D. Hrivnak and R. Kalus, *THE JOURNAL OF CHEMICAL PHYSICS*, 125, 104315 (2006)
4. I. Janecek, S. Cintava, D. Hrivnak, R. Kalus, M. Farnik, and F. X. Gadea, *THE JOURNAL OF CHEMICAL PHYSICS* 131, 114306 (2009)
5. P. Pukowiecova, F. X. Gadea and R. Kalus, *THE JOURNAL OF CHEMICAL PHYSICS* 133, 214302 (2010)

Elastic Image Registration with Rigid Parts Solved by TFETI

Alena Vasatova

Department of Applied Mathematics, FEECS,
VŠB – Technical University of Ostrava, 17. listopadu 15, 708 33 Ostrava – Poruba
alena.vasatova@vsb.cz

Abstract. Given two images, the goal of image registration is to find an optimal transformation in such way that one image becomes, in a certain sense, similar to the second one. This paper describes elastic image registration method. Elastic means that registration is based on physical motivation of deforming body, thus linearized elastic potential is used as the regularizer. Driving forces are derived from image intensity using suitable distance measure. The optimal transformation is then gain by solution of Navier–Lamé equation. This equation is solved by TFETI method which is a variant of the FETI domain decomposition method for parallel numerical solution of elliptic PDE.

Keywords: elastic image registration, rigid parts, TFETI

1 Introduction

Image registration is a crucial step of image processing if there is a need to compare or integrate information from two (or more) images, a reference R and template T . The main task is to find an optimal transformation such that T becomes, in a certain sense, similar to R . These images usually show the same scene, but taken at different times, from different viewpoints or by different sensors.

Image registration is used in various areas. In medical applications it serves to obtain more complete information about the patient, for example to monitor tumor growth, to verify treatment or to compare the patient's data with anatomical atlases [1],[2].

Elastic potential of deformation in connection with image registration has been introduced by Broit [3]. His method can register images with local non-rigid geometric differences. Broit use it to automatically find an optimal mapping between a CT image and an atlas of brain anatomy. The external forces have been derived by correlating intensity-based properties in local regions in the source and target image.

2 Problem Formulation

To design a suitable distance measure \mathcal{D} and to minimize the distance between images with respect to searched transformation φ is the most intuitive way

$$\mathcal{D}[R, T; \varphi] := \mathcal{D}[R, T_\varphi] \stackrel{\varphi}{\rightarrow} \min. \tag{1}$$

But this approach has its drawbacks: a solution is not necessarily unique and it actually may not exist. Thus the problem (1) is ill-posed. Moreover additional implicit preconditions can emerge, for example in medical images no additional cracks or folding of the tissue are allowed (the transformation should be diffeomorphic). Adding regularizer can solve both situations.

2.1 Regularization

Elastic registration is based on physical motivation that the images are two different observations of an elastic body, one before and one after a deformation. The transformation $\varphi : \mathbb{R}^2 \rightarrow \mathbb{R}^2$ is splitted into the trivial identity part and the displacement $u : \mathbb{R}^2 \rightarrow \mathbb{R}^2$

$$\varphi(x) = x - u(x). \tag{2}$$

As the regularizer we use linearized elastic potential

$$\mathcal{P}[u] = \int_{\Omega} \frac{\mu}{4} \sum_{j=1}^2 \sum_{k=1}^2 (\partial_{x_j} u_k + \partial_{x_k} u_j)^2 + \frac{\lambda}{2} (\operatorname{div} u)^2 dx, \tag{3}$$

where λ and μ are the so-called Lamé constants. The regularizer has the meaning of internal forces which implicitly constrain the displacement to obey a smoothness criteria. We gain regularized problem, which is a starting point for a stable numerical implementation (parameter α control the strength of the smoothness of the displacement versus the similarity of the images)

$$\mathcal{J}[u] = \min_{v: \mathbb{R}^2 \rightarrow \mathbb{R}^2} \mathcal{J}[v], \text{ where } \mathcal{J}[v] := \mathcal{D}[R, T; v] + \alpha \mathcal{P}[v]. \tag{4}$$

Disadvantage of this linear model is that it assumes small deformations. For larger deformations it can be replace by the viscous fluid model [4].

2.2 Distance measure

Distance measure represents external force, so it pushes the deformable template into the direction of the reference. We choose so-called sum of squared differences (SSD)

$$\mathcal{D}[R, T; u] := \frac{1}{2} \|T_u - R\|_{L_2(\Omega)}^2, \tag{5}$$

where $T_u(x) := T(x - u(x))$. And the forces $f : \mathbb{R}^2 \times \mathbb{R}^2 \rightarrow \mathbb{R}^2$ are derived from its Gâteaux-derivative

$$f(x, u(x)) := (R(x) - T_u(x)) \nabla T_u(x). \tag{6}$$

The images are represented by the compactly supported mappings $R(x), T(x) : \Omega \rightarrow \mathbb{R}$, where $\Omega = (0, 1)^2$. Hence, $T(x)$ and $R(x)$ denotes the intensities of images at the spatial position x , we set $R(x) = 0$ and $T(x) = 0$ for all $x \notin \Omega$.

If the images are monomodal, i.e. the intensities of corresponding pixels are supposed to be identical, SSD is a reasonable measure for applications. But if the images are multimodal SSD then probably fail. More suitable choices are the mutual information (MI) or the normalized gradient field (NGF). MI is based on measuring the entropy of the joint density [5] and NGF considers two images to be similar if intensity changes occur at the same locations [6].

2.3 Navier–Lamé equation

The partial differential operator associated with the Gâteaux–derivative of the elastic potential is the well-known Navier–Lamé operator. The displacement of the elastic body is then obtained from solution of partial differential equation

$$\mu \Delta u + (\lambda + \mu) \nabla \operatorname{div} u = -f. \quad (7)$$

The additional constraints can be added to force the displacement to satisfy explicit criteria, like for example landmark, volume preserving imposed constraints or rigid body motion for rigid parts (in medical images bones).

3 Problem Solution

TFETI (Total FETI) method is a variant of FETI (Finite Element Tearing and Interconnecting), which is one of the most successful methods for parallel solution of elliptic partial differential equations. This method is based on the decomposition of the spatial domain into non-overlapping subdomains that are "glued" by Lagrange multipliers. So that, after eliminating the primal variables, the original problem is reduced to a small, relatively well conditioned, typically equality constrained quadratic programming problem that is solved iteratively. Its drawback is difficulty to determine the kernels of stiffness matrices reliably in the presence of rounding errors.

A new variant of the FETI method which is easier to implement and which preserves efficiency of the coarse grid of the classical FETI was proposed in [7]. The basic idea of TFETI is to simplify the inversion of stiffness matrices of subdomains by using Lagrange multipliers not only for gluing of the subdomains along the auxiliary interfaces, but also to enforce the Dirichlet boundary conditions. Thus, all the subdomains are floating and their stiffness matrices will have a priori known kernels – bases of rigid body motion. This approach allows us to incorporate other linear constraints such as rigidity for bones simply by adding other Lagrange multipliers.

To apply the FETI based domain decomposition, we partition Ω into N_s subdomains Ω_s as in Fig. 1 (now λ denotes vector of Lagrange multipliers) and we denote by K_s , f_s and u_s for $s = 1, \dots, N_s$, respectively the subdomain stiffness matrix, the subdomain force and displacement vectors.

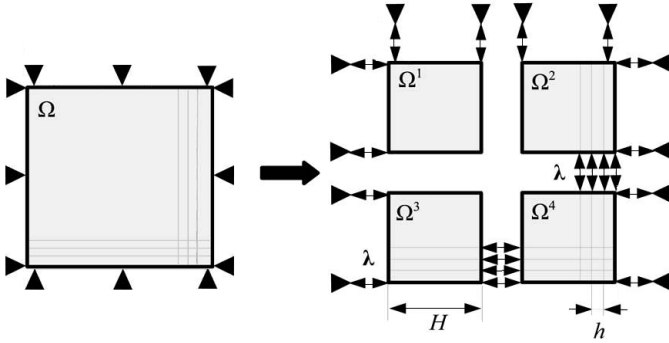


Fig. 1. TFETI domain decomposition.

We shall get the discretized problem

$$\min \frac{1}{2} u^T K u - u^T f \text{ s.t. } B u = c, \tag{8}$$

where $K = \begin{bmatrix} K_1 & & \\ & \ddots & \\ & & K_{N_s} \end{bmatrix}, f = \begin{bmatrix} f_1 \\ \vdots \\ f_{N_s} \end{bmatrix}, u = \begin{bmatrix} u_1 \\ \vdots \\ u_{N_s} \end{bmatrix}, B = [B_1, \dots, B_{N_s}].$ (9)

The matrix B and the vector c enforce the prescribed displacements on the part of the boundary with imposed Dirichlet condition, the continuity of the displacements across the auxiliary interfaces and rigid motion on rigid parts. For easy implementation we choose Dirichlet condition on whole boundary. We shall introduce the Lagrangian associated with problem (8) by

$$L(u, \lambda) = \frac{1}{2} u^T K u - u^T f + \lambda^T (B u - c) \tag{10}$$

and equivalent saddle-point problem

$$\begin{bmatrix} K & B^T \\ B & 0 \end{bmatrix} \begin{bmatrix} u \\ \lambda \end{bmatrix} = \begin{bmatrix} f \\ c \end{bmatrix}. \tag{11}$$

By substituting $R^T(f - B^T \lambda) = o, u = K^\dagger(f - B^T \lambda) + R \alpha$ we gain dual formulation

$$\begin{bmatrix} B K^\dagger B^T & -B R \\ -R^T B^T & 0 \end{bmatrix} \begin{bmatrix} \lambda \\ \alpha \end{bmatrix} = \begin{bmatrix} d \\ e \end{bmatrix}, \tag{12}$$

where $d := B K^\dagger f - c, e := -R^T f$ and K^\dagger denotes a generalized inverse matrix satisfying $K K^\dagger K = K$.

As mentioned the kernels R_s of the local stiffness matrices K_s are bases of rigid body motion and can be formed directly

$$R_s^\top = [(R_s^1)^\top, \dots, (R_s^{n_s})^\top]^\top, R_s^i = \begin{bmatrix} 1 & 0 & -y_i \\ 0 & 1 & x_i \end{bmatrix}, \tag{13}$$

where $(x_i, y_i), i = 1, \dots, n_s$ are coordinates of the nodes of Ω_s . Using R_s , we can easily assemble the block diagonal basis R of the kernel of K as

$$R = \begin{bmatrix} R_1 & & \\ & \ddots & \\ & & R_{N_s} \end{bmatrix}, \tag{14}$$

Let us denote $F = BK^\dagger B^T, G = -R^T B^T$, thus we gain the same saddle-point structure

$$\min \frac{1}{2} \lambda^T F \lambda - \lambda^T d \text{ s.t. } G \lambda = 0, \tag{15}$$

however, its size is considerably smaller and the diagonal block F is much better conditioned than K .

The problem is equivalent to

$$\min \frac{1}{2} \lambda^T P F P \lambda - \lambda^T P d \text{ s.t. } G \lambda = 0, \tag{16}$$

where $P = I - Q$ and $Q = G^T(GG^T)^{-1}G$ denote the orthogonal projectors on the image space of G^T and on the kernel of G , respectively. This problem may be solved effectively by the conjugate gradient method.

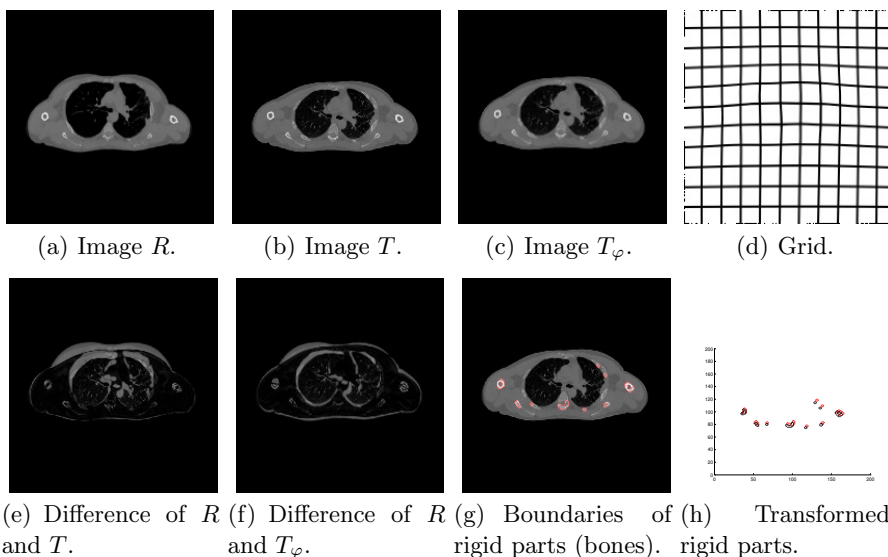


Fig. 2. Registration of images from department of Oncology at the University Hospital of Ostrava. The images show the cuts in the chest in exhalation and inhalation obtained by CT method.

4 Conclusion

This paper presents elastic image registration with rigid parts solved by TFETI. Elastic registration is based on physical motivation of deforming body, thus it fits to register images with local non-rigid differences. We use SSD distance measure for deriving external forces from intensities of monomodal image. Navier–Lamé equation are solved by TFETI, a variant of the FETI method for parallel numerical solution of elliptic PDE, which use Lagrange multipliers also to enforce the Dirichlet boundary conditions, so the inversion of stiffness matrices is simplified. We encompass rigidity for bones simply by adding other Lagrange multipliers.

5 Publications

List of publications in which the results were presented:

- A. Vasatova. Elastic image registration with rigid parts solved by TFETI. Submitted to Proceedings of the 28th Spring Conference on Computer Graphics.
- A. Vasatova. Elastic image registration with rigid parts solved by TFETI. Submitted to Proceedings of MENDEL 2012 – 18th International Conference on Soft Computing. Mendel Journal series.

References

1. Zitova B., Flusser J. Image registration methods: a survey. *Image and Vision Computing*, Vol.21, No.11, 2003, pp. 977–100. ISSN: 0262–8856.
2. Modersitzki J. *Numerical Methods for Image Registration*. Oxford : Oxford University Press, 2004. ISBN 0198528418, 9780198528418.
3. Broit C. *Optimal Registration of Deformed Images*, PhD thesis, University Pennsylvania, 1981.
4. Christensen G. E., *Deformable Shape Models for Anatomy*, PhD thesis, Washington University, 1994.
5. Maes F., Collignon A., Vandermeulen D., Marchal G., Suetens P., Multimodality Image Registration by Maximization of Mutual Information. *IEEE TRANSACTIONS ON MEDICAL IMAGING*, Vol.16, No.2, 1997, pp. 187–198. ISSN: 0278–0062.
6. Haber E., Modersitzki J., Intensity gradient based registration and fusion of multi-modal images. *Methods of Information in Medicine*, Vol.46, No.3, 2007, pp. 292–299. ISSN: 0026–1270.
7. Dostal Z., Horak D., Kucera R., Total feti – an easier implementable variant of the feti method for numerical solution of elliptic pde, *Communications in Numerical Methods in Engineering*, Vol.22, No.12, 2006, pp. 1155–1162. ISSN: 1099–0887.

Modelling of Risk to Safety Personnel in Process Industries by Simulation Method

Adam Zdráhala

Department of Computer Science, FEECS,
VŠB – Technical University of Ostrava, 17. listopadu 15, 708 33 Ostrava – Poruba
adam.zdrahala@vsb.cz

Abstract. Risk to safety of personnel in process industries is normally modelled in the application of Event Trees, where the risk is defined as a product of event frequency and its consequences. This method is steady state whilst the actual event is time dependent, comprising, for a gas release, as for example, the size of gas cloud being released, probabilities of ignition, fire or explosion, fatality, escalation to new releases and fire and/or explosion, and the probability of fatality, all varying with time. This paper presents a method whereby the time-dependent events and the time-dependent probability of fatality are modelled by means direct Monte Carlo simulation method. Using this method the modeled scenarios change with relevant probabilities at defined times to configurations with appropriate probabilities of fatalities. The paper uses a realistic example from the offshore industry.

Keywords: Offshore Industry, Time-Dependent Risk Modeling, Hydrocarbon-Related Fire Risk

1 Introduction and problem definition

Process industry, such as an offshore production installation, exposes personnel to risk of injury or fatality. Probability of fatality in real practical situation depends on many random events that may occur during a potential accident, which are difficult to quantify at a specific time instant or in the course of a time interval. This results in over- or under-estimation of risk.

Figure 1 shows an example of typical offshore production installation consisting of a wellhead platform (WHP), production and riser platform (PRP), and accommodation platform (AP), all connected by bridges. The installation is sub-divided into 10 Zones according to the nature of the plant or activities. Hydrocarbons being produced come up from a reservoir onto WHP in the form of multi-phase fluids, which are piped across the bridge to the PRP, where they are separated into oil, gas, and water and sand. Produced oil and gas are piped through risers and pipelines to a terminal located on-shore. Living quarters are provided on the AP, which is connected to PRP by a bridge. The installation is provided with a standby vessel, which would be located 100m away from the installation.

The main risk on the installation is from potential leaks of the produced hydrocarbons on WHP or PRP. The primary escape and evacuation route from the installation is to the AP, where installation personnel evacuate by free-fall lifeboats. The three lifeboats shown in the Figure 1 are of the minimum capacity of the capacity of the installation. The secondary escape and evacuation route is to the WHP, which is equipped with one free-fall lifeboat. The WHP lifeboat capacity would be based on number of personnel on WHP plus PRP at any one time. Tertiary evacuation capacity is provided on WHP and PRP by life rafts.

In case of evacuation the evacuees are transferred by the lifeboats and life-rafts to the standby vessel.

This paper focuses on the hydrocarbon-related risk, whereas the highest risk is in the wellheads and manifolds area on the WHP (Zone 3) and then in the separation and compression area on the PRP (Zone 8).

Leak frequencies in Zone 8 based on statistical observations may be estimated as for example:

- Small leaks 609 per 10000 years,
- Medium leaks 234 per 10000 years, and
- Large leaks 216 per 10000 years.

A leak in Zone 8 would initiate the following actions:

1. activation of fire & gas system, which in turn would simultaneously activate Alarm,
2. emergency shutdown of process and electrical systems,
3. blowdown of hydrocarbon plant inventories,
4. start of emergency power generation,
5. start of fire pumps, and personnel would make their workplace safe, start to escape.

These actions normally happen within the first 1 minute on the leak detection. The probability of ignition of the leaking hydrocarbon would be minimized by the shutdown and blowdown, but the leaking hydrocarbon may still ignite, immediately, or with some delay. Immediate ignition of leaking pressurised gas would result in jet fire, whilst a relatively large gas cloud may accumulate and explode following a delayed ignition. Explosions or prolonged jet fires may damage the plant and structures of the installation. Calculations and trials show that personnel should be able to escape to the lifeboats and evacuate from the installation to the sea within 30 minutes after the start of the leak.

1.1 Problem formulation and application example

It is important to know the possible development/escalation of incidents on the installation, and the implication on escaping personnel in first phases of the accident, as personnel may be trapped or injured by collapsing plant or structures with resultant fatalities. Table 1 summarizes such events with associated probabilities for a person working and escaping from separation and compression Zone 8 on Level 2 of the PRP, related to small, medium and large leaks respectively. Pis, Pim and Pil, Pfs, Pfm and Pfl, and Pes, Pem and Pel, denote the respective probabilities of ignition, hydrocarbon-related fatality and escalation to bridge for small, medium and large releases.

Pf denotes the probability of fatality related to the escape to sea by jumping into the sea. In Table 1, as for example, an immediate ignition of a medium release with $P_{im} = 0.03$ may result in an immediate fatality of $P_{fm} = 0.1$. As an alternative, the person may escape unhurt from the leak area behind the nearest fire/blast wall and continue to the PRP-AP bridge, but the bridge may lose support due to the fire damage of PRP. As a result, the escaping person may be trapped by the PRP on fire and the damaged bridge and he/she may need to escape by jumping into the sea the secondary route to WHP. In this case, $P_{im} = 0.03$, $P_{em} = 0.1$ and $P_f = 0.7$.

Personnel escaping on the basis of scenarios described in Table 1 may be exposed to an insufficient condition for evacuation (ICFE), which results in fatality, probability of which is to be computed. The objective of this paper is quantification of probability of fatality of a person working and escaping from separation and compression Zone 8. We are particularly interested in behavior of the function during initial part of the accident. The initial event of the accident is a hydrocarbon leak and we are considering three sizes of the leak: small, medium and large. As Table 1 illustrates, the leak is detected during the 1st minute, personnel start to escape, but the time of ignition varies and so also varies the time of fatality with its associated probability.

Table 1. Person and Installation actions at various times

	0 to 1min	1min to 2mins	2 to 5mins	5 to 8mins
Plant	Leak in Zone 8: -Leak detection. -Alarm activated -Installation shutdown -Depressurisation starts -Ignition: $P_{is}=0.004$; $P_{im}=0.03$; $P_{il}=0.1$. -Fire starts.	-Fire continues impinging on flanges and structure. -Installation being depressurised.	-Flanges lose their tightness resulting in escalation to additional fire(s). - damage of the PRP-AP bridge. $P_{es}=0.05$, $P_{em}=0.1$, $P_{el}=0.5$.	
Person	-Person working in Zone 8. -Considering the situation, deciding which way to escape. -Fatality, $P_{fs}=0.05$; $P_{fm}=0.1$; $P_{fl}=0.3$.	-Escaping person located behind the nearest fire/blast wall. -Fatality: $P_{fs}=0.01$; $P_{fm}=0.02$; $P_{fl}=0.06$.	-Escaping via stairs to the PRP-AP bridge. -Person trapped - Person escapes to the sea. -Fatality, $P_f=0.7$.	Escaping person on the PRP-AP bridge. -Person trapped. -Person escapes to the sea. -Fatality, $P_f=0.7$.
Plant	-Leak in Area 8. -Leak detection. -Alarm activated. -Installation shutdown. -Depressurisation starts.	-Ignition, $P_{is}=0.006$; $P_{im}=0.04$, $P_{il}=0.2$. -Fire impinging on flanges and structures.	-Flanges lose their tightness resulting in escalation to additional fire(s).	-Loss of strength of PRP topside resulting in damage of the PRP-AP bridge. $P_{es}=0.05$, $P_{em}=0.1$, $P_{el}=0.5$.

Person	-Person working in Zone 8. -Making working area safe. -Considering the situation, deciding which way to escape and starting to escape.	-Escaping person located behind the nearest fire/blast wall. -Fatality, Pfs=0.01; Pfm=0.02; Pfl=0.06.	-Person escaping via stairs to the PRP-AP bridge. -Fatality, Pfs=0.005; Pfm=0.01; Pfl=0.03.	-Escaping person on the PRP-AP bridge. -Person trapped escapes to the sea. -Fatality, Pf=0.7.
Plant	-Leak in Zone 8. -Leak detection. Alarm activated. Installation shutdown. Depressurisation starts.	-Un-ignited leak continues. -Installation being depressurised.	-Ignition, Pis=0.007; Pim=0.05, Pil=0.2. -Fire impinging on flanges.	-Flanges lose their tightness resulting in escalation to additional fire(s).
Person	-Person working in Zone 8. -Considering the situation, deciding which way to escape and starting to escape.	-Escaping person located behind the nearest fire/blast wall.	-Person escaping to the PRP-AP bridge.-Fatality, Pfs=0.003; Pfm=0.005; Pfl=0.02.	-Escaping person on the PRP-AP bridge.

2 Direct Monte Carlo method

The Monte Carlo simulation method has formally existed since early 1940's, but only with increasing computer technology and power, became widely used. The MC method enables modelling of complex processes without the need of making unrealistic simplifying assumptions, as is inevitably done when using analytical methods. With the increasing availability of fast computers, MC methods become more and more powerful and feasible.

The basis of MC simulation method is described in many references, as for example in Marseguera and Zio [2]. Each "trial" of the MC simulation (a "trial" is one simulation of a system history during a mission time) consists of generating a random walk which guides the system from one configuration to another, at different times. During a trial, starting from a given system configuration, we need to determine when the next transition occurs and which is the new configuration reached by the system as a consequence of the transition. This can be done by two ways which give rise to so-called "indirect" and "direct" MC method.

The indirect MC simulation method consists of sampling first the time of a system transition from the corresponding system conditional probability density $f_S(t|k_0)$ of the system performing one of its possible transitions out of a state k_0 at time t . Then, the transition to the new configuration k' actually occurring is sampled from the conditional probability $q_S(k'|k_0, t)$ that the system enters the new state k' given that a transition has occurred at time t starting from the system in the state k_0 . The procedure then repeats from k_0 at time t to the next transition.

The direct MC simulation method differs from the previous one in that the system transitions are not sampled by considering the distributions for the whole system but rather by sampling directly the times of all possible transitions of all individual components of the system and then arranging the transitions along a timeline, in accordance with their times of occurrence.

The probability of each event in our example is given by Table 1. Events occur in specific time intervals in what can be identified as transition times of components in context with the description above. We can assume that probability density functions of events within specified intervals are piece-wise rectangular. So we construct these functions and use them to generate occurrence time of each event. One Monte Carlo trial consists of the ignition time which is generated first. Resulting from the simulated ignition time, appropriate scenario (set of events) is selected and occurrence times of next events are generated. This is repeated until the mission time is over. All MC trials are finally evaluated to obtain time dependent probability of ICFE (Insufficient Condition For Evacuation).

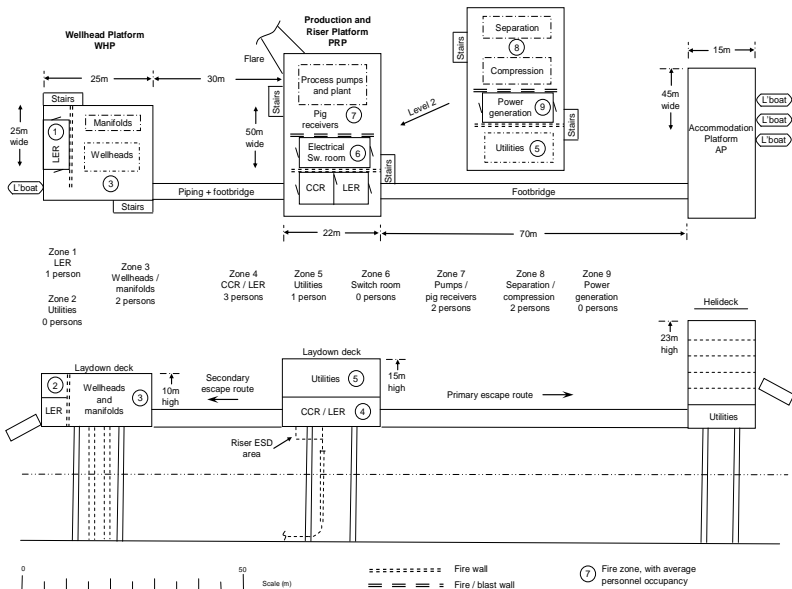


Fig 1. Typical Offshore Production Installation

3 Results

Let us assume suppose that the fire & gas detection system is properly activated whenever a leak in Zone 8 occurs. Using the data from Table 1, the time dependent probability of occurrence of ICFE within $(0, t)$ can be computed and evaluated, for small, medium and large leaks.

Figure 2 compares probabilities of ICFE based on type of leak. Probability axis is in logarithmic scale, for better resolution and understanding.

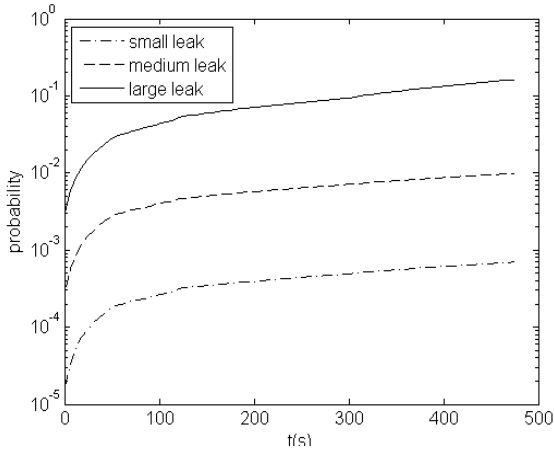


Fig 2. Probability of ICFE for Small, Medium, Large Leak, Computed by MC Simulation Method

A large leak is very dangerous, because its associated probability of fatality increases approximately evenly within each minute and very rapidly too (at about 0.1 per one minute).

4 Conclusion

Data in Table 1 have been used to compute a time dependent probability of ICFE for individual leaks in Zone 8. Based on the dynamic evolution of the probability of ICFE, it can be concluded that most dangerous is the large leak. Probability of fatality increases very rapidly within first 5 minutes.

If we wish to represent the probability for ICFE per annum, we have to multiply these probabilities by leak frequencies in Zone 8 based on statistical observations, see above the paragraph 1.1.

Acknowledgements: This Paper has been prepared in the framework of the IT4Innovations Centre of Excellence project, reg. no. CZ.1.05/1.1.00/02.0070 supported by Operational Programme 'Research and Development for Innovations' funded by Structural Funds of the European Union and the Government of Czech Republic.

References

1. Kumamoto H and Henley E J. Probabilistic Risk Assessment and Management for Engineers and Scientists, IEEE Press, New York, 1996. ISBN 0-7803-10004-7.
2. Marseguera M and Zio E. Monte Carlo approach to PSA for dynamic process systems. Reliability Engineering and System Safety. 52, 227-241, 1996.
3. Bris R. Parallel simulation algorithm for maintenance optimization based on directed Acyclic Graph. Reliability Engineering and System Safety. 93, 874-884, 2008.
4. Bris R. Exact reliability quantification of highly reliable systems with maintenance. Reliability Engineering and System Safety. 95, 1286-1292, 2010.

Polyaniline – Electrical Resistance

Jiří Bocheza and Stanislav Hejduk

Department of Telecommunications, FEECS,
VŠB – Technical University of Ostrava, 17. listopadu 15, 708 33 Ostrava – Poruba
{jiri.bocheza, stanislav.hejduk}@vsb.cz

Abstract. This article discusses other measurements, which were focused on research of basic properties of conducting polymer – Polyaniline (PANI). Measurements were focused on measuring of changes of electrical resistance in depending on time.

1 Introduction

This article follows the article [1], where was made a short list of what are conducting polymers, their properties and where was evaluated the first set of basic measurements of individual potentially interesting optical, electrical or magnetic properties of this conducting polymer.

Polyaniline belongs to the group of conductive polymers [2] [3]. Electrical conductivity is its main feature. PANI can occur in two basic forms. The first form is polyaniline salt, which is conductive and has a green color. The second form is polyaniline base, which is non-conductive and has a blue color. Change between these two forms is done by changes of the pH of the environment.

As noted, the major feature of this polymer is conductivity. Therefore, additional measurements of the behavior of PANI were focused on measurement of electrical resistance R [Ω]. Measurements of alone electrical resistance would not be so interesting, therefore was realized measurement of the electrical resistance of PANI layer in depending to time. The results of these measurements and their evaluation will be described in this article.

2 Measurements of change of electrical resistance in depending on time

This measurement was performed in order to find the behavior of electrical resistance of PANI layer during long-term effects of electric current. Schema of measurement of changes electrical resistance in depending on time is shown in Figure 1.

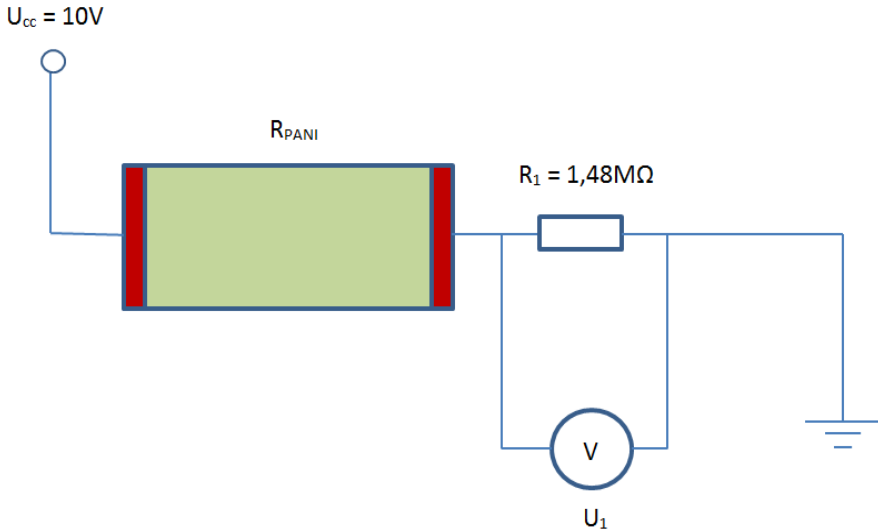


Fig. 1. Schema of measurement of changes of electrical resistance in depending on time

For measurement was used DC voltage power supply with voltage $U_{cc} = 10V$. The resistor $R_1 = 1,48M\Omega$ and resistor of PANI layer (R_{PANI}), which was applied to a laboratory micro-glass, were connected to this power supply. For connection of micro-glass with a PANI layer was used a special holder, which was manufactured at the Department of Telecommunications at VŠB - TU Ostrava. Resistor R_1 was connected parallel with PC USB measuring card from National Instruments. Measuring of a change voltage on the resistance R_1 in dependence on time was executed with program LabVIEW Signal Express 2011. The voltage and time from the measurements were automatically saved to a file for later processing.

For the calculation of electrical resistance PANI layer R_{PANI} was derived formula: $R_{PANI} = (U_{cc} - U_1) / (U_1 / R_1)$.

3 Waveforms of electrical resistance in dependence on time

Measurements were performed on several selected samples, which were created in provisional conditions at the Department of Telecommunications at VŠB - TU Ostrava and also with controlled procedure by chemists from the Center of nanotechnology at VŠB - TU Ostrava.

Measurements were performed by description in chapter 2. Electrical resistances of PANI layer were calculated from the measured values by the derived formula $R_{PANI} = (U_{cc} - U_1) / (U_1 / R_1)$. In Figure 2 are plotted waveforms of change of electrical resistance of PANI layer in dependence on time when they are exposed to electric current.

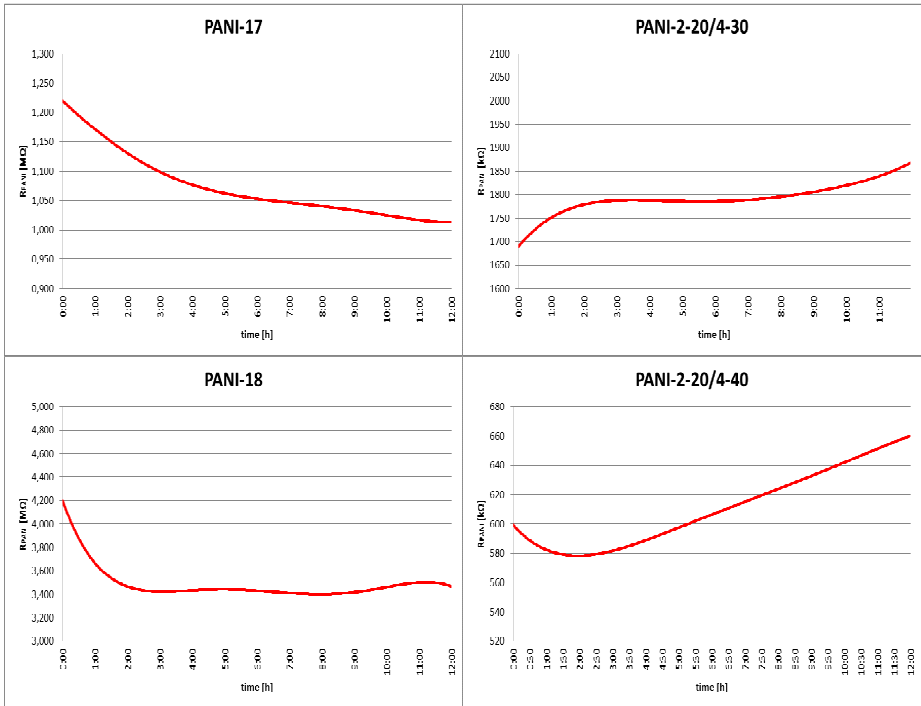


Fig. 2. Changes of electrical resistance of PANI layer in dependence on time when they are exposed to electric current.

From the measured waveforms we can see that each sample has a different character of the electrical resistance during long-term effects of electric current. Small similarity is seen in samples of PANI-17 and PANI-18 and in samples of PANI-2-20/4-30 PANI-2-20/4-40. This similarity can be explained by the fact that the samples PANI-17 and PANI-18 were created in provisional conditions at the Department of Telecommunications at VŠB - TU Ostrava and samples PANI-2-20/4-30 and PANI-2-20/4-40 were created by controlled procedure by chemists from the Center of nanotechnology at VŠB - TU Ostrava.

Differences in waveforms of individual samples are probably caused by slightly different methods of production of individual samples.

4 Repeated measurements of one PANI sample

The difference of individual waveforms of PANI samples (Figure 2) is probably caused by different methods of production. For this reason, it was carried out repeated measurements of the selected sample of PANI. Figure 3 shows waveforms of sample of PANI-17, which were measured at time intervals of 1 month.

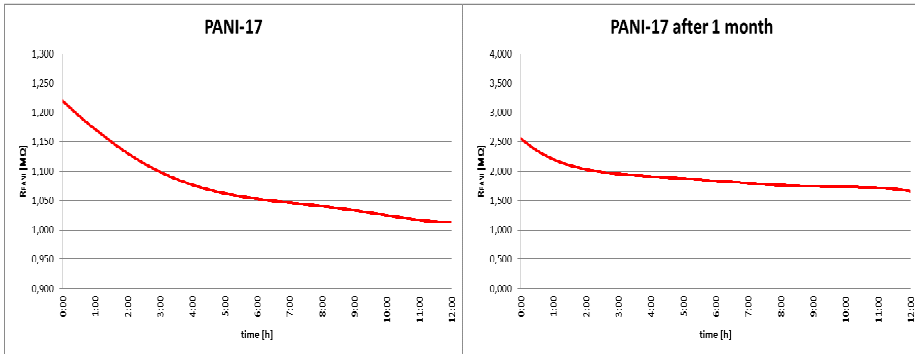


Fig. 3. Waveforms of changes of electrical resistance in dependence on time. Measurements were performed on one sample of PANI at time intervals of 1 month.

It is seen that the measured waveforms are very similar. The major difference is in different sizes of electrical resistance $R_{\text{PANI}} [\Omega]$. We can notice at the first waveform that the electrical resistance is lower than at second measurement, which was measured one month later. This difference is caused by the gradual conversion of conducting form (polyaniline salt) of PANI layer on the non-conducting form (polyaniline base). This change results in increase of electrical resistance. This transformation is spontaneous when the layer of PANI is exposed to the outside environment.

5 Conclusion

This article was focused on measuring changes of electrical resistance of PANI layer during long-term effects of electric current.

Measurement has shown that the electrical resistance of PANI layer is not constant and is changeable, when exposed to activity of electrical current.

Furthermore, it is seen from the measured waveforms that for individual samples, which are made by different procedures, are different waveforms. From this we can deduce that the manufacturing process has an effect on the waveform of electric resistance.

By repeated measuring of the same sample of PANI was found that the waveforms are very similar. The difference was mainly in an increase of electrical resistance. This increase is caused by the gradual conversion of conducting form (polyaniline salt) of PANI layer on the non-conducting form (polyaniline base). This conversion is caused by effect of the outside environment on the PANI layer.

References

1. Bocheza, J., Hejduk, S., Vitásek, J. Conducting Polymers – Polyaniline. In *WOFEX 2011 : 9th annual workshop: proceedings of papers*. 1st edition. Ostrava : VSB - Technical University of Ostrava, 2011.
2. Stejskal, J., Sapurina, I., Prokeš, J., Zemek, J.: In-situ polymerized polyaniline films. *Synthetic Metals*. 1999, 105, pp. 195-202. ISSN 0379-6779.
3. Prokeš, J., Nešpůrek, S., Stejskal, J.: Vodivé polymery: Inteligentní materiály pro nové století. *Vesmír*. January 2001, 80, pp. 35-38. ISSN 1214-4029.

Study of Edge Detection Algorithms

Miroslav Bureš and Jaroslav Zdrálek

Department of Telecommunications, FEECS,
VŠB – Technical University of Ostrava, 17. listopadu 15, 708 33 Ostrava – Poruba
{miroslav.bures, jaroslav.zdralek}@vsb.cz

Abstract. The article deals with the basic properties of algorithms for detecting edges in the image. This article aims to compare their properties when algorithms were applied to images with degraded properties, such as images with more details or overexposed images. For comparison, it has been selected five types of edge detectors. The tests were made on three images on those were applied edge detectors. For visualization and comparison was used software MATLAB.

1 Introduction

In image processing are frequently used algorithms for the edge detection in the image (edge detectors). Their aim is to filter out only the image points which are important for further processing. It is an image preprocessing, which it does not change the information in the image.

The edge detection in image can be used in many specialization, such as medicine, security, reconstruction of 3D scenes and more. Based on detected edges it is possible to search for particular shapes or automatically recognizing content, such as automatic detection of explosives.

2 Edges and their detection

The edge of the object need not coincide with the boundary between objects in the scene, the edges can arise and disappear depending on your point of view. The edges in the image are most often defined as a place where there is a step change in brightness function. According to the brightness function its shape can be divided into several sections: jump, roof, lines and noisy edge. The first three are highly idealized and in real world conditions do not occur. The most common course of the brightness function is noisy.

If the edge is defined as a large change in brightness function, at the place of edge is large value of derivative of brightness function. The maximum value of the derivative in the direction perpendicular to the edge. This is actually a partial derivative of the function of two variables and change its function allows the gradient ∇ , which determines the direction of greatest growth of brightness function and slope of this growth:

$$\|\nabla f(x, y)\| = \sqrt{\left(\frac{\partial f}{\partial x}\right)^2 + \left(\frac{\partial f}{\partial y}\right)^2}, \quad \psi = \arctan\left(\frac{\partial f}{\partial x} / \frac{\partial f}{\partial y}\right) \quad (1)$$

Because image processing is working with discrete data values, it is necessary to select the appropriate method of discrete approximation of partial derivatives. This problem can be two basic approaches:

- the reconstruction of continuous functions and calculate its derivative
- approximation of derivative with finite differences

The first option is not used in practice for its demands and computational complexity. The second option is used in the most cases. The principle is approximation of derivative by convolution with a suitable core. Selection of convolution cores can influence the properties of facet detector. The simplest approximations are:

- Unsymmetrical (derivative at the point $i - \frac{1}{2}$):

$$f' \approx f(i) - f(i - 1) \quad (2)$$

- Symmetrical (neglecting the effect of pixel i):

$$f' \approx f(i + 1) - f(i - 1) \quad (3)$$

If we express this approximation by convolution, we obtain the simplest convolution cores:

$$f' \approx [-1, +1] * f, \quad f' \approx [-1, 0, +1] * f \quad (4)$$

$$[-1, +1], \quad [-1, 0, +1] \quad (5)$$

3 Edge detectors

There are three types of edging detectors based on:

- search of maxim of first derivative (Roberts, Sobel, Prewittov)
- search of zero-cross of second derivative (Laplacian of Gaussian, Marr-Hildreth)
- a local approximation of image function with parametric model, such as polynomial of two variables (Haralick)

3.1 Roberts operator

Roberts convolution mask size is only 2x2. The most commonly used for grayscale images, the calculation is very fast, but it is also very prone to mark random noise in the image as the edge. The size gradient is calculated as:

$$|g(x, y) - g(x + 1, y + 1)| + |g(x, y + 1) - g(x + 1, y)| \quad (6)$$

Convolution cores are:

$$h_1 = \begin{bmatrix} 1 & 0 \\ 0 & -1 \end{bmatrix}, \quad h_2 = \begin{bmatrix} 0 & 1 \\ -1 & 0 \end{bmatrix} \quad (7)$$

3.2 Sobel operator

Sobel operator is often used to detect horizontal and vertical edges. Convolution cores h_1, h_3 are useful for this application.

$$h_1 = \begin{bmatrix} 1 & 2 & 1 \\ 0 & 0 & 0 \\ -1 & -2 & -1 \end{bmatrix}, \quad h_2 = \begin{bmatrix} 0 & 1 & 2 \\ -1 & 0 & 1 \\ -2 & -1 & 0 \end{bmatrix}, \quad h_3 = \begin{bmatrix} -1 & 0 & 1 \\ -2 & 0 & 2 \\ -1 & 0 & 1 \end{bmatrix}, \quad \dots \quad (8)$$

3.3 Prewitt operator

The size of matrix of Prewitt operator is 3x3, for edge detection in different directions:

$$h_1 = \begin{bmatrix} 1 & 1 & 1 \\ 0 & 0 & 0 \\ -1 & -1 & -1 \end{bmatrix}, \quad h_2 = \begin{bmatrix} 0 & 1 & 1 \\ -1 & 0 & 1 \\ -1 & -1 & 0 \end{bmatrix}, \quad h_3 = \begin{bmatrix} -1 & 0 & 1 \\ -1 & 0 & 1 \\ -1 & 0 & 1 \end{bmatrix}, \quad \dots \quad (9)$$

3.4 Laplace operator

Maximum of the first partial derivatives of discrete brightness functions correspond to the zero crossing second partial derivatives. Laplacian is preferably used for this.

$$\nabla^2 f(x, y) = \frac{\partial^2 f(x, y)}{\partial x^2} + \frac{\partial^2 f(x, y)}{\partial y^2} \quad (10)$$

Omni-directional linear Laplace operator (Laplacian) is useful if we want to detect edges in an image, but we do not care about the direction of edges. This operator gives the same response for all directions, so no information about the direction of edges. It can be used to focus the image. The disadvantages are its high sensitivity to noise and double response to a thin line. Examples of possible convolution cores (8-neighborhood, highlighting the center):

$$\begin{bmatrix} 1 & 1 & 1 \\ 1 & -8 & 1 \\ 1 & 1 & 1 \end{bmatrix}, \quad \begin{bmatrix} 2 & -1 & 2 \\ -1 & -4 & -1 \\ 2 & -1 & 2 \end{bmatrix}, \quad \begin{bmatrix} -1 & 2 & -1 \\ 2 & -4 & 2 \\ -1 & 2 & -1 \end{bmatrix} \quad (11)$$

Since the Laplace operator is very sensitive to noise, first step is exterminate the image from the noise and then try to detect edges. So we accept the image blurring with the Gaussian and use the second derivative estimate directional Laplacian. This procedure is known as LoG operator (Laplacian of Gaussian).

Values of derivative of Gaussian can precalculated because is not dependent on the input image. LoG operator can be approximated by the difference of two images smoothed using a Gaussian with differen σ . This operator is called a DoG (Difference of Gaussians).

The disadvantage of this operators is blurring sharp shapes (corners of objects) and edges tend to concentrate in an enclosed shapes. Another problem is once again setting the appropriate values of σ .

3.5 Canny edge detector

Canny edge detector is an algorithm which includes several steps to achieve the best result in the detection of edges in the image. The basic requirements include reliable detection (so that it found most of the existing edges), the exact location of the edges (so that the edge position is identified as accurately as possible) and clarity (not to detect nonexistent edges).

During edge detection Canny edge detector usually proceeds as follows: first step is to eliminate noise in the image (usually a Gaussian filter, but we can also use another filter), then finds the approximate directions of gradient for each pixel in the direction of the derivative of gradient with a suitable convolution masks. In the next step, we find local maximum of these derivatives and edges are obtained by thresholding with hysteresis. In the last step (mostly not used) are merged edges, which we have gained in various large extermination.

4 The simulation results of edge detectors

To test the five selected edging detectors were selected three types of image. The first is a nontrivial image with standard properties. This image serves as a control. The second image is a group photo with lots of small details. The last chosen is overexposed photograph of the corner of room with a lot of noise. Edge detection results of individual detectors can be seen in figures 1, 2, 3.

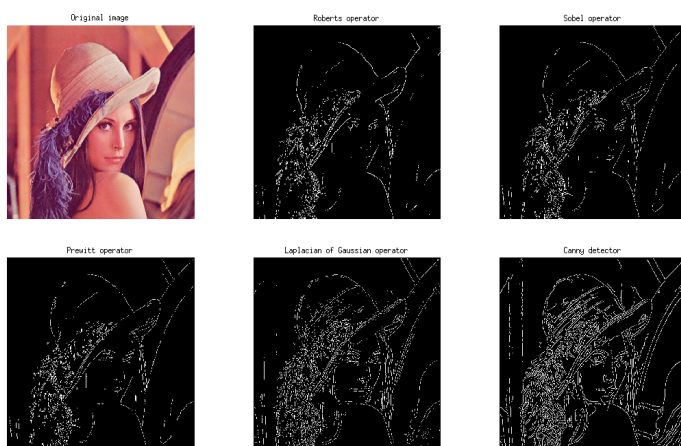


Fig. 1: The control image

For control image is achieved the best results of simulations with Canny detector. The operator's detectors are worst, especially Roberts and Prewitt operator. This is due to the simplicity of these detectors, which occurs only for convolution. Edge detection is significantly improved using a Gaussian filter.

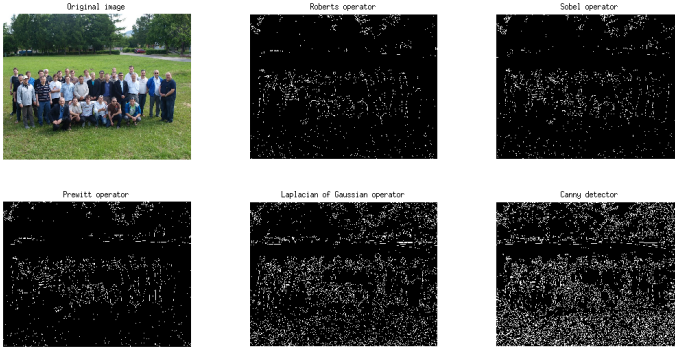


Fig. 2: Image with a large number of small details

Applying the same algorithms on the image with a lot of details is a better result for simple detectors. The best seems to be a Prewitt and Sobel operator. Use of Laplacian of Gaussian and Canny detector is edge detection worse due to noise. The resulting edges are short and coalesce.

Edge detection in overexposed image is the same as in the previous case. The last two methods are due to the large amount of noise in an overexposed image unusable. For their use is necessary to apply a larger filtration.

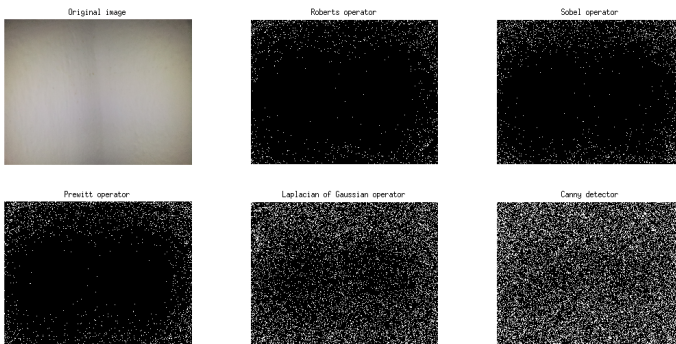


Fig. 3: Overexposed image with noise

5 Conclusion

The article described five most common edging detectors and their basic properties. The simulation results confirmed that for quick search of specific shapes can be simply used operator detectors. In future work we would like to continue and

tried to create a set of test images for the purpose of detection and automatic recognition of suspicious objects such as explosives.

Thanks

The research leading to these results has received funding from the European Community's Seventh Framework Programme (FP7/2007-2013) under grant agreement no. 218086.

References

1. J. R. Parker, *Algorithms for Image Processing and Computer Vision*, Wiley, 2010, ISBN 978-0470643853.
2. R. Louban, *Image Processing of Edge and Surface Defects: Theoretical Basis of Adaptive Algorithms with Numerous*, Springer , 2009.
3. S. Price, *Edges: The Canny Edge Detector*, 1996, available on www: http://homepages.inf.ed.ac.uk/rbf/CVonline/LOCAL_COPIES/MARBLE/low/edges/canny.htm
4. E. Nadernejad, S. Sharifzadeh, H. Hassanpour, *Edge Detection Techniques: Evaluations and Comparisons*, Applied Mathematical Sciences, Vol. 2, 2008, no. 31, 1507-1520.

Software for Visualization of Measured Data from Mach – Zehnder Interferometer

Jan Doricak, Stanislav Kepak, and Jakub Cubik

Department of Telecommunications, FEECS,
VŠB – Technical University of Ostrava, 17. listopadu 15, 708 33 Ostrava – Poruba
{jan.doricak.st, stanislav.kepak, jakub.cubik}@vsb.cz

Abstract. This document describes script that was created in Matlab, designed for visualization and processing of data measured at Mach-Zehnder interferometer output captured using National Instruments measuring card and LabView. It summarizes the various development stages of this script and its planned expansion.

Keywords: Matlab, script, visualization of data.

1 Introduction

The primary impulse to create this script was requirements for data processing of Mach-Zehnder interferometer (MZI) output signal and its visualization. Aim of this application is to facilitate the interpretation of the MZI output signal. As a development environment for creating this script was chosen Matlab and its 2010 version (later 2011). Matlab environment was selected because it provides a broad base of functions for working with any data that considerably facilitates the work of developing many different scripts. Above all, Matlab is very powerful tool to perform various mathematical operations.

2 Measuring of Mach-Zehnder interferometer output signal

On Figure 1 is shown block diagram of measuring process, which captures the MZI output signal. The electro-optical conversion provides Thorlabs detector. The output from the detector is through asymmetric coaxial cable with impedance of 50Ω . This analog signal $u(t)$ is applied to first order high-pass filter with selectable cutoff frequency 17 or 34 Hz. In this block is also removed DC component from signal. Next follows the amplifying block with optional amplification from 0 to 30 dB with 10 dB step and symmetrical output. This symmetrical output is then fed to analog input of measuring card with input voltage range of 0-10 V. Measuring card performs AD conversion of analog signal $u(t)$ to digital output stream $s[n]$ with sampling speed of 250 kS/s and output data word length of 16 bits. Data stream $s[n]$ represents the voltage at the detector and is further processing in LabView. On the captured signal $s[n]$

is applied 5th order high-pass IIR filter with cutoff frequency of 10 Hz. Output from this filter is then stored in *.txt file. This file is one of data inputs to the script. Behind the IIR filter is on the signal applied Fourier transformation (FFT block) with Hanning window function to convert $s[n]$ from time to frequency domain. From calculated frequency-amplitude spectrum of the original signal are selected only spectral components from range 0 to 1000 Hz, which are also saved as *.txt file. This file will be further used as a next input data file for previously mentioned script to display calculated spectrum and its time dependence.

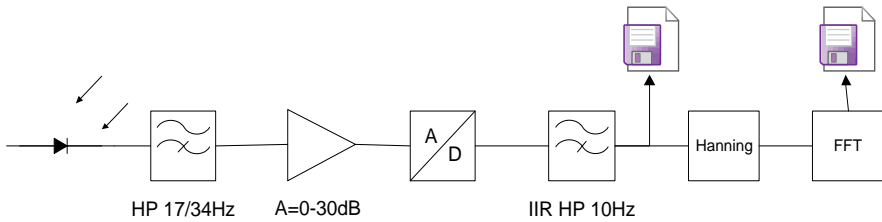


Fig. 1. Block diagram of the signal capturing method

3 Development stages of the script

3.1 The first version of the script

The first version of application was simple script for plotting graphs waveforms of measured MZI output signal at detector. Script loads data previously captured using LabView. This data had a plain text form. This data were converted from text form to integer or double data type then can be easily plotted in graphs and performed other mathematical operations with it. Script plots a graph of voltage over time with correct descriptions of all axes. As input vector for x axes were used data derived from the number of data captured in *.txt file and sampling rate of measuring card. Plotted waveform of voltage over time was automatically saved in PNG format (Fig. 2). Created script was not intended to use only for visualization of MZI output data. If we assume that the same structure of data files is captured with measuring card and saved with similar configuration of LabView software, the script can also display data which are not measured on MZI, but are measured in another experiment. [2]

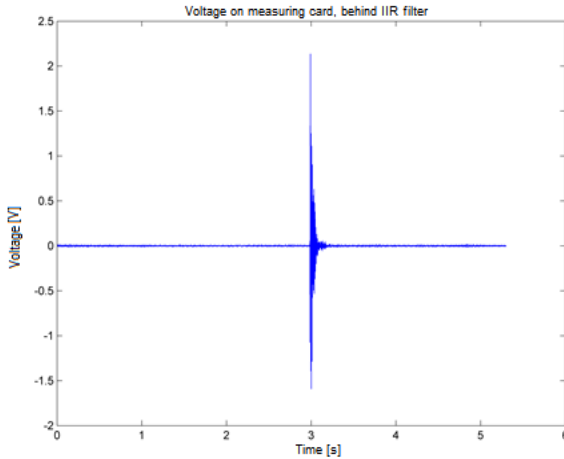


Fig. 2. Graph of voltage waveform over time

3.2 The second version of the script

Second version of the developed application extends the previous version with feature, which could load data that represents the Fourier transformation of the voltage on optical detector. The captured data includes captured spectra varying in time as one column vector. This vector must be transformed into matrix whose columns contain data of each captured spectra and rows contains data of varying each frequency component in time. This matrix is then visualized as 2D or 3D graph (Fig. 3). These graphs can be also exported to PNG format. Axes labels must be also extracted from raw data so they correspond to reality.

For more detailed analysis of measured data was implemented extension, which allows display Fourier transformation in one time. This time was specified in popup window and after that was plotted. Because calculated spectrums are not continuous in time it is necessary to choose values of time in specified steps. The final plot is shown on Figure 4.

Another modification was the implementation of dialog boxes to find exact path to files, which contains input voltage and spectral data.

The next feature of the script was CSV data output. This feature could export actually loaded data to CSV file, which could be executed in MS Excel. Waveform spectra data of each measurement were stored in common directory. The script automatically reads data from each measurement. Time delay between measurement start and event, which spectrum will be analyzed was eliminated by choosing of appropriate value. Selected spectrum was written to column in the CSV file. In analyzing sub-folders, which contains spectra data of further measurements, selected spectra were written to next columns in the CSV file. By this way could be compared repeated measurements. [1], [2], [3], [4], [5]

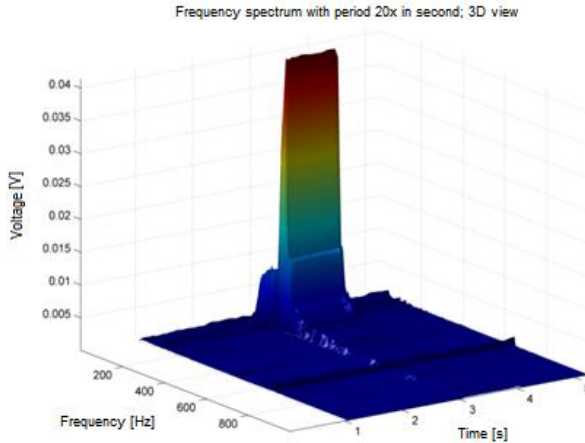


Fig. 3. 3D graph of spectrum varying in time

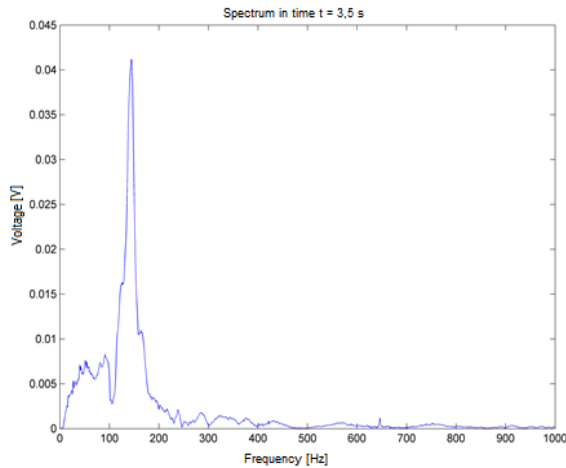


Fig. 4. Graph showing spectrum in selected time

3.3 Third version of the script

To simplify work with script, it is currently implemented a graphical user interface (GUI), which contains all previously mentioned features. The aim of this GUI is primarily permit work with this application to users who do not know the structure of used script or never seen the Matlab environment. The current application state is shown on Figure 5.

The new properties increased the size of script and decreased clarity and intelligibility. Therefore the script was divided into several external functions that are called when the script need them. This has improved readability of the script and its availability on individual provisions. [1], [2]

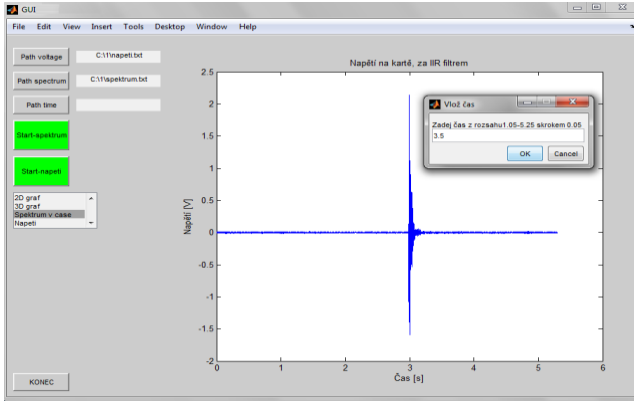


Fig. 5. GUI of the script

4 Planned expansions

After implementing all features of the previous versions to the current version with GUI, the application still will be further developed. First of all will be add a possibility of setting parameters of input files such as sampling frequency of recorded voltage. Further will be implemented loading of the file, which contains set of times of analyzed events, or application could be set to find proper time automatically. So that users will be no longer need to manually insert these event times.

Matlab also contains the functions, which allows performing of Fourier transformation on data stored in memory. This feature will be also added to application. After that the user will have to load only one file containing the voltage over time. [1], [2]

5 Summary

The designed application satisfies the current requirements for visualization of measured data. Further planned modifications of this application may include performance improvement or implementing other features that facilitate work with measured data.

Acknowledgement

This paper and research has been supported by the VG20102015053 - The modern structure of photonic sensors and new innovative principles for intrusion detection systems, integrity and protection of critical infrastructure – GUARDSENSE. This work was supported by the Grant Agency of the VSB-Technical university of Ostrava, grant No. SP2012/160, SP2012/165.

Bibliography

1. Karel Zaplatilek, Bohuslav Donar: MATLAB tvorba uzivatelskych aplikaci. Technicka literatura BEN, Praha 2004, ISBN: 80-7300-133-0
2. MathWorks Inc.: MATLAB User's Guide,
http://www.mathworks.com/help/techdoc/matlab_product_page.html
3. Dana Majerova: Vyuka MATLAB Lekce 1-9,
<http://uprt.vscht.cz/majerova/matlab/>
4. Blanka Heringova, Petr Hora: MATLAB Díl I. – Prace s programem. Plzen 1995,
<http://www.cdm.cas.cz/czech/hora/vyuka/mvs/tutorial.pdf>
5. Petr Pesik: Uvod do Matlabu.
<http://labe.felk.cvut.cz/~posik/y33aui/uvod-do-matlabu/>

FBG Temperature Sensor with Two Braggs Gratings with Mutually Overlapping Spectra

Marcel Fajkus, Andrej Liner, and Martin Papes

Department of Telecommunications, FEECS,
VŠB – Technical University of Ostrava, 17. listopadu 15, 708 33 Ostrava – Poruba
marcel.fajkus@vsb.cz

Abstract. The fiber-optic sensors are more and more replaced by the standard sensors. In the field of measuring mechanical stress and temperature are at the forefront of the fiber-optic sensors based on FBGs. These sensors reported excellent properties. They are resistant to external conditions and achieve very precision measurements. The FBG sensors like sensors of mechanical stress and temperature can be used as a single or multipoint (quasi-distributed) sensors.

Keywords: Braggs grating, edge filter, fiber-optic sensor, wavelength.

1 Introduction

The optical fibers with uniform Braggs gratings are special optical fibers in which cores is a periodic change in refraction index designed. On the interfaces of these refractive index changes are reflecting specific wavelengths. The reflected wavelength depends on the period of changes in the refractive index and on the effective refractive index of the core.

$$\lambda_B = 2n_{eff}\Lambda$$

2 Braggs Grating

The Braggs gratings are characterized by a very narrow selective reflection with the peak on wavelength λ_B high reflectivity approaching to 100% and width of the reflected spectrum between $0,1$ to 2 nm . The spectrum of a uniform FBG is shown in the figure 1.

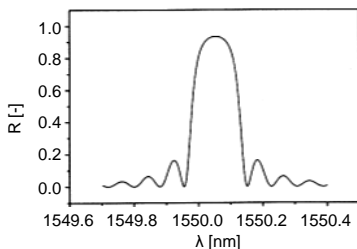


Fig. 1. The spectrum of a uniform FBG.

The light from LEDs guided to the FBG will be partially reflected and partially released. The wavelengths corresponding to the central wavelength of the Bragg grating will be reflected, others will be released as show in figure 2. These FBGs are used as temperature sensors and mechanical stress sensors. Due to the mechanical stress or temperature influence the period of the refractive index is changed which moves the FBGs reflected spectrum. The change of mechanical stress or temperature leads to the change in the reflected wavelength. The dependence of wavelength shift on the temperature change is around $1.3 \text{ pm}/^\circ\text{C}$ and on the mechanical stress change is around $13 \text{ pm}/\mu\text{e}$ [1].

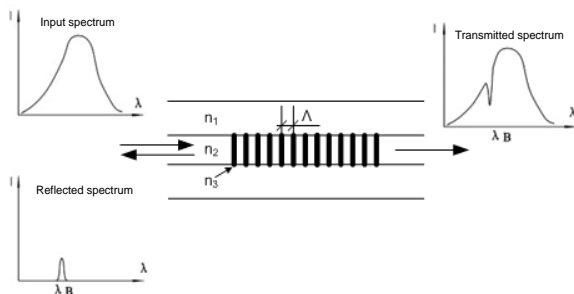


Fig. 2. The principle of FBGs: light from a broadband source enters the grating. The wavelengths corresponding to the central wavelength of FBGs are reflected, others are released.

The disadvantage is that the central wavelength shift is dependent on temperature and mechanical stress simultaneously. By measuring with one FBG it is impossible to distinguish between the size of stress influence and influence of temperature. This problem can be solved in three ways. The ideal solution is the use of FBG, which is sensitive only to temperature or only to stress. It is also possible to use the references grating, which is located so as to be influenced by the same temperature as the main measuring grating, but not to be loaded with mechanical stress. By subtracting the measured value from the reference grating from the value on the measuring grating will provide the value of mechanical stress influence [2]. The last solution is the use of two different FBGs that have different sensitivities to temperature and mechanical stress. [3], [4]. This two gratings sensor can be described by the following equation:

$$\begin{pmatrix} \Delta\lambda_1 \\ \Delta\lambda_2 \end{pmatrix} = \begin{pmatrix} K_{1\varepsilon} & K_{1T} \\ K_{2\varepsilon} & K_{2T} \end{pmatrix} \begin{pmatrix} \Delta\varepsilon \\ \Delta T \end{pmatrix}$$

Where K_ϵ is stress coefficient and K_T is temperature coefficient, $\Delta\epsilon$ is mechanical stress change, ΔT is temperature change and $\Delta\lambda_1, \Delta\lambda_2$ are caused changes of the wavelengths on gratings 1 and 2 [5]. If the determinant of the matrix of the coefficients is not zero, we can express the measured values of mechanical stress and temperature as follows:

$$\begin{pmatrix} \Delta\epsilon \\ \Delta T \end{pmatrix} = \frac{1}{K_{1\epsilon}K_{2T} - K_{2\epsilon}K_{1T}} \begin{pmatrix} K_{2T} & -K_{1T} \\ -K_{2\epsilon} & K_{1\epsilon} \end{pmatrix} \begin{pmatrix} \Delta\lambda_1 \\ \Delta\lambda_2 \end{pmatrix}$$

The advantage of sensors based on Bragg’s gratings is that the measured quantity is encoded into the reflected wavelength and not into the reflected intensity, which is by the distribution thought the fiber absorbing. To detect the wavelength shift can be used spectrometer. But the spectrometer is very expensive, and therefore are new ways how to detect the wavelength changes looking. The simplest technique is to transfer the wavelength changes into intensity. Converting of the wavelength changes to the intensity change can be achieved by using forward edge filter, which has a linear relation between the change in wavelength and intensity of out light (Fig. 3) [6]. The distribution of the reflected light into two branches, and placing the edge filter into one branch can eliminate the power fluctuations of the source.

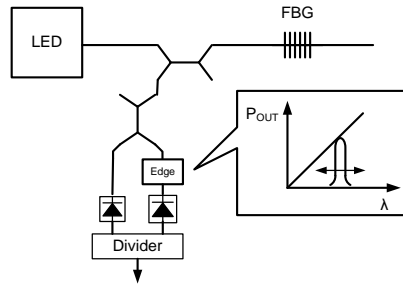


Fig. 3. Transfer of the wavelength shift to the amplitude by using edge filter.

Another option is the use of two FBGs with the same properties, where one is sensing and the second is receiving (Fig. 4) [7], [8]. The temperature or mechanical stress changes lead to detuning of the sensing grating. Using of piezo-element leads to the retuning of the sensing grating until the maximum reflected power from receiving grating and photodiode is detected. At the moment of maxim detected power, the central wavelength of receiving grating correspond to the central wavelength of sensing grating. Assuming that the relation between control voltage and wavelength of receiving grating is known, the wavelength of the sensing grating can be determined..

The simplest technique is the used of two identical gratings placed in a row, which spectra overlap. In the case that the gratings will not be influenced by temperature or even mechanical stress will be on the photodiode certain power of reflected light detected.

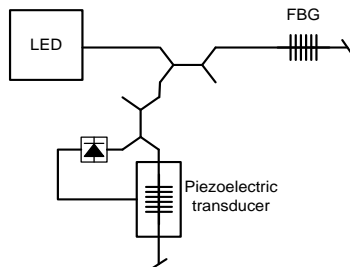


Fig. 4. Converting of the wavelength shift to the amplitude by using two identical FBGs.

If the gratings will have mutually overlapping spectra, than by shifting one spectrum to lower or higher wavelengths due to the temperature or stress changes will occur the changes of the overlapping surfaces of the both spectra. As a result, the reflected power from both gratings will change. The connection scheme is shown in figure 5.

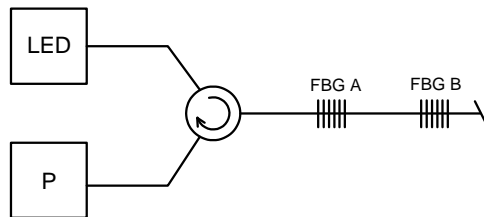


Fig.5. Converting of the wavelength shift to the amplitude by using two FBGs with mutually overlapping spectra.

The simulation of dependence of reflected power on central wavelength change of the grating A in range from 1550 to 1550.7 nm was performed. As a source was used a broadband LED at 1550 nm and output power of 1 mW. The result is shown in figure 6.

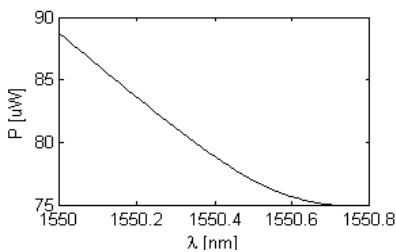


Fig. 6. The simulation of the power dependence on central wavelength of FBG A change.

2 Experiment

In the experiment was the investigation technique of wavelength shift by using two Bragg gratings with mutually overlapping spectra verified. Two FBGs were used in experiment. FBG A had central wavelength at 1553.59 nm , spectral width at half maximum power at 3.117 nm , and reflectivity of 85.9% . FBG B had central wavelength at 1554.21 nm , spectral width at 2.597 nm and reflectivity of 80.9% . Measured results are shown in figure 7.

Four measurements were performed. In figure 7 are shown four courses that follow the shape of the curve in the simulation. The problem is that the individual courses do not overlap each other and are shifted. This inaccuracy was caused by very high sensitivity of LEDs on the ambient temperature. And because no thermostat was used to stabilize the temperature of the LEDs in the environment, there were fluctuations in LEDs output.

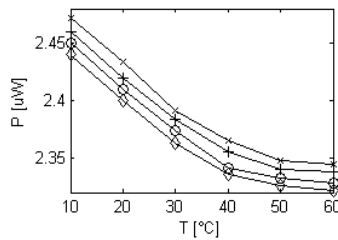


Fig. 7. The dependence of power on temperature change applied on FBG A.

In the accompanying measurement was measured the dependence of the LEDs output power on the ambient temperature, shown in figure 8. The temperature change of $1 \text{ }^\circ\text{C}$ leads to a change of LEDs output power about $3.37 \text{ } \mu\text{W}$, which corresponds to of 4.7% original value. The measured values in figure 7 are shifted by about $0.1 \text{ } \mu\text{W}$, which corresponds to a change of 0.4% . The change in reflected power about 0.4% corresponds to a temperature change about $0.085 \text{ }^\circ\text{C}$. This shows that the LED in this sensor scheme is very sensitive to ambient temperature.

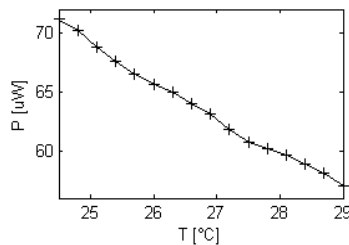


Fig. 8. Dependence of LED output power on ambient temperature.

3 Conclusion

In this paper has been verified the functionality of investigate technique based on two FBGs with mutually overlapping spectra. It was shown that by using

two FBGs can convert the wavelength shift to amplitude change, which is very appropriate for practical applications, particularly in terms of simple design and low cost financial solutions.

By measurements was the stabilization of the ambient temperature imperfect. This issue significantly affected the LEDs output power, which was reflected in the results as not overlapping courses as shown in figure 7. This issue can be eliminated by improving the LEDs power stabilization.

Acknowledgements

This article was supported by project VG20102015053 - The modern structure of photonic sensors and new innovative principles for intrusion detection systems, integrity and protection of critical infrastructure – GUARDSENSE. This work was supported also by the Ministry of Education of the Czech Republic within the project no. SP2012/165 of the VSB - Technical University of Ostrava.

References

- 1.Y. J. Rao, In-fiber Bragg grating sensors, *Measurement Sci. Tech.*, 8, pp. 355–375, 1997.
- 2.G. W. Yoffe, P. A. Krug, F. Ouellette, and D. A. Thorncraft, Passive temperature-compensating package for optical fiber gratings, *Appl. Opt.*, 34, 30, pp. 6859–6861, 1995.
- 3.M. G. Xu, J. L. Archambault, L. Reekie, and J. P. Dakin, Discrimination between strain and temperature effects using dual-wavelength fiber grating sensors, *Electron. Lett.*, 30, 13, pp. 1085–1087, 1994.
- 4.S. W. James, M. L. Dockney, and R. P. Tatam, Simultaneous independent temperature and strain measurement using in-fiber Bragg grating sensors, *Electron. Lett.*, 32, 12, pp. 1133–1134, 1996.
- 5.Morey, W.W., G. Meltz, and W.H.Gleen, Fiber optic Bragg grating sensors, Society of Photo-Optical Instrumentation Engineers, *Fiber Optic and Laser Sensors VII*, 1989, Vol. 1169, pp. 98-107.
- 6.S. M. Melle, K. Liu, and M. Measures, A passive wavelength demodulation system for guided-wave Bragg grating sensors, *IEEE Photon. Technol. Lett.*, 4, 5, pp. 516–518, 1992.
- 7.D. A. Jackson, A. B. L. Ribeiro, L. Reekie, and J. L. Archambault, Simple multiplexing scheme for a fiber-optic grating sensor network, *Opt Lett.*, 18, 14, pp. 1192–1194, 1993.
- 8.L. A. Ferreira, J. L. Santos, and F. Farahi, Pseudoheterodyne demodulation technique for fiber Bragg grating sensors using two matched gratings, *IEEE Photon. Technol. Lett.*, 9, 4, pp. 487–489, 1997

Comparison of Communication via IR and Visible Light Spectrum in Mobile Indoor FSO Networks

Stanislav Hejduk, Jiri Bocheza, Jan Vitasek, and Karel Witas

Department of Telecommunications, FEECS,
VŠB – Technical University of Ostrava, 17. listopadu 15, 708 33 Ostrava – Poruba
{stanislav.hejduk, jiri.bocheza, jan.vitasek, karel.witas}@vsb.cz

Abstract. In this paper we compare two different types of light spectrum which can be used for mobile free-space-optical (FSO) communications. First system is using white (visible) light spectrum and the second system uses IR (invisible) spectrum. Aim is to describe the main differences between these two systems in terms of observed optical noise, range and their influence on the transmission speed.

1 Introduction

Nowadays, FSO communications aren't widespread as RF communications and development is limited to few industrial applications. Mobile FSO communications are used even less. Main reasons are probably the problems with complex coverage (compared with RF) and lower speeds. On the other side, there are also few advantages like unlicensed band and essentially zero interference between systems. We can also precisely define coverage area and divide area into different networks with same communication wavelength, which is impossible with RF technology. But it is accompanied by large demands on accuracy and requires complex management system which is able to tracking the mobile station across the area [1]. Easier way is to use a diffuse network. That means flooding of the room with strong optical signal that is strong enough to work even through reflection from walls and other obstacles. With this system we can use LEDs in the room for lighting and communication at the same time [2].

Our target is to compare the differences between the use of visible light and IR light. Both systems have their pros and cons. They are different in terms of optical power, demands on the modulation scheme, optical noise and some other parameters.

Another thing that we must pay attention is power consumption, because our communication system should be mobile, it means that it will work with a limited supply of energy. For both systems we consider use of high power LEDs to achieve sufficient communication range.

2 Communication via visible light

Using of visible light for communication brings in the first place demands on the stability of light intensity, especially when we use the lighting systems. If the human eye will be able to perceive changes in the light intensity, illumination may become unpleasant. To meet this condition we are strongly encouraged to careful choose of the used modulation and coding.

And of course light will be activated whenever the system will communicate.

2.1 Modulation

Since the light intensity must be constant we must use the modulation that maintains a stable mean value. Also the difference in communication signal should be as large as possible.

The best and easiest to implement is On-Off Keying (OOK), so the light have just two states: On or Off. But for stable mean value we must add the appropriate coding, like Biphase or Manchester. Examples of them are shown in Figure 1.

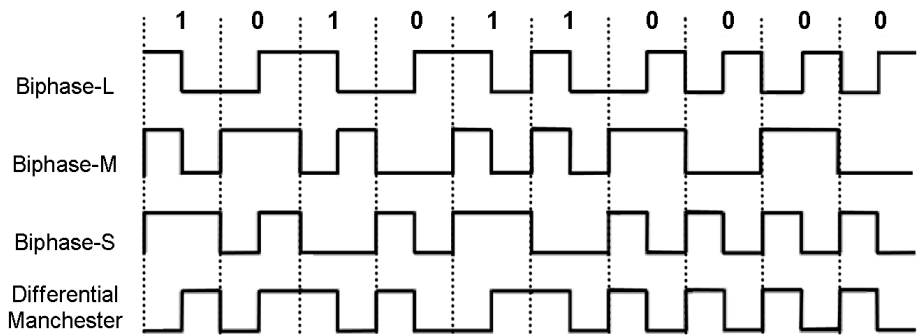


Fig. 1. Coding examples for use in the visible spectrum communications

2.2 Optical power

Patterns used in Fig.1 are easy to transmit, synchronize and receive, but optical power drops to 50%. Only way to suppress this decline is to increase the transmission power. The best part about it is increasing the range of the system. However, we need to modulate light source with higher current which is always more difficult and causes modulation frequency limitations.

2.3 Speed

Achieved bit rate is equal to used modulation frequency (1MHz = 1Mbit/s). But with more sophisticated modulation methods is possible to make the communication more efficient and therefore faster, like MIMO systems [3] or OCDMA [4].

3 Communication via invisible (IR) light

When we are using infrared part of the light spectrum, the communication isn't detectable with human eye. So we don't have to use special coding schemas or keep light active while no data are present at system output. This feature saves a lot of valuable energy, especially in mobile applications.

3.1 Modulation

Since the modulation does not depend on special requirements of human eye, we can use whatever we need for the necessary energy saving.

3.2 Optical power

With optical power we will observe an improvement in signal-to-noise ratio, due to the lower optical noise in this region of light spectrum.

But the propagation of light is the same. Which means that each time you double the distance between transmitter and receiver, the optical power drops to a quarter. Which is described in the following formula, light from LED disperses conically and at any cross section of this cone can be emitted power calculated as [1]:

$$\frac{SA_R}{SA_T + \pi/4 (\theta R)^2} \quad (1)$$

Where SA_R is the surface area of receiver, SA_T is the surface area of the transmitter, θ is divergence angle and R is range in meters.

4 Main problems

Before we try to make a proposal of Mobile FSO system, we must consider some general limitations of optical communications.

4.1 Optical noise

Optical noise from the surroundings causes a significant problem, because it is more difficult to recognize the original signal on photodetector. Hence the problem with the choice of suitable working wavelength comes. Optical noise is different for various wavelengths and photodetector itself is unable to distinguish signal from the noise. It just converts all the light that is able to accept due to the composition of the PN junction to an electrical signal. So it is worth to use appropriate optical filter on the photodetector side, which suppress the redundant noise of unused wavelengths.

On the following figure we can see the example of optical noise coming from daylight and its differences across the spectrum.

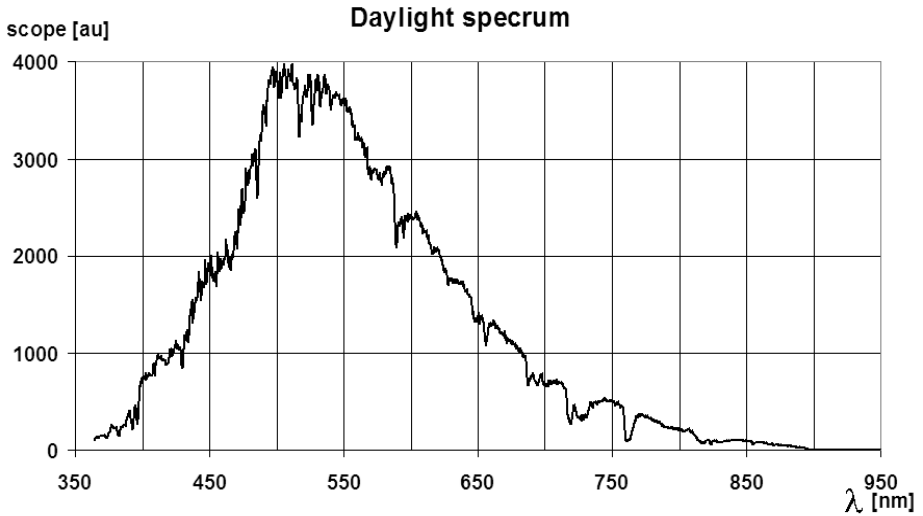


Fig. 2. Spectrum of the daylight for individual wavelengths

As a result we can see that the noise of the visible spectrum is much higher than in infrared. This means that for the same SNR ratio in the visible spectrum we need a much larger transmission power than in case of IR spectrum.

4.2 Bandwidth vs. sensitivity tradeoff

It's logical that we expect two things of this system. First is the high sensitivity of the receiver, which means higher communication distance and second thing is maximum possible bandwidth for faster communication. Unfortunately, these two parameters act against each other. And of course higher sensitivity leads to a higher noise. This is due to the photodetector circuit principle [5]. Where capacity $C_{par.}$ of the PN junction limits the communication speed and load resistor R controls the sensitivity.

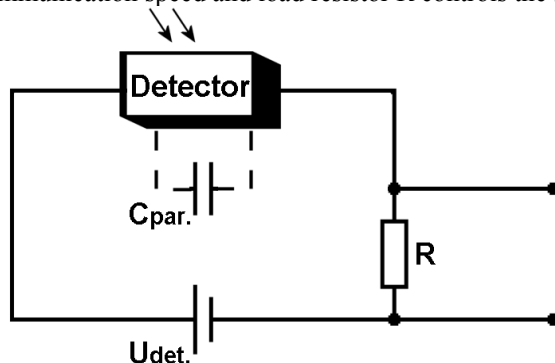


Fig. 3. General circuit of the quantum photodetector

If we look at Figure 3, we see that output signal has a high frequency cutoff given by:

$$B = 1 / 2\pi RC \quad (2)$$

So if we want high bandwidth, we must use small resistor R. Nevertheless, small value of R also means that output signal will be smaller, so we need to increase transmission power or increase the gain of the photodetector amplifier which can be difficult. Another thing is high value of the load resistor. It is an ideal solution for low speed and low power transmitters, but we must not forget the SNR ratio.

4.3 Multipath signal propagation

In the end we must solve the question how to cover the area with optical signal. The best performance will be achieved with point-to-point solution. But when it comes to mobility and easy realization, we come back to the diffuse network, where transmitted light evenly covers the entire area due to the reflections from obstacles. These reflections bring us to the problem in terms of delay and expansion of optical pulses, which limits the bitrate.

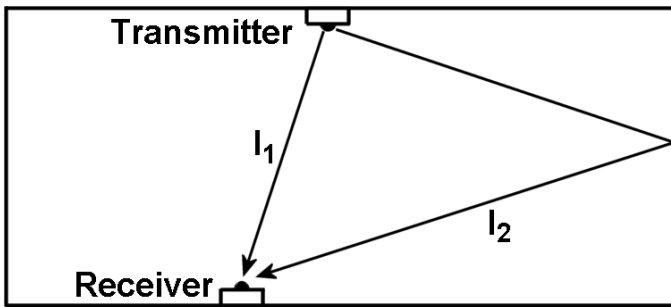


Fig. 4. Consequences of multipath signal propagation

Light needs a lot of time before it gets from the transmitter to the receiver and because light goes to the receiver in different ways simultaneously, the receiver gets the same signal in different times [6]. This difference in time is given by:

$$\Delta t = \frac{\Delta l}{c} [s] \quad (3)$$

So if the difference between the paths of light is 1 meter, the difference in time is approximately 3 nanoseconds, which can be problematic at high frequencies.

5 Mobile FSO system proposal

Due to differences between the use of visible and IR spectrum, there is the possibility of using a combination of their advantages. Because LED lighting in visible spectrum works with high optical power, it's suitable for use like base stations. On the other side the IR spectrum is more convenient for mobile stations as shown below.

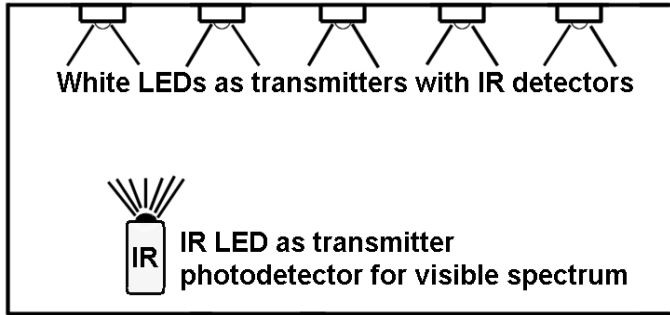


Fig. 5. Mobile FSO system proposal

As we can see in Figure 5, we used combination of both systems. White LEDs have enough power to supply the photodetector of mobile station with sufficient power to allow high speed communication and sensitive IR detectors can receive slow weak signals from low power mobile station.

6 Conclusion

Combination of white and IR light have its advantages and disadvantages, for example it solves the problem with full duplex communication, because communication channels are divided into different wavelengths and there is minimum optical noise at IR spectrum around 950nm. But the lights must be activated whenever the system will communicate and it does not matter whether it is day or night. So it must be turned on continuously.

References

1. Jayasri Akella, Chang Liu, David Partyka, Murat Yuksel, Shivkumar Kalyanaraman, and Partha Dutta.: Building Blocks for Mobile Free-Space-Optical Networks. Proceedings of IFIP/IEEE WOCN, Dubai, United Arab Emirates, March 2005
2. T.D.C.Little, P.Dib, K.Shah, N.Barraford, B. Gallagher.: Using LED Lighting for Ubiquitous Indoor Wireless Networking, IEEE International Conference on Wireless & Mobile Computing, Networking & Communication (2008)
3. Raed Mesleh, Rashid Mehmood, Hany Elgala, Harald Haas.: Indoor MIMO Optical Wireless Communication Using Spatial Modulation. Communications (ICC), IEEE International Conference 2010.
4. Radu Lucaciu, Adrian Mihaescu, Calin Vladeanu.: Dynamic OCDMA Coding for Indoor Wireless Optical Communications, 8th International Conference on Communications, Bucharest, Romania, 2010
5. Silvano Donati. Photodetectors: Devices, Circuits, and Applications, ISBN 0-13-020337-8, Prentice Hall, Inc. USA, (2000)
6. Adrian Mihaescu, Pascal Besnard: Indoor Wireless Optical Communications, 8th International Conference on Communications, Bucharest, Romania, 2010

The Method for Real-time Content Transmission Measurement in Mobile Networks

Lukas Kapicak and Pavel Nevlud

Department of Telecommunications, FEECS,
VŠB – Technical University of Ostrava, 17. listopadu 15, 708 33 Ostrava – Poruba
{lukas.kapicak, pavel.nevlud}@vsb.cz

Abstract. The paper deals with transmission video calls in mobile networks. It describes transmission speed in different mobile networks in connection with video calls. We have developed method for comparing transmitted video content based on the size of the video calls. The paper describes differences in video content affected by the transmission speed or by packet loss. There are factors described in this paper, which influence the transmission characteristics. The video calls are tested as a data transmission not as a video call service available only in UMTS mobile networks.

Keywords: Real time video transmission, mobile networks, data transmission, H.263, Asterisk.

1 Introduction

Video calls are not nowadays widely spread service in spite of a mobile operators' effort to expand video calls among more users. We can consider both video and voice transmissions together as next revolution in telecommunication services. Although the most of users think that mobile networks are not able to operate video calls, the true is that the mobile networks offer a sufficient transmission capacity for real-time video calls.

To define the sufficient transmission parameters of mobile networks used to real-time video transmission, we need to know both properties of mobile networks and transmitted video content. There are transmission line capacity limits with 2.5 generation networks. Third generation networks offer sufficient bandwidth for transmitting video calls with higher data stream.

This publication focuses on determining sufficient transmission capacity for specific video content and for defining test of line. The service [1] for video calls transmission used in 3G mobile networks was not chosen. All tests were created by data transmissions and Asterisk [3] represented a multimedia gateway.

2 Testing configuration

Mobile networks

There are very variable conditions in mobile networks. They are affected by weather, aggregation, the number of connected users, etc... Therefore we were obliged to make a measurement separately and to average results. At first, we measured the properties of CSD, HSCSD, GPRS, EDGE and 3G [2] mobile networks. Later, according to the real properties, we chose video codecs used later in video calls tests. We have found out that CSD, HSCSD and GPRS [2] networks are not useable for video transmission. The minimum requirements for video transmission are data connection via EDGE technology.

Measuring system

To ensure objectivity of measurement, there were 2 Asterisks [4] chosen as the end-points for video transmission – Figure 1. We had to add a special module and libraries to learn Asterisk recording and playing saved video call records.

One Asterisk sent a video call to another Asterisk, which answered a call and recorded it. The same attitude can be used in future for testing more than one video calls together.

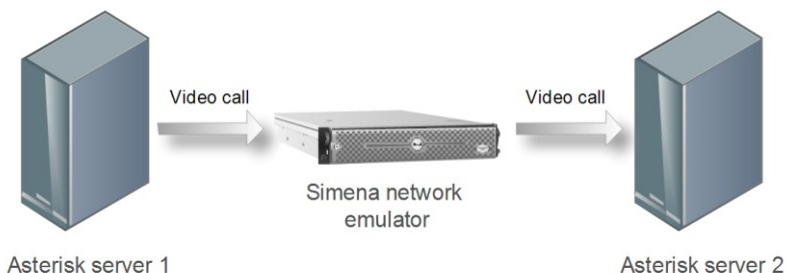


Fig. 1. System architecture.

3 Modification of Asterisk

Asterisk supports video calls transmissions; it becomes a gateway among individual clients talking together. Asterisk supports H.263, H.263p and H.264 [5] codecs. Asterisk doesn't work with video streams. It only verifies whether the codec is allowed to be used in the client account.

There are two ways of measuring a video call transmission. Can be used either comparing source and destination video file or source and destination data stream. We chose the first option, comparing source and destination video file. We have installed `app_mp4.c` module into Asterisk. Module adds 2 functions to `extensions.conf`, `mp4play` and `mp4save`.

There is a scheme of video call recording in Figure 1. The call between Asterisk 1 and Asterisk 2 is established by CLI interface of Asterisk 1. The Asterisk 2 had to be registered on Asterisk 1 as a user and special dialplan rules were created to establish the call.

There was a network emulator Simena [6] located between Asterisk servers. Video was saved in 176x144 resolutions in H.263 codec. Data stream of video was 304 kbps.

4 Testing results

After the test, the size of the streamed video file in Asterisk 1 was compared with the size of recorded video file in Asterisk 2. We assumed that the size of the file would not be changed during faultless transmission. However, the size decreased with growing packet loss during the transmission. In this test, latency should not influence over size of the recorded file.

Table 1. Dependence of the size of the video file on latency and mobile network – original video file size is 991129 B

H263	128kbps	218kbps	1990kbps
Latency (ms)	Size [B]	Size [B]	Size [B]
0	478198	748112	991129
50	529798	837544	991129
150	463514	743340	991129
250	516075	711935	991129
350	407041	688161	991129
500	530520	962987	991129

Table 2. Dependence of the size of the video file on packet loss and on mobile network - original video file size is 991129 B

H263	128kbps	218kbps	1990kbps
Packet Loss (%)	Size [B]	Size [B]	Size [B]
5	574935	793403	944177
15	460507	672654	791849
25	572034	757362	746104
35	468005	656917	661522
45	439112	560021	548463
55	370665	379394	353694

In the first case, bandwidth 128 kbps was set. It represents EDGE technology. The measurement shows that EDGE technology is not able to serve adequate bandwidth for video transmission.

In the second case, we set up bandwidth 218 kbps. Bandwidth is corresponding with bandwidth of UMTS TDD network. This network could not serve adequate conditions for faultless video transmission either. During latency measurement, the size of file was nearly constant. The size of destination video file was more negatively influenced by packet loss.

In the last case, we set up bandwidth 1990 kbps. Bandwidth is corresponding with bandwidth of 3G networks in UMTS FDD configuration. We have decided there is no influence of latency to transmitted video file. But in the real video call, the level of latency higher than 400ms means that users are not able to communicate well. The size of destination video file is negatively influenced by packet loss.

Video call quality tests

The individual video files are compared with software Video Quality Measurement Tool (MSU) [7]. This software offers techniques for comparing two or more video files according to codecs and lost frames field. MSU VQMT consists of many plugins. We have chosen plugin SSIM - Structural Similarity [8].

SSIM video tests

SSIM value defines similarity between the original video picture and transmitted video picture. Table 3 and table 4 describe average SSIM value for specific transmission characteristics. If the SSIM value equals 1.0000 it means that transmitted video has 100% similarity compared with original video frame.

Table 3. SSIM values for video calls affected by latency

H263	218 kbps	218 kbps	1990 kbps	1990 kbps
Latency	Frames	Avg. SSIM	Frames	Avg. SSIM
0	255	0.99954	391	0.99985
50	305	0.89954	391	0.99985
150	253	0.99947	391	0.99985
250	241	0.94062	391	0.99985
350	226	0.99911	391	0.99985
500	374	0.98782	391	0.99985

Table 3 shows SSIM values for transmission affected by latency. Latency does not affect changes in video content. Insufficient bandwidth cause changes at the end of the video call.

Table 4. SSIM values for video calls affected with packet loss

H263	218 kbps	218 kbps	1990 kbps	1990 kbps
Packet Loss(%)	Frames	Avg. SSIM	Frames	Avg. SSIM
0	255	0.99954	391	0.99985
5	297	0.75648	366	0.35738
15	266	0.33385	319	0.32075
25	297	0.27950	298	0.28947
35	260	0.28148	263	0.25502
45	225	0.24798	230	0.24841
55	158	0.27858	122	0.28791

Table 4 shows SSIM values for transmission line, which loses packets. There are not significant differences in SSIM between line with bandwidth 218 kbps and line with 1990 kbps.

We have defined these categories according to occurred errors

- Video call file has the same size compared with original video file. Bandwidth covers transmission demands of the video calls. Transmission delay caused by latency is not found.
- Video call has the smaller size compared with original video file and there are SSIM values nearby value 1. Bandwidth does not cover demands of the video calls.
- Video call has the smaller size compared to original video file and there are SSIM values close to zero. All broadcasted packet do not achieve destination and the packets are lost during transmission.

5 Conclusion

Our results can be used in many cases. It can be extended to measure not only latency and packet loss, but also in other networks beside mobile networks. It is basic scenario which can be used to prove that the measured line can serve real-time video transmission.

It is obvious from the measured data, that we can't identify latency in transmission line. However, we are able to decide packet loss in line. We can calculate the percentage of lost packet from the saved data.

For purpose of modeling real transmission line, we can compare measured data and data from real traffic. There can be a script prepared, which will establish test call in definite time, system or line status.

Measured data can be used in later analysis. We can calculate packet loss of a line or actual bandwidth during the measurement. We can analyze that by controlling saved video file content.

Our method informs which properties influent transmission of video calls. Nowadays, the method will be extended for:

- automatic analysis of video content,
- searching defects in image,
- testing other transmitting networks,
- searching of mathematical dependencies of packet loss on size of video file,
- testing of H.264 high resolution video in mobile networks HSPA and HSPA+.

References

1. Jörg Eberspächer, Hans-jörgVögel, Christian Bettstetter, Christian Hartmann, GSM-Architecture, Protocols and Service, 3.edition, West Sussex, England: John Wiley & Sons, Ltd, 2002, pp. 58, 108, 139, 212, 234, 264, 266. ISBN 978-0-470-03070-7.
2. Timo Halonen, Javier Romero, Juan Melero, GSM, GPRS and EDGE Performance Evolution Towards 3G/UMTS, 2.edition, West Sussex, England: John Wiley & Sons, Ltd, 2003, pp. 11, 14, 49. ISBN 0-470-86694-2.
3. M. Voznak, Voice over IP. VSB-Technical University of Ostrava: College book, 1st. ed., Ostrava, 2008.
4. Jim Van Meggelen, Jared Smith, Leif Madsen, Asterisk: The Future of Telephony, O'Reilly Media, pp. 15 - 48, September 2005. ISBN 978-0-596-00962-5.
5. S. Zoi, D. Loukatos, L. Salakis, P. Stathopoulos, N. Mitrou, Extending an Open MPEG-4 Video Streaming Platform to Exploit a Differentiated Services Network, In: High-Speed Networks and Multimedia Communications 6th IEEE International Conference, HSNMC 2003, July 2003, pp. 385-405.
6. Simena, Simena network emulator, [online], <http://www.simena.net/>
7. MSU, MSU Quality Measurement Tool: Metrics information, [online], http://www.compression.ru/video/quality_measure/info_en.html
8. SSIM, Information about SSIM, [online], <https://ece.uwaterloo.ca/~z70wang/research/ssim/>

New Method of Analysis of Crystallizer Temperature Profile Using Optical Fiber DTS

Petr Koudelka, Jan Látal, Jan Vitásek, Martin Pápeš, and Andrej Líner

Department of Telecommunications, FEECS,
VŠB – Technical University of Ostrava, 17. listopadu 15, 708 33 Ostrava – Poruba
{petr.koudelka, jan.latal, jan.vitasek,
martin.papes, andrej.liner}@vsb.cz

Abstract. Continuous casting is a modern and advanced technology of steel production, which product is a blank as an intermediate product for further processing. One of the most important parts of this whole process is crystallizer. At present most methods, describing how to analyze the temperature profile of crystallizer in operation, were published and experimentally verified. These methods include the use of thermocouples or Bragg's grids. New sophisticated method of analysis of crystallizer temperature profile is the use of optical fiber DTS based on stimulated Raman dispersion. This paper contains the first experimental measurement and method's verification, which are necessary for the deployment this method into industrial practice.

1 Introduction

The optical fiber DTS (Distribution Temperature Systems) are unique distributed temperature systems using optical fiber as a sensor. Due to advantageous features of optical fiber these sensory systems begin to be utilizing in industry [1]. In some cases optical fiber DTS is indispensable helper today:

- monitoring of outflow from oil pipeline,
- monitoring of outflow from product pipeline,
- monitoring of water percolatin from hydraulic structure,
- temperature profile measurement of borehole in rock pillar (heat pumps).

The optical fiber DTS uses nonlinear effects in optical fiber, Raman or Brillouin nonlinear effect respectively. Optical-Fiber DTS using Brillouin stimulated scattering is able to measure temperature and tension along optical fiber in distance of 50 km, nevertheless due to higher purchase cost the industry rather uses systems based on Raman nonlinear effect.

Technologically, the optical fiber DTS is based on optical reflectometer principle. In the optical fiber a light pulse is transmitted with wavelength of 975 nm, 1064 nm or 1550 nm (in dependence on construction of DTS) and with width of 10 ns.

2 Optical-fiber DTS Based on Raman Stimulated Scattering

The main function of crystallizer is to ensure stiffening of the surface shell of such a thickness and strength, to keep the content of a liquid core at the entrance of the stream to the secondary cooling zone. The key elements are shape, shell thickness, the same temperature of the shell by the shift and this all without the internal and surface defects with minimal porosity and a small number of non-metallic foreign inclusions [2].

Cooling of the blank in crystallizer is a combination of heat transfer by convection, conduction and radiation. In the crystallizer is the largest amount of heat per unit time from the blank taken away and that is 10 to 30 % of all heat. In most cases is the crystallizer cooled by water flowing in the milled grooves or drilled channels of the plates, or the crystallizer is constructed like tubular, and it's on whole outer surface washed with water.

2.1 The Coefficients of Heat Transfer in the Crystallizer

Heat flow Q_m exhausted from the blank is given by (1) implying that this flow is taken away by cooling water, passing through to crystallizer [3],

$$Q_m = c_w \rho_w F (T_{out} - T_{in}), \quad (1)$$

where F is the flow ($\text{kg}\cdot\text{s}^{-1}$), c_w is the specific heat capacity of cooling water ($\text{J}\cdot\text{kg}^{-1}\cdot\text{K}^{-1}$), ρ_w is the density of cooling water ($\text{kg}\cdot\text{m}^{-3}$), T_{out} is temperature at the output of the crystallizer (K), and T_{in} is temperature at the input of the crystallizer (K).

The average heat transfer coefficient on the border blank – crystallizer can be determined from the equation

$$htc_m = \frac{Q_m}{A(T_{solidus} - T_{out})}, \quad (2)$$

where htc_m is the heat transfer coefficient of the crystallizer ($\text{W}\cdot\text{m}^{-2}\cdot\text{K}^{-1}$), Q_m is the heat flow of the crystallizer, A is the area of the work surface of the crystallizer (m^2), $T_{solidus}$ is the temperature of the solid phase (K) and T_{out} is the temperature at the output of the crystallizer (K).

From the experimental measurement, in which was 44 thermocouples in two lines into the crystallizer installed, it is possible to observe that the temperature at the spot T_m is about values 100 °C and not exceed 200 °C [2].

3 Optical Meanders in Point

If it is necessary to ensure accurate localization in the measurement process, it is appropriate to apply optical meanders in the point mode. Point mode means that some point is created sensory ring of optical fiber. In practice, it is often required the sensory ring to have the smallest sizes (inner diameter and length of the optical fiber in the

ring). It is obvious that the dimensions of the sensory ring will vary with different parameters of optical fibers [4].

Experimental measurement revealed that for multimode optical fiber with primary protection (outer diameter 250 μm) is critical inner diameter of the sensory ring 3 cm, as shown in Fig. 1, [5].

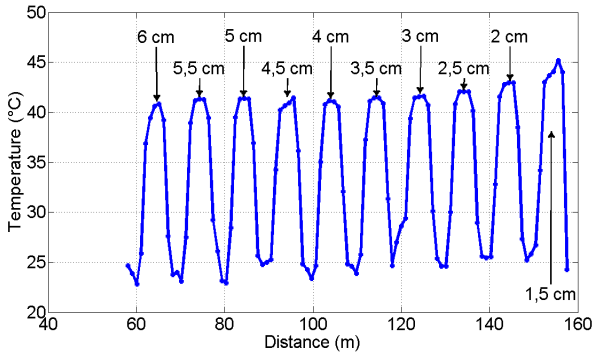


Fig. 1. Effect of the inner diameter of the sensory ring on the measured temperature of the water bath (measured together, optical fiber with primary protection, outer diameter 250 μm), [5]

According to another experimental measurement the length of multimode optical fiber in the sensory ring has a critical value of 3 m [5].

3.1 Experimental verification of the implementation of sensory rings on the crystallizer model

For experimental verification, were the sensory rings placed on the model of the crystallizer by special epoxy adhesive designed for high temperatures (Loctite 9492, operating temperature from $-55\text{ }^{\circ}\text{C}$ to $180\text{ }^{\circ}\text{C}$). The location of sensory rings on the crystallizer was chosen so that on each side of the crystallizer at one level were placed sensory rings (Fig. 2).

At the bottom part of the crystallizer model was placed a kettle with water that was heated by hot plate. In order to ensure a measurable increase of temperature on the surface of the crystallizer model was the upper part of the model covered with a metal plate. The experimental measurement of the temperature profile through the sensory rings with primary protection was such that the model of crystallizer stood near a window that was opened. Side turn to the window should be cooler during the whole experimental measurement. On the contrary, the reverse side from the window should be warmer. Side turn to the window is labeled as side A, reverse side from the window as C, the other two sides B and D within the meaning counterclockwise. On the side A fiber began and each new level here. Level always ended on the side D, as well as the fiber. At the beginning of the experimental measurement in the room was

measured at 25.7 °C, at the window closed. Just after the beginning of the experimental measurement window was open.

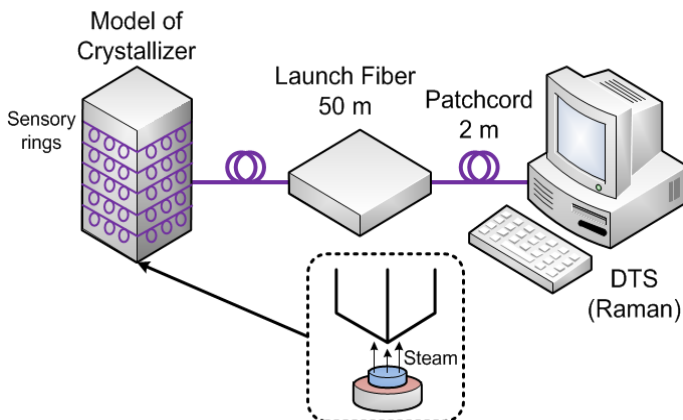


Fig. 2. Experimental verification of the implementation of the sensory rings on the crystallizer model

Hot plate was turned on after measuring the first iteration, after three minutes of the start of measurement. Measurement lasted for 42 minutes, i.e. 14 iterations. The measurement results are shown in Fig. 3. The temperature was increased on crystallizer over time. The fiber had its beginning in the upper level of crystallizer, so the temperature of the upper level of crystallizer is visible on the left side of Fig. 3, temperature of the lower levels of crystallizer on the left.

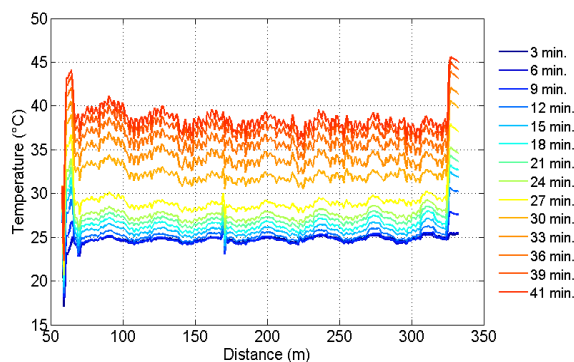


Fig. 3. The measurement results of the experimental verification (measurement lasted for 42 minutes, i.e. 14 iterations)

Through sensory rings can also accurately identify the place of the temperature anomalies. The model shows always two sides of the crystallizer. They are divided

into squares each square represents the place of measurement of sensory ring. Examples of results of experimental measurements transformed into the temperature model of crystallizer are shown in Fig. 4 and Fig. 5. Transformed measured results show the temperature profile of crystallizer model.

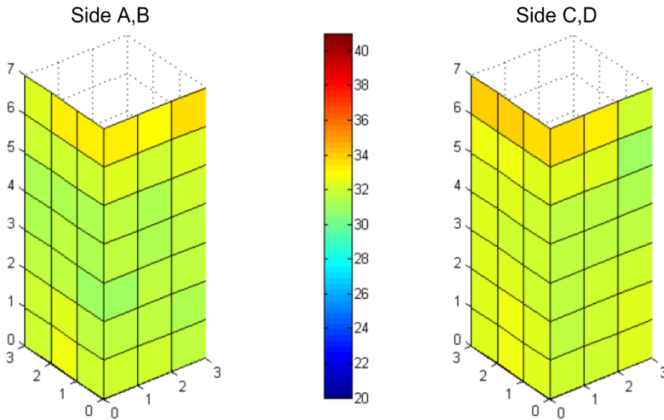


Fig. 4. Transformed measured results show the temperature profile of crystallizer model – 30. minute

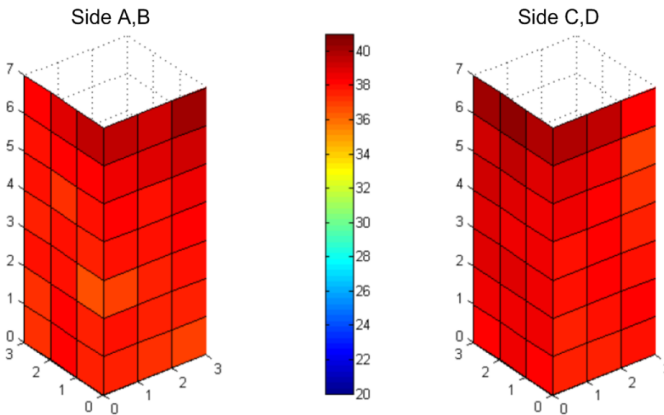


Fig. 5. Transformed measured results show the temperature profile of crystallizer model – 42. minute

5 Conclusion

Experimental measurements were supposed to verify the applicability of optical meanders in the spot mode (sensory rings) to measure the temperature profile of the crystallizer. For implementation in real conditions are under consideration milled slots into the outer shell of the crystallizer. After embedding of milled slots by the help of high temperature adhesive a continuous surface will arise for better heat dissipation by flowing water. Through sensory rings can also accurately identify the place of the temperature anomalies.

References

1. Koudelka, P., et al., "Optical fiber distributed sensing system applied in cement concrete commixture research," *Radioengineering*, 19(1), 172-177 (2010)
2. Štětina, J., "Dynamicky model teplotního pole plynule odlevané bramy," VUT Brno, (2007)
3. Delhalle, A., Larrecq, M., Petegnief, J. and Radot, J. P., "Control of the first shell formation during continuous casting of steel," *Revue de métallurgie*, 86(6), 483-489 (1989)
4. Skapa, J., et al., "Optical fiber distributed temperature sensor in cardiological surgeries," *Proceedings of SPIE - The International Society for Optical Engineering*, (2010)
5. Koudelka, P., et al., "New Sophisticated Analysis Method of Crystallizer Temperature Profile Utilizing Optical Fiber DTS Based on the Stimulated Raman Scattering," *Advances in Electrical and Electronic Engineering*, 10(2), 106-114 (2012)

Practical Simulation Phenomenon of the Helmholtz Coils and Its Calculation

Lukáš Paulínský and Pavel Svoboda

Department of Electrical Power Engineering, FEECS,
VŠB – Technical University of Ostrava, 17. listopadu 15, 708 33 Ostrava – Poruba
ok2pzp@centrum.cz, pavel.svoboda@vsb.cz

Abstract. Practically, flux density on Helmholtz coils is measured by the help of Halls probe and teslametre that is calibre voltmeter right in values of magnetic inductance B. We have available basic programming languages for various levels of implementing advanced methods of simulation. With computer simulation we can simulate this phenomena easilly and understand this effect. We have an available programming language from Comsol AB company for various levels of implementing advanced methods of simulation.

Keywords: magnetic field, flux density, current, Helmholtz coils, magnetic inductive lines.

1 Introduction

A Helmholtz coil is a parallel pair of identical circular coils which place one radius apart and wind so that the current flows through both coils in the same direction. This winding results in a uniform magnetic field between the coils with the primary component parallel to the axis of the two coils. The uniform field is the result of the sum of the two field components which parallel to the axis of the coils and the difference between the components is perpendicular to the same axis.

As recognition magnetic inductance B has to measure three components B_x, B_y, B_z. With regard to axial geometry coils and recognition magnetic inductance in axial level, only axial and radial directions are enough.

$$B = \frac{\Phi}{S} = Q \frac{R}{NS}$$

To create magnetic field on Helmholtz coils, it is necessary to bring up periodic pulse current (voltage) which creates pulsating magnetic field.

By using Biotov-Savartov law, it is possible to demonstrate that the flowing, which is caused by two circular conductors that have radius a , certain distance b and same axis x with the same current, will be the homogeneous field between the coils. If we want to get a strong magnetic field, we have to place conductors which use two coils. Therefore, flux density in proximity centre between coils, where distance coils grade their radius, is calculated:

$$B = \left(\frac{4}{5}\right)^{\frac{3}{2}} \mu_0 N \frac{I}{a}$$

It follows the deduction of relation for the size of the magnetic inductance at point A on axis x (Fig 1.):

$$B_A = \frac{\mu_0 N I a^2}{2} \left\{ \left(a^2 + \left(x - \frac{b}{2} \right)^2 \right)^{-\frac{3}{2}} + \left(a^2 + \left(x + \frac{b}{2} \right)^2 \right)^{-\frac{3}{2}} \right\}$$

Where:

μ_0 – permeability of vacuum (1,257 x 10-6 T.m.A-1)

a - radius coils

I – current in scroll of coils

x – x-axis point A

N – count of scroll

b – distance coils

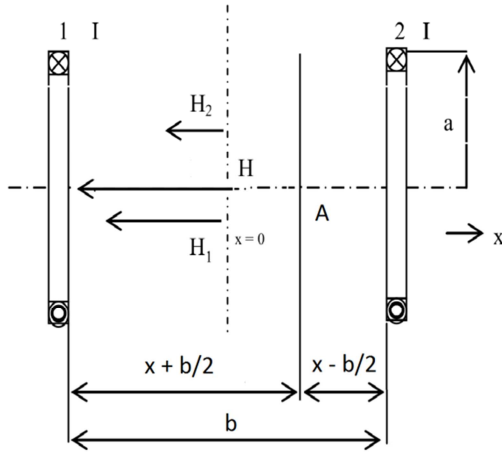


Fig 1. – Size magnetic induction in point A

2 Non-consonant direction currents in coils

Magnetic field with non-consonant direction currents is imaged in Fig 2. Here the electric current runs through the upper and lower scrolls contrariwise. These non-consonant direction currents have an intensity magnetic field on the axis coils that has consonant gradient. Dipole moments of both scrolls have an opposite orientation. Magnetic field scroll is added and in the middle of scrolls the target field is zero. In spite of scroll stationary, the operation on them repulses force, which creates pressure field between scrolls.

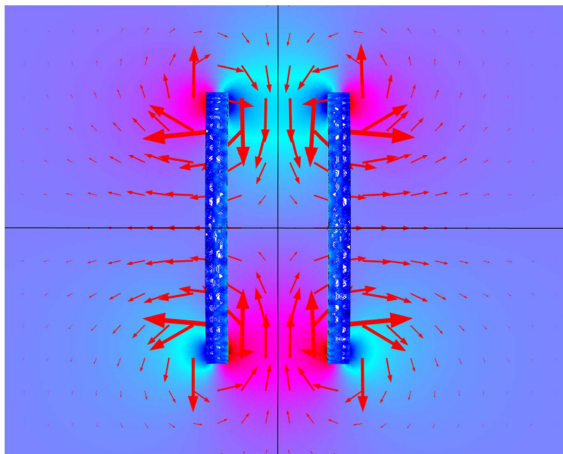


Fig 2. – Helmholtz coils with different direction currents – magnetic field visible by the help of surface darts.

Gauge is introduced at nanotesla (nT), where blue shows the smallest value and red shows the highest value. Fig 3. shows the declining of magnetic inductance at non-consonant direction currents is about 0,49 nT compared to coils with consonant direction (see Fig 5.). The next declining magnetic inductance below 0,02 nT occurs in the middle graph. Due to opposite orientation currents in coils, magnetic field, which is away from coils – repulse, is created. This phenomenon can be seen with red darts routing out.

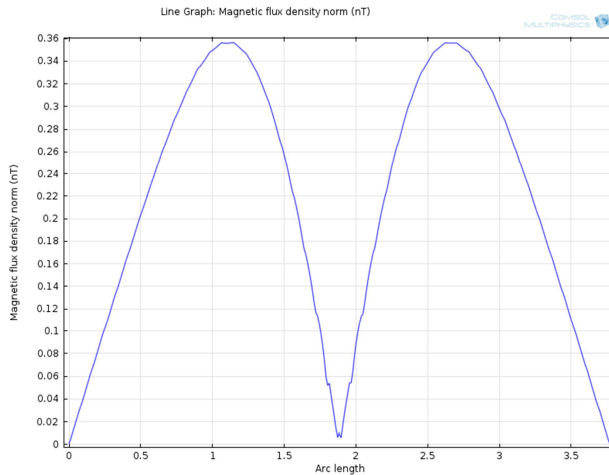


Fig 3. – Measured flux density depending on zoom factor (cm) – different polarity currents.

3 Consonant direction currents in coils

Magnetic field of Helmholtz coils with consonant direction is visible in the next figure where their size and direction can be seen by the red darts. Upper and lower scrolls run through electric current of even direction and same sizes. Current density is attached only in double-direction axial symmetry coils. Dipole moments of both scrolls have the same orientation. The fields of both scrolls pile up and create resulting field that is constant in the centre scrolls. Despite scrolls stationary, the force of gravity, which stretches magnetic lines between scrolls, still works on them.

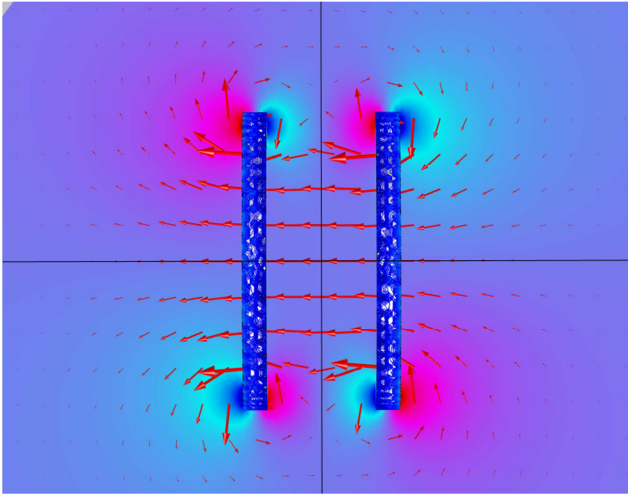


Fig 4. – Helmholtz coils with agreeing direction currents – magnetic field visible by the help of surface darts.

The next visible diagram shows total magnetic induction in both coils. Therefore, it is the highest value which is almost two times more than the value in the figure from previous chapter. Fig 5 shows us one coil with zero decline in the centre axis. Because the real field from both coils is added, it cannot come to any declining inductance like in the previous case. Therefore, at the first sight it can look like the only one to behave one coil. The centre axis is approximately 2 cm and attains maximum flux density at 0,84 nT.

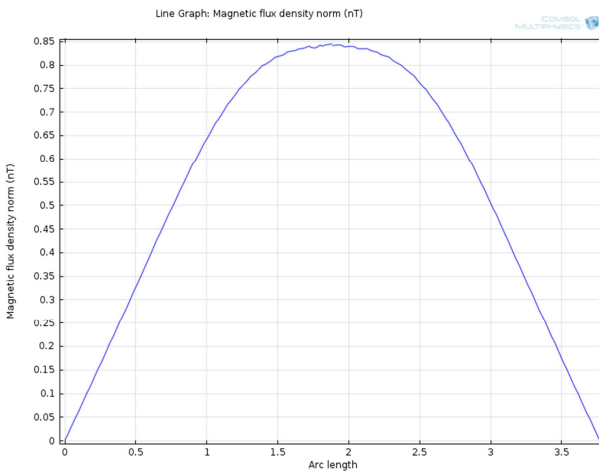


Fig 5. – Measured flux density depending on zoom factor (cm) – same polarity currents.

4 Conclusion

It can be possible to conclude that to attain an acceptable magnetic field in the round coils, it depends very much on the quantity of scrolls which are coils twisted as well as the options of acceptable consonant current. From measured values, the best (stability) process of magnetic inductance near Helmholtz coils will come when their distance from straight radium coils $b=a$. That also points out the attainment of simulation that Fig 5 shows. Therefore, it would be said that the magnetic field around centre coils is almost constant. The direction passing the currents has a big influence on the magnetic field around coils. The non-consonant direction current field in coils is repelled. This fact we can see in Fig 3, where small values are in center axis x (repulsive field). Same currents can be found in coils of total larger field. Coils are placed in the air environment and adjusted to such values which are typical for laboratory conditions. Moreover, with current density we have to adjust two conditions for each coil. The size of current is adjusted to 1 A/m^2 .

References

1. Kulda, J.: Magnetické pole v silnoproudé elektrotechnice, ACADEMIA Praha1974
2. COMSOL AB, *Comsol Multiphysics*. USA: Comsol Publishing, October 2010.
3. Sedlák, B.,Štoll,I.:Elektřina a magnetismus, Academia, Praha2002.
4. Ivánek, L.: Elektromagnetismus – učební texty, v rámci operačního programu Rozvoj lidských zdrojů spolufinancováno z prostředků ESF a státního rozpočtu ČR: Ediční středisko VŠB – TUO Ostrava, 2007.
5. Shepherd, M. R.: Electricity and Magnetism, October 2008.

CUDA Attacks and Their Effect on Security in SIP

Jan Rozhon, Karel Tomala, and Martin Mikulec

Department of Telecommunications, FEECS,
VŠB – Technical University of Ostrava, 17. listopadu 15, 708 33 Ostrava – Poruba
{jan.rozhon, karel.tomala, martin.mikulec}@vsb.cz

Abstract. Session Initiation Protocol (SIP) incorporates several authentication algorithms that can be viewed as a potential security risk. One of them is MD5 digest access authentication which is commonly used and represents the most widespread method of authentication in SIP nowadays. Since the technology of parallel computing has undergone a huge leap since the SIP standardization, it can now pose a huge threat to this kind of authentication and SIP communication in general. This paper presents examples of the possible passwords and the time needed to break them to fill in the gap in the common knowledge about how long it takes to break an MD5 hash function.

1 Introduction

The security of modern communications lies on the series of algorithms, which can be split into two groups – hash functions and ciphers. While the former is mainly used for authentication and integrity checks the main purpose of the latter is to encrypt the communication so that only rightful recipient can access the content of the message. Both groups have long history and both are being improved all the time. However, due to the standardization and the slower implementation of newly proposed standards these algorithms are often used even when their weaknesses are discovered. The typical example is the MD5 Message-Digest algorithm. This hash function is widely used in various implementations of web services and applications, VoIP (Voice over IP) communication and others although it is well known that the procedures for “cracking” this tool exist and are very efficient. The main reason for this is the fact that although the original plain text input or the appropriate text string that would produce the same hash (collision) can be obtained by well-known procedures, the time to obtain them is usually very long, or at least long enough not to cause any security risk.

As we are going to describe in the following text, the technology evolved faster than the area of securing the digital communications. In this paper we are going to present several measurements illustrating the actual amount of time necessary to crack the MD5 hash function of password with typical length and characters that are commonly used. Moreover, we are going to present the time consideration regarding the “cracking” of digest access authentication, which is the most common method for user authentication in SIP. To steal user passwords we are going to use open-source tools

Hashcat and cudaSIPcracker, which can utilize the CUDA cores in the graphic cards and thusly make the brute force attacks very efficient.

2 Behind the Scene

In this section, we are going to describe the basics of MD5 and its implementation in digest access authentication as well as some basics of CUDA technology to provide the user with necessary background information for complete understanding of the topic.

2.1 MD5

The MD5 Message-Digest Algorithm is widely used cryptographic hash function producing the 16-byte long hash values from input of an arbitrary length. It was designed in 1991 and is used in modern communications for data integrity checks and authentication mechanisms used to conceal the plaintext passwords and prevent its transmission over insecure networks.

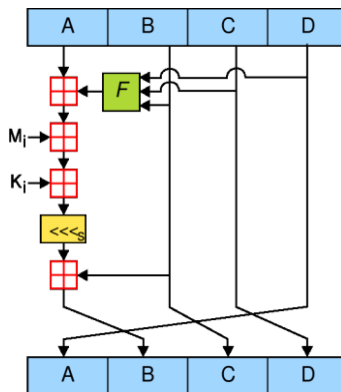


Fig. 1. Schematic operation of MD5 hash function according to [1].

Since its design several flaws of MD5 have been discovered allowing for creation of collisions (different inputs produce same output) or even breaking the cipher, which is why this hash function is not recommended for SSL certificates or digital signatures and should be replaced by other and more secure hash functions.

Despite this recommendation, MD5 still can be seen in production environments even in situations where the possible attack can cause significant damage. The example of this is the SIP communication, where the MD5 is used for authentication and if the attacker is able to capture network traffic, he can relatively easily steal the user account. The illustration of this attack and the security considerations will be presented later.

The MD5 algorithm splits the input into 512 bit chunks on which the given mathematical operations are performed. If the data cannot be divided, the input is zero padded and the 64-bit information about the original length is appended. Each chunk is then processed in 4 rounds as it is outlined on the Fig. 1 [1,2].

2.2 Digest Access Authentication

The Digest Access Authentication Scheme is widely used to prevent the plaintext passwords to be transmitted over the insecure network. In SIP we can encounter a digest authentication based on the MD5 algorithm. Basically, we can state that the client transmits the MD5 hash calculated from its credentials and the message headers. In greater detail we can distinguish three stages of calculation:

- $H(A1) = \text{MD5}(\text{username}:\text{realm}:\text{password})$,
- $H(A2) = \text{MD5}(\text{method}:\text{sip_uri})$,
- $\text{Response} = \text{MD5}[H(A1):\text{nonce}:H(A2)]$.

All the parameters required for the response calculation are transmitted over network insecurely. To be more precise, the required information can be obtained by examination of SIP headers in the authentication request. Method and sip_uri can be obtained from the request line of the SIP header. For example the following request line:

```
REGISTER sip:localhost SIP/2.0
```

results in method equal to "REGISTER" and sip_uri equal to "sip:localhost". All the other parameters for the response calculation can be found in authentication header, which may look as follows:

```
Digest username="100", realm="asterisk", \
nonce="16f24eb8", uri="sip:localhost", \
response="729cf3487af16529195ea7867ee3d883", \
algorithm=MD5
```

From this it is obvious that if the attacker manages to capture the SIP message containing this content, he could try to gain knowledge about the original client password.

2.3 CUDA

CUDA is the abbreviation for the Nvidia's Compute Unified Device Architecture, which allows for running high level programs written for instance in C/C++ on a graphic card. The graphic cards are designed to contain so called stream processors (or CUDA units), the main purpose of which is a calculation of graphical information. However, since 2006 and the Nvidia chip G80 these processors can be used for general calculations such as weather modeling, molecular dynamics modeling and so on. The main advantage of using graphic card (GPU) over processor (CPU) is the number of stream processors, which is very high even for mainstream GPUs and which allows for massive parallelization. Whereas the CPU can offer 4 to 8 cores capable of han-

dling complex operations using the modern instruction sets such as SSE, the GPU offers simple cores in high quantities. The basic difference between CPU and GPU is depicted on the Fig. 2 [3,4,5].

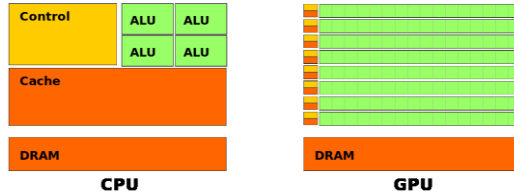


Fig. 2. Comparison of simplified CPU and GPU architectures[3].

There are several tools that use the power of CUDA architecture or its AMD counterpart STREAM to maximize their computational power. In our case, we are going to use Hashcat and CudaSIPcracker.

3 Experiment

To find out how quickly the attacker can steal the pass-word from the communication we have prepared a testing platform with massive computational power. The cornerstone of this platform are two dual-core GPUs nVidia GTX590, which provide 1024 stream processors (CUDA cores) working at 607 MHz. The theoretical computational power according to the manufacturer reaches 2.5 TFLOPS.

The other important data about the measuring platform summarizes following list:

- CPU Intel 3930K @ 3.2GHz (6 cores),
- 16 GB DDR3 RAM @ 1600 MHz,
- OS Windows 7 SP1 x64.

From the given we can state that the platform is the current high-end. On this platform two MD5 cracking tools were installed. First, the Hashcat in its CUDA variant. Second, the CUDA SIP Cracker.

3.1 cudaHashcat

Hashcat is an open-source software tool for breaking the hash functions in vast variety of implementations ranging from MD5 and salted MD5 to such special implementations such as Joomla hash, or even DES.

In our case we focused on using hashcat to break the MD5 hash values of password of reasonable length and character set. We used two assumptions: first, the password to be remembered can contain only numbers, lower and upper case letters, not special characters. Second, the password length was determined to 8 characters because of the compromise between password efficiency and the easiness to remember it. Of course longer or shorter passwords can be used; however the former need more time to be cracked, while the latter can be broken in matter of minutes, which is very insecure.

The special character can be used for passwords as well; however it is not likely because of the need to configure the telephones. In general, same approach can be used even for passwords with special characters.

To generate passwords we used strong password generator to generate three passwords of a length 8 and from the given characters. This way we created three groups of passwords – from lowercase characters, from lower and uppercase characters and from the lower and uppercase letters and digits. These three groups of passwords were then exposed to attack using hashcat, which resulted in the data contained in the table 1.

Table 1. Plaintext passwords and the time needed to get them from their MD5 Hash value

Plain Password	Time to Crack [s]	Theoret. Max. [s]
nrlcwelm	13	
ryvbbwlo	7	35
skxznpvw	31	
vCcZDrrU	4920	
YbmfeCFp	7320	8500
QiqcRWsd	1935	
CDoXEGcr	3599	
aTszJRL2	5280	34700
fAD9cBy9	5580	

It is clear that breaking the relatively secure password en-coded by the MD5 hash is the question of hours due to the usage of high performance GPU computing. The maximal computational power of the measuring platform was estimated to 6 300 M/s, which can give us the theoretical maximum for each group of password using the following equation.

$$T_{\max} = N / v, \text{ where } N = N_{\text{char}}^l \quad (1)$$

In (1) the N specifies the total number of possible passwords of the given length and character set and v is the computational speed of the platform. N_{char} is the number of characters in the given character set and l is the password length.

Although the character set between second and third group increased by 10 numbers to 62 total characters, the three given hashes from the third group had similar breaking times as the hashes from the group 2.

To complete the picture it is necessary to say, that the first hash with only lowercase characters as the character set took 9 138 seconds to be cracked using the CPU. From this it is obvious that for calculations such as hash computation the graphic cards are superior to CPUs.

3.2 cudaSIPcracker

The Hashcat provided us the means to calculate the plaintext password from the given hash values. It is one of the best tools for this, but it did not give us the needed pass-

word from the SIP communication. For this purpose, the CUDA SIP Cracker comes to the scene.

This tool can calculate the password from the strings contained in the SIP header as stated in the section 2. However it is not well optimized and in our environment it allowed only one GPU core to be utilized. Therefore the Hashcat was chosen as the main tool for this paper. Still the calculation of the last given hash took almost 7 days, which is of course a high value, however still easily reachable.

4 Conclusion

This paper did not try to come up with the breath-taking new technology; it was rather focused on bringing some enlightenment to VoIP community. In present days many people know about the computational capacity of the massively parallel applications using the CUDA, STREAM or OpenCL technology, but quite few know what the relation between this computational power and the time scale for cracking the passwords is. By this paper we wanted to show that even seemingly strong password can be broken in matter of hours using commonly available software, not mentioning the speed and efficiency of some proprietary solutions. The speeds reached in our experiment could still be increased using AMD graphic cards, which seem to tend to a better performance in this type of calculations. With this in mind the standard digest access authentication in SIP should always be enhanced by other security precautions like SIPS, IPsec, or other when communicating over the insecure network.

Acknowledgement

This contribution was supported by the grant of Ministry of Education, Youth and Sports No. 1974/2012/G1 FRVS (Fund of Development of Czech Universities) and by the project OPVK No. CZ.1.07/2.2.00/28.0062, Joint activities of BUT and TÚO while creating the content of accredited technical courses in ICT.

References

1. Ius Mentis, MD5, [Online], available at: <http://www.iusmentis.com/technology/hashfunctions/md5/>.
2. IETF, RFC1321: The MD5 Message-Digest Algorithm, [Online], available at: <http://tools.ietf.org/html/rfc1321>.
3. Wikipedia, CUDA, [Online], available at: <http://cs.wikipedia.org/wiki/CUDA>.
4. nVidia, Introducing CUDA 5, [Online], available at: http://www.nvidia.com/object/cuda_home_new.html.
5. J. Sanders, E. Kandrot, CUDA by Example: An Introduction to General-Purpose GPU Programming. 1st Edition, Addison-Wesley Professional (2010).

Development and Implementation of IP Telephony Solution on Embedded Platform and Integration of YANG/NETCONF to OpenWRT

Jakub Safarik, Jiri Vychodil, and Pavol Partila

Department of Telecommunications, FEECS,
VŠB – Technical University of Ostrava, 17. listopadu 15, 708 33 Ostrava – Poruba
{jakub.safarik.st1, jiri.vychodil, pavol.partila}@vsb.cz

Abstract. The paper deals with a development of an embedded SIP communication server within the scope of BESIP project (Bright Embedded Solution for IP Telephony). The BESIP project was formally launched in mid-2011 and brings a modular architecture with additional functionality such as speech quality monitoring and security of IP telephony. We come up with an idea of unified configuration of individual components based on NETCONF protocol. In order to be able to implement the idea into OpenWRT, we have developed the complex support NETCONF configuration protocol and YANG as a language used to model configuration and data manipulated by the NETCONF. Our modifications were accepted by OpenWRT community and have been included in OpenWRT/Trunk branch. The BESIP consists of four modules, their features are described in the paper as well as the entire concept.

1 Introduction

BESIP aims to become VoIP PBX system available for anybody, the users need not know complex software features and hidden internals of VoIP software. BESIP offers the prepared solution with integrated key components. The entire system is distributed as an image or individual packages could be installed from SVN and users do not care about dependencies, they just configure VoIP system. Every software solution includes own configuration and management. BESIP aims to be scalable solution with security and unified configuration in mind [1]. After research and project discussion, we made these decisions:

- OpenWRT for good scalability and easy embedding
- Kamailio for reliability and high availability
- Asterisk as PBX factory
- YUMA as NETCONF server
- OpenWRT UCI as configuration backend

Choosing OpenWRT as operating system has a problematic porting of applications into OpenWRT buildroot [2]. On the other hand, BESIP could run on a small device

(32MB RAM, MIPS) or on x86 machine with 1024MB of RAM. Of course, not all modules are supported on all platforms.

2 Platform of BESIP project

Choosing the right software distribution was a crucial step. Because final device is considered as small embedded solution, we cannot modify Debian distribution, which is not suitable for embedding. There are other possibilities like FreeWrt, OpenWrt and DebWrt. After discussion and projects observations, OpenWrt was selected as a primary platform. OpenWrt is well-known for great support, ticket system, relatively well documentation and mail-list server.



Fig. 1. BESIP main page.

We created basic administration page which directs the user to right configuration module. For OpenWrt basics, there is LuCI frontend and Asterisk-GUI for Asterisk [3]. Next to this, there is a link to our application for monitoring of the call quality and the administration page is depicted on Fig. 1.

3 Architecture and technology

The BESIP architecture is depicted in Fig. 2. It is created entirely from open-source parts or software developed by our team right for BESIP. There are four basic modules: Core, Security, Monitoring and PBX. Core is divided into following parts:

- OpenWRT as build platform;
- NETCONF For administration of entire system, YUMA implementation was adopted;
- Web GUI for easier configuration;
- SUBVERSION as revision control system providing a support and better orientation for developers, it is not a part of the released BESIP image.

The security module is based on SNORT, SNORTSam and iptables [7]. In addition to this, the Kamailio ratelimit and pike module is used for defending attacks. The moni-

toring module exploits a tshark package and our java code which interprets its results and gives information about particular speech quality. The Zabbix agent is used to report basic states of the entire system and finally the PBX module is made from kamailio in conjunction with Asterisk.

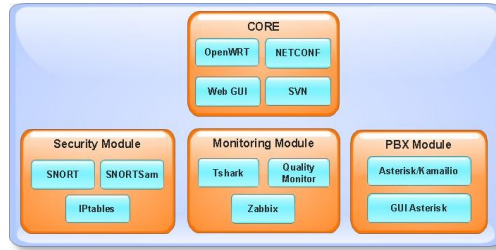


Fig. 2. BESIP architecture.

4 Configuration module

The NETCONF protocol serves as a mechanism for exchanging a configuration data among an administrator and target devices. It relies on sending XML documents via RPC (Remote Procedure Call) paradigm [5]. While requests proceed, client is blocked until it receives a RPC reply from NETCONF server [4]. Whole communication is secured through SSH2 protocol (RPC calls over SSH tunnel).

Internally run NETCONF in YUMA package. YANG module then defines a semantic and syntax of management feature. It provides complex data structures for various requirements of developers. Main reason for using NETCONF is in its universal configuration approach. Many systems today are configurable through different protocols. NETCONF brings us universal configuration of the whole device with no need for developing new configuration mechanisms.

5 PBX

The PBX module is a key part of the BESIP project. It operates as SIP B2BUA or SIP Proxy, depending on configuration. Asterisk is used for call manipulation and PBX functions. Kamailio is used for the proxying SIP requests, the traffic normalization and for the security [11], [12]. There are always two factors when developing VoIP solution, the first one is a high availability and reliability, the second one is an issue of advanced functions. BESIP adapts both solutions for serving different user's requirements. The BESIP offers users an option to choose how system will work. From this reason, the BESIP includes both Kamailio and Asterisk. Today, only one of these engines can be configured, but in the future, both engines will work together and will be configured by common NETCONF server. Kamailio will route requests even if Asterisk will be out of order, only advanced PBX functions will be unavailable in such situation [13], [15].

5.1 Asterisk GUI

Asterisk-GUI is very flexible web solution of Asterisk management. Even if it is not NETCONF based, Asterisk-GUI was added to the first BESIP release. The reason was, that there was not completed interoperability between NETCONF and Asterisk. It is available in the next release and the implementation involved highly complex task.

In the future version we would like to remove the Asterisk-GUI package from BESIP image and the configuration will be accessible only through a newly developed NETCONF based management.

6 Security module

Security module is an important part of BESIP and all the time, it was considered to make the developed system as secure as possible. Next to this, entire system has to be fault-tolerant, monitored and protected from attacks. BESIP solution uses a pre-configured firewall rules and contains IPS (Intrusion Prevention System). This IPS system is based on open-source intrusion detection system Snort in combination with SnortSam. If an attack is detected, a source IP address of the attacker is blocked via firewall rule. Whole system of blocking has built-in auto-recovering mechanism. After 10 minutes could blocked IP address communicate again, but only if attacker stop his malicious actions. Self-recovery serves well in case of false positive attacks.

This is flexible, reliable and effective implementation with no need of human interaction. Dropping attack based on IP directly in the Linux kernel is much more efficient than to check messages on the application level.

Administrators can use Zabbix or NAGIOS agent inside BESIP to gather all information directly into their monitoring system. The monitoring is especially important part of the security module and BESIP team was focused on the issue in early design [14].

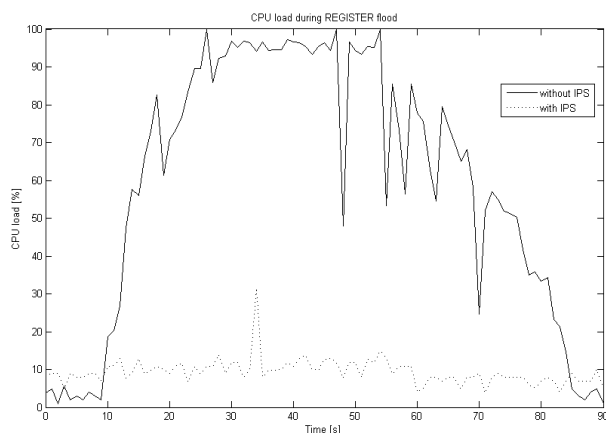


Fig. 3. Attack effectivity based on REGISTER flood. [12]

Partially, BESIP is resistant to some DoS attacks. It depends also on hardware used. If hardware is strong enough to detect some security incidents on application level, the source IP is immediately dropped. For a weak hardware it can be a serious problem. There should be other security mechanisms in the production network, security on BESIP serves as a last line of defense.

The features of our security module were verified in test-bed and result for REGISTER flood attack is depicted in Fig. 3. The CPU load was monitored during trivial SIP attacks. The attack starts at 10s and stops at 60s. Last 30 seconds show recovery of server after attack. Fig. 3. clearly prove the ability of the security module to mitigate the performed attack.

7 Monitoring module

The overall solution of the monitoring system consists of several different open-source components and also of the part that was directly developed for this purpose to meet the defined requirements.

The system itself consists of three logical components – web interface that serves the administrators (Web GUI), part of the script that controls the obtaining the information necessary to calculate the E-model. Last component is part of the Quality Monitor, which contains the logic for calculation itself and performs processing of data obtained by scripts.

Web interface is written entirely using a scripting language PHP, because of the need for starting or stopping the monitoring system through OpenWRT shell, since it depends on shell applications such as tshark. Scripts are launched through the web interface of monitoring tool enabling the monitoring itself. Practically, this means starting network traffic capture with tshark tool where RTP filter is activated. A usage of RTP filter makes the work with RTP streams much easier, because these streams contain some valuable statistical data (packet loss, jitter) and other data (source/destination IP, codec) needed to calculate the E-model.

The collected data is stored in text form and then is started the calculation of quality. After processing, results are saved in SQLite3 database, and text files are erased from disk.

The E-model is based on the “equipment impairment factor” method and was developed by the SG12 group under ITU-T, and it was published in ITU-T recommendation G.107 as the E-model [16].

8 Conclusion

The contribution of our work is entire BESIP concept and its implementation. As we have mentioned, BESIP consists of several components, which are distributed under GPL as an open-source solution. A few of them have been fully adopted such as components in Security and PBX modules, some of them modified, concerning the CORE module and finally we have developed own tool for Speech quality assessment. The contribution of our work is not only several hundred of hours spent on the

development, on the coding BESIP system. We bring a new idea of the unified configuration management, with unified CLI syntax which enables to configure different systems, Asterisk and Kamailio in our case. We perceive that we need to solve a lot of issues. Individual packages are working, and after several pre-releases, the version 1.0 was released in November 2011. BESIP is distributed as a functional image for x86 platform but is possible to run it on VMware or KVM. Configuration is available through web-browser or SSH client. Today, there is a trunk version in SVN, which is actively developed and individual improvements are included in next subversions. After testing, version 2.0 will be released. New release 2.0 will be based entirely on NETCONF with one API to configure entire system. Next to this, CLI syntax will be connected to NETCONF. CLI will be independent of internal software so if some internal software is modified, there will be no change in configuration. Even more, CLI and NETCONF configuration will be independent on hardware and version. To export configuration from one box and to import it to the next one will be an easy task. Users will modify only one configuration file to manage entire box. After this step, all internals of configuration will be hidden as was mentioned in the introduction.

References

1. P. Thermos, A. Takanen, "Securing VoIP Networks: Threats, Vulnerabilities, and Countermeasures", Addison-Wesley Professional; 1 edition, 2007, ISBN-13: 978-0321437341.
2. L. M. Surhone, M. T. Tennoe, "OpenWrt", Betascript Publishing, 2011, ISBN-13: 978-6135271591.
3. J. Loeliger, "Version Control with Git: Powerful Tools and Techniques for Collaborative Software Development", O'Reilly Media; 1 edition, 2009, ISBN-13: 978-0596520120.
4. R. Enns, "NETCONF Configuration Protocol", RFC 474, URL: <http://tools.ietf.org/html/rfc4741>.
5. K. Tomala, J. Rozhon, F. Rezac, J. Vychodil, M. Voznak, J. Zdralek, "Interactive VoiceXML Module into SIP-Based Warning Distribution System", Conference Proceedings MCSS 2011, In SPRINGER Communications in Computer and Information Science 2011, Vol. 149 CCIS, pp. 338-344. ISSN 18650929, ISBN 978-364221511-7.
6. A. Bogus, "Lighttpd", Packt Publishing, 2008, ISBN-13: 978-1847192103.
7. Voznak M., Rezac F., SIP Threats Detection System, Advances in Data Networks, Communications, Computers, pp. 125-130, University of Algarve, Faro, Portugal, November 3-5, 2010, ISBN 978-960-474-245-5, ISSN 1792-6157.
8. Voznak M., Rezac F., Tomala, K. SIP Penetration Test System, In Conference Proceedings TSP 2010, pp. 504-508, August 17th-20th 2010, Baden near Vienna, Austria, ISBN 978-963-88981-0-4.
9. N. C. Zakas, J. McPeak, J. Fawcett, "Professional Ajax", Wrox, 624 p., 2007, ISBN-13: 978-0470109496.
10. D. Flanagan, "JavaScript: The Definitive Guide", O'Reilly Media, 1100 p., 2011, ISBN-13: 978-0596805524.
11. Voznak M., Rezac F., Security Risks in IP Telephony, Networking Studies 2010 Selected Technical Reports, p. 91-100, CESNET, May 2010, ISBN 978-80-904173-8-0
12. Voznak, M., Safarik, J., DoS Attacks Targeting SIP Server and Improvements of Robustness, INTERNATIONAL JOURNAL of MATHEMATICS AND COMPUTERS IN SIMULATION, ISSUE 1, VOLUME 6, 2012, ISSN 1998-0159, pp. 177-184.
13. S. Wintermezer and S. Bosch, "Practical Asterisk 1.4 and 1.6: From Beginner to Expert". Addison-Wesley Professional; 1 edition, 2009, ISBN-13: 978-0321525666.
14. W. Barth, "Nagios: System and Network Monitoring", No Starch Press; Second Edition, 2008, ISBN-13: 978-1593271794.
15. F. E. Goncalves, "Building Telephony Systems with OpenSIPS 1.6", Packt Publishing, 2010, ISBN-13: 978-1849510745.
16. RAAKE, Alexander. *Speech Quality of VoIP: Assessment and Prediction*. New York: Wiley, 2006. ISBN 978-0470030608.

The USRP Devices in LabVIEW

Martin Tomis

Department of Telecommunications, FEECS,
VŠB – Technical University of Ostrava, 17. listopadu 15, 708 33 Ostrava – Poruba
martin.tomis@vsb.cz

Abstract. This article deals with attributes of the USRP devices, solves problems caused by cheap construction and problems with program threading.

1 Introduction

In the market with high-frequency measurement devices, for some time there is device called USRP - Universal Software Radio Peripheral. It is universal software-programmable radio transceiver, controlled by a PC. The device is designed as separated direct-conversion transmitter and receiver. Bandwidth in both directions can be adjusted by changing the sampling frequency of transmitted data in the range of 200 kS/s to 50 MS/s. Sampling rates of A/D and D/A converters in the baseband, however, are significantly higher in the hundreds of MS/s. High sample rate of converters to the lower sampling rate for data transfer and back converts the FPGA processor. Few years ago students simulated real RF signals using software simulators such as Matlab or LabView [1], due to the extremely high cost of RF generators and analyzers, which could be used with LabView for real measurement. On the contrary the USRP device is significantly cheaper, but does not reach such parameters as RFSA, which is modular system PXI measurement plug-in card from National Instruments.

2 Parameters of USRP

USRP devices are being sold by the original developer and manufacturer Ettus Research, and also more recently National Instruments began their production of USRP. Version from National Instruments is redesigned,

as I've been told by their sales engineers. All PCBs from Ettus Research needs to be redesigned because of bugs (further in the article) and to comply with NI quality and precision standards. Version NI USRP-2922 [2] (same as USRP with SBX module from Ettus Research [3]) is not out yet because of redesigning. Ettus Research sells USRP as a case with motherboard [4]. User needs to buy RF modules separately. There are three main series of USRP motherboards differing in control interfaces. There is USB 2.0 version, 1 Gb/s Ethernet version, and standalone version with DSP and ARM processor with Linux. On the contrary, National Instruments sells fixed closed configurations. For both manufacturers frequency range covers part of the range from 0 MHz to 5.9 GHz, depending on the version. Transmitter maximum output power varies from 50 mW to 200 mW.

The most limiting parameter of USRP is a control interface [5]. The data can be transmitted through 1 Gb/s Ethernet interface in several formats. From 8-bit integers of immediate amplitude level, up to 2 * 16-bit floating-point complex I/Q components. The interface is a limiting factor because of the data throughput. (The following information applies to the USRP N-210 with WBX module) USRP has a separate transmitter and receiver part, each has the theoretically up to 50 MS/s sample rate at 8-bit sample or up to 25 MS/s sample rate at 16-bit sample. Both modes are based on 14-bit A/D and 16-bit D/A converters, and those data it is necessary to adjust for transmission through interface to and/or from PC. Both modes are a compromise between higher resolution and greater bandwidth. A compromise could be solved by the compression of data stream in the FPGA processor. From the above mentioned values the required bandwidth of the control interface for maximum sustained transmission bandwidth in real-time can be calculated:

$$\begin{aligned} 25 \text{ MS/s} \cdot 16 \text{ bit} \cdot 2 \text{ complex components} &= 800 \text{ Mb/s} \\ 50 \text{ MS/s} \cdot 8 \text{ bit} \cdot 2 \text{ complex components} &= 800 \text{ Mb/s} \end{aligned}$$

Calculated theoretical maximum throughput is required in both directions. This throughput with the significant assistance of data transfer is necessary in both directions between PC and USRP. For the calculated throughput it would be appropriate to use interface with at least 2 Gb/s of throughput in both directions. The consequence of 1 Gb/s limit of Ethernet is the limit of maximum sampling rate in real-time, which varies from 8 to 17 MS/s

at 16-bit resolution in one direction only mode. The value cannot be accurately determined, as the drivers and the FPGA image are still unstable and in development. Limit of the maximum transferred bandwidth decreases with the performance of controlling computer. Mentioned real-time throughput of 17 MS/s, followed by simple processing was achieved on the water-cooled high-end computer, overclocked to 5 GHz. Much more complex data processing can be achieved with the same bandwidth, but application must use other cores of CPU - multithreaded application. The actual data transfer runs on one processor core, as the most demanding process of the measurement program, and the processor must be powerful enough and have enough computing time to switch between threads. At the time of interrupt for next data transfer, processor must respond immediately. If the processor is unable to respond or fails to transfer so wide bandwidth, further adjustment or division of program will not help. Therefore the sampling rate for continuous reception and simple processing on the new standard PC or laptop decreases to 12 - 4 MS/s.

For immediate response of PC the application needs to be separated into threads. Threaded program with shift registers achieves considerably higher data throughput than serial-oriented program. Easiest way to separate application into multiple threads is to use shift registers in one loop. This way the application is time-linear, but all threads must be less time demanding than the data transferring thread. Time delay between input and output is recording time multiplied by number of shift registers, and it is constant.

The best performing solution is to divide application into short loops by First In First Out memory buffers. Serial-oriented program is divided into several independent loops which are interconnected by several buffers. More demanding programs must be composed of at least three loops. Each loop solves part of the measurement. The first loop, which performs data transfer, must not contain any further calculations. Despite the fact that application divided by FIFO buffers is best performing, and manages to analyze the largest bandwidth, its disadvantage is a variable delay between the input and output due to fluctuations in the buffer. If there is a buffer overflow, it is necessary to discard some blocks from the buffer. In this case the measurement is not continuous.

When attempting to capture a wider bandwidth than the bandwidth transferable by control interface and processable by PC, it is necessary to insert time gaps between records for data transfer, otherwise hardware buffer of USRP overflows. In this case, although it is not a continuous transmission, even a standard computer can process the maximum bandwidth (50 MS/s) with a sufficiently long time gap for data transfer and processing. Due to limited size of hardware buffer, with the maximum bandwidth it is impossible to transfer more than cca 400 kS continuously. The actual value varies due to instability of the drivers and USRP firmware.

There are many applications where it is possible to use the device. USRP device with a sufficiently powerful computer can replace almost any radio equipment not exceeding the maximum allowed bandwidth of USRP device. Eg.: GPS receiver or transmitter, mobile phone, mobile phone base station (project OpenBTS), remote controls, RF data links, radar, amateur radio transceiver, broadcast radio / television, capturing RF data transmission, aircraft position data, etc. Some applications, such as car remote control code capture to unlock the vehicle, may be illegal.

3 Problems of cheaper construction

USRP device was designed as a cheaper substitute of RF vector signal analyzers and generators. To reduce the cost of production, several rules for the production of high-frequency devices have been violated. USRP is shielded only by the outer cover of the device and the ground in the printed circuit boards, uses cheaper parts, and uses method of direct mixing. These weaknesses and several others are the cause of some problems. In the preset with separate transmitter and receiver, the signal from transmitter section enters a receiver section with attenuation of only few decibels. For full duplex operation it is necessary to use sufficiently distant frequency channels. Input sensitivity of receiver section is very low. Setting the receiver preamplifier to a different level than the maximum level is useless for the most of omnidirectional antennas. (NI devices are redesigned with significantly higher sensitivity.) Because of the direct mixing the oscillator frequency is reflected in receiver antenna and returned to the mixer, after which the frequency is measured as a DC component in the baseband. For the most of digital modulations, this phenomenon

does not matter, but the frequency spectrum shows a significant DC component. In the frequency spectrum of the device itself without the antenna, there are several other peaks, probably caused by internal oscillators of the device. Internal interference peaks are found on all multiples of 100 MHz frequency and a few others.

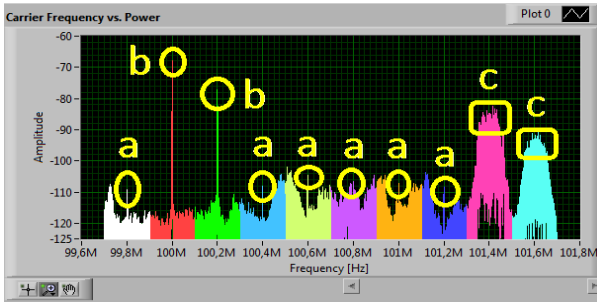


Fig. 1. Problems in the frequency spectrum

Using LabVIEW, the FFT frequency spectrum was measured ten times with step of 200 kHz. Individual measurements are drawn in different colors. Antenna was used with a preamplifier. Peaks are marked in the picture:

- a) Interfering DC component produced by the direct mixing method. When using the antenna without preamplifier, the useful signals around the DC component decreases as much as 20 dB, but the amplitude of the DC component is almost unchanged.
- b) Multiples of the internal oscillators are also undesirable.
- c) Useful signals of the nearby radio stations.

Even if the antenna with preamplifier is used, the unwanted DC components affect the frequency spectrum, and multiples of internal oscillators also have large amplitude. In NI devices those problems are partially reduced by redesigning. Identified serious problems of Ettus Research USRP devices were eliminated as follows.

Known multiples of the internal oscillator frequencies were removed programmatically. The entire widths of the peaks of a known internal oscillator's frequency multiples in the spectrum were replaced by a constant level of the nearest spectral lines. The method is inaccurate, but worse results than false spectral lines with large amplitude should not be achieved.

DC components in the spectra were mathematically eliminated by averaging spectrum with shifting frequency axis of spectrum. Each frequency sub-spectrum of the total measured spectrum is measured several times and averaged. This way a wideband frequency spectrum of any width in the frequency range of USRP is created, with many unwanted DC components a) as in the Fig.1. By repeating the measurement several times with a steady shift of the center frequency of sub spectra by the fraction of the width of the sub spectrum, and then properly shifted averaging, DC components are spread between averaged spectra and then reduced by shifted averaging. This way the wideband frequency spectrum accuracy is improved.

4 Conclusion

USRP is a powerful, much cheaper device for measurement of current high-frequency radio systems, but also for designing and testing new systems. For practical familiarization of students with high frequency radio signals, the device with its price may be included among the commonly used measuring instruments in lessons. The lower price, however, correspond with slightly worse parameters.

References

1. ŽÍDEK, J., Grafické programování ve vývojovém prostředí LabVIEW (výuková skripta). Ostrava : VŠB-TU Ostrava, 2006.
2. National Instruments. USRP 2920 Specifications [online]. < <http://www.ni.com/pdf/manuals/375839a.pdf> >
3. Ettus Research. Transceiver Daughterboards [online]. < <https://www.ettus.com/product/details/SBX> >
4. Ettus Research. USRP Networked Series [online]. < <https://www.ettus.com/product/details/UN210-KIT> >
5. National Instruments. USRP Help [online]. < <http://zone.ni.com/reference/en-XX/help/373380B-01/> >

The Radiation Pattern Shaping of Power LED Diode

Jan Vitásek, Stanislav Hejduk, Artem Ganiyev, Jan Látal, and Jiří Bocheza

Department of Telecommunications, FEECS,
VŠB – Technical University of Ostrava, 17. listopadu 15, 708 33 Ostrava – Poruba
{jan.vitasek, stanislav.hejduk, artem.ganiyev.st,
jan.latal, jiri.bocheza}@vsb.cz

Abstract. This article deals with a development of future fiberless data transmitters. These transmitters would provide room lighting and information transmitting at the same time. These transmitters will be based on using white power LED diodes. The radiation of these diodes has to be shaped for achievement of maximal possible efficiency. In this article there is described the shaping of power LED by parabolic reflector. The shaped radiation pattern was measured by power meter and it was simulated in software LightTools. The obtained results are compared each other.

1 Introduction

Free space optics (FSO) links represent progressive and fast developing field of telecommunications. These FSO links are able to replace current wireless technologies which are reaching a peak of their possibilities. FSO links are useful for data transmission between places, where it is very difficult to build optical fiber connection, e.g. natural obstacles. The next field of application of these transmitters is in building interior, where they gradually replace WiFi technology. On the ceiling of room it will be placed a transmitter which will provide data to all users indoor. The advantage is that the data can't penetrate into adjacent room. Further, the FSO links are usable for communication between cars in traffic, the cars will exchange important data. The one of directions of FSO communications is direction based on using a visible spectrum of optical radiation, Visible Light Communications (VLC). The development of this field is enabled by progress in production of white power LED diodes. White power LED diodes are divided into two types. The first type uses blue emitted chip (450 nm) whereon it is deposited a layer of yellow luminophore YAG (Yttrium, Aluminium, Garnet). The other type uses a triplet of chips RGB (red, green, blue) which make together a white light [1]. The first research results in this field summarize IEEE 802.15.7 norm effective from December 2011 [2]. For maximal usage of power LED diode it is necessary to shape their radiation pattern whereto serves collimators.

1.1 Power LED Diode LUXEON Star

The transmitter for indoor will include white power LED diode. It was chosen type Luxeon 5W Star marked LXHL-LW6C. This diode is typically supplied by voltage 6,84V, thereof it comes up color temperature 5500K, optical power 120lm, viewing angle 120° [3]. This power LED diode was mounted on cooler due to great heating. The measured spectrum of white power LED diode is on Fig. 1.

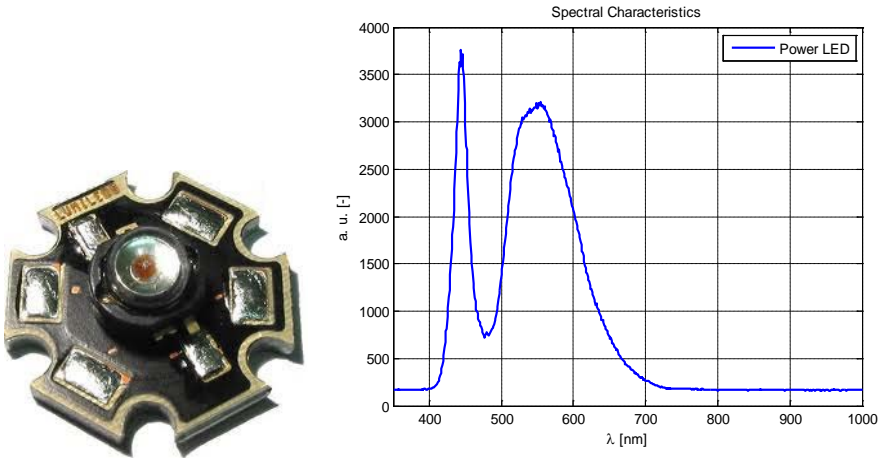


Fig. 1. White power LED diode Luxeon 5W Star LXHL-LW6C and its spectral characteristic

1.2 Reflector CLP20CR

To the power LED diode it was set parabolic reflector purchased from seller Roithner LaserTechnik GmbH [4]. It is 6° reflector for Lambertian power LED diodes with aluminium reflective coating with protective clear-coat. The seller couldn't tell us other data about this reflector, therefore it had to be calculated. The aim was to obtain the equation of a parabola, which shapes the reflector.

From real reflector it was measured three proportions, input diameter $a_1 = 6$ mm, output diameter $a_2 = 20$ mm and the height of reflector $y_1 = 15,1$ mm. The draft in on Fig. 2.

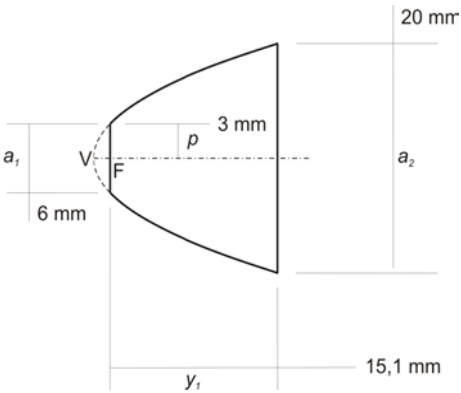


Fig. 2. The draft of parabolic reflector

It results from the geometry of parabola if the input aperture goes to focus, than the parameter of a parabola p equals to a half of input diameter a_1 . Due to knowledge of parameter of a parabola it was set the equation of a parabola which forms the parabolic reflector. The general equation of a parabola is $y^2 = 2p \cdot x$, where p is parameter of a parabola. The final result is $y^2 = 6x$.

2 Measurement

2.1 Linear travels

Measurement of optical power distribution was realized by two linear travels NRT150/M by Thorlabs company [5], which enable moving in horizontal and vertical direction. The maximal shift in one direction is 150mm. These travels were controlled by software supplied by manufacturer. In this software it was set a step distance 1cm.

2.2 Power meter

For optical power measurement it was used power meter PM100 with photodetector S120B, both by Thorlabs Company. The wavelength range of sensor is 400-1100 nm. To the power meter it is set wavelength correction, which tell power meter, which wavelength of light is measured. This caused the first problem, because white power LED diode is wide-spectrum source and hence it isn't possible to choose dominant wavelength. It was done several measurements for different wavelengths. The greatest values of power were measured for wavelength correction 400 nm even if according Fig. 1 white power LED diode emits minimal power at wavelength 400 nm. This error is caused due to the fact that the power meter considers the all incident light as light

with wavelength 400 nm and according calibration curve it adjusts measured values. By shaping of radiation pattern the absolute values are not important, relative values are sufficient. The measured values were divided by maximal value and thereby we obtained radiation pattern. We calculated relative values of power measured at different wavelengths and we obtained the same shapes of radiation pattern.

2.3 Measuring application

The power meter PM100 can be connected with computer via serial port RS232. This possibility was used for easier and more effective measurement. In Matlab it was written an application, which enables save values of optical power in text file. In this application the user chooses communication port COM, whereto is connected the power meter, sets wavelength correction and initializes the connection. If the user presses button Save Value the application save actual value into text file. Separated power values are saved inline.

2.4 Realization of measurement

The measurement run in semiautomatic mode. The linear travels were controlled by software supplied by manufacturer. If the appropriate button was pressed the linear travels moved 1 cm in required direction. At first, the linear travels moved to starting position. Then it was saved the first value by press button in measuring application. After that, the linear travel moved 1 cm in horizontal direction a then it was again pressed button for saved value. Thereby semiautomatic procedure it was measured a grid 10x10 cm with 121 points. Photodetector S120B has circular aperture with diameter 9,5 mm. The distance between active area of photodetector and chip of power LED diode was 114 mm.

2.5 Simulation of power LED diode with reflector in LightTools

In software LightTools it was created a reflector with parameters, which was calculated in chapter 1.2. This reflector was set to power LED diode. The power LED diode was chosen from LED library, which is included in LightTools. The parameters of this diode are identical to parameters written in datasheet of real power LED diode LXHL-LW6C [3]. The measuring plane was placed in distance 114 mm like in real measurement. On Fig. 3 is the whole configuration of simulation with reflector, power LED diode and measuring plane.

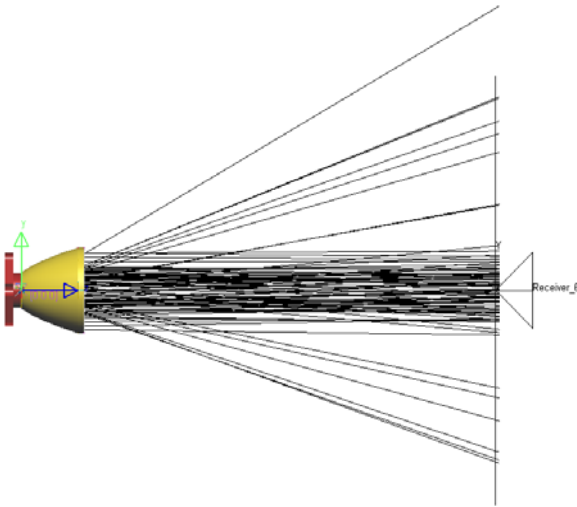


Fig. 3. Simulation in LightTools

3 Results

Measuring application saved the power value inline. In Matlab it was created square matrix from this line. The square matrix comes up to measured grid. Matlab drew 3D figures.

Simulation in software LightTools calculated optical power distribution. The data was exported into text file and loaded by Matlab so that measured and simulated results could be compared.

3.1 Measured results

The reflector CLP20CR was set to power LED diode LXHL-LW6C. The diode was supplied by voltage 6,84 V. The wavelength correction of power meter was set at wavelength 450 nm. By the help of measuring application measured values were saved. Finally, the saved values were load in Matlab which drew 3D figure of relative optical power distribution, Fig. 4.

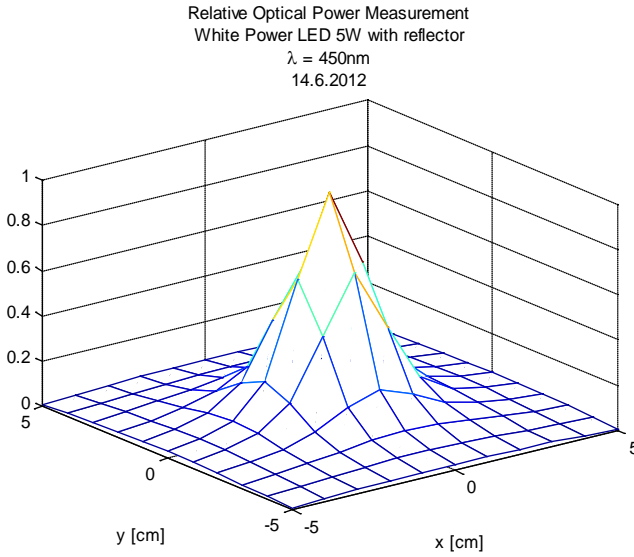


Fig. 4. Relative optical power distribution

By the help of command `contourf` it was created other type of figure displayed relative optical power distribution.

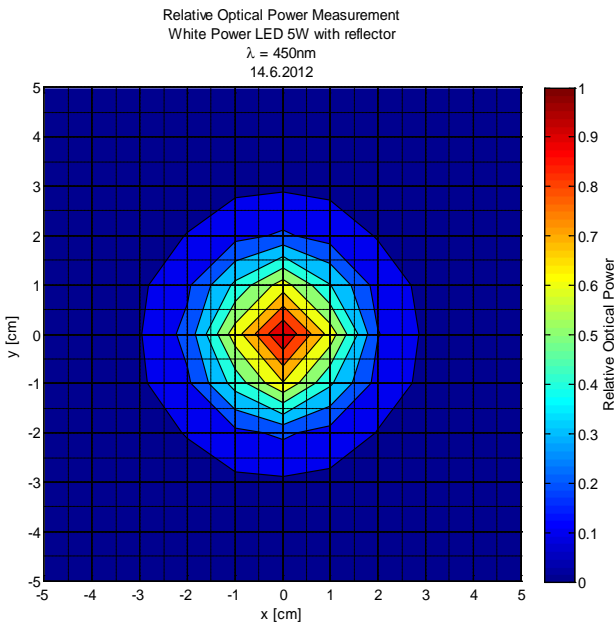


Fig. 5. Relative optical power distribution

3.2 Simulated results

Software LightTools offers several types of figures, which it can calculate. It was chosen 3D and 2D figure of optical power distribution.

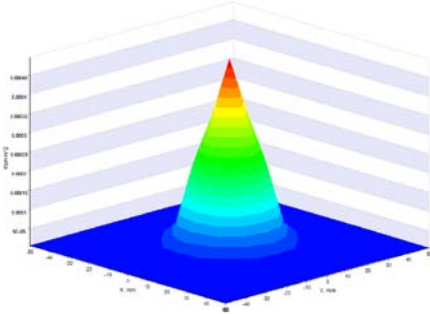


Fig. 6. Simulation of optical power distribution

3.3 Comparison of results

The simulated values of optical power distribution were exported into text file for loading in Matlab therefore the results are comparable. The next figure compares measured and calculated results. It is figures of relative optical power distribution in cross-section, Fig. 7.

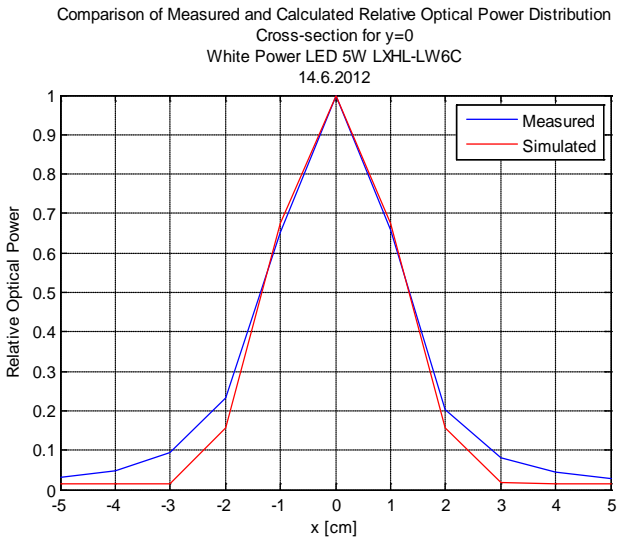


Fig. 7. Comparison of measured and simulated optical power distribution

4 Conclusion

This article deals with shaping of radiation pattern of white power LED diode by help of parabolic reflector. To the measurement it was needed to create measurement application written in Matlab so that the measurement of optical power distribution was considerably simplified. Next it was set the equation of a parabola according which was made a parabolic reflector. These data are necessary for reflector modelling in software LightTools. Thereby it could be created a simulation of real measurement. Thanks to data export from LightTools it was able to load these data in Matlab and compare real and measured data. From the last figure it is obviously that the difference between measurement and simulation is insignificant. The curves begin diverge in distance 2cm from the middle, when it is only 20% of optical power.

Acknowledgement

This article was created with the active support of projects SP2012/160 and SP2012/165.

References

- [1] Schubert, E. Fred. Light-emitting diodes. 2nd ed. New York: Cambridge University Press, 2006. ISBN 05-218-6538-7.
- [2] IEEE 802.15.7. Short-Range Wireless Optical Communication Using Visible Light. New York, USA: IEEE Computer Society, 2011.
- [3] LUXEON. *Luxeon 5W Star: Technical Data DS30*. 2012. Available at: http://www.roithner-laser.com/datasheets/led_single/hexagonal/lxhl_5w.pdf.
- [4] ROITHNER. *CLP series Reflectors for Lambertian*. 2012. Available at: http://www.roithner-laser.com/datasheets/led_optics/CLP17_20CR.pdf.
- [5] NRT150/M - 150 mm Travel. THORLABS. *Thorlabs* [online]. 2012. Available at: <http://thorlabs.com/thorProduct.cfm?partNumber=NRT150/M>.

High-resolution Images Reconstruction Based on the Standard Thermograms

Mirosław Lasar

Opole University of Technology,
Faculty of Electrical Engineering, Automatic Control and Computer Science,
Institute of Power Plants and Measuring Systems,
ul. Prószkowska 76, 45-758 Opole, Poland
mirek.lasar@gmail.com

Abstract. This paper presents a method to obtain high-resolution thermal image sequences using thermograms shifted pixels. The article describes the methodology for obtaining thermograms. The described apparatus has been used and has been built to obtain the position of thermograms. We presented the results obtained using the method used.

1 Introduction

In recent years we can observe an increasing interest in the problem of obtaining images with high resolution (High Resolution - HR) from images of lower resolution (Low Resolution - LR). Getting High Resolution images has technological and financial aspects. Of particular importance for obtaining HR images occurs in the infrared, where technological progress in obtaining the FPA matrix has already reached its capacity. Currently the market offers thermal imaging cameras have a maximum resolution of up to 1 megapixel. One of the companies offer camera with 1.3 megapixel sensor. Such high resolution obtained with a matrix with a resolution of 320×240 pixels installed on positioner. All lenses introduce geometric distortions in the form of radial distortion - more or less. These distortions are particularly visible in the wide-angle lens. They can also be seen on the standard lens. They are revealed through distortion, visible especially in the most remote from the axis of the optical sections (Fig. 1). For the correction was used the polynomial method, and the results are presented in [1].

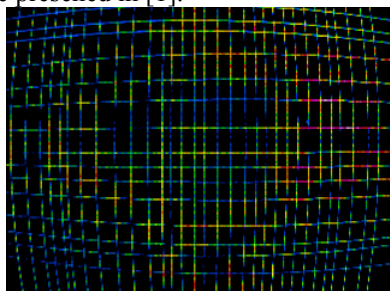


Fig. 1. Wide-angle lens distortion thermogram 320x240 pixels resolution

2 Reconstruction of the HR thermograms

There are a few methods for receiving the HR image. The most popular techniques include the transformation in the frequency domain. These methods use the following transformations [2]:

- Moving the Fourier transform,
- Aliasing, the relationship between discrete and continuous Fourier transform,
- Limitations of the original band image.

Using the above transformations is possible to formulate equations that combine discrete Fourier transform coefficients of low-resolution images of the continuous Fourier transform of the unknown high resolution image, which can be written using the vector equation (1)

$$Y = \Phi X \quad (1)$$

where:

Y - discrete Fourier transform column vector

X - samples of the continuous Fourier transform

Φ - the relationship between a set of LR images and HR images.

HR image reconstruction requires the identification the Φ and solution of the problem (1). One method of solution is to use a recursive least squares method [3]. In the second group of methods images reconstruction for high-resolution it using the transformation in space. One method is iterative back projection [4]. The idea of this method are presented in Figure 2.

This method requires to describing the mathematical model transformation of HR image (in the transmitter FPA) marked function $f(x,y)$ and set out in the field of $S = \{(x,y) \in \mathbf{R}^2, 0 \leq x \leq K\Delta x, 0 \leq y \leq L\Delta y\}$ to the LR image labeled of function $g(m,n)$ in the field $S = \{(m,n) \in M \times N, 1 \leq m \leq M, 1 \leq n \leq N\}$. Having i -images we create a system $i \times M \times N$ equation (2).

$$g_k(m,n) = \sigma_k(h(f(x,y)) + \eta_k(x,y)) \quad (2)$$

It occurs in the blur operator h and non-linear function σ_k , which represents the processes of quantization and decimation of the image in pixels and includes moving sequence of images. During the process of acquisition image with natural noise and interference represented by the function $\eta(x,y)$. The realization of the blur, as a consequence of sampling, is a source of additional information for the HR image reconstruction.

The number of the establishment of equations resulting from the implementation of the transformation (2) of the transducer sequence of images uniformly shifted in the directions X and Y is less than the number of occurring variables. Resetting the missing data in Figure 2 as the value of $f_{0,i}$ and $f_{i,0}$. Solving this system of equations is an iterative method by determining the minimum feature set by equation (3), where g_k are the original images obtained from the camera, and $g_k^{(n)}$ is another simulation outputs the image pickup operation in subsequent iterations the playback HR.

$$e^n = \sqrt{\sum_k \sum_{(m,n)} (g_k(m,n) - g_k^{(n)}(m,n))^2} \tag{3}$$

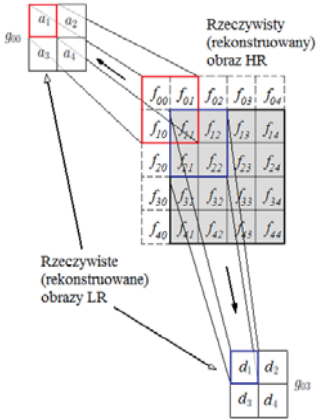


Fig. 2. The transformation of the real and the reconstructed HR images to LR images

Missing data were supplemented by various methods [5]. It is assumed that outside the analyzed area of the function f is periodic, symmetric or zero. Creating a HR image from the LR sequence is shown in Figure 3.

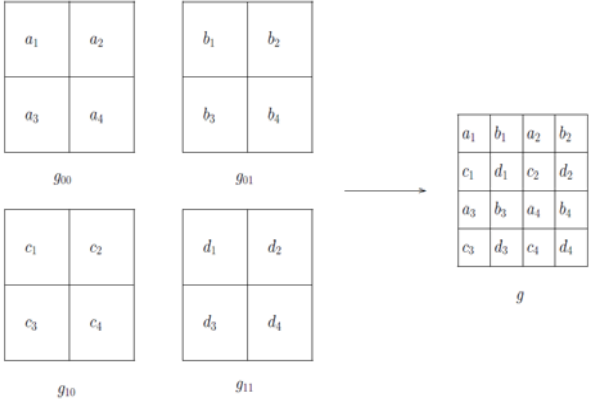


Fig. 3. Construction of the observed high-resolution image

To get a better picture of the observation matrix g averaging effect should be considered in each pixel, which for the transducers in the FPA can be described by equation (4).

$$g(m,n) = \frac{1}{\Delta x \Delta y} \int_{x-\Delta x}^x \int_{y-\Delta y}^y f(x,y) dx dy + \eta(m,n) \tag{4}$$

A / D Converter of FPA matrix infrared camera corresponds to the 14 bit transmitter, thus in equation (4) is not modeled quantization, because the resolution of the camera (0.08 K) is much smaller than the smallest possible to obtain the

uncertainty of temperature measurement (2 K). Zakładając funkcję h realizowaną przez przetwornik, sprawdza się jakość rekonstrukcji porównując oryginalny obraz wysokiej rozdzielczości z obrazem zrekonstruowanym, przy użyciu wskaźnika błędu PSNR oceniającego efektywność rekonstrukcji obrazu. Assuming the function h implemented by the transmitter, verifies the quality of the reconstruction of the original image by comparing the high resolution of the image reconstructed using the PSNR error rate performance evaluation of image reconstruction. The used methods are computationally complex and time needed to obtain satisfactory effects are relatively long [5].

$$\begin{aligned} f_{11} &= 4a_1 - f_{00} + f_{01} + f_{10} \\ f_{12} &= 4b_1 - f_{01} + f_{02} + f_{11} \\ f_{21} &= 4c_1 - f_{10} + f_{20} + f_{11} \\ f_{22} &= 4d_1 - f_{11} + f_{12} + f_{21} \end{aligned} \quad (5)$$

Proceeding similarly, continuing the calculations for successive columns and rows can be determined reconstructed all the missing values of the matrix f . Requires a computational effort $J^2 \times M \times N$ activities described one of the equations (5). If we assume zero value f_{0i} and f_{i0} is the solution to obtain an iterative method.

3. Apparatus and measurement system application

Measuring equipment consisted of a thermal imaging camera VarioCAM Head with a resolution of matrix 320×240 pixels characterized by a sensitivity of 0.08 K. The uncertainty of the measurements is 2 K at a measurement range from -40° C to 120° C. The camera can operate in temperatures between -15° C to 50° C and is equipped with three lenses:

- Standard (focal length $f = 25$ mm, angle $32^\circ \times 25^\circ$),
- Wide angle (focal length $f = 12.5$ mm, viewing angle $64^\circ \times 50^\circ$),
- Telephoto (focal length $f = 100$ mm, viewing angle of $8^\circ \times 6^\circ$).

P70530 stepper motor controllers and modules NI9512 allow to obtain resolution of 51 200 steps per revolution step motor with 1.8° .

With such precision devices it was possible to rotate the camera with an angular resolution of 0.35 seconds, with an angular resolution of a single pixel camera of 6 minutes of arc. Another precision device used in the draft was sliding platform NRT100 100mm long and a resolution of 2 microns. The platform allowed the shift of the camera lens focal length to the axis of rotation of the motor. Figure 4 shows a picture turntable NR360S placed on a NRT100 sliding platform. The combination of two turntables allows you to turn the camera on two axes.



Fig. 4. Rotation stage NR360S on linear stage NRT100 - Thorlabs Company

Turntables and a motor control system was used a linear feed real time system cRIO 9022 with software written in LabVIEW 2009. Figure 5 shows a portion of the application that shows the control panel one of the axes of stepper motor, which is determined the size of a single step.

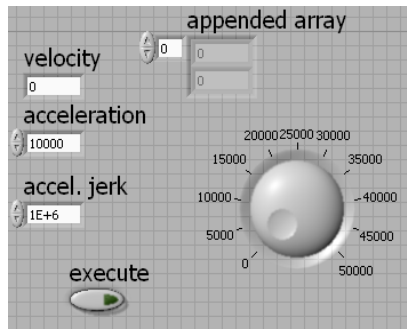
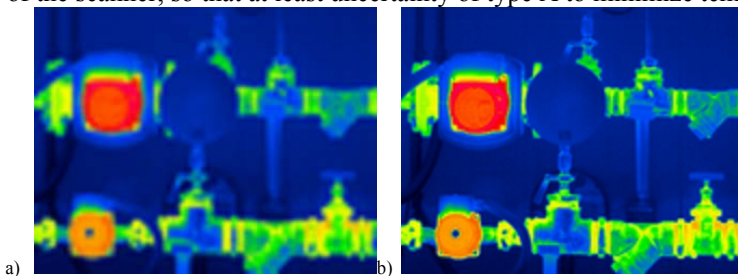


Fig. 5. Dialog box for stepper motor control

4. The results

Figure 6a shows one of the four low-resolution thermal images made with the infrared camera lens $32^\circ \times 25^\circ$. Figure 6b shows the result of HR image reconstruction, while Figure 6c shows the HR thermogram obtained from the assembly 4 thermograms made camera with lens $8^\circ \times 6^\circ$ by the method described in [1]. In the proposed method, it is advisable to use the thermograms averaged for each position of the scanner, so that at least uncertainty of type A to minimize temperature.



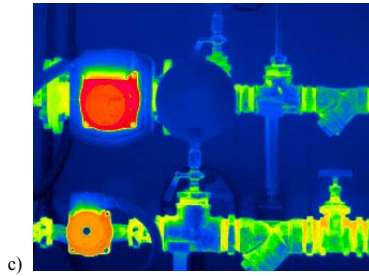


Fig. 6. The results obtained a) one of the 4 thermogram LR b) reconstructed thermogram HR c) original thermogram HR

5. Summary

The proposed method of high-resolution image reconstruction from low-resolution images requires precise motor for J^2 sequences of images uniformly shifted in X and Y with known angle corresponding to $1 / J$ pixel in each direction. The system is dedicated to transducers FPA infrared cameras, which can be inserted into a test scene object with known temperature, geometry and position relative to the camera. The obtained thermograms do not have as good resolution as with the turntable and a telephoto lens, but they are clearly better than the thermogram of the basic resolution of the camera.

Bibliography

- [1] Zator S., Lasar M.: Uzyskiwanie termogramów wysokiej rozdzielczości, PAK 2011 nr 12, s. 1480-1482
- [2] Park S.C., Park M.K., Kang M.G.: Super-Resolution Image Reconstruction, IDE Signal Processing Magazine, vol.20, 2003, s. 21-36
- [3] Bose N.K., Kim H.C., Velenzuela H.M.: Recursive implementation of total least squares algorithm for image reconstruction from noisy, undersampled multi-frames, IEEE Conference Acoustic, Speech and Signal Processing, Mineapolis 1993
- [4] Irani M., Peleg S.: Improving Resolution by Image Registration, Graphical Models and Image Processin, Vol. 53, 1991, s. 231-239
- [5] Chan R.H., Chan T.F., Shen L., Shen Z.: Wavelet algorithms for high-resolution image reconstruction, J. Sci. Comp. Vol 24, No 4, pp. 1408-1432



Photo and Thermal Image as an Additional Information for the Point Cloud Data

Paweł Michalski

Opole University of Technology,
Faculty of Electrical Engineering, Automatic Control and Computer Science,
Institute of Power Plants and Measurement Systems,
ul. Prószkowska 76, 45-758 Opole, Poland
p.michalski@doktorant.po.opole.pl

Abstract. The article presents the possibility of integration of different measurement techniques to obtain information about the surface of the object. In the first section measurement equipment used during the measurement are presented. In the second chapter the measurement methodology is described. Next the sample results obtained during implementation are presented and the process of preparing the data and their subsequent integration are shown.

1 Introduction

Integration of different measurement techniques generates a new quality. This article presents the integration of different data acquisition techniques such as laser scanning, photo documentation and thermography. These techniques are intended to reproduce the shape of the object with a maximum available precision. The shape of the object is one of the basic features used in the construction of the model used in numerical calculations [3]. Currently scanning technique allows precise reconstruction of surface geometry to the nearest tenth of a millimeter. So the exact reconstruction of the surface captures elements such as splice site or deformation caused by mechanical or thermal treatment of the object. The exact reproduction of the shape is usually not enough to build a digital model of the object. It is necessary to frequently integrate different measurement techniques, such as creating compact measuring systems that generate multi-level description of the test object. A good example is the registration data in the form of images, not only in the visible, but also in the infrared and ultraviolet, which often provide valuable information about boundary conditions of the object. While the integration of information about the changes occurring on the surface of the thermal facility with spatial data from laser scanning can serve as a spatial model diagnostics [1]. The information about the color at a given point can also serve as a simple filter to select specific points of the point cloud.

2 Measurement devices

For the geometry measurement Trimble FX laser scanner was used (Fig. 1). Measurements performed within the scanner are performed by the phase shift. The device has a large field of view, which is $360^{\circ} \times 270^{\circ}$ (this parameter allows the operator to do the surround scan).

Maximum measurement range is 70 m scanner for single scanning and 140 m for the double scan. Scanner space coordinates apart also provides information on the energy reflected radiation, which depends among others from the reflectance of the surface. At time 1 seconds, the device performs an average of 216 000 measurements of distance. The surround scan, which takes about 5 minutes generates a very large amount of data for analysis. The scanner is very accurate, for example, for an object 11 meters away, offers a distance measurement uncertainty of 0.6 mm for a single scan and 0.45 mm for the double scan. Ambient temperature operating range from the device (5-45) °C. The scanner is presented on figure 1.



Figure 1. Trimble FX laser scanner



Figure 2. VarioCam infrared camera

Temperature measurement was made using Head VarioCam infrared camera with a resolution of 320×240 matrix of pixels. The IR camera is presented on figure 2. The standard lens can capture all the examined objects, usually from a large distance from the object which reduces the precision of the measurements. Resolution used to measure lens allows for a 16-fold increase in resolution, but at the expense of the small field of view ($6^{\circ} \times 8^{\circ}$).

There is a need to produce thermal images of large objects with high resolution [2] brought forth the idea of using a thermal imaging camera with a telephoto lens placed on the turntable biaxial. The control system consists of two precision stepper motors NR360SP9 / M, which were controlled by a controller CompactRIO Real-Time Controller with modules NI 9512 and 9022, and P70530.

To carry out photographic documentation digital SLR Canon EOS 30D with a standard lens was used. The camera was also placed on the turntable.

3 Methodology

Base element is to carry out a measurement, a few sessions with laser scan measurement from various locations to get the maximum amount of information about the geometry of the object. There is the possibility of varying the density of points in selected areas of the scanned scene. This feature allows you to precisely reproduce the essential elements of the facility and keep the less important elements such as the geometry of the room in which the test object. An important advantage of this function is that different densities can occur in a single scan which excludes the appearance of errors in matching several independent scans of each other. The process of registering scans from different positions were performed using spheres that are indicative of the examined object. Registration is done on the basis of calculating the distance to the sphere and determining the position of the scanner. In each of the scans, the operator is obliged to indicate the scan, which will serve as a reference scan for all the others. For each measurement session performed a series of photographs from camera mounted on a precision biaxial turntable. This approach allows the operator to create panoramic photos for each measurement session. Then the motor is mounted infrared camera and a measuring cycle is repeated. It is extremely important to both sessions performed with a digital camera and thermal imaging camera were made from the same point where previously was the laser scanner. This approach enables you to capture the same area on both the scan and raster graphics, raster graphics also are oriented to scan by identifying sections or characteristic points on both the scan and raster graphics [4]. The bitmap and the point clouds integration process has to be performed manually by the process operator.

The broadcast chromatics points based on raster maps (image, thermograms) requires a statement of the same control points in scan and the map and determine the optical parameters of the camera (focal length, viewing angles, resolution, et al Correction) [5]. On the basis of their orientation is fixed relative to the map object and the camera. In the software example RealWorks is satisfactory when used at least 10 points will be binding. The conception of broadcasting bitmap pixels to the point cloud points is presented on Figure 3.

For a full analysis of the behavior of the plant used:

- 3D object models,
- verification of the measuring techniques evolving topology of the technical infrastructure,
- data acquisition systems and monitoring the results of working in real time.

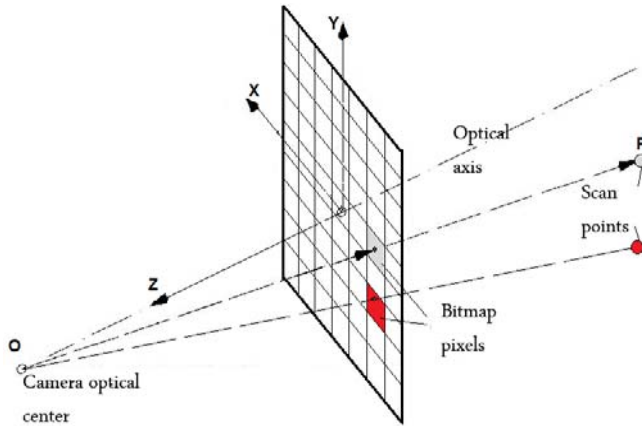


Figure 3. The idea of broadcasting chromatic points

In Figure 4 can be seen a point cloud with the mapped thermography image. Figure 5 shows the thermogram mapped on a triangular mesh created on the basis of the point cloud seen in Figure 4. The 2D image mapping process is performed independently for each of the stations even before they are registered in one scan of the output. A single station does not keep a complete picture of the 3D depth map and only known in the literature as an image of $2\frac{1}{2}$ D.

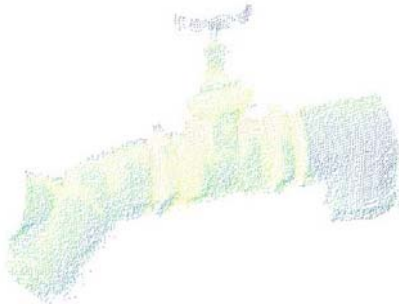


Figure 4. Sample point cloud with imposed thermogram

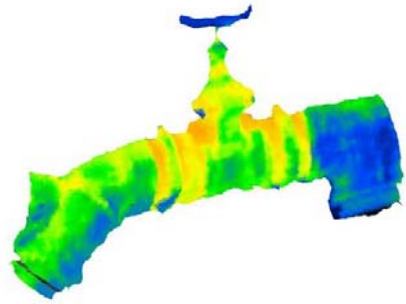


Figure 5. Sample triangle mesh model with imposed thermogram

Both the thermal and photographic documentation obtained during the measurement can be used as filters for point cloud. Points to the added thermal information in most cases, you can quickly filter out the points which are in the background. This is because the temperature of such objects in the thermograms is not correct until you take the temperature correction. If the point is not aware of the thermal information it could be filter out from the background, this is a semiautomatic welding process, which is based on segmented point groups according to the given criterion.

Using this method, performed a series of projects designed to demonstrate its strengths and weaknesses. One of the projects was the reconstruction of the lattice support structure pole Z52 series. Scanning was performed from 6 different positions to give a point cloud containing about 1 million points. Because of the large dimen-

sions of the test object and a simple design, which allows for a precise indication of the characteristic points necessary for the mapping, it was decided to perform digital and infrared images at a distance, to partially compensate for lens distortion.

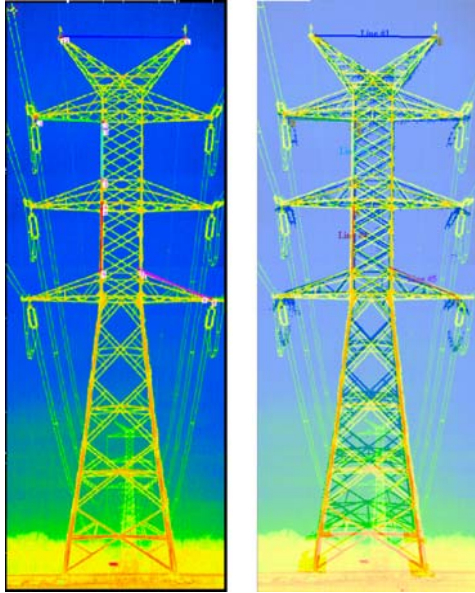


Figure 6. Thermogram of the column (left), the pole model with imposed thermogram (right)

The thermograms on Figure 6 are created by merging Moreover, the resulting thermogram lattice structure shown on Figure. 6 can be used as a filter for the point clouds located on the pole in relation to those outside it.

4 Summary

The combination of laser scanning with the measurements of thermal imagers and digital images allow for quick determination of geometric distortion due to wear or deformation of materials and their association with changes such as temperature.

Analysis of the resulting model allows to determine critical points where there may be deformation, deformation leading to failure. 3D model of the imposed temperature distribution can be used as data and boundary conditions for numerical computations such as finite element program ANSYS and also to compare the results of model calculations with the measurements obtained on the real object.



KAPITAŁ LUDZKI
NARODOWA STRATEGIA SPÓJNOŚCI



UNIA EUROPEJSKA
EUROPEJSKI
FUNDUSZ SPOŁECZNY



References

1. Zator S., Ryszczuk M.: Korekta pomiaru termowizyjnego w oparciu o trójwymiarowy model obiektu, *Przegląd Elektrotechniczny*, 89 (2008), nr 12, 323-325
2. Zator S., Lasar M.: Uzyskiwanie termogramów wysokiej rozdzielczości, *PAK 2011* nr 12, 1480-1482
3. Rabbani T., van den Heuvel F. A., Vosselmanc G.: Segmentation of point clouds using smoothness constraint, *ISPRS Commision V Symposium 'Image Engineering and Vision Meteorology'*, September 2006
4. Alam M.S., Bognar J.G., Hardie R.C., and Yasuda B.J.: Infrared Image Registration and High-Resolution Reconstruction Using Multiple Translationally Shifted Aliased Video Frames, *IEEE Trans. Magn.*, 49 (2002), n. 5,
5. Borman S., Stevenson R.: Spatial Resolution Enhancement of Low-Resolution Image Sequences A Comprehensive Review with Directions for Future Research, July, 1998

Thermal Analysis of Induction Motor

Piotr Mynarek and Marcin Kowol

Opole University of Technology,
Faculty of Electrical Engineering, Automatic Control and Computer Science,
Institute of Electromechanical Systems and Industrial Electronics,
ul. Prószkowska 76, 45-758 Opole, Poland
piotr_mynarek@o2.pl, m.kowol@po.opole.pl

Abstract. The work describes a method of thermal calculations for an induction motor. Thermal model of the analyzed motor was built based on the thermal network method and was implemented in PLECS package. Simulation results, were verified by measurements performed on the physical model of the motor.

1 Introduction

Thermal phenomena constitute an aspect of the utmost importance while designing electrical machines and determining their load capacity. These phenomena determine to the large extent reliability and life time of an electrical motor. Additionally, thermal calculations allow to determine the level of use of a machine and effectiveness of construction solutions. In spite of the enumerated aspects much less attention is devoted to thermal analysis than to electromagnetic phenomena. This asymmetry is particularly vivid in case of motors of small and medium power. Recently however, one may observe change in this trend which results in numerous publications [1, 2, 3]. It is caused mainly by growing demand concerning achieving as great power as possible from a given size of a machine. Additionally, each increase in efficiency of a motor is connected with a notable economic effect. Therefore, works connected with determining temperatures in particular elements of electrical machines in various phases of their work become appropriate.

2 Thermal model of the motor

The work adopted a three-phase motor Sh80-6B produced by Besel with power of 0.55 kW as the object of research. Individual elements of the analyzed machine is assigned a value of thermal resistance [2]. As a source of heat in the motor adopted occurring power losses in the copper (1) and iron (2).

$$\Delta P_{Cu} = I^2 R_0 (1 + \alpha \Delta \vartheta) \quad (1)$$

where: I – phase current, R_0 – phase resistance at reference temperature ϑ_0 , α – temperature coefficient, $\Delta \vartheta$ – temperature change.

$$\Delta P_{Fe} = k_{kt} \Delta p_{B,f} \left(\frac{f}{f_p} \right)^{\frac{4}{3}} \left(\frac{B}{B_p} \right)^2 m_{Fe} \tag{2}$$

where: k_{kt} – construction-technology factor (stator, rotor teeth $k_{kt}=1,5$, stator, rotor core $k_{kt}=1,7$), $\Delta p_{B,f}$ – maximum specific total core loss at B_p i f_p , f – frequency, B – magnetic flux density in the core at f , m_{Fe} – mass of core.

In order to determine the value of magnetic induction in various parts of the motor core developed numerical model in FLUX3D environment, based on FEM [3].

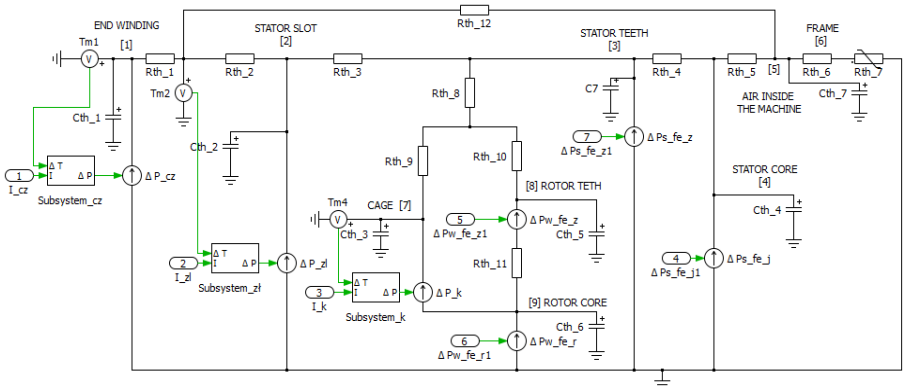


Fig. 1. Thermal model of the analysed motor in PLECS toolbox.

3 Measurements

In order to verify results of the simulation the measurements were performed on the real object. For this purpose a test bench was made (Fig. 2). Whereas data acquisition system was designed based on LabVIEW and National Instruments hardware – controller PXIe-8130 with card PXI-4353 and PXI-6133 [1]. Temperature measurements were performed using type K thermocouples, pyrometer and infrared camera.

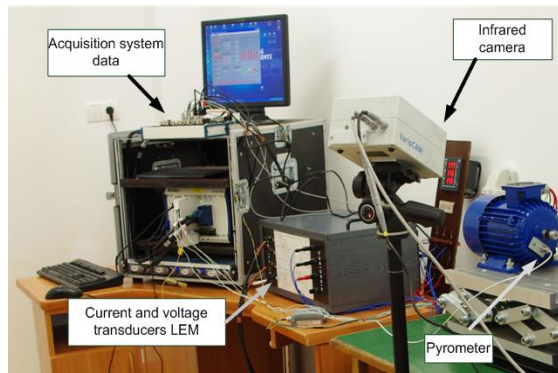


Fig. 2. Test bench

4 Results of analysis

Based on the lumped-parameter thermal model, a number of computer simulations for different motor operating conditions were performed. Fig.3 shows the temperature changes at selected measuring points which were obtained from computer simulations for the object of research at no-load operation. The calculation results were compared with measurements performed on the model of a real motor. Fig. 4 shows the temperature changes at short-circuit condition at reduced supply voltage ($U=130V$). The computer simulations adopted two values of the heat transfer coefficient: $h=30 \text{ W}/(\text{m}^2\text{K})$ for forced convection and $h=15 \text{ W}/(\text{m}^2\text{K})$ for natural convection.

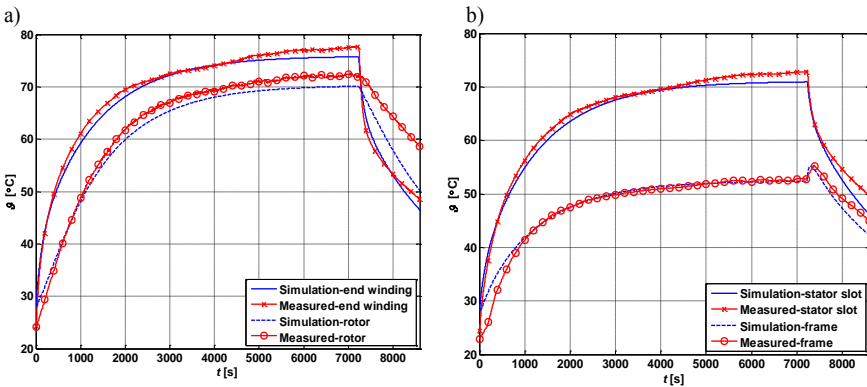


Fig. 3. Measured and simulated temperatures at no-load operation ($\vartheta_0=24,5^{\circ}\text{C}$)

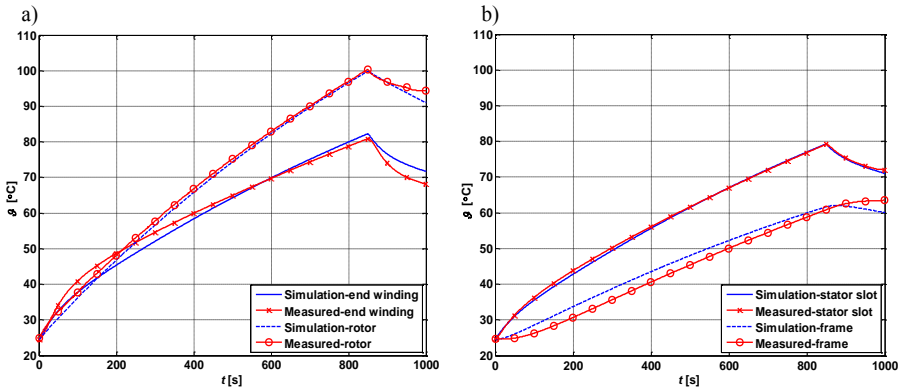


Fig. 4. Measured and simulated temperatures at short-circuit condition ($\vartheta_0=24,5^{\circ}\text{C}$)

Fig. 3 can be seen that at no load the highest temperature occurs in end winding. While the short-circuit condition (Fig. 4) is the highest temperature in the rotor, which is due to increased losses in this element. As a measure of error between calculations and measurements (Tab. 1) were adopted δ error defined as follows (3):

$$\delta = \frac{1}{n} \sqrt{\sum_{i=1}^n (\vartheta_{mi} - \vartheta_{si})^2} \tag{3}$$

where: n – number of samples, ϑ_m – temperature measurement, ϑ_m – temperature of the simulation

Tab. 1. The value of δ error for the individual characteristics of heating at no-load operation and short-circuit condition

	End winding	Stator slot	Rotor	Frame
No-load	2,83	2,15	3,47	1,61
Short circuit	2,13	0,54	2,31	1,14

5 Summary

The results of thermal analysis of an induction motor of small power on the basis of a thermal model which were presented in the work show high compliance with results of measurements. Error δ between results of calculations and measurements does not exceed 3,5°C both for no-load operation and state of short-circuit of the motor. This concurrence proves correctness of the designed thermal model of the motor. Errors which occur result from adopted simplifying assumptions and difficulty in determining characteristics of particular materials the motor is built of. Another cause of occurring divergences may be the fact, that microscopic slits which occur between two elements of the motor, e.g. between grooved insulation and stator core, were ignored in the model.

The method of analysis used is characterized by low numerical cost. With the use of the constructed model one may fast and at the same time with sufficient precision determine temperature in particular elements of a motor. These quantities are extremely important as far as operation and load capacity of motors is concerned.

References

1. Barański M.: Laboratory stand to investigation of influence of temperature on the electromagnetic transient in a squirrel cage induction motor, Poznan University of Technology Academic Journal Electrical Engineering, No. 72, 129-140, 2012.
2. Kylander G., Thermal modelling of small cage induction motors, Ph.D. thesis, Göteborg, 1995.
3. Lefik M.: Obliczenia cieplne silników indukcyjnych małej mocy metodami polowymi, Rozprawa doktorska, Łódź, 2011.



UNIA EUROPEJSKA
EUROPEJSKI
FUNDUSZ SPOŁECZNY



Praca powstała dzięki współfinansowaniu ze środków Europejskiego Funduszu Społecznego

The Possibility of the Implementation of the Gaussian Puff Model in the Parallel Architecture

Tomasz Przybyła

Opole University of Technology,
Faculty of Electrical Engineering, Automatic Control and Computer Science,
Institute of Automatic Control and Computer Science,
ul. Sosnkowskiego 31, 45-272 Opole, Poland
tom.info.dok@gmail.pl

Abstract. The number of computing processes related with the simulation of dispersion of pollutants for the global scale do not allow to obtain results in acceptable time, that is why the methods which can accelerate the air pollution modeling are searched. In this article the problem of air pollution dispersion modeling for huge scales has been introduced. Additionally, the conceptions of the implementation of the air dispersion model, related to the Gaussian puff models in parallel architecture and massively parallel architecture, are presented.

1 Introduction

Simulation of the complex and global processes, which appear in the reality, is very time consuming that is why there is the need of the use of modern, high-speed computing systems. Among such complicated problems there are for instance the process of transport and dispersion pollutants in the air [1, 4].

The peculiarity of modeling dispersion of the pollution in atmosphere, especially in the case of those huge scenarios, require high-performance computing systems. The bigger and bigger requirements according to the precision and the time of getting the results of the simulation implicate the must of finding efficient methods for computing which are adjusted to the contemporary hardware platforms of the parallel architecture or the massively parallel architecture.

2 Gaussian dispersion model

The simulation of the pollution dispersion processes can be performed by the use of many models which differ in the spatial scale, the time scale, the transport equation and the destination. Classification by the mathematical base and the frame of reference distinguishes two main types of models: Eulerian model and Lagrangian

model [3]. In additions, the Gaussian models are available, which can be introduced both by the Eulerian and Langrangian model [1]. Among the Gaussian models there are two kinds of them: the plume models and segment plume/puff models. The proper choice of the model plays the crucial role both in the process of credible analysis of the current condition of the air and in the process of the forecast of the concentrations of pollutants.

Gaussian plume model describes the transport and the dispersion of the pollution via the plume moving with the wind direction, while maintaining the stationary meteorological condition and continuous pollution emission [1]. Because of the restriction due to some simplified presumptions the plume models are used for individual emitters [5].

In the Gaussian puff model the amount of pollution emitted into the atmosphere is divided into puffs which move in the area of the modeling. The movement is determined by the local meteorological conditions. The necessity of records each generated puff in the area of the simulation causes very high computational costs [1, 2].

3 CALPUFF

CALPUFF (CALifornia air research board PUFF air dispersion model) is a multilayer, non-steady-state model which can be used in the air quality simulation model system. The CALFUFF system consists of three main elements: the meteorological preprocessor (CALMET), the computing module of dispersion and chemical conversion (CALPUFF) and the tool for processing the results (CALPOST) [3].

The model CALPUFF is based on the Gaussian puff model. The dispersion of the pollution inside the puff is described by equations 1, 2.

$$C = \frac{Q}{2\pi\sigma_y\sigma_z} g \exp\left[-\frac{1}{2}\left(\frac{d_a}{\sigma_x}\right)^2\right] \exp\left[-\frac{1}{2}\left(\frac{d_c}{\sigma_y}\right)^2\right] \quad (1)$$

$$g = \frac{2}{(2\pi)^{\frac{1}{2}}\sigma_z} \sum_{n=-\infty}^{+\infty} \exp\left[-\frac{(H_e + 2nh)^2}{2\sigma_z^2}\right] \quad (2)$$

where: C - the ground-level concentration, Q - the pollutant mass in the puff, σ_x , σ_y , σ_z - the standard deviation of the Gaussian distribution in the along-wind direction, cross-wind direction and vertical direction, d_a , d_c - the distance from the puff center to the receptor in the along-wind direction and cross-wind direction, g - the vertical term of the Gaussian equation, H - the effective height above the ground of the puff center, h - the mixed-layer height.

The computing in the CALPUFF model is made via diffusion ratios which are designated by one of the methods: measured values of turbulence σ_v , σ_w , internally calculated σ_v , σ_w with the use of the standard deviation of vertical and horizontal component of the wind and with the Monin-Obukhov length, the dependence of Pas-

quill Gifford's (rural areas) and McElroy-Poller's (urban areas) and computed using the MESOPUFF II equation [3].

The CALPUFF is a model which realizes calculations sequentially what in the case of huge scenarios of modeling makes the time of simulation takes much longer. To make the process faster some certain methods have been prepared but none of them changes any program code. One of the methods assumes parallelization of computing according to the emission source [6]. In this particular method the computing is made for single emission source or the group of sources. To make the processors balanced it is very important to use multicriterial division of emission sources. At first, there is the division because of the type of the emission sources, next, depending on the available number of the processors, in the area one of the sources [6]. This method can be used only when the chemical transformation isn't taken into consideration.

4 Parallelization

To make such model as CALPUFF more parallel there is the need to know very deeply how the computing is made in particular modules. To identify the procedure which is characterized the highest computing cost the profiling has been performed. To analyse the program code of CALPUFF the tools of Lahey-Fujitsu Fortran 7.3 (Windows 7) and Lahey-Fujitsu Fortran 8.1 (Ubuntu 12.04) have been used. The modeling for the purpose of profiling was performed on a very small area (grid 4 x 4 km), in which only 87 area sources were defined. What is more the limit of the maximum number of the puffs which appear in the grid has been increased to 300 thousands. In the vertical relation the area of modeling has been divided into 11 layers and restricted to 4000 m. The computing has been made via the Intel Core i7-2630QM 2,0 GHz processor.

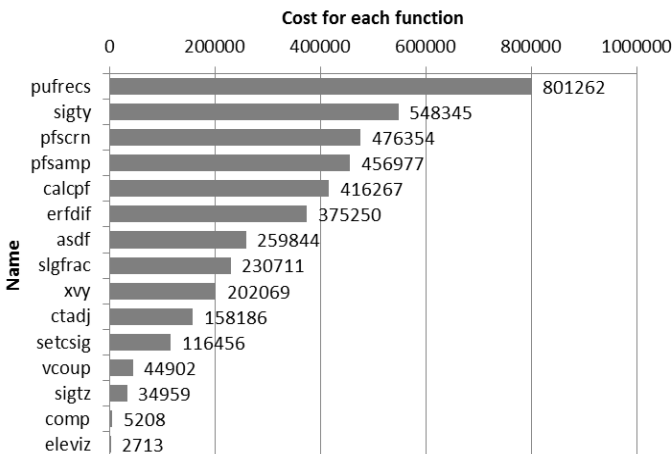


Fig. 1. Profiling results

The results show that the procedures responsible for the evidence of the puffs and computing the σ worth for particular receptors (pufrec, pfscrn, pfsamp) are characterized by the biggest cost of computing. This makes a chance to make a division according to the receptors. Because of this that the computing of the concentration for each of the receptors are not related to each other they can be compute in the parallel way both in the parallel architecture and the massively parallel architecture.

5 Summary

The modeling of dispersion of the air pollution, which occurs in various area and time scales, is extremely important in the managing system of the air quality. One of the universal models, which can be used to air pollution modeling, is the CALPUFF. In this work the conception of fastening the computing via the use of multiprocessors architecture has been shown.

In the further scientific work the concepts discussed in this article will be realized. What is more the verification of possible benefits due to the use of the heterogeneous computing systems in the modeling processes of the space-time dynamics.

References

1. Markiewicz M. T.: Podstawy modelowania rozprzestrzeniania się zanieczyszczeń w powietrzu atmosferycznym. Oficyna Wydawnicza Politechniki Warszawskiej, Warszawa 2004.
2. Szczygłowski P.. Ocena przydatności wybranych modeli gaussowskich w obliczaniu stanu zanieczyszczeń powietrza, Rozprawa doktorska, Akademia Górniczo-Hutnicza im. Stanisława Staszica w Krakowie, Kraków 2007.
3. Scire J.S., Strimaitis D.G., Yamartiono R.J.: A User's Guide for the CALPUFF Dispersion Model (Version 5), Earth Tech, Inc. Concord, 2000.
4. Alexandrov V.N., Owczarz W., Thomson P. G., Zlatev Z.: Parallel runs of a large air pollution model on a grid of Sun computers, Mathematics and Computers in Simulation 65, pp. 557-577, 2004.
5. Łobocki L.: Wskazówki metodyczne dotyczące modelowania matematycznego w systemie zarządzania jakością powietrza, Ministerstwo Środowiska, Główny Inspektorat ochrony Środowiska, Warszawa 2003.
6. Smolczyk A., Rosicki M.: Wykorzystanie wielu procesorów w modelowaniu rozprzestrzeniania zanieczyszczeń w atmosferze, Nauka i praktyka - staże zawodowe w przedsiębiorstwach, Politechnika Opolska, Opole 2009.



KAPITAŁ LUDZKI
NARODOWA STRATEGIA SPÓJNOŚCI



UNIA EUROPEJSKA
EUROPEJSKI
FUNDUSZ SPOŁECZNY



Effect of Rounding Duty Cycle on the PWM Modulation

Tomasz Pyka

Opole University of Technology,
Faculty of Electrical Engineering, Automatic Control and Computer Science,
Institute of Electric Power Stations and Measuring Systems,
ul. Prószkowska 76, bud. nr 1, 45-758 Opole, Poland
t.pyka@doktorant.po.edu.pl

Abstract. This paper presents simulation of Pioneer 2DX mobile robot motion including regulator for: pulse width modulation (PWM), without PWM control and with a constant corrector factor. The simulation was carried out taking into account the actual parameters of the DC motor.

1 Introduction

Supply system for mobile robots is usually achieved by using H-bridge with PWM. Constant voltage is mapped on the basis of the pulse duty factor, which is defined as an integer. The issue is still present, considered in the article, is to determine the method of calculating the duty cycle factor in such a way as to commit the slightest error.

The article presents the impact of rounding error resulting from the pulse duty factor of unipolar PWM while moving the mobile robot along a trajectory. Were analyzed cases: without PWM controller, with the controller and for a constant value equal to 0.4.

2 Mobile robot model

The simulation was conducted for the three-wheeled mobile robot Pioneer 2DX with the following equations [1]:

$$(2m_1l_1^2 + m_4l_2^2 + I_{z5} + 2I_{y1} + 2I_{z1}l_1^2)\ddot{\beta} - m_4l_2r\dot{\alpha}\dot{\beta} = (M_1 - M_2 - N_1f_1 + N_2f_2)h_1, \quad (1)$$

$$[(2m_1 + m_4)r^2 + 2I_{z1}]\ddot{\alpha} + m_4l_2r(\dot{\beta})^2 = M_1 + M_2 - N_1f_1 - N_2f_2, \quad (2)$$

where: m_1 – mass of the drive wheel, m_4 – mass of the robot, f_1f_2 – varying coefficients friction wheel of the ground, N_1, N_2 – wheel pressure to the ground, I_{z1}, I_{z5}, I_{y1} – moments of inertia, M_1, M_2 – driving torque, h_1 – height of axis to the drive wheel, $\ddot{\alpha}, \ddot{\beta}$ – angular acceleration, $\dot{\alpha}, \dot{\beta}$ – angular velocities, α – angle of the drive wheel, β – angle of a robot construction.

The simulation was carried out for the actual DC motor with the following parameters: $U_n=24.0\text{V}$, $I_n=2.7\text{A}$, $\psi=0.06\text{ Nm/A}$, $R_t=1.2\ \Omega$, $L_t=0.0029\text{ H}$, where: U_n – related voltage, I_n – related current, ψ – exciting flux, R_t – armature resistance, L_t – armature inductance.

Furthermore, it was assumed that transmission efficiency is 80% and the varying coefficients friction wheel of the ground f_1 and f_2 , were selected from the normal distribution $N(0.01, 0.0058)$. The simulation does not include the impact of the passive wheel to the robot motion trajectory.

Pulse duty cycle factor of the unipolar PWM was described as:

$$k = V_d / V_{\max}, \quad (3)$$

where: V_d – desired voltage, V_{\max} – source voltage, k – pulse duty cycle factor, which is defined as an integer.

3 Simulation results

PWM modulation was modeled based on [2] [3] and the simulation was carried out with simplified switching between the semiconductor elements.

Below was presented a fragment of the output voltage waveform:

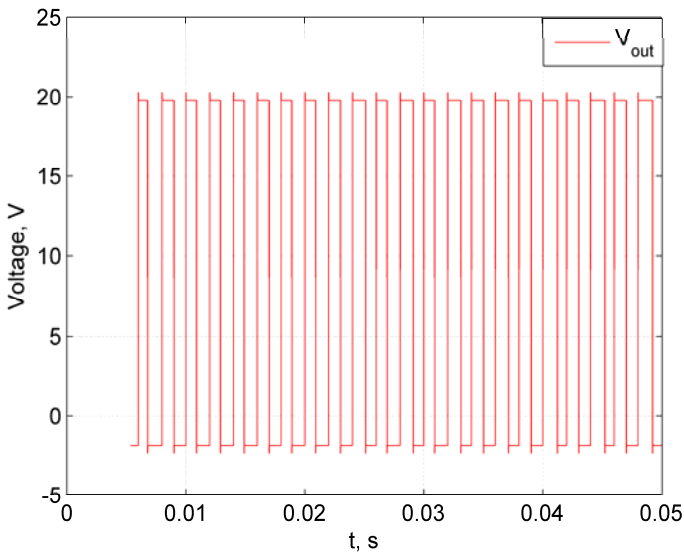


Fig. 1. Output voltage (fragment).

In the present case, reference trajectory was the accelerating during 1s in a straight line. It is a very important part of motion for the proper mobile robot control, because too large errors made at this stage, can cause even greater errors in the next phases of robot motion.

In Table 1 was shown the root mean square errors and maximal errors calculated as [4]:

Table 1. Simulation results.

Kind of simulation	Root mean square error		Maximal error	
	$\dot{\alpha}$ [rad / s]	α [rad]	$\dot{\alpha}$ [rad / s]	α [rad]
Without controller	$4.83 \cdot 10^{-2}$	$8.96 \cdot 10^{-2}$	$5.69 \cdot 10^{-2}$	$2.00 \cdot 10^{-1}$
With controller	$7.90 \cdot 10^{-3}$	$1.38 \cdot 10^{-2}$	$9.81 \cdot 10^{-3}$	$3.58 \cdot 10^{-2}$
With constant corrector factor	$4.04 \cdot 10^{-2}$	$8.21 \cdot 10^{-2}$	$5.20 \cdot 10^{-2}$	$1.86 \cdot 10^{-1}$

Fig. 2 shows the difference between the average desired voltage and average output voltage calculated as:

$$\Delta V = V_d - V_{out} \quad (4)$$

where: V_d – desired voltage, V_{out} – output voltage.

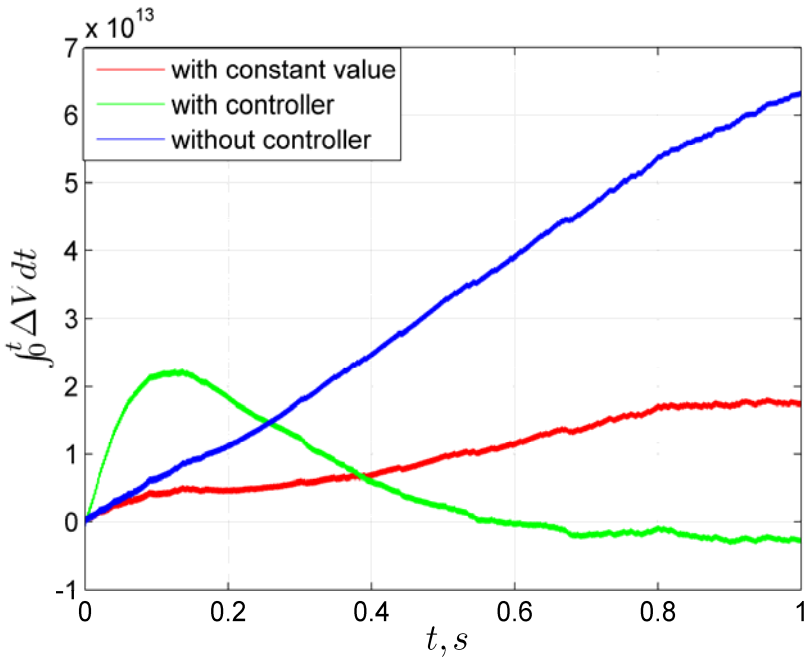


Fig. 2. Integration of the difference between desired and output voltage.

The difference between the modulations are quite significant and skipped the rounding effect in pulse duty factor, causes greater errors on the trajectory, which was confirmed by simulation results presented in Fig. 2 and Table 1.

A constant value corrector significantly improves the result of mapping the desired voltage only at the beginning of the movement.

Using the controller in PWM causes the error voltage mapping tends to zero, in other kind of modulation analyzing in this paper it is quite impossible.

4 Summary

Using the controller with an integrating part significantly improves mapping given by the PWM voltage, which also translates directly into smaller errors during tracking move on the trajectory. It should be noted that this kind of control in the initial phase produced a significant traffic controller errors, and therefore can be at the beginning of movement round the duty cycle with a constant value, then switch the control kind on the controller included in the PWM.

References

1. Giergiel M. J.,Hendzel Z., Żylski, W.: Modeling and control of wheeled mobile robots, Warsaw, Polish Scientific Publishers PWN, 2002
2. Boudreaux R. R. Nelms R. M., Hung J. Y.: Simulation and modeling of a DC-DC converter by an 8-bit microcontroller, Applied Power Electronics Conference and Exposition, 1997, pp. 963-969
3. Maksimović D., Stanković A. M., Thottuvelii J. V., Verghese G. C., Modeling and Simulation of Power Electronic Converters, Proceedings of the IEEE Vol. 89, No. 6, 2001, pp. 898-912
4. Beniak R, Pyka T: Control stepsize optimization for tri-wheel mobile robot, 3rd International Students Conference Electrodynamics and Mechatronics (SCE III), 2011, pp. 73-76

This work was co-financed by the European Social Fund



Detection and Classification of Two-dimensional Images Based on the Hilbert Method of Digital Optical

Sławomir Stemplewski¹ and Adam Sudol²

¹Politechnika Opolska, Instytut Układów Elektromechanicznych i Elektroniki
Przemysłowej ul. Prószkowska 76, 45-758 Opole, Polska
stempell@gmail.com

²Uniwersytet Opolski, Wydział Przyrodniczo-Techniczny
Katedra Technologii, 45-365 Opole, ul. Dmowskiego 7-9, Polska
dasiek@dasiek.info

Abstract. This article presents one of many currently investigated ways to minimize the description of objects intended to do the greatest possible reduction of computational complexity and the adaptation of the calculation procedure for the implementation in the flying machines as part of the identification track and classification of ground facilities.

1 Introduction

Identification of objects and textures is very wide issue, mainly because of the countless number of domains in which it is currently used [4], [5]. The final phase of identifying consists several stages. One of which is the process of acquiring, or acquisition of signals, which are the basis for further identification procedure [6]. During acquisition images can be obtained with different information capacity [2]. In natural conditions can be difficult to obtain images of adequate quality. Some may be low resolution, while others are burdened with noise. In such situations it is necessary to analyze the image one of the ways:

- Artificially increasing the informative of images by pre-treatment to reduce noise, histogram filtration or increase local contrast by using filters such as Unsharp Mask or by submitting multiple images into one.
- Application of the methods showing a high efficiency, enabling to identify the object with sufficient, founded probability of an image with reduced naturally informative (resolution, noise).

This last methodology include Digital Hilbert optics, which consists of a large set of methods responsible for secondary processing of the analyzed images [10].

2. Implementation methods of Hilbert's digital optics for the classification of "flat" objects (two-dimensional)

Below shows sample implementation of procedures to identify objects according to specific, pre-defined criteria.

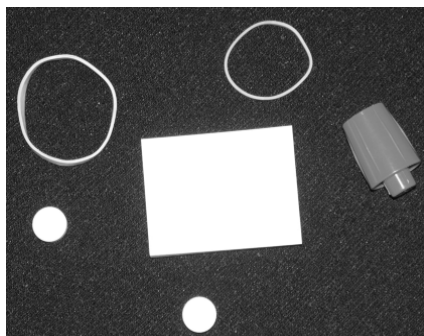


Fig. 1. The test scene

The first part of this exercise (stages 1-5) was taken from the Matlab tutorial and because of its wide availability, this part of the task will be discussed only in fragments, whose knowledge is essential to carry out the second part - step 6 The Identifying round objects procedure is a very good example of the applicability of hybrid Hilbert transformation for advanced identification of objects in digital images. Below shows the steps preceding the advanced stage of identification of objects, namely the search for the object most similar to the pattern:

Stage 1 – **Read Image.**

Stage 2 – **Threshold the Image.**

Stage 3 – **Remove the Noise.**

Stage 4 – **Find the Boundaries.**

Stage 5 – **Determine which Objects are Round.**

Stage 6 – **Finding a shape similar to the pattern.**



Fig. 2. The wanted object - a pattern

In the previous stage, where the most round areas was determined, assumed that "roundness" area can be defined by the formula:

$$m = \frac{4\pi s}{o^2}$$

where: m – roundness factor. For a perfect circle $m = 1$

s – surface of the test shape







o – circuit of the test shape

In the sixth stage is necessary to use correlation methods to determine the segment of the test image, where the correlation coefficient of transformed form and transformed in the same way as the pattern is the highest. To demonstrate the benefits of using hybrid Hilbert transformation, the experiment was divided into several sequences of correlation:

- Correlation of the primary objects (NTR),
- Radon correlation vectors for the original images (RdNTR),
- Correlation of objects subjected to a hybrid HTA,
- Correlation of objects undergoing a HTA-Radon hybrid (RdHTA).

The correlation coefficients relative to the pattern shown below.

Table. 1. Table of correlation coefficients of the image and the tested object for the various transformations.

Shape Transformation						
NTR	0,657	0,648	0,429	0,630	0,654	0,412
RdNTR	0,963	0,965	0,971	0,970	0,964	0,993
HTA	0,805	0,810	0,732	0,797	0,795	0,528
RdHTA	0,355	-0,223	-0,416	-0,200	-0,459	0,652

The most important is that the image of the sought object is 135% size of the object in the test stage and is rotated by 30°. The above table shows, however, that only the HTA hybrid Radon transform gives the highest correlation coefficient in comparison to the object sought.

3. Final, the conclusions and the prospect of further research

The article is an introduction to create the most complete set of transformations that reduce the descriptive capacity of the test objects by various techniques of research - in particular the methods and correlation with neural networks. Hybrids Hilbert transformation described in this article may be used in all domains, in which the process of identification and classification based on comparison with the pattern. The analysis of the subject and the results show the path of potential future research on:

- Optimizing of identification procedures for shortening the time of their execution. In particular, the iterative calculation of the correlation, the execution time without optimization algorithms operation is unacceptably long;
- Adapting some of the most time-consuming calculations for parallel execution. Authority on x86 microprocessors and RISC [3] indicates the possibility of using parallel processing techniques, which give the modern computer processors. Equally high hopes may be linked with the needs of parallel computing, GPU - especially processors from nVidia, which has been implemented CUDA technology, which can dramatically reduce the time needed to calculate the correlation, but also on the earlier stages - that is, processing steps pre-formed models where Hilbert and Fourier transformation. GPUs are designed to maximize efficiency in compression and

decompression domain of images in JPEG format, which is based on Fourier transform.

Literature

- [1] STEMPLEWSKI S., *Identification of chemical compounds on the basis of their chemical spectra in infrared*, Zeszyty Naukowe Politechniki Opolskiej – Elektryka nr 63 (335), 2010, **53-54**
- [2] STEMPLEWSKI S. SUDOŁ A., *Tworzenie opisów sygnaturowych na potrzeby identyfikacji z użyciem sieci neuronowych*, Zeszyty Naukowe Politechniki Opolskiej
- [3] STANISLAWSKI W., RACZYŃSKI D., *Programowanie jednostek wektorowych procesorów rodziny x86*, Politechnika Opolska, Opole, 2009
- [4] VLASENKO V., SUDOŁ A., *Modelowanie systemów informatycznych analizy i identyfikacji scen dynamicznych opartych na cyfrowej optyce Hilberta*, Zarządzanie Wiedzą i Technologiami Informatycznymi, PWNT, Gdańsk, 2009
- [5] VLASENKO V., SUDOŁ A., *Identyfikacja elementów scen dynamicznych: zastosowania cyfrowej optyki Hilberta w modelowaniu procesów obróbki obrazów i sygnałów w systemach optoelektronicznych*, Przegląd Telekomunikacyjny i Wiadomości Telekomunikacyjne, Warszawa, 2009
- [6] VLASENKO V., SUDOŁ A., *Digital Hilbert optics methodology for complex shape objects and textures at dynamic scenes identification: structure design, modeling and verification*, Systems Science, Vol. 35, No. 3, 2009
- [7] SUDOŁ A., STEMPLEWSKI S., VLASENKO E., *Design of video-information systems based on digital Hilbert-optics methods for objects identification: analysis and modeling as stages of project management process*, DidMatTech, Radom 2010
- [8] SUDOŁ A., STEMPLEWSKI S., VLASENKO E., *Information engineering as principal aspect of MDHO based video-information systems and technologies design project management: some examples of application*, DidMatTech, Radom 2010
- [9] SUDOŁ A., STEMPLEWSKI S., VLASENKO N., VLASENKO V., *Identification based on objects' generalized 2-d phase images correlation algorithms: MDHO-IIT-HOES design and effectiveness comparative study*, ISAT, 2010
- [10] HAHN, STEFAN L., *Hilbert Transforms in Signal Processing*, Artech House, USA, 2009



KAPITAŁ LUDZKI
NARODOWA STRATEGIA SPÓJNOŚCI



UNIA EUROPEJSKA
EUROPEJSKI
FUNDUSZ SPOŁECZNY



Praca współfinansowana ze środków Europejskiego Funduszu Społecznego



eu
european
social fund in the
czech republic



EUROPEAN UNION



MINISTRY OF EDUCATION,
YOUTH AND SPORTS



OP Education
for Competitiveness

INVESTMENTS IN EDUCATION DEVELOPMENT

BIOM Workshop

BIOM workshop – organized as a part of WOFEX 2012 workshop – have been realized as a part of BIOM project (CZ.1.07/2.3.00/20.0073). This project is co-financed by ESF and Czech state budget.



Acknowledgement

Following papers were supported by the Bio-Inspired Methods: research, development and knowledge transfer project, reg. no. CZ.1.07/2.3.00/20.0073, co-financed by ESF and state budget of the Czech Republic:

- Alisa Babskova. *Finding and Recommendation of Suitable Persons in Social Networks*
- Petr Berek, Jan Platoš, and Václav Snášel. *Similarity Measurement of Text Documents using Signatures*
- Pavel Dohnálek. *Non-negative Matrix Factorization as Massively Parallel Algorithm for Brain Computer Interfaces*
- Jaroslav Hořejší. *Hardware, Software, Questionnaires and Conferences for the Handicapped*
- Ondřej Koběorský, Jakub Štolfa, and Martin Kopka. *Methodology for Estimating Working Time Effort in the Software Projects*
- Tomáš Kocyan. *Using Case-based Reasoning with Time-warped Data Collections*
- Martin Kopka, Jakub Štolfa, and Ondřej Koběorský. *Estimation of the Project or Use Case Parameters Using SOM and Fuzzy Rules*
- Jonáš Krutil, and Miloš Kudělka, and Václav Snášel. *Analysis of Web Pages Using Schema.org Collection*
- Michal Prílepok, Jan Platoš, and Václav Snášel. *Compression – based Similarity*
- Jakub Štolfa. *Business Process – Formal Modeling in Graphical Ontology Tool – Functional View*
- Lukáš Zaorálek. *EEG Cognitive Action Recognition Based on Singular Value Decomposition Accelerated by GPU*

Finding and Recommendation of Suitable Persons in Social Networks

Alisa Babskova

Department of Computer Science, FEECS,
VŠB – Technical University of Ostrava, 17. listopadu 15, 708 33 Ostrava – Poruba
`alisa.babskova.st@vsb.cz`

Abstract. Finding and recommendation of suitable persons based on their characteristics in social or collaboration networks is still a big challenge. The purpose of this paper is to discover and recommend suitable persons or whole community within a developers' network. The experiments were realized on the data collection of specialized web portal used for collaboration of developers - Codeplex.com. We have used the approach for extraction of initial metadata, and we have used modified Jaccard coefficient for description of the strength of relations between developers.

Keywords: Social Network, OSS, Codeplex.com, graph

1 Introduction

Recently the concept of social networks and online communities is becoming still more and more popular. As a result, the number of their users significantly increasing.

OSS (Open Source Software) is an example of a dynamic network, as well as a prototype of complex networks emerging on the Internet. By working through the Internet, interactions between developers can be considered as relations in the synthetic network of collaborators. These relations arise when the developers join the project and begin to communicate with others. OSS network consists of two entities - developers and projects. An example of such OSS social network established on the basis of interaction between the participants is CodePlex.

In this paper we try to determine the strength of relationship or similarity between CodePlex developers in the context of projects they work on. To determine the context, we used project key words, which in the case of the CodePlex are extracted from project descriptions. We would find some developers or some community, which is specified by key words, for a recommendation.

* This paper is based on an article named 'Method for Identification of Suitable Persons in Collaborators' Networks'. Therefore I would like to thank co-authors, namely Jan Martinovic, Pavla Drazdilova and Katerina Slaninova, for cooperation with this article and agreement to its publication.

2 Codeplex

CodePlex is Microsoft's open source project hosting web site. You can use CodePlex to find open source software or create new projects to share with the world. CodePlex is mainly used by developers for collaboration on projects, sharing source codes, communication and software development. Generally, registered users can participate in multiple projects, discussions, adding the source code and documentation, issue a release, etc. Some of the users have defined a specific role within the project for which they work. Each user has his own page, where he can share information about himself, his projects on which he currently works, and the most recent activities. The CodePlex projects themselves can be considered as a very interesting source of information. In addition to the list of users and roles, CodePlex enables register keywords, add description of the project, the number of visits, status, date of creation, url and other information about the project. All activities are carried out on CodePlex by a particular user within a specific project.

Database which was created as a result of data obtained from CodePlex.com, consists of 6 main tables: User, Project, Discussions, RecentActivity, Membership and SourceCode (see Table 1).

Table 1. The CodePlex database tables

Table	Number of lines
User	96251
Project	21184
Discussions	397329
RecentActivity	72285
Membership	126759
SourceCode	610917

In CodePlex, we can see two types of entities: users and projects. Both are represented by tables that contain specific characteristics. The undirect connection between the user and the project is implemented through activities within the scope of the project. These activities are in the database CodePlex divided into different types: SourceCode, Discussion, RecentActivity and Membership.

The main attribute, carrying the largest set of information, is the project Description – the description of the project itself.

Using activities such as user links to the projects, we are able to determine with some probability an area of specialization and a work of each user. For example, if a user is working on three projects written in .NET and one in Java, we could include him in .NET programmers with high probability, and less likely recommend him as a Java programmer.

In other words, terms or description of the project may not only help us to provide more information about projects, but also to determine the user's area of

interests or abilities. As a result, the way we are able to compare user attributes determines the similarity to other network participants.

3 Collaborators network

Whenever we think about collaboration between two persons, we not only look at the relationship itself, but also at the context. It is clear that depending on context, the strength of relationship changes. Therefore, we divide collaboration into two main parts *Developers' Relationship* and *Developers' Context*.

3.1 Developers' and Context Relationship

We describe a developers' relationship as commutative operation on cartesian product of developer's attribute $X \times X$, where output is mapped to the set of real numbers \mathbb{R} .

We use Jaccard coefficient ([2]) for evaluation of developers relations using their attributes.

$$Attribute_{Score}(CP_{D_i}, CP_{D_j}) = \frac{|CP_{D_i} \cap CP_{D_j}|}{|CP_{D_i} \cup CP_{D_j}|} \tag{1}$$

The whole process of obtaining term sets is described in [5], so we just reminding (t_k in T_{D_i}) stands for the number of terms t_k by T_{D_i} and (t_k in T) stands for the number of terms t_k in descriptions of all projects by T .

We can evaluate association between the selected term $t_k \in D_T$ and a developer $D_i \in D$:

$$R(T_{D_i}, t_k) = \frac{(t_k \text{ in } T_{D_i})}{(t_k \text{ in } T) + |T_{D_i}| - (t_k \text{ in } T_{D_i})} \tag{2}$$

Evaluation of the whole relationship context of two persons D_i and D_j has two steps. First, we compute association between D_i and select term t_k , and between the second developer D_j and t_k separately and we obtain equation for the $Context_{Score}$:

$$Context_{Score}(T_{D_i}, T_{D_j}, t_k) = R_{Norm}(T_{D_i}, t_k) R_{Norm}(T_{D_j}, t_k) \tag{3}$$

The last step is to define Whole Score, which consists of $Attribute_{Score}$ and $Context_{Score}$. This equation evaluates the relation between developers depending on the selected words, which represent the context. So we get a evaluation for the new subnet, which is specified by selected terms.

$$Score(CP_{D_i}, CP_{D_j}, T_{D_i}, T_{D_j}, t_k) = Attribute_{Score}(CP_{D_i}, CP_{D_j}) Context_{Score}(T_{D_i}, T_{D_j}, t_k) \tag{4}$$

3.2 Construction of the Collaborators Graph

To describe the network of collaboration, we use standard weighted graph $G_D(V_D, E_D)$, where weighted function is defined as $w_D : E_D(G) \mapsto \mathbb{R}$, when $w_D(e) \geq 0$.

When we construct graph based on developers' projects relationship, we use $Attribute_{Score}(CP_{D_i}, CP_{D_j})$ as w_D .

The function $Score(CP_{D_i}, CP_{D_j}, T_{D_i}, T_{D_j}, t_k)$ is used for evaluating the edges in the context of the term. The only difference is, that majority of developers has not chosen term in their description text, so the result will be 0 and no edge would exists. The function $Score(CP_{D_i}, CP_{D_j}, T_{D_i}, T_{D_j}, t_k)$ is used for evaluating the edges in the context of the term. The only difference is, that majority of developers has not chosen term in their description text, so the result will be 0 and no edge would exists.

4 Experiments

In one of experiments, we have calculated the keywords for the developers "moder", "raja4567" and "raouf". We have selected only the some terms for illustration. In the Figure 1 is whole network of collaborators for the selected terms "iphone", "wp7", "android". The edge weights are evaluated by $Score$. This subnetwork has 199 connected components (communities) with collaborating developers.

Second part of Figure 1 shows graph of the connected component which contain selected and highlighted developers. We can see that selected developers are not in the one community of collaborators. They are connected, but the relation is too weak. They are not suitable for recommendation.

We used our algorithm for spectral clustering [7] and we detect communities of more collaborated developers. Than we can recommend the "green" community, which contain developers with the stronger relation in the context of selected words.

5 Conclusion

Research presented in this article is oriented to the strength extraction between persons based on their context in the CodePlex. The method was presented using the data collection from the CodePlex database, which contains information of the activities of developers in the project. The proposed method is usable for the development of collaboration network. The description of this network is based on the set of terms (as the input), which are used in the description of projects by the given developer. Using this method, we have obtained the new weight in the synthetic collaborators network. By means of the set of selected term, belonging to one (or more) persons, we can construct the subnetwork with only the context-related collaborators. This subnetwork can be very helpful in searching of the persons who are interested in the same area, defined by the selected term. It is usable for members of the project management, who need to find suitable developers specialized to certain area.

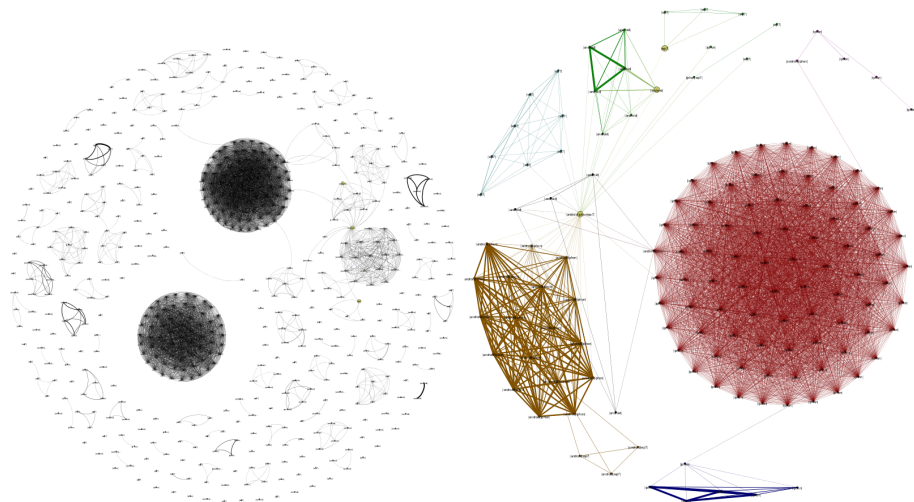


Fig. 1. Synthetic collaborators network for the terms "iphone", "wp7", "android" and selected subnetwork with developers "modder", "raja4567" and "raouf"

6 List of publications

Developers Cooperation based on Terms of Project Description. Minks S., Martinovic J., Drazdilova P., Babskova A., Slaninova K. DATESO, 2012

Method for Identification of Suitable Persons in Collaborators Networks. Drazdilova P., Babskova A., Martinovic J., Slaninova K., and Minks S. CISIM 2012, 2012

References

1. Chen J., Geyer W., Dugan C., Muller M., Guy I. Make new friends, but keep the old. *Proceedings of the 27th international conference on Human factors in computing systems CHI 09*, (1):201, 2009.
2. Deza M.-M., Deza E. *Dictionary of Distances*. Elsevier Science, Amsterdam, The Netherlands, Oct. 2006.
3. Konchady M. *Text Mining Application Programming*. Charles River Media, 1 edition, May 2006.
4. Long Y., Siau K. Social network structures in open source software development teams. *Journal of Database Management.*, 18(2):2540, 2007.
5. Minks S., Martinovic J., Drazdilova P., Slaninova K. Author cooperation based on terms of article titles from dblp. *IHCI2011*, 2011
6. Porter M.F. An algorithm for suffix stripping. *Program*, 14(3):130137, 1980.
7. Vojacek L., Martinovic J., Slaninova K., Drazdilova P., and Dvorsky J. Combined method for effective clustering based on parallel som and spectral clustering. *DATESO*, 2011

Similarity Measurement of Text Documents using Signatures

Petr Berek, Jan Platoš, and Václav Snášel

Department of Computer Science, FEECS,
VŠB – Technical University of Ostrava, 17. listopadu 15, 708 33 Ostrava – Poruba
{petr.berek, jan.platos, vaclav.snasel}@vsb.cz

Abstract. In this paper we describe how to use signatures and S-Tree data structure for measurement similarity of small text documents. Signature contains a lot of information from source documents. Many techniques for signature creation as well as for signature indexing was developed in the past. The most interesting signature storing and indexing data structure is S-Tree. Similar signatures should be in same nodes in S-Tree. In our work, we are interested in the ability of S-tree in grouping similar documents into same node or into nodes with the same parent.

Keywords: signatures, similarity, S-Tree

1 Introduction

The amount of large textual dataset (newspaper, email, articles from conferences, etc.) is growing as well as the need of managing documents inside datasets. One aspect of the management is plagiarism detection. The plagiarism detection is a method which detects similar documents or its parts. We need to inspect whole collection for each new document to detect possible plagiarism. This technique is very time consuming and we need a tool, which helps us do this task more efficiently. One possible solution is signatures. Signatures contain information extracted documents. But they are much smaller and we can measure them and do any other operation with them. Signatures should be organized into data structures for efficient searching, adding, removing, etc.

2 Signature generation techniques

There are two main methods for signatures generation. The first is word fragmentation. In this method, word is broken into pairs or triplets of characters.

Second method is pseudo-random generation. This method uses pseudo-random number generator for selection of active bits in the signature. Every word is sent to hashing function which produces an integer number, which is

used as a seed to a pseudo-random number generator. Signature is created by setting bits on positions taken from k words and their corresponding values from pseudo-random number generator to one.

Pseudo-random method has two major advantages over word fragment approach[3]:

- The number of bits set to one is not function of the length of word. It means that each word generates the same number of bits. Therefore, this method has shorter signatures than word fragmentation method.
- Bits are distributed evenly along the length of the signature and not clustered around bits that correspond to frequently used tri-gram patterns.

We used Floyd algorithm which belong to the second group of algorithms in our work. The Floyd algorithm clearly distributes bit positions evenly throughout the length of the signature as well as distinguishing quite well between anagrams. This algorithm is described in [3].

Optimal bit proportion in signature is 0.5 - 50% of ones and 50% of zeros. We used equation 1 to computation of the signatures length. N is size of the signature, k is number of bits set to one and D is number of distinct words. [3]

$$\frac{N}{k} = \frac{D}{\ln(2)} \tag{1}$$

Number of different bits set for each word is given by equation 2.[3]

$$k_{opt} = \frac{N \ln 2}{D} \tag{2}$$

3 Data structures for saving signatures

Many data structures which support efficient handling with large signatures exist. In our work we used a structure called S-Tree. This structure is a tree similar to B-tree.[1] In this structure we have leaf nodes and non-leaf nodes. Leaf nodes contain similar signatures. Parents of leaf nodes are non-leaf nodes which contain signatures created by merged signatures of its child nodes using bitwise OR operation.[2]

Parent of non-leaf node is again non-leaf node. On the top of the tree is a root. Root is non-leaf node which has no parent. Each non-leaf node has k child nodes. Each leaf node has k items.

In our work we used two function of s-tree - adding and splitting. When node of tree is full (has k items), it must be divided. The problem of node splitting is in bitwise OR operation on signatures in child nodes. Nodes near root could have signatures with a lot of ones and nodes near leaf nodes will have only few of them.[1] The following procedure is used for node splitting:

1. We look for signature S with heaviest signature weight. This is signature for first new node

2. We look for signature S' with heaviest signature weight but where S contains ones S' must have nulls and where S contains nulls S' must have ones. S' is signature for second new node.
3. For each remaining signature s we compare s with S and S'
 - if s is near S then s is added into first new node
 - if s is near S' then s is added into second new node
4. A parent node is assigned to the new nodes. The signature of the parent node is recalculated using signatures of new nodes and remaining child nodes. If the parent full after addition of new nodes, it must be split.

When we are adding a new item into tree we start in a root node. We compare signature s with each signature in node. Then, we choose way where result of comparison is the smallest. We follow the path from the root to the leaf node and then we added a new item into leaf node. Then, we must update all signatures of the parent nodes along the path from the root.

4 Experiment

The experiments were performed on a small text collection. This collection allows a comparison and evaluation of algorithms for similarity detection of text documents.

4.1 Collection

The testing collection contains randomly picked articles from news server. Each article has several paragraphs. Selected base articles were different from each other. To each base article five other articles were generated using minor changes and substitution from other articles.

We select five base articles. Five variants of each article were generated. Therefore, we have 30 testing articles.

We used an algorithm described above in our experiments. In each article we used up to 1000 unique trigrams. The size of the signature was set to 10104 bits according to the equation 1 and the number of ones set by each trigram was set according to the algorithm above.

4.2 Comparison of signatures

Two methods were used for signature comparison. The first method compared every document to each other. Results of this method give an overall view on the collection.

The second algorithm used a S-Tree structure for storing signatures. We set number of items per node to six and we looked for groups of signatures/articles in nodes of S-Tree.

The comparison of the signatures uses two bit-wise operation - AND and NOT. The NOT operation represents a bit-negations - converts one to zeros and

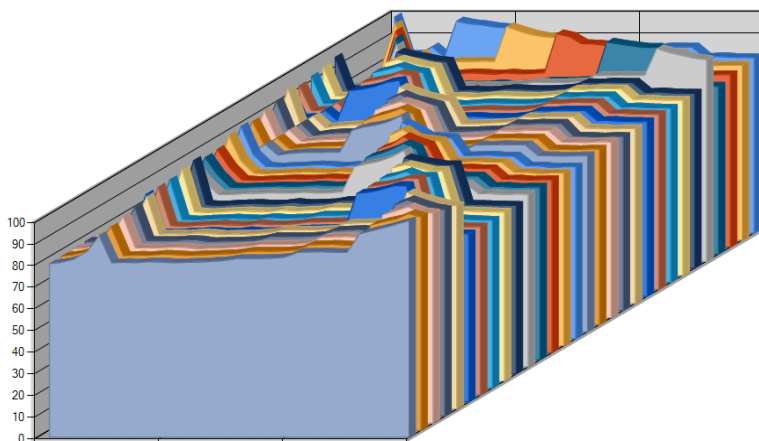


Fig. 1. Graph for each with each signature comparison

zeros to ones. The AND operation preserve one only when both signatures has ones on corresponding position. When we have two signatures S_1 and S_2 , the results signature S_3 is computed as follows:

$$S_3 = S_1 \& !S_2$$

The and operation is represented using symbol $\&$ and negation using a $!$.

S_3 contains zeros on all positions when S_1 is equal to S_2 , and is more or less similar to one of the compared signature otherwise.

Bit-wise operators are the most expensive part of the algorithm. Therefore, we precomputed a table which contains results of the comparison operation on bytes ($b_1 \& !b_2$) and OR operation used in S-Tree data structure.

Another improvement in efficiency may be done be pre-computation of ones in bytes after operation. This operation is important in signature comparison because comparison operation between two identical signatures result in all zeros and same operation between two different signatures result in a number of ones equal to the number of ones of one of the signatures.

5 Results

Results achieved on testing collection are depicted on Figure 1. Percentage of similarity of articles is depicted on Y-axis as values between 0 and 100. Documents are depicted on X and Z-axis. The graph with results has no defined marks. But the diagonal shows the similarity between corresponding articles. The similarity between corresponding documents is 100%. Around diagonal may be seen high similarity of documents derived from the set of base documents.

The resulting S-Tree is depicted on Figure 2. In the figure may be seen the number of groups of similarity. The first number in a node for each signature is number of ones. The second number is a rate of ones, i.e. the ration of number of ones to the size of the signature. The last number is number of article. Three of five groups depicted in the figure are closed.

The open groups remained for articles derived from article 3 and article 2. As may be seen in parent node, article 33, which is derived from article 3, has less ones than other articles derived from article 3. Therefore, group of documents was split correctly. The second open group of similarity - articles derived from article 2 has different reason. All of the signatures has similar rate of ones. But they are split onto different groups and even the parent nodes are not the same. This was caused by the initial setup of the S-tree. Node which contains documents 23, 24 and 25 was created as a last node and contains documents remained after splitting of the previous node.

6 Conclusion

We used signatures and data structure s-tree for measurement similarity of small text data. Documents from collection have been grouped onto nodes of s-tree by their similarity. As Figure 1 shows comparison every document with each other has similarity result as Figure 2 shows. But comparison every document with each other is $O(n^2)$. It is not efficient for large documents collection. In the contrary, S-Tree has complexity $O(n \log n)$ and comparison signatures in one each node is linear. It can improve efficient in large documents collection.

Acknowledgment

This work was partially supported by the SGS in VSB - Technical University of Ostrava, Czech Republic, under the grant No. SP2012/58, and was supported by the European Regional Development Fund in the IT4Innovations Centre of Excellence project (CZ.1.05/1.1.00/02.0070) and by the Bio-Inspired Methods: research, development and knowledge transfer project, reg. no. CZ.1.07/2.3.00/20.0073 funded by Operational Programme Education for Competitiveness, co-financed by ESF and state budget of the Czech Republic.

References

1. Deppisch, U.: S-Tree: A Dynamic Balanced Signature Index for Office Retrieval
Computer science department, Technical university Darmstad, D-6100 Darmstad, West-Germany
2. Korčák, Z.: Signaturní soubory se signaturami proměnné délky. Vysoké učení technické v Brně, Fakulta informačních technologií. 2002
3. Campbell, M.: The Design of Text Signatures for Text Retrieval Systems, Dekain university, School of computing mathematics, 1994

Non-negative Matrix Factorization as Massively Parallel Algorithm for Brain Computer Interfaces

Pavel Dohnálek

Department of Computer Science, FEECS,
VŠB – Technical University of Ostrava, 17. listopadu 15, 708 33 Ostrava – Poruba
`pavel.dohnalek@vsb.cz`

Abstract. The goal of this paper is to explore options of massive parallelism to be used in the design of brain computer interfaces (BCIs). In general, brain computer interfaces are based on pattern matching techniques that require a great deal of computing power. Massive parallelism is cheap and efficient way of significantly speeding up the computations. In this paper we propose using a GPU accelerated non-negative matrix factorization (NNMF) to construct a BCI. The approach shows promising results in terms of computation speed, allowing for real-time classification and pattern recognition.

Keywords: Matrix factorization, pattern matching, graphics processor, electroencephalography, signal processing

1 A brief introduction

Massive parallelization is a state-of-the-art technique used to significantly boost the computation speed of various algorithms. Combined with BCI being a heavily explored area of human-computer interaction, it seems reasonable to merge these two concepts. To utilize massive parallelism, one must use a suitable algorithm. Since BCIs consist mainly of signal processing algorithms, we chose short-time Fourier transform (STFT) to preprocess the signal, NNMF to extract features from it and simple Cosine Similarity Measure to classify the query pattern. Describing STFT is beyond the scope of this paper, so we encourage the reader to study the matter in [4], where it is well described. Let us begin by stating the NNMF problem and its description.

2 The NNMF Problem

Many algorithms (and their versions) exist to efficiently compute NNMF, two of the arguably most used ones originally proposed by Lee and Seung in [3]. First, let us formally state the NNMF problem:

Given the input matrix $V_{M \times N}$, $M \geq 0, N \geq 0$, and the rank $K \ll \min(M, N)$, minimize the error matrix E in the equation

$$V = WH + E, \tag{1}$$

where W and H , subjects to non-negativity constrains $W \geq 0, H \geq 0$, are factor matrices with dimensions $M \times K$ and $K \times N$. The algorithms proposed by Lee and Seung use multiplicative update rules to iteratively update the factor matrices, minimizing an error function. One such function is the Frobenius Norm:

$$\|V - WH\|^2. \tag{2}$$

In [3] Lee and Seung prove that the Frobenius Norm is non-increasing if the factor matrices are updated using the following multiplicative update rules:

$$H_{xa} \leftarrow H_{xa} \frac{(W^T V)_{xa}}{(W^T W H)_{xa}}, \tag{3}$$

$$W_{bx} \leftarrow W_{bx} \frac{(V H^T)_{bx}}{(W H H^T)_{bx}}, \tag{4}$$

where a denotes a row of matrix H and a column of matrix W , x represents a column of matrix H and y is the row index of matrix W . We utilize these update rules to compute the factor matrices used later to recognize patterns belonging to particular actions in our EEG signal. Many more algorithms to compute NNMF along with other versions of the NNMF problem such as Sparse NNMF or Large-scale NNMF can be found in [2]

2.1 Pattern Recognition

Once we have obtained the factor matrices from our training data set using the equations (3) and (4), we compute the Moore-Penrose pseudoinverse matrix of W using Singular Value Decomposition [5]. This pseudoinverse matrix is then used to convert any incoming query vector \mathbf{q} to the required dimensionality and vector space by the following formula:

$$\mathbf{h}_q = W^\dagger \mathbf{q}, \tag{5}$$

where \mathbf{h}_q denotes the query vector converted into the vector space of matrix H while W^\dagger is the Moore-Penrose pseudoinverse of W [1].

Once we have obtained the \mathbf{h}_q vector, we can then compare it to all vectors (columns) of matrix H and measure its similarity to them. To measure the similarity, we use Cosine Similarity Measure defined as

$$\frac{\mathbf{h}_q^T \cdot \mathbf{h}_x}{\|\mathbf{h}_q\| \|\mathbf{h}_x\|}, \tag{6}$$

where \mathbf{h}_x denotes a column vector of matrix H . We seek the maximum of the above expression iterating over all column vectors \mathbf{h}_x , of which there are N , obtaining the final formula of the action recognition step:

$$\max_{0 \leq x < N} \left\{ \frac{\mathbf{h}_q^T \cdot \mathbf{h}_x}{\|\mathbf{h}_q\| \|\mathbf{h}_x\|} \right\}. \tag{7}$$

3 Dataset

During data recording, 203060 different values were collected from one of the EEG sensors and stored for brainwave pattern recognition. There is a total of 14 relevant EEG sensors in the headset, yielding 14×203060 values to process. When the data is obtained, it is then preprocessed using STFT. This transformed data is then used to assemble a training matrix in the following manner: every column represents data processed in one STFT window for each sensor. Let M be the number of rows in the matrix, x be the amount of computed Fourier coefficients and y be the number of EEG sensors used to collect the data. M is then determined as $(\frac{x}{2} + 1) \times y$. We only store $(\frac{x}{2} + 1)$ Fourier coefficients since the rest is duplicate and carries no new information. Having constructed the training matrix, we only need to choose the number of features we are looking for by NNMF. Let K be this number. We learned that for given data the best results in terms of both speed of computation and accuracy in pattern recognition are obtained when $K = 10$.

4 Experiments

We conducted several experiments to determine the performance of our accelerated implementations. Results of the experiments are summarized in tables below, with the abbreviations having the following meaning:

- **TMD** - Training matrix dimension
- **# test vectors** - Number of test vectors
- **STFT** - Short-Time Fourier Transform
- **NNMF** - Non-negative Matrix Factorization
- **LP** - Learning Process (STFT+NNMF)
- **CT** - Classification time for the whole data set
- **CTR** - Classification time for a single input vector
- **ACC** - Classification accuracy

All time values are expressed in milliseconds. Table 1 shows the computation times for different numbers of FFT coefficients. It should be noted that the coefficients themselves compose the training matrix, hence the increase in one of the matrix dimensions. While there is a significant increase of classification time for 1024 coefficients, the time is still well within acceptable boundaries.

As shown in table 2, we learned that window size used for STFT has no significant impact on the performance. Note that training matrix dimensions are not dependent on STFT window size - the increase is caused by the change in the number of FFT coefficients that was necessary for certain window sizes.

Table 3 expresses results similar to 2. It is obvious that while the increase in the number of features certainly impacts performance, the impact is of no great import. It might be interesting to measure the performance for even more features, 320 features is, however, arguably the reasonable maximum number

Table 1. Computation times given in milliseconds showing the performance dependency on the number of Fourier coefficients being computed for the input data

	Number of FFT coefficients				
	64	128	256	512	1024
TMD	462 x 2026	910 x 2026	1806 x 2026	3598 x 2026	7182 x 2026
# test vectors	3656				
STFT	5975	5226	5413	5351	5569
NNMF	1264	1295	2371	4352	8065
LP	7239	6521	7784	9703	13634
CT	19235	21044	23525	30154	178714
CTR	5.26	5.76	6.43	8.25	48.88
ACC	64.21%	59.74%	51.37%	41.96%	44.26%

Table 2. Computation times given in milliseconds showing the performance dependency on the size of the window used in STFT. Note that input matrix dimensions are not dependent on the window size. The input matrix is bigger for certain window sizes because for these sizes it was necessary to adjust the number of FFT coefficients computed.

	Size of the STFT window				
	50	100	150	200	250
TMD	462 x 2026	910 x 2026	1806 x 2026	1806 x 2026	1806 x 2026
# test vectors	3656	1828	1219	914	732
STFT	5975	5366	5570	5382	5460
NNMF	1264	1326	2293	2356	2340
LP	7239	6692	7863	7738	7800
CT	19235	10186	9052	5257	3993
CTR	5.26	5.57	7.42	5.75	5.46
ACC	64.21%	60.40%	47.15%	42.84%	41.94%

Table 3. Computation times given in milliseconds showing the performance dependency on the number of features that NNMF looks for.

	Number of features					
	10	20	40	80	160	320
TMD	462 x 2026					
# test vectors	3656					
STFT	5975	5547	5211	5367	5507	5273
NNMF	1264	1202	1513	2215	3806	7442
LP	7239	6749	6724	7582	9313	12715
CT	19235	19719	20185	20640	22073	25538
CTR	5.26	5.39	5.52	5.65	6.04	6.99
ACC	64.21%	61.74%	53.12%	57.48%	44.17%	45.70%

Table 4. Computation times given in milliseconds showing the performance dependency on the number of features that NNMF looks for.

	Number of NNMF iterations					
	1	10	100	1000	10000	100000
TMD	462 x 2026					
# test vectors	3656					
STFT	5413	5257	5975	5258	5367	5444
NNMF	390	437	1264	5741	53944	535986
LP	5803	5694	7239	10999	59311	541430
CT	19640	19595	19235	19312	19734	19484
CTR	5.37	5.36	5.26	5.28	5.40	5.33
ACC	29.24%	57.26%	64.21%	61.83%	59.14%	67.59%

Table 5. NNMF computation times given a square matrix with the number of desired features equal to half the dimension of the matrix.

	Matrix dimension				
	256	512	1024	2048	4096
GPU	577	1326	6833	49530	392200
CPU	5912	57751	503107	6544050	not tested

Table 6. NNMF computation times given a square matrix with the number of desired features being exactly 200.

	Matrix dimension				
	256	512	1024	2048	4096
GPU	811	1450	3416	11747	41449
CPU	9844	38875	167289	979518	not tested

of features to look for in our application. Experiments have shown us that 10 features is the best choice in terms of performance, as stated in chapter 3.

Number of NNMF iterations (table 4) seem to have the greatest impact on the performance, but it should be noted that NNMF converges well within 100 iterations and therefore, once again, number of iterations have very little influence on practical usefulness of our solution.

We also performed experiments on NNMF computation times alone for different training matrix dimensions. The results can be seen in tables 5 and 6. It can be clearly seen that our GPU implementation of the NNMF algorithm is far superior to its CPU counterpart with the worst case of GPU performance being 10 times better than that of the CPU.

5 Future research and Conclusion

Both the performance and price of graphics processing units show great promise for use in the BCI field. Our next efforts will focus on creating BCIs with more advanced EEG devices, increasing the performance by utilizing multiple GPUs and improving the recognition accuracy, which still remains a great challenge to solve. We presented a method of creating a BCI capable of real-time pattern recognition in brainwaves using a low-cost hardware, resulting in a very cost-efficient way of solving the problem, and we certainly feel this method to be worth further elaboration.

Acknowledgement

This work was supported by the Bio-Inspired Methods: research, development and knowledge transfer project, reg. no. CZ.1.07/2.3.00/20.0073 funded by Operational Programme Education for Competitiveness, co-financed by ESF and state budget of the Czech Republic.

References

1. E Benetos, M Kotti, and C Kotropoulos. Musical instrument classification using non-negative matrix factorization algorithms and subset feature selection. *Circuits and Systems 2006 ISCAS 2006 Proceedings 2006 IEEE International Symposium on*, 5:4, 2006.
2. Andrzej Cichocki, Anh Huy Phan, and Rafal Zdunek. *Nonnegative Matrix and Tensor Factorizations: Applications to Exploratory Multi-way Data Analysis and Blind Source Separation*. Wiley, Chichester, 2009.
3. Daniel D. Lee and H. Sebastian Seung. Algorithms for Non-negative Matrix Factorization. In Todd K. Leen, Thomas G. Dietterich, and Volker Tresp, editors, *Advances in Neural Information Processing Systems 13*, pages 556–562, The MIT Press, 55 Hayward Street Cambridge, MA 02142-1493 USA, April 2001. MIT Press.
4. Shuhei Okamura. *The Short Time Fourier Transform and Local Signals*. PhD thesis, 2011.
5. G. W. Stewart. On the early history of the singular value decomposition, 1992.

Hardware, Software, Questionnaires and Conferences for the Handicapped

Jaroslav Hořejší

Department of Computer Science, FEECS,
VŠB – Technical University of Ostrava, 17. listopadu 15, 708 33 Ostrava – Poruba
jaroslav.horejsi@vsb.cz

Abstract. In this article I am informing you about the hardware, options of the facilitation in Windows for physically disabled people, about the results of the questionnaire survey, standards for physically disabled people and about the context of the conferences INSPO 2012 and ICCHP 2012, too. They deal with the adaption of the software tools for the people with the health disabilities. The Conference ICCHP 2012 direct on assistive technologies, too.

Keywords: INSPO 2012, ICCHP 2012, BMI, Krizovatka.cz, Prague, Linz, Jaroslav Winter, Web accessibility, WCAG 1.0, WCAG 2.0, BITV 2.0, Windows, hardware, assistive technologies(AT), options of the facilitation, W3C, PDF, PDF/UA, Qatar

1 Introduction

In this text you will find out which the hardware and standards physically disabled people use and you will learn about the questionnaire survey. You will learn about the content of the conferences INSPO 2012 that took place in Prague and the conference ICCHP 2012 that took place in Linz, too. People with physical disabilities practically daily use the computing technology for their fun or their work. Computers can be for them the only option how to communicate with the world ,too. That is why various standards for the web accessibility and further hardware and software tools are being created for them. So as experts could mutually inform themselves in this field, they participate in various conferences, where they deal with hardware and software tools for people with specific needs, like for example conferences INSPO and ICCHP. Both these conference are directed on the facilitation of the work with the computing technology and consumable electronics. The conference ICCHP 2012 is aimed for the education of the people with disabilities, too and next on assistive technologies(AT) that help the handicapped.

2 The view of various facilitation on the computer for the handicapped

Various software and hardware tools for the handicapped are being created to facilitate the life of the handicapped. Besides this there exists standards for the adaptation of web, so it would be barrier-free from the view of the handicapped. On the other hand these adaptations principally concern visual and deaf impairment of disabled people, but very a little for physically disabled people. In the following part of the article you will learn about the basic information about standards, hardware and software tools. Because I needed to find out what tools physically disabled people use, I have been making the questionnaire survey you will get acquainted with in the next paragraph.

2.1 Standards and hardware and software tools

In the United States of America the community W3C was created the standard Web Content Accessibility Guidelines 1.0 (WCAG 1.0) and subsequently it was created as the modernized variant WCAG 2.0. In Germany the standard BITV (Barrierefreie-Informationstechnik-Verordnung) arises 1.0 and subsequently it was created to the modernized variant BITV 2.0. In the Czech Republic the rules web accessibility were created. These standards deal with the web accessibility for the visually disabled people and deaf disabled people above all. These standards are obliged to the servers of the public management. But in today's time these standards are kept by internet shops and news servers.

Various hardware tools for the better control of the computer programs have been originating for the people with health disabilities. They are various mice (convertible device) keyboards, communicators, adapters, switches, brackets of buttons and armrests. Communicators serve for the communication for the people with various limits of abilities to speak. Switches serve to the control of the computer for the human with the hard health disability. In the operating system Windows also exist various options for the facilitation of the work for the people with the physical disability, visual impairment or deaf impairment.

2.2 The questionnaire survey

I accomplished the questionnaire survey to find out, what assistive technologies the physically disabled people use at the control of the computer. This questionnaire action concerned lecturers and the physically disabled people. At the lecturers, that learn the handicapped I found out what experiences they have with the teaching the physically disabled people on computers. I learned from physically disabled people, what tools for the control of the computer they use the most often.

I asked the lecturers what programs they teach, whether at the learning they use some assistive technology when teaching. My next question was whether they know in what line of work then the people with disabilities work. My next question was, whether at the teaching of internet they use the rules of web accessibility and the center facilitation in Windows.

The result of the questionnaire survey From the answers of the questionnaire given to the lecturers it arises, that they try to use the normal keyboard etc because the lecturers assume that the physically disabled people should use the normal device because at work they do not usually have assistive technologies. From the hardware they use the most often BigTrackBall, MID MEDIUM, and MID BIG. They do not have the influence at the learning of the Rules of web accessibility.

I asked again the disabled people about it whether they use some assistive technologies or they know the rules of web accessibility. the majority of the disabled people try to use the normal keyboard and they do not know the Rules of web accessibility and they do not almost use the center facilitation in Windows.

3 Conferences

Because I wanted to get acquainted with the newest technologies namely hardware and software that have been implementing today, I joined two conferences. The first conference INSPO 2012 took place in Prague and the second international conference ICCHP 2012 in Linz.

3.1 Conference INSPO 2012

The conference INSPO - Internet and information systems for the people with Specific Needs. It is the only conference in the Czech Republic that specialises in the use of Internet and information technology for the people with Specific Needs. This conference takes place by BMI association with the president Jaroslav Winter, Association of information systems for citizens with specific needs and Kri-zovatka.cz This conference is regularly held in Congress Center in Prague. This year it was held on 17.March 2012.

3.2 The schedule of the conference

The conference lasted one day and it was divided into the morning program, that all attended and into the afternoon program that was divided into sections. These sections were:

- Web (not only) Accessibility - This part concerned the web accessibility and further programs or libraries
- Education and Employment of the people with health disabilities - the section dealt with the education and the employed opportunities for the people with specific needs.
- Information and communication technologies for the people with the deaf impairment - This section dealt with technologies for people with the deaf impairment

The interesting information for me There were a lot of the interesting presentations at the conference, that is why I chose such presentations that have the most important meaning for me. From my point of view I am interested in presentations concerning the physically disabled people. (I am the physically disabled person) But there were also other interesting presentations as for example *Hybrid book* [4] or *free space for the web for disabled people* [5].

3.3 The conference ICCHP 2012

The conference ICCHP - International Conference on Computers Helping People with Special Needs is the conference that took place in Linz at the Kepler's university. This conference was organized by Kepler's university Linz and Masaryk university Brno. This conference deals with the facilitation of accessibility to the information technology for the people with health disabilities. It also deals with the learning of the various handicapped and next assistive technologies. This conference also deals with the life of the handicapped in various countries. This conference was between 11-13 July 2012.

The schedule of the conference The conference lasted three days. The conference was divided into the sections. Every section deals with the other part of needs for people with specific needs. Besides it contained three big talks. Everybody was present. This conference is the one most important in Europe. The attendance was really intentional. I chose such presentations, that concerned physically disabled people. There was not much of such contributions. There were such that they were related to the web accessibility and various next documents for example PDF files etc.

The interesting information for me There were a lot of the interesting presentations at the conference but I could not be present at each presentation. As at the first conference I chose such presentations according to my aim of the study. Some presentations were together as for example

Creating an Entertaining and Informative [6]

The next presentations were separated according to the interest of participants. That is why I was going into such sections, that dealt with physically disabled people. There were presentations as for example

Makind the Play Station 3 Accessible with AsTeRICS [3]

Indoor and Outdoor Mobility for an Intelligent Autonomous Wheelchair [7]

Identifying Barriers to Accessibility in Qatar [8]

Applying WCAG 2.0 principles to the world of PDF documents [9]

MainStreaming the creation of accessible PDF documents by rule-based transformation from Word to PDF [10]

4 Conclusion

At the meeting with standards I found out that they are principally concerned with visually disabled people and deaf disabled people and less mentally disabled

people. Next, I got acquainted you with the recent results of the questionnaire survey. I could learn thanks to my directing with hardware tools and tools in the operating system Windows.

Because I carried out the questionnaire survey I learned what assistive technologies physically disabled people use and whether they know the rules of web accessibility. I tried to meet with the progress in the world, that is why I participated in two conferences INSPO 2012 and ICCHP 2012.

Thanks to this I found out what assistive technologies and programs are created for the people with disabilities. But on both conferences there were the little presentations which concerned physically disabled people.

References

1. <http://www.helpnet.cz/inspo> (last access 31.7.2012)
2. <http://www.icchp.org/> (last access 31.7.2012)
3. <http://www.asterics.eu> (last access 31.7.2012), Ossman Roland, Making the Play Station 3 Accessible with AsTeRICS, Computers Helping People with Special Needs, 13th International Conference, ICCHP 2012, Linz, Austria, July 11-13, 2012, Proceedings, Part I, page 443
4. Hybrid book, Tomáš Gůra, Petr Hladík, Masaryk university Brno, Electronic collection INSPO 2012, Prague, Czech republic, March 17
5. Hosting services for NNO firm HEXAGEEK.CZ, Jan Kachlík, Masaryk university Brno, Electronic collection INSPO 2012, Prague, Czech republic, March 17
6. Creating an Entertaining and Informative Music Visualisation, Fels Deborah, Ryerson University, Toronto, Computers Helping People with Special Needs, 13th International Conference, ICCHP 2012, Linz, Austria, July 11-13, 2012, Proceedings, Part I, page 451
7. Indoor and Outdoor Mobility for an Intelligent Autonomous Wheelchair, Lin C.T, Kalifonsk sttn Universita, Computers Helping People with Special Needs, 13th International Conference, ICCHP 2012, Linz, Austria, July 11-13, 2012, Proceedings, Part II, page 172
8. Identifying Barriers to Accessibility in Qatar, Erik Zetterstrom, Computers Helping People with Special Needs, 13th International Conference, ICCHP 2012, Linz, Austria, July 11-13, 2012, Proceedings, Part I, page 235
9. Applying WCAG 2.0 principles to the world of PDF documents, Olaf Drmmer, firma Axaio, Computers Helping People with Special Needs, 13th International Conference, ICCHP 2012, Linz, Austria, July 11-13, 2012, Proceedings, Part I, page 587
10. MainStreaming the creation of accessible PDF documents by rule-based transformation from Word to PDF, Erle Marcus, Computers Helping People with Special Needs, 13th International Conference, ICCHP 2012, Linz, Austria, July 11-13, 2012, Proceedings, Part I, page 595
11. Computer and Handicaped, Jaroslav Hořejší, VŠB - Technical University of Ostrava, Wofex 2011, September 9-10, 2011, page 371

Methodology for Estimating Working Time Effort in the Software Projects

Ondřej Koběorský, Jakub Štolfa, and Martin Kopka

Department of Computer Science, FEECS,
VŠB – Technical University of Ostrava, 17. listopadu 15, 708 33 Ostrava – Poruba
{ondrej.kobersky, jakub.stolfa}@vsb.cz, martin.kopka@c4u.cz

Abstract. The precise estimation of the time effort of the project is one of the key limits of its success. One of the ways how to achieve a correct valuation of the project is developing of a detailed analysis, which output is a structured solution that uses use cases. This paper focuses on developing a methodology for estimating working time effort of the project for one particular company. An important part of the methodology is to build up and maintain comparative database of valued use cases and time progress of realized projects. The aim of the methodology is to deliver data for evaluating a new project.

1 Introduction

The proper estimation of the project is a goal which wants to achieve almost every project manager. It is hard task which takes a lot of effort to do it right and there are several ways how to fulfill it. Which one is the best is depending on the concrete company, concrete types of the projects etc.

1.1 Basic principles of estimations

Since our method is based on the use cases, we will mention only some methods utilizing the use case approach here.

The COCOMO methodology [1] computes the effort of the software projects as a function of program size and a set of cost drivers on separate project phases, it's described in [4].

Methodology introduced by [3] computes the project estimation using complexity of use cases and its transactions applying the set of adjustment factors.

Almost all methods, which use estimation based on use case points, are based on method of Gustav Karner. He first described use case points in [2]

We can say that our methodology is even based on the use case point, but it looks more precisely on the use case realization, that means text of the use case.

1 Definition of the problem

Our goal was to set up an estimation working time effort of projects in the particular company. Even that the company has 130 workers and lot of finished projects, people in this company were not used to estimate by some methodology. We tried to come with methodology or let's say supporting tool for estimating time effort of new projects. Our approach can help workers to estimate a new project by showing them average project progress of similar projects.

1.1 Initial state

The analysis in the company is made by use cases. These use cases are standardized. That means, if the use case deals with same repeatable issue, then it is almost similar to other use cases that are dealing with the same issue.

The capturing of the project progress is made by CRM system. In the CRM system you can see how much time was spent on each activity.

2 Proposal of the methodology

Methodology consists of two main processes. Rectangle is an activity; oval is input or output data to the activity.

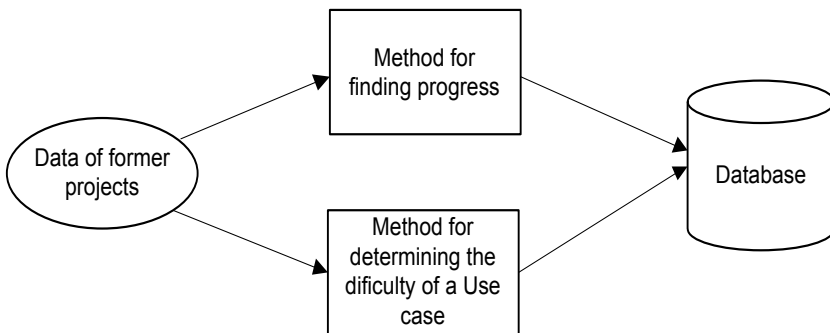


Fig. 1. Filling of the database.

The first process name is “Filling of the database” (Fig. 1). Here data about a recent project are filled into the database. These data are separately executed in two main methods as you can see.

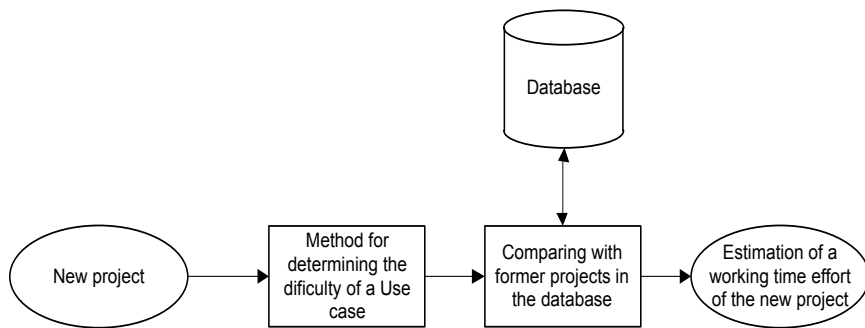


Fig. 2. Estimation of the new project

In case, that database is filed by the first process, the second process can be run. The Name of this process is “Estimation of the new project”, input is a finished analysis of new project with all required use cases. These use cases are elaborated in the activity “Method for determining the difficulty of a Use case”. It is the same method like in the process named “Filling of the database”. In second step process continues with the method named “Comparing with former projects in the database. The method compares former project in the filled database with data of the new project, finds similar project and estimate working time effort based on the similar projects progress. When the project is finished, the database could be extended by the new finished project. Next sections of this paper introduce particular steps of both processes.

Our method tracks progress of five main activities of the project as follows Consultation (with shortcut PORA), Analysis (ANAL), Programming (PROG), Testing (TEST), Implementation (IMPL).

Steps of the method finding progress.

- 1) **Input project data.** We need to know number of worked hours in each day for particular activities
- 2) **Setting number of segments.** Because every project last for different time period we split them for normalization. Methodology set default number of segments to 10.
- 3) **Evaluation of time period.** It means that we count all days – from the first day to the last day, when some of tracked activities were performed. Duration of project (number of days) is divided by number of segments (default 10). So that we know how many days the segment contains.
- 4) **Calculation.** We count number of hours spent on particular activity in each segment.
- 5) **Saving a result to the database.** Saving the result of the methodology is made by vectors. We can group these vectors and so that we can find out similar projects. Vectors are easily transferable to the graphs. Vector contains 5 segments as

follows name of the project, three numbers of particular difficulty of use cases contained in this project and worked hours of the activity in each segment.

2.1 Method for determining the difficulty of a Use case

Complexity of a project is given by the difficulty of UC realizations. The difficulty of UC is hard to determine, there is no easy benchmark for their comparison. We decided to determine the complexity based on number of rows, words and paragraphs in every UC. We have set 3 levels of difficulty for each criteria. For example we present criteria for number of rows:

- E (easy) – number of rows < 70
- M (medium) – number of rows $\in \langle 70; 110 \rangle$
- H (hard) – number of rows > 110

We declare overall difficulty, which is calculated from rows, words and paragraphs. Difficulty of words is considered as the most important aspect.

2.2 Comparing to former projects in the database

After we find that recent project are in the database which have almost similar difficulty of a use cases. We declare that two projects are similar if their particular difficulties differ by ± 2 . This simple differ was set up by several experiments made on real data in the company.

3 Conclusion and Future Work

Our methodology was tested on the 20 past projects made by the company. Fifteen projects were taken to the process of filling the database. Five projects were proclaimed as new projects. The result of our methodology was compared to the historical data of these projects. The difference between the predicted progress and the actual data for the tested projects was approximately 30%. The 30% inaccuracy seems not to be a good, but the previous ad-hoc human based estimation had inaccuracy of 40%. We found out these data by comparing their original estimations on the beginning of the projects with result of these projects at their ends. In 40 percent there was huge deflection of estimation and the real execution. Therefore our methodology brings approximately 10% improvement, which is a good result of the methodology.

In the future, we plan to improve our methodology by using neuron nets (SOM) and fuzzy rules as tools which find out groups of similar projects. In any case the topic of estimation project's effort is huge place for research and improvements. Our goal is to develop methods and that will be widely usable.

4 References

1. Boehm, B., Abts, Ch., Brown, W., Chulani, S., Clark, B., Horowitz, E., Madachy, R., Reifer, D., Steece, B.: *Software Cost Estimation with COCOMO II*. Englewood Cliffs, NJ:Prentice-Hall, 2000. ISBN 0-13-026692-2
2. Cohn, M.: *Estimating With Use Case Points, Methods and Tools*, Fall 2005 (Volume 13, number 3), ISSN 1661-402X.
3. Ochodek, M., Nawrocki, J., and Kwarciak, K.: *Simplifying effort estimation based on Use Case Points*. *Information and Software Technology*, 53(3):200–213, 2011.
4. Boehm B.: *Software Engineering Economics*, Prentice Hall, 1981.

Using Case-based Reasoning with Time-warped Data Collections

Tomáš Kocyan

Department of Computer Science, FEECS,
VŠB – Technical University of Ostrava, 17. listopadu 15, 708 33 Ostrava – Poruba
tomas.kocyan@vsb.cz

Abstract. This paper discusses possibilities of using the Voting Experts algorithm enhanced by the Dynamic Time Warping (DTW) method for improving performance of Case-Based Reasoning (CBR) methodology used with time-warped data collections. CBR, in general, is the process of solving new problems based on the solutions of similar past problems. Success of this methodology strongly depends on the ability to find similar past situations. The main goal of this paper is to provide suitable mechanism for retrieving typical patterns from distorted time series and thus improve the usability of CBR.

Keywords: Voting Experts, Segmenting, Information Retrieval, Episode-Based Reasoning, Case-Based Reasoning

1 Introduction

Many types of existing collections often contain repeating sequences which could be called as patterns [1]. If these patterns are recognized they can be for instance used in data compression or for prediction. Extraction of these patterns from data collections with components generated in equidistant time and in finite number of levels is now a trivial task. The problem arises for data collections that are subject to different types of distortions in all axes. This paper will focus on processing of measured river discharge volume, especially on finding typical patterns in this data collection. In my future research, such found patterns will be used for simulation of the rainfall runoff process and for prediction of discharge volumes in basins outlet cross section via CBR. The CBR methodology belongs to a group of artificial intelligence methods and it can be simply described as a process of solving new problems based on the solutions of similar past problems [2]. For achieving the best results using CBR, it is necessary to successfully manage the first algorithm's step - Retrieve the most similar cases. Many supervised and unsupervised methods for looking for patterns and similar situations exist, but the most of them have a common problem: they cannot handle searching for patterns of different lengths and they are not resistant to distortion. The Voting Experts algorithm is one of the algorithms that are able to handle these problems.

2 Voting Experts Algorithm

The Voting Experts Algorithm is a domain-independent unsupervised algorithm for segmenting categorical time series into meaningful episodes. It was first presented by Cohen and Adams [3] and it is based on the simple hypothesis that natural breaks in a sequence are usually accompanied by two statistical indicators [4]: low internal entropy of episode and high boundary entropy between episodes. For detailed explanation of each of mentioned steps see [3].

Proposed solution for Voting Experts improvement takes the task of using Dynamic Time Warping algorithm (introduced below) and high precision cuts as a starting point for looking for typical patterns located in the input. The basic idea is to refine the sparse set of high precision cuts into regular sequences as correctly as possible. The mentioned refinement will be done by simple principle (as shown in Fig. 1). If there are high precision cuts in the input (such as cuts A, B, C and D in Fig. 1) and if the shorter sequence (bounded by cuts C and D) is a subsequence of the longer one (bounded by cuts A and B), we can deduce new boundaries E and F by projecting the boundaries of common subsequence to the longer sequence. In this very simplified example the sequences were composed by definite number of values and limited length, so the evaluation is quite straightforward.

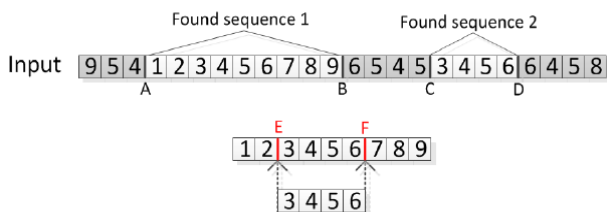


Fig. 1. The Longest Common Subsequence

In the case of application of previously mentioned process on distorted data, it is necessary to slightly modify it. Typical episodes of measurement of natural phenomena (such as precipitations, measured discharge volume etc.) are unfortunately subject to distortion in both time and value axes. For this reason, it is necessary to find out suitable mechanism that is able to deal with this deformation. The Dynamic Time Warping (DTW) algorithm can be used for this purpose. The DTW is a technique to find an optimal alignment between two given sequences under certain restrictions[5]. The sequences are warped in a nonlinear fashion to match each other. First DTW was used for comparing two different speech patterns in automatic speech recognition. In information retrieval it has been successfully applied to dealing with time deformations and different speeds associated with time-dependent data. For purposes of this paper, the DTW algorithm was modified for finding the longest common subsequence

of two sequences [6]. The main idea of the Voting Experts DTW Post-Process is summarized into the following steps:

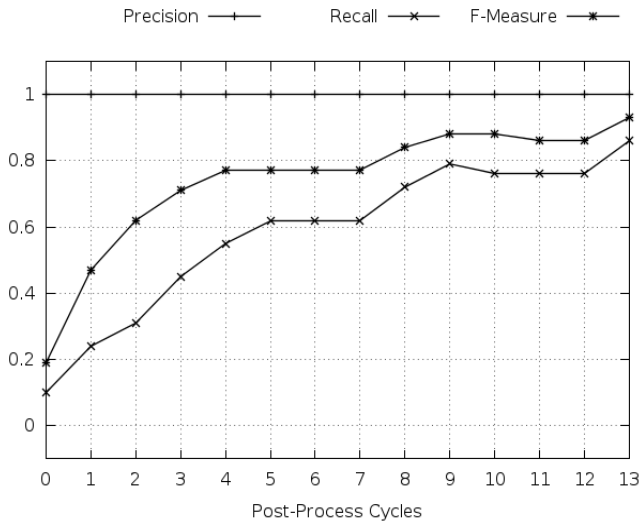
1. The high precision (but not complete) cuts are created by splitting the input with high level of threshold.
2. Let's suppose that there are m unique sequences which were created in step 1 and $m \times m$ distance matrix is build. For each pair in this matrix, where the length of sequence s_1 is bigger than length of sequence s_2 :
 - (a) The optimal mapping of s_2 to the s_1 is found by using modified DTW.
 - (b) If the mapping cost does not overcome selected threshold, the sequence s_1 stores the shorter sequence s_2 into its own list of similar sequences.
 - (c) Each of the shorter sequences points to positions in the longer sequence, where it should be split. Because there is usually more than one similar shorter sequence, it is pointed to several locations. For this reason, the votes are collected into internal vote storage.
 - (d) After these votes are collected, the local maximums are detected. These places are suggested as new cuts in original input.
3. The granted votes from step 3(d) are summed with votes of frequency and entropy experts in the input. Subsequently, the local maximums of votes are searched again. The cuts are made in locations where the number of granted votes is higher than the specified threshold.
4. Algorithm ends or it can continue with step 2 for further refinement.
5. After each post-process iteration, all found patterns can be received from the 3(b) step. Actually, the found patterns are groups of similar chunks.

3 Experiments

First of all, the algorithm was tested on artificial collection. This collection was generated from simple patterns, which were randomly repeated to the total input's length of 200 elements. On this data collection, the original Voting Experts algorithm was executed with many configurations and the best result was taken. Then, with the same data, the proposed algorithm was tested in many configurations and also the best result was taken. For the evaluation of proposed algorithms performance, precision and recall coefficients were defined. In this case, the precision coefficient will be understood as the ratio of the amount of correct spaces induced by algorithm to the entire number of induced spaces. Recall will represent the ratio of the amount of correct induced spaces to the entire amount of spaces in input. To get high precision cuts for post-processing, the value of threshold had to be increased and followed by particular count of post-process cycles. The comparison of both versions of algorithm's success is presented in Table 1. It is evident that proposed algorithm significantly outperforms the basic version of Voting Experts in all evaluation indicators and increases its performance. The fact that the precision indicator still takes the value of 1 means that algorithm did not make any wrong cuts. Graphical representation of the progress of all indicators after each post-process cycle is in Fig. 2.

Table 1. Evaluation with Normal Collection

Algorithm	Precision	Recall	F-Measure
Basic VE	0.71	0.68	0.70
VE with Post-Process	1.00	0.86	0.93

**Fig. 2.** Progress of Evaluation Indicators

The second experiment was executed on distorted version of the previous data collection. Applied distortion randomly manipulated with length of patterns (elements of patterns were repeated or omitted) and its amplitude. The results of the experiment are shown in Table 2. It is evident that the original Voting Experts algorithm cannot work with distorted data and its accuracy rapidly decreases. The proposed solution's accuracy decreases too, however it still provides better result with distorted input than the basic version on regular input.

Table 2. Evaluation with Distorted Collection

Algorithm	Precision	Recall	F-Measure
Basic VE	0.48	0.58	0.53
VE with Post-Process	0.91	0.72	0.81

The last experiment was executed with river data obtained from the U.S. database - USGS (U.S. Geological Survey) Water Data for the Nation. The discharge data (CFS - cubic feet per second) from stations located on the main rivers in the U.S.A. (years from 1986 to 2007, 30 min. step) was used for practical

demonstration of proposed algorithm. For this data collection, the exact real boundaries are not known, so it is impossible to numerically evaluate success of the algorithm. For this reason, the results of the algorithm will be evaluated only visually and the examples of found patterns will be presented. The algorithm was executed with the same configuration as in the example above. The found patterns are shown in Fig. 3.

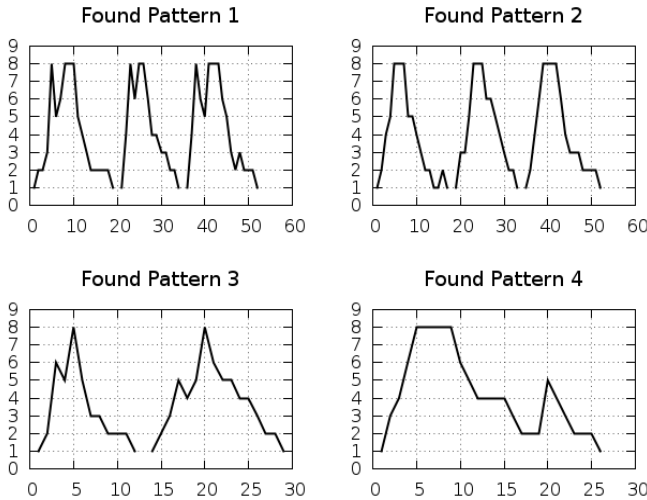


Fig. 3. Segmentation of English Text.

4 Conclusion

The tests showed that proposed algorithm is able to successfully split input data into the meaningful episodes and then find characteristic patterns in both regular and distorted collections. Proposed alternative approach outperforms the original Voting Experts algorithm in all evaluation indicators and moreover, it is more immune to working with distorted inputs. Future research will be focused on optimizing and improving proposed algorithms performance, especially on automatic settings of configurations parameters, which have to be set manually for now. Additionally, the research will focus on the modification of DTW for receiving characteristic patterns from a group of similar episodes.

5 List of Relevant Publications

FLOREON⁺: Using CBR in System for Flood Predictions.

Kocyan, T., Martinovic, J., Unucka, J., Vondrak, I.,
Disaster Management and Human Health Risk: Reducing Risk, Improving Outcomes.

Hydrometeorologic Social Network With CBR Prediction.

Kocyan T., Martinovic J., Valickova A., Sir B., Horinkova M., Rihova V.,
ECMS 2010, Kuala Lumpur 2010-07-31.

Competency-based human resources allocation in business process simulations.

Kuchar S., Martinovic J., Kocyan T.,
ESM 2011, Guimaraes, Portugal, August 2011.

Czech text segmentation using voting experts and its comparison with Menzerath-Altmann law.

Kocyan, T., Martinovic, J., Dvorsky, J., Snasel, V.,
In Proceedings of CISIM 2011, India, December 2011.

Unsupervised Algorithm for Post-Processing of Roughly Segmented Categorical Time Series.

Kocyan, T., Martinovic, J., Kuchar, S., Dvorsky, J.,
In Proceedings of Dateso 2012. Žernov, Czech Republic, April 2012.

Dynamic Time Warping in Analysis of Student Behavioral Patterns.

Slaninova, K., Kocyan, T., Martinovic, J., Drazdilova, P., Snasel, V.,
In Proceedings of Dateso 2012. Žernov, Czech Republic, April 2012.

References

1. Theodoridis, S., Koutroumbas, K.: *IPattern Recognition. Third Edition.* Academic Press., 2006.
2. Aamodt: *Case-Based Reasoning: Foundational Issues.* Methodological Variations & System Approaches, AI Communications, Vol. 7 Nr. 1, March 1994.
3. Cohen, P. R., Adams, N.: *An Algorithm for Segmenting Categorical Time Series into Meaningful Episodes.* Proceedings of the Fourth Symposium on Intelligent Data Analysis, Lecture Notes in Computer Science. 2001.
4. Cohen, P. R., Adams, N., Heeringa, B.: *Voting Experts: An Unsupervised Algorithm for Segmenting Sequences.* To appear in Journal of Intelligent Data Analysis. 2007.
5. Muller, M.: 2007. *Dynamic Time Warping.* Information Retrieval for Music and Motion, Springer, ISBN 978-3-540-74047-6, 69–84.
6. Kocyan, T., Martinovic, J., Podhoranyi, M., Vondrak, I.: *Unsupervised Algorithm For Retrieving Characteristic Patterns From Time-Warped Data Collections,* EMS 2012, Vien

Estimation of the Project or Use Case Parameters Using SOM and Fuzzy Rules

Martin Kopka, Jakub Štolfa, and Ondřej Koběřský

Department of Computer Science, FEECS,
VŠB – Technical University of Ostrava, 17. listopadu 15, 708 33 Ostrava – Poruba
martin.kopka@c4u.cz

Abstract. Many decisions realized during project estimation and planning are based on previous experience and competency of the manager. Evaluated realized/completed projects provide rich knowledge about similar decisions and reality. This paper focuses on the approach how to estimate value of specific parameters of the projects utilizing parameterized use case model. The proven methods are used for this estimation – SOM for grouping similar use-cases and fuzzy rules for calculating the search parameter value. An important part of the approach there is to build up and maintain comparative database of valued use cases.

1 Introduction

Many decisions during project estimation and planning are based on previous experience, competency, and even intuition of project managers. There are many parameters that can help managers with this decision process, especially in case when knowledge about previous similar projects is available. It is possible to find analogy among planned project and previous (evaluated) projects and utilize it for the estimation of work effort, risk factors, and other parameters of the new project.

It is important to mention that presented decision support approach takes place after the analysis phase of the software development process.

The approach was evaluated on several specific software development projects. We obtained a knowledge base of parameterized real world project use cases created by certain software development company. Most parameter values were set at project analysis phase but some of parameter values (specifically the unexpected additional work, testing complexity) were updated after projects completion to reflect the real state of the project.

When a new use case is to be planned and calculated, it is important to estimate the risk of additional work and level of potential complexity. An accurate estimation of needed work effort is important for project scheduling, pricing, resource allocation, and project management.

The project estimation methodologies and approaches are usually based on software project parameter analysis and rely on known static relationship between parameters. In contrast, the presented approach is based on data mining and machine learn-

ing. The method learns the relations and rules from provided knowledge base and in reality it creates a model of particular company with its business processes, software development processes, team management etc.

The paper is organized as follows: Section 2 introduces the methods used for the estimation and describes the logic of our approach: the parameterization of the recent use cases, the parameterization and adding of the new use case, the clustering the data by SOM, the processing of the cluster by fuzzy rules, and the estimation of the extra work parameter; Section 3 depicts realized experiment; concluding Section 4 provides a summary and discusses the planned future research.

2 Description of the logic of the approach

The Fig. 2 depicts simplified view of process of current approach. In the left side of the figure are values parameterizations of the particular use cases. This set of the use cases is divided to the two parts. The first part is fulfilled by use cases of recent projects. The second part is fulfilled only by one use case of a new project. The process continues by processing of the use cases by self-organizing map. There you can see a map with the dots and one cross. The cross represents the current new use case. Then cluster, which contains this new use case, is chosen and processed by fuzzy rules. That is a step how to predict parameters of a use case that we can know even after project. It means that we can predict parameter “extra work”.

Step 1 – The parameterization of the recent use cases

We set values of particular use cases of recent projects. This step is important to be executed only one time.

Step 2 – The parameterization and adding of the new use case

The new project is started. It means that we have its particular use cases, which has particular parameterization that is made after writing of the use case. It has set of all the parameters besides of extra work parameter, which we really know only after project closing.

1. We add current use case of the new project. Like it was mentioned above, current use case has set of all parameters besides extra work parameter.
Note that, if the project has more use cases, we run the steps of the approach individually for each particular use case. It means that if the new project has 50 use cases, steps of the approach are run 50 times.
2. We have stored data about recent use cases. We have reached these data in the step 1.

Step 3 – The clustering of the data by SOM

We cluster the data, which we reached in the step 2, by SOM algorithm. Then we find out that which cluster contains that new use case.

For the extra work prediction we want to know which use-cases are “similar” to the new one. We cluster the new use-case with all, already implemented use cases. It is important to note that the extra work is known for all historical use cases. Kohonen’s maps are used for use case clustering.

In all experiments we present $X + 1$ parameterized use cases to SOM algorithm. X are historical use cases with known the extra work, $+1$ represents one new use case for which we want to predict the extra work.

SOM algorithm sorts input use-cases into the clusters. There are two possibilities:

- Use case felt somewhere outside of the main clusters. We don't estimate its extra work, because the new use case is too different from the historical use cases.
- Use case felt in one of the clusters and the approach continues with next step

Step 4 – The processing of the cluster by fuzzy logic

In this step we take only recent use cases, which are in the particular cluster with a new use case. Then we include one more parameter. It is extra work parameter. We find out fuzzy rule to estimation of the extra work parameter by fuzzy logic.

Step 5 – The estimation of the extra work parameter

We have the fuzzy rule that has some probability of the estimation of an extra work parameter. We are able to estimate the probability of the estimation. The more the probability of estimation is higher, the more proper estimation we will reach.

3 Realized experiment

The following experiment was realized with the aim to confirm the approach described in chapter 2. The data was collected from a software development company that systematically created use cases for the number of their projects.

In summary, the knowledge base contained a collection of 135 parameterized use cases from analyzed projects. We took 130 of them as a base for clustering and knowledge database; the remaining 5 use-cases were used as a test set (i.e. they acted as new use cases although we already knew their extra work – xwork).

We use following parameters of use cases for the clustering: difficulty rows, difficulty paragraphs, difficulty words, overall difficulty, NSC, concerned processes and testing level. We will use following process for each use case from this set:

1. make a new clustering including this new use case, for example

	Dif. Rows	Dif. Parag	Dif. Words	Overall dif.	N/S /C	Testing level
Example 1	2	2	2	2	1	1

2. specify to which cluster the new use case belongs, for example

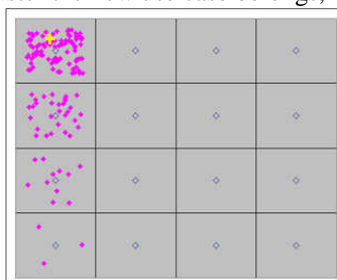


Fig. 1. SOM output grids for Example 1

3. calculate the fuzzy rule for estimation of the xwork for this cluster and
4. apply the rule for estimation of xwork for the new use case

Kohonen maps

We set used SOM algorithm as follows: number of observations is 131, number of variables is 6, n-square of neurons is 4, number of training cycles is 500 with randomize presenting of input to the algorithm. Learning parameter is set to start value 0,9 and end value 0,1.

Fuzzy rules

The xwork parameter was estimated by the artificially evolved fuzzy rules. The training data was for each verification record clustered using the SOM algorithm and a fuzzy rule was evolved for each cluster. The verification record was evaluated by the rule found for the class it belonged to. Finally, predicted and real xwork were compared.

Due to the stochastic nature of the artificial evolution, all experiments were repeated 10 times. Table 1 summarizes the results of artificial evolution of fuzzy rules for clusters in all five examples mentioned above. It shows that the algorithm was able to extract the rules describing the presence of extra work in different clusters in the training data set with good precision of 80% and more (however, we note that especially the small clusters might not contain enough information).

The extra work estimation of a use case by fuzzy rule requires the substitution of the feature names by (normalized) feature values from the use case. Then, the rule evaluation is done according to the formulas given in [6, 5] and it results into a single real number from the range [0, 1]. A value greater than 0.5 is interpreted as extra work, value bellow 0.5 is interpreted as no extra work. Obviously, the evaluation of new use cases by the fuzzy rule is inexpensive and fast. The summary of the precision of extra work estimation for previously unknown use cases is given in table 1. The table shows for each test use case (example) whether the best found rule classified the extra work correctly (2nd column) and the percent of fuzzy rules evolved by the genetic programming that at the end correctly estimated the xwork for the use case (3rd column).

Apparently, the genetic programming was able to find fuzzy rules that estimated the extra work for examples 1, 2, 4 and 5 correctly in 80 – 100 percent. An exception was the example 3 for which all evolved fuzzy rules featured the same training fitness of approx. 87 percent (i.e. the best fuzzy rule could not be determined) and only 3 out of the 10 evolved rules correctly estimated the xwork for the test use case.

Table 1. Results of verification use case classification

Example	Classification by best fuzzy rule	Pct. of successful rules
1	Correct	80
2	Correct	90
3	NA	30
4	Correct	90
5	Correct	100

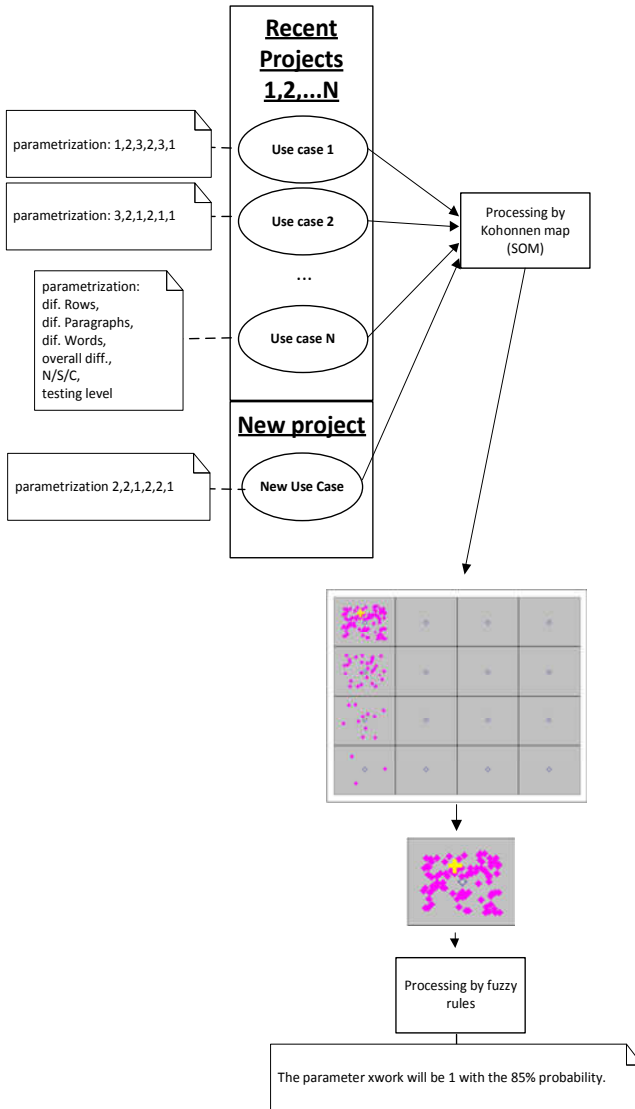


Fig. 2. The logic of the approach

4 Conclusion and future works

The introduced approach showed how the parameterized use case driven model can be used for the estimating of the really evaluated parameters (values) of new use case. The procedure of the estimating is based on clustering of the set of known use cases and the new one by the SOM method. Derived fuzzy rule for the known use cases

from the cluster containing also the new use case helps us to calculate the really evaluated parameter for the new use case.

The chosen methods of SOM and evolutionary fuzzy rules yielded promising results but a number of other soft and hard clustering (e.g. fuzzy c-means clustering, k-means clustering, NMF based clustering), and soft and hard prediction methods (e.g. ANFIS, Flexible Neural Trees) and their combinations can be evaluated for software project features.

References

1. Crestani, F., Pasi, G.: Soft information retrieval: Applications of fuzzy set theory and neural networks. In: N. Kasabov and R. Kozma, editors, *Neuro-Fuzzy Techniques for Intelligent Information Systems*, pages 287–315. Springer Verlag, Heidelberg, DE, 1999.
2. Klir, G.J., Yuan.B.: *Fuzzy Sets and Fuzzy Logic. In; Theory and Applications*. Prentice Hall, Upper Saddle River, N. Y., 1995.
3. Kraft, D. H., Petry, F. E., Buckles B. P., Sadasivan, T.: Genetic Algorithms for Query Optimization in Information Retrieval: Relevance Feedback. In: E. Sanchez, T. Shibata, and L.A. Zadeh, editors, *Genetic Algorithms and Fuzzy Logic Systems*, Singapore, 1997. World Scientific.
4. Krömer, P., Platoš, J., Snášel, V., Abraham, A., Prokop, L., Mišák, S.: Genetically evolved fuzzy predictor for photovoltaic power output estimation. In: 2011 Third International Conference on Intelligent Networking and Collaborative Systems (INCoS), pages 41 – 46. IEEE, 2011.
5. Krömer. P., Snášel, V., Platoš, J.: Learning patterns from data by an evolutionary-fuzzy approach. In: *Soft Computing Models in Industrial and Environmental Applications*, 6th International Conference SOCO 2011, volume 87 of *Advances in Intelligent and Soft Computing*, pages 127–135. Springer Berlin / Heidelberg, 2011. 10.1007/978-3-642-19644-7-14.
6. Snášel, V., Krömer, P., Platoš, J., Abraham, A.: The evolution of fuzzy classifier for data mining with applications. In: SEAL, volume 6457 of *Lecture Notes in Computer Science*, pages 349–358. Springer, 2010.
7. Zadeh, L.A.: Fuzzy sets. In: *Information and Control*, 8:pp. 338–353, 1965.
8. Kohonen, T.: The Self-Organizing Map. In *Proceedings of The IEEE*, vol. 78, NO. 9, September 1990
9. Vesanto, J., Alhoniemi, E.: Clustering of the Self-Organizing Map. In: *IEEE Transactions on neural networks*, vol. 11, NO. 3, May 2000
10. Cohn, M.: *Estimating With Use Case Points, Methods and Tools*, Fall 2005 (Volume 13, number 3), ISSN 1661-402X
11. Heemstra, F.J.: Software cost estimation. In: *Information and Software Technology*, Vol. 34, No 10, October 1992, Elsevier.
12. Ochodek, M., Nawrocki, J., and KwarciaK, K.: Simplifying effort estimation based on Use Case Points. In: *Information and Software Technology*, 53(3):200–213, 2011
13. Bente, A, Hege, D., Dag, I., Sjoberg, K., Jorgensen, M.: Estimating Software Development Effort Based on Use Cases-Experiences from Industry. In: 2011 Proceedings of the 4th International Conference on The Unified Modeling Language, Modeling Languages, Concepts, and Tools (UML'01). Springer-Verlag, London, 2001.
14. Štolfa, J., Štolfa, S., Koběřský, O., Kopka, M., Kožuszník, J., Snášel, V.: Methodology for Estimating Working Time Effort of the Software Project, In: 2012 Databases, Texts, Specifications, and Objects (DATESO), pages 25-37, 2012

Analysis of Web Pages Using Schema.org Collection

Jonáš Krutil, Miloš Kudělka, and Václav Snášel

Department of Computer Science, FEECS,
VŠB – Technical University of Ostrava, 17. listopadu 15, 708 33 Ostrava – Poruba
{kru178, milos.kudelka, vaclav.snasel}@vsb.cz

Abstract. Internet provides access to a huge amounts of information. Unfortunately these information can be structured-viewed-formatted in various and not formal ways. The result is that extracting relevant data from more than one known source is very difficult. In this article we want to introduce the identification and extraction of relevant information from the web pages using collection of schemas — schema.org. Our work is focused on use of schemas collection to classify these various web pages. We expect this procedure can be used to improve the accuracy of web search query. Genres of web pages can be clearly identify and classify as the results of our experiments with schemas collection which provide a clear semantic structure of source code. Our approach can be easily extend to other formats such as microformats, RDFa, data-vocabulary.org and more.

1 Introduction

Internet can be considered as the world's largest information library. We can imagine single books in the library as an individual web pages. There is no one who can classify them according to specific topics in the shelves. It's not an easy way to be and stay oriented in the amount of unstructured information.

Our aim is offer to users more effective way of orientation and assigned to each webpage with schema collection new auxiliary labels as „Movie“, „Person“, „Recipe“, „Blog“ or „Price information“. Identify web page genres and microgenres and offer to users more detailed search possibilities which can lead to much more relevant content. Existing web pages globally lack a better semantics to provide similar advanced search options to the user.

In order to provide detailed and relevant information on the web search content, collection of microdata schemas schema.org was created in 2011. It extend family of existing RDF [1], Microformats [2] and microdata [3] to their gradual replacement [4]. This collection gives us an uniform and formal set of rules and recommendations that allow us to add significantly better semantic information to the web page source code.

Major global web search engines Bing, Google, Yahoo! and Yandex who overarching schema.org project, committed to support microdata future. Their search algorithms are extended to support microdata schemas gradually. Currently most widely used and supported schema is the recipe.

Our work focuses on the unique identification of specific genres and microgenres [5] using the microdata schema collection. Extraction of semantic information and classifying web pages. About the content of web pages we analyzed, we can determine the amount of additional information which can be used to expand web search options, more accurate search results and others.

2 Related work

Apart from schema.org microdata schemas collection is there several other formally defined rules for the semantic web. These semantic web languages are presented in [9]. Also systems for web information extraction which transform web pages into program-friendly structures such as a relational database are important to us. This approach analyzes the structure and the templates of the web page. The survey of major web information extraction approaches is presented at [10]. Concept of Genres and MicroGenres is introduced at [5] as ambiguous categories without fixed boundaries and are especially formed by the sets of conventions. Authors of paper [7] analyze web pages using a web patterns and introduces a method for semantic analysis of web pages.

3 Our research

In contrast to the above approaches is the information located in the source code by tags and attributes essential to us and our approach cannot be applied to plain text only. Our algorithm uses a specific semantic attributes and the information they marked.

For our experiments we chose schema of Recipe, the most widely used schema and being supported by web search engines mentioned above.

Our aim was to analyze the source code of a sufficient number of web pages that publish articles about cooking. We want try to clearly identify the Recipe schema and obtain on the basis of our analysis additional semantic information about a particular web page. We went manually through hundreds of international and domestic recipe web sites, looking for pages that contain information about the Recipe schema, possibility rate the recipe by stars and have option write a user review. Our results from human browsing were compared with our results from algorithm using a microdata collection schema.org.

4 Microdata collection — Schema.org

Schema.org goal is to get back unambiguous meaning of the information that is lost during the transfer from the database (information in database is clearly divided and described in the tables, their columns and rows) to the application presentation layer.

Collection of schemas is used to restore that lost information back into the source code of web pages and offers the possibility to extend the semantic meaning even further. If we are talking about semantically unstructured data, we imagine them as plain text with some html tags:

```
<h1>Mom's World Famous Banana Bread</h1>
By John Smith
May 8, 2009

This classic banana bread...

<strong>Nutrition facts:</strong>
240 calories, 9 grams fat

<strong>Ingredients:</strong>
- 3 or 4 ripe bananas, smashed
- 1 egg
...
```

People can read this information and understand the meaning of its individual parts, but search engine crawler will not understand the meaning so well. Information will be stored in a search engine database as a plain text inside some general table probably. Maybe just add to some words more weight thanks to the importance of html tag. If you assign a schema to our data above, the result for the search engine crawler will be much more readable:

```
<div itemscope itemtype="http://schema.org/Recipe">
  <h1 itemprop="name">Mom's World Famous Banana Bread</h1>
  By <span itemprop="author">John Smith</span>,
  <meta itemprop="datePublished" content="2009-05-08">May 8, 2009
  
  <span itemprop="description">This classic banana bread...</span>

  <div itemprop="nutrition"
    itemscope itemtype="http://schema.org/NutritionInformation">
    <strong>Nutrition facts:</strong>
    <span itemprop="calories">240 calories</span>,
    <span itemprop="fatContent">9 grams fat</span>
  </div>

  <strong>Ingredients:</strong>
  - <span itemprop="ingredients">3 or 4 ripe bananas, smashed</span>
  - <span itemprop="ingredients">1 egg</span>
  ...
</div>
```

The information described using microdata is much better semantically structured [6]. We can see that the text belongs to the genre of Recipe has its own name, author, published date and recipe description. Also we have clearly listed the individual ingredients and nutritional information. Now we can store these semantic results into recipe tables with appropriate properties.

4.1 Algorithm

The algorithm parses source code of web pages that is divided into several blocks by `itemscope` and `itemtype` attribute. With this procedure we obtain clear information if the recipe schema is on the website or is not. Because we are searching for recipe schema, algorithm at first seeks for `itemscope` with "Recipe" and then inside the returned data blocks is looking for additional information (`aggregateRating`, `Review`) using values in `itemprop` attribute.

```
<div itemscope itemtype="http://schema.org/Recipe">
  <div itemprop="aggregateRating" itemscope itemtype="http://sche-
ma.org/AggregateRating">
    <span itemprop="ratingValue">4</span> stars - based on
    <span itemprop="reviewCount">250</span> reviews
  </div>

  <div itemprop="review" itemscope itemtype="http://schema.org/Re-
view">
    <span itemprop="name">Great recipe</span> - by
    <span itemprop="author">Ellie</span>,
    <div itemprop="reviewRating" itemscope
itemtype="http://schema.org/Rating">
      <meta itemprop="worstRating" content = "1">
      <span itemprop="ratingValue">4</span>/
      <span itemprop="bestRating">5</span>stars
    </div>
    <span itemprop="description">Delicious!</span>
  </div>
</div>
```

This procedure clearly identify the web page containing the microdata schema with the recipe, ratings and reviews of users. It should be noted that the algorithm is language independent and if the schema is written according to specifications then detection achieves 100% success rate. Algorithm can be easily extended to other schemas of the collection and we are able to identify and extract all the information that are described within the collection. It gives us the possibility to easily extract specific information that is important to us within a web page. This information can be used for advanced search features, personalization results [8] or for other applications working with structured data.

4.2 Genres & MicroGenres

Web pages that use collection of schemas are logically divided into blocks and clearly describing genres and some microgenres [5] for every website. For example, we can obtain "information about the price" for a particular product. This microgenre is usable if you are considering buying a product and your search results are only the product reviews and message boards. The content of such a web pages we do not want to include because there is no shopping possibility. We can offer to the user the ability

to view only web pages that contain "information about the price," and other web pages are filtered out in favour of the relevant results.

Actual genre of web page can then be determined by the name of the collection. Also we obtain the individual labels "Movie," "Person", "Recipe" and others as mentioned above. The search can become much more comfortable for users.

We also mentioned that the recipe genre is currently the the most widely used schema. Its implementation by Google and Yahoo! is shown in the figures (Fig. 1, Fig 2).



Fig. 1. Recipe schema by Google.com



Fig. 2. Recipe schema by Yahoo.com

5 Conclusion

Due to the dependence of the schemas and semantic structure of source code our approach is not universal. Also schemas can be currently found only in a limited number of web pages. However it is clear already that web search engines will be pushing web developers to write their source code with microdata. Web developers should want to create semantic source code, because their website will be more visible

in search engine results. We think that in the collection of schemas schema.org is the future of web semantics.

In the near future, we want to focus on web pages that contains no schema information but they should because they belongs to any of them. We will be analyze these web pages and trying to find a way to recommend add schema by the text semantic meaning.

References

1. Brickley, D., Guha, R. V.: RDF Vocabulary Description Language 1.0: RDF Schema, (2004, February). World Wide Web Consortium (W3C). Retrieved from <http://www.w3.org/TR/rdf-schema/>
2. About Microformats, Retrieved from <http://microformats.org/>
3. Hickson, I.: HTML Microdata, (2012, March). World Wide Web Consortium (W3C). Retrieved from <http://www.w3.org/TR/microdata/>
4. Schema.org FAQ, (2012, January). Google Inc. Retrieved from <http://support.google.com/webmasters/bin/answer.py?hl=en&answer=1211158>
5. Kudelka, M., Snasel, V., Horak, Z., Abraham, A.: MicroGenre: Building block of web pages, Networked Digital Technologies (2009, July)
6. Bradley, S.: Why (And How) You Should Use HTML5 Microdata, (2011, August). Van SEO Desig. Retrieved from <http://www.vanseodesign.com/web-design/html5-microdata/>
7. Kudelka, M., Snasel, V., Lehecka, O., El-Qawasmeh., E.: Semantic Analysis of Web Pages Using Web Patterns, Web Intelligence (2006) 329–333
8. Eirinaki, M., Vazirgiannis, M.: Web mining for web personalization, ACM Transactions on Internet Technology (TOIT), Vol. 3 Issue 1 (2003) 1–27
9. Bailey, J., Bry, F., Furche, T., Schaffert, S.: Web and Semantic Web Query Languages: A Survey. In J. Maluszinsky and N. Eisinger, editors, Reasoning Web Summer School 2005, pages 35–133. Springer-Verlag, LNCS 3564, (2005)
10. Chang, C.-H., Kayed, M., Girgis, M. R., Shaalan, K. F.: A survey of Web information extraction systems. IEEE Transactions on Knowledge and Data Engineering, 18(10):1411–1428, (2006, October)

Compression – based Similarity

Michal Prílepok, Jan Platoš, and Václav Snášel

Department of Computer Science, FEECS,
VŠB – Technical University of Ostrava, 17. listopadu 15, 708 33 Ostrava – Poruba
{michal.prilepok, jan.platos, vaclav.snasel}@vsb.cz

Abstract. One of the important areas of data mining is ability to determine similarity between files. To determine similarity rate we can use different methods, to sort files into groups and extract best candidates to reach our goal. This paper describes experiments in this direction, and compares the results of few metrics and compression algorithms. Successful rate of an individual metric depends on used compression method.

Keywords: data compression, similarity, metric

1 Introduction

Vitanyi and his co-workers have reported some success using a universal similarity metric based on Kolmogorov complexity for a variety of classification tasks for example music, images, genre recognition or texts. This paper describes experiments in this direction, and compares the results of few metrics and compression algorithms.

Successful rate of an individual metric depends on used compression method. We compared following metrics: Universal Similarity Metric, Normalized Compression Distance, Compression-based Dissimilarity Measure and Compression-based Cosine [1].

The organization of this paper will be as follows. Section 2 describes used similarity metrics. Selected compressions are described in Section 3. The results of our experiments are described in Section 4 and Section 5 contains conclusion of this paper.

2 Metrics

Formally, a distance is a function D with nonnegative real values, defined on the Cartesian product $X \times X$ of a set X . It is called a metric on X , if for every $x, y, z \in X$:

- $D(x, y) = 0$ if $x = z$ (the identity axiom);
- $D(x, y) + D(y, z) \geq D(x, z)$ (the triangle inequality);
- $D(x, y) = D(y, x)$ (the symmetry axiom).

A set X provided with a metric is called a metric space. For example, every set X has the trivial discrete metric $D(x, y) = 0$ if $x = y$ and $D(x, y) = 1$ otherwise. [1]

2.1 Universal Similarity Metric

The most outstanding metric based on Kolmogorov complexity is the Universal Similarity Metric (USM) proposed by Li et al.

This USM has been used for detect similarity mitochondrial genomes, cluster SARS virus, musical pieces, image, detect plagiarism of student assignments. But it fails to compare TOPS diagrams. [2]

Resulting rate of probability distance is calculated by the following formula:

$$USM(x, y) = \frac{\max(C(xy) - C(x), C(yx) - C(y))}{\max(C(x), C(y))}$$

Where:

- $C(xy)$ is length of compression concatenation of x and y ;
- $C(x)$ is length of compression of x ;
- $\max(x, y)$ is maximum of values x and y ;
- $\min(x, y)$ is minimum of values x and y .

The USM is in the interval $0 \leq USM(x, y) \leq 1$. If $USM(x, y) = 0$, then files x and y are equal. They have the highest difference when the result value of $USM(x, y) = 1$.

2.2 Normalized Compression Distance

Normalized Compression Distance (NCD) is a mathematical way for measuring similarity of objects. Measuring of similarity is realized by the help of compression where repeating parts are suppressed by compression. It is based on algorithmic difficulty of the Normalized Information Distance (NID) developed by Andrey Kolmogorov. NCD may be used for comparison of different objects, such as images, music, texts or gene sequences. NCD has requirement to compressor. Compressor meet the condition $C(x) = C(xx)$ within logarithmic bounds. [3] We may use NCD for detection of plagiarism and visual data extraction. [4]

Resulting rate of probability distance is calculated by the following formula:

$$NCD = \frac{C(xy) - \min(C(x), C(y))}{\max(C(x), C(y))}$$

Where:

- $C(x)$ is length of compression of x .
- $C(xy)$ is length of compression concatenation of x and y .
- $\min\{x, y\}$ is minimum of values x and y .
- $\max\{x, y\}$ is maximum of values x and y .

The NCD is in the interval $0 \leq NCD(x, y) \leq 1$. If $NCD(x, y) = 0$, then files x and y are equal. They have the highest difference when the result value of $NCD(x, y) = 1$.

2.3 Compression-based Dissimilarity Measure

Compression-based Dissimilarity Measure (CDM) is response to NCD. It is called "simpler measure", but avoiding theoretical analysis.

$$CDM(x, y) = \frac{C(xy)}{C(x) + C(y)}$$

Authors of this metric are aware that CDM is nonmetric, failing the identity property. CDM give values in the range of $[\frac{1}{2}, 1]$, where $\frac{1}{2}$ shows pure identity and 1 shows pure disparity.[3]

2.4 Compression-based Cosine

$$CosS(x, y) = 1 - \frac{C(x) + C(y) - C(xy)}{\sqrt{C(x)C(y)}}$$

This measure is normalized to the range $[0,1]$, with 0 showing total identity between the files x and y , and 1 total dissimilarity. [3]

3 Compression algorithms

Compression allows us to eliminate recurring parts in the file. The resulting size of the compression can be considered as the minimum amount of information in the file. This value is used in the calculation of metric.

All metrics were tested with following compression methods LZW, Adaptive Huffman, BurrowsWheeler, LZ77 and LZSS with various settings. List of all compressions and their settings is listed below.

1. LZW
2. Adaptive Huffman
3. BurrowsWheeler with Adaptive Huffman Encoding
4. BurrowsWheeler with Adaptive Huffman Encoding, RLE and Fibonacci Encoding
5. LZ77, DirectBit, 256
6. LZSS lazy, DirectBit, 256
7. LZ77, Huffman, 256
8. LZSS, Huffman, 256
9. LZSS lazy, Huffman, 256

4 Results

These algorithms and metrics were tested in database of 48363 spam email files. Individual file was sequentially compared with other files from file database. The results are depicted in tables 1, 2, 3 and 4.

Theoretical results range in USM metric met LZW, Adaptive Huffman, BurrowsWheeler with Adaptive Huffman Encoding and BurrowsWheeler with Adaptive Huffman Encoding, RLE and Fibonacci Encoding compression algorithms. The best success in the same files detection achieved BurrowsWheeler with Adaptive Huffman Encoding algorithm with success 54.49%.

In NCD metric useful are following algorithms: LZW, Adaptive Huffman, BurrowsWheeler with Adaptive Huffman Encoding and BurrowsWheeler with Adaptive Huffman Encoding, RLE and Fibonacci Encoding. Highest success rate (54.49%) in detection of the same files was by same BurrowsWheeler with Adaptive Huffman Encoding compression as in USM metric.

Applicable algorithms for CDM metric are LZW, Adaptive Huffman, BurrowsWheeler with Adaptive Huffman Encoding and BurrowsWheeler with Adaptive Huffman Encoding, RLE and Fibonacci Encoding. The best success in the same file detection achieved BurrowsWheeler with Adaptive Huffman Encoding algorithm with success 54.49%.

None of selected compression algorithms reached theoretical results CosC metric. Selected compressions are not usable with CosC metric.

Table 1. Results of USM metric

Compression method	Successful rate		Failure rate		Minimum USM	Maximum USM
1	25875	53.50%	22488	46.50%	0.473	0.899
2	22846	47.24%	25517	52.26%	0.590	0.996
3	26354	54.49%	22009	45.51%	0.185	0.843
4	26210	54.19%	22153	45.81%	0.081	0.861
5	20161	41.69%	28202	58.31%	-0.827	37.1
6	17645	36.48%	30718	63.52%	-0.902	18.1
7	19954	41.26%	28409	58.74%	-0.884	13.461
8	17347	35.87%	31016	64.13%	-0.947	32.333
9	17386	35.95%	30977	64.05%	-0.947	32.333

5 Conclusions

In the realized experiments we got the following results. Usable compression for USM, NCD and CDM metrics are LZW, Adaptive Huffman, BurrowsWheeler with Adaptive Huffman Encoding and BurrowsWheeler with Adaptive Huffman Encoding, RLE and Fibonacci Encoding compression. Best success rate give BurrowsWheeler with Adaptive Huffman Encoding compression in all metrics. Success rate is for all metrics same 54.49%.

LZ77, LZSS algorithms with various settings gives results outside of estimated theoretical range of metrics.

None of selected compressions are usable with CosC metric.

Table 2. Results of NCD metric

Compression method	Successful rate		Failure rate		Minimum NCD	Maximum NCD
1	25875	53.50%	22488	46.50%	0.473	0.899
2	22846	47.24%	25517	52.26%	0.590	0.996
3	26354	54.49%	22009	45.51%	0.185	0.843
4	26210	54.19%	22153	45.81%	0.081	0.861
5	20161	41.69%	28202	58.31%	-0.827	37.100
6	17645	36.48%	30718	63.52%	-0.902	18.100
7	19954	41.26%	28409	58.74%	-0.884	13.461
8	17347	35.87%	31016	64.13%	-0.947	32.333
9	17386	35.95%	30977	64.05%	-0.947	32.333

Table 3. Results of CDM metric

Compression method	Successful rate		Failure rate		Minimum CDM	Maximum CDM
1	25875	53.50%	22488	46.50%	0.736	0.949
2	22846	47.24%	25517	52.26%	0.795	0.998
3	26354	54.49%	22009	45.51%	0.592	0.921
4	26210	54.19%	22153	45.81%	0.540	0.930
5	20161	41.69%	28202	58.31%	0.086	19.050
6	17645	36.48%	30718	63.52%	0.048	9.55
7	19954	41.26%	28409	58.74%	0.057	7.230
8	17347	35.87%	31016	64.13%	0.026	16.666
9	17386	35.95%	30977	64.05%	0.026	16.666

Table 4. Results of CosC metric

Compression method	Successful rate		Failure rate		Minimum CosC	Maximum CosC
1	1020	2.10%	47343	97.9%	-0.150	0.500
2	1743	3.60%	46620	96.40%	-0.410	0.155
3	1085	2.24%	47278	97.76%	-0.183	0.802
4	1037	2.14%	47326	97.86%	-0.130	0.893
5	887	1.83%	47476	98.17%	-83.333	1.827
6	1503	3.11%	46860	96.89%	-39.142	0.992
7	1321	2.73%	47042	97.27%	-30.700	0.938
8	1094	2.26%	47269	97.74%	-47.571	0.987
9	1077	2.23%	47286	97.77%	-45.571	1.000

References

1. M. Li, X. Chen, X. Li, B. Ma, and P. M. B. Vitányi. The similarity metric. *IEEE Transactions on Information Theory*, 50(12):3250–3264, 2004.
2. J. Rocha, F. Rosselló, and J. Segura. Compression ratios based on the universal similarity metric still yield protein distances far from cath distances. *CoRR*, abs/q-bio/0603007, 2006.
3. D. Sculley and C. E. Brodley. Compression and machine learning: A new perspective on feature space vectors. In *DCC*, pages 332–332, 2006.
4. P. M. B. Vitányi. Universal similarity. *CoRR*, abs/cs/0504089:5, 2005.

Business Process – Formal Modeling in Graphical Ontology Tool – Functional View

Jakub Štolfa

Department of Computer Science, FEECS,
VŠB – Technical University of Ostrava, 17. listopadu 15, 708 33 Ostrava – Poruba
jakub.stolfa@vsb.cz

Abstract. There exist many modeling approaches in the domain of process modeling. We can use many semi-formal or formal approaches and notations. The advantage of the formal specification and modeling is in the precisely defined semantics. We are using an approach based on the first order logic, but the big issue for us is the form of the description of the particular models. Text based tools for the ontology descriptions are good, but even the description of the simplest model can be very complicated. The solution is to have a graphical tool that is able to define the necessary views of the model by the particular diagrams and then transform them to the ontology model. In this paper, we focus on the transformation of the functional view to the ontology description. Elements, their relations and attributes are described in the diagrams and then transformed to the ontology description.

1 Introduction

Modeling of the process is always driven by the specific goal. The goal has to be selected before the modeling is performed, because the modeling approach depends on the desired point of view and that point of view depends on the goal. Our intention is to develop a modeling approach that can be used, at least at the beginning of the modeling, without the knowledge of the real goal. We have decided to use an ontology based approach that could fulfill some necessary properties:

- iterativeness – the model can be modeled from the abstract viewpoint and then refined;
- transformation between different types of model approaches;
- integration of approaches – avoiding duplicities when modeling by one approach and then switching to another.

We have already discussed benefits of knowledge based modeling in [1, 2] and demonstrated the possibility of import of existing models into environment of ontologies where other transformation or integration can be executed. We used results presented in [3] here.

Since we have our own tool for the modeling of the processes, we have decided to adapt this tool for this purpose. Our tool supports three different views of the process – functional, coordination and object. In this paper, we focus on the transformation of the functional view to the ontology description and back.

The paper is organized as follows: Section 2 introduces the state of the art in the field of study, connects the paper to our previous research and introduces our tool method. Section 3 – Functional model example - describes the simple process example; Section 4 describes the fundamental tenets of the model transformation to the ontology description. Section 5 presents the transformation of the example to the ontology description. Finally, concluding Section 6 provides a summary and discusses future research.

2 BP Method

Modeling and simulation of software processes and business processes in general presents some specific problems which lead to the creation of specialized modeling methods. BPM Method ([5]) is one of these methods that is based on the Petri Nets approach and is used in the case study presented in this paper. BPM Method looks at the three elemental views of the process – architecture of the process, objects and resources utilized in the process and the behavior of the process. Each of these aspects is described by one of the models included in the BPM Method.

Functional model identifies the process architecture and its customers and products. The primary focus of the functional model is to answer which processes are cooperating with the main process and which subprocesses are used to perform specific tasks in the main process.

Object model identifies static structure of all objects and resources that are essential for the enactment of the process. This model captures all workers employed in the process and their communication channels. It also contains information about all artifacts (documents, products, material, etc.) that are manipulated or created in the process. Each worker and artifact can be characterized by various optional attributes.

Coordination model specifies the behavior of the process as a sequence of activities, what resources the activities demand and which artifacts are consumed and produced. This model is based on the Petri Nets formalism and is the most important part of the simulation.

BP Method is implemented in the BP Studio software tool [6] used for modeling, simulation and enactment of the processes and used for the simulation of the software process.

3 Functional model example

The example is made in the BP Studio. This diagram shows architecture of a process Car Sale, where salesman sells a car to customer. This process contains another process which is named Financing. Process Car Sale has some Customers, which are required. Then it has Salesman, which owns current process. Output of a process is a handed over Car. This example is a typical representative of a functional view model in the BP Studio. It is depicted in the Figure 1.

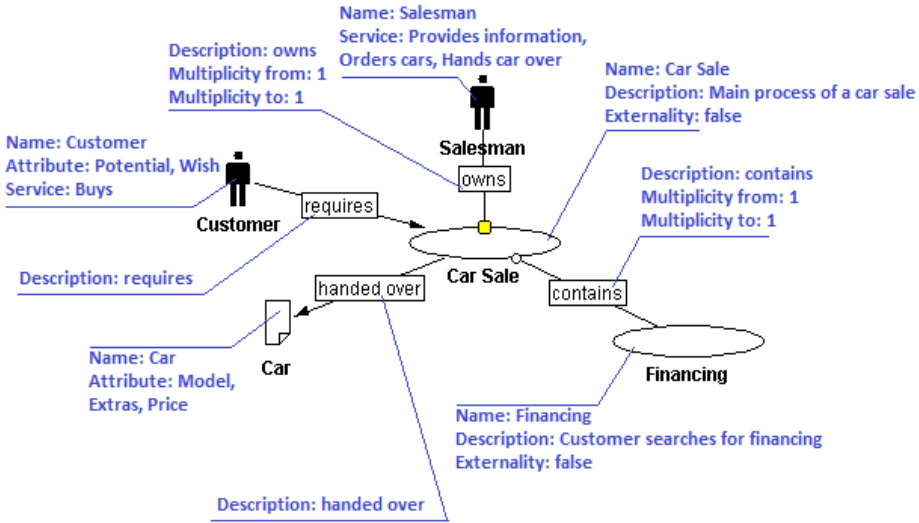


Fig. 1. The example of the functional view diagram made in the BP Studio software tool

4 Mapping elements of the BP Studio to the ontology

We can represent all graphical elements of the BP Studio by ontology. The ontology has three main elements, which correspond to main graphical elements of the BP Studio software tool. It is Process, Object and Connection. Common feature of these classes is that they are disjunct. It means if element belongs to one on them, it could not belong to another one. For example process element could not be connection element in same time. Described structure is shown in the Figure 2.

Description of Classes

There are two types of objects in the BP Studio. It is active object and passive object. That is the reason why class Object is extended by two subclasses – *Active* and *Passive*. And as well as types of classes, these subclasses are disjunct. It means that no element can be active and passive in one time.

The same logic is used for the Connection class. There are a lot of particular types of connection, which are disjunct against each other. It is depicted in the Figure 2.

Description of the data properties

Element Process has attribute name, description and an option, which define externality of the process. These attributes are represented by data properties in the ontology. Data property *hasName* defines name of the process, *hasDesc* defines description of the process and *hasExternality* defines externality of the process.

In case that we would like to preserve even graphical information about particular elements, it is possible to have data value, which describes graphical positions of particular elements. Graphical information about particular elements is important during importing model to the BP Studio, because it determines the position of particular elements. Data properties for the position of the graphical elements are *hasCoord*-

dinateX and *hasCoordinateY*, which describe horizontal and vertical coordinates of particular elements. A graphical representation of classes and their data properties are depicted in the Figure 2.

Description of the object properties

So far, we have described the static view of elements. It is important to depicture connection between elements in the ontology. Some of the object properties are *hasConnectionFrom* and *hasConnectionTo*. Their values are particular elements, which are connected.

Other object properties are *hasAttribute* and *hasService*, which describe relationship between elements. We need those elements, because so far we have described particular elements and no particular relationships.

Description of the domain and the range

The definition of the ontology is set up by the specification of boundaries that preserve consistence and uniqueness of the ontology. Boundaries are set up by the definition of domain and range.

Domain and range are set up for individual properties. The domain of the current property determines the set of the classes that the current property can use. The range of the current property determines the set of values that the current property can reach.

Table 1. Domain and ranges

Type of property	Property	Domain	Range
Object	<i>hasAttribute</i>	Active, Passive	Attribute
Object	<i>hasService</i>	Active	Service
Object	<i>hasConnectionFrom</i>	All types of Connection	Process, Active, Passive
Object	<i>hasConnectionTo</i>	All types of Connection	Process, Active, Passive
Data	<i>hasCoordinateX</i>	Process, Active, Passive	integer
Data	<i>hasCoordinateY</i>	Process, Active, Passive	integer
Data	<i>hasDesc</i>	Process, Attribute, Service, all types of Connection	string
Data	<i>hasExternality</i>	Process	boolean
Data	<i>hasName</i>	Process, Active, Passive, Attribute, Service	string
Data	<i>hasMultiplicityFrom</i>	All types of Connection	string
Data	<i>hasMultiplicityTo</i>	All types of Connection	string

5 The example - transformation of BP Studio elements to the ontology

The example of conversion of BP Studio elements to the ontology is based on the example that is depicted in the Figure 1. It is a Car Sale process. We have to go through three main steps of the conversion.

For the demonstration purpose we have chosen the OWL language [7]. OWL language provides a tool for capturing all classes, data properties and object properties of our determined ontology.

A. First step - instances

In the first step, particular instances of the classes are created.

B. Second step – data properties

Next step contains the definition of data properties of particular elements. For instance, process Car Sale, which has name “Car Sale”, description "Main process of a car sale", and externality

is false. The example 1 shows a definition of that process and its data properties in OWL language.

Example 1:

```

1 <ClassAssertion>
2 <Class IRI="#Process"/>
3 <NamedIndividual IRI="Process1328184291769"/>
4 </ClassAssertion>
5 <DataPropertyAssertion>
6 <DataProperty IRI="#hasDesc"/>
7 <NamedIndividual IRI="Process1328184291769"/>
8 <Literal datatypeIRI=" XMLSchema#string">Main process of
  a car sale</Literal>
9 </DataPropertyAssertion>
10 <DataPropertyAssertion>
11 <DataProperty IRI="#hasExternality"/>
12 <NamedIndividual IRI="Process1328184291769"/>
13 <Literal datatypeIRI=" XMLSchema#boolean">>false</Literal>
14 </DataPropertyAssertion>
15 <DataPropertyAssertion>
16 <DataProperty IRI="#hasName"/>
17 <NamedIndividual IRI="Process1328184291769"/>
18 <Literal datatypeIRI="XMLSchema#string">Car
  Sale</Literal>
19 </DataPropertyAssertion>
  
```

Example 2:

```

1 <DataPropertyAssertion>
2 <DataProperty IRI="#hasName"/>
3 <NamedIndividual IRI="Active1328184665717"/>
4 <Literal
  datatypeIRI="XMLSchema#string">Salesman</Literal>
5 </DataPropertyAssertion>
6 <DataPropertyAssertion>
7 <DataProperty IRI="#hasName"/>
8 <NamedIndividual IRI="Service1728182665789"/>
9 <Literal datatypeIRI=" XMLSchema#string">Hands car
  over</Literal>
10 </DataPropertyAssertion>
11 <DataPropertyAssertion>
12 <DataProperty IRI="#hasDesc"/>
13 <NamedIndividual IRI=" Service1728182665789"/>
14 <Literal datatypeIRI=" XMLSchema#string"></Literal>
15 </DataPropertyAssertion>
16 <ObjectPropertyAssertion>
17 <ObjectProperty IRI="#hasService"/>
18 <NamedIndividual IRI=" Service1728182665789"/>
19 <NamedIndividual IRI=" Active1328184665717"/>
20 </ObjectPropertyAssertion>
  
```

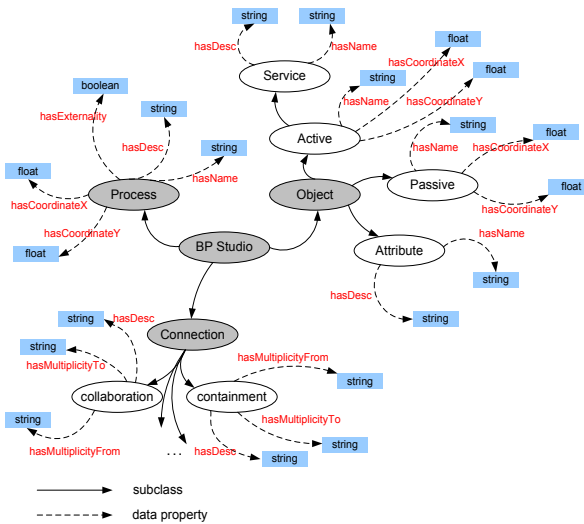


Fig. 2. The data properties in the ontology

C. Third step – object properties

Properties of all elements are made the same way like for the process Car Sale. For example, the element Salesman has more complex definition. We cannot record everything only by data properties, so we have to use object properties.

Element Salesman contains name "Salesman" and service "Hands car over". In that case it is necessary to create instance of the class Active (Salesman) and instance of the class Service (Hand car over) and their particular data properties. Then, we have to make connection between these elements by object properties. It is made by the object property *hasService*. The example 2 shows a definition of that element and its data and object properties in OWL language.

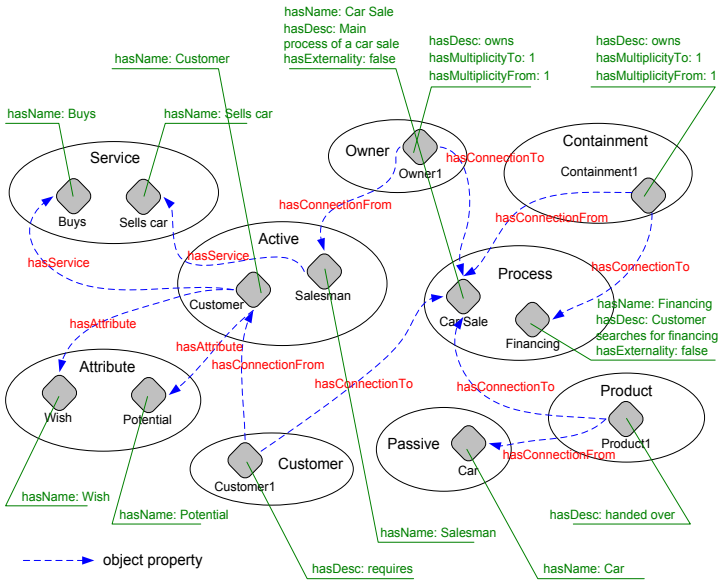


Fig. 3. The complete ontology of an example

6 Conclusion and future work

This paper described an approach to the transformation of the functional model of the process to the ontology based description. Our work on that tool is driven by the fact that text based formal ontology descriptions are not easy to follow for the humans. Thus, one of the solutions is to have a graphical tool that is supported by the ontology description in the background. The transformation described in this paper is the first step of the creation of such a tool. The next step is to create the transformation for the coordination and object models.

Our intention is develop a tool that would be able support the ontology description from different views of the process modeling, but this is not the end. The presented tool is one of the interfaces of our order logic based modeling and simulation environment. The near future work is dedicated to the creation of modeling mechanisms that will be used for the description of the reality and used in the knowledge base capable to store complex “know-how“.

References

- [1] J. Kożusznik, and S. Štolfa, "Knowledge based approach to software development process modeling." pp. 16-28.
- [2] J. Kożusznik, and S. Štolfa, "Basic Constructions for the Definition of the Software Development Process with Formal Method ". pp. 45-47, 2011.
- [3] W. Scacchi, "Experience with software process simulation and modeling," Journal of Systems and Software, vol. 46, no. 2-3, pp. 183-192, Apr, 1999.
- [4] H. Knublauch, R. W. Ferguson, N. F. Noy et al., "The Protege OWL Plugin: An open development environment for Semantic Web applications," Semantic Web - Iswc 2004, Proceedings, Lecture Notes in Computer Science S. A. McIlraith, D. Plexousakis and F. VanHarmelen, eds., pp. 229-243, 2004.
- [5] I. Vondrák, R. Szturc, and M. Kružel, "Company Driven by Process Models," in European Concurrent Engineering Conference ECEC '99, Erlangen-Nuremberg, Germany, 1999, pp. 188-193.
- [6] I. Vondrák, "Business Process Studio, version 3.0.," VŠB – Technical University of Ostrava, 2000.
- [7] W3C. "OWL 2 Web Ontology Language.," <http://www.w3.org/TR/owl2-overview/>.

EEG Cognitive Action Recognition Based on Singular Value Decomposition Accelerated by GPU

Lukáš Zaorálek

Department of Computer Science, FEECS,
VŠB – Technical University of Ostrava, 17. listopadu 15, 708 33 Ostrava – Poruba
lukas.zaoralek@vsb.cz

Abstract. In this paper, we describe real-time pattern recognition of EEG signals using Singular value decomposition. Today's graphics processors are able to processing obtained EEG signals in real-time and therefore we use GPU to recognise several type of EEG actions. We also measure performance between GPU and CPU EEG-action recognition.

Keywords: Electroencephalography, cognitive signal, pattern recognition, graphics processors, singular value decomposition

1 Introduction

EEG is a non-invasive technique used in the diagnosis and management of brain diseases such as epilepsy. EEG is also used in the diagnosis of coma, encephalopathies, alertness and brain-death. Moreover, areas of damage following head injury, stroke tumour can also be located.[4]

Brain computer interface (BCI) is a communication system that recognizes users command only from his or her brainwaves and reacts according to them. For this purpose PC or/and subject is trained. Simple task can consist of desired motion of an arrow displayed on the screen only through subjects imaginary of the motion of his or her left or right hand. As the consequence of imaging process, certain characteristics of the brainwaves are raised and can be used for users command recognition, e.g. motor mu waves (brain waves of alpha range frequency associated with physical movements or intention to move) or certain ERPs.[5] In other words, the BCI provides a solution to convert brain signals to usable control commands.[1]

1.1 Singular value decomposition

SVD is an algebraic extension of classical vector model. It is similar to the PCA method, which has been the first method used for the generation of eigenfaces. Informally, SVD discovers significant properties and represents the EEG signals

as linear combinations of the base vectors. Formally, we decompose the matrix of EEG signals A by singular value decomposition (SVD), calculating singular values and singular vectors of A .

We have a matrix A , which is an $n \times m$ rank- r matrix and values $\sigma_1, \dots, \sigma_r$ are calculated from eigenvalues of matrix AA^T as $\sigma_i = \sqrt{\lambda_i}$. Based on them, we can calculate column-orthonormal matrices $U = (u_1, \dots, u_r)$ and $V = (v_1, \dots, v_r)$, where $U^T U = I_n$ and $V^T V = I_m$, and a diagonal matrix $\Sigma = \text{diag}(\sigma_1, \dots, \sigma_r)$, where $\sigma_i > 0, \sigma_i \geq \sigma_{i+1}$. [2]

$$A = U \Sigma V^T. \quad (1)$$

1.2 Action Recognition

Let us have k ($0 < k < r$) and singular value decomposition of the matrix A . We call $A_k = U_k \Sigma_k V_k$ a k -reduced singular value decomposition (rank- k SVD) (U_0, Σ_0 , and V_0 represent matrices filled with zeros). Instead of the A_k matrix, a matrix of EEG signal vectors in reduced space $D_k = \Sigma_k V_k$ is used in SVD as the representation of EEG signals collection. The EEG signal vectors (columns in D_k) are now represented as points in k -dimensional space (the feature-space). To execute a query Q in the reduced space, we create a reduced query vector $q_k = U_k q$. Instead of A against q , the matrix D_k against q_k is evaluated. [2]

2 Dataset

We chose the EPOC headset to measuring EEG signals. We had obtained 203060 values per one sensor during 20 minutes. The EPOC SDK has own data structure known as chunk for EEG signal process. We had divided EEG collection of signals into two sets, one of them was a training set and second of them was a test set. The training set was dedicated to calculating singular value decomposition (SVD). We had verified the action recognition on the test set of the EEG collection using results of SVD as describe below.

Because of non-stationary character of EEG signals we had calculated Short-time Fourier transformation (STFT) thus we converted EEG signals from time domain to frequency domain. There was one sliding window of STFT per one sensor in our collection. After preprocessing EEG collection applying STFT we had made singular value decomposition of the training set of the EEG collection. In other words, the input matrix of SVD consists of precalculated sliding windows belong to the training set. Let r be number of rows of the input matrix, w be length of one sliding window and s be amount of sensors, then we have $r = w * s$. The number of columns of the input matrix is equal to number of sliding windows.

After decomposition we had calculated reference matrix using matrices Σ and V^T which where parts of SVD as described 1.2. Let RM be reference matrix, U be left column-orthonormal matrix, Σ be diagonal matrix, V^T be right column-orthonormal matrix, then $RM = \Sigma * V^T$. Let c be one column of RM and q

be one column of preprocessed test set, then each column c of matrix RM is comparing with each vector q in the following manner: $Q = q * U^T$. In other words, we had measured similarity vector Q to vector c . If we get consensus between vector Q and vector c we compare assigned cognitive actions between vector Q and vector c .

3 Experiments

We had tested our approach of EEG pattern recognition using SVD and massive parallel computation on GPU hardware. We concretely used NVIDIA tesla C2050 graphics card. For details on how are threads distributed for computing and how they are executed, we encourage the reader to further study the matter in [3]. The parameters such as size of STFT window or number of FFT coefficients had directly impact on performance and also on results of pattern recognition. The meaning of abbreviations which are part of this paper are listed in following statement:

- **TMD** - Training matrix dimension
- **STFT** - Short-Time Fourier Transform
- **SVD** - Singular value decomposition
- **LP** - Learning Process (STFT+SVD)
- **CT** - Classification time for the whole data set
- **SM** - percentage similarity between our approach and EPOC SDK

As you can see on a table 1 if we increase the number of FFT coefficients we get better similarity to EPOC SDK. On the other hand it noticeable increase classification time for whole collection with rising number of FFT coefficients.

The size of the STFT window has impact on the similarity as shown in table 2. However if we set the size of the STFT window at 150 or higher the classification time is significantly growing up.

The table 3 shows performance comparison between CPU and GPU pattern recognition. The GPU is 2-3 times faster than CPU as we expected.

Table 1. Time spent shows performance of the SVD approach depending on the number of FFT coefficients.

	Number of FFT coefficients				
	32	64	128	256	512
TMD	238 x 729	462 x 725	910 x 719	1806 x 726	3598 x 613
STFT	3848	4213	3767	3229	4077
SVD	270	545	1259	1883	3303
LP	4118	4758	5026	5112	7380
CT	8683	19952	25412	69651	101642
SM	56.57	56.13	56.32	56.63	60.46

Table 2. Time spent shows performance of the SVD approach depending on the size of the STFT window.

	Size of the STFT window				
	50	100	150	200	250
TMD	462 x 697	910 x 722	1806 x 717	1806 x 712	1806 x 707
STFT	3806	4313	3249	4470	3723
SVD	475	883	1728	1693	1638
LP	4281	5196	4977	6163	5361
CT	19571	35145	68964	67815	68985
SM	59.52	57.22	56.40	56.67	58.96

Table 3. Time spent shows performance between CPU and GPU pattern recognition of the SVD approach.

	Matrix dimension				
	910 x 989	910 x 1989	910 x 3989	910 x 7989	910 x 14989
GPU	1267	2033	5604	19560	56733
CPU	9123	12408	22393	86391	not tested

Note that, each value in the tables above represents measured time in milliseconds.

4 Future research and Conclusion

In this paper we presented the performance of EEG pattern recognition on the GPU hardware and also comparison results with EPOC device. The GPU provides pattern recognition on huge collection of EEG signals in real time. We can see several interesting future research based on this paper. In future work, we plan to use advanced EEG device and increase ability to detect different cognitive actions. We want to use multiple GPUs as well as use several times greater collection of EEG signals than it is now.

Acknowledgement

This work was partially supported by the Ministry of Industry and Trade of the Czech Republic, under the grant no. FR-TI1/420, SGS in VSB-Technical University of Ostrava, Czech Republic, under the grant No. SP2012/58, and has been elaborated in the framework of the IT4Innovations Centre of Excellence project, reg. no. CZ.1.05/1.1.00/02.0070 supported by Operational Programme 'Research and Development for Innovations' funded by Structural Funds of the European Union and state budget of the Czech Republic.

References

1. A. Ahmadi, O. Dehzangi, and R. Jafari. Brain-computer interface signal processing algorithms: A computational cost vs. accuracy analysis for wearable computers. In *Wearable and Implantable Body Sensor Networks (BSN), 2012 Ninth International Conference on*, pages 40–45, may 2012.
2. P. Gajdos and, P. Moravec, and V. Snasel. Preprocessing methods for svd-based iris recognition. In *Computer Information Systems and Industrial Management Applications (CISIM), 2010 International Conference on*, pages 48–53, oct. 2010.
3. David B. Kirk and Wen-mei W. Hwu. *Programming Massively Parallel Processors: A Hands-on Approach (Applications of GPU Computing Series)*. Morgan Kaufmann, 1 edition, February 2010.
4. S. Suja Priyadharsini and S. Edward Rajan. An efficient soft-computing technique for extraction of eeg signal from tainted eeg signal. *Applied Soft Computing*, 12(3):1131–1137, 2012.
5. M. Teplan. Fundamentals of EEG measurement. Number 1, pages 1–11, 9 2002.



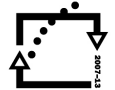
euROPEAN
social fund in the
czech republic



EUROPEAN UNION



MINISTRY OF EDUCATION,
YOUTH AND SPORTS



OP Education
for Competitiveness

INVESTMENTS IN EDUCATION DEVELOPMENT

SoftComp Workshop

SoftComp workshop – organized as a part of WOFEX 2012 workshop – have been realized as a part of SoftComp project (CZ.1.07/2.3.00/20.0072). This project is co-financed by ESF and Czech state budget.



Acknowledgement

Following papers were supported by the Development of human resources in research and development of latest soft computing methods and their application in practice, reg. no. CZ.1.07/2.3.00/20.0072, co-financed by ESF and state budget of the Czech Republic.

- Stanislav Böhm and Ondřej Meca. *From Petri Nets to Octave Modules*
- Patrik Dubec and Jan Plucar. *Floreon JavaScript Framework for Data Visualization in Web Application*
- Adam Farnik. *Current Trends in Object Constraint Language (OCL) Use*
- Michal Holiš and Martin Plaček. *Detecting Frayed Edge in Steel Plate using Multi Scale Retinex Algorithm*
- Lenka Skanderová. *Investigation on Evolutionary Algorithms Dynamics*
- Ondřej Takács, Jana Šarmanová, and Kateřina Kostolányová. *Dynamic Control of Adaptive e-Learning*
- Lukáš Vojáček, Zbyněk Janoška, and Jiří Dvorský. *P Systems for Traffic Flow Simulation*

From Petri Nets to Octave Modules

Stanislav Böhm and Ondřej Meca

Department of Computer Science, FEECS,
VŠB – Technical University of Ostrava, 17. listopadu 15, 708 33 Ostrava – Poruba
{stanislav.bohm, ondrej.meca}@vsb.cz

Abstract. We are developing a tool Kaira intended for modelling, simulation and generation of parallel applications. A developer is able to model parallel programs and different aspects of communication using Kaira. Models are based on our own variant of Coloured Petri Nets. Petri nets are a well established graphical and mathematical modelling language for a description of concurrent systems, but Petri nets are rarely used in the area of high performance computing. An important feature of our tool is an automatic generation of standalone parallel applications from models. In this paper we focus on the new Kaira's feature, the ability to generate parallel libraries. Kaira supports C++ libraries and also it is possible to generate parallel libraries for Octave. Their usage is demonstrated on a real example, parallelization of Total-FETI domain decomposition method.

1 Introduction

We are developing the tool Kaira¹[1–4], this tool is an open source project released under GPL. Our goal is to develop a practically usable general-purpose high-level programming tool for the area of High Performance Computing (HPC), especially for distributed memory systems. We feel that there is a space for this research. Tools used by practitioners in this area are low-level ones (like Message Passing Interface – MPI) or they are domain specific tools.

An important aspect of our tools is a usage of an *abstract computation model*. Our efforts aim for a tool that can be used (at the basic level) by non-experts in the parallel/distributed programming. The model should provide sufficient abstraction so it can be used without knowing low-level details of used technologies and solving low level issues. On the other hand our goal is *not* to develop an automatic parallelizing tool. So Kaira does not automatically discover parallelisms in an application and a user has to explicitly define them. But parallelisms can be defined in a high level way and the tool can derive implementation details. We also want to use an abstract model to communicate in the opposite way, from a program to a user. We want to show what happens inside of a developed program through abstract model and without using specialized low level tools.

¹ <http://verif.cs.vsb.cz/kaira>

One of our design goals is to support *prototyping*. In other words, we want to offer an easy way how a user can develop a working prototype of an application in a short time. We want to achieve this by two basic features. First of them is a possibility to run simulations and to observe behaviour of incomplete applications from a very early stage of a development cycle. This feature is natural part of modelling tools, but when tools like MPI are used, it often takes a long time to get a working prototype. The second feature that supports prototyping is integration of existing source codes into models. It is a common approach in parallel programming to start from a sequential solution. Our tool respects this approach and therefore it is possible to link together models of parallelism and communication with sequential codes in common programming languages. Also, we use an abstract model that is not commonly used in the area of HPC. But we do not want to force users to abandon existing solutions and start from the scratch in a different paradigm. The current implementation supports integration of codes written in C++ and we also started to work on Java support.

Our goal is to build a practically usable programming environment and in contrast to many high-level modelling tools, Kaira is able to generate standalone parallel applications. The resulting applications use MPI and pthreads as parallel backends. So these applications can be directly executed on HPC computers.

In this paper, we want to introduce another possibility for a fast prototyping and for reusing of existing codes, but in the reverse direction. As we said, it is possible to generate a standalone application from models created in Kaira and existing codes can be used as building blocks. New features introduced in the latest version allows another view, Kaira can create building blocks for other environments. In the other words, we offer a possibility to create parallel libraries from our models. We do not want to restrict this feature only for C++ but also we want to generate libraries to other high level tools. Therefore the current implementation offers to generate beside C++ libraries also modules for Octave².

This feature of Kaira allows us quickly interchange time-consuming parts by parallel running functions without modifying the rest of a program. The same idea of parallelizing only performance demanding parts appears in existing tools like OpenMP³, but our solution do not need a special compiler, it works with distributed memory and we offer visual programming tool where parallel parts can be modelled, simulated and tested independently of the rest of a program. To demonstrate these new features we show how can be a part of Octave's application replaced parallel version generated by Kaira.

2 Kaira's libraries

We start this section with C++ libraries because it is a crucial feature and others are built on it. For defining libraries we are using a infrastructure of modules (described in [4]). In a case of a standalone application, there is a "main" net

² <http://www.gnu.org/software/octave/>

³ <http://openmp.org/>

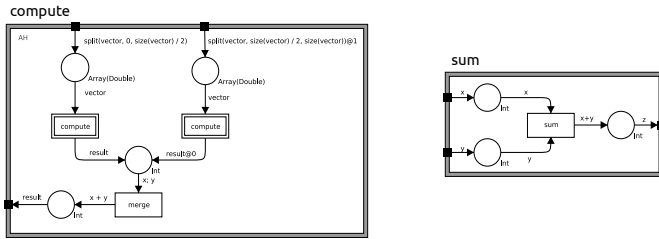


Fig. 1. The example of Kaira's modules

and optionally other modules. If we are developing a library then there are only modules without the main net. Application interface (API) of a resulting library will be defined by an interface of modules.

Let us consider two simple examples of modules depicted in Figure 1. The first module sums two numbers. The second one performs a computation on a vector of numbers. The vector is split into two parts and computation is performed in parallel on first two MPI processes and results are summed at the end. Kaira generates a C++ library with the following interface from these modules:

```
void calib_init(int argc, char **argv);
void sum(const int &x, const int &y, int &z);
void compute(const std::vector<double > &vector, double &result);
```

The function `calib_init` is always present and a user is obligated to call this function as a first function in a program. The other two functions are derived from modules in the model. These functions can be freely executed in any sequential program. A usage can look like this:

```
int main(int argc, char **argv) {
    calib_init(argc, argv);
    int z; double d;
    sum(3, 2, z); // call of generated function
    std::vector<double> v;
    v.push_back(3); v.push_back(2); v.push_back(5);
    compute(vector, d); // call of generated function
    return 0;
}
```

When functions `sum` or `compute` are called, then a program starts executing (in parallel) a function defined by a module in the model. When such function is finished (i.e. the module is finished) then the program continues again sequentially. Such program can be also used with MPI without any modification (except a compilation with `mpicc`). In a case of running via MPI, the function `calib_init` initiates MPI and ensures that the main program is executed only once in a process with the rank 0. Other processes just wait until a function generated

by Kaira is called. When it happens then a computation is executed according to a module's structure through all MPI processes.

Beside this type of libraries, our tool can also generate libraries that work in the Remote Procedure Call (RPC) mode. Kaira generates both server and client part. The client side is a library that has the same interface as was described in the example above, but when a function is called then it sends a request through a network to the server where a requested computation is executed. It is useful when you want to execute the main sequential program on a different computer then rest of computations or when we need to run the main application exactly once, using only one instance (for example due to a program licensing).

2.1 Octave libraries

Generating Octave libraries from models and their usages are very similar to C++ libraries. An equivalent Octave code from the previous example:

```
source generated-library.m # Load module
z = sum(3, 2)
v = [3, 2, 5]
z2 = compute(v)
```

Calling Kaira's modules from Octave is straightforward like in case of C++ libraries. Important issue of such integration is an interoperability between data types. We have to exchange values between Kaira's inscription language and Octave. Basic data types likes numbers or vectors are translated automatically. But inscription language types can be extended by C++ types from external libraries, therefore we offer an option to define two special functions `from_octave_value` and `to_octave_value` for each external type. With these functions Kaira performs all conversions between types when necessary.

3 Case study

In this section we want to demonstrate features described above. As an example we have chosen a variant of Finite Element Tearing and Interconnecting (FETI) domain decomposition method [5] – Total-FETI [6]. The key idea of FETI method is decomposition of the spatial domain into non-overlapping sub-domains. After this decomposition we can get final result by combine results from each sub-domain. Each sub-domain can be calculate independent and thus in parallel but finding an optimal solution for parallelization of Total-FETI method is still an open problem. For this problem several studies were published (for example [7, 8]). There are different problems like an appropriate number of sub-domains, a level of preprocessing (the coarse problem, mentioned in [7]) or if certain matrices should be distributed or used only by a master process. And as usual in area of HPC, an optimal solution also depends on aspects like a target platform or used libraries. All in one, finding the optimal solution is not an easy task and it is hard to predict performance of a specific solution without experiments.

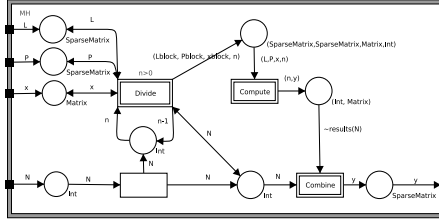


Fig. 2. Module *Kplus_par*

3.1 Experiments and Results

At the beginning we had a working sequential implementation of Total-FETI for Matlab/Octave. Using a profiler we have discovered that the most expensive operation is a computation of generalized inverse \mathbf{K}^+ of stiffness matrix \mathbf{K} with vector \mathbf{x} . So we have made Kaira’s library (Figure 2) for calculation this operation and generate interface with function `Kplus(x)`. For test this library’s performance we solve a displacement of a 1D string that is fixed on both ends. We prepare stiffness matrix \mathbf{K} where each sub-domain has 500 000 discretization steps and we use 30 sub-domains. Using these settings function `Kplus(x)` consumed approximately 34 percent of the whole execution time.

The measurement was performed at computer with 8 processors AMD Opteron/2500 (in total it is 32 cores). A computation of `Kplus(x)` takes in average 21.79 seconds in pure Octave solution. We measured runs of library generated our model of `Kplus(x)`. The test was performed RPC mode, where both client and server run on the same computer. The measured times for thread and MPI back ends can be found in Table 1.

Table 1. Running times (in seconds) of *Kplus(x)* by using threads and MPI

Computing nodes	1	2	4	8	16	30
Threads with RPC	25.30	19.87	10.32	8.02	7.70	7.76
MPI with RPC	25.19	20.88	16.89	15.36	16.55	16.39
Threads without RPC	21.71	11.05	6.51	4.35	4.06	3.93

4 Conclusion

This text briefly introduces new features of our tool Kaira that moves it toward our goal to create programming environment for HPC applications with extensive support of prototyping. We think that our tool can be useful because the parallel computers became more common and accessible, therefore also more scientific

and engineering applications can profit from this hardware, but not all of them require optimized handmade solutions. Moreover as far as we know any tool is able to do what we presented in this paper, generate parallel C++ libraries that can be used as modules in Octave.

As we show on our example – parallelization of Total-FETI method, our tool can be used to obtain parallel running functions that can be used directly in Octave. One of big issues that we wanted to solve in the near future, is preserving data on computing nodes between each library calls. We feel that formalism of Petri nets can be the right way how to manage such task.

We would like to thank to T. Kozubek, co-author of paper [8] that provides us his Matlab Total-FETI method implementation.

References

1. Böhm, S., Běhálek, M.: Kaira: Modelling and generation tool based on Petri nets for parallel applications. In: UkSim 13th International Conference on Computer Modelling and Simulation. (2011) 403–408
2. Böhm, S., Běhálek, M., Garncarz, O.: Developing parallel applications using Kaira. In: Digital Information Processing and Communications. Volume 188 of Communications in Computer and Information Science., Springer (2011) 237–251
3. Běhálek, M., Böhm, S., Krömer, P., Šurkovský, M., Meca, O.: Parallelization of ant colony optimization algorithm using Kaira. In: 11th International Conference on Intelligent Systems Design and Applications (ISDA 2011), Cordoba, Spain (2011)
4. Böhm, S., Běhálek, M.: Usage of Petri Nets for High Performance Computing. In: ACM SIGPLAN Workshop on Functional High-Performance Computing, FHPC'12. (2012) to appear.
5. Farhat, C., Roux, F.X.: An unconventional domain decomposition method for an efficient parallel solution of large-scale finite element systems. *SIAM J. Sci. Stat. Comput.* **13**(1) (1992) 379–396
6. Dostál, Z., Horák, D., Kučera, R.: Total FETI-an easier implementable variant of the FETI method for numerical solution of elliptic PDE. *Communications in Numerical Methods in Engineering* **22**(12) (2006) 1155–1162
7. Horák, D., Dostál, Z.: Parallelization of the total-FETI-1 algorithm for contact problems using PETSc. In: Proceedings of the Second International Conference on Parallel, Distributed, Grid and Cloud Computing for Engineering, Civil-Comp Press, Stirlingshire, UK (2011)
8. Vondrák, V., Kozubek, T., Sadowská, M., Dostál, Z.: TBETI and TFETI algorithms for contact shape optimization problems. In: Proceedings of the Second International Conference on Parallel, Distributed, Grid and Cloud Computing for Engineering, Civil-Comp Press, Stirlingshire, UK (2011)

Floreon JavaScript Framework for Data Visualization in Web Application

Patrik Dubec and Jan Plucar

Department of Computer Science, FEECS,
VŠB – Technical University of Ostrava, 17. listopadu 15, 708 33 Ostrava – Poruba
{patrik.dubec, jan.plucar}@vsb.cz

Abstract. This paper deals with new architectural design of Floreon project web application. In this paper an approach to development of a modular web application is described. The new approach should improve performance of entire application and it should help developers with faster development and subsequent maintenance. New architecture supports extend-ability thanks to support for adding plugins.

Keywords: MEF, ASP .NET MVC3, Google Maps

1 Introduction

Data visualization is the key functionality of numerous applications, where such visualized data could help to understand core of the given problem. In this day and age we can come across visualization in areas such as medicine, graph theory, social networks and financial markets.

One of the projects that use data visualization is called Floreon. The goal of this project is to build a prototype system as a platform for modeling and simulation of adverse situations caused by natural phenomena using modern computing and Internet technologies. The primary phenomenon, which became a bearing element of the project, is in our country quite frequently occurring floods. Results of those simulations may dramatically help with early warnings of flood-affected areas, which could save lives and decrease material loss. Results are presented in a form of graphical visualization into the common map in order to be understandable to wide range of public.

This publication focuses on design of modular well-maintainable and performing architecture [1] for Floreon web application.

2 Solution requirements

Previous solution was based on Microsoft technologies so it would be best to hold on to the platform. The biggest problem to overcome was the use of Silverlight technology, which requires additional plugin to be installed. Installation itself could be problematic in various environments. Typical examples are companies with employ-

ees restricted from installing new software or mobile environment, which does not have to support Silverlight technology.

Application should bring the support for adding plugins from various sources [3]. Additional plugins will be able to use map framework methods in order to visualize and describe data into the map. Whole project is quite complex so it is natural that several teams will be generating data that are necessary to be displayed (water level, cloudiness, wind). In order to accomplish this goal we have to prepare architecture which would be able to handle various modules (plugins) in well-defined way. It is the only way, how to ensure independent development for several development teams.

2.1 Architecture description

To ensure all of those requirements we have designed the base architecture that you can see in the Figure 1. As you can notice the solution is divided into layers.

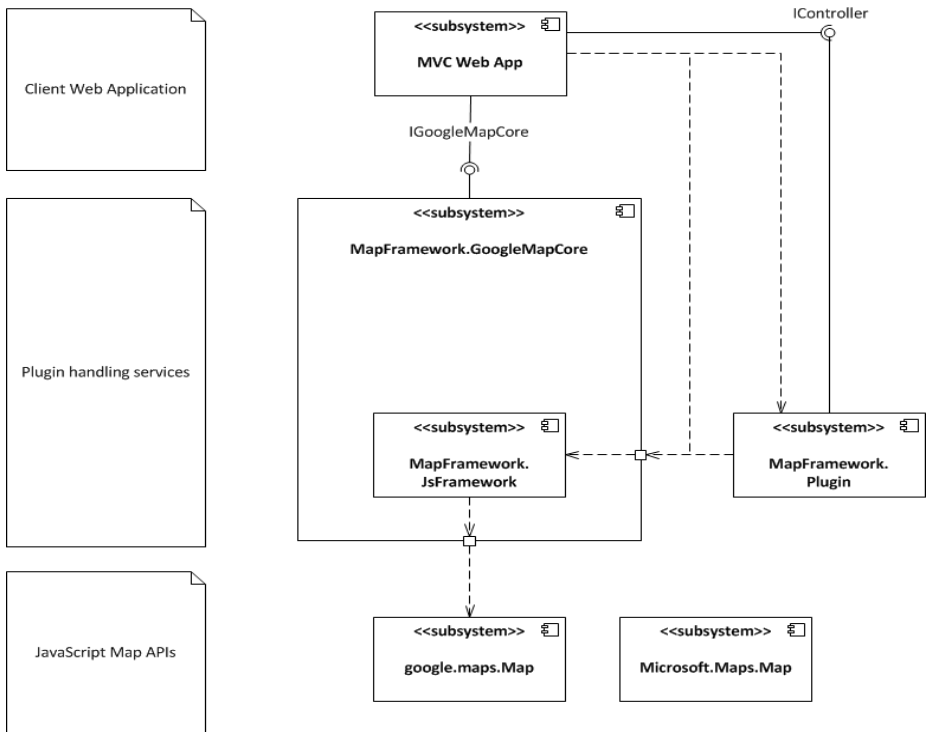


Fig. 1. Web application architecture.

Map source layer

This layer represents a map that is used as a background to display the data on (i.e. river-basins, rainfall, place of accident etc.). The map that is active has to implement all the methods from given interface. This allows us to change the map provider for

another provider, for example Google maps for Bing maps. Both map solutions provide JavaScript based API [2] which allows us to work with several map entities. The most useful entities are points of interests, routes, heat maps and events that could be bind to them. Google maps and Bing maps are platform independent and do not require any additional web-browser plugins.

Our JavaScript framework

It was necessary to define a custom abstract layer for different map sources. At first, basic set of operations that are used to work with map and map entities has to be defined.

Using JavaScript operated map sources lightened server's load. Map itself is now rendered on the client's side and the map source is downloaded from different server. However it is necessary to obtain data, mostly in JSON format [2], computed on our server. Amount of data could slow down visualization considerably, so the application is able to chunk the data and load them asynchronously in background thread. It is also possible to download appropriate amount of data according to the zoom level. The rest of data could be pre-fetched.

Map core layer

This layer is primarily responsible for loading all necessary plugins. Plugins provide business logic, required functionality and implementation of abstract JavaScript layer for Google Maps (Bing Maps) too.

There is no doubt that it is necessary to strictly separate application logic from the application view and from data representation. This idea is depicted in MVC pattern [3] and directly used in ASP.NET MVC [1] programming language.

To ensure plugin-able architecture new feature of .NET framework 4 called MEF (Managed Extensibility Framework) was used. The MEF is a composition layer for .NET that improves the flexibility, maintainability and testability of large applications. MEF can be used for third-party plugin extensibility, or it can bring the benefits of a loosely-coupled plugin-like architecture to regular applications. Use of the MEF is shown in Figure 2, which describes the process of plugin registration.

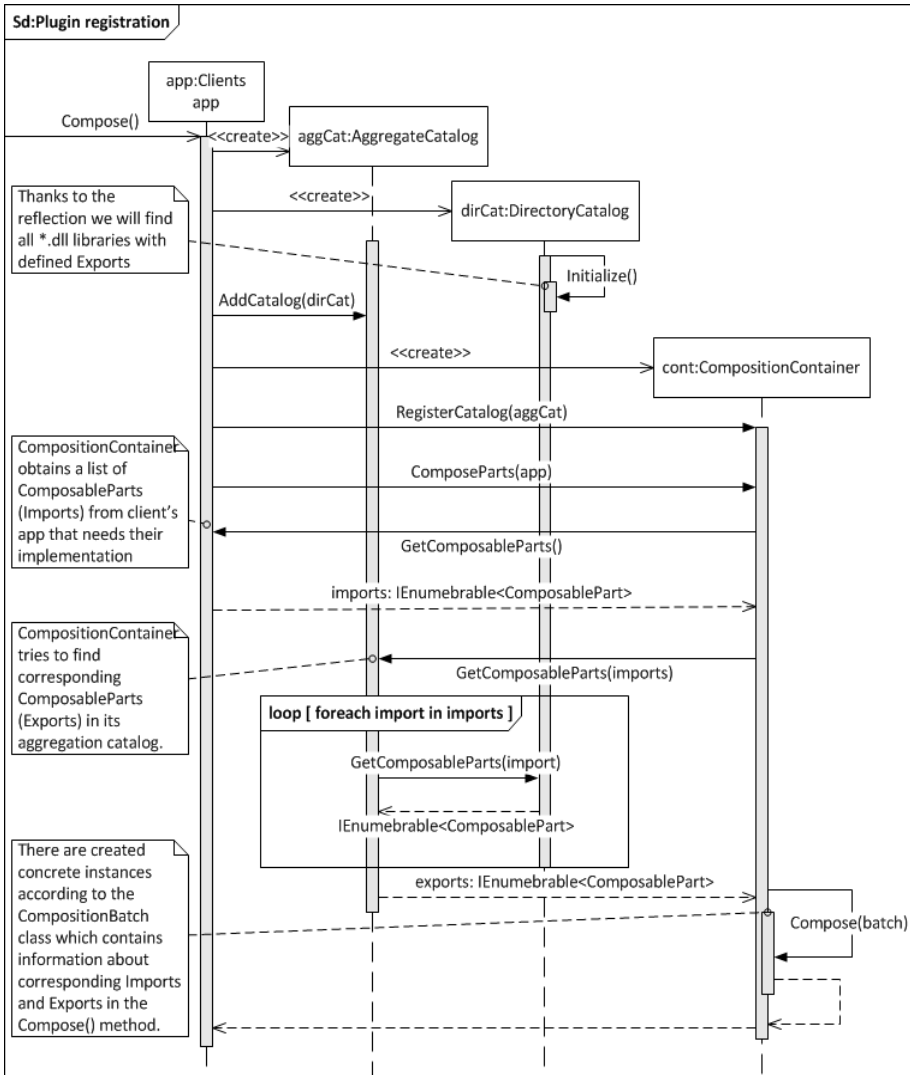


Fig. 2. Sequence diagram of a plugin registration.

Client’s web application

Last layer represents standard ASP.NET MVC3 [1] web application which can provide its own application logic or integrate several external plugins.

Those plugins may extend business logic and view with its own view and JavaScript methods that control map elements. Google map core itself is provided as one of our plugins so it can be easily reused everywhere.

3 Conclusion

Floreon Map JavaScript Framework provides means to:

- implement visualization layer into any ASP.NET MVC web site
- fast and easy plugin creation, thanks to ready to use methods that encapsulate JavaScript code controlling the map
- development in several teams, since all plugins are well described by interfaces
- quick change of map provider thanks to abstract map layer and business logic separation

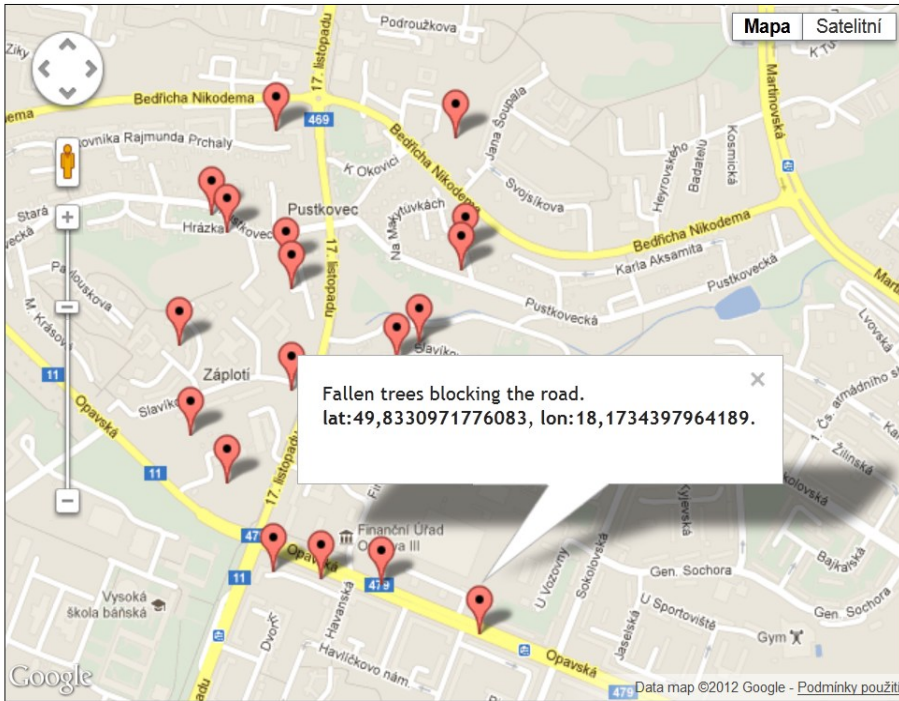
In conclusion, new map framework match all specified requirements and is ready to be used and extended by third party programmers.

Next step in development of Map Framework will be performance testing when displaying large amount of data by hundreds of users at the same time (e.g. browsing the map during floods)

Floreon MVC pluginable web application

- [Home](#)
- [Maps](#)

Google map plugin



External plugin - InterestingPlaces

Fig. 3. Client’s web application screen shot showing two plugins. One is Google map plugin and other plugin provides buttons able to load and display somehow interesting places.

4 References

1. Steven Sanderson, Adam Freeman, Pro ASP.NET MVC3 Framework 3rd edition, New York, July 11, 2011, chapter 4, 5, 16, 17, 18. ISBN 978-1-4302-3404-3
2. Nicholas C. Zakas, Professional JavaScript for Web Developers, 2nd Edition, West Sussex, England: John Wiley & Sons, Ltd, January 2009, chapter 12, 17, 20. ISBN 978-0-470-22780-0
3. Judith Bishop, C# 3.0 Design Patterns, O’Reilly Media, December 2007, chapter 5, 6. ISBN 978-0-596-52773-0

Current Trends in Object Constraint Language (OCL) Use

Adam Farnik

Department of Computer Science, FEECS,
VŠB – Technical University of Ostrava, 17. listopadu 15, 708 33 Ostrava – Poruba
adam.farnik@vsb.cz

Abstract. Object Constraint Language has been developed by Object Management Group into version 2.3.1 recently. This paper conveys a search of few recent contributions to the OCL world, covering topics ranging from the language's use in automated testing to its proposed alternative.

1 Introduction

Software engineering has long been associated with Unified Modeling Language. Object Constraint Language (OCL) [1] provides it with means for specifying constraints that its graphical notion cannot express. This paper concerns in study of recent development in the world of OCL. Its main part covers a search of recently published papers on OCL.

Structure of the paper is as follows: After introduction, in the second chapter there is a brief description of OCL including example. Following is history of OCL specifications. Fourth chapter is structured into sub-sections, each covering one recent paper about OCL, and finally comes the conclusion.

2 OCL

The Object Constraint Language is a declarative language used to specify constraints in Unified Modeling Language (UML) diagrams. It is based on mathematic set theory and predicate logic, which allows it to extend UML class diagrams by rules that cannot be expressed in its graphical notion. By introducing invariants (structural constraints) and pre- and post-conditions (behavioral constraints), OCL provides software designers with means to describe the model's semantics. Each OCL expression is always linked to specific context – a meta-class, on which instances the expression is validated. OCL is designed as side-effect-free, which means that execution of its statements will not change the state of the system. This allowed it to develop into rather declarative language, strongly influenced by functional programming languages [2].

To illustrate the use of OCL, I use a simple and well know example, described in UML diagram on Figure 1 [3], which shows two classes – Customer and Account.

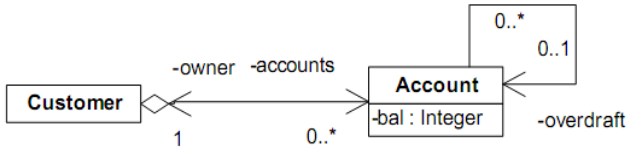


Figure 1. UML class diagram

Customer can have one or more accounts and an account can be linked to another account for overdraft protection. What the class diagram is unable to show is that the account cannot be linked to itself. To specify this, OCL invariant is needed such as:

```

context Account
  inv: self <> overdraft
  
```

Keyword `self` is one constructs defined in OCL. This particular one denotes an instance of the meta-class (in this case instance of `Account` class).

Following expression specifies behavioral constraint of operation `Customer::addAccount`, using collection operations defined in OCL: `includes` (testing presence of element in collection) and `including` (adding element to collection), and the postfix operator `@pre`, denoting the property's value from before the operation execution:

```

context Customer::addAccount(acc: Account): void
  pre: not accounts->includes(acc)
  post: accounts = accounts@pre->including(acc)
  post: acc.owner = self
  
```

The meaning of above is:

- The operation cannot be parameterized with instance of `Account` class, which already is in `accounts` collection of `self`
- After the operation, the `accounts` collection of `self` has to be exactly the same as before the operation, just with the `acc` added
- The `owner` property of `acc` has to be `self`

3 Evolution of OCL

The definition of OCL was first introduced as a part of UML version 1.3 in 1999 [4], yet its actual use in the industry was almost negligible [5]. In 2003 revision 2.0 was adopted, but as it came earlier, than UML 2.0, it was still building upon UML 1.x, which nearly led to its withdrawal [4], further damaging the OCL position. It was only in 2006, when the 2.0 revision of OCL was completed, which amongst other improvements, most importantly adjusted the OCL metamodel to UML2 concepts.

Since then, two new revisions were published – version 2.2 in 2009 introducing number of enhancements and fixing some inconsistencies left by the previous revision and version 2.3.1 from January 2012, which only cleaned the previous revision of some minor flaws.

Further maintenance of OCL specification became much harder as companies see little reason in assigning manpower to work on already adopted specifications, rather focusing on creating new ones [4].

4 Current development and perspectives

As the researchers are rather focusing on creating new specifications a broad range of projects based on OCL has emerged, from adaptations into another models, to extensions and proposals for further development. This chapter goes through 3 such cases, illustrating OCL's current use and possible future horizons.

4.1 Automated testing

A case of employing OCL as is, into project taken further into practice is described in [3]. The paper by two researchers from Texas University at El Paso describes automated Java program testing using combination of random testing and OCL.

To do that, they are using OCL to AspectJ [6] translator, converting OCL constraints into aspect-oriented code. Aspect Oriented Programming (AOP) is a programming paradigm aiming at separation of *crosscutting concerns*, thus increasing modularity of code. Crosscutting concerns are pieces of code of minor importance, which need to repeat in many program modules. AOP addresses the resulting knottiness of such code by introducing *join points* – sets of execution points, at which specific behavior is required, and *advices* – pieces of code providing such behavior. Advices, somewhat reminding triggers used in SQL, can be specified to be executed *before*, *after* or *around* the join points.

The OCL pre- and post-conditions correspond with AOP's before and after join point advices. In practice, however, the OCL to AspectJ translator uses `OclChecker` framework class translates all conditions to around advices and verifies conditions by methods `checkPre` and `checkPost`.

The testing itself consists of generating random data and invoking the tested methods with it (for which random testing tool JET [7] was used). If such test execution results in a pre-state constraint violation, the data is rejected as inappropriate for testing. If on the other hand, the test results in a post-state violation, it is considered a test failure. Elsewise the test runs without exceptions and is thus considered successful.

In a case study, where 30 different unrelated faults were introduced into program, such testing was able to detect 27 of them, giving it a success rate of 90%. For the remaining 3 undetected faults the OCL constraints were not defined strong enough.

4.2 Pragmatic extension for OCL

As stated previously (Chapter 3), even though the UML is being used extensively, OCL is not quite as popular. One commonly quoted reason for being so is that it is designed for use at modeling level, yet its syntax is closer to programming languages. Hence it often appears too formal for designers and too abstract for programmers.

In order to make it easier for designers to use, a paper [8] proposes pragmatic extension for OCL consisting of collection (library) of OCL expressions (*OCLLib*), set of test cases for OCL expressions (*OCLUnit*) and documentation of OCL expressions (*OCLDoc*). The idea for the library is to provide large number of relatively small OCL expressions that would be easy to reuse by parameterization and modularity. Expressions forming the library need to be validated before being put to use, and so the library should be supplemented with set of test cases, proving that the expressions passed the validation. Furthermore, each test case is a simple scenario with known result and as such can lead to better understanding of what the expression means. Finally the library should be documented, to support its usability and simplify the knowledge transfer to the developers and designers using it. The practice has shown that documenting is best done by the developer of the expressions directly into the code then generating the documentation from the code by an automatic tool.

The paper [8] reports that putting the described extension into practice brought higher effectiveness into development of OCL extensions even among people with low previous experience with OCL.

4.3 Epsilon Validating Language

The fact that currently the efforts to create new specifications based on OCL are more supported comparing to the efforts to manage the existing specification, was already mentioned in chapter 3. Epsilon Validating Language (EVL) [9] is an example of such new specification, although it is not meant to be a rival of OCL.

The authors of EVL argue that unlike the OCL language and types, which were revised and improved during the evolution of the language, the *invariants* remained practically unchanged since its inception. They identified a group of shortcomings of OCL (some of them already identified by both commercial and open-source programming groups) and proposed the solution implementing it as EVL. The list of criticized properties is as follows:

- Poor support for user feedback – there is no message being passed in case of invariant failure, but the failure itself.
- No warnings support – there is only one level of reports: errors.
- No support for dependent constraints – if the invariant is only applicable on the basis of another invariant's successful evaluation, it has to contain whole body of the invariant it is dependent on.
- Limited complexity in context definition – refining once defined context in the invariant body is hard and confusing.

- No support for repairing inconsistencies – OCL as a side-effect free language lacks constructs for code modification. However, in many cases the inconsistencies causing the invariant to be evaluated as failed are easy to repair and therefore introducing the hints for repairing errors, as is common in many development tools, would be useful for the programmers.

Those drawbacks were addressed by implementing a prototype validation language – EVL. The authors view it as a flexible tool for evaluating novel approaches to model constraints and possible contributor to the evolution of OCL, but not its replacement.

Syntax of EVL is very much different from the one of OCL, as it uses the Epsilon Object Language (EOL) [10] proposed by the same authors. EOL is procedural language and as such is closer to the programmers than the declarative OCL. EOL also supports user input and output, which allows sending diagnostic messages. EVL introduces further specifics:

- *Context* as is known from OCL can be optionally refined by a *guard*, limiting invariant's applicability to a subset of instances of the context type.
- *Invariant* is a parent class for *constraint* (critical errors) and *critique* (warnings, with 3 levels of importance)
- *Fix* can be optionally assigned to an invariant, suggesting the way of correcting the problem that caused its failure.
- *Pre* and *post* blocks that can optionally be executed before or after evaluating invariant.

Although EVL is not meant to rival OCL, its execution engine was already implemented in Eclipse IDE [11] and it was also added to open-source modeling tool ArgoUML [12], so that it is possible for anyone to try it in a real life scenario.

5 Conclusion

Although not much has changed in the OCL specification since 2009, it has proved its functionality and usability, being commonly used within projects following scope that OCL was never designed for. Its use as a standalone language is however still not that frequent while critics are and the fact that different companies have introduced their own closed standards instead of contributing to the development of the open one is also not helping. Its future now depends on projects incorporating it into larger practical scope.

References

1. Object Management Group. Object Constraint Language 2.3.1
<http://www.omg.org/spec/OCL/2.3.1/PDF>
2. Chiorean, D., Bortes, M., Corutiu, D.: Proposals for a Widespread Use of OCL. In: Proc. Tool Support for OCL and Related Formalisms - Needs and Trends, Models/UML 2005, Montego Bay, Jamaica (October 2005)

3. Cheon, Y., Avila, C.: Automating Java Program Testing Using OCL and AspectJ. In: Seventh International Conference on Information Technology, Las Vegas, Nevada, USA (2010)
4. Belaunde M.: Evolution of the OCL OMG Specification. In: Invited talk at the Workshop on OCL and Textual Modelling, collocated with MODELS 2010 conference, Oslo, Norway (2010)
5. Pandey, R. K.: Object Constraint Language (OCL): Past, Present and Future. In: ACM SIGSOFT Software Engineering Notes, Volume 36, Number 1 (January 2011)
6. Kiczales, G., Hilsdale, E., Hugunin, J., Kersten, M., Palm, J., Griswold, W. G.: An overview of AspectJ. In: Springer-Verlag, June 2001, vol. 2072, Berlin, Germany (2001)
7. Cheon, Y., Rubio-Medrano, C.E.: Random test data generation for Java classes annotated with JML specifications. In: SERP, Volume II, Las Vegas, Nevada, USA (2007)
8. Chimiak-Opoka, J.: OCLLib, OCLUnit, OCLDoc: Pragmatic Extensions for the Object Constraint Language. In: MODELS 2009, Springer-Verlag, Berlin, Germany (2009)
9. Kolovos, D. S., Paige, R. F., Polack, F. A. C.: On the Evolution of OCL for Capturing Structural Constraints in Modeling Languages. In: Börger Festschrift, LNCS 5115, Springer-Verlag, Berlin, Germany (2009)
10. Kolovos, D. S., Paige, R. F., Polack, F. A. C.: The Epsilon Object Language (EOL). In: ECMDA-FA 2006. LNCS, vol. 4066, Springer, Heidelberg, Germany (2006)

Detecting Frayed Edge in Steel Plate using Multi Scale Retinex Algorithm

Michal Holíš and Martin Plaček

Department of Computer Science, FEECS,
VŠB – Technical University of Ostrava, 17. listopadu 15, 708 33 Ostrava – Poruba
michal@holis.cz

Abstract. In this paper we propose technique that is suitable for detection of frayed edges on grain oriented electrical steel. Technique is based on preprocessing of source image using Multi Scale Retinex algorithm and detects frays using preprocessed image data analysis. Method is fast and suitable for real-time detection of frayed edges during the manufacturing process.

1 Introduction

Goal of this paper is to present method for frayed edges on grain oriented electrical steel detection. Frayed edge is small crack like damage on edge of the steel plate.

Main problem, making detection of this defect very hard, is it's inconspicuousness. By naked eye the frayed edge in input image appears as only small variance in natural noise of the image.

Many image normalisation methods have been tried in pursuit to solve this problem and variant of Multi Scale Retinex algorithm was chosen for image preprocessing. In this paper are described some of the methods that have been tried for preprocessing and algorithm for frayed edges detection in preprocessed image is proposed.

2 Image normalization methods

2.1 Histogram equalization

Histogram equalization aims to increase global contrast of processed image to adjust local intensities. This method is useful when image is composed mainly of close values as it spreads the most frequent values of the image and allows areas with close values to gain much higher contrast. More detailed description of this method can be found in [1].

2.2 Self-Quotient Image

The Self Quotient Image is an extension of The Quotient Image technique first introduced by Riklin-Raviv and Shashua in [7]. This method was first proposed by Wang, Li and Wang in [2].

These methods are both class recognizing methods and they are widely used for object classifications (for example in face recognition [3]).

Original method (Quotient Image) uses series of bootstrap images to identify ideal illumination free representation of recognized class of objects. Quotient Image of two objects belonging to the same class is then defined as ratio of their albedo functions, thus being illumination free and normalising lightning conditions and luminance variations.

Self-Quotient Image is extension of previous method that doesn't need training set of images, instead it derives Quotient Image directly from analysed image. This means, that it can be used purely as image preprocessing method, since no direct knowledge of object's class is required.

2.3 Anisotropic diffusion

Anisotropic diffusion (also referred to as Perona-Malik diffusion) is technique first proposed by P. Perona and J. Malik in [6] that reduces noise and preserves important details of the image that are necessary for correct interpretation of the image. It is based on generating family of parametrized images, where each of these images is combination of the original image and selected filter.

3 Retinex

Technique, that appears to be most suitable for our application and for solving our problem is "Retinex" based preprocessing filter.

3.1 Introduction to Retinex

In real life huge difference in color quality of observed scene and detail of recorded image can often be perceived. The most apparent difference is loss of color accuracy and image detail, especially in darker areas covered by shadows. As a result recorded images often seem dimmed compared to observed scene. This is caused mainly by inability of camera to distinguish between ambient illumination of the scene and reflectance. Illumination is by its nature independent of the scene, so all the characteristics of observed objects are described only by reflected light component. Recorded image is product of these two components and once it has been evaluated, there is no way we can separate these two values and obtain reflectance, which is critical for correct visual representation of the scene, but human eye still seems to be able to do so.

In 1986 Edwin Land [5] proposed image processing method that tries to simulate behaviour of human eye and called it "Retinex". Retinex is a compound

of two words – Retina and Cortex – as retina and primary visual cortex are thought responsible for color constancy of final image. Since then the method has developed and can now be considered family of three main techniques:

- Single Scale Retinex,
- Multi Scale Retinex,
- Multi Scale Retinex with Color Restoration (MSRCR).

4 Multi Scale Retinex with Color Restoration

MSRCR can be considered most advanced of these techniques and is thoroughly described in [4]. Simply put MSRCR can be described with equation:

$$R_i(x, y) = \sum_{s=1}^N (w_s \log I_i(x, y) - \log [F(x, y) * I_i(x, y)]), \tag{1}$$

where i is the index of color band of the image, $R_i(x, y)$ is resulting value of pixel (x, y) of i -th color band, $I_i(x, y)$ is value of i -th color band of original image, $F(x, y)$ denotes Gaussian function and $*$ represents convolution.

Basically MSRCR performs set of Gaussian filter operations on input image and computes difference between the filtered and unfiltered image. Each of the steps performed is dependent on so called “scale”. Images filtered with smaller scales contain strong details and dynamic compression, but fail to provide faithful color representation. Large scales behave the opposite. MSRCR merges all of these images and combines strengths of each scale to provide best image detail and color quality possible.

Great advantage of MSRCR is that once desired input parameters are found technique performs constantly well with any image provided.

Example of MSRCR applied to color image can be seen in Fig. 1. Notice how all the details (mainly bricks on the tower) became clearly visible.

5 Detecting frayed edges on grain oriented electrical steel

Retinex as the most appropriate image normalization technique was chosen for preprocessing of images in inspection of quality in grain oriented electrical steel making process.

Frayed edges detection is part of surface quality monitoring system. Goal of the system is to monitor grain oriented electrical steel plate’s surface during manufacturing process and to detect set of defects degrading quality of final product.

Steel plate is coiled up into the coils. Approximate length of one coil is 4000 meters.

Steel plate continuously runs through the de-carbonization line and it’s surface is monitored by set of cameras from both sides. System then analyses input images for defects in real-time.

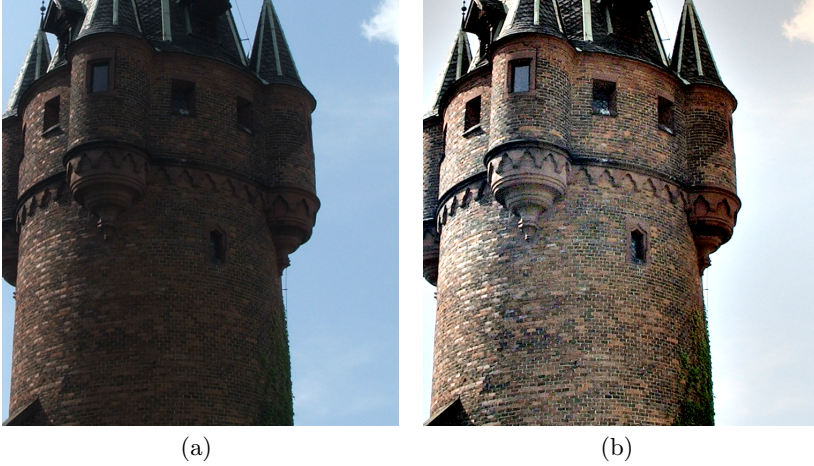


Fig. 1. MSRCR applied to color image. Figure (a): original image, Fig. (b): image processed with MSRCR.

One of the most problematic defects to detect is frayed edge. In the input image it appears only as a small deviation in brightness in horizontal direction (see Fig. 2). This type of defect is captured from one side of the plate only (as it is visible from both sides) using monochrome digital camera. Resolution of one image is 2400×600 pixels. Width of area captured by one camera is approximately 50 cm, which means that each millimeter of captured area is represented almost by 5 pixels in final image. Images are automatically archived so they can be worked with to improve quality of defect detecting algorithms and now we currently have base of more than two million test images.

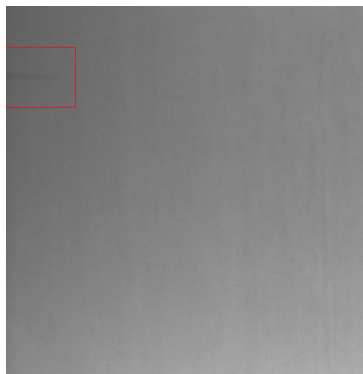


Fig. 2. Frayed edge.

Frayed edges arise on a plate because of insufficient MgO powder coverage of the edges. In the annealing process the uncovered edges are stuck together, because of high annealing temperature, and the defect is formed on a plate when it is unwinded on the next processing line and stuck edges are torn off.

Common edge detecting algorithms used on non-preprocessed images don't provide any meaningful results because frayed edge appears only as very small deviation in input image and is suppressed by noise that is introduced into the image due to low exposition time requirements and environmental conditions that don't allow for better lighting of the scene.

To highlight our area of interest – the frayed edge – and to suppress the light non-constancy is the core of the problem.

5.1 Retinex implementation

To solve this problem Multi Scale Retinex for grayscale images was implemented. Implementation for grayscale images is easily achievable since the algorithm operates independently on each color channel of the image.

Color restoration part of the process was skipped, as although it introduces some gain to the final image, it doesn't contribute fundamentally enough to final quality of processed grayscale image and is relevant only when processing color images.

Most time-consuming operation of whole computation is definitely convolution operation used to apply Gaussian filter to original image. Recursive implementation of Gaussian filter described in [8] was chosen as it's computation time is independent on selected σ parameter, which is often high for MSRCR and is cause of poor performance of many other algorithms.

5.2 Detecting frayed edge in preprocessed image

After Retinex algorithm is applied to source image frayed edges are recognizable by naked eye.

Figure 3 shows us comparison between original image and image preprocessed with MSRCR. Red line on image with MSRCR indicates edge of steel plate that is initially analysed to obtain location of fray.

By averaging all the values of each column for each row in image preprocessed with MSRCR plot shown in Fig. 4 can be obtained. Data from this plot can be easily analysed programmatically as frays appear as local minimums in function displayed in this plot. By finding these local minimums frays can be detected and evaluated. Each of those minimums represents one single fray. This approach exploits fact that there are no other defects appearing on the edge of the plate that would contain sharp horizontal edge.

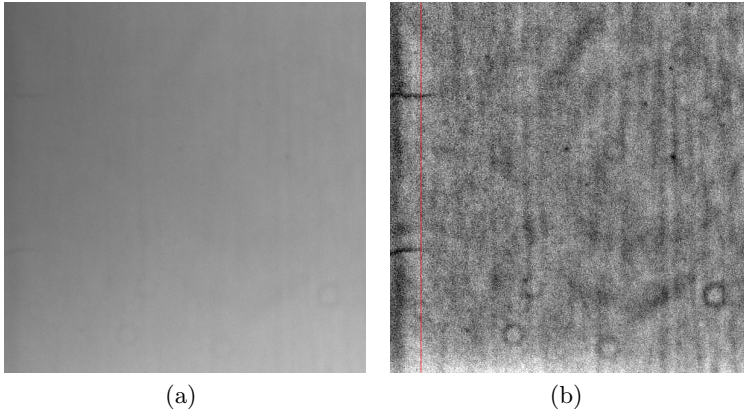


Fig. 3. MSRCR applied to monochrome image. Figure (a): original image, Fig. (b): image processed with MSRCR.

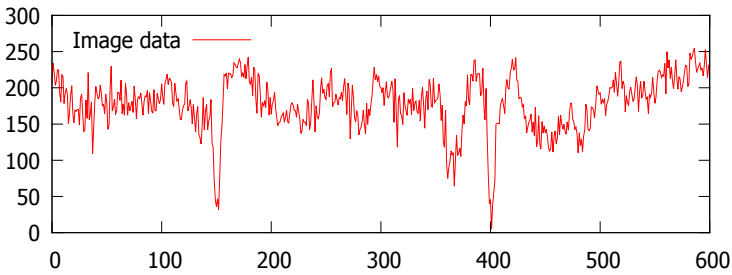


Fig. 4. Plot built from data of the image.

6 Conclusion

Approach for frayed edge detection proposed in this paper is based on heavy preprocessing of input image using variant of Multi Scale Retinex algorithm and on analysis of image data obtained from preprocessed image. Analysis performs detection of local minimums in collected data and locates frayed edges using these minimums.

Technique presented in this paper is suitable for real-time applications and can be used for detection during manufacturing process. Usage of recursive implementation of Gaussian filter allows for constant performance of filter no matter how big σ parameter is used and so it allows Retinex to generate and use highly blurred images with no additional performance cost.

This method is planned to be extended with various edge detection algorithms and comparison between various methods of frayed edge detection in preprocessed image is planned.

References

1. Acharya and Ray. Image processing: Principles and applications. *Wiley-Interscience*, 2005.
2. S. Li H. Wang and Y. Wang. Face recognition under varying lighting conditions using self quotient image. *IEEE International Conference on Automatic Face and Gesture Recognition*, 2004.
3. Guillaume Heusch, Fabien Cardinaux, and Sebastien Marcel. Lighting normalization algorithms for face verification. 2005.
4. D.J. Jobson, Z. Rahman, and G.A. Woodell. A multiscale retinex for bridging the gap between color images and the human observation of scenes. *IEEE Transactions on Image Processing*, 6:965 – 976, 1997.
5. E. Land. An alternative technique for the computation of the designator in the retinex theory of color vision. *Proc. Nat. Acad.*, 83:3078–3080, 1986.
6. P. Perona and J. Malik. Scale-space and edge detection using anisotropic diffusion. *IEEE Transactions on Pattern Analysis and Machine Intelligence*, 12(7), 1990.
7. A. Shashua and T. Riklin-Raviv. The quotient image : Class based re-rendering and recognition with varying illuminations. *IEEE Transactions on Pattern Analysis and Machine Intelligence*, 23(2), 2001.
8. Ian T. Young and J. Van Vliet. Recursive implementation of the gaussian filter. *Signal Processing*, 1995, 44.

Investigation on Evolutionary Algorithms Dynamics

Lenka Skanderová

Department of Computer Science, FEECS,
VŠB – Technical University of Ostrava, 17. listopadu 15, 708 33 Ostrava – Poruba
`lenka.skanderova.st@vsb.cz`

Abstract. This paper describes using of evolution algorithms (EAs) to generate complex networks structure (CNS). There are many evolution algorithms, this paper is specialized in Self organizing migrating algorithm (SOMA) and differential evolution (DE). It shows how the complex network structure is established and how parameters of evolution algorithms (SOMA and DE) influence the results.

1 Introduction

EAs work with the population of individuals, which are developing (improving) during the evolution. In this paper it is shown how these algorithms make CNS during the process of searching the cost function minimum. It is focused on Schwefel, de Jong's and Ranna functions. Complex networks appear in many areas of the research and in practical life (e.g. [2], [3], [4], [5], [6]). Complex networks are based on two basic elements - vertices and edges. This article is trying to show how these elements are established during the process of searching of function minimum. Individuals of evolution algorithms are represented by vertices and the edges symbolize relationships among these individuals.

2 Evolution algorithms

SOMA and DE are based on evolution of individuals in population. Population can be represented as a matrix $N \times M$, where columns represent individuals. At the beginning of algorithm the population is generated. Each individual may consist of real or integer numbers. The count of these numbers represents dimension of the problem (cost function dimension – D). The value of cost function is called fitness. Fitness shows how the individual is suitable for next development of population. Value of fitness is not covered in the evolution process. EAs make new population in the cycle and the old population is replaced by the new one.
[1]

2.1 SOMA - Self organizing migrating algorithm

SOMA works on the nature principle, where intelligent individuals of group collaborate on solving of the common problem. Philosophy of SOMA states on space individuals migration. Individuals are moving in the space of possible solutions. Each individual is influenced by another one during the better solution searching process [1]. New population is understood as a moving of the old population’s individuals. There are many strategies of SOMA - all to one, all to all etc. In this paper *all to one* strategy is presented. Migration of the current individual to the leader is represented by the equation:

$$x_{i,j} = x_{i,j,start}^{MK+1} + (x_{i,j}^{MK} - x_{i,j,start}^{MK})tPRTVvector; \tag{1}$$

$$t \in < 0, byStepto, PathLength >$$

2.2 Differential evolution

Differential evolution (DE) is a population – based optimization method that works on real – number – coded individuals [7]. Unlike SOMA, DE creates new individuals and ancestors are replaced by them, if new individuals have better parameters than ancestors. New individual arises from four parents - actual individual and three randomly chosen individuals. When the new individual is creating, for each individual other three randomly chosen individuals are taken from the population (r_1, r_2, r_3). By means of them noisy vector v is created. Noisy vector is a mutation of these three chosen parents. Mutation is done such that difference of two randomly chosen parents is multiplied by the mutation constant F . And the result vector is added to the third randomly chosen parent, see 2.

$$v_j = x_{r3,j}^G + F \times (x_{r1,j}^G - x_{r2,j}^G) \tag{2}$$

3 Experiment design

It is known that DE has many types as well as SOMA. In this article new individual has been created by the equation 2. Schwefel 3, 1st de Jong’s 4 and Rana 5 functions have been chosen as the cost functions. Twelve sets of experiments have been designed. Each evolution algorithm has been tested on each function. And for each function two sets of parameters have been created (see table 1). For each generation new graph in tool Gephi 0.8.1 has been constructed. At the same time experiments in [7] have been done.

$$\sum_{i=1}^D -x_i \sin(\sqrt{|x_i|}) \tag{3}$$

$$\sum_{i=1}^D x_i^2 \tag{4}$$

$$\sum_{i=1}^{n-1} \left[(x_{i+1} + 1) \cos \left(\sqrt{|x_{i+1} - x_i + 1|} \right) \sin \left(\sqrt{|x_{i+1} + x_i + 1|} \right) + x_i \cos \left(\sqrt{|x_{i+1} + x_i + 1|} \right) \sin \left(\sqrt{|x_{i+1} - x_i + 1|} \right) \right] \tag{5}$$

Table 1: Differential evolution parameters setting.

Parameter	DE set 1	DE set 2	Parameter	SOMA set 1	SOMA set 2
PopSize	50	500	PopSize	50	500
Dimension	20	100	Dimension	20	100
Generations	200	1000	Migrations	200	1000
Low bound	-512	-512	Low bound	-512	-512
High bound	512	512	High bound	512	512
F	0.5	0.5	PathLength	3	3
CR	0.7	0.7	Step	0.11	0.11
			PRT	0.1	0.1

4 Results

We can say that evolution algorithms are very good tool for generating of CNS. These complex networks can show us many things relating with population and it’s individuals. We can observe relations among individuals. Look at the figure 1(a). As you can see the vertex 38 is the darkest green one. It’s degree is the biggest from the all vertices. From the view of DE that means that this vertex has participated in the biggest number of improvements.

In the experiment with DE, current individual and three parents have been saved in the text file. If the individual had been improved, it was saved with plus. If not, it was saved with minus. In the case of the vertex 38 we can see that this individual participated eight times in developing of other individuals as a parent. From these eight participations, individual 38 was used five times to improve of another individual (it was saved as a parent) and three times the individual with the parent 38 was not improved. The individual 38 has the biggest out – degree. The out – degree is 5. In our file mark plus means the out – degree, minus represents in – degree. Look at the figure 1(b). All green vertices (individuals) have been improved in this generation, all pink vertices (individuals) have not been improved.

When we compare the figure 2 and the figure 1(b) we can see relationships which correspond with statements above.

The principle of graph establishing in SOMA was different. In the experiment leaderes and the improved individuals have been saved to the text file. When we

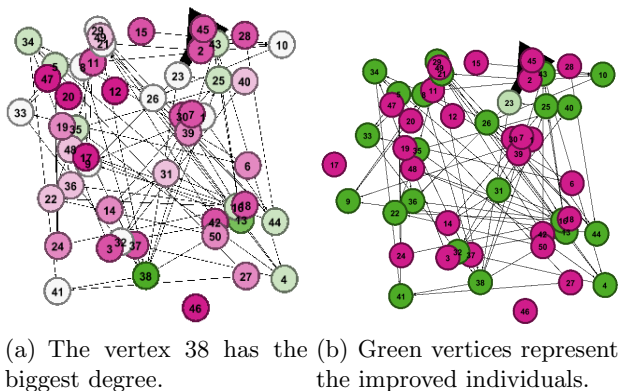


Fig. 1: DE, Schwefel’s function, 1st generation.

```
#Date and time: 23.6.2012 15:15:18
#Used algorithm: Differential evolution
# Population size: 50
# Dimension: 20
# Number of generations: 500
# Low border: -512
# High border: 512
# Mutation constant (F): 0,5
# Threshold of crossing (CR): 0,7
# Test function: Schwefel
#
-1, {50,34,25},-2, {47,26,42},-3, {48,34,32},4, {26,35,43},5, {8,24,41},-6, {7,20,17},-7, {40,25,48},8, {37,9,6}
```

Fig. 2: DE, Schwefel’s function, 1st generation in text file. We can see marks plus and minus which correspond with the figure 1(b).

look at the figure 3(a), we will see that in the second generation, two leaders were chosen. The green vertices 38 and 39 represent leaders. Pink vertices represent individuals which was improved during the path to the leader (see the figure 3(b)). In this graph we are interesting in the weight of the edge too, because weight will say us how many times the current vertex was improved during the path to the leaders. In SOMA one individual can be chosen as a leader many times. And when other individual migrates to it, the weight of the edge is increasing. When we look at the figures 4(a) and 4(b) we can see the phenomenon that the individual in population have not to be the leader during evolution at all.

5 Conclusion

During the experiments some conclusions have been done (some of them are presented in [7]):

1. If the number of generations is too small and the function dimension too big, the algorithm can not reach the global minimum of the function. But if the number of generation is very big, we can observe the phenomenon the rich become to be the richer. In SOMA after current number of migration

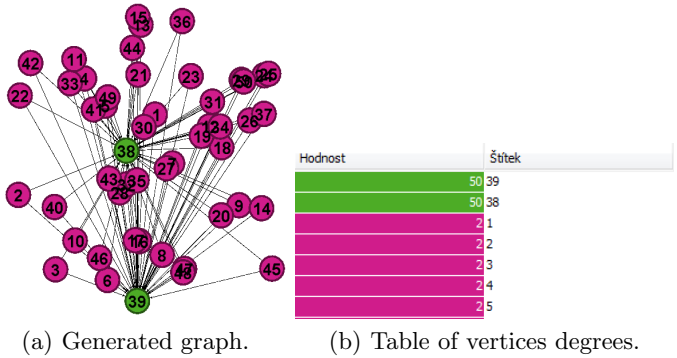


Fig. 3: SOMA, 1st DE Jong's function, the 2nd migration cycle.

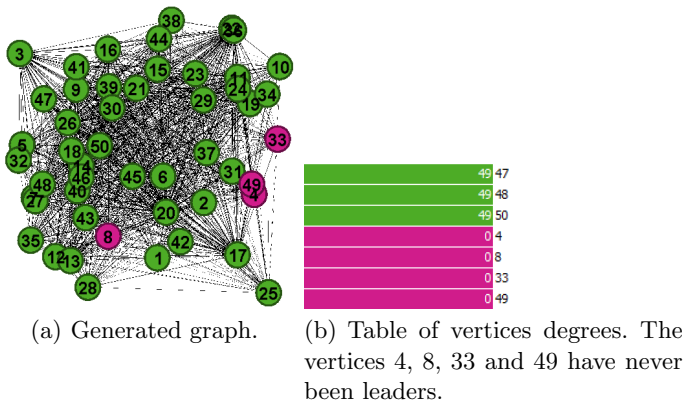


Fig. 4: SOMA, 1st DE Jong's function, the 200th migration cycle.

cycle all individuals will reach the global minimum. The evolution cycle stagnates, because the goal was reached and one individual is chosen as a leader repeatedly.

2. Differential evolution: From the complex network point of view we can say that vertices are divided into two sets. The first set is the set of improved individuals, the second one is the set of not improved individuals. We can see how many times the actual vertex has participated on another individual improving. Next we can see which individual was used most frequently in the process of other individuals improving.
3. SOMA: Complex network system is very good tool to display the relationship between leader and the rest of population. We can observe how the improved individuals were adding during the evolution to the graph. We can see how many times the actual vertex was leader and how many individuals have been improved during the way to this leader.

4. Population size: CNS forming was observed usually from population size of 100 and more individuals for dimensions 50. It is parameter, which does not influent CNS forming alone, but in the combination with other parameters [7].
5. Functions: It depends which function is chosen for creating of CNS (how much the cost function is jagged). If we are trying to find the global minimum of the 1st De Jong's function, we will find it faster than in the Schwefel's function. In Rana's function no global minimum is described in the literature. And during the evolution in these experiments no global minimum was found.

References

1. Zelinka, I., Oplatkova, Z., Seda, M., Osmera, P., Vcelar, F., (ed.): Evolucni vypocetni techniky, Principy a aplikace, BEN - Technical literature, Czech republic (2008)
2. Ren, J.,(ed.): Complex Network Study of Yantai Tourism Industry,International Conference on Artificial Inteligence and Computational Intelligence, 2009
3. Zhuo, L., Changping, L., (ed.): Study on Simulation of Mobile Phone Virus Spreading Based on Complex Network Theory, 978-1-61284-840-2, IEEE, 2011
4. Zelinka, I., Davendra, D., Snasel, V., Jasek, R., Senkerik, R., Oplatkov, Z.,(ed.): Preliminary Investigation on Relations Between Complex Networks and Evolutionary Algorithms Dynamics, 978-1-4244-7818-7, IEEE, 2010
5. Jiang, H., Gao, J., Chen, F., (ed.): System Failure Analysis Based On Complex Network Theory, 1-4244-2509-9, IEEE, 2009
6. Yao, Y., Huang, S., Hu, B., Liu, X., (ed.): Research on Network of Relationship in the Large Software Research Development Team Based on Complex Network Theory,978-0-7695-4047-4, IEEE, 2010
7. Zelinka, I., Davendra, D., Chadli, M., Senkerik, R., Dao, T., Skanderova, L. (ed.): Evolutionary Dynamics and Complex Networks, Mendel Conference, Brno, 2012

Dynamic Control of Adaptive e-Learning

Ondřej Takács¹, Jana Šarmanová¹, and Kateřina Kostolányová²

¹Department of Computer Science, FEECS,
VŠB – Technical University of Ostrava, 17. listopadu 15, 708 33 Ostrava – Poruba
{ondrej.takacs, jana.sarmanova}@vsb.cz

² University of Ostrava, Pedagogical faculty, Department of Information and
Communication Technologies, Dvořakova 7, 70103, Ostrava, Czech Republic
katerina.kostolanyova@osu.cz

Abstract. The goal of adaptive e-learning is to adjust e-learning content and environment to student's properties and achieve more effective learning by doing so. This paper focuses on dynamic adjustment of content of teaching. This adaptation is done on base of analysis of learning process with focus on student's success rate of answering testing questions and on student's requests to alter the form of teaching. If student's success rate is too low, easier variant of content is shown to him. And if student's success rate is high, more challenging parts are added to the learning content.

1 Introduction

Adaptive e-learning is focused on the student and it adjusts the teaching style to the student's needs. The teaching style is defined by the content, form of and the way of teaching. This teaching style is altered on the basis of student's knowledge and properties that has influence on his learning.

This article follows the system Barborka [1] that can adapt learning content by the student's properties. This system is working with very structured learning content that is prepared by the author in different forms and difficulty levels (called depth). The teaching is controlled by algorithm called virtual teacher [2] that can be parameterized by expert on adaptive teaching.

1.1 Learning Content Structure

Learning content has hierarchical structure formed by lessons, frames, variants and layers. *Lesson* is learning unit with the size of teaching hour. It doesn't have to be of equal size of the textbook chapter. Lesson is composed of frames.

Frame is a part of lesson and it contains one teaching topic. For the purpose of adaptive teaching is frame divided to variants and layers.

Variants of frames are different ways of teaching and testing the same topic. They differ in sensual form and the depth of teaching. The *sensual forms* are divided to visual (with pictures and schemes), auditive (with sound information) verbal (with text) and kinesthetic (with interaction elements). The depth of teaching describes the detail and level of difficulty of teaching. The depth is divided to three levels. The depth 2 is most often used level of detail and difficulty. The depth 3 teaches the same information but in lower difficulty. The depth 1 has additional, more complex information that is not in depth 2 and is not required from students at any exam.

Layer of frame is part of frame that has clearly defined purpose in the learning process (explanation, fixation, examination, motivation...).

1.2 Virtual Teacher

Virtual teacher displays appropriately ordered layers of chosen frame in suitable form to student. Work of virtual teacher is controlled by set of rules that are designed by expert for adaptive teaching. Each rule is composed of the presumptions and conclusions. The presumptions are formed by the levels of student's properties. The conclusions are formed by the sensual form and depth of each type of layer and the order of layer types.

The original algorithm of virtual teacher was changed in order to follow the new theory and concepts [3] and to better react to student's requests and to missing variants of layers.

The work of virtual teacher is now divided to three phases. Appropriate rules, which apply to given levels of student's properties, are chosen first. This set of chosen rules is called personal teaching style. After the student chooses the frame, the virtual teacher creates actual teaching style (ordered set of layers in appropriate form) on the base of personal teaching style and available variants of frame. In the last phase appropriate frame (composed of parts specified in actual teaching style) is gradually displayed to student, who can anytime ask to display the layer in different form or depth.

In this paper is described the automatic data analysis of teaching process that creates recommendations to alter the rules of virtual teacher. It also creates recommendations for authors of learning content. In the following part is described the design of algorithm for dynamic control of teaching process.

2 Automatic Analysis of Teaching Process

Dynamic adaptation of teaching process is based on the information gathered by analysis of teaching process. Correctness of student's answers is recorded together with requested changes in form and depth. All these data are stored in already designed teaching process log [4].

Analysis of this log is divided to two levels. On first level are analyzed data of all students and on the second level are analyzed data of individual students. This separa-

tion is useful because the results of analysis will be used in different cases. First level will be used for general recommendation and the second level will be used for immediate adaptation of teaching style for individual students.

2.1 Teaching Process Analysis of All Students

Results of this analysis will be used by two groups of users: experts on adaptive teaching (who can alter the parameters of adaptive teaching algorithm) and authors (who can see parts of learning content that was difficult for many students).

Authors of adaptive textbooks can view statistics about how successful were student's answers to questions in different frames. And they can also see in which frames students frequently requested easier depth.

Experts on adaptive teaching can change the way of adaptive teaching by altering adaptive rules. Following information will be available to support this process:

1. statistics of successfulness of existing rules
2. proposals to alter existing rules
3. proposals to add new rules

Statistics of successfulness of existing rules will be mostly represented by reliability of each rule. This reliability is given by computing average successfulness of all students for whom the virtual teacher used this rule in their teaching.

Proposals to alter or add rules will be based on the association analysis. The log of the teaching process must be supplemented with ID of used rules for the needs of this analysis.

This preprocessed data can now be analyzed by association method. Student's properties, ID of used rule and layer type will be used as antecedents. Student's requested change will be used as consequent. Proposals for altering the rules are given by associations with ID of used rule. Proposals for adding new rules are based on associations with no ID of used rule.

2.2 Teaching Process Analysis of Individual Students

Results of this analysis will be used in real time by algorithm of dynamic control of adaptive teaching process. That's why the computation of this analysis must be fast and large log of teaching process can't be used. Only following aggregated data will be logged in for each student: total number of student's requested changes for each type of layer and total number of correctly and incorrectly answered questions. This data can be computed fast and easily by incrementing counters during the teaching process.

3 Design of Algorithm for Dynamic Control of Adaptive Teaching

This algorithm displays learning content tailored to the student's properties and actual learning situation. Algorithm that adjusts learning content to the student's properties is

already done [2]. That's why we will now focus on adaptation to the learning situation that is described by following parameters:

1. type, form and depth of layers that are already displayed to student in actual frame
2. total number of correct and wrong answers of student for actual subject
3. total number of student's requests to change form or depth of each type of layer

Following processes will be altered on the basis of above parameters:

1. immediate reaction to student's wrong answer
2. reaction to student's average successfulness
3. altering of student's properties

3.1 Immediate Reaction to Student's Wrong Answer

If the student gives wrong answer to some question in some frame, then there is a chance that he didn't learned enough from some part of this frame. That's why it's important to give quick and useful feedback. First is displayed the reaction to wrong answer (that can be prepared by the author), then will the student be encouraged to read again what he need from already displayed layers and then he can try to answer the same question again. If he answers it incorrectly again, then the system will display reaction to the wrong answer together with easier variant of the frame (depth 3) and the student can try to answer the same question again. If he answers incorrectly for the third time, then the correct answer will be displayed together with its explanation (if the author prepared it).

3.2 Reaction to Student's Average Successfulness

The virtual teacher also alters the way of teaching on the basis of the long term successfulness in actual subject. Student's successfulness in subject is given by his answers. If he almost always answers correctly, then variant with additional and more challenging content and questions (depth 1) is displayed to him together with usual content. Better students can now study more difficult content and will not be bored by things that are easy for them. On the contrary, if the student almost always answers incorrectly, then the more carefully explained variant of content with easier questions (depth 3) is displayed to him. In this case the students, who have some difficulty with studying this subject, will have opportunity to better understand it. The algorithm follows these rules:

1. if the student answered correctly more than 75% of depth 2 questions of actual subject, then display depth 1 of given layer type after each teaching or testing layer
2. if the student answered incorrectly more than 75% of depth 2 or 3 questions of actual subject, then display all teaching and testing layers in depth 3

3.3 Altering of Student's Properties

Student's properties are measured by short and inaccurate questionnaire that is filled only at the beginning of the study. But the properties can be measured incorrectly even under the best circumstances, when long questionnaire with many questions is used and the final evaluation is done by psychologist and not the computer program. Because of this it's appropriate to measure the student's properties with multiple methods. And one of the more accurate methods that we can use in e-learning is to watch the student's teaching process.

Virtual teacher is adapting the teaching process on the basis of student's properties. So, if the student's property is changed, the way of teaching is also changed. The goal is to display the learning content in the most appropriate form for the student, so he can learn quickly and easily. We can assume that the form of content that the student is often requesting is good for him and he will learn better from it. It is the student who has the major responsibility for his learning, so it is suitable to give him more control over his learning. That's why the student's properties will be altered by the student's repeated requests and the requested form will be displayed by default. Form of the content is given by adaptive rules that are based on student's properties. And for each student's repeated request can be found either exactly one rule, which can fulfill the request, or none. If none rule is found, nothing is changed. If one rule is found, then the student's properties are changed so they are closer to the properties in condition of the found rule. The more often the student will repeat this request the closer will be his properties to the properties used in found rule. In time will be the student's properties close enough to the properties in rule's condition. Then the rule will be used and the requested form will be displayed to the student by default.

4 Conclusion

Automatic data analysis described above will enable to easily assess the feedback from adaptive e-learning study. This analysis also allows the system to react on this feedback and adapt the learning content in real time.

The goal of this work is not to find the most effective way of teaching, but to create system, which can effectively help in finding it. For these reasons is the system designed very generally, so it's easy to change its behavior in various ways.

This system is now being implemented in PHP and MySQL. The release date of basic adaptive version that can do all tasks described here is scheduled at the end of year 2012. Then it will be used in limited teaching of subjects prepared in adaptive form and the collected data will be closely analyzed.

References

1. Takács, O., Kostolányová, K., Šarmanová, J.: Adaptation of Presentation and Structure of e-Learning Material. In: IASK, (2010) 215-222

2. Holub, L.: Automatizované řízení adaptivní výuky v e-learningu podle stylů učení studenta. VŠB-TUO (2010)
3. Kostolányová, K.: Teorie adaptivního e-learningu, University of Ostrava (2012)
4. Kristiánová, O.: Datový sklad procesů e-learningu, VŠB-TUO (2011)

P Systems for Traffic Flow Simulation

Lukáš Vojáček¹, Zbyněk Janoška², and Jiří Dvorský^{1,2}

¹Department of Computer Science, FEECS,
VŠB – Technical University of Ostrava, 17. listopadu 15, 708 33 Ostrava – Poruba
`lukas.vojacek@vsb.cz`

²Department of Geoinformatics, Palacký University,
Třída Svobody 26, 771 46 Olomouc, Czech Republic
`zbynek.janoska@cdiv.cz`

Abstract. Membrane computing is an emergent branch of natural computing, taking inspiration from the structure and functioning of a living cell. P systems, computing devices of this paradigm, are parallel, distributed and non-deterministic computing models which aim to capture processes taking place in a living cell and represent them as a computation. In last decade, a great variety of extensions of model, introduced by Paun in 1998, were presented. In this paper, we focus on modelling the traffic flow by the means of P systems. P systems enable mesoscopic representation of traffic flow with individual modelling of each cars behaviour. Theoretical model is presented together with an XML scheme to store the output of the model.

Keywords: membrane computing, P systems, traffic flow, XML

1 Introduction

Membrane computing represents new and rapidly growing branch of natural computing, which starts from observation that the processes taking place in a living cell can be understood as a computation. Membrane computing and its computational device – *P system* – were introduced by Păun [6] and gained a lot of interest in last decade. P systems start from observation, that membrane plays a fundamental role in the functioning of a living cell. Membranes act as three-dimensional compartments which delimit various regions of a living cell. They are essentially involved in a number of reactions taking place inside cell and moreover act as selective channels of communication between different compartments of a cell [2].

P systems take inspiration from cell on two levels – the structure and the functioning. Structure of cell is represented by its membranes and functioning is governed by biochemical reactions. Every P system therefore has three main elements: a *membrane structure*, where *object* evolve according to given *evolution rules* [8]. Some authors add fourth basic element of membrane systems – *communication* [2, 7]. Communication is always encoded in rules (they are called

communication rules instead of evolution rules) and will be dealt with later in the text. From the point of view of transportation modelling, communication (e.g. topology) is essential feature.

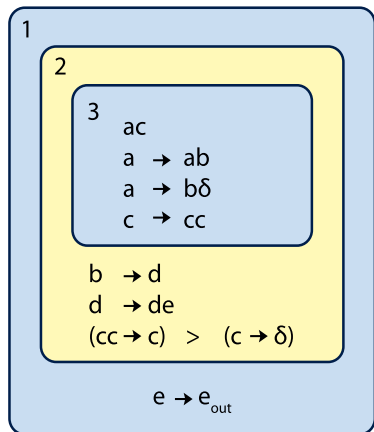


Fig. 1. Graphical representation of P system, [13]

Simple example of P system is depicted in Fig. 1. Membrane structure is hierarchically arranged set of membranes, contained in a distinguished outer membrane, called *skin* membrane. System is surrounded by the *environment*, which may collect objects leaving the system, or in some variants of P systems, the environments can actively support system with objects [1, 3]. Membranes delimit *regions*, with which they are in one-to-one relation. Therefore the terms *membrane* and *region* are mostly interchangeable. Each membrane is identified by its *label*, which can be with membranes in one-to-many relation. The position of inner membranes does not matter; we assume, that in membrane *there is no ordering, everything is close to everything else* [8].

Second basic element of P systems are *objects*. By objects in biological sense are meant chemicals, ions, molecules etc. Those substances are present in a cell in enormous amounts, but the ordering again does not matter. What matters is the concentration, the population, the number of copies of each molecule [8]. Abstracting from biological reality, we represent each substance by a symbol from given alphabet and since the multiplicity matters, instead of objects we use *multisets* of objects. Common notation of multisets in P systems is following: if, for example, objects *a, b, c* are present in 7, 2 and 5 copies, they will be represented by multiset $a^7b^2c^5$.

2 Transition P system

P systems based on application of *multiset-rewriting rules* are called *transition P system*. Formally, transition P system is a construct of the form:

$$\Pi = (O, C, \mu, w_1, w_2, \dots, w_m, R_1, R_2, \dots, R_m, i_o), \tag{1}$$

where:

- *O* is the finite and non-empty alphabet of objects,
- $C \subset O$ is the set of catalysts,
- μ is a membrane structure, consisting of *m* membranes, labeled 1, 2, ..., *m*; one says, that the membrane structure, and hence the system, is of degree *m*,
- w_1, w_2, \dots, w_m are strings over *O* representing multisets of objects present in regions 1, 2, ..., *m* of membrane structure,

- R_1, R_2, \dots, R_m is finite set of evolution rules associated with regions $1, 2, \dots, m$ of membrane structure,
- i_o is either one of the labels $1, 2, \dots, m$ and then the respective region is the *output region* of the system, or it is 0 and then the result of the computation is collected in the environment of the system.

A sequence of transitions of P system constitutes a *computation*. A computation is successful if it halts, it reaches a configuration where no rule can be applied to the existing objects, and output region i_o still exists [8].

The rules are of form $u \rightarrow v$, where $u \in O$ and $v \in (O \times Tar)$, where $Tar = \{here, in, out\}$. Target indications Tar extend transition P system in following way: rule $ab \rightarrow c_{here}d_{in}e_{out}$ consumes one instance of each a and b and produces one copy of c in current membrane, one copy of d in a child of current membrane and one copy of e in the parent of current membrane. If current membrane is skin membrane, object e is send to environment of the system. If current membrane does not have a child, rule can not be applied.

Another extension comes from the existence of *catalysts*. Catalysts are objects, which participate in a chemical reaction, but are not consumed or produced by it. They just enable the application of rule. Rule with catalysts takes following form: $ac \rightarrow bc$, with object c being the catalyst.

3 P system based model of traffic flow

In this section we describe P system model of traffic flow. This model aims to capture detailed behaviour of cars at the intersection, while ignoring behaviour at road segments.

3.1 Definition of a system

Within P systems paradigm, road network can be described as a graph with membranes at the nodes. This representation is similar to the one of communication P systems [11]. There are three types of membranes, based on their function. *White holes* act as generators of cars. If the systems represents, say, a city, than white holes will be the roads, bringing cars to the city. Opposite reactions take place in *black holes*, where the cars leave the system. White and black holes does not necessarily have to be only at the periphery of the system – also residential, industrial or business areas within the city can act as white or black holes, and they can therefore be placed arbitrarily in the graph. The third type of nodes is an *intersection*. At intersection, cars are distributed to other parts of the network.

Within this paradigm, cars are represented as objects. For the sake of brevity, we will consider only one type of object – an arbitrary vehicle. In praxis, however, different types of vehicles (cars, buses, motorcycles etc.) can be represented by different objects.

The behaviour of objects is described by a set of rules. In classical P systems, rules enable objects to be created, destroyed or qualitatively changed. In

the proposed system, each of these is encapsulated in one type of membranes. In white holes, objects are created, in black holes, they are removed from the system, and at the intersections, they are changed (meaning they can change their state from moving to stopping or vice versa). At the intersections, objects are communicated to other membranes in the system.

Clearly, the behaviour of cars is not strictly deterministic, therefore stochasticity must be introduced at some point. There are two ways to represent the behaviour of a car in the network.

- When an object is introduced to the system at white hole A , a target destination B is chosen from set of available black holes. The shortest path between nodes A and B is calculated and vector of intersection, which must be passed by an object is assigned to it. For each white hole, a set of probabilities is assigned to all available black holes. Therefore, some paths are preferred by the cars then others.
- For each intersection, a set of probabilities is assigned to all intersecting roads. When a car is present at the intersection, a road is chosen and car is send to next node of a graph. Each road is associated with a certain probability of being chosen, therefore some links are more preferred by cars than others.

First approach is preferable in case, where the preferences of cars in the network are well known. If we lack the knowledge about drivers preferences and know only vehicle intensities at the roads, second approach seems more suitable.

Also, travel time have to be taken into account. Time necessary to travel from one node of a graph to another is represented by a cost of the link. Graph is oriented, therefore travel time between two nodes can differ in both directions.

Last issue is associated with representation of traffic lights. At intersection, only cars approaching from a certain direction are allowed to pass. Within P systems framework, membrane polarizations are suitable tool for selective allowance of objects into a membrane. The polarization of each intersections represents red/green lights and periodically changes, therefore simulating real world situation.

3.2 Formal definition of a model

Traffic P system is a construct:

$$TrafficP = (O, \mu, syn, (s_{(i,j,t)})_{(i,j) \in syn; t \in \mathbb{N}}, R), \tag{2}$$

where:

- $O = \{veh, veh_s\}$ is an alphabet of objects, veh representing moving vehicle and veh_s representing stopping vehicle,
- μ is a membrane structure, consisting of m membranes, labeled WH, BK, INT ; representing white holes, black holes and intersections,

- $syn \subseteq \{(i, j, t) | i, j \in \{0, 1, 2, \dots, m\}, i \neq j, t \in \mathbb{N}\}$ is a subset of synapses – links between the membranes, where i and j are membranes from the set μ and t is time constant associated with each synapse.
- R is a set of rules associated with membranes from μ . The rules differ for membranes labeled as white holes, black holes and intersections.

- White holes – vehicles veh are generated and sent to one of neighboring membranes.

$$[]_{WH} \xrightarrow{t_i} [veh^{WH}]_k,$$

where $\{k, WH, t_i\} \in syn$ and application of a rule takes t_i time steps. A label of white hole will be associated with a vehicle veh when approaching intersection k , which will be used to decide, whether a vehicle should stop or pass the intersection.

- Black holes – vehicles veh are removed from the system.

$$[veh]_{BH} \xrightarrow{t=1} []_{WH},$$

application of such rule takes 1 time unit.

- Intersection – several rules are associated with intersections. Here we describe a situation, where car makes a decision about its target destination at each intersection.

Rule:

$$[veh^k]_m \xrightarrow{t_i, p_i} [veh^m]_n$$

describes a situation, where car coming from membrane k approaches an intersection m with polarization k . Since the polarization and label of veh correspond, a veh can pass the intersection and proceed to membrane n , with probability p_i . veh will be assigned with label of passed membrane m . Application of rule will take t_i time units.

Rule:

$$[veh^k]_m \xrightarrow{t=1, p=1} [veh_s]_m^l$$

describes a situation, where moving car veh coming from membrane k approaches an intersection m with polarization l . Since the polarization and label of veh do not agree, the vehicle veh must stop and therefore changes to veh_s , with probability 1 and taking 1 time step.

Rule:

$$[veh_s^k]_m \xrightarrow{t_i, p_i} [veh]_n$$

describes a situation, where stopping car veh_s from membrane k is in membrane m with polarization k ; it can pass the intersection and continue to membrane n . This is enabled by changing polarizations of membranes.

Global clock for the system are assumed. The polarization of membranes changes according to a given schedule. All other parameters of the system - creation rate at white holes, probabilities and time constants associated with the synapses can also be time-dependent.

4 Publications

1. Lukas Vojacek, Zbynek Janoska, Jiri Dvorsky, : P Systems for Traffic Flow Simulation. In *The 11th International Conference on Computer Information Systems and Industrial Management Applications (CISIM 2012)*.
2. Lukas Vojacek, Jan Martinovic, Katerina Slaninova, Jiri Dvorsky, Ivo Vondrak: Parallel Hybrid SOM Learning on High Dimensional Sparse Data. In *The 10th International Conference on Computer Information Systems and Industrial Management Applications (CISIM 2011)*.

Acknowledgement

This article is based on paper published on CISIM 2012.

References

1. Bernardini, F., and Manca, V. Dynamical aspects of P systems. *BioSystems* 70 (2). 2003. Pages 85-93.
2. Bernardini, F., and Gheorghe, M., and Krasnogor, N., and Muniyandi R.C., and Perez Jimenez, M.J., and Romero-Campero, F.-J. On P Systems as a Modelling Tool for Biological Systems. *Pre-Proc. of the sixth Workshop on Membrane Computing*. Vienna, Austria, 2005. Pages 114-133.
3. Cavaliere, M. Evolution-Communication P Systems. Proceeding WMC-CdeA '02 Revised Papers from the International Workshop on Membrane Computing. 2003. Pages 134-145.
4. Hoogendoorn, S.P., and Bovy, P.H.L. State-of-the-art of Vehicular Traffic Flow Modelling. *Delft University of Technology, Delft, The*. 2001. Pages 283-303.
5. Obtulowicz, A., and Păun, Gh. (In search of) Probabilistic P systems. *Biosystems* 70 (2). 2003. Pages 107-121.
6. Păun, Gh. Computing with Membranes. *Technical report, Turku Center for Computer Science-TUCS*. Turku, Finland, 1998.
7. Păun, A., and Păun, Gh. The Power of Communication: P Systems with Symport/Antiport. *New Generation Computation* 20 (3). 2002. Pages 295-306.
8. Păun, Gh. Introduction to Membrane Computing. *First brainstorming Workshop on Uncertainty in Membrane Computing*. Palma de Mallorca, Spain, 2004. Pages 1-42.
9. Pescini, D., and Besozzi, D., and Mauri, G., and Zandron, C. Dynamical probabilistic P systems. *International Journal of Foundations of Computer Science* 17 (1). 2006. Pages 440-447.
10. Peeta, S., and Ziliaskopoulos, A.K. Foundations of dynamic traffic assignment: The past, the present and the future. *Networks and Spatial Economics* 1. 2001. Pages 1233-1265.
11. Verlan, S., and Bernardini, F., and Gheorghe, M., and Margenstern, M. Generalized communicating P systems. *Theoretical Computer Science* 404 (1-2). 2008. Pages 170-184.
12. The P Systems Web Page. <http://ppage.psystems.eu/>. Last revision: 2012-03-18.
13. P system - Wikipedia, the free encyklopedia. http://en.wikipedia.org/wiki/P_system. Last revision: 2012-03-18.

Author Index

- Al Fatlawi, Amer Kareem, 239
- Babskova, Alisa, 559
Bašniar, Václav, 309
Bednář, Pavel, 314
Berek, Petr, 564
Bílek, Pavel, 114
Bilík, Petr, 213, 251, 257
Blaheta, Radim, 379
Böhm, Stanislav, 625
Bocheza, Jiří, 453, 476, 518
Burda, Pavel, 373
Bureš, Miroslav, 458
Byczanski, Petr, 379
- Campos, Filipe, 201
Carbol, Zbyněk, 3
Cubik, Jakub, 464
- Diviš, Daniel, 9
Dobrovsky, Marek, 120
Dohnálek, Pavel, 570
Doricak, Jan, 464
Dubec, Patrik, 631
Dvorský, Jiří, 662
- Đurica, Maroš, 14
- Fajkus, Marcel, 470
Farnik, Adam, 637
Folvarčný, Aleš, 126
Friedrich, Jiří, 132
Friedrichová, Kristýna, 207
Fusek, Radovan, 320, 349, 355
- Ganiyev, Artem, 518
Grunt, Ondrej, 361
- Hajduková, Zdeňka, 399
Hapla, Václav, 367
Hasal, Martin, 373
Hejduk, Stanislav, 453, 476, 518
Hercík, Radim, 201
Holčáková, Regina, 138
Holiš, Michal, 643
Holmbacka, Simon, 239
Holuša, Michael, 325
Horák, Bohumil, 207
- Horák, David, 367
Horinek, Marek, 213
Hořejší, Jaroslav, 576
Houdek, Vít, 20
Hromják, Michal, 143
Hrtus, Rostislav, 379
Hrvolova, Barbora, 303
- Chupáč, Luboš, 343
Chvalek, Roman, 239
- Janoška, Zbyněk, 662
Janurová, Kateřina, 195
Jarošová, Marta, 385
Jirka, Jakub, 220, 291
- Kabelíková, Pavla, 423
Kapicak, Lukas, 482
Kepak, Stanislav, 464
Kijonka, Jan, 227
Klein, Lukas, 165
Koběorský, Ondřej, 581, 592
Kocian, Jiri, 233
Kocyan, Tomáš, 586
Konecny, Jaromír, 239
Kopka, Martin, 581, 592
Kostolányová, Kateřina, 656
Košínar, Michal, 331
Kotas, Petr, 392
Koudelka, Petr, 488
Kowol, Marcin, 538
Koziorek, Jiri, 233, 285
Kozubek, Tomáš, 385
Krňa, Petr, 149
Krohova, Jana, 303
Krutil, Jonáš, 598
Kučera, Radek, 405
Kudělka, Miloš, 598
Kuráňová, Pavlína, 399
- Lasar, Miroslaw, 526
Látal, Jan, 488, 518
Líner, Andrej, 470, 488
- Macek, Jakub, 337
Mañas, Jakub, 245
Marek, Martin, 49
Markopoulos, Alexandros, 385

Meca, Ondřej, 625
Menšík, Marek, 343
Menšík, Martin, 385
Merta, Michal, 367
Michalski, Paweł, 532
Michna, Viktor, 291
Mikulec, Martin, 500
Motyčková, Kristina, 405
Mozdřeň, Karel, 320, 349, 355
Mynarek, Piotr, 538

Nemec, Lili, 201
Nevlud, Pavel, 482

Odlevák, Lukáš, 154
Opluštil, Josef, 171, 177

Pápeš, Martin, 470, 488
Partila, Pavol, 506
Paulinský, Lukáš, 61, 494
Penhaker, Marek, 227, 303
Pětvaldský, Petr, 251
Plaček, Martin, 643
Platoš, Jan, 564, 604
Plucar, Jan, 631
Pokorný, Viktor, 26
Pospíšil, Lukáš, 411
Praks, Pavel, 399
Praužek, Michal, 220
Prílepok, Michal, 604
Przybyła, Tomasz, 542
Pustková, Radka, 291
Pyka, Tomasz, 546

Rapant, Lukas, 417
Ronovský, Aleš, 423
Rozehnal, Petr, 32
Rozhon, Jan, 500

Řepka, Pavel, 257

Safarik, Jakub, 506
Santana – Alonso, Alejandro, 201
Silva, Dorotea Bueno, 239
Skalny, Pavel, 429
Skanderová, Lenka, 650
Slabý, Roman, 262
Slíva, Ladislav, 159
Smoček, Martin, 37
Smondrk, Maros, 303

Snášel, Václav, 564, 598, 604
Sojka, Jaroslav, 43
Sokanský, Karel, 3
Stachoň, Martin, 435
Stankus, Martin, 267
Staš, Peter, 49
Stemplewski, Sławomir, 550
Stuchlý, Jindřich, 55
Sudoł, Adam, 550
Svoboda, Pavel, 61, 494

Šarmanová, Jana, 656
Šnobl, Jaroslav, 67
Šofer, Michal, 49
Šprlák, Roman, 177, 183
Šrámek, Jan, 73
Štolfa, Jakub, 581, 592, 610
Šumpich, Jan, 3
Šurkala, Milan, 320, 349, 355

Takács, Ondřej, 656
Tomala, Karel, 500
Tomis, Martin, 512
Tutsch, Michal, 273
Tvrdoň, Martin, 189

Uher, Marián, 84
Unger, Jan, 90

Vaculík, Jan, 96
Valová, Lucie, 279
Vasatova, Alena, 441
Vavrla, Tomas, 285
Vích, Lukáš, 343
Vitásek, Jan, 476, 488, 518
Vlach, Karel, 291
Vo, Tien Trung, 79
Vojáček, Lukáš, 662
Vojčinák, Petr, 297
Vondrák, Vít, 423
Vozda, Michal, 303
Vramba, Jakub, 102
Vychodil, Jiri, 506

Witas, Karel, 476

Zach, Petr, 108
Zaorálek, Lukáš, 616
Zdráhala, Adam, 447
Zdrálek, Jaroslav, 458

Editors: Michal Krátký, Jiří Dvorský, Pavel Moravec
Dept. of Computer Science
VŠB – Technical University of Ostrava

Title: WOFEX 2012

Place, year, edition: Ostrava, 2012, 1st

Page count: 688

Edit: VŠB – Technical University of Ostrava,
17. listopadu 15, 708 33 Ostrava-Poruba
Czech Republic

Print: Tiskárna Tiskservis
gen. Sochora 1764, 708 00 Ostrava-Poruba
Czech Republic

Impression: 200

Not for sale.

ISBN 978-80-248-2769-8